

Geotechnical Engineering and Soil Testing

AMIR WADI AL-KHAFAJI
Bradley University

ORLANDO B. ANDERSLAND
Michigan State University

New York

Oxford

OXFORD UNIVERSITY PRESS

OXFORD UNIVERSITY PRESS

Oxford New York
Athens Auckland Bangkok Bombay
Calcutta Cape Town Dar es Salaam Delhi
Florence Hong Kong Istanbul Karachi
Kuala Lumpur Madras Madrid Melbourne
Mexico City Nairobi Paris Singapore
Taipei Tokyo Toronto

and associated companies in
Berlin Ibadan

Copyright © 1992 by Oxford University Press, Inc.

Published by Oxford University Press, Inc.
198 Madison Avenue, New York, New York 10016

Oxford is a registered trademark of Oxford University Press

All rights reserved. No part of this publication may be reproduced, stored in a retrieval system, or transmitted, in any form or by any means, electronic, mechanical, photocopying, recording, or otherwise, without the prior permission of Oxford University Press.

CIP data available upon request

ISBN 978-0-19-510719-7

1 3 5 7 9 8 6 4 2
Transferred to Digital Printing 2007

Preface

Geotechnical Engineering and Soil Testing is intended for use in the first of a two-course sequence usually taught to third- and fourth-year civil engineering students. The text introduces students to soil materials as they relate to geotechnical engineering problems. Soil exploration with retrieval of samples permits evaluation of the soil behavior by use of laboratory tests. With preparation of a general picture of the underlying soil conditions at a site (soil profile) and a working knowledge of how soil behaves as a material, civil engineering technology can be applied to the design of foundations, slope stability problems, earth dams, and retaining structures. The design aspects are introduced in the final chapters and are covered extensively in subsequent courses. Students are assumed to have a working knowledge of undergraduate mechanics (statics, mechanics of materials, and fluids). Some knowledge of basic geology is desirable.

APPROACH

An introduction to the nature and properties of soil materials builds on the knowledge of mechanics and geology. The *language* of geotechnical engineering is presented in terms of the classification and engineering properties of soils. A working knowledge of how soil behaves is acquired from a study of known behavior along with laboratory work on properties important to geotechnical engineering problems. Innovative instructors can add supplementary design examples to the final

chapters should they so desire. The integration of introductory geotechnical topics along with laboratory methods into one textbook attempts to meet a longtime need in the field. The laboratory portion of a first course is an essential part of the new engineer's experience with soils as a unique engineering material. An emphasis on laboratory and field testing is provided by the 29 experiments. The order of laboratory experiments or field tests closely follows the organization and development of the text material.

ORGANIZATION

The early chapters introduce soil materials, soil exploration, and index properties of soils. Laboratory topics parallel class work with initial emphasis on phase relations, classifications of soils, and simple classification tests. A practical discussion of compaction is given in Chapter 4. Permeability and seepage serve as background on effective stress (Chapter 6), on volume change in soils (Chapter 7), and on shear strength (Chapter 8). Stresses within a soil mass are thoroughly reviewed in Chapter 6. The stress deformation and strength characteristics of soils are discussed relative to practical engineering applications. Immediate and consolidation settlement theories are introduced in Chapter 8. Closed form and numerical solutions are thoroughly discussed. The finite difference and Eigen methods for solving time rate of settlement problems are presented. Both single and multilayer time rate of settlement problems are covered. Laboratory work is directed to the more common compression and strength tests. A discussion of experimental work with example results is provided for each laboratory test. Design aspects, including lateral earth pressure problems, bearing capacity, and slope stability are introduced in Chapters 9, 10, and 11. Laboratory data sheets and a glossary of soil terms are found at the end of the textbook.

LEARNING AIDS

The many fully worked example problems and laboratory experiments make the book user friendly. In a formal course, this aspect of the book will free the instructor from the necessity of working examples during lectures. The instructor will have more time to concentrate on basic principles and specific engineering applications. Problems are provided at the end of each chapter. Questions for further study are included at the end of each experiment and may be used for independent study topics, honors work, or to provide a challenge to the more advanced students. The instructor's solution manual provides full documentation of the solution to the problems found at the end of each chapter. For convenience to the reader, engineering properties for a wide variety of soils are included in the text. Also, basic definitions of terms used in geotechnical engineering are included with information on SI units and conversion factors. Examples are worked using SI or U.S. customary units enabling the reader to gain insights into the concepts irrespective of the units being used. Most of the figures and the tables have both SI

and U.S. customary units. The data forms used in each of the 29 laboratory experiments are included at the end of the textbook. Students should make copies of these forms when conducting an experiment. It is suggested that the forms be copied and, if necessary, enlarged by the instructor, then made available to students. The basis and recommendations relative to several commercially available geotechnical computer programs are provided.

ACKNOWLEDGMENTS

The authors are grateful to the many colleagues and students who have contributed significantly and often indirectly to their understanding of geotechnical engineering. Contributions by many individuals are given credit by reference to their published work and by quotations. The source of photographs is indicated in each case. This book has been written on the proposition that good judgment comes from experience and that experience comes from poor judgment. The quality of this book has been and will continue to be judged by our students and colleagues whose comments and suggestions have contributed greatly to the successful completion of the final manuscript. We are indebted to Professor Ted Vinson of Oregon State University who provided several examples and insights during the development of this book. We are grateful to Professor Farzad Shahbodaghlou of Bradley University and his wife Moji for their significant help in finalizing the manuscript. Our sincere thanks to Julie Dell for her help in preparing some of the figures. Our families and especially our wives Wilma Al-Khafaji and Phyllis Andersland deserve our appreciation and respect for their tolerance and dedication. We would not have been able to complete this project without their support and encouragement.

The authors appreciate the efforts of the following reviewers who, by their criticisms and helpful comments, have encouraged us in the preparation and finalization of the manuscript.

Joseph Martin, Drexel University

Wayne A. Charlie, Colorado State University

Bernard D. Alkire, Michigan Technological University

George P. Korfiatis, Stevens Institute of Technology

Sukhmander Singh, Santa Clara University

Robert D. Krebs, Virginia Polytechnic Institute and State University

Our thanks to Laura Shur, Barbara Gingery, and Martha Brown of Saunders College Publishing. They deserve special acknowledgment for their dedication and hard work.

Amir Wadi Al-Khafaji
Orlando B. Andersland
February 1992

Contents

PREFACE vii

1 SOIL MATERIALS 1

- 1.0 Introduction 1
- 1.1 Soil Composition 5
- 1.2 Soil Deposits 15
- 1.3 Soil Profile 22
- 1.4 Soil Engineering Problems 24

2 SOIL EXPLORATION 33

- 2.0 Introduction 33
- 2.1 Scope of Subsurface Exploration 34
- 2.2 Exploratory Investigation Using Geophysical Methods 38
- 2.3 Exploratory Subsurface Investigation Using Direct Methods 43
- 2.4 Detailed Subsurface Investigation 47
- 2.5 Presentation of Results and Reports 59

3 INDEX PROPERTIES OF SOILS 64

- 3.0 Introduction 64
- 3.1 Water in Soils 65
- 3.2 Grain Size and Shape 75
- 3.3 Soil Aggregate 77
- 3.4 Consistency and Sensitivity of Clays 86
- 3.5 Organic Soils 90
- 3.6 Soil Classification 93
- 3.7 Typical Values and Uses of Soil Parameters 106

4 SOIL COMPACTION 113

- 4.0 Introduction 113
- 4.1 Compaction Theory 113
- 4.2 Properties of Compacted Soils 116
- 4.3 Field Compaction and Ground Modification 119
- 4.4 In-Place Determination of Soil Density 128

| | | |
|----------|---|------------|
| 5 | WATER FLOW THROUGH SOILS | 132 |
| 5.0 | Introduction | 132 |
| 5.1 | Darcy's Law | 133 |
| 5.2 | Permeability Measurement—Laboratory | 136 |
| 5.3 | Permeability Measurement—Field | 139 |
| 5.4 | Hydraulic Heads in Soil | 145 |
| 5.5 | Basic Equation for Fluid Flow in Soil | 152 |
| 5.6 | Analytical Methods for Solving Fluid Flow Problems | 155 |
| 5.7 | Flow Net for One-Dimensional Flow | 160 |
| 5.8 | Flow Net for Two-Dimensional Confined Flow | 164 |
| 5.9 | Flow in Anisotropic Soil | 168 |
| 5.10 | Unconfined Flow | 170 |
| 5.11 | Seepage Force and Critical Gradient | 178 |
| 6 | STRESSES WITHIN A SOIL MASS | 187 |
| 6.0 | Introduction | 187 |
| 6.1 | The Effective Stress Concept | 188 |
| 6.2 | Mohr Circle of Stress | 198 |
| 6.3 | The Pole Method of Stress Computation | 201 |
| 6.4 | Stress Due to a Point Load | 204 |
| 6.5 | Stress Due to an Infinite Line Load | 208 |
| 6.6 | Stress Due to an Infinite Strip Load | 212 |
| 6.7 | Stress Due to a Linearly Increasing Infinite Strip Load | 213 |
| 6.8 | Stress Distributions Due to an Asymmetrical Triangular Load | 216 |
| 6.9 | Stress Due to a Vertical Embankment Load | 217 |
| 6.10 | Stress Due to a Uniformly Loaded Circular Area | 218 |
| 6.11 | Stress Due to a Uniformly Loaded Rectangular Area | 221 |
| 6.12 | Stress Increment Approximation Using Newmark's Chart | 226 |
| 6.13 | Stress Due to any Loaded Area | 231 |
| 7 | VOLUME CHANGE IN SOILS | 244 |
| 7.0 | Introduction | 244 |
| 7.1 | Soil Compressibility | 245 |
| 7.2 | Consolidation and Oedometer Test | 247 |
| 7.3 | Constant-Rate-of-Strain Consolidation | 261 |
| 7.4 | Settlement Analysis | 264 |
| 7.5 | Numerical Solution of Time Rate of Settlement | 281 |
| 8 | SHEAR STRENGTH OF SOILS | 306 |
| 8.0 | Introduction | 306 |
| 8.1 | Soil Deformation Behavior and Strength | 307 |
| 8.2 | Measurement of Soil Stress-Strain Properties | 311 |
| 8.3 | Shear Strength of Soil Materials | 333 |

9 LATERAL EARTH PRESSURE 353

- 9.0 Introduction 353
- 9.1 Earth Pressure at Rest 353
- 9.2 Rankine's Earth Pressure Theory 356
- 9.3 Coulomb's Earth Pressure Theory 364
- 9.4 Culmann's Graphical Method of Solving Coulomb's Theory 376
- 9.5 Point of Application of Earth Pressure Force 382
- 9.6 Wall Movement versus Tilt 382
- 9.7 Effects of Water on Earth Pressure 384
- 9.8 Soil Properties 386

10 BEARING CAPACITY 392

- 10.0 Introduction 392
- 10.1 Factor of Safety 393
- 10.2 Terzaghi's Bearing Capacity Theory for Shallow Foundations 395
- 10.3 Effect of Groundwater Table and Eccentricity 401
- 10.4 Ultimate Bearing Capacity on Two-Layer Cohesive Soil 402
- 10.5 Nominal Bearing Pressure 405
- 10.6 Allowance Settlement versus Allowable Bearing Pressure 405
- 10.7 Bearing Capacity of Deep Foundations 410

11 SLOPE STABILITY 424

- 11.0 Introduction 424
- 11.1 Slope Types and Failure Theories 425
- 11.2 Causes of Instability 427
- 11.3 Stability of Infinite Slopes in Cohesionless Soils 428
- 11.4 Stability of Infinite Slopes in Cohesive Soils 431
- 11.5 Stability of Homogeneous Slopes 433
- 11.6 Method of Slices for Nonhomogeneous Slopes 435
- 11.7 Wedge Method of Analysis 444
- 11.8 Recommended Factors of Safety 445

Experiment 1 Refraction Survey 450

Experiment 2 Field Soil Sample Collection and Description 455

Experiment 3 Laboratory Water Content Determination 458

Experiment 4 Field Water Content Determination 462

Experiment 5 Salinity of Soil Pore Water 466

Experiment 6 Grain Size Analysis—Mechanical Method 472

Experiment 7 Grain Size Analysis—Hydrometer Method 482

| | | |
|----------------------|--|------------|
| Experiment 8 | Specific Gravity of Soil Solids | 493 |
| Experiment 9 | Volumetric–Gravimetric Relationships for Cohesionless Soils | 498 |
| Experiment 10 | Volumetric–Gravimetric Relationships for Cohesive Soils | 502 |
| Experiment 11 | Liquid Limit | 507 |
| Experiment 12 | Plastic Limit | 515 |
| Experiment 13 | Shrinkage Limit | 519 |
| Experiment 14 | Ignition Test | 526 |
| Experiment 15 | Standard Proctor Compaction Test | 530 |
| Experiment 16 | Modified Proctor Compaction Test | 535 |
| Experiment 17 | Relative Density | 540 |
| Experiment 18 | Soil Density—Sand Cone Method | 545 |
| Experiment 19 | Soil Density—Rubber Balloon Method | 551 |
| Experiment 20 | Soil Density—Nuclear Method | 556 |
| Experiment 21 | Coefficient of Permeability—Constant-Head Method | 559 |
| Experiment 22 | Coefficient of Permeability—Falling-Head Method | 564 |
| Experiment 23 | Oedometer Test | 568 |
| Experiment 24 | “Quick” Oedometer Test | 579 |
| Experiment 25 | Direct Shear Test | 585 |
| Experiment 26 | Unconfined Compression Test | 591 |
| Experiment 27 | Consolidated-Undrained Triaxial Test | 598 |
| Experiment 28 | Consolidated-Drained Triaxial Test | 612 |

xiv CONTENTS

Experiment 29 Vane Shear Test 619

Appendix A SI Units and Conversion Factors 623

Appendix B Laboratory Forms 627

Glossary 665

References 678

Index 684

1

Soil Materials

1.0 INTRODUCTION

The term **soil** is used by civil engineers and most geologists to describe the relatively loose agglomeration of mineral and organic materials extending from the ground surface down to solid rock. These soils were formed by weathering and disintegration from solid rock and differ depending on the parent material and the weathering processes involved. Subsequent transportation of these soils by glaciers, wind, and/or water may alter the soil profile and is responsible for the formation of various landforms. These landforms are topographic features that can be recognized in air photos and are often used for engineering soils evaluation of a site. Soil is the oldest building material known. It serves as the support for virtually all structures. For detailed knowledge of soils at a site soil, samples must be obtained on which physical and mechanical properties can be measured.

Geotechnical engineering concerns the application of civil engineering technology to some aspect of the earth. It is one of the very young disciplines within civil engineering. Geotechnical engineering has two main broad areas of emphasis: *soil mechanics* and *foundation engineering*. **Soil mechanics** is concerned with the engineering mechanics and properties of soil materials. **Foundation engineering** applies soil mechanics, structural engineering, geology, and other related sciences to the design of foundations for structures and the construction of earthen structures. Soil mechanics is a science as compared to foundation engi-

neering, which is an art. Geotechnical engineering was not recognized as a discipline until the 1920s, when Terzaghi published his famous first book on soil mechanics. The following examples may provide a perspective on the types of problems with which a geotechnical engineer might be involved.

The Case of the Heaving Freezer

In 1976 a light building was built as a freezer for a fish import firm in southern Indiana. Three years after going into full operation, problems developed. First the floor system began to heave, then cracks appeared in the concrete floor. The local builder who had constructed the whole facility was called back, but he was unable to effect any substantial improvement. By January 1982 it was clear that the freezer would have to be closed. The walls had suffered substantial outward rotation, the roof leaked, and the concrete floor was heaving badly. With no solution to his problems, the owner sued, and a geotechnical engineer was hired as an expert witness.

A preliminary site investigation revealed that the groundwater table was only 7 ft below ground surface. Furthermore, the heaving was most pronounced (2.7 ft) under the center of the concrete floor, as shown in Figure 1.1. Consideration of the architectural plans revealed that the foundation system was not designed to prevent freezing of the ground below. Because the operating temperature was -5°C , it was clear that part of the water table could have been frozen. Utilizing available methods of analyzing frozen soils, the engineer was able

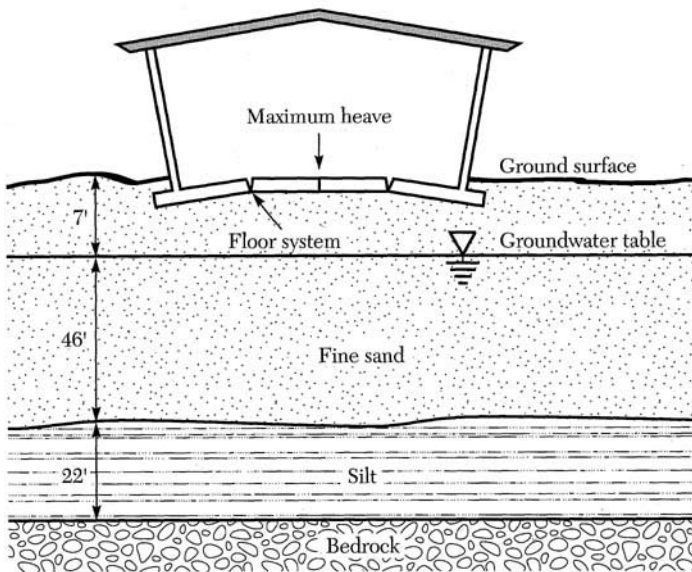


FIGURE 1.1 Exaggerated sketch of freezer and soil cross section.

to verify that part of the water table did freeze. The reason it took seven years to cause the distress in the building was attributable to the freeze and thaw cycle that took place as a result of seasonal temperature changes. The builder settled out of court, and the structure was ultimately used for storage purposes.

The Case of Moving Oil Storage Tanks

While working at a geotechnical firm in Detroit, Michigan, an engineer was asked to investigate an urgent cry for help from a company located at the Detroit River. It was bitter cold, and snow covered much of Detroit. The problem was that several large cracks had appeared on the walls surrounding three oil storage tanks, which were in danger of total collapse.

A quick inspection of the site revealed the existence of several tension cracks on the ground surface that were hidden from view by snow. The engineer immediately placed several markers at critical locations and measured the distances between them. The oil tanks were separated from the river by a berm. The manager of the facilities indicated that during the preceding summer the Detroit River had been dredged so that ships could dock closer to shore. Consequently, the soil profile hidden from view by the river was explored. A cross section of the site was ultimately established, as is shown in Figure 1.2.

Since this facility had existed for several decades without any problems, it became immediately clear that the difficulty had been caused by the removal of soil through dredging. Examination of the distances between markers placed on the site showed appreciable movements (a few inches per day). Using a slope-

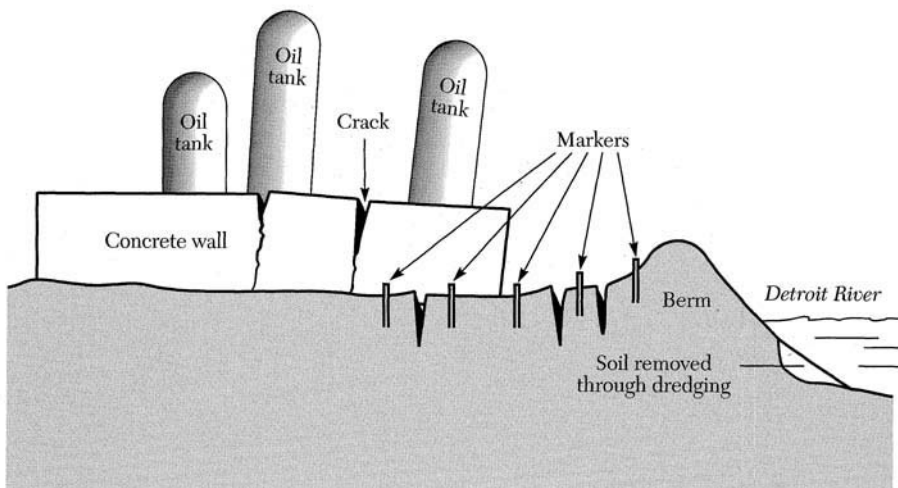


FIGURE 1.2 Exaggerated sketch of the oil storage facility.

stability-analysis computer program, it was possible to examine several solution alternatives. Ultimately, the oil tanks were stabilized by removing part of the soil and then leveling it. This helped reduce the force that had caused the slope to fail in the first place.

The Case of the Unhappy Homeowner

A prominent doctor in Southfield, Michigan, was delighted with his new home when he moved into it with his wife and children in June 1985. The cost was relatively low in spite of the beautiful lakeside view, because he had acquired the land very cheaply. As time passed, the family found a few of the usual faults — skewed door frames, a leaking sewer pipe, and cracking plaster — and the builder rectified all of them. In subsequent years, however, several cracks appeared and were covered with plaster and paint. During 1989 a large crack appeared that seemed to divide the house into two parts, as is depicted in Figure 1.3.

The crack quickly widened to a maximum of 2.25 in. (57 mm) at roof level, tapering to 0.0 in. at ground level. The doctor immediately had the builder inspect the damage. The builder recommended that a consulting geotechnical engineer be hired to investigate the problem. The first task was to gather information relative to site conditions prior to construction. Unfortunately, there were no borings or any other type of information that could be used to analyze the soil. Consequently, three borings were drilled at the locations shown in Figure 1.3. Borings 1 and 2 showed that the soil was mostly silty clay. Boring 2 revealed the existence of an organic soil layer 14 ft thick at a depth of 6.5 ft below ground surface. Laboratory tests indicated that the organic soil layer was highly compressible and could

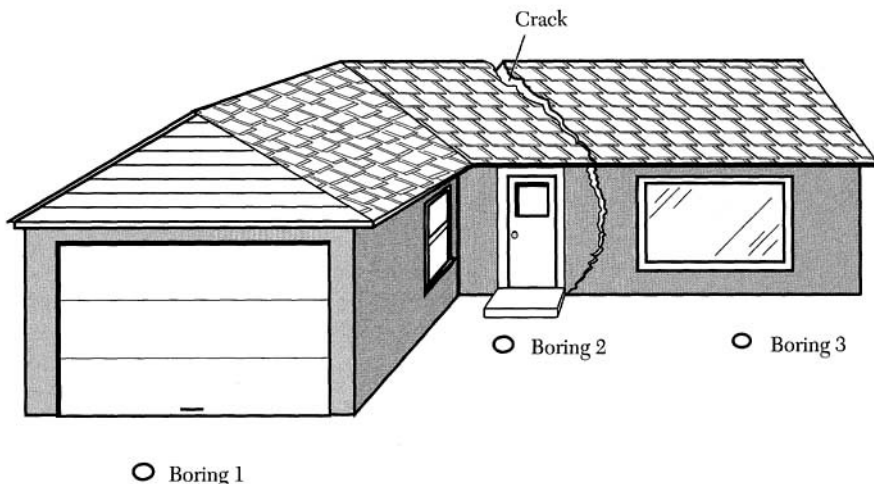


FIGURE 1.3 Sketch of the house, boring locations, and crack.

account for the resulting cracks. Consequently, the doctor sued the person who had sold the property, and the case was settled out of court.

The application of civil engineering technology to some aspect of design and construction with or on soil materials requires that the engineer be able to distinguish among the various soil deposits, identify the principal soil types, and determine their physical and mechanical properties. In a general way, soils can be classified into groups that have somewhat similar engineering properties — *gravel, sand, silt, and clay*. Classification may also be based on mineralogical composition or on the basis of the process (residual soils, glaciation, wind, or water) responsible for their current status. The Unified Soil Classification System (see Section 3.6) utilizes particle size distribution along with selected physical soil properties. Topics introduced in this chapter include the origin and composition of soils, soil deposits, the soil profile, and soil engineering applications.

1.1 SOIL COMPOSITION

1.1.1 Origin and Formation of Soils

All mineral soils are derived from rock as a result of weathering. The parent rocks can be classified according to their mode of formation. Igneous rocks are formed on or at various depths below the earth's surface by the cooling of hot molten material (magma). Sedimentary rocks are formed in layers from sediments that have settled in large water masses. Metamorphic rocks are formed by the alteration of existing igneous or sedimentary rocks under high temperatures and/or high pressures. Rocks included under each class and their essential mineral composition are given in Table 1.1.

The processes of weathering involved in soil formation can be subdivided into those that cause disintegration and those that cause decomposition. Disintegration refers to the weathering of rock by physical agents, such as (1) periodic temperature changes, (2) freezing and thawing, and (3) the prying action of ice, plants, and animals in small cracks. The prying action causes flakes of rock to split away, producing sharp and angular particles. Decomposition refers to the changes in rocks produced by chemical action, such as (1) oxidation, (2) hydration, (3) carbonation, and (4) the chemical effects of plants. Potassium feldspars combine with carbon dioxide to form potassium carbonate or potash, an important soluble plant food. Solution and leaching remove lime and other carbonates from rocks, as well as large amounts of silica. These chemical changes are aided by high temperatures and the presence of organic acids. Where the main process is of a chemical nature, certain minerals in the rock will disintegrate and others will prove resistant. Quartz is exceedingly resistant to chemical decomposition and will usually emerge from the process unchanged. The processes responsible for formation of soil material from the parent rock are outlined in Table 1.2. Note that several factors — including climate, topography, time, geologic history, and rock type — influence the resulting soil type.

| | | | | | | | | | | | | | |
|-----------------------|-----|-----|-----|-----|------|-----|-----|----|-----|------|-----|-----|----------------|
| Metamorphic rocks | | | | | | | | | | | | | |
| Granite gneiss | 169 | 34 | 35 | (4) | — | — | 20 | — | — | — | — | — | 7 |
| Hornblende gneiss | 18 | 10 | 16 | 15 | (3) | 45 | (4) | — | — | — | — | — | 7 |
| Mica schist | 59 | 36 | 14 | (1) | — | — | 40 | — | — | — | — | — | 9 |
| Chlorite schist | 23 | 11 | — | 10 | — | (5) | — | — | 39 | — | 28 | (4) | 3 |
| Hornblende schist | 68 | 10 | (3) | 12 | — | 61 | — | — | — | — | (7) | — | 7 |
| Amphibolite | 22 | (3) | — | 8 | — | 70 | — | — | — | — | 12 | — | 7 |
| Slate | 71 | 29 | (4) | — | — | — | 55 | — | — | — | — | (5) | 7 |
| Quartzite | 61 | 84 | (3) | — | — | — | (4) | — | — | — | — | — | 9 |
| Feldspathic quartzite | 22 | 46 | 27 | — | — | — | (7) | — | (3) | (10) | — | — | 7 |
| Pyroxene quartzite | 11 | 29 | 19 | 15 | (15) | — | — | — | — | — | — | (5) | 8 ⁵ |
| Marble | 61 | (3) | — | — | — | — | — | 96 | — | — | — | — | 1 |

¹ Values shown in parentheses indicate minerals other than those essential for the classification of the rock.

² Includes 10–20% rock glass.

³ Limestone contains 8% of the minerals dolomite; the rock dolomite contains 82% of this mineral.

⁴ Includes 3% opal.

⁵ Includes 3% garnet.

(After U.S. Dept. of Commerce, 1960.)

Sources
(parent rock)

| | | |
|-------------------------|--|--|
| Igneous rock | Formed by solidification of molten materials that originated within the Earth | { Surface or near surface --- { Volcanic ash, pumice, rhyolite, andesite, basalt { Deep seated --- { Granite, diorite, gabbro |
| Sedimentary rock | Formed of material that has settled out of a transporting medium such as water | --- { Sandstone, shale, limestone |
| Metamorphic rock | Formed by creation of new features (minerals and structures) in preexisting rocks by increased temperature and pressure (without passing through a molten state) | --- { Quartzite, gneiss, marble, slate, schist |

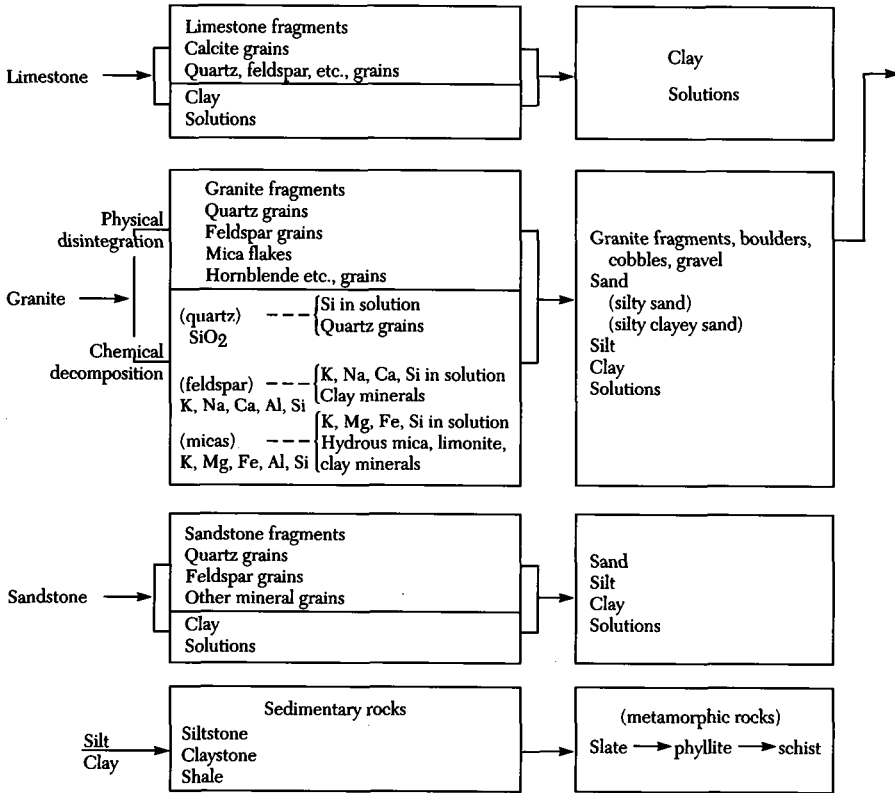
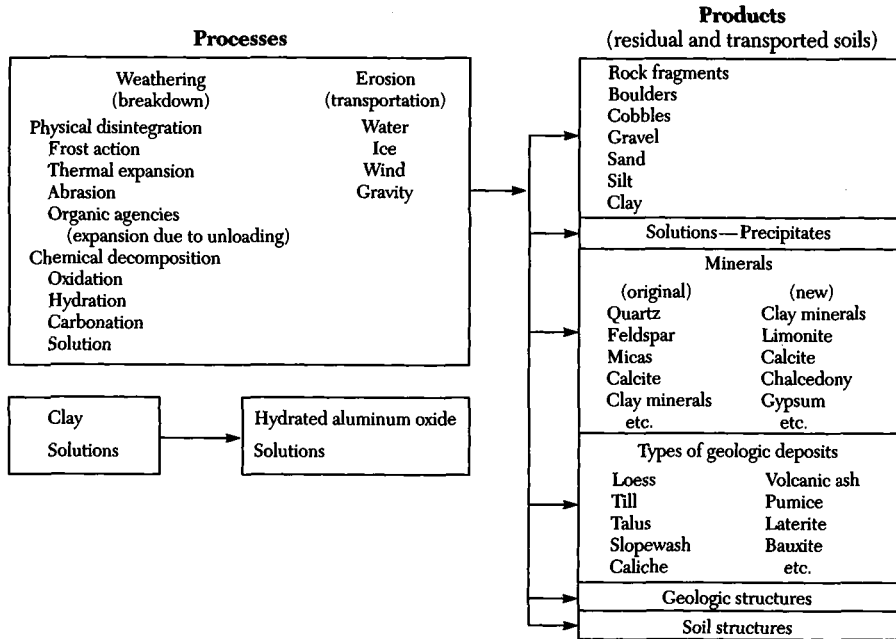
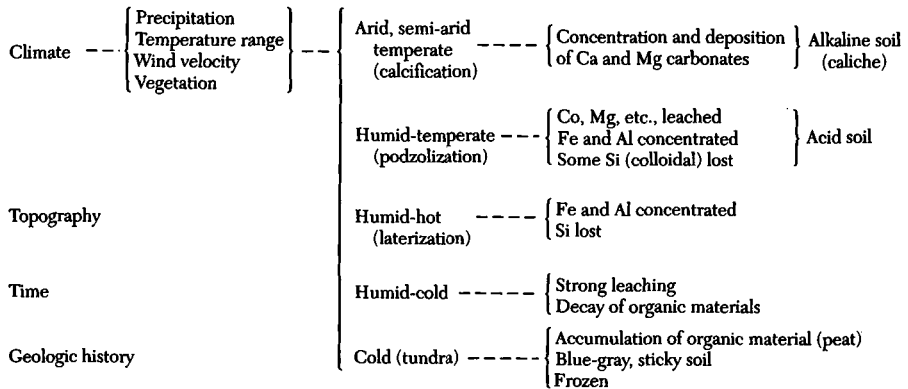


TABLE 1.2 Soil-Forming Processes (U.S. Dept. of Commerce, 1960.)



Factors influencing soil type



Rock type (mineralogy, grain size, hardness, solubility, specific gravity, etc.)

1.1.2 An Assemblage of Particles

The large majority of soils consist of an assemblage of mineral particles together with some water and air. It is convenient to visualize soil as a particulate system composed of solid particles with gas (air) and liquid (usually water) dispersed in the voids between particles. Figure 1.4a represents the three phases as they might typically exist in an element of natural soil. The voids are continuous, so water

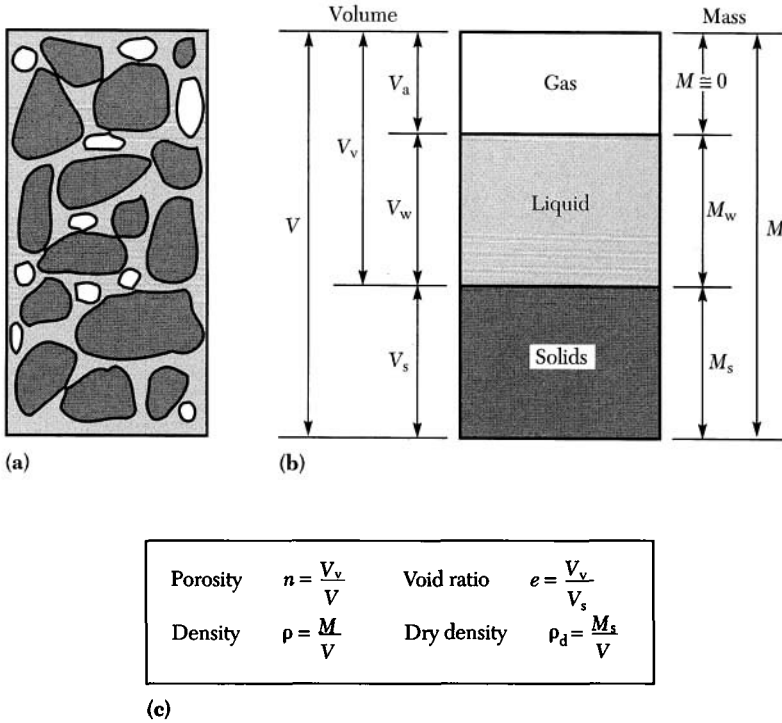


FIGURE 1.4 Three-phase soil system: (a) natural soil sample; (b) separation into phases; (c) definitions.

movement through a soil leads to problems of seepage and permeability. Water has no shear strength, is almost incompressible, and thus transmits fluid pressures within the soil mass. Water can dissolve and carry in solution various salts, some of which alter the soil behavior. The soil mass can be dry (no pore fluid) or fully saturated (no air voids). The process of compaction reduces air voids by packing soil particles more closely together. The phases have been separated in Figure 1.4b in order to simplify the formulation of volumetric and gravimetric proportions. Note that certain basic terms, including *porosity*, *void ratio*, and *density*, are defined in terms of the volumes and masses shown in Figure 1.4b. Phase relationships needed to solve a variety of soil problems are introduced in Section 3.3.

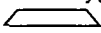
The solid part of the soil mass consists primarily of mineral particles and organic matter in various sizes and amounts. Rock fragments are identifiable pieces of the parent rock containing several minerals. These fragments are fairly large (>1 mm) and can be observed in sands and gravels. The overall soundness of these particles will depend on the extent of decomposition. Mineral grains are separate particles of a particular mineral and may range in size from 2 mm down to 1 μm . Soils may contain a mixture of different minerals or may consist almost entirely of

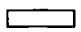
one mineral — for example, sand deposits in which the predominant mineral is quartz.

Soil organic matter originates from plant and/or animal remains and is often observed in various stages of decomposition. The process of decomposition involves microbial activity with the formation of gases, water, new bacterial cells, and volatile acids and a decrease in the organic solids fraction. The end product is known as **humus**, a complex mixture of organic compounds. Prolonged periods of marsh development can result in deposits of organic soil (peat) with a thickness as great as 25 m. The lower portions of the peat layer generally consist of highly decomposed organic material mixed with mineral portions. The middle and top portions contain large amounts of fibrous vegetation. These organic deposits are highly compressible under load; with their low shear strength, they normally have a low bearing capacity.

1.1.3 Clay Minerals

Clay minerals, commonly found in soils, result primarily from the weathering of feldspars and micas, as is indicated in Table 1.2. They usually occur in small particle sizes and thus have considerable surface area per unit mass. These surface areas have a residual negative charge and, when mixed with limited amounts of water, exhibit a plastic behavior. The more common clay mineral groups include kaolin, montmorillonite, illite, and palygorskite. Fringe groups include chlorite, vermiculites, and halloysites. For a classic treatment of clay mineralogy, the reader is referred to Grim (1953).

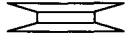
A review of the clay layer–lattice structure helps provide an understanding of clay mineral properties. Layer silicates can be considered in terms of the tetrahedral and octahedral structural units illustrated in Figure 1.5. The tetrahedral unit consists of four oxygens (or hydroxyls, if needed to balance the electrical charge) that enclose a silicon atom. The tetrahedra combine into a sheet structure with all tips pointing in the same direction. The oxygens, at the base of all tetrahedra, are in a common plane and each oxygen atom is shared by two tetrahedrons. The tips of the tetrahedra are hydroxyls in a silica sheet. The layer of silicon atoms between a layer of oxygens and a layer of hydroxyls is conveniently represented by the symbol  with the lower plane corresponding to the base of the tetrahedra.

The octahedral unit shown in Figure 1.5b consists of an aluminum, iron, or magnesium atom enclosed by six hydroxyls. These octahedral units are combined into sheets that may be considered as a layer of aluminum, iron, or magnesium atoms between two layers of densely packed hydroxyls in octahedral coordination. This sheet structure (Figure 1.5b) is represented by the symbol .

The spacing between outer ions in the tetrahedral and octahedral sheets is sufficiently similar for them to link together via mutual oxygen or hydroxyl ions. In a two-layer lattice, tetrahedral and octahedral layers alternate, as is indicated by the symbol for kaolinite in Table 1.3. Kaolinite mineral particles consist of a series of units linked together to form stacks with the approximate length and thickness given in Table 1.3. Hydrogen bonds between layers are comparatively strong,

hence the kaolinite crystal is relatively stable. Water cannot enter between the sheets to expand (or shrink) the unit cells. In the presence of water some hydroxyls dissociate and lose hydrogen atoms, leaving the kaolinite crystal with a small residual negative charge. The exchange capacity, listed in Table 1.3, provides a measure of this residual negative charge.

Halloysite is similar to kaolinite, being composed of the same two-layer lattice units (Table 1.3). The successive units are more randomly packed and may be separated by a single molecular layer of water. When this water layer is removed by drying, the mineral exhibits different properties. In contrast to most other clays, which have a platelike shape, halloysite particles take the form of elongated units (tubes or rods).

The montmorillonite mineral is represented by an octahedral sheet sandwiched between two silica sheets, hence the symbol  is used. The octahedral sheet may contain aluminum, iron, magnesium, or some combination of these atoms. Some of the silica atoms in the tetrahedral sheets (<15%) may be replaced by aluminum atoms. These replacements (by isomorphous substitution) result in the unit having a residual negative charge. Cations in the water (Na^+ , Ca^{++} , or K^+) are attracted to the unit and satisfy a large fraction of the residual charge. The clay particle consists of individual units stacked one above the other

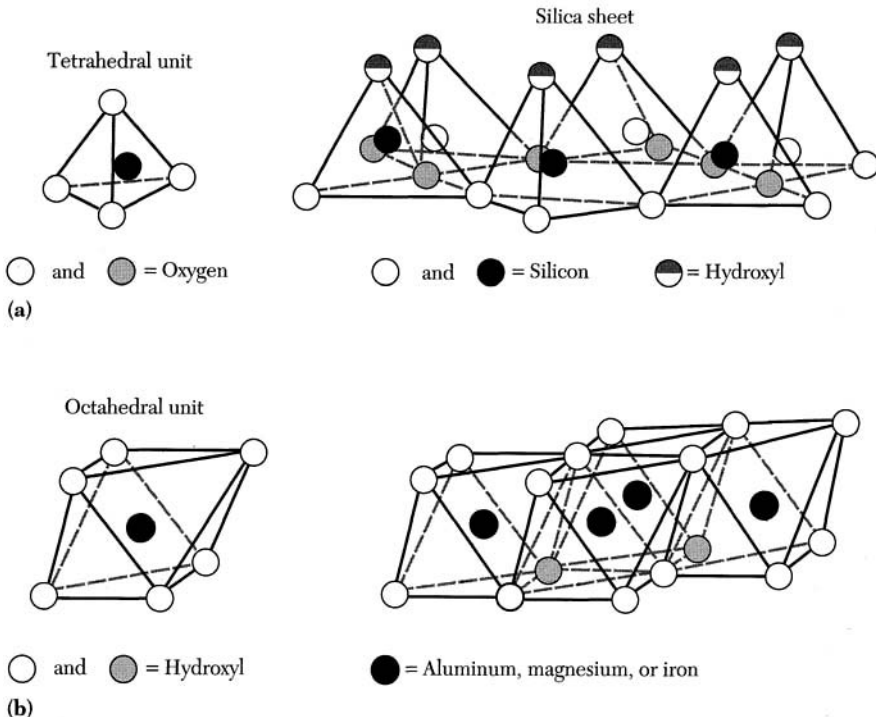
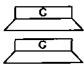
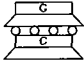
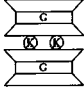
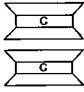
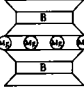


FIGURE 1.5 Clay mineral structural units: (a) silica sheet; (b) octahedral sheet.

TABLE 1.3 Descriptive Information on Several Common Clay Minerals

| Mineral Name | Structure Symbol | Linkage between Sheets | Approximate Particle Size (μm) | Specific Surface (m^2/g) | Approximate Exchange Capacity ($\text{meq}/100\text{g}$) [*] |
|-----------------|--|---------------------------------------|---|--|---|
| Kaolinite |  | H-bond + secondary valence | $L = 0.2-2.0$ $t = 0.05-0.2$ | 10-20 | 5 |
| Halloysite |  | Secondary valence | (tubular) $L = 0.5$ $t = 0.05$ | 40-50 | 15 |
| Illite |  | Secondary valence + K linkage | $L = 0.2-2.0$ $t = 0.02-0.2$ | 80-100 | 25 |
| Montmorillonite |  | Weak cross-linkage between Mg/Al ions | $L = 0.1-1.0$ $t = 0.001-0.01$ | 800 | 100 |
| Vermiculite |  | Secondary valence + Mg linkage | $L = 0.15-1.0$ $t = 0.01-0.1$ | 5-400 | 150 |

^{*} L = length, t = thickness, meq = milliequivalents

with bonding between units being mutual attraction for the (exchangeable) cations plus weak van der Waals forces. These bonds are comparatively weak, so water can enter between sheets, causing them to expand. Soils containing montmorillonite minerals will exhibit high swelling and shrinkage characteristics, the amount depending on the types of exchangeable cations present.

A number of engineering properties are attributable to the size, shape, high surface area, and negative surface charge carried by all clay particles. Two basic types of particle orientations, flocculated (edge-to-face) and dispersed (face-to-face), are observed for clay minerals. Natural clay sediments will have more or less flocculated particle orientations (Figure 1.6). Some bulky silt particles may be present within the soil deposit. In laboratory testing of clay soils for particle size distribution, a flocculated structure can be dispersed by supplying cations from a suitable salt solution, such as sodium hexametaphosphate (see Experiment 6).

A clay soil has some equilibrium water content under a constant ambient pressure and temperature. A change in ambient conditions will bring about a tendency for a change in the water content. Swelling will occur with an increase in

water content, and shrinkage will occur when suction is induced by drying. Soils containing substantial proportions of montmorillonite or illite demonstrate high swelling characteristics. In areas where these surface soils are subject to seasonal wetting (high rainfall) and drying (no rainfall), foundations are placed at a depth below the zone of volume change to reduce structural problems.

The plastic consistency of a clay-water mixture will vary with change in water content (see Experiment 11). Clays such as montmorillonite, with a high specific surface area as well as a residual electrical surface charge, are more highly plastic and more compressible. When the water content is reduced and particles are closer together, interparticle attractive forces become more effective, giving the soil mass an internal tension labeled **cohesion**. As a result, air-dried clay, when crushed between the fingers, will be relatively hard in comparison to a silt with few clay particles. This characteristic becomes useful for field identification of clay soils in comparison to nonclay soils (see Section 3.7).

In natural clay, the actual clay-size material (smaller than $2\ \mu$) constitutes only a fraction of the total soil mass. The degree to which the soil behaves like a clay depends upon the character of the clay-size component present. Examination of several clay samples (Skempton, 1953) showed that a linear relationship exists

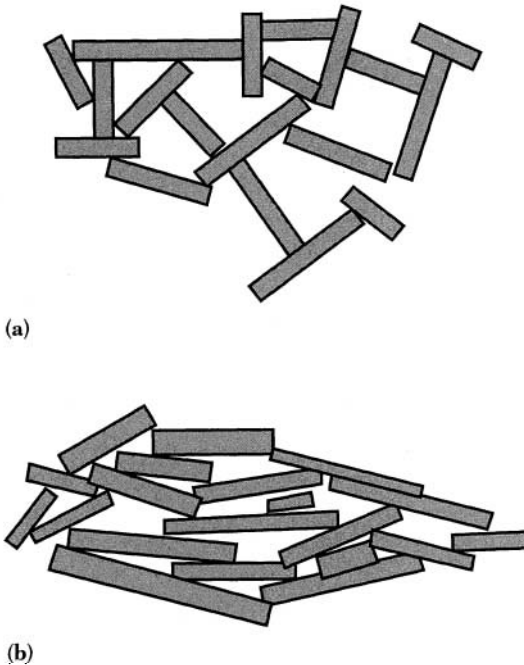


FIGURE 1.6 Schematic diagram of clay particle orientations: (a) flocculated-type structure (edge-to-face contact); (b) dispersed-type structure (face-to-face contact). (Redrawn after Lambe, 1958.)

between the weight fraction of a given clay-size material and its plasticity index. The ratio of the plasticity index (Section 3.4) to the percentage of clay (less than 2 μ) by weight is termed activity, A_c . The activity of a clay is a measure of the degree to which it exhibits colloidal behavior.

Experience shows that for soils having a particle size less than one micron, surface forces begin to exert a distinct influence on the soil's behavior. Most clay particles fall within the colloidal range in terms of both size and importance of surface forces. Consequently, the smaller the particle size, the larger the surface area and corresponding surface forces. The surface area per unit mass of soil is termed the **specific surface** and is used to compare clay surface forces and behavior. Montmorillonite, one of the clay minerals, exhibits a specific surface of approximately 800 m^2/g (89.7 acres/lb). If all the particles contained in 10 g of this clay could be spread out side by side, they would cover a football field.

1.2 SOIL DEPOSITS

The geological origin of a soil deposit often furnishes insight into its physical characteristics. Based on their origin, the more common natural soil materials can be divided into four groups: (1) residual soils, (2) water-transported soils, (3) wind-transported soils, and (4) soils of glacial origin.

1.2.1 Residual Soils

Soils that were formed by disintegration and decomposition of bedrock in place are termed **residual soils**. Some of the surface products of weathering have been removed by erosion and glacial action. The texture of residual soil is determined by the environmental conditions under which it was formed and by the type of parent rock. In warmer regions (tropics), with gently sloping terrain, residual soils formed from igneous rock may be over 20 m thick. In cold regions, such as Greenland, weathering is much slower and the soil blanket may be only a few meters thick. In other areas, such as the Canadian Shield, glacial action has carried away the residual soil accumulations, leaving igneous rocks bare except for local pockets of soil cover. Granites produce sandy silts and silty sands with varying amounts of mica and clays of the kaolinite group. Basalt yields highly plastic montmorillonite clays.

The degree of weathering varies with depth. Feldspars, micas, and ferromagnesium minerals at the surface are largely converted into clay minerals. At larger depths they are only partially altered and may retain some of their interparticle bonding. Joints and shear zones in the rock help weathering advance more quickly. The deeper residual soils often retain the fabric of the parent rock in mineral concentrations and grain orientation, as is shown in Figure 1.7. The depth of weathering penetration is largely dependent on rock type, permeability, and degree of cementation. One would expect porous sandstones to weather throughout more easily than relatively impervious igneous rocks. Significant depths of residual soils are found in the following areas:

| Area | Depth (ft) | Depth (m) |
|-------------------|------------|-----------|
| Southeastern U.S. | 20–75 | 6–23 |
| Angola | 25–30 | 7.5–9 |
| South India | 25–50 | 7.5–15 |
| West Africa | 33–66 | 10–20 |
| South Africa | 30–60 | 9–18 |
| Brazil | 33–83 | 10–25 |

Sedimentary rocks occur in a wide variety of forms depending on their mode of deposition. Many limestones consist of almost pure CaCO_3 , which is dissolved and removed by groundwater. The insoluble impurities that remain form the residual soil: clay (including kaolinite to montmorillonite); silica in the form of chert, silica sand, and silt; and iron oxides. The transition between soil and sound bedrock depends to a large degree on the solubility of the parent rock and is generally relatively abrupt. The contact is often very irregular because solution of the limestone occurs preferentially along joints. At intersections of bedding plane

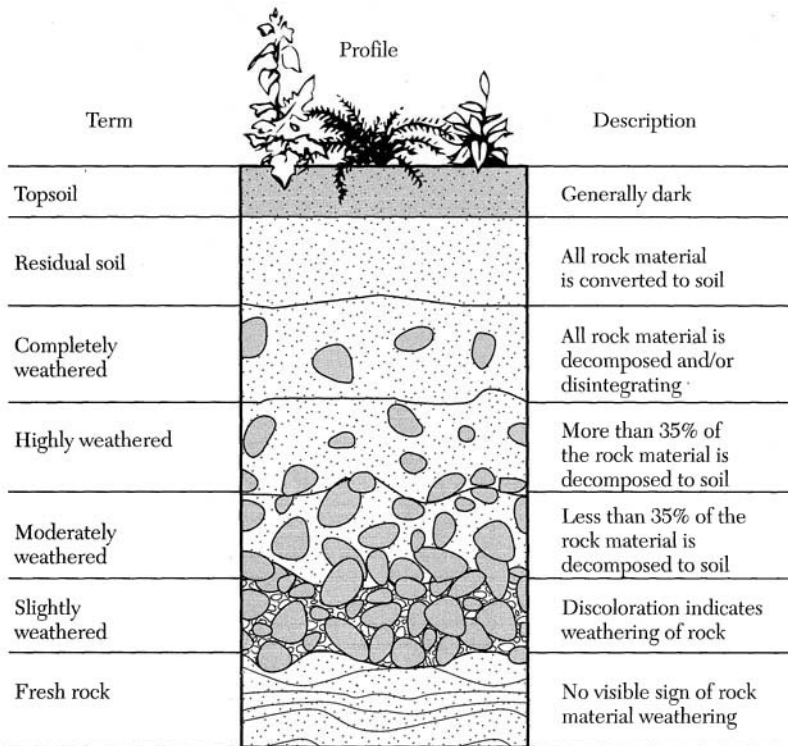


FIGURE 1.7 Typical residual soil profile.

joints with other systems, solution may extend laterally to form extensive cavities or caves; some of these may remain, whereas others may collapse to form sink-holes filled with rock debris, clay residue, and surficial materials. The extent and degree of continuity of these solution features must be investigated prior to construction in limestone areas.

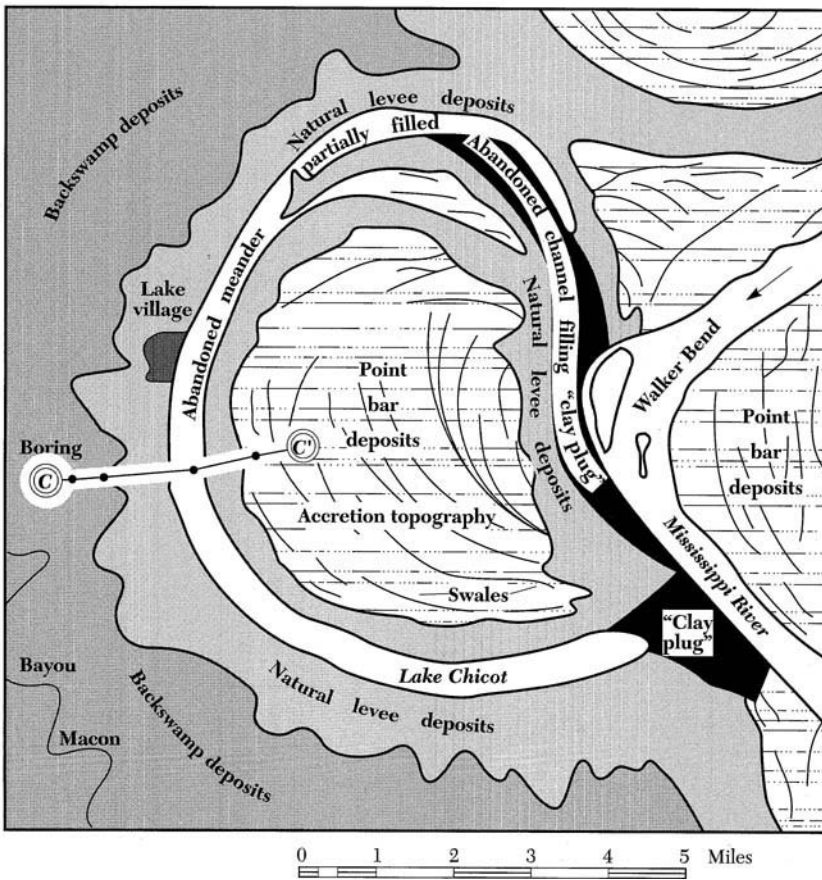
Residual soils developed from metamorphic rocks vary from sandy silts to silty sands, with varying amounts of mica in those derived from gneiss and schist. The soils may be deep for humid climate conditions. Marble weathers by solution, giving residual soils similar to those derived from nonporous limestones. Other metamorphic rocks weather in much the same way as igneous rocks: decomposition decreases with depth, and there is no sharp boundary between residual soil and the parent rock. The mass of unweathered rock may include seams of partially weathered material along old joints or along some less resistant material. Pinnacles or sawtooth projections of hard, slightly weathered rock may exist within the soil.

1.2.2 Water-Transported Soils

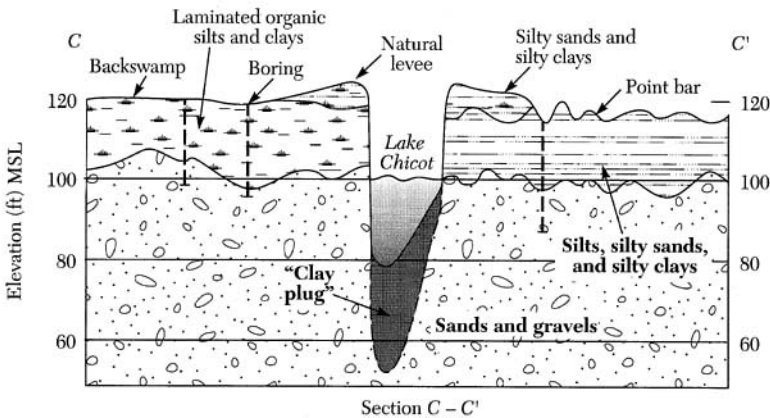
Large areas of the United States are covered with soils transported by and sedimented from water, such as river deposits (alluvium), lake (lacustrine) deposits, and marine deposits. Moving river water lifts smaller particles and carries them downstream with little physical change. Larger particles — sand, gravel, and boulders — are transported or rolled along the riverbed and rounded by abrasion. The river erodes its channel until its ability to transport materials is satisfied. When stream velocity decreases due to decreased flow or flatter slopes, the larger particles are dropped first. Large alluvial fans are formed where mountain streams enter the flat country and stream velocity is greatly decreased. A succession of these fans may be formed as the deposit builds up and the river shifts its course.

In flat valleys during periods of low flow the river is confined to its channel and deposition is balanced by erosion. During flood periods it may overflow its banks to form large, flat sheets of slowly moving water. Rapid deposition along the riverbanks forms natural levees. Broad overflow areas act as settling basins in which fine particles are deposited. As the flood subsides, finer particles are deposited until evaporation reduces the remaining puddles to dust. A floodplain and meander belt in the lower Mississippi Valley (Lake Chicot) are illustrated in Figure 1.8. The lake formed when the river forged a new channel, leaving the old channel behind. The complexity of this soil deposit is shown in the Lake Chicot area (Figure 1.8).

Lacustrine deposits form when lakes serve as sedimentation basins for water carrying suspended soil material supplied by local rivers. In arid regions, during periods of high stream flow, large quantities of gravel, sand, and silt are deposited in deltas due to a decrease in velocity when water enters the lake. New stream channels are continually forming in the region of the delta so that soil deposits are seldom homogeneous. The delta may be thin or it may be massive, extending several hundred meters in depth. Smaller particles are transported into deeper



(a)



(b)

FIGURE 1.8 Lower Mississippi meander belt for the Lake Chicot area: (a) distribution of soil deposits; (b) cross section for part of the deposit. (After Fisk, 1947.)

water, where sedimentation forms alternating layers of fine- and coarse-grained particles. If the water basin contains salts (sodium chloride or calcium chloride), the finer clay particles flocculate, thereby increasing the bulk volume of the sediment. Lakes in arid regions soon fill with sediment, become shallow, and may dry out during the dry season. The lake deposits possess practically horizontal surfaces and the fine-grained soils are often *varved* — that is, they consist of intermittent, very uniform laminae of silt and clay. The varve thickness can vary from fractions of a centimeter to over 1 cm. Varves do not form in saltwater, because the electrolytic action makes the clay particles flocculate and settle with the silt.

In humid regions, as the lake fills up and becomes shallow, plant life around the edges increases. Decomposing plant material produces organic solids, which are deposited with the silts and clays to form organic soils. Small diatoms contribute their silica skeletons, and other organisms add their calcium carbonate shells to the deposit. At later stages the lake may be covered with vegetation so that only partial decomposition occurs. The result is a covering of fibrous organic matter known as **peat**. At this stage the lake has become a marsh or bog.

Marine sediments were initially carried away by stream action and eventually deposited in the oceans, seas, or gulfs, with coarser particles near the shore and finer particles at some distance. Offshore conditions are similar to those in lakes in that deposition takes place in relatively still water below the zone of wave action. Fine-grained particles deposited in saltwater form a flocculent, low-density structure and have properties that are influenced by the salt content of the pore water. After these deposits emerge above sea level, leaching of the salts by natural groundwater permeation produces marine clays of high sensitivity.

Due to the mixing and transport activities of wave action and shore currents, shore deposits are complex. Spits or bars form when sediment brought to the sea by rivers is washed from the sea by wave action and swept along the shore by shore currents. Spits or bars may close off portions of the beach from the sea to form shore or tidal lagoons. These lagoons may become permanent lakes that rise and fall with the tide or in other cases may become flat tidal marshes. Organic deposits similar to those in shallow lakes form in the marshes. Mangrove swamps develop along subtropical and tropical shores that are protected from wave action. Marine sands and gravels are good sources of cohesionless materials for construction. Marine clays are normally soft, highly compressive, and capable of supporting only light loads.

1.2.3 Wind-Transported Soils

The movement of wind across large sand- and/or silt-covered areas moves the sand and silt-sized particles but leaves larger particles behind. Particles coarser than 0.05 mm (sand) are rolled along or lifted into the air for short distances and piled up to form dunes. Silt-sized particles are blown greater distances. The wind sorts the sand into deposits with a *relatively uniform grain size* and in some cases an extremely loose condition. Dunes take the form of ridges or irregular hills with steeper slopes (equal to the angle of repose) on the leeward side and with flat

slopes on their windward side. Sand dunes normally show a continual migration in the direction of the prevailing wind unless stabilized by vegetation.

Windblown silt may be transported many kilometers before a decrease in wind velocity permits deposition over large areas. The deposits accumulate slowly such that grass growth may keep pace with deposition. The result is a high vertical porosity combined with a very open structure, resulting in a soil material termed **loess**. Deposits of calcium carbonate and iron oxide, which line the former root-holes, make loess a relatively hard material. On saturation loess becomes soft and erodes very easily. Vertical cleavage permits loess to assume nearly vertical slopes in stream banks, gullies, and highway cuts. If loess does not become saturated, it provides good foundation support. It is difficult to obtain samples by means of borings because the natural structure of loess is altered by the sampling process.

1.2.4 Soils of Glacial Origin

During our geological past, large continental glaciers covered much of the land surface area north of the 40th parallel. The expanding ice sheets excavated, mixed materials, and transported and redeposited loose rocks and soils in different ways. Materials deposited directly by the ice are called **till**. Till deposits on the south shore of Lake Michigan are illustrated in Figure 1.9. Glacial tills vary widely in texture, including particles ranging from boulders to clay. Meltwater flowing from the ice sheet carried sand and gravel, which was deposited in broad sheets in front of the glacier as outwash. In some cases meltwater was dammed between high ground and the glacier, creating lakes in which glacial lake deposits were formed. As meltwater flowed into these basins, the coarser particles deposited near shore formed large deltas of sand and gravel. The finer particles were carried to open water, where thick beds of silt and clay formed in the still water. During cold periods, when melting and inflow ceased, the finer clay particles continued to settle, giving banded deposits known as **varved clays**.

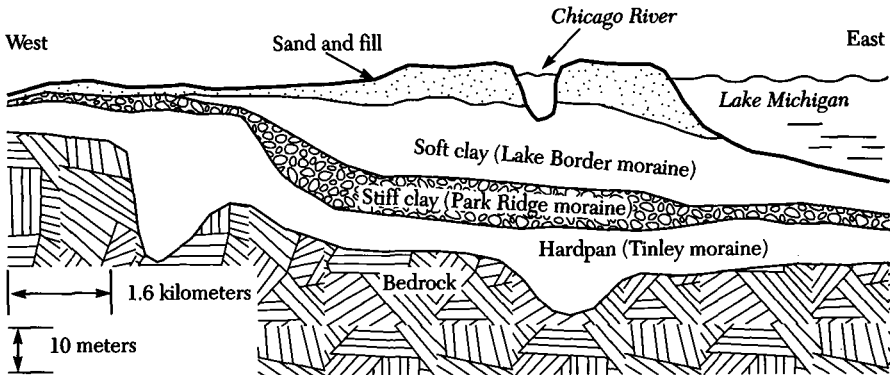


FIGURE 1.9 Glacial deposits below Lake Street in Chicago, Illinois.

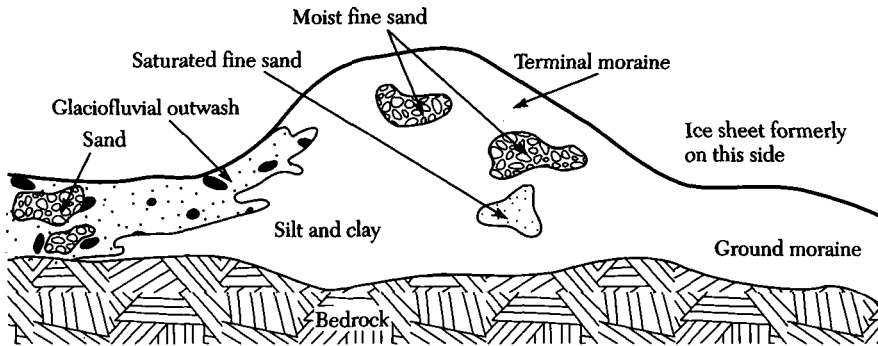


FIGURE 1.10 Typical terminal moraine cross section.

When the ice front remained stationary for several years, drift would accumulate in a ridge at the face of the glacier. These deposits, known as *terminal* or *end moraines*, consist largely of till, as is illustrated in Figure 1.10. Outwashes of sand, gravel, and clay or silt are shown on the moraine side that slopes away from the ice. The remains of rivers that flowed in tunnels beneath the ice or in crevasses near the ice front formed sinuous ridges, now called *eskers*, or conical hills called *kames*. These deposits provide ideal sources of coarse granular material.

1.2.5 Special Soils

The behavior of soil deposits is occasionally governed by the presence of a relatively small percentage of special soil material. Such soil material includes expansive soil, collapsing soil, limestone soil, quick clays, and organic soil. The presence of any one or more of these soils in a given soil deposit even in small amounts could profoundly influence foundation design. Consequently, the geotechnical engineer should be able to characterize and identify these soils so that potential disasters are avoided. A brief description of the special types of soils normally encountered in engineering practice follows:

Expansive soils are distinguished by their potential for great volume increase when exposed to water. Soils exhibiting such behavior are mostly montmorillonite clays and clay shales.

Collapsing soils are distinguished by their potential for great volume decrease upon increase in moisture content. The volume reduction occurs without any change in the external loads. Examples of such soils include loess, weakly cemented sands and silts where the cementing agent is soluble. The cementing agent is generally gypsum or halite. Collapsing soils are normally found in the arid regions of the world.

Limestone and related materials are characterized by their solubility and potential for cavity development. Such soils are noted for their erratic behavior in sustaining external loads.

Quick clays are characterized by their great sensitivity to disturbance. Such soils undergo significant strength reduction when disturbed or remolded. All quick clays are of marine origin and have sensitivities greater than 15. Note that *sensitivity* is defined as the ratio of the undisturbed strength to the disturbed strength.

Organic soils are present in many surface soils and in some cases deep soil deposits. They occur where the environment is not conducive to rapid decomposition, such as cold regions.

The distribution and physical properties of soils may change with time and local geologic conditions. The geotechnical engineer is required to provide the necessary recommendation relative to the expected soil behavior based on experience and on soil testing. The methods used in the identification and classification of problematic soils are covered later in this textbook. For example, the identification of collapsible soil is based on its plasticity characteristics, which are covered in Chapter 3.

1.3 SOIL PROFILE

The term **soil profile** indicates a vertical section through a soil deposit that shows the thickness and sequence of individual soil strata. Over the years, engineering terminology has developed by which the geotechnical engineer, boring foreman, and soil technician can equally describe the materials shown on the soil profile. These topics are introduced in this section.

1.3.1 Engineering Terminology

Three broad groups of soils are present in most natural soil deposits: granular (or cohesionless) soils, including sands and gravels; fine-grained soils, including inorganic silts and clays; and organic soils, such as peat, muck, organic silts, and organic clays. Usage has established the terms *gravel*, *sand*, *silt*, and *clay* as basic elements of a soil name. In practice the names are qualified by selecting adjectives to make the descriptions more complete. For example, the term *silty clay* denotes clay as the predominate soil type with some silt. Soil classification systems (Section 3.6) provide definitions of particle size, size ranges, and symbols for granular soils. Fine-grained soils are those with particle sizes smaller than about 0.1 mm. The unaided eye cannot readily distinguish the fine-grained particles. Silt and clay particles may be similar in appearance but exhibit different physical properties. **Clay** can be made to exhibit plastic properties by adjusting its water content, and it acquires considerable strength when air-dried. **Silt** cannot be made plastic and has little or no strength when air-dried. This behavior provides a basis for defining the terms *silt* and *clay* and also provides a simple method for distinguishing between these two soil types.

In general, soils will contain some combination of gravel, sand, silt, and clay. Hence, other details are needed so that the soil description conveys as complete a picture as possible to individuals who have not examined it. A number of soil physical characteristics that are important to the geotechnical engineer can be determined by visual and manual inspection. Color and homogeneity should be recorded for all soil types. Characteristics important to granular soils include grain size, grain shape, gradation, the presence of fine material, and the state of compaction. Characteristics needed for fine-grained soils include the degree of plasticity, consistency in the undisturbed state, the change due to remolding, and the natural water content. Details on these soil characteristics are given in later chapters. Simple visual and manual tests to provide the soil characteristics listed are a useful basis for field identification of most soil materials.

With urban development, man-made deposits (**fills**) constructed of natural soil are being utilized more and more for building sites. When the site is prepared and the fill soil is properly placed, the fill will provide the necessary support for additional loads. Random fills, such as old basement excavations or filling of low areas, will normally be at equilibrium under their own weight and will experience considerable settlement under any additional loads. These sites are indicated when foreign matter such as twigs, turf, and/or topsoil are observed at some depth in soil borings. Particularly troublesome are those fills containing broken concrete, debris from old buildings, rubbish, and waste materials. These sites are normally covered with a layer of soil after completion and may have vegetation on the ground surface. Fill of unknown character should always be investigated as part of the normal planning process.

1.3.2 Soil Profile from Site Exploration

A reasonably accurate description of a soil deposit, including the physical properties of the soils involved, is needed before the design of a foundation can be made in an intelligent and satisfactory manner. Before the appropriate design theories are applied, two independent operations are undertaken. First, the physical properties of the soil deposit must be determined by boring and testing. Second, an idealized soil profile (Figure 1.11) consisting of a few homogeneous soil units with simple boundaries must be prepared for the more complex soil profile. In many cases, the real soil profile is reasonably approximated by the idealized profile, so theory combined with the results of soil testing makes possible a prediction of the performance of soil-supported foundations. Limits of the proposed foundation have been superimposed on the soil profile shown in Figure 1.11.

Exploration of soil deposits usually involves a reconnaissance of the site, borings made to permit sampling of the subsoils for laboratory testing, and field tests. Depending on the type, importance, and nature of the project, the program of soil exploration may range from penetration tests at a number of boreholes to a careful collection of undisturbed soil specimens for laboratory tests. The engineer must decide on the depth, number, and location of borings required at the site. The types of samples and sampling intervals will depend on soil type and physical

properties to be measured. Details on methods of soil exploration are presented in Chapter 2. In special cases large-scale field tests may follow the usual site exploration. The nature of the exploration program is governed not only by the project to be undertaken but also by properties of the soil deposit.

The soil profile shown in Figure 1.11 represents five borings located approximately in a straight line through the proposed foundation area. Based on approximate limits shown for each boring, a soil cross section has been drawn showing the four soil types and depth to rock. Information from standard penetration resistance of the sand and the unconfined compressive strengths for the clay has been noted adjacent to each boring location. The groundwater level falls entirely in soil 4. The soil profile represented in Figure 1.12 includes somewhat different but perhaps much more complete information from that shown in Figure 1.11. The information is derived from four boreholes. A much more variable soil deposit is shown, with layers of clay, peat, silty clay, and sand. The shear strengths reflect the effects of preconsolidation of the upper 12 ft. The right-hand half of the profile summarizes information on water contents, densities, soil sensitivity, and plasticity of the various clay layers. Later chapters will discuss the laboratory testing needed to obtain much of the information included in Figure 1.12.

1.4 SOIL ENGINEERING PROBLEMS

Geotechnical properties of soils are required for the application of civil engineering technology to the design of foundations, earth dams, excavations, earth-retain-

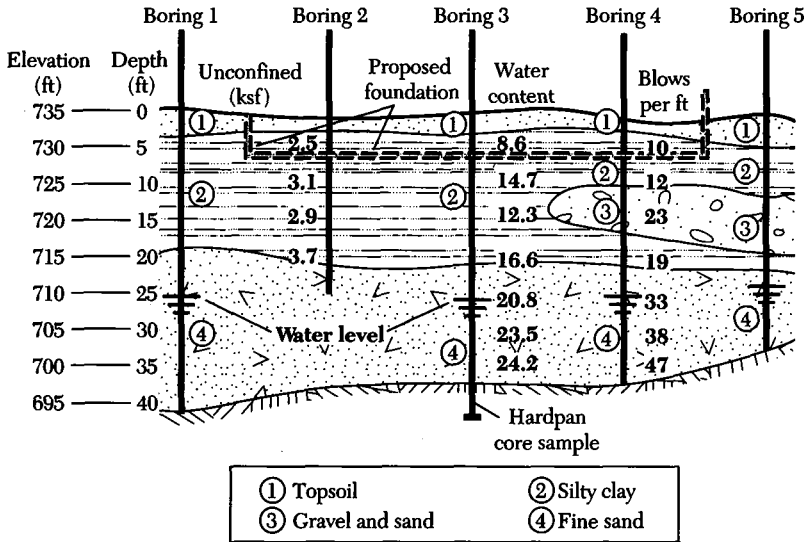


FIGURE 1.11 Soil profile from site exploration data.

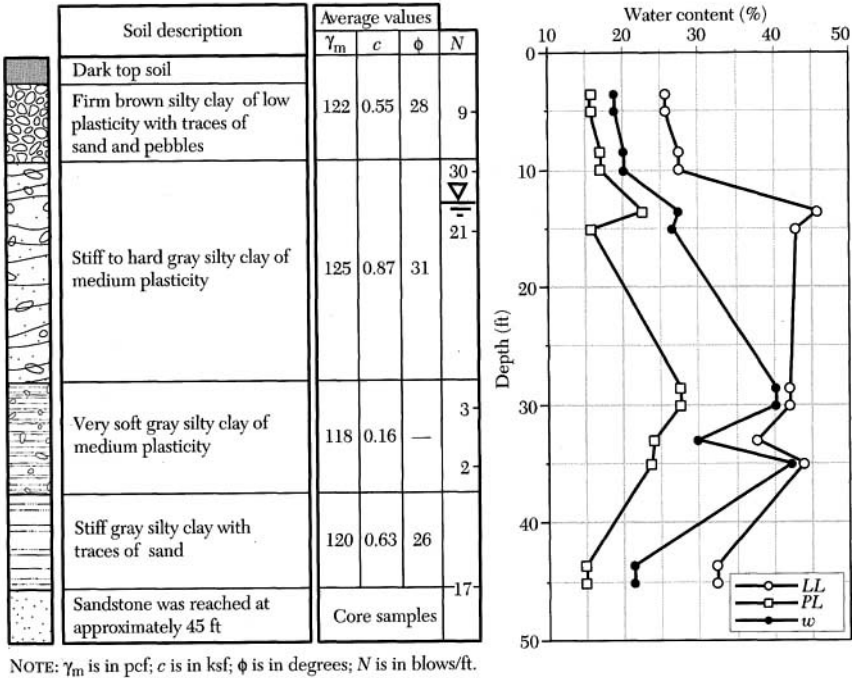


FIGURE 1.12 Results from an actual boring log for a site in Winslow, Indiana.

ing structures, and other special soil engineering problems. Several illustrations are introduced in this section.

1.4.1 Volume Change and Settlement

Settlement analysis is one of the more important soil engineering problems, particularly when less desirable sites are used for construction. The site may be brought up to grade by placement of fill, which in turn increases loads on lower soil strata. This condition is illustrated in Figure 1.13a where a soft clay underlies the upper sand layer. Due to the increase in load, water will drain from the clay until a new equilibrium void ratio e_1 is established. Using a soil element, this relationship is shown in Figure 1.13b for the initial condition and in Figure 1.13c for the final compressed condition. The settlement resulting from this one-dimensional volume change of the clay results in a surface settlement, ΔH . The ratio of change in volume to the initial volume of the soil element times the initial thickness of the clay layer gives the predicted settlement. This approach becomes more meaningful if the soil element represents a soil sample taken from the clay strata. As is shown in Chapter 6, the sample is placed in a consolidation ring and incremental vertical loads are placed on the sample. Measurement of change in sample

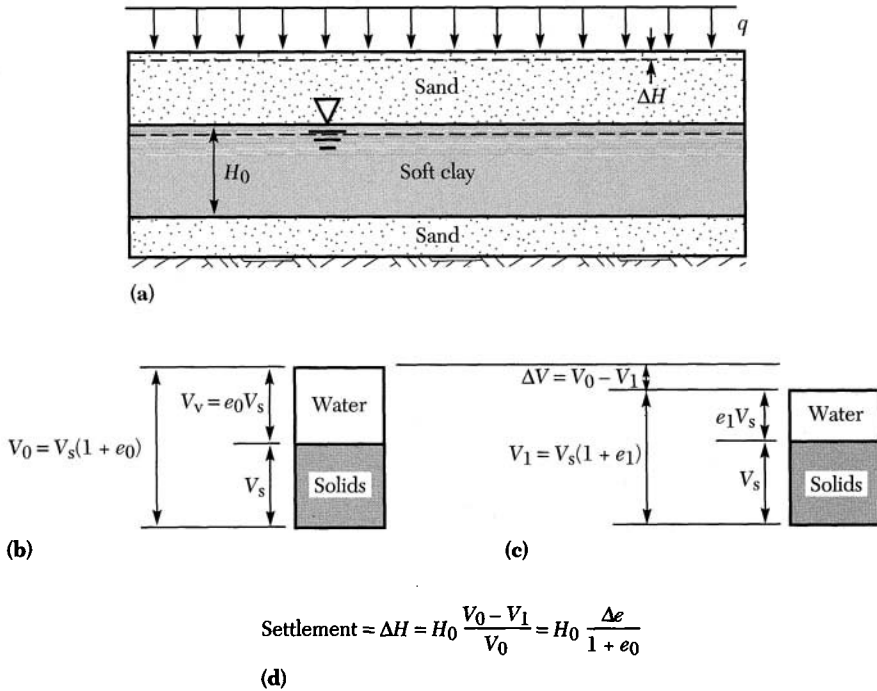


FIGURE 1.13 One-dimensional volume change and settlement in soft clay: (a) soil deposit; (b) initial conditions; (c) compressed conditions; (d) settlement ΔH .

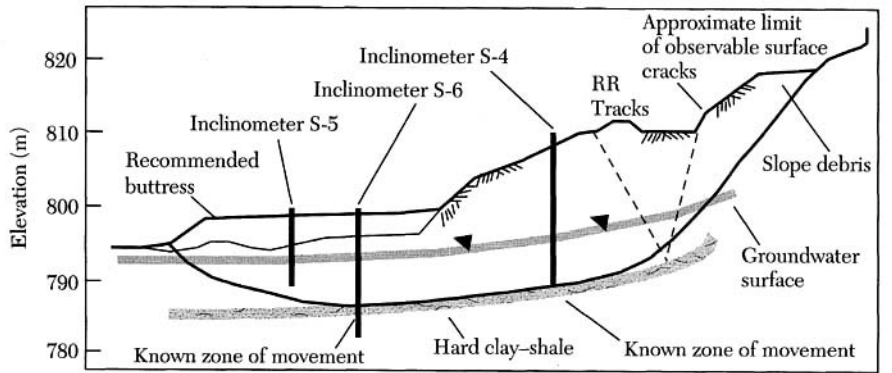
height provides the data needed for the prediction of settlement due to clay compression in the field for the increase in pressure due to the fill.

If in a loose condition, the sand strata will also be compressed due to the increase in pressure from the fill. This volume change is normally small and occurs immediately on placement of the fill due to the higher permeability of the sand. If this volume change is significant, it can be accounted for immediately by placement of additional fill. The much lower permeability of the clay may extend the period for this settlement to several months or more. The problem now becomes one of predicting the rate of settlement (consolidation) of the clay. If expensive structures are to be placed on the fill, it is important that the settlement be kept to a minimum during and after their construction. The owner and contractor may not wish to wait for completion of consolidation in the clay. The problem now becomes one of using extra fill (a surcharge) to speed up the settlement process. The surcharge is removed when the predicted settlement is attained and the project then proceeds as planned. As suggested by this illustration, the settlement of structures can be a major problem. Information needed for measurement of the soil properties used in prediction of volume change and settlement is presented in later chapters.

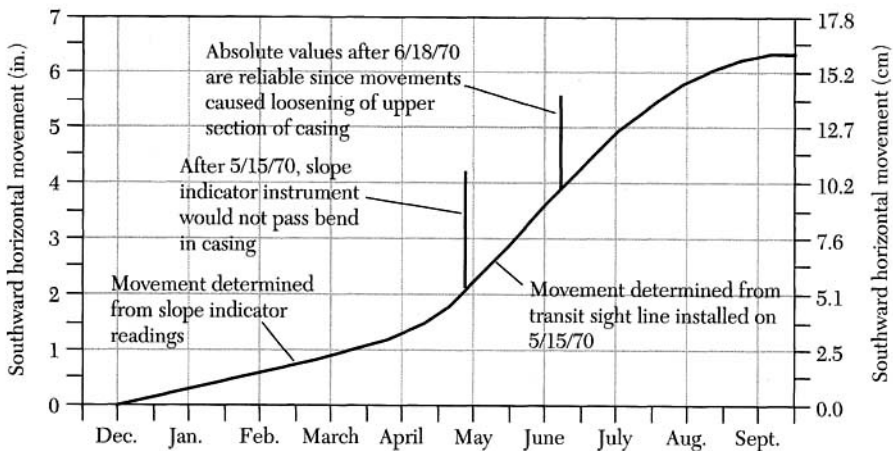
1.4.2 Stability of Soil Masses

Soils located beneath hillsides or the sloping sides of an excavation have a tendency to move downward and outward under the influence of gravity. The initial movement may be caused by some external disturbance such as undercutting the foot of an existing slope or digging an excavation with unsupported sides. This soil movement along some failure surface is counteracted by the shearing resistance of the soil. Slope failure would be predicted when the shear stress on this failure surface equals the soil shear strength (factor of safety = 1). The material involved in a slide may consist of natural soil deposits and/or a man-made fill.

Many of the problems involving slope stability are associated with the excavation of cuts for highways and railroads. Railroad tracks situated on a sidehill fill on



(a)



(b)

FIGURE 1.14 Fort Benton slide in western Montana: (a) slide cross section; (b) movement of top of inclinometer S-4. (After Wilson and Mikkelsen, 1978.)

the Burlington Northern rail line in western Montana had experienced vertical and horizontal movement over many years. Continuing realignment and restoration of the tracks was necessary for uninterrupted rail service. A soils investigation provided the subsurface conditions at the site summarized in Figure 1.14a. Soils beneath the slope consisted of stiff to hard silts and clays of low to medium plasticity with intermittent zones or pockets of sand and gravel down to about 16 m below the crest and 5 m below the toe. At greater depths a hard, mottled dark gray clay was encountered. Movement recorded by inclinometer S-4 indicated that the surface of the hard clay–shale was at a depth close to 18 m beneath the tracks.

Over a period of several years vertical movement at the tracks had accumulated to about one meter. Horizontal movement observed at the top of inclinometer S-4 from December 1969 through September 1970 is summarized in Figure 1.14b. Movement was greatest during the summer months. Data from the inclinometers showed that movement was occurring within a relatively thin zone, probably only a few centimeters thick, close to the surface of the hard clay–shale strata. With the approximate location of the failure surface established from the inclinometer data, the design of corrective measures was started. The most practicable means of stabilizing this hillside was the buttress shown above the toe of the moving soil mass in Figure 1.14a. This example demonstrates how borings, laboratory tests, and field tests were required to arrive at a satisfactory solution.

1.4.3 Load Transfer and Bearing Capacity

All structures, including buildings, bridges, earth dams, and towers, consist of a superstructure and a substructure (or foundation). The substructure interfaces with the supporting ground. For earth dams and embankments there may not be a clear line of demarcation between the superstructure and the substructure. Foundations serve the purpose of load transfer from the superstructure to the soil in a safe and economical manner. The term *safe* means that any settlement must be tolerable and the bearing capacity of the soil must be sufficient to avoid lateral expulsion of soil material from beneath the foundation. In addition, the structural

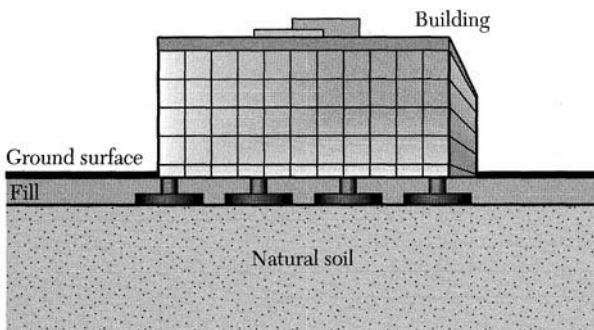


FIGURE 1.15 Spread footings supporting a building.

system must be safe against overturning, rotation, and sliding. Other criteria for foundation design may involve the depth of seasonal ground freezing, corrosion due to harmful constituents in the soil, and the method of construction.

Spread footings (Figure 1.15) are used for transferring concentrated loads from the walls or columns of a building to firm soil near the ground surface. The arrangement of footings illustrated in Figure 1.15 is called a *spread foundation*. These footings are normally constructed of reinforced concrete. For soil strata with low bearing capacity and/or column loads so large that more than 50% of the area is covered by the spread footings, a mat foundation may be used. A mat foundation is a large reinforced concrete slab that supports several columns. Placement of the mat below the ground surface introduces the technique called *flotation*, whereby the building load is partly compensated for by soil removed during excavation for the foundation. With either spread footings or a mat foundation, the engineer must decide how deep into the soil the foundation should be placed. Site information required involves a soil profile for the site with properties of each soil type and depth of the water table. Other questions involve stability of the excavation walls, whether it will be necessary to lower the water table in order to construct the foundation, and if there is danger of possible damage to adjacent buildings during construction.

When firm soil is not near the ground surface, the foundation may involve the use of piles for transfer of the load down to rock (Figure 1.16). No part of the building load is applied to the soft soil. Piles are structural members of steel, concrete, or timber that transfer their load to the soil by a combination of side resistance with the soil and/or point bearing to rock. Design of the pile foundation requires information on the in situ soil type and properties. This data, along with information on available piles, allow selection of the length and number of piles required on a project. More advanced texts on foundation engineering provide detailed information on foundation design.

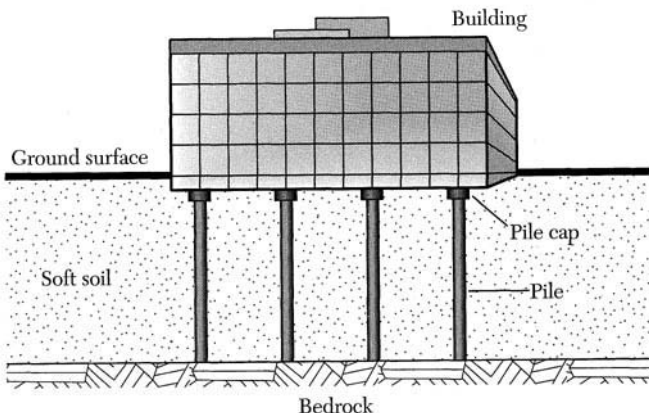


FIGURE 1.16 Pile foundation supporting a building.

1.4.4 Seepage and Flow of Water

Water present in soil voids is continuous and is free to move under the influence of gravity. Below the groundwater table, a degree of saturation approaching 100% is implied. The water table (surface) takes many shapes and may change with

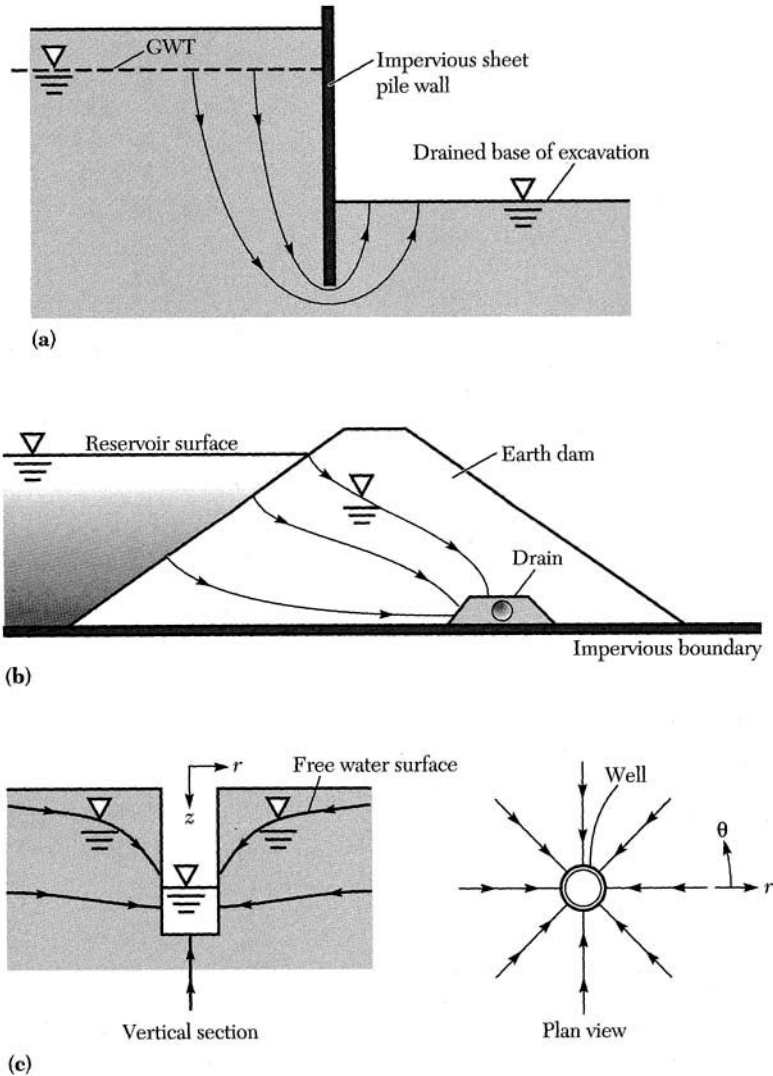


FIGURE 1.17 Seepage problems: (a) flow around a sheet pile wall; (b) flow through an earth dam; (c) flow into a well.

time, depending on the pattern and size of voids, the sources of water, and the points of discharge. During wet weather the water table will rise; during dry weather or periods of water depletion by drainage it falls. Water movement (flow) at low velocities involves an orderly procession of molecules in the direction of flow. This movement is characteristic of most soils except uniform coarse gravels with larger voids. Darcy's law (Section 5.1) describes the relationship between discharge velocity, hydraulic gradient, and a soil parameter labeled the **coefficient of permeability**. Methods used for permeability measurement are outlined in Section 5.2. This coefficient describes the ease with which water passes through a soil and depends on the viscosity and density of the pore fluid and on the size, shape, and area of the conduits (voids) through which the water flows. Viscosity is a function of temperature, hence a number of soil parameters involving water movement depend on soil temperature.

The flow of water molecules through a saturated soil can be represented pictorially by flow lines (Figure 1.17). In this case a water molecule, initially outside the sheet pile wall at the groundwater table (GWT), travels a flow path into the excavation similar to those shown. These flow lines are curved, roughly parallel, and often form segments of ellipses or parabolas. The impervious sheet pile wall (Figure 1.17a) serves to retain the soil on the sides and partially interrupts the flow of water into the excavation. If the sheet pile wall were to intercept a clay layer with a much lower permeability, flow through this layer and around the sheet piles into the excavation would be reduced. In some cases the reduction would permit construction to proceed within the excavation with little or no dewatering required. Methods presented in Chapter 5 permit estimates to be made of water flow into the excavation and how changes in wall pressure caused by this seepage may be computed.

Seepage through a man-made embankment (earth dam) is illustrated in Figure 1.17b. For this case, the upper flow line represents the groundwater table as the water molecule travels from the reservoir surface, through the dam, and into the drain. The quantity of flow will be controlled by the soil permeability and the drop in hydraulic head. The drain provides a collection point for seepage from all the flow lines and prevents any flow line from intercepting the downstream slope. Should this occur, a spring would form, followed by softening of the soil and possible erosion. This condition, which is prevented by the drain, would lead to unstable soil conditions and possible failure of the dam.

Flow into a partially penetrating well and the drop in the groundwater table (Figure 1.17c) result in three-dimensional seepage as well as unsteady flow. The upper flow line coincides with the free water surface. Flow lines radiate from the well as shown by the plan view (Figure 1.17c). Soil permeability and drop in hydraulic head are again the primary factors controlling the yield of a well. More advanced textbooks analyze this flow by mathematical approximations. The importance of having information on the soil deposit of interest and the properties of each soil type that apply to the engineering problem has been emphasized in each illustration.

PROBLEMS

- 1.1 Describe the main difference between kaolinite and montmorillonite clay minerals.
- 1.2 Explain why the flat surfaces of a clay mineral have a negative charge.
- 1.3 Define the term *isomorphous substitution*.
- 1.4 Explain why some clays swell when water is available.
- 1.5 For each of the following sedimentary soils identify the main transportation agent: (a) sand dunes, (b) beach sand, (c) alluvium, (d) glacial till, (e) loess, (f) talus.
- 1.6 In what areas would you expect to find the following soil deposits: (a) dune sand, (b) beach sand, (c) alluvium, (d) glacial till, (e) glacial erosion, (f) loess.
- 1.7 Sand dunes are observed to be encroaching on a housing area. Suggest two ways for stabilizing the dunes and describe how they work.
- 1.8 Define the activity and surface area of clay, then explain their relevance to geotechnical engineering practice.
- 1.9 For areas containing limestone with sinkholes and/or solution cavities, discuss problems related to (a) foundations and (b) dams.
- 1.10 Describe two soil profiles and two building characteristics that would make a pile foundation preferable to a spread foundation.

2

Soil Exploration

2.0 INTRODUCTION

An engineer must have reasonably accurate information on the extent and physical properties of underlying soil strata before it is possible to properly design a structure. The purpose of an exploration program is to ascertain that the ultimate capacity of the underlying soil is greater than the loading to be imposed by the foundations. In addition, the total and differential settlements must be limited to within acceptable tolerances under the structure in question and under adjacent buildings, roads, and other facilities. The types of structures normally encountered in practice may be divided into three separate categories:

1. Structures that interact with the surrounding ground. These include foundations, retaining walls, bulkheads, tunnels, buried pipes, and underground installations.
2. Structures constructed of earthfills, such as earth dams, bases and subbases for pavements, embankments, and backfill for foundations and retaining walls.
3. Structures of natural earth and rock such as natural slopes and cut slopes.

Besides selecting the most economical foundation system, the geotechnical engineer must provide information relative to foundation behavior and anticipated construction problems. These problems may include but are not limited to a high water table, an artesian condition, soft ground, frozen fill, the presence of

organic soils, and topography. The soil exploration program for a given site may be divided into three broad yet interdependent categories: reconnaissance, preliminary subsurface investigation, and detailed subsurface investigation. For small projects these phases are conducted concurrently, whereas for large projects these activities are nearly independent of each other.

2.1 SCOPE OF SUBSURFACE EXPLORATION

Soil characteristics for a given site may be highly variable and could change sharply within limited lateral distances and depths. The purpose of soil reconnaissance is to determine the stratigraphy and physical properties, both in plan and profile, of the soils underlying a given site. The subsurface investigation is normally carried out by making borings or test pits from which soil samples are recovered for identification and testing. These may then be supplemented by geophysical and geological studies. The strength, permeability, and compression properties are of particular importance in the design of economical and safe foundations. For some sites, the chemical properties of soil and groundwater may be needed to provide data for evaluating the hazards of corrosion of foundation piling and for designing drainage dewatering systems. In addition, information pertaining to adjacent structures, roads, sidewalks, or underground facilities that could be affected by the proposed construction should be obtained prior to the design and construction of the project.

Exploratory investigations are normally made in areas where little or no previous subsurface data are available, where there are no existing structures for comparison, where the proposed structure is drastically different in design from existing structures, or where the soil is known to have extreme variability in terms of properties and thicknesses. Often in dealing with large structures such as nuclear power plants, a preliminary investigation using boring and/or geophysical methods is conducted to plan a more detailed subsurface exploration program and to determine the number, depth, and spacing of subsequent borings.

2.1.1 Depth of Soil Borings

The basic criteria used in establishing the depths to which soil borings are extended is to ensure that the pressures imposed on the soil by the proposed construction at these depths are not of significant magnitude. Just where the pressures cease to be significant is a matter of opinion and experience. Rules of thumb, such as "boring depths should be at least twice the width of the largest footing," are sometimes used. Generally, one should extend borings through any unsuitable or questionable soil materials and sufficiently deep into firm soils that significant settlement will not result from compression of underlying soils. A commonly used rule is to carry borings to such depths that the net increase in soil stress caused by the proposed construction is less than 10% of the maximum value. A second technique employs the concept of drilling to depths where the net increase in soil stress caused by the proposed construction is limited to less than

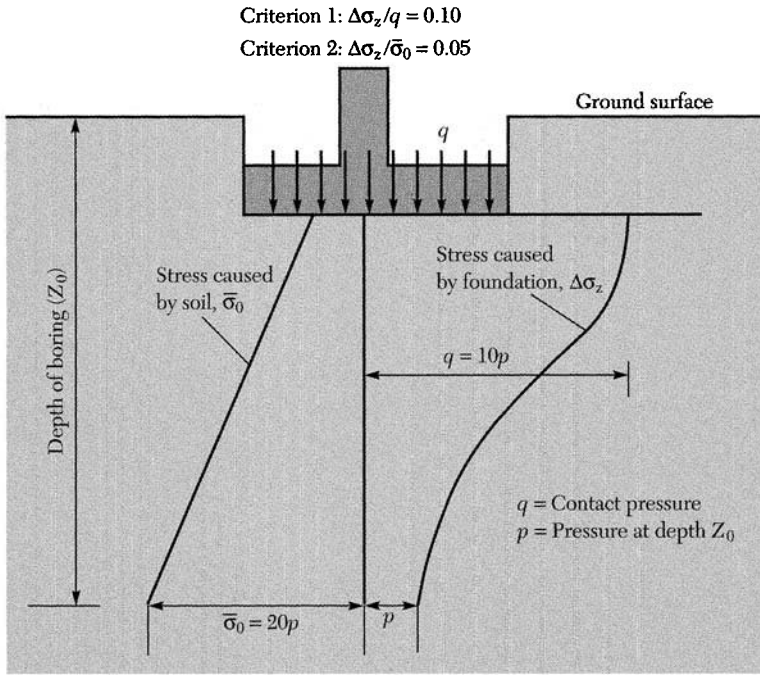


FIGURE 2.1 Graphical illustration of procedures used to approximate drilling depths.

5% of the effective stress caused by the soil's weight. These concepts are illustrated graphically in Figure 2.1.

The methods used to compute effective stresses and stresses caused by foundations are treated later in this text. Note that in general, the depth of a given boring is taken as the lesser depth obtained using the procedures referred to earlier. Such depths may have to be adjusted based on conditions disclosed during additional drilling, or even during construction. In dealing with deep excavations, boring depths should be at least 1.5 times the depth of the excavation in order to establish soil properties and water levels. This is necessary to properly plan dewatering that may be required if water levels are higher than the proposed excavation.

2.1.2 Number of Borings and Spacing

Because of limitations on cost and time, it is not generally practical to carry out the detailed exploration program needed to permit definitive evaluation of most job sites. Consequently, most foundation designs incorporate some degree of risk. The degree of risk associated with a given project is directly related to the sensitivity of the proposed construction to weaknesses in the soil. For example, for a given site, a foundation system for a warehouse used for storing materials is less critical than one for a building where sensitive instruments are housed. The amount of

money spent on soil exploration is generally dictated by the function of the structure being proposed for a given site, so one must make use of all available data to minimize cost to an acceptable level without sacrificing accuracy. Generally, an adequate number of borings is needed to locate any soft pockets or layers in the supporting soil and to provide a reasonably accurate assessment of the thicknesses of the bearing strata.

Because there is no scientific approach for determining the number of borings for a given site, there is no substitute for common sense and experience. However, a reasonable approach would be to use widely spaced borings if soil conditions are well known and the stratifications are simple. For such cases, borings may be placed at 30–40 m (100–130 ft). If soil conditions vary appreciably, then borings should be spaced at 5–10 m (15–30 ft). Borings for highways and roads may be spaced at 30–120 m (100–400 ft). This is also true for large parking lots found near shopping malls. The justification is that such facilities are not subjected to the extremely high loading values associated with buildings.

2.1.3 Type of Samples and Sampling Intervals

Soil borings are the most commonly used means for subsurface soil investigations. Borings are advanced by drilling at predefined intervals, where soil samples are obtained by driving or pushing a suitable sampling device into the soil. In some cases continuous sampling may be used; in which case no drilling is necessary. Bored holes are normally vertical unless otherwise specified. Inclined borings are possible for cases where the geological conditions dictate that such borings are desired. A bored hole is drilled using augers or with a bit, removing the cuttings with fluid (normally water) circulating through the drill stem and up around it or the reverse.

Characteristics of the soil materials, the type of sampler, and the experience of the drilling crew determine the quality of the soil samples obtained. Both disturbed and undisturbed soil samples can be obtained for a variety of laboratory and field soil tests. For most jobs, a standard procedure is used to obtain soil samples at depths of 2.5, 5, 7.5, 10, 15, 20, and 30 ft unless otherwise specified by the geotechnical engineer. Section 2.4 will discuss this topic further.

2.1.4 Site Geology and Seismicity

For small jobs, geological studies are omitted when conducting soil investigations. However, knowledge of the general geology of the proposed site is helpful in interpreting and correlating borings, especially for large projects where soil conditions may be highly variable. Geological data could be helpful in relating site conditions to other areas, and geological studies may be essential in areas of seismic activity. In such cases, the relation of the structure to active faults is of extreme significance. The geology of a given site could provide relevant information concerning problematic soils, such as those involving slides.

Geological studies are usually initiated by reviewing published data. The United States Geological Survey and various state geological surveys are often

used for such studies. Additional sources may include individual geologists, mining and petroleum companies, and publications found at libraries of most major institutions. Unfortunately, the correlation of such geological studies can be difficult, expensive, and time-consuming, especially when the studies have extended over long time periods. Items of special interest such as faults and joints are frequently omitted, and names may be changed by different investigators.

When dealing with earthquake-resistant designs, the geology of the site in question and its distance from major faults are extremely important in determining the foundation system to be used. There are many areas of the globe where earthquakes occur with frequency. In the United States, the Midwest and much of the area west of the Rocky Mountains are considered active earthquake zones with varying degrees of seismic activities. In some cases, local codes are in place for the purpose of controlling building design so that fatalities and building damage are minimized during an earthquake. Several great earthquakes (magnitude > 8.0) have occurred in the United States. These include the New Madrid, Missouri, earthquake of 1887, the San Francisco earthquake of 1904, and the Alaskan earthquake of 1964.

2.1.5 Hydrology

The effects of proposed construction on groundwater conditions are normally considered before construction commences. The water pressure (piezometric level) and its seasonal variations are important in determining dewatering procedures to be used, the effect of dewatering on adjacent structures, uplift pressure to be expected, and the effect of dewatering on water supplies. Meaningful data on groundwater and climatic factors are difficult to obtain, and conditions often vary over short distances. Data may be obtained from local, state, and national geologic surveys and from technical literature.

In some cases, heavy rain may cause flooding by surface runoff, erosion, contamination, or collapse of excavations and slopes. Evaluation of meteorological data may provide information relative to the probability of such hazards before, during, and after construction. Climatic factors are important wherever landslides and/or cold climates are expected. In the United States, hydrological data are usually obtained from local weather bureaus or from the National Weather Service.

2.1.6 Site Conditions and Existing Structures

Engineers often ignore site conditions in planning a soil investigation program. Information relative to site accessibility, drainage, and topography is important in the proper characterization of a given site. One should be aware of the presence of obstacles such as trees, buildings, and utilities. Drilling equipment including rigs may be lost for long time periods because site conditions are not adequate to support the drilling rig being used. It is easy to specify on paper the location and depth of the borings to be drilled in a given site. It is a different matter when site conditions are such that the specified locations are impossible to reach because of

TABLE 2.1 Checklist for a Subsurface Soil Investigation Program

| Project | Site | Project and Site |
|--------------------------|-----------------------|-------------------------------|
| Size of structure | Size of site | Location of structure on site |
| Shape of structure | Location of site | Existing buildings |
| Foundation system | Access and obstacles | Previous reports |
| Basement | Geology | Local code requirements |
| Column loads and spacing | Topography | Cut and fill requirements |
| Type of construction | Drainage | Cost |
| Starting date | Existing utilities | Site visit/photos |
| Completion date | Hydrology | Plans |
| Contractor | Previous soil reports | Owner |

difficult topography and/or because of the presence of obstacles. Consequently, one may have to compromise on such matters as boring location and depth, and even the number of borings.

The scope of work associated with a given site is determined, in part, by the size of the proposed structure and its intended function. However, the performance of existing structures may provide information relative to troublesome soil conditions. Thus, it is desirable to obtain information pertaining to past subsurface soil investigations, the foundation systems being used, and the behavior of existing structures. Such information may include boring logs, settlement, groundwater conditions, and construction problems. In addition, an existing structure may be affected by the proposed construction. This may include additional settlement, caused by increased stresses (due to the new structure) within the soil, pile driving, and dewatering. In such cases, a thorough investigation of existing structures is necessary. One may look for cracks, distortion, and the type of foundations being used.

It is evident that the more information available at the start of a project the more efficient the subsurface investigation program will become. Information needed for the fact-finding survey falls into three broad categories. The first pertains to the proposed structure only, the second pertains to the site only, and the third deals with the proposed structure and how it relates to the site. A checklist for the type of information desired is given in Table 2.1. Each project is unique and must be handled as such. The list provided in Table 2.1 is meant to assist the reader in identifying those items that are common to most projects.

2.2 EXPLORATORY INVESTIGATION USING GEOPHYSICAL METHODS

These methods deal with the use of artificially generated elastic waves to locate soil deposits, soil layer thicknesses, and water. They can provide information relative to the structure and distribution of rock types. Geophysical methods alone cannot determine many of the physical soil properties needed for geotechnical engineering analysis and design. Their use is more widespread in the exploration for petroleum. For large job sites, geophysical methods can be used for direct measurement of soil and rock formations without borings. Normally, these indirect



FIGURE 2.2 Portable refraction seismograph. (Courtesy of Soiltest, Inc.)

techniques will supplement direct assessment of site conditions (borings, pits, trenches, etc.). Two methods that have been found useful for site investigations are seismic and electrical resistivity techniques.

2.2.1 Seismic Survey

Seismic methods performed at the ground surface (Figure 2.2) yield wave propagation and profile information for soil and rock materials situated at lower depths. A compression wave (elastic vibration) is introduced by hammer blows to a steel plate placed on the ground surface. The wave moves out from the source on an expanding spherical front, with a velocity dependent on soil properties. Some of the energy will travel directly from the impact point to the detection point, a geophone embedded at the soil surface. In some instruments the hammer blow starts an electric timer and the geophone stops it, and the wave arrival time may be read directly from the timer. The geophone or the hammer is moved successively to different locations along a straight line. At each position (Figure 2.3a), the test is repeated to give the time–distance relationships shown in Figure 2.3b for horizontally layered soils.

For a small distance x from the source S to a receiver R , the travel time t_d for arrival of the direct wave can be written as

$$t_d = x/V_1 \quad (2.1)$$

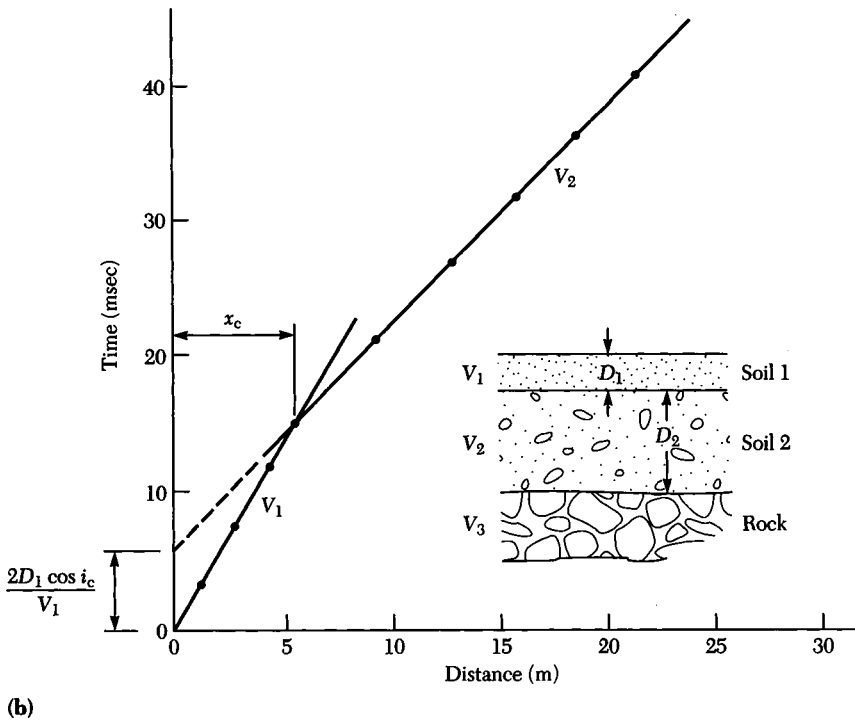
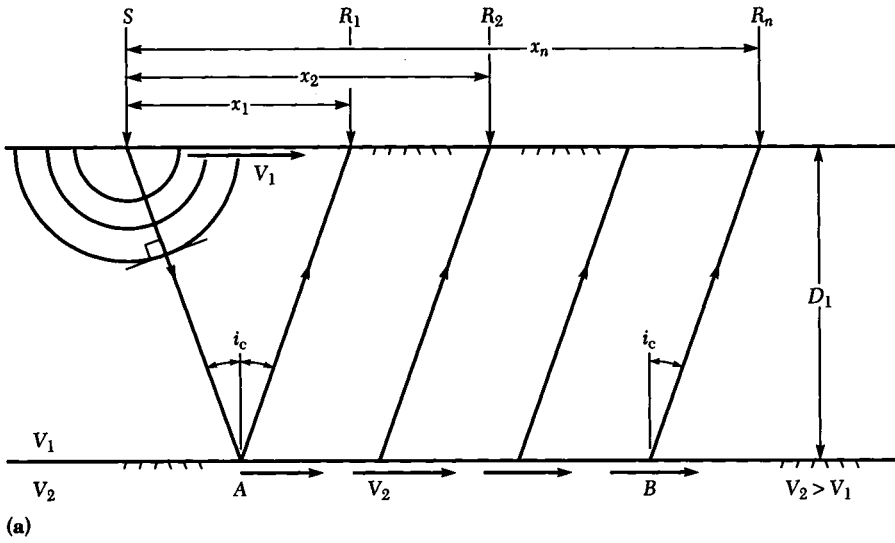


FIGURE 2.3 Refraction survey: (a) ray paths for direct and head waves; (b) travel time curves for direct and head waves.

where V_1 is the compression wave velocity in the upper soil layer. A plot of travel time versus distance gives the straight line through the origin in Figure 2.3b with a slope of $1/V_1$. With increase in distance x a point is reached at which the direct wave and a refracted wave (path SAR_1) arrive at the same time. The travel time t_h for the refracted wave can be written as

$$t_h = \frac{D_1}{V_1 \cos i_c} + \frac{1}{V_2}(x - 2D_1 \tan i_c) + \frac{D_1}{(V_1 \cos i_c)} \quad (2.2)$$

where D_1 is the thickness of the upper layer, V_2 is the wave velocity in the second layer, and i_c is the critical angle for the refracted wave. Using $\sin i_c = (V_1/V_2)$ and $\cos i_c = [1 - (V_1^2/V_2^2)]^{1/2}$ Eq. (2.2) can be reduced to

$$t_h = \frac{x}{V_2} + \frac{(2D_1 \cos i_c)}{V_1}$$

or

$$t_h = \frac{x}{V_2} + 2D_1 \left[\frac{1}{V_1^2} - \frac{1}{V_2^2} \right]^{1/2} \quad (2.3)$$

Equation (2.3) represents the straight line in Figure 2.3b with a slope of $1/V_2$ and an intercept on the t -axis at $(2D \cos i_c)/V_1$. The distance x_c (crossover distance) represents the point at which $t_d = t_h$. Substituting x_c for x in Eqs. (2.2) and (2.3), setting these equations equal, and rearranging terms gives the depth D_1 of the upper layer:

$$D_1 = \frac{x_c}{2} \left[\frac{(V_2 - V_1)}{(V_2 + V_1)} \right]^{1/2} \quad (2.4)$$

Up to this point seismic methods (refraction survey) have provided three important unknowns: V_1 , V_2 , and D_1 . Note that the condition $V_1 < V_2 < V_3, \dots$ must be satisfied for the method to work. Further refinements in the seismic method permit determination of velocities for additional soil layers, their depths, and the inclination of soil or rock surfaces (Richarts et al., 1970; Dobrin, 1976). Typical seismic compression wave velocities for several materials are summarized in Table 2.2. The elastic properties (E and G) of these soil and rock materials are related to seismic wave velocities. More advanced texts (Richarts et al., 1970; Dobrin, 1976; U.S. Dept. of the Army, 1979) provide information on other seismic techniques suitable for measurement of both compression and shear wave velocities along with the theory needed for computation of the moduli of elasticity (E and G) and Poisson's ratio.

2.2.2 Resistivity Exploration

Resistivity surveys are used to locate or outline gravel deposits and buried aquifers, find depths to a water table or bedrock, or locate a change in soil conditions. Resistivity exploration operates on the principle of measuring the electrical resistance per unit length of a unit cross-sectional area of the ground. For example, if resistivity could be measured directly on a one cubic meter block of

TABLE 2.2 Representative Compression Wave Velocities

| Materials | Velocity (m/sec) | Velocity (ft/sec) |
|---------------------------|---------------------|----------------------|
| Fresh water, 20°C | 1,480 | 4,850 |
| Dry sand | 460–915 | 1,500–3,000 |
| Clay | 915–1,830 | 3,000–6,000 |
| Saturated loose sand | 1,525 | 5,000 |
| Weathered rock | 1,525–3,050 | 5,000–10,000 |
| Shale | 3,660 | 12,000 |
| Hard granite or limestone | 6,700 | 22,000 |
| Steel | 6,100 | 20,000 |

(After U.S. Dept. of the Army, 1979.)

soil by applying a voltage to two opposite sides, the resistivity ρ would equal $(V/I)(\text{cross-sectional area}/\text{length}) = (V/I)(1 \text{ m}^2/1 \text{ m})$. If V is in volts and I in amps, ρ will be in ohm-meters. Soil resistivity relates primarily to water content and concentration of dissolved ions. Clay soils with higher ion concentrations give lower resistivities. Dry soils and solid rock will have a higher resistivity, with saturated granular soils giving an intermediate resistivity. Representative data are summarized in Table 2.3.

In resistivity surveying, four metal electrodes are driven into the ground at intervals along a straight line (Figure 2.4). An electric current is sent into the earth through two of these electrodes, and a voltage drop or potential difference between these and the other two electrodes is measured. These electrical measurements plus distance measurements between electrodes are the data used to determine subsurface conditions. The depth of investigation is controlled by moving the electrode probes farther and farther out from the center of the survey area. The two outer probes (Figure 2.4) are the current electrodes, feeding electrical current into the survey area. The inner two are the receiving (or potential) electrodes. When current is fed through the two outer probes a bowl-shaped volume of electrical activity is formed around each electrode.

TABLE 2.3 Representative Electrical Soil Resistivities of Earth Materials

| Material | Resistivity (ohm-meters) |
|--------------------|-----------------------------|
| Clay | 1–20 |
| Sand, wet to moist | 20–200 |
| Shale | 1–500 |
| Porous limestone | 100–1,000 |
| Dense limestone | 1,000–1,000,000 |
| Metamorphic rocks | 50–1,000,000 |
| Igneous rocks | 100–1,000,000 |

(After U.S. Dept. of the Army, 1979.)

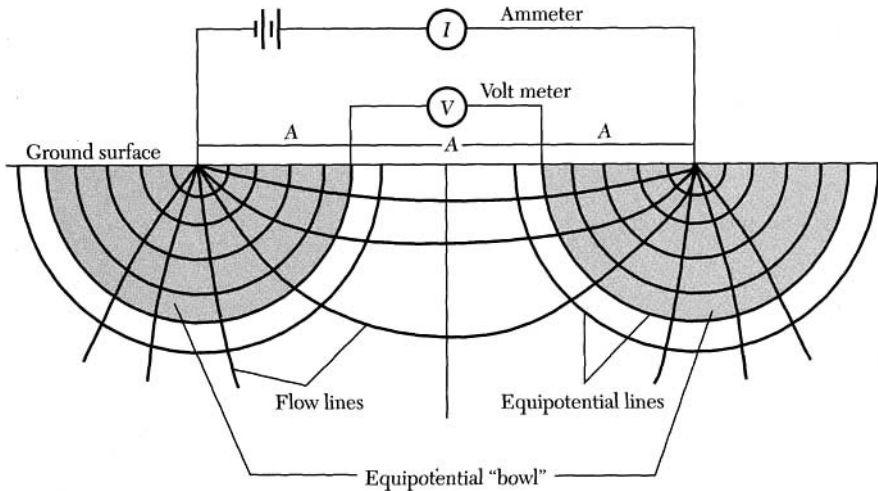


FIGURE 2.4 Wenner electrode arrangement, used in resistivity surveys, with a flow net for a homogeneous soil.

As the electrode spacing A is increased, the ratio of measured voltage V to current I decreases proportionately if the soil is homogeneous. When the induced electrical volume is interrupted by underground features such as gravel, bedrock, or groundwater, certain known resistivity values register on the resistivity meter. The soil involved in resistivity measurements is not a cube, but it can be shown by calculus that with the Wenner arrangement the effective resistivity for any spacing A (meters) between two adjacent electrodes is

$$\rho = 2\pi A(V/I) \quad (2.5)$$

with units of ohm-meters.

For shallow depths in variable soils, resistivity data interpretation involves a plot of $\Sigma\rho$ versus spacing A (Figure 2.5). If ρ is constant with depth, the result is a straight line with slope ρ_1/A where ρ_1 is the resistivity of the upper soil layer. With an increase in electrode spacing a different material is encountered, giving a second line with slope ρ_2/A . Intersection of the two lines gives the boundary depth between the two materials, usually within 5% to 10%. A test pit showed rock at a depth of 4.27 m (14 ft) in Figure 2.5. The advantage of a cumulative resistivity curve over a plot of ρ versus depth is shown by the individual-test-value curve in Figure 2.5.

2.3 EXPLORATORY SUBSURFACE INVESTIGATION USING DIRECT METHODS

Depending on the size of the proposed development, this phase of the soil investigation program consists of drilling one or more borings (holes) for the purpose of

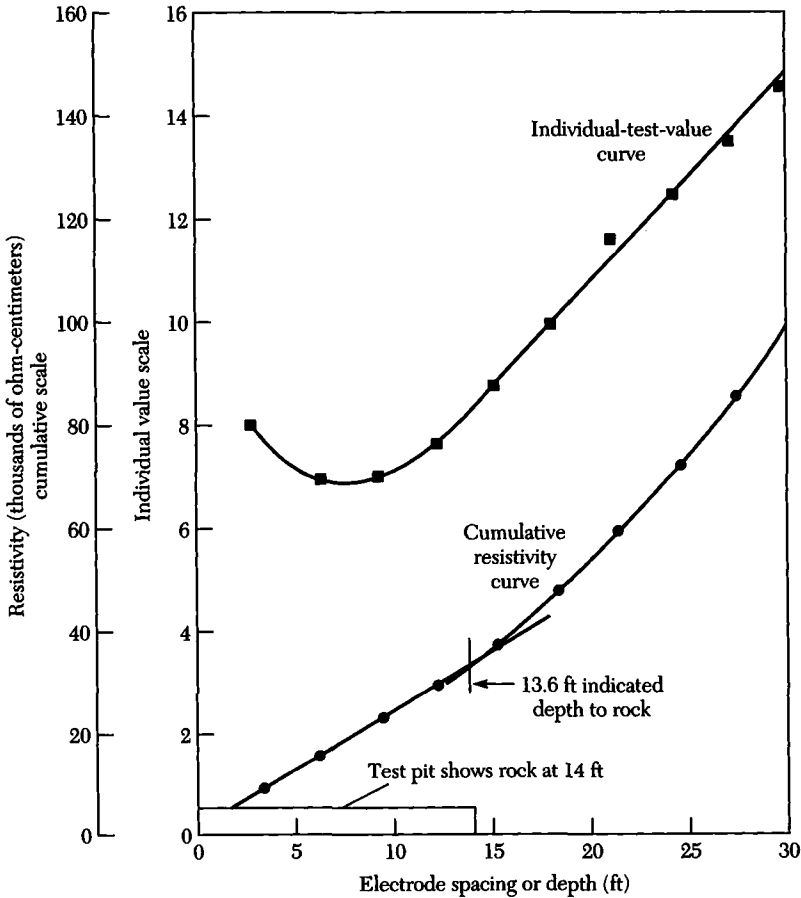


FIGURE 2.5 Typical resistivity data and method of analysis using the cumulative resistivity curve. (From Moore, 1961.)

obtaining soil samples and describing the general characteristics of the underlying soils. The information obtained during this phase may provide a basis for selecting the foundation system. It could also provide valuable information relative to soil layers and properties. Such information can then be used to determine appropriate drilling and sampling methods for the detailed subsurface exploration phase. Although such information is necessary for preliminary planning, it is not generally intended for final design.

2.3.1 Hand-Operated Sampling Tools

One of the most popular tools for hand-operated drilling is the Iwan auger. This tool is used when dealing with firm soil deposits where the hole remains open. The Iwan auger is available in sizes of 7.6 to 20.3 cm (3 to 8 in.) in diameter and

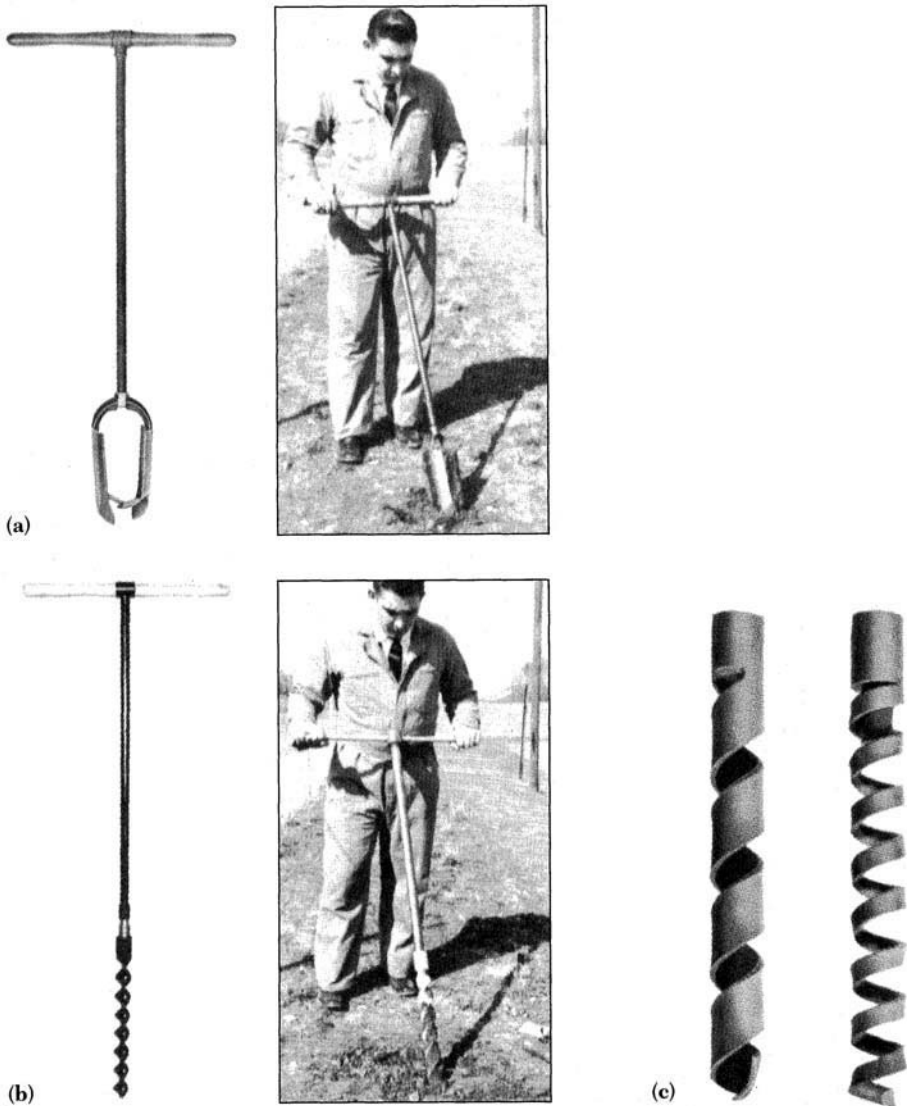


FIGURE 2.6 Types of manual augers: (a) Iwan auger; (b) ship auger; (c) spiral auger. (Courtesy of Acker Drill Co., Inc.)

can be used to depths of 7 m (23 ft). A soil sample is obtained by pressing the auger into the ground and simultaneously turning it. The tool is then removed and the sample is recovered. Because the soil sample has been disturbed, it should be used only for identification tests. Deep samples can be recovered by advancing the hole downward and adding extensions to the auger. These are pipes measuring 76 to 122 cm (2.5 to 4 ft) in length and 2 to 3.3 cm ($\frac{3}{4}$ to $\frac{15}{16}$ in.) in diameter.

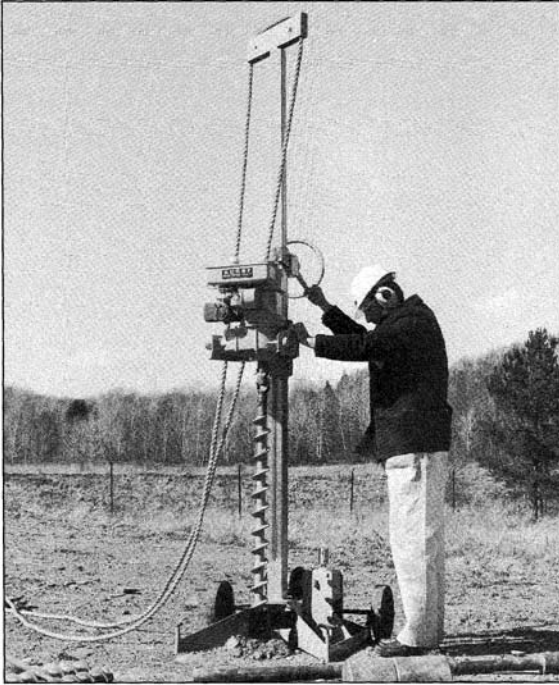


FIGURE 2.7 Lightweight motorized augers. (Courtesy of Acker Drill Co., Inc.)

The ship auger is a second hand-operated sampling tool. The operation of this tool is similar to that of the Iwan auger. However, it is easier to advance due to its screwlike design. The ship auger is most effective in cohesive soil deposits and is available in a 5.1-cm (2-in.) diameter. The Iwan and ship augers are shown in Figure 2.6.

These tools are extremely simple to operate and inexpensive; they can save the client money because the information they provide may be such that the proposed site is not suitable for supporting the proposed structure. This is possible if the recovered samples indicate the presence of organic soil deposits, soft and/or loose layers, or a high water table.

2.3.2 Lightweight Motorized Tools

These are drilling tools that can be transported by one person to the proposed site. Although these tools can be used in conjunction with the hand-operated tools, they provide more accurate information about subsoil conditions. Holes can be drilled faster than those drilled using hand-operated tools. Depending on site accessibility and soil conditions, this type of equipment can provide information relative to soil deposits at shallow to intermediate depths. Figure 2.7 shows one type of lightweight motorized drill. Obviously, one must exercise utmost care when using this equipment, especially when dealing with soil deposits containing gravel and/or rocks.

2.3.3 Test Pits and Trenches

Often the availability of rotary bucket augers, backhoes, bulldozers, or clamshells makes it possible to explore a given site inexpensively by digging pits and trenches. Test pits are used to facilitate in-place examination or sampling of soils at shallow to medium depths. Bucket augers used to drill caisson holes can provide information relative to site subsurface conditions at great depths. In most cases test pits or trenches are used where soil conditions at shallow depths are essential to the design of the foundation system. Although there are no general rules as to where test pits should be located, it is important to place them at the intended positions of shallow foundations.

2.4 DETAILED SUBSURFACE INVESTIGATION

Detailed subsurface investigation involves a comprehensive subsoil survey, which will provide all boring details, field test data, and laboratory data required to complete the analysis and to make foundation design recommendations. Detailed explorations fall in two broad classifications. The first classification, referred to as *drive sampling* or *dry sampling*, is made by driving a thick wall sampler. Such samplers produce representative but disturbed soil samples that might be adequate for estimating a number of important soil parameters. The second classification, referred to as *undisturbed sampling*, is made with one of many thin-walled tube samplers. Samples obtained with such samplers are relatively undisturbed and may be suitable for compression and strength tests.

Decisions must be made relative to number of holes, drilling methods, type of samples, depth of borings, sampling intervals, rock coring, and boring locations. Information relative to site accessibility and the type of drilling equipment to be used should be made available to the drilling crew.

2.4.1 Disturbed Soil Sampling

Detailed subsurface investigations of soil deposits are often made using disturbed sampling techniques. In practice, such samples are identified and classified preliminarily in the field and then preserved in moisture-proof jars for more precise identification, testing, and analysis. Disturbed samples are useful for identification

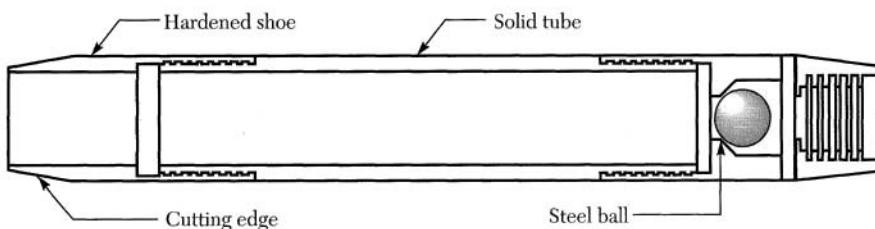


FIGURE 2.8 Solid-tube soil sampler.

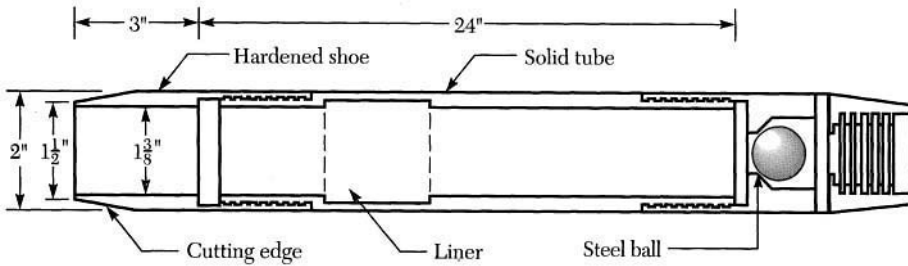


FIGURE 2.9 Split-spoon soil sampler.

and index property tests. The sampling intervals are normally specified as 2.5 ft in the first 10 ft, 5 ft in the second 10 ft, then at every 10 ft. Deviations from these specifications are often made to investigate soft, organic, or other types of difficult subsoil layers. The samplers used may be solid, thick-walled tubes or of the split-barrel type.

Common Soil Samplers

Disturbed sampling involves driving samplers ranging in size from 2" outside diameter (O.D.) to 4.5" O.D. into the soil at the specified depths. The standard size used most often is the 2" O.D., which has an inside diameter (I.D.) of $1\frac{3}{8}$ ". These samplers are normally 18 in. or 24 in. long and may be connected using connecting coupling for extra long samples. This is seldom done, however, and similar results can be achieved using continuous sampling.

The solid-tube samplers, as the name suggests, are solid steel tubes that can be attached to a drilling rod (Figure 2.8). These samplers are advantageous from the point of view of simplicity and ruggedness. However, the soil samples must be pushed out of the tube, resulting in further disturbance and even broken samples.

Split-spoon samplers are the most widely used devices for obtaining disturbed soil samples. This sampler is similar in construction to the solid-tube sampler except that the barrel is split longitudinally so that the sample can be readily exposed (Figure 2.9).

A groove can be made on the inside of the split spoon to house liners of different sizes. The most popular size is the $1\frac{3}{8}$ " I.D. and 3 in. long brass liner. The liner is placed in the groove, then the two halves are closed. Once the spoon is driven and retrieved, the two halves are opened and the liner removed with the soil sample, which can then be placed in a jar for testing. The liner has the advantage of having a known volume and height, which makes it easy to approximate the unit weight of the soil sample. Furthermore, the sample is ideal for the unconfined compression test.

Often, the soil strata may be too soft for the soil sample to remain inside the soil sampler, so an attachment is placed inside the sampler to prevent the sample from falling out. The trap valve retainer, spring sample retainer, and Lad sample

retainer are different devices normally used to keep the sample from sliding out of the sampler.

Standard Drilling Method

Over the years, contractors and geotechnical engineers developed many different procedures for soil sampling. The majority of these methods specified a driving distance of one foot. However, they differed in terms of the type of sampler and the weight used to drive it, and there were differences relative to the distance the weight must travel before impacting the sampler.

One of the most popular and most economical drilling methods is the American Society for Testing and Materials (ASTM) standardized SPT method (D 1586). It involves driving a 2" O.D. ($1\frac{3}{8}$ " I.D.) sampler using a 140-lb weight falling freely a 30-in. distance. The number of blows required to drive the sampler 18 in. is recorded in three successive 6-in. increments. The number of blows required to drive the sampler the first 6 in. is used to seat the sampler. The number of blows required to drive the sampler the second and third 6-in. increments are added to give the blow count (N). There are many reasons why the numbers are recorded in three different 6-in. increments, the most obvious being the fact that some soil deposits may be too hard to drive the sampler through. The number indicates whether there are any soft sublayers, hard sublayers, or obstacles such as rocks within each 6 in. of driving. If the number of blows required to drive the

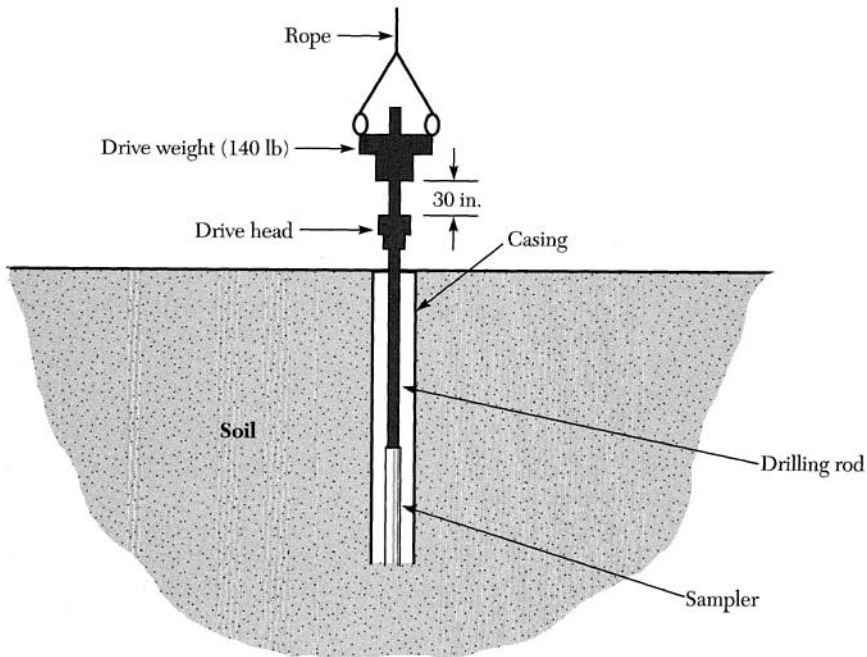


FIGURE 2.10 Cross section of a typical boring hole and drilling equipment.

TABLE 2.4 Standard Drilling Rods and Casings Used in Soil Exploration

| Boring Diameter (in.) | Drill Rod | O.D. (in.) | Casing | O.D. (in.) |
|--------------------------|-----------|------------------|--------|------------------|
| $1\frac{1}{2}$ | E | $1\frac{15}{16}$ | EX | $1\frac{7}{16}$ |
| 2 | A | $1\frac{5}{8}$ | AX | $1\frac{7}{8}$ |
| $2\frac{1}{2}$ | B | $1\frac{7}{8}$ | BX | $2\frac{3}{8}$ |
| 3 | N | $2\frac{3}{8}$ | NX | $1\frac{15}{16}$ |

sampler the second 6 in. is appreciably different from that recorded for the third 6 in., then one must investigate the reasons. The N -value is normally recorded on the lid of the jar in which a soil sample recovered at that depth is stored. The depth, the boring number, and the sample number are recorded as well.

The drilling is begun by using an auger to drill a hole to a specific depth and cleaning the hole down to that depth. The drilling auger is then removed and replaced with a drilling rod with a standard spoon sampler attached at its end. The sampler is then driven 18 in. using the standard weight freely falling 30 in. If the sampler cannot be driven a 6-in. distance because of cemented hardpan, very dense/hard soil, or rocks, the N -value is reported as number blows/number of inches driven. For example, if 80 blows were required to drive the sampler a distance of 3 in., then the blow count is reported as 80/3. Drilling operations are normally stopped at refusal or when the blow count is 50 blows/1 in. ASTM defines refusal as 100 blows/ft. This is also referred to as *hard driving* and is very expensive to the client. A typical boring cross section is shown in Figure 2.10.

The N -value is extremely important and is widely used in estimating many physical soil properties. Unfortunately, its determination may be subject to significant errors. These are attributable to such factors as inexperience of the drilling crew, variation in the 30-in. height of weight drop, distorted samplers, inadequate cleaning of holes, obstacles, and interference with the free fall of the weight. More important, the blow count could be influenced by the type of soil deposits in which drilling is taking place. More information is given in Section 8.2.4. Note that the N -values are those obtained using a standard 140-lb weight with a free fall of 30 in. and a standard 2" O.D. by $1\frac{3}{8}$ " I.D. sampler.

In addition to the factors mentioned earlier, the type of drilling rod and its length may drastically influence the N -value. Studies by Mclean et al. (1975) have shown that the blow count may be higher than it should be up to 14 blows/ft when long drill rods are used. Table 2.4 shows a number of standard drilling rods and casings for different applications.

It is evident that one must exercise utmost caution when dealing with empirical values developed from correlations between the N -values recorded for a given soil type and its mechanical properties.

2.4.2 Undisturbed Soil Sampling

The equipment and methods for obtaining undisturbed cohesive and/or semi-cohesive soil samples vary in terms of procedures and type of sampler used. How-

ever, they share the same objective in that they all attempt to cause the least amount of disturbance possible to the soil sample. These soil samples are generally needed for testing soil strength and compression. Because sample disturbance is influenced by such factors as sampler type, rod type and length, type and rate of penetration, and soil type, it is impossible to meaningfully quantify the extent of disturbance that a given sample undergoes. It is clear that one cannot totally eliminate and can only hope to minimize the effects of these factors on the soil sample extracted from the field. The implication is that “disturbance” refers to the degree rather than the absolute magnitude of the effect on the behavior of a given soil sample.

Sampling Cohesionless Soils

Regardless of the method and equipment used in obtaining soil samples, good engineering judgment and experience must be relied upon to interpret the test results. Strength and compression tests must be corrected for disturbance even though an “undisturbed” sample was used in these tests!

Undisturbed samples in cohesionless soil deposits are extremely difficult to obtain. Such samples are generally recovered by cutting a trench around the soil sample and boxing the soil sample, then pouring paraffin or wax to fill the voids around the sample and cutting the sample at its bottom with a shovel. The box is then turned over and more paraffin is poured to fill the rest of the voids, after which the box is enclosed (Figure 2.11).

The box can then be carefully transported to the laboratory and frozen. The soil sample can be taken out and trimmed to the dimensions needed for specific strength or compression testing. This approach to soil sampling should only be used when the soil deposit is moist, so that when the box is frozen there will not be excessive expansion of the sample, which may result if the soil sample contains an appreciable amount of water. Such sampling methods are expensive and time-consuming and are limited to shallow and medium depths.

Sampling Cohesive Soils

Unlike cohesionless soils, cohesive soils can be sampled with relatively less disturbance because of the cohesion that exists between the individual soil particles. The degree of disturbance associated with sampling in cohesive soil deposits may

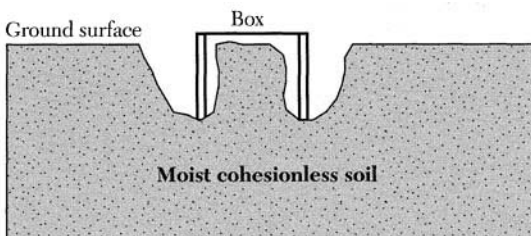


FIGURE 2.11 Typical setup for undisturbed sampling in cohesionless soil deposits.

be expressed in terms of the dimensions of the sampler used and ignoring other factors contributing to disturbance. This will only reflect the effects of one of the many factors influencing soil sample disturbance. For a soil sample of length L , the **area ratio** AR is often used to indicate the relative degree of disturbance associated with a given soil sampler. AR is determined by relating the volume of soil displacement to the volume of the soil sample collected as follows:

$$AR = \frac{\frac{\pi d_o^2}{4}L - \frac{\pi d_i^2}{4}L}{\frac{\pi d_i^2}{4}L} \times 100 = \frac{d_o^2 - d_i^2}{d_i^2} \times 100$$

where d_o is the outside diameter of the sampler being used and d_i is its inside diameter. This expression relates the cross-sectional area of the displaced soil to the recovered cross-sectional area of the sample. Samplers used for undisturbed sampling should have an area ratio of approximately 10%. To meet this requirement, the wall thickness of a sampler should not exceed 0.07 in. (1.8 mm) for a soil sample 3 in. (76.2 mm) in diameter.

Thin-Wall Tube Sampler This is by far the simplest and most widely used of the undisturbed samplers. It is referred to as *Shelby tube* and is shown in Figure 2.12. The sampler consists of a thin-wall tube with a sharp cutting edge and can be attached to a drilling rod.

The steel ball valve in the head section vents the inside of the tube to the outside, permitting air and/or water to escape as the tube is pushed into the soil strata. Sampling with Shelby tubes involves drilling a borehole to a predefined depth with an auger, then cleaning the hole. The auger is removed and replaced with a drilling rod. The Shelby tube is attached to the bottom of the drilling rod and then lowered back into the open hole (sometimes casing is used to prevent the hole from caving in). The Shelby tube is then pushed to a depth approximately equivalent to the length of the tube using the hydraulic system on the drill rig. Sometimes, the Shelby tube cannot be pushed, in which case the sampler is driven with the weight normally used with the SPT test. This is not preferred and should be avoided when possible because extensive sample disturbance may re-

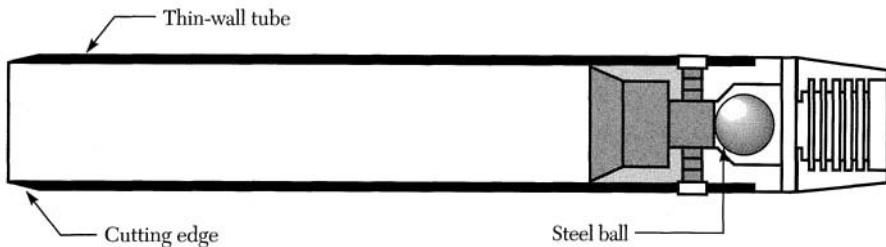


FIGURE 2.12 Shelby tube used for undisturbed sampling in cohesive soil deposits.

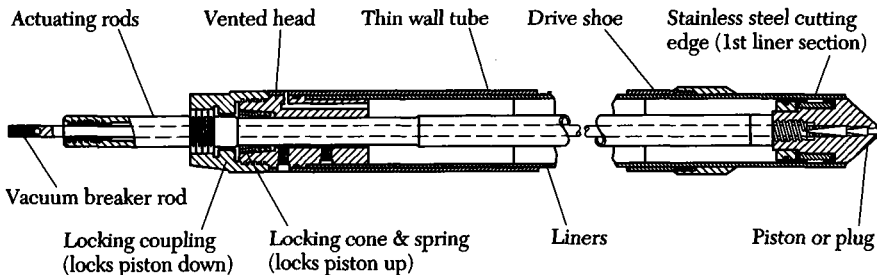
TABLE 2.5 Standard Shelby Tube Sizes (ASTM D-1587)

| Outside Diameter (in.) | Outside Diameter (mm) | Inside Diameter (in.) | Inside Diameter (mm) | Wall Thickness (in.) | Wall Thickness (mm) | Tube Length (in.) | Tube Length (cm) |
|------------------------|-----------------------|-----------------------|----------------------|----------------------|---------------------|-------------------|------------------|
| 2 | 50.8 | 1 $\frac{7}{8}$ | 47.6 | 0.049 | 1.24 | 36 | 76.2 |
| 2 $\frac{1}{2}$ | 63.5 | 2 $\frac{3}{8}$ | 60.3 | 0.065 | 1.65 | 36 | 76.2 |
| 3 | 76.2 | 2 $\frac{7}{8}$ | 73.0 | 0.065 | 1.65 | 36 | 76.2 |
| 3 $\frac{1}{2}$ | 88.8 | 3 $\frac{3}{8}$ | 85.7 | 0.065 | 1.65 | 36 | 76.2 |
| 4 $\frac{1}{2}$ | 114.3 | 4 $\frac{3}{8}$ | 111.1 | 0.065 | 1.65 | 36 | 76.2 |
| 5 | 127.0 | 4 $\frac{3}{4}$ | 120.6 | 0.120 | 3.05 | 54 | 137.2 |

sult. In any event, if driving is necessary due to the presence of stones or strata of hard or dense soil, this fact should be reported. Information relative to depth, sample number, sample length recovered, and borehole number should be recorded on each tube.

Shelby tubes have been standardized by the ASTM and are available in different sizes. These sizes are shown in Table 2.5. Shelby tubes are also available in lengths of 20 $\frac{3}{4}$ " (52.7 cm), 24" (61.0 cm), 26 $\frac{1}{2}$ " (67.3 cm), 30" (76.2 cm), 36" (91.4 cm), and 54" (137.2 cm). Regardless of the tube length used, soil samples are normally extracted by first cutting the Shelby tube (with the sample still inside) in lengths appropriate for the particular test to be conducted, then extracting the sample using an extruder. This will minimize the disturbance due to friction between the inner surface of the tube and the outside surface of the soil sample. It is recommended that Shelby tube samples should be extracted soon after they arrive in the laboratory, because adhesion might become a problem when dealing with cohesive soil samples, making it difficult to extract the soil sample without causing needless sample disturbance.

Stationary Piston Sampler This instrument is available in several variations. The construction of these samplers is similar to that of the Shelby tube sampler

**FIGURE 2.13** Stationary piston sampler. (Courtesy of Acker Drill Co., Inc.)

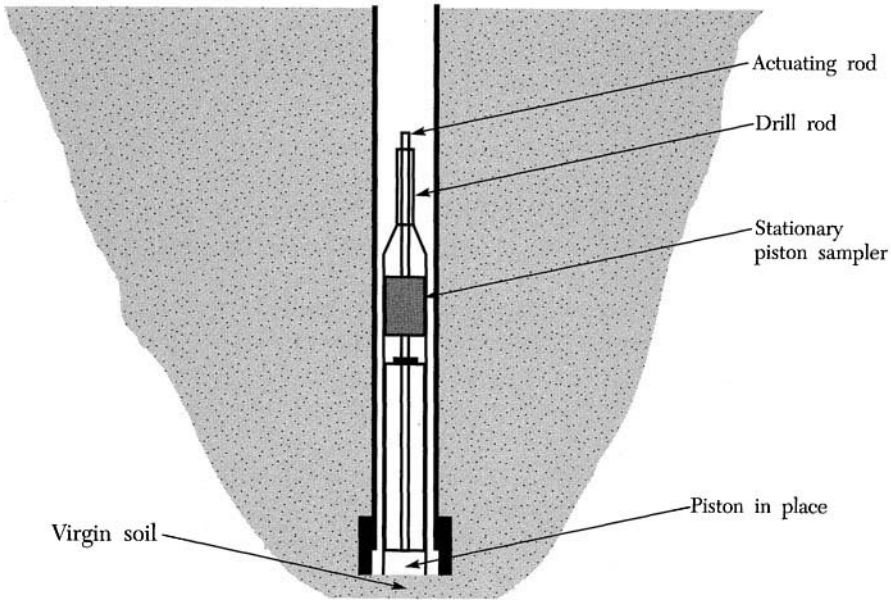


FIGURE 2.14 Stationary piston sampler set.

except for the addition of a sealed piston and a locking cone in the head to prevent the piston from moving downward (Figure 2.13). The use of the stationary sampler involves preparing the borehole in the same manner as for the Shelby tube sampler. The piston sampler is then placed on the bottom of the borehole with the thin-walled tube flush with the piston (Figure 2.14), and the sample tube is pushed past the stationary piston using the actuating rod. The drilling rod and the tube are then removed from the borehole and the tube is separated from the sampler apparatus for safe storage.

Piston samplers have two main advantages over the Shelby tube sampler: (1) They are fully sealed, making it possible to lower the sampler into fluids and cuttings without fear of sample contamination, and (2) the top of the soil sample is protected from any distorting pressure. Improved versions of stationary samplers that will enable operations in uncased boreholes are now available. The Lowe Acker stationary piston plug sampler is one good example of such samplers.

Denison Sampler This is a third type of sampler generally accepted for undisturbed soil sampling (Figure 2.15). It is available in four sizes with outside diameters of $3\frac{1}{2}$ ", 4", $5\frac{1}{2}$ ", and $7\frac{3}{4}$ ". These devices are useful in difficult soils such as hardpan, hard clay, highly cemented soils, or other soil deposits where hard driving is needed. In these cases, the Shelby tube and the stationary piston samplers are ineffective in that significant pressures are required to push the sampler. This may result in damage to the thin-wall tubes normally used in undisturbed sampling.



FIGURE 2.15 Denison soil sampler. (Courtesy Acker Drill Co., Inc.)

In the field, the Denison sampler is rotated into the virgin soil at a given depth within a cased or an uncased borehole. The inner barrel is a full swivel type mounted on antifriction bearings. The barrel protrudes below the cutting bit carried by the outer barrel. This ensures that the soil sample is recovered from materials undisturbed by cutting action of the rotating bit. The sampler is designed to seal off the sample from water or drilling fluid normally discharged at the bit face. The fluid is used to facilitate drilling operations by reducing friction. As the Denison core barrel is forced into the soil with gradually increasing pressure, the sample passes through the core retainer into the inner barrel and the thin-walled liners. There are two basic types of retainers used with the Denison sampler: (1) the split-ring type for hard materials, and (2) the basket-spring type for soft soils.

2.4.3 Rock Coring

Often, when the foundations are carried by or into bedrock, rock core samples are taken to test for the physical characteristics and the quality of the rock materials. This is especially true when dealing with earth and concrete dams, piles, and caissons. In addition to elevation of the rock surface, rock type, and permeability, one may have to determine the degree of weathering, depth, solution channel (especially in limestones), discontinuities, folds, and cleavage. Geological standards are generally used in the classification of rocks for engineering use (Table 2.6). The strength of rocks can be determined using uniaxial compression tests. However, such tests are limited by the fact that the overall strength is limited by the rock character, spacing, distribution of discontinuities, and partial weathering. These factors could also have a significant influence on the permeability and the deformation properties of rocks.

The Rock Quality Designator (RQD) as defined by Deere (1967) is often used as an indicator for discontinuities in rocks of most types. This criterion is not applicable for fissile rocks such as shales. The RQD value is defined as the ratio of the sum of intact pieces greater than 10 cm (4 in.) in length in a core sample (L_s) to the length of the core advance (L_c). That is

$$\text{RQD} = \frac{L_s}{L_c} \times 100$$

This equation is applicable only if double-tube N -size core barrels of 3 in. (76 mm) nominal O.D. with fixed inner barrels are used in obtaining the sample. The N -size drill usually gives good recovery. A smaller drill-rod size (A or B)

TABLE 2.6 Recommended Procedures of Rock Classification*

| Weathering | | |
|--|--|------------------------------|
| Fresh | Few joints may show slight staining. | |
| Very slight | Joint stained, some joints may show clay layers. | |
| Slight | Joint stained and discoloration may extend 1 in. into rock. | |
| Moderate | Significant portion of rock show discoloration and other weather effects. | |
| Moderately severe | All rock except quartz is discolored with moderate loss of strength. | |
| Severe | All rock except quartz is discolored with severe loss of strength. | |
| Very severe | All rock except quartz is discolored and is effectively reduced to soils. | |
| Complete | Rock is reduced to soil. | |
| Hardness | | |
| Very hard | Rock cannot be scratched with a knife and would require several hard blows to break if impacted with a geologist's pick. | |
| Hard | Rock can be scratched with knife with a lot of effort. | |
| Moderately hard | Rock can be scratched with a knife and shallow grooves can be made. | |
| Medium | Rock can be scratched with a knife and grooved with firm hand pressure. | |
| Soft | Rock can be readily grooved and gouged with a knife. | |
| Very soft | Rock can be carved with a knife. | |
| Joint Bedding and Foliation Spacing | | |
| Spacing | Joints | Bedding and Foliation |
| Less than 2 in. | Very close | Very thin |
| 2 in. to 1 ft | Close | Thin |
| 1 ft to 3 ft | Moderately close | Medium |
| 3 ft to 10 ft | Wide | Thick |
| More than 10 ft | Very wide | Very thick |

*(*Technical Procedures Committee, ASCE, 1962*)

should be used where massive rocks such as granite are sampled. The recovered core rock sample should be carefully stored in specially constructed wooden boxes. Information pertaining to borehole number, sample depth, voids, and core losses should be properly recorded on each box. The RQD value obtained for a given rock core sample can be used to approximate some of its physical properties. Table 2.7 gives information relative to the ratio of field Young's modulus of elasticity (E_f) of rocks to the laboratory value (E) and the corresponding RQD value. It is evident that the descriptive terms used in classifying rocks are subjective and can only provide qualitative measures of the expected behavior of rocks as a bearing material. However, with experience, that might be sufficient for many applications.

In unweathered and/or cemented rocks, core samples are normally obtained using one or more of many bits and sampling methods. The Denison sampler dis-

TABLE 2.7 Relationship between the RQD and the E_t

| RQD | Rock Description | E_t/E (%) |
|-------|------------------|-------------|
| < 25 | Very poor | 15 |
| 26–50 | Poor | 20 |
| 51–75 | Fair | 25 |
| 76–90 | Good | 30–70 |
| > 90 | Excellent | 71–100 |

cussed earlier in undisturbed sampling of soil is often used to obtain rock core samples. It is ideal in formations of gravel, soft shales, and hard clay with gravel. The Denison sampler must be equipped with a carbide or diamond bit when coring harder materials. A standard diamond core bit, normally used for rock coring, is shown in Figure 2.16.

In the drilling operation, the bit and core barrel rotate while pressure is applied and fluid (normally water) is circulated to carry the cuttings out of the borehole and to cool the bit and the rock. The water may have to be brought in a tank if no water is available on the job site.

2.4.4 Field Water Level Observation

The recording of water levels at drilling sites is an important aspect of subsurface exploration. Failure to obtain an accurate water level may invalidate otherwise useful boring data. This is because groundwater may occur due to a free water surface, artesian conditions, or a perched water table. Consequently, groundwater may significantly affect various aspects of foundation design and construction.

Artesian conditions are difficult to handle especially when dealing with a project that requires an excavation to be made below the water level. In such cases, proper precautions must be taken so that excess water is removed by pumping or trenching. This type of water occurs due to the presence of sloping confined aquifers as shown in Figure 2.17. In this case, water is first encountered at the



FIGURE 2.16 Standard diamond core bit. (Courtesy Acker Drill Co., Inc.)

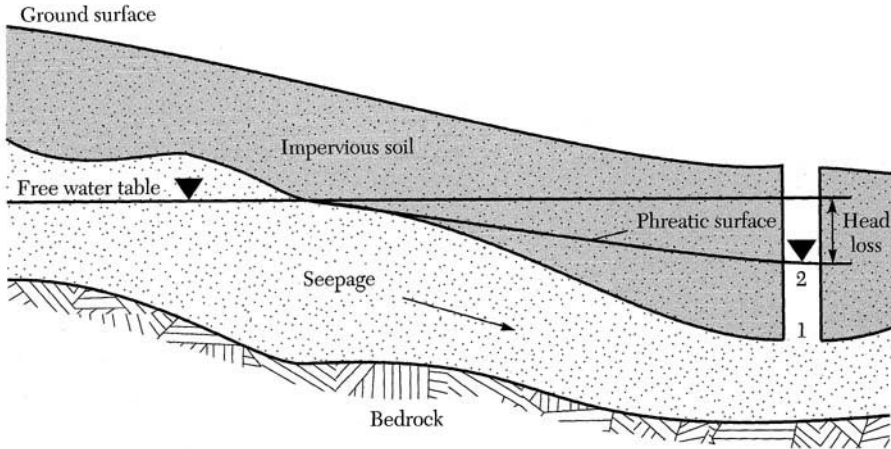


FIGURE 2.17 Artesian groundwater.

bottom of the borehole (level 1 in Figure 2.17), then rises to a stable elevation (level 2 in Figure 2.17). The difference between the free water table and level 2 is due to energy loss caused mainly by friction between water and the soil particles.

Perched water is generally of no consequence during construction but is of extreme importance when one is calculating the effective overburden pressures within a given soil deposit. The implication is that if perched water is erroneously assumed to be the free water table, then estimates of settlements and the bearing capacity of the foundation will be in error. A perched water table is developed when the water is an accumulation above a sagging impervious formation (Figure 2.18).

It is evident that in this case, the free water table may be located several feet below the perched water level. Perched water generally disappears a few hours after the borehole is extended through a permeable soil layer and will not rise as free water would. Note that in coarse sand and gravel formations, the groundwater level may rise and fall due to changes in weather, discharge, and recharge. In such deposits, the free groundwater surface would normally slope in the same manner as the ground surface. These variations in the water table are not as pronounced in impervious formations such as clay and silt.

Water levels in a borehole can be estimated by the drilling crew by lowering a float attached to a tape measure. For good results to be obtained, the borehole should be cased and left open and the water level recorded at least two different times (preferably at 24-h increments). In most cases, the final water level recorded is assumed to be the depth of the free water table. One can use the procedure proposed by Hvorslev (1949) for estimating the correct water table depth. This procedure involves bailing water out of the borehole, then recording the depth of the water level D_0 at time t_0 . The water level at times $t_0 + \Delta t$ and $t_0 + 2 \Delta t$ is recorded as D_1 and D_2 respectively, where Δt is the time increment ($\Delta t =$

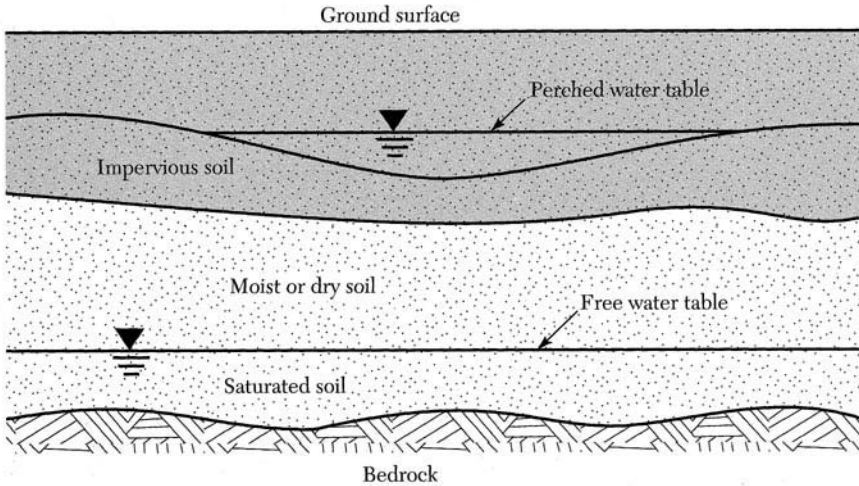


FIGURE 2.18 Perched groundwater.

24 h is recommended). This approach is illustrated graphically in Figure 2.19. Note that although the water is shown to rise in the borehole, it can also fall. The recorded depth values D_1 and D_2 can then be used to approximate the water table depth as follows:

$$D_w = \frac{D_0 + D_1}{2} - \frac{1}{2} \left[\frac{Z_1^2 + Z_2^2}{Z_1 - Z_2} \right] \quad (2.6)$$

where D_w is the depth of the free water table, $Z_1 = D_0 - D_1$, and $Z_2 = D_1 - D_2$. Clearly Z_1 and Z_2 must not be equal for Eq. (2.6) to be valid. Additionally a **piezometer**, an instrument for measuring pressure head in soil deposits (see Section 5.4), should be used for water level determination if more precise field data are required.

2.5 PRESENTATION OF RESULTS AND REPORTS

The need for well-written reports, test data, and logs cannot be overemphasized. The effort and money expended on sampling, testing, and planning for subsurface exploration must ultimately result in a well-prepared and well-documented report. Clarity, accuracy, and completeness are a must. This is basically the responsibility of the driller and the geotechnical firm involved in the soil exploration aspect of the project. The following outline, which is based on the ASTM D-18 Committee of Standards, can be used as a guide when preparing a report relative to a subsurface exploration program.

- I. Text
 - A. Cover letter
 - B. Scope and purpose of the investigation

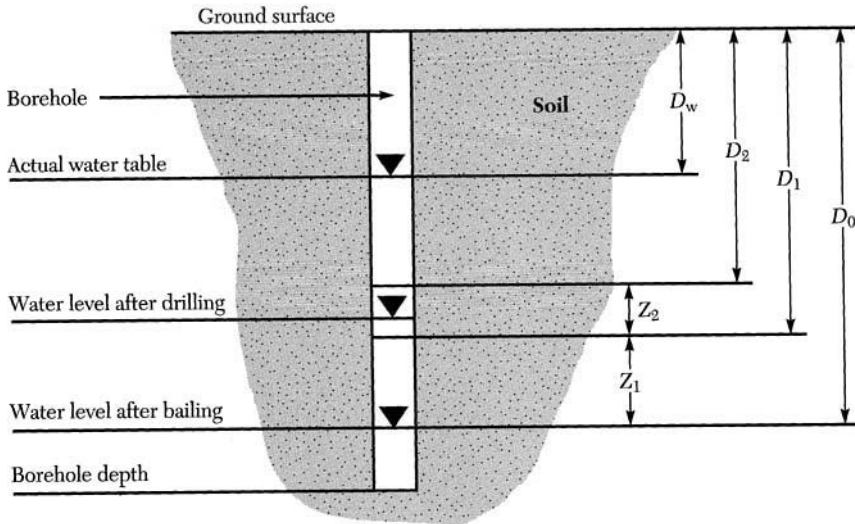


FIGURE 2.19 Method of estimating the actual water table.

- C. Proposed structure(s)
- D. Geological information
- E. Adjacent structures
- F. Methods used in drilling and sampling
- G. Laboratory tests, procedures, and equipment used
- H. Discussion of field and laboratory test results
- I. Recommendations for foundation alternatives
- J. Recommendations for construction procedures
- K. Limitations of the exploration program
- L. Site location map
- II. Laboratory data
 - A. Laboratory test results
 - B. Testing procedures (if different from ASTM)
 - C. Subsurface engineering profile showing soil types and properties
- III. Logs
 - A. Plan of boring/test pits/locations
 - B. Boring/test pits logs
 - C. Subsurface profile based on field examinations
 - D. Groundwater information
 - E. Unusual field conditions

Although this list is by no means exhaustive, it does provide an overall picture of the extent of work to be done before a subsurface exploration program is completed. Furthermore, there are other items relating to drilling that must be included in the report. Typical field and laboratory boring log forms are shown in Figures 2.20 and 2.21 respectively.

Remarks pertaining to problems encountered during the drilling operations should be included on the back of the boring log. Loss of circulating water, rocks and/or boulders encountered, casing conditions, loss of sample, and cavities and voids should all be reported. Although some of the items may not be essential, let the engineer in the office decide that. Do not assume the responsibility yourself.

PROBLEMS

- 2.1 Describe the criteria normally used in determining boring depth.
- 2.2 List the factors considered when specifying boring numbers and spacing in a subsurface site exploration.
- 2.3 What is meant by *continuous sampling*?
- 2.4 Why is it important to investigate site geology and hydrology when the subsurface investigation is conducted?
- 2.5 Describe briefly why existing structures must be taken into account in subsurface investigation.
- 2.6 Why should geophysical methods be used in subsurface exploration when other methods may provide more informative data?
- 2.7 Describe the differences between seismic surveys and resistivity exploration.
- 2.8 Describe briefly the differences between the various methods used in the exploratory subsurface investigations.
- 2.9 List the major differences between the exploratory and the detailed methods of subsurface investigation techniques.
- 2.10 Describe briefly the SPT method of soil sampling.
- 2.11 List the basic factors influencing the accuracy of the field N -value in as far as the soil type is concerned.
- 2.12 In evaluating the disturbance associated with a given soil sampler, one may use the area factor to approximate it. Determine the area factor for the standard split-spoon sampler.
- 2.13 Determine the area factors associated with the tubes listed in Table 2.5. Which tube is likely to have the least amount of disturbance?
- 2.14 Determine the RQD factor for a core advance in rocks of 100 cm that produced a sample of 85 cm consisting of dust, clay, and pieces of rock. The sum of the lengths of pieces 10 cm or larger is 72 cm. How will you rate such a rock from the standpoint of engineering behavior?
- 2.15 Describe the main differences between the distinct types of groundwater conditions that might be encountered in the field. What are the dangers associated with artesian water?
- 2.16 It is desired to approximate the water table location in a silty clay deposit. The borehole was extended to 45 ft, then bailed to a depth of 40 ft below ground surface. The water rise was then recorded on two separate times as follows:

$$D_1 = 33 \text{ ft} \quad 12 \text{ h after bailing}$$

$$D_2 = 30 \text{ ft} \quad 24 \text{ h after bailing}$$

Determine the depth of the water table for this profile.

3

Index Properties of Soils

3.0 INTRODUCTION

Soils are a heterogeneous accumulation of mineral particles. The term *soil* includes almost every type of uncemented or partially cemented inorganic and organic material found in the ground. Only hard rock, which remains firm after exposure, is excluded. To the engineer engaged in design and construction of foundations and earthwork, the index properties of soils are of primary importance. These properties include their water content, unit weight, particle size and shape, the soil aggregate including its texture and structure, soil consistency and sensitivity, and organic content. To enable an engineer to describe and discuss a soil with brevity and the assurance that the description would mean the same soil to another engineer, it was necessary to establish a classification system. Logs of explorations containing adequate soil classifications and descriptions can be used in making preliminary design estimates, in determining the extent of additional field investigations needed for final design, and in extending test results to additional explorations. A soil classification system can best be understood by considering the index properties of soils.

3.1 WATER IN SOILS

3.1.1 Free Water and Hydration Water

The soil mass consists of a collection of solid particles with voids between them. The soil solids are small grains of different minerals, and the voids can be filled with water or air, or partly filled with both air and water (Figure 3.1). The engineer wants to know how much water is present in the voids relative to the amount of solid particles. The water content of a given soil specimen, in both the natural state and under defined test conditions, may provide extremely useful information about its engineering behavior. In addition, it is essential in solving the phase diagram problem and for classifying cohesive soils (clays). The effort required for its determination is by no means indicative of its importance.

It is convenient to define the ratio of mass of water M_w to mass of soil solids M_s as the **water content** (or **moisture content**) w , thus,

$$w = (M_w/M_s) \times 100 \quad (3.1)$$

This ratio of water present in a soil volume to the amount of soil grains is based on the dry mass and not the total mass. The dry mass of solids is normally determined by drying soil in an oven to a constant mass at a temperature of 110°C. The actual drying time needed depends on the soil type and amount, and the shape of the soil specimen used. For convenience, the sample is often dried overnight in an oven. The water content can be expressed as a fraction or as a percentage and may range from zero (dry soil) to several hundred percent. For most soils, w is well under 100%, although it can range up to 300% or more for some organic and marine soils.

Care must be exercised in selecting representative field samples for a water-content determination. In layered soil strata (sedimentary clays) there can be a large difference in water content between adjacent strata. To minimize the effects

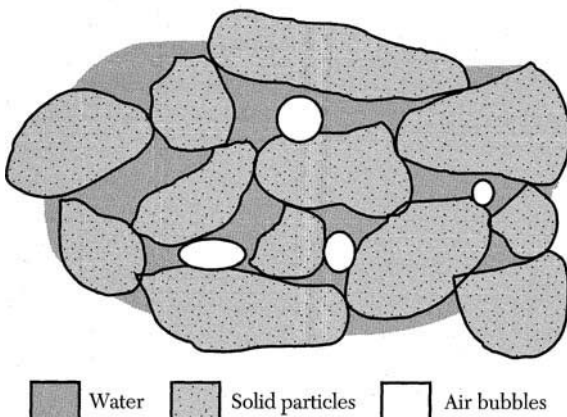


FIGURE 3.1 Soil skeleton containing water, solid particles, and air bubbles in the voids.

of drying, the total soil mass should be determined as soon as possible after the sample has been secured. Soil samples in storage may have partially dried at the surface. It is desirable to determine the water content for several layers that have not undergone surface drying to obtain a representative value. The amount of soil required for a water content determination depends on the soil type and the quantity of soil available. For fine-grained soils, ASTM D 2216 recommends that the minimum soil mass be 100 g to 200 g. For larger particle sizes, a representative sample will require a larger soil mass. Attempts to refine test methods in order to obtain high precision may not be possible when water contents are between adjacent strata in a sedimentary clay. In other cases, a high precision is desired for a homogeneous clay or when the mass of dry soil is measured in a specific gravity test.

Three categories of water are normally recognized in soils: (1) pore water (free and oriented water), (2) interlayer water between the basic structural units of montmorillonite and halloysite (adsorbed water), and (3) water present in the clay mineral crystal lattice (hydration water). These categories are shown in Figure 3.2. Only pore water has a primary influence on soil behavior. Free water comprises the greater portion of water in most soils. Oriented water can be described as a thin layer, three or four molecules in thickness, on particle surfaces. In frozen soils the first one or two layers of oriented water retain their liquid properties and represent an unfrozen water content. The amount of oriented water depends on the specific surface area of the soil particles, the mineral type, and the presence or absence of solutes in the pore water. For granular soils (sand, gravel, etc.) the standard procedure used for water content determination removes all free water without affecting the individual particles' structure. For cohesive soils (clays) and organic soils, the individual particles can be affected by oven drying.

The hydration water is part of the crystal structure. Except for gypsum and some tropical clays, the hydration water cannot be removed by oven-drying at 110°C. Significant dehydration may occur in soil samples containing allophane, montmorillonite, and to a lesser extent halloysite, when oven-dried at 110°C. The loss of dehydration water at 110°C may approach 13% by weight. That is, a dry soil sample of allophane clay may show a water content of 13% when the actual free water content is zero. Organic soils may present similar problems. The or-

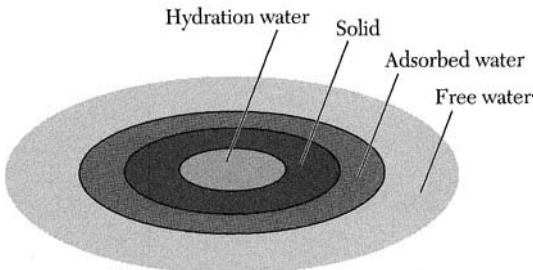


FIGURE 3.2 Water zones in a clay particle.

ganic fraction in a given soil sample could experience substantial weight losses even at 60°C. The authors (1981) have reported that organic soils containing cellulosic substance lose approximately 7% by weight of the organic fraction when oven-dried at 100°C. For clays the removal of interlayer water is not reversible, and the hydrated form of the mineral cannot ordinarily be formed by rewetting. Removal of interlayer water does influence soil properties where large amounts of allophane, halloysite, and montmorillonite are present in the soil. Lattice water is strongly attracted to mineral particles, and temperatures of about 300°C are required to remove it, as is shown in Figure 3.3. Lattice water has little significance from an engineering standpoint but is of considerable importance in ceramics.

For some projects, particularly for ground freezing, it is important to determine the salinity of the pore water. The importance of following standardized test procedures (ASTM D 2216) relative to drying temperatures is illustrated in Figure 3.3.

3.1.2 Capillarity

Capillarity arises from a phenomenon associated with fluids known as *surface tension*, which occurs at the interface between different material surfaces. In soil deposits, it occurs between soil solids and water. Surface tension results from differences in the forces of attraction between water molecules and those on solid-particle surfaces. Capillarity plays a rather important role in geotechnical engineering, especially with silty soils. The heaving of pavements in cold regions may

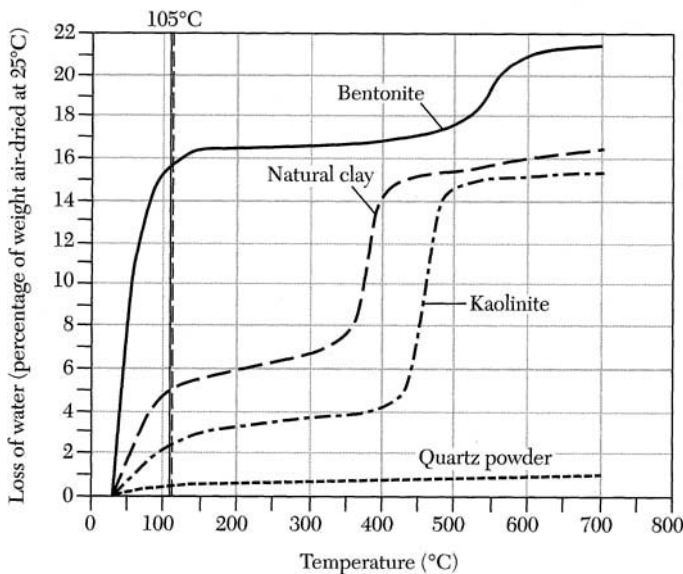
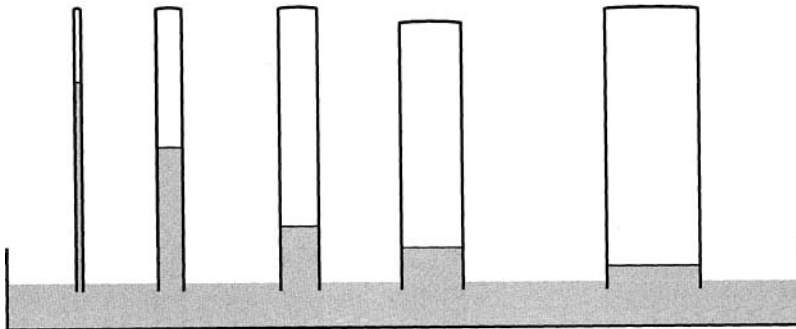


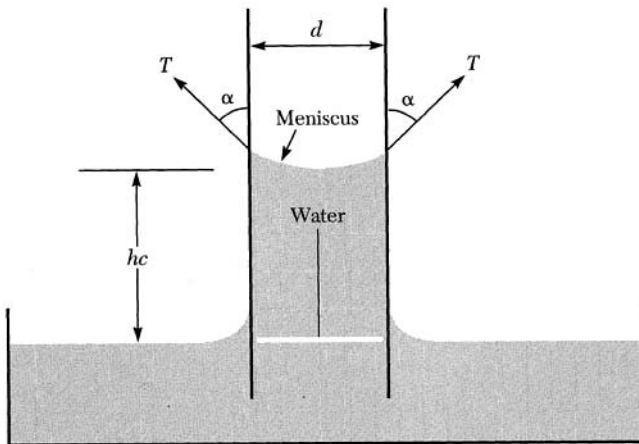
FIGURE 3.3 Dehydration curves showing loss of surface hydration and lattice water. (After Kelly et al., 1936.)

be attributable to the freezing of water transported by capillary action to the ice lens.

The phenomenon of capillarity as it relates to soil can be demonstrated using the analogy of a small-diameter tube inserted in a water container. The water will rise a distance inversely proportional to the diameter of the tube — that is, the larger the diameter the smaller the capillary rise. Capillary rise is affected by the roughness, cleanliness, and type of the inner tube surface. For practical purposes, the diameter of the tube is the parameter of most concern in estimating capillary rise. Figure 3.4 illustrates derivation of the relationships needed for its calculation. Fluids such as water form a concave meniscus on top of the capillary water column inside the tube. Equating the forces due to the weight of the water column to the surface tension forces around the circumference of the water column



(a)



(b)

FIGURE 3.4 Capillary rise: (a) tubes of different diameters; (b) geometry showing parameters used in the derivation of capillary rise formula.

using the principle of static equilibrium gives

$$\gamma_w h_c \frac{\pi d^2}{4} = \pi d T \cos \alpha$$

where γ_w is the unit weight of water (9.807 kN/m³), d is the diameter of the tube, α is the angle between the surface tension forces and the vertical direction, T is the surface tension of water, and h_c is the capillary rise. Solving for the capillary rise (h_c) yields

$$h_c = \frac{4T}{\gamma_w d} \cos \alpha \quad (3.2)$$

In soils, the shape, size, and configuration of void spaces between solid particles are unlike those of a glass capillary tube. Therefore, accurate prediction of capillary rise is impossible. Equation (3.2) provides information needed for the basic understanding of the factors involved in capillarity. While it is impossible to accurately assess each of the parameters appearing in Eq. (3.2), experimental work by a number of researchers has shown that reasonable values for capillary rise can be estimated. For soils, the value of α is taken as 0, the diameter as 20% of the effective particle size (D_{10}), and the surface tension force as 75 dyn/cm. The effective size of a given soil is calculated using grain size analysis (discussed later in this chapter). Substituting these values into Eq. (3.2) gives

$$h_c = 1.50/D_{10} \quad (3.3)$$

where h_c and D_{10} are measured in centimeters. Equation (3.3) shows that the smaller the grain size of a given soil, the higher the capillary rise. This is true because the void spaces are of the same order of magnitude as the particle sizes. The temperature in a given soil plays an important practical role. Unfortunately, it is not possible at this time to quantify its influence. However, the height of capillary rise should be higher with lower temperatures. This may increase the difficulty in handling soil materials and may create a situation where the movement of equipment from and to construction sites becomes rather challenging. Typical capillary rise values for different soil types are listed in Table 3.1.

At first it would appear that clay soils are the most difficult to deal with. Despite the fact that their potential for capillary rise is greater than that of any other soil, this is not true. The reason lies in the fact that the time required to achieve

TABLE 3.1 Typical Capillary Rise for Different Soils

| Soil Type | Capillary Rise, h_c (cm) | Capillary Rise, h_c (ft) |
|--------------|-------------------------------|-------------------------------|
| Small gravel | 2 to 10 | 0.1 to 0.4 |
| Coarse sand | 15 to 25 | 0.6 to 1.0 |
| Fine sand | 30 to 100 | 1 to 3 |
| Silt | 100 to 1000 | 3 to 30 |
| Clay | 1000 to 3000 | 30 to 90 |

maximum capillary rise is much longer for clay than it is for silts. Based on typical soil constants, silts are the most difficult to handle. This is because the time required to achieve maximum capillary height for clay may be on the order of years, so evaporation and temperature variations would have to be considered. That is, water may achieve its maximum capillary height in a clay soil because of evaporation. The time required for achieving a specific capillary rise can be estimated using

$$t = \frac{nh_c}{k} \left[\ln \left(\frac{hc}{h_c - Z} \right) - \frac{Z}{h_c} \right]$$

where n is soil porosity, k is the coefficient of permeability, and Z is the distance to which water will rise in time t . The implication is that for a given Z , h_c , and n the time required to achieve capillary rise is inversely proportional to the coefficient of permeability.

3.1.3 Seasonal Ground Freezing

Temperatures near the ground surface undergo annual and daily fluctuations in response to changes in energy transfer at the surface. In cold regions, the arrival of freezing air temperatures in the fall leads to the penetration of a freezing front into the ground (Figure 3.5). The depth reached by this front depends on the intensity of winter temperatures along with a number of other factors (structural and textural composition of the soil and the insulation effect of vegetation and/or snow cover). When the air temperature again becomes positive in the spring, there is a simultaneous penetration of a thawing front into the ground and a retreat of the previous freezing front. The freezing front, represented by the 0°C isotherm, has been superimposed on a highway structure in Figure 3.5. The loss of bearing capacity of the pavement is most critical in the spring during thawing of the foundation soils.

Frost Action With the advance of the freezing front into the foundation soils (Figure 3.5), water contained in the voids of a moist or saturated sand or gravel will freeze in situ. The freezing is associated with a volume expansion of water by almost 10%. This expansion does not necessarily lead to a 10% increase in the voids, because water is expelled during freezing. For a saturated silt or silty sand the effects of freezing depend on the rate of temperature decrease. Rapid cooling of a saturated soil sample in the laboratory causes the water to freeze in situ. If the temperature is lowered slowly, a large part of the frozen water accumulates as clear ice layers oriented parallel to the pavement or ground surface exposed to the freezing temperature.

Under field conditions, ice layers formed in silty soils can grow to several centimeters or more in thickness. The formation of these masses of clear ice requires that water migrate through the soil voids toward the freezing front. This behavior is illustrated in Figure 3.6, which shows three cylindrical samples of fine silt. Sample A rests on a firm base and samples B and C have their lower ends im-

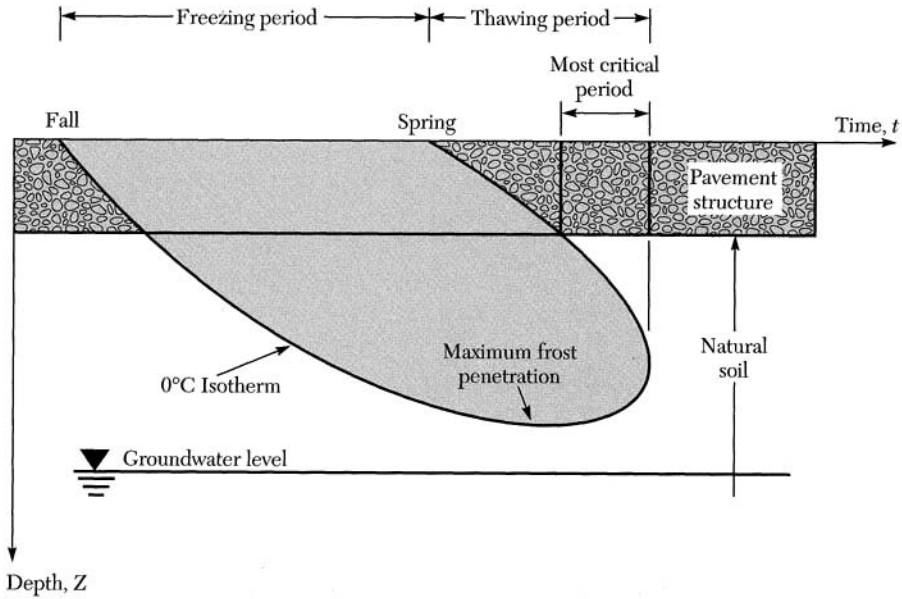


FIGURE 3.5 Seasonal change of the freezing front depth.

mersed in water so as to simulate a high groundwater table. The temperature at the upper surface of each sample is lowered below freezing. Ice layer growth in sample A is limited to the water drawn out of the lower part of the specimen. The lower part consolidates in the same manner as if the water were pulled by capillarity toward an evaporation surface at the top of the sample. The ice layer growth will continue until the water content in the lower part of the soil cylinder is re-

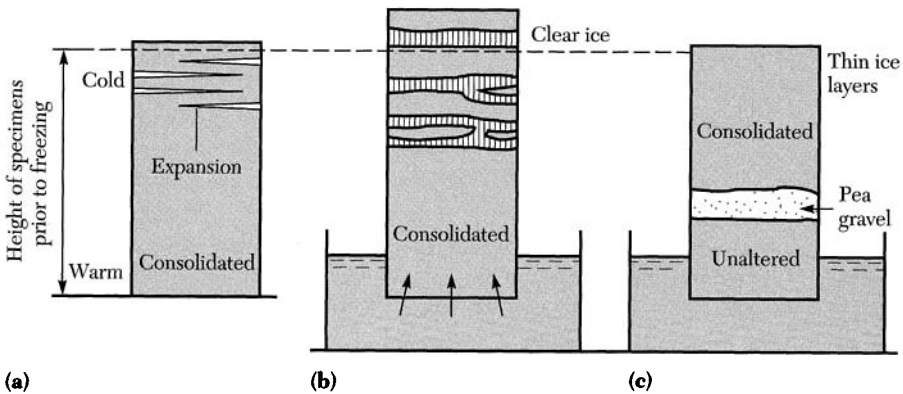


FIGURE 3.6 Frost action in soils: (a) closed system; (b) open system; (c) pea gravel stops capillary flow making upper soil a closed system. (Adapted from Terzaghi, 1952.)

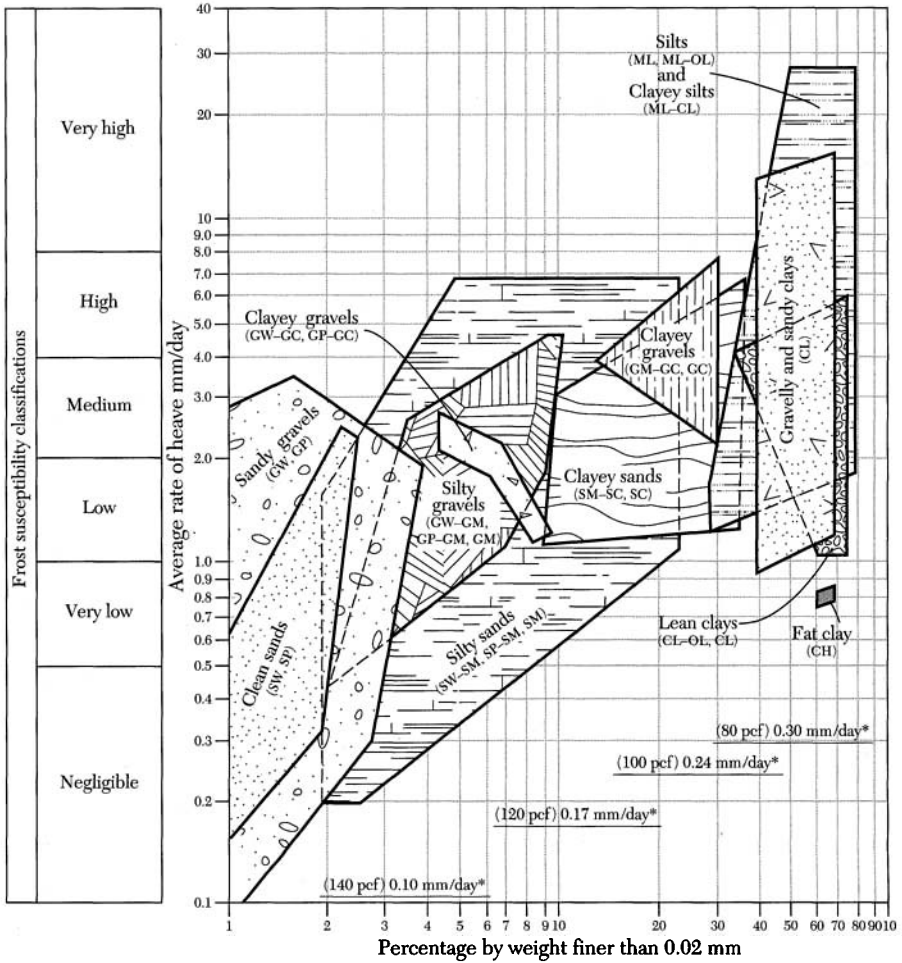
duced to the shrinkage limit. Sample A is referred to as a *closed system*, because all water forming the ice layers comes from within the specimen. The volume increase will be less than 10% of the pore water volume contained in the system.

In sample B, water required for the initial ice layer growth is also drawn out of the silt. As consolidation progresses in the lower part of the sample, water is drawn from the free water located below the sample. With time, both the rate of flow toward the freezing zone and the water content of the unfrozen zone through which water percolates become constant. Sample B constitutes an open system. The ice lens formation in an open system can theoretically increase to several meters in thickness. Insertion of a coarse-grained layer between the freezing zone and the water table (Figure 3.6) transforms the open system (sample B) into a closed system (sample C). Water cannot rise by capillary action through the pea gravel, hence the upper part of sample C represents a closed system. If the freezing front penetrates below the pea gravel, the lower part of sample C will be subjected to ice lens formation. In clay specimens the low permeability limits the rate of water movement toward the freezing front, resulting in a reduced ice lens formation.

In the field, open systems are encountered wherever the vertical distance between the water table and the freezing front is smaller than the height of capillary rise for the soil. Because water that migrates from the water table is continually replenished, ice lenses grow continually during freezing periods and the ground surface (pavement) located above the freezing zone rises. This behavior is labeled *frost heave*. Frost heaves of up to 150 mm are reasonably common in regions with a moderate winter climate. Variations in the underlying soil permeability control ice lens thickness, so frost heave is usually nonuniform. Highway structures located above the frost heave zone can experience increased roughness. As warmer spring air temperatures arrive, the frozen soil and ice lenses are transformed into a zone of supersaturated soil with a reduced strength. The resultant loss in bearing capacity can severely impair pavement performance.

Soil Frost Susceptibility Frost action in soils includes both heaving and thaw-weakening effects, both of which are related to the formation of ice lenses near or at the freezing front. Increased surface roughness is attributed to nonuniform soils and the resultant variation in ice lens thickness. Thaw-weakening involves loss in strength after retreat of the freezing front. The two phenomena are not directly proportional; field experience shows that some clay soils develop segregated ice (and hence thaw-weakening) while exhibiting little or no heave. The shrinkage of compressible soils may cancel the heave associated with ice segregation where the water supply is restricted by low permeability. Chamberlain (1981) stated that both kinds of frost damage (heaving and thaw-weakening) should be addressed in any frost susceptibility criterion.

The range in soil frost susceptibility for most soil types is given in Figure 3.7 relative to the percentage of particles finer than 0.02 mm. The ordinate includes numerical values (heave in mm/day) for each frost susceptibility classification. Data summarized include the results of extensive laboratory frost heave tests and



| | | | | |
|---|----|----|----|----|
| Gravelly soils | F1 | F1 | F2 | F3 |
| Sands (except very fine silty sands) | | F2 | | F3 |
| Very fine silty sands | | | | F4 |
| All silts | | | ← | F4 |
| Clays (PI > 12) | | | ← | F3 |
| Clays (PI < 12), varved clays and other fine-grained banded sediments | | | ← | F4 |

NOTES: Standard tests performed by Cold Regions Research and Engineering Laboratory; specimens 6 in. dia. by 6 in. high, frozen at penetration rate of approximately 0.25 in. per day, with free water at 38°F continuously available at base of specimen. Specimens compacted to 95% or better of applicable standard, except undisturbed clays. Saturations before freezing generally 85% or greater.

*Indicated heave rate due to expansion in volume, if all original water in 100% saturated specimen were frozen, with rate of frost penetration 0.25 inch per day.

FIGURE 3.7 Range in the degree of frost susceptibility of soils according to the U.S. Army Corps of Engineers (1965).

field observations of reduced bearing capacity after thaw. All soil types in Figure 3.7 have been placed into four frost groups (F1 through F4) based on the percentage of particles finer than 0.02 mm. All silt soils are placed in group F4 with a frost susceptibility ranging from low to very high. Table 3.2 lists the different soils with their frost group classification.

Results of laboratory tests, summarized in Figure 3.7, show that there is a considerable range in the degree of frost susceptibility within frost groups. The standard tests performed by the Cold Regions Research and Engineering Laboratory (Chamberlain, 1981) involved soil specimens 152.4 mm (6 in.) in diameter by

TABLE 3.2 U.S. Army Corps of Engineers (1965) Frost Design Soil Classification System

| Frost Susceptibility* | Frost Group | Kind of Soil | Amount Finer than 0.02 mm (% by weight) | Typical Soil Type under Unified Soil Classification System† |
|-----------------------|-------------|---|---|---|
| NFS‡‡ | None | (a) Gravels | 0–1.5 | GW, GP |
| | | (b) Sands | 0–3 | SW, SP |
| Possibly§ | ? | (a) Gravels | 1.5–3 | GW, GP |
| | | (b) Sands | 3–10 | SW, SP |
| Very low to high | F1 | (a) Gravels | 3–10 | GW, GP, GW–GM, GP–GM |
| Medium to high | F2 | (a) Gravels | 10–20 | GM, GM–GC, GW–GM, GP–GM |
| | | (b) Sands | 10–15 | SW, SP, SM, SW–SM, SP–SM |
| Medium to high | F3 | (a) Gravels | >20 | GM, GC |
| Low to high | | (b) Sands, except very fine silty sands | >15 | SM, SC |
| Very low to very high | | (c) Clays, $PI > 12$ | — | CL, CH |
| Low to very high | F4 | (a) All silts | — | ML, MH |
| Very low to high | | (b) Very fine silty sands | >15 | SM |
| Low to very high | | (c) Clays, $PI < 12$ | — | CL, CL – ML |
| Very low to very high | | (d) Varved clays and other fine-grained, banded sediments | — | CL and ML; CL, ML, and SM; CL, CH, and ML; CL, CH, ML, and SM |

*Based on laboratory frost heave tests.

†G = gravel, S = sand, M = silt, C = clay, W = well graded, P = poorly graded, H = high plasticity, L = low plasticity.

‡‡Nonfrost-susceptible.

§Requires laboratory frost heave test to determine frost susceptibility.

152.4 mm (6 in.) high frozen at a penetration rate of about 6.35 mm (0.25 in.) per day with free water at 3.3°C (38°F) continuously available at the specimen base. Specimens were compacted to 95% or better of applicable standards, except undisturbed clay samples representative of field conditions. Saturation before freezing was generally 85% or greater. The variability shown in Figure 3.7 reflects possible differences in grain size distribution, density, and mineralogy. These differences are not included in the basic frost susceptibility classification system. The Corps of Engineers do not consider this variability necessarily a problem, because the properties of the soil in question may be compared with those of the most similar soil (Appendix B in Chamberlain, 1981) used in preparation of Figure 3.7. In this manner the relative frost susceptibility can be determined without conducting the frost heave test.

3.2 GRAIN SIZE AND SHAPE

Soil is a nonindurated aggregation of minerals and/or organic particles containing gases and/or liquids. Mineral soils result from the agencies of weathering, erosion, transportation and deposition. Organic soils, such as peat, form as an assemblage of vegetable and animal remains that have not been destroyed by decomposition. This sequence of events is generally referred to as the *geologic cycle*. Soils are engineering materials that are used to support foundations, backfill with, cut slope in, or even build with.

Soil particles in nature may range in size from a 12-in. boulder to a fine silt or clay particle that cannot be seen by the unaided eye. The different materials (gravel, sand, silt, clay) are generally associated with a given size range; however, the limits for different ranges will vary depending on the agency involved. Furthermore, the range of sizes of soil particles is quite large. Two common ways for determining particle size are (1) the sieve analysis, for particles larger than 0.075 mm, and (2) the hydrometer analysis, for particles smaller than 0.075 mm.

Mineral soils are classified primarily on the basis of particle size. Each particle will fall into a prescribed size range. Particle size is a parameter that can be measured in the laboratory using standard test methods. The dominant particle size controls many aspects of the engineering behavior of soil. A number of grain size designations have been adopted by various agencies, the most important of which are shown in Table 3.3. The unified and the USDA systems classify soil whose grain size is 75 to 100 mm as **cobbles**, while the AASHTO system classifies them as **boulders**. The variations between different systems are to a large extent minor when compared to the expected engineering behavior for a given soil. Further subdivisions for each of the soil types are also possible. That is, gravel, sand, silt, and clay may be subdivided into coarse, medium, or fine grained based on the relative proportions present within a size range in a given sample.

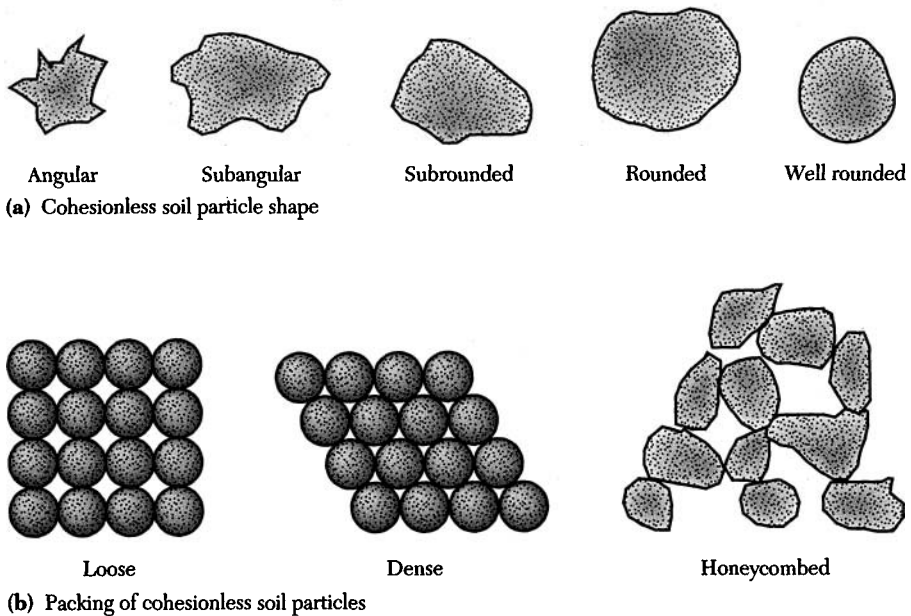
Unlike clay, which is cohesive, sand, gravel, and to a lesser extent silt are considered cohesionless soils; that is, they do not become plastic when mixed with water. This distinction is based on the assumption that the soil in question contains the dominant particle size present. The physical properties of cohesionless

TABLE 3.3 Grain Size Designation for Various Soils

| Classification System | Grain Size (mm) | | | |
|-----------------------|-----------------|------------|--|---------|
| | Gravel | Sand | Silt | Clay |
| Unified | 4.75–75 | 0.075–4.75 | Clay and silt are identified by their plasticity characteristics | |
| AASHTO | 2.00–75 | 0.050–2.00 | 0.002–0.050 | < 0.002 |
| MIT | 2.00–100 | 0.060–2.00 | 0.002–0.060 | < 0.002 |
| ASTM | 2.00–100 | 0.075–2.00 | 0.005–0.075 | < 0.005 |
| USDA | 2.00–75 | 0.050–2.00 | 0.002–0.050 | < 0.002 |

soils depend on a number of geological factors such as particle shape, packing, and particle size. These concepts are illustrated in Figure 3.8.

Cohesive soil particles are generally flat in shape (Figure 3.9). The internal arrangement of cohesive particles depends largely on the types of clay minerals present, the nature of the water in which the clays were sedimented, and the cohesive forces between the particles. Consequently, if the forces of repulsion dominate in a freshwater environment, then the clay particles align themselves to offer the maximum face-to-face area and thereby develop the maximum grain-to-grain distance. This results in a dense and watertight dispersed structure. A flocculated clay structure will result when the forces of attraction are stronger than those of repulsion. This situation occurs normally in saltwater where the particles collect

**FIGURE 3.8** Packing and shape of cohesionless soil particles.

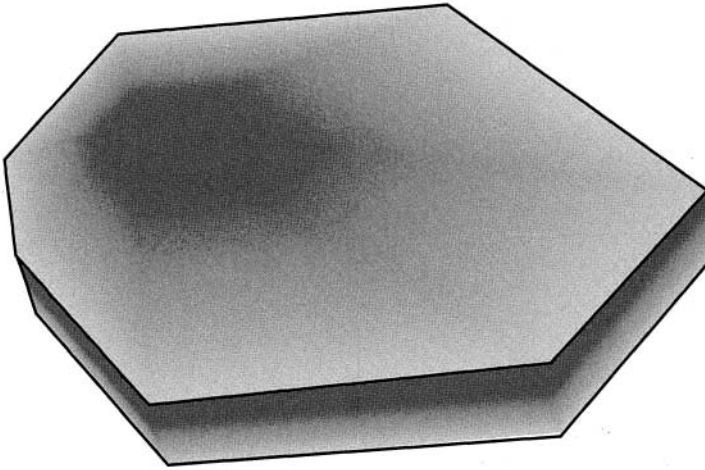


FIGURE 3.9 Idealized clay particle shape.

together randomly, trapping water within the large pore spaces between the particles. Flocculated soils are highly compressible and have lower densities. However, they normally possess high strength and have more resistance to vibration. Dispersed and flocculated clay structure were discussed in Section 1.1.3.

Very few clay deposits consist entirely of clay minerals. They are more likely to consist of an array of particle sizes including silt, sand, and/or gravel. A given soil deposit may exhibit cohesion if the clay particle size dominates.

3.3 SOIL AGGREGATE

In its natural state, soil is generally a three phase particulate system consisting of solids, liquids, and gas. The solids phase may include minerals and/or organic matter. The relative proportions of each phase in a given soil sample depend on, but are not limited to, geographic location, depth, stress, and geologic history. The discussion included in this section is directed to those soils in which the solids are of mineral origin, the liquid is water, and the gas is air. This is appropriate since most naturally occurring soils encountered in geotechnical engineering contain little if any organic matter.

The solution of geotechnical engineering problems requires knowledge of basic soil parameters pertaining to the three phase soil constituents. The phase diagram offers a convenient tool in the derivation of important phase relationships as shown in Figure 3.10, where V is total volume, V_a is volume of air, V_w is volume of water, and V_s is volume of solids, W is total weight, W_a is weight of air, W_w is weight of water, W_s is weight of solids. For a given soil sample, the weights, volume of solids, water, and air cannot be directly measured in a practical manner as indicated in Figure 3.10a. Instead, the volumes and weights of each of the con-

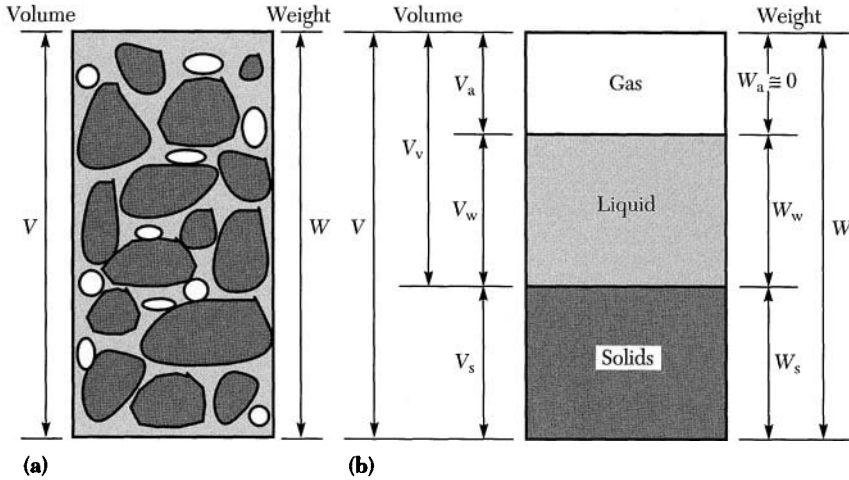


FIGURE 3.10 Schematic representation of soil: (a) natural soil; (b) phase diagram.

stituents can be more appropriately designated using the phase diagram as indicated by Figure 3.10b. The remaining task is to formulate a practical procedure through which the various weights and volumes and their interrelationships can be determined.

Consideration of Figure 3.10 clearly shows that the phase diagram involves six unknown parameters. Consequently, a total of six equations are needed for its solution. For all practical purposes the weight of air in a given soil sample is negligible when compared to that of water or solids. Therefore, it can be assumed to equal zero. Hence, the number of unknowns is reduced to five: V_a , V_w , V_s , W_w , and W_s . These can be interrelated by introducing new dimensional and dimensionless parameters.

Dimensional Parameters

These are useful quantities that occur frequently in the course of solving geotechnical engineering problems. The following definitions are meant to establish a link between the various weights and volumes appearing in the phase diagram:

Water unit weight, γ_w

$$\gamma_w = W_w/V_w \tag{3.4}$$

Solids unit weight, γ_s

$$\gamma_s = W_s/V_s \tag{3.5}$$

Soil bulk unit weight, γ_m

$$\gamma_m = W/V \tag{3.6}$$

Soil saturated unit weight, γ_{sat}

$$\gamma_{\text{sat}} = W/V \quad \text{with } V_a = 0 \quad (3.7)$$

Soil dry unit weight, γ_d

$$\gamma_d = W_s/V \quad (3.8)$$

Soil buoyant unit weight, γ_b

$$\gamma_b = \gamma_{\text{sat}} - \gamma_w \quad (3.9)$$

Soil effective unit weight, γ'

$$\gamma' = \gamma_m \quad \text{if } V_a > 0 \quad (3.10a)$$

$$\gamma' = \gamma_b \quad \text{if } V_a = 0 \quad (3.10b)$$

Density, ρ

$$\rho = \gamma/g \quad (3.11)$$

where γ is the unit weight and g is the gravitational acceleration ($g = 9.81 \text{ m/s}^2 = 32.2 \text{ ft/s}^2$). Note that the dimensional parameters provide the only link between weights and volumes of air, water, and solids. The density relates mass rather than weight to volume. Hence, dry density is the ratio of the mass of solids to the total soil volume, water density is the ratio of mass of water to its volume, and so on. Keep in mind that weight is equal to the product of mass and gravitational acceleration.

Dimensionless Parameters

Unlike dimensional parameters, dimensionless parameters are independent of the system of units used. Therefore, it is possible to use masses instead of weights as long as consistent units are used for all parameters appearing in a given expression. For example, the water content was defined earlier [Eq. (3.1)] as the ratio of the mass of water to the mass of solids. It is equally valid to define water content as the ratio of the weight of water to the weight of solids as indicated by Eq. (3.15).

Void ratio, e

$$e = V_v/V_s \quad (3.12)$$

Porosity, n

$$n = (V_v/V)100\% \quad (3.13)$$

Degree of saturation, S_r

$$S_r = (V_w/V_v)100\% \quad (3.14)$$

Water content, w

$$w = (W_w/W_s)100\% \quad (3.15)$$

Solids specific gravity, G_s

$$G_s = \gamma_s / \gamma_w \quad (3.16)$$

It is evident that once V_a , V_w , V_s , W_w , and W_s are determined, then the various dimensional and dimensionless parameters given by Eqs. (3.4) through (3.16) can be readily evaluated. Generally, solving the phase diagram problem involves the determination of one or more of the dimensional and/or dimensionless parameters using standard laboratory tests, after which the remaining unknowns are calculated. The implication is that for a given problem different solution procedures may be possible. Therefore, good judgment, experience, cost, and common sense are important factors that should be considered when solving soil phase problems. For example, if for a given phase problem, one has a choice between evaluating the water content and the specific gravity, then the obvious choice would have to be to evaluate the water content. This is much simpler and less costly.

In practice, a soil sample is retrieved from the field using standard sampling methods. The total volume and total weight of the sample can then be evaluated in the laboratory. This gives rise to the following two equations:

$$V_a + V_w + V_s = V \quad (3.17a)$$

$$W_w + W_s = W \quad (3.17b)$$

In addition, water content (w) and specific gravity (G_s) can be readily determined using standard testing methods. Therefore, by introducing the basic definitions given earlier for G_s and w , two additional equations can be formulated, thus,

$$w = W_w / W_s \quad (3.17c)$$

$$G_s = \gamma_s / \gamma_w = W_s / (V_s \gamma_w) = (W_s / V_s) / (W_w / V_w) \quad (3.17d)$$

The fifth equation needed for solving the phase diagram problem is given by the unit weight of water. For all practical purposes, its value can be assumed to be 9.81 kN/m^3 (62.4 lb/ft^3). Hence,

$$\gamma_w = W_w / V_w \quad (3.17e)$$

The relationships given by Eq. (3.17) represent a system of algebraic equations in the five unknowns V_a , V_w , V_s , W_w , and W_s . Solving for the unknowns gives

$$W_s = W / (1 + w) \quad (3.18a)$$

$$W_w = w W_s = w W / (1 + w) \quad (3.18b)$$

$$V_s = W_s / (G_s \gamma_w) = W / [(1 + w) G_s \gamma_w] \quad (3.18c)$$

$$V_w = W_w / \gamma_w = w W / [\gamma_w (1 + w)] \quad (3.18d)$$

$$V_a = V - V_w - V_s = V - W(w G_s + 1) / [\gamma_w G_s (1 + w)] \quad (3.18e)$$

These equations are useful in the derivation of important phase interrelationships. They can be directly applied in solving practical phase problems when V , W , G_s , w , and γ_w are known. Otherwise, alternative forms of the solution procedure must be developed. Note that for dry soil and saturated soils only four unknowns exist.

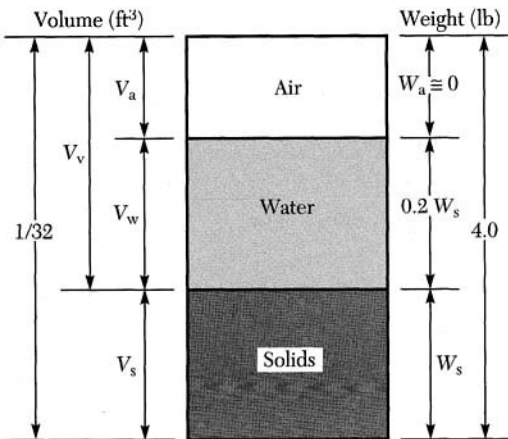
The implication is that fewer soil laboratory tests will be required, as is demonstrated in the following examples.

EXAMPLE 3.1

A soil sample has a bulk unit weight of 19.62 kN/m^3 and a dry unit weight of 17.66 kN/m^3 . If the specific gravity of its solids is 2.70 , compute the soil sample void ratio, porosity, degree of saturation, saturated and buoyant unit weight, and dry density.

Solution

Before proceeding with the solution, it is important to point out that the basic definitions for the dimensional and dimensionless parameters given earlier must be carefully studied. Furthermore, it is good practice to draw the phase diagram and to place the known values in the diagram. For this problem, we have



The weight of water is determined from the total weight and the dry weight. That is

$$w_w = 19.62 - 17.66 = 1.96 \text{ kN}$$

Therefore, the volumes of water and solids are calculated as follows:

$$V_w = W_w / \gamma_w = 1.96 / 9.81 = 0.19979 \text{ m}^3$$

$$V_s = W_s / (\gamma_w G_s) = 17.66 / [(9.81)(2.70)] = 0.66674 \text{ m}^3$$

Finally, the volume of air is computed from the total volume and the volume of solids and water. Hence,

$$V_a = 1 - V_s - V_w = 1 - 0.19979 - 0.66674 = 0.13347 \text{ m}^3$$

The phase diagram is now solved. Therefore, the various parameters needed to complete the solution of the problem can be readily determined:

$$V_v = V_a + V_w = 0.13347 + 0.19979 = 0.33326 \text{ m}^3$$

$$e = V_v / V_s = 0.33326 / 0.66674 = 0.49983$$

$$n = V_v/V_t = (0.33326/1.0)100\% = 33.33\%$$

$$S_r = V_w/V_v = (0.19979/0.33326)100\% = 59.95\%$$

$$\gamma_{sat} = (W_w + W_s + \gamma_w V_a)/V_t$$

$$\gamma_{sat} = [19.62 + 9.81(0.13347)]/1.0 = 20.93 \text{ kN/m}^3$$

$$\gamma_b = \gamma_{sat} - \gamma_w = 20.93 - 9.81 = 11.12 \text{ kN/m}^3$$

$$\rho_d = \gamma_d/g = (17.66)(1000)/9.81 = 1800 \text{ kg/m}^3$$

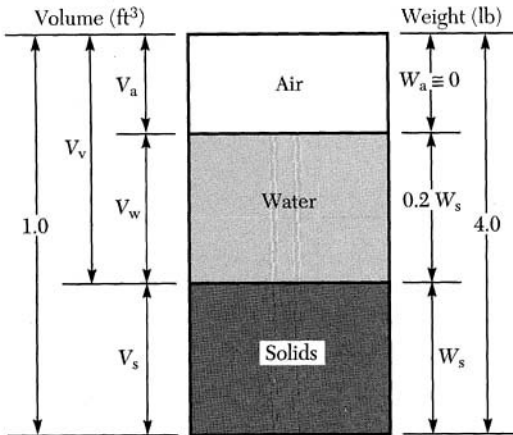
Note that 1.0 kN = 1000 N. The solution of this problem can also be achieved using Eq. (3.18) directly. ■

EXAMPLE 3.2

A soil sample is compacted in a mold whose volume is $\frac{1}{30} \text{ ft}^3$. The wet weight of the soil sample is 4 lb. If the water content is 20% and the specific gravity of the solids is 2.65, calculate n , e , S_r , and γ_{sat} .

Solution

The corresponding phase diagram can be easily drawn and the solution obtained in the same manner as is outlined in Example 3.1. However, let us apply Eqs. (3.18) instead. The corresponding phase diagram is



It is clear that it is appropriate to deal first with the weights, then with the volumes.

$$W_s = W/(1 + w) = 4/1.2 = 3.333 \text{ lb}$$

$$W_w = wW_s = 0.20(3.33) = 0.667 \text{ lb}$$

$$V_s = W_s/(G_s \gamma_w) = 3.333/[(2.65)(62.4)] = 0.02016 \text{ ft}^3$$

$$V_w = W_w/\gamma_w = 0.667/62.4 = 0.01069 \text{ ft}^3$$

$$V_a = V - V_s - V_w = 1/30 - 0.02016 - 0.01069 = 0.00248 \text{ ft}^3$$

$$V_v = V_w + V_a = 0.01317 \text{ ft}^3$$

The solution for n , e , S_r , and γ_{sat} is obtained by directly applying the definitions given earlier.

$$n = (V_v/V)(100) = [0.01317/(1/30)](100\%) = 39.52\%$$

$$e = V_v/V_s = 0.01317/0.02016 = 0.6533$$

$$S_r = (V_w/V_v)(100) = (0.01069/0.01317)(100\%) = 81.17\%$$

$$\gamma_{\text{sat}} = W/V \quad \text{with} \quad V_a = 0$$

$$\gamma_{\text{sat}} = (W_s + V_v\gamma_w)/V$$

$$\gamma_{\text{sat}} = [3.333 + 0.01317(62.4)]/(1/30) = 124.64 \text{ lb/ft}^3$$

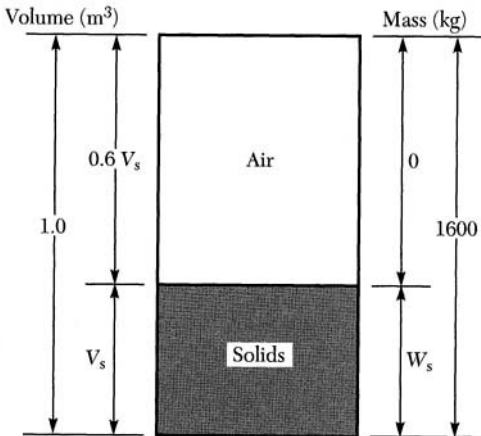
Note that $V_v\gamma_w$ is the weight of water required to fill the voids, thus guaranteeing that V_a is equal to zero. ■

EXAMPLE 3.3

The dry density of a natural clay sample is 1700 kg/m^3 . Given $e = 0.60$, determine the specific gravity of soil solids and the saturated unit weight of the sample.

Solution

Consideration of the following phase diagram shows that in this case it would be best to solve first for the volumes, then for the weights. The dry unit weight is evaluated as follows:



$$\gamma_d = \rho_d g = 1650(9.81) = 16,677 \text{ N/m}^3 = 16.677 \text{ kN/m}^3$$

It is evident that the volume of voids is equal to the volume of air. Thus,

$$V = V_v + V_s = V_a + V_s = 1.0$$

The void ratio is given. Hence, solving for the volume of air in terms of the volume of solids gives

$$e = V_v/V_s = V_a/V_s = 0.60$$

$$V_a = 0.6 V_s$$

The volume of solids is now determined:

$$\begin{aligned}0.6 V_s + V_s &= 1.0 \\ V_s &= 1.0/1.6 = 0.625 \text{ m}^3 \\ V_a &= 1.0 - 0.625 = 0.375 \text{ m}^3\end{aligned}$$

The specific gravity of solids is given by Equation (3.17d). Thus,

$$G_s = \gamma_s / \gamma_w = W_s / (V_s \gamma_w) = 16.677 / (0.625) / (9.81) = 2.72$$

The saturated unit weight is determined by filling the air voids with water. That is,

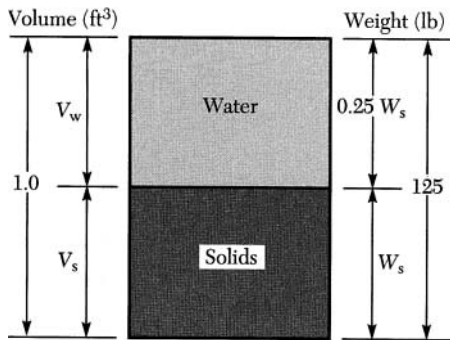
$$\gamma_{\text{sat}} = (V_a \gamma_w + W_s) / V = [(0.375)(9.81) + 16.677] / 1.0 = 20.36 \text{ kN/m}^3 \quad \blacksquare$$

EXAMPLE 3.4

The saturated unit weight of a natural clay sample is 125 lb/ft^3 . Given $w = 25\%$, determine the specific gravity of soil solids and the void ratio of the sample.

Solution

The corresponding phase diagram for the saturated soil sample is given here:



Note that in this case only water and solids are present in the soil sample. This should simplify the solution. It is evident that the weight is equal to the sum of the weight of water and the weight of solids. Thus,

$$W = W_w + W_s = 125$$

The water content is given. Solving for the weight of water in terms of the weight of solids gives

$$\begin{aligned}w &= W_w / W_s = 0.25 \\ W_w &= 0.25 W_s\end{aligned}$$

The weight of solids is now determined:

$$0.25 W_s + W_s = 125$$

$$W_s = 125/1.25 = 100 \text{ lb}$$

$$W_w = 125 - 100 = 25 \text{ lb}$$

The volume of water is readily calculated using a unit of water of 62.4 lb/ft^3 . Thus,

$$V_w = W_w/\gamma_w = 25/62.4 = 0.40 \text{ ft}^3$$

$$V_s = 1.0 - 0.40 = 0.60 \text{ ft}^3$$

The specific gravity of solids is given by Eq. (3.17d). Thus,

$$G_s = \gamma_s/\gamma_w = W_s/(V_s \gamma_w) = 100/(0.60)/(62.4) = 2.67$$

The void ratio is then determined:

$$e = V_w/V_s = 0.4/0.6 = 0.667 \quad \blacksquare$$

EXAMPLE 3.5

Derive an expression for the saturated unit weight in terms of G_s , w , and γ_w .

Solution

Recall that by definition, the saturated unit weight is the ratio of total weight to total volume when the volume of air is equal to zero. Using Eq. (3.18e), write

$$V_a = 0 = V - W(wG_s + 1)/[\gamma_w G_s(1 + w)]$$

Solving for the unit weight as the ratio W/V gives

$$W/V = \gamma_{\text{sat}} = \gamma_w G_s(1 + w)/(wG_s + 1)$$

or more simply

$$\gamma_{\text{sat}} = \gamma_w(1 + w)/(w + 1/G_s)$$

Note that w is the water content when the sample is saturated. \blacksquare

EXAMPLE 3.6

Derive an expression for the void ratio e in terms of w , G_s , and γ_m .

Solution

Recall that by definition $e = V_v/V_s$. Rewriting gives

$$e = V_v/V_s = (V - V_s)/V_s = V/V_s - 1$$

Then, substituting Eq. (3.18c) into the expression, we get

$$e = [VG_s\gamma_w(1 + w)/W] - 1$$

$$e = (G_s\gamma_w/\gamma_m)(1 + w) - 1$$

Note that one may choose to express a given equation in different forms depending on the type of problem being solved. For example, the preceding expression

can also be used to determine the bulk density γ_m in terms of e , G_s , and w :

$$\gamma_m = G_s \gamma_w (1 + w) / (1 + e) \quad \blacksquare$$

EXAMPLE 3.7

Derive a relationship between e and n .

Solution

From the basic definition for void ratio, we have

$$e = V_v / V_s = V_v / (V - V_v)$$

Dividing the numerator and denominator by V_v and noting that $n = V_v / V_t$ gives

$$\begin{aligned} e &= 1 / [(1/n) - 1] \\ e &= n / (1 - n) \quad \blacksquare \end{aligned}$$

EXAMPLE 3.8

Derive an expression relating the degree of saturation S_r to e , G_s , and w .

Solution

Recall that by definition

$$S_r = V_w / V_v$$

and

$$G_s = \gamma_s / \gamma_w = W_s V_w / V_s W_w$$

Solving for V_w and then substituting into the degree of saturation expression gives

$$\begin{aligned} V_w &= G_s V_s W_w / W_s = w V_s G_s \\ S_r &= w V_s G_s / V_v \\ S_r &= w G_s / e \end{aligned}$$

Additional relationships between dimensional and dimensionless parameters pertaining to the phase diagram problem can be developed. A summary of some of the more useful ones is given in Table 3.4. The reader should be aware that these interrelationships are meant to aid in the solution of the phase diagram problem. They do not represent a substitute for basic understanding of the various definitions presented. \blacksquare

3.4 CONSISTENCY AND SENSITIVITY OF CLAYS

The presence of water in fine-grained cohesive soils may significantly affect their engineering behavior. The degree of influence depends on the amount of water and the type of soil in question. For a given water content, different clay types exhibit varying behaviors depending on their composition, grain size, and specific surface area. Under static loads cohesionless soils are basically unaffected by the

TABLE 3.4 Dimensional and Dimensionless Parameter Interrelationships

| Water Content, w | | |
|---|---|---|
| $S_r e / G_s$ | $S_r (\gamma_w / \gamma_d - 1 / G_s)$ | $\gamma_m / \gamma_d - 1$ |
| $\gamma_m (1 + e) / \gamma_w G_s - 1$ | $(\gamma_w - \gamma_{sat} / G_s) / (\gamma_{sat} - \gamma_w)$ | $(\gamma_w - \gamma_{sat} / G_s) / \gamma_b$ |
| $(1 - 1 / G_s) \gamma_w / \gamma_b - 1 / G_s$ | $(\gamma_w - \gamma_m / G_s) / (\gamma_m / S_r - \gamma_w)$ | $[\gamma_m / \gamma_w G_s (1 - n)] - 1$ |
| Void Ratio, e | | |
| $w G_s / S_r$ | $G_s \gamma_w / \gamma_d - 1$ | $n / (1 - n)$ |
| $(G_s - 1) \gamma_w / \gamma_b - 1$ | $\gamma_w / (\gamma_d - \gamma_b) - 1$ | $\gamma_{sat} - \gamma_d / (\gamma_d - \gamma_b)$ |
| $(G_s \gamma_w - \gamma_{sat}) / \gamma_{sat} - \gamma_w$ | $(\gamma_w G_s - \gamma_m) / (\gamma_m - S_r \gamma_w)$ | |
| Porosity, n | | |
| $e / (1 + e)$ | $1 - \gamma_d / G_s \gamma_w$ | $(\gamma_{sat} - \gamma_d) / \gamma_w$ |
| $1 / (1 + S_r / w G_s)$ | $1 - \gamma_m / [\gamma_w G_s (1 + w)]$ | $1 + (\gamma_b - \gamma_d) / \gamma_w$ |
| Degree of Saturation, S_r | | |
| $w G_s / e$ | $\gamma_m (1 / e + 1) / \gamma_w - G_s / e$ | $\gamma_m / n \gamma_w - G_s (1 / n - 1)$ |
| $w / (\gamma_w / \gamma_d - 1 / G_s)$ | $w / [\gamma_w (1 + w) / \gamma_m - 1 / G_s]$ | |
| Specific Gravity, G_s | | |
| $e S_r / w$ | $\gamma_d (1 + e) / \gamma_w$ | $\gamma_d S_r / (S_r \gamma_w - w \gamma_d)$ |
| $\gamma_{sat} (1 + e) / \gamma_w - e$ | $\gamma_m (1 + e) / [\gamma_w (1 + w)]$ | $(\gamma_b + \gamma_w) / (\gamma_w - w \gamma_b)$ |
| $n S_r / [w (1 - n)]$ | | |
| Bulk Unit Weight, γ_m | | |
| $\gamma_d (1 + w)$ | $\gamma_d (1 + e S_r / G_s)$ | $(G_s + e S_r) \gamma_w / (1 + e)$ |
| $\gamma_w (1 + w) / (w / S_r + 1 / G_s)$ | $(1 + w) \gamma_w G_s / (1 + e)$ | $(\gamma_{sat} - n \gamma_w) (1 + w)$ |
| Dry Unit Weight, γ_d | | |
| $\gamma_m / (1 + w)$ | $G_s \gamma_w / (1 + e)$ | $G_s \gamma_w / (1 + w G_s / S_r)$ |
| $\gamma_b + \gamma_w / (1 + e)$ | $\gamma_{sat} / (1 + w)$ | $G_s \gamma_w (1 - n)$ |
| Saturated Unit Weight, γ_{sat} | | |
| $\gamma_d + n \gamma_w$ | $\gamma_d + e \gamma_w / (1 + e)$ | $(G_s + e) \gamma_w / (1 + e)$ |
| $(1 + w) \gamma_w / (w + 1 / G_s)$ | $\gamma_m / (1 + w) + n \gamma_w$ | $\gamma_d (1 + w)$ |
| $e (1 + w) \gamma_w / [w (1 + e)]$ | | |

presence of water. The implication is that engineering properties of such soils are to a large extent independent of the water content. For example, the shear strength of a given saturated cohesionless soil is approximately equal to its shear strength when dry. An important exception is the case where water is present in a loose sandy deposit located in an earthquake zone. In this case, the soil deposit may liquefy during an earthquake, resulting in considerable settlement and damage to buildings and other facilities placed on it.

Although the water content of a given soil can be readily measured in the laboratory, this is not sufficient to adequately describe cohesive soils behavior. One needs to compare the water content relative to an established engineering standard. This is precisely what Atterberg proposed in 1911. This Swedish scien-

tist proposed six limits against which the water content of a fine-grained soil can be compared. The Atterberg limits are water contents taken at critical stages in soil behavior. These limits of consistency are

1. Upper limit of viscous flow
2. Liquid limit
3. Sticky limit
4. Cohesion limit
5. Plastic limit
6. Shrinkage limit

In current geotechnical engineering practice the term *Atterberg limits* refers only to the liquid limit *LL*, the plastic limit *PL*, and the shrinkage limit *SL*. These consistency limits permit an evaluation of the degree to which a given soil can be deformed. The **liquid limit** represents the lower limit of viscous flow, whereas the **plastic limit** represents a lower limit of the plastic state and the **shrinkage limit** represents a lower limit of volume change. Atterberg also defined a very important parameter called the **plasticity index** *PI*, which is the difference between the liquid and plastic limits. That is

$$PI = LL - PL \tag{3.19}$$

The **liquidity index** *LI* was introduced later to scale the natural water content w_n of a given soil relative to the Atterberg limits. This is defined as follows:

$$LI = \frac{w_n - PL}{PI} \tag{3.20}$$

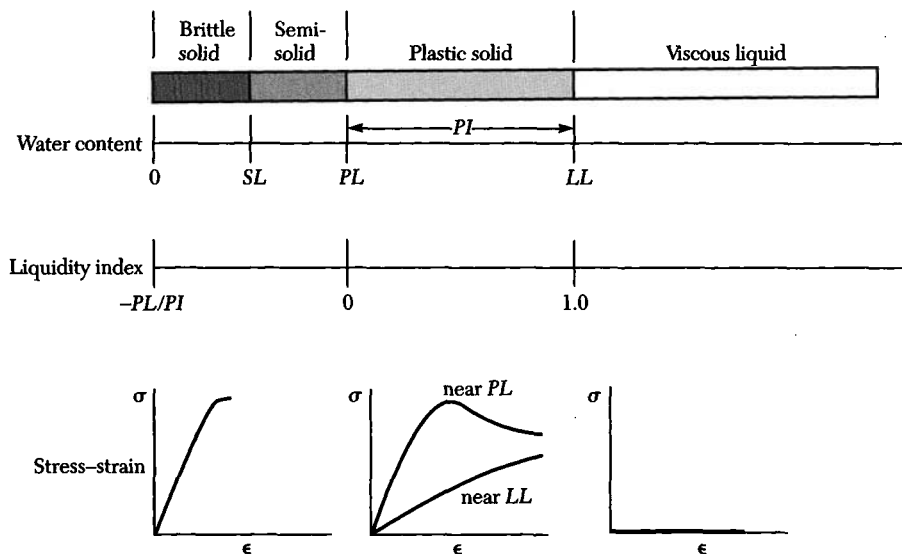


FIGURE 3.11 Schematic representation of the Atterberg limits and the liquidity index.

3.4 CONSISTENCY AND SENSITIVITY OF CLAYS 89

The liquidity index provides insight into expected soil behavior. For a given soil sample it is possible to determine whether the soil behavior will be liquid, plastic, or brittle. If the LI is negative, the soil will behave as brittle material. On the other hand, if the LI is between zero and one, then the soil will behave as plastic material. Values of LI greater than one indicate that the soil will behave as a viscous liquid. These limits along with the Atterberg limits are shown schematically in Figure 3.11.

It is evident that the Atterberg limits could serve a useful purpose in the identification and classification of cohesive soils. This is precisely what Karl Terzaghi and A. Casagrande did. While working for the U.S. Bureau of Public Roads, they proposed new standardized testing methods for evaluating the LL , PL , and SL . The liquid limit device developed by Casagrande is less operator dependent than the one used in the plastic limit test. The plastic limit test is somewhat more arbitrary and requires experience to get reproducible results.

The Atterberg limits and the plasticity and liquidity indices play an important role in the classification of soils. Such classification may include coarse-grained soils with fines and fine-grained soils. These limits have been correlated empirically to a number of physical properties of soils. Such correlations were developed over a period of time and thus provide insight into the expected behavior of a given soil. The plasticity index versus the liquid limit for a variety of clays is shown in Figure 3.12.

Clays may also be identified using the activity index. The activity of a given soil was defined by Skempton as

$$A = PI/PC \quad (3.21)$$

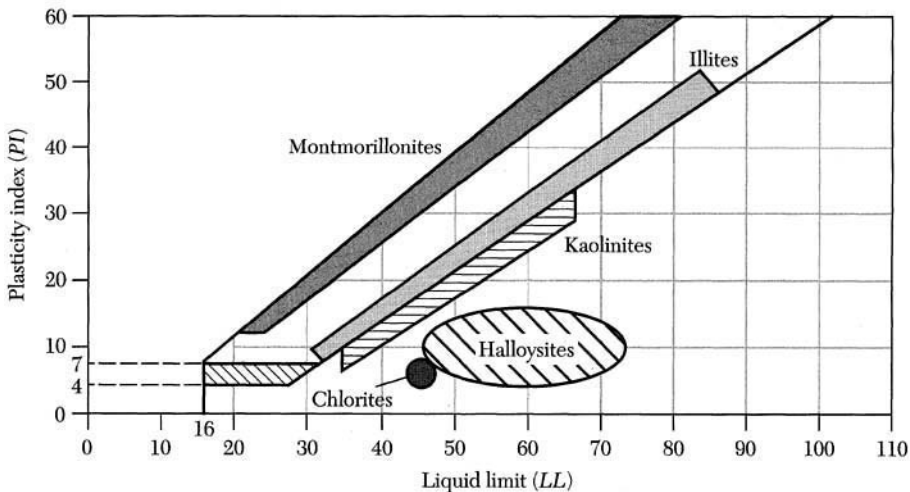


FIGURE 3.12 Plasticity index versus liquid limit for common clay minerals. (Adapted from Casagrande, 1948 and data in Mitchell, 1976.)

4

Soil Compaction

4.0 INTRODUCTION

The soils at a given site are often less than ideal from the viewpoint of soil engineering. The site may require soil improvement for several reasons: reduced compressibility (for structural foundations), increased strength (for pavement structures), and reduced permeability (for earth dam foundations). In the past, potential soil problems were avoided by relocating the structure or facility. Considerations other than geotechnical ones often govern the location, so the design must account for existing soil conditions. Soil improvement (or soil stabilization) involves the alteration of a soil property to improve its engineering performance. The more common techniques available for soil improvement are (1) **compaction** (densification with mechanical equipment), (2) **preloading** (densification by placement of a temporary surface load), and (3) **dewatering** (the removal of pore water and/or pore pressures). This chapter will be limited to soil improvement by densification with mechanical equipment — including laboratory methods, field compaction control, and specifications.

4.1 COMPACTION THEORY

The theory pertaining to soil compaction is relatively new. While working for the Bureau of Waterworks and Supply in Los Angeles, R. R. Proctor proposed the basic principles of compaction. He established that compaction of soils involves four

major factors: (a) dry unit weight γ_d , (b) water content w , (c) compactive effort, and (d) soil type and gradation. The ability of any rational design method to predict the compression and strength behavior of soil deposits is often limited by the quality of the bearing soil. Additionally, the density of fills placed around and beneath foundations must be controlled to assure the fill's quality and performance. Therefore, it is essential that laboratory and field monitoring be planned whenever soil density is in question.

It has been recognized that the soil compaction process affects a variety of soil properties that can be broadly categorized into two interrelated groups: (a) physical properties and (b) engineering properties. The physical properties, such as moisture and density, can be used to analyze the effectiveness of the compaction process used in the field. The engineering properties include compression, permeability and flow, and strength. It has been demonstrated that soils compacted to a given density and at a given moisture content exhibit different engineering properties depending on their dry density.

In the field, compactive effort relates to the number of passes of a roller of a certain weight on a given volume of soil. This is not easy to determine, because the volume of soil is unknown. In the laboratory, impact or kneading compaction is normally used to obtain certain densities. Impact compaction is accomplished by dropping a hammer several times on a soil sample in a mold of known volume. The soil is placed in several layers and each layer is impacted with a hammer of known weight falling a prescribed distance. The corresponding compactive effort

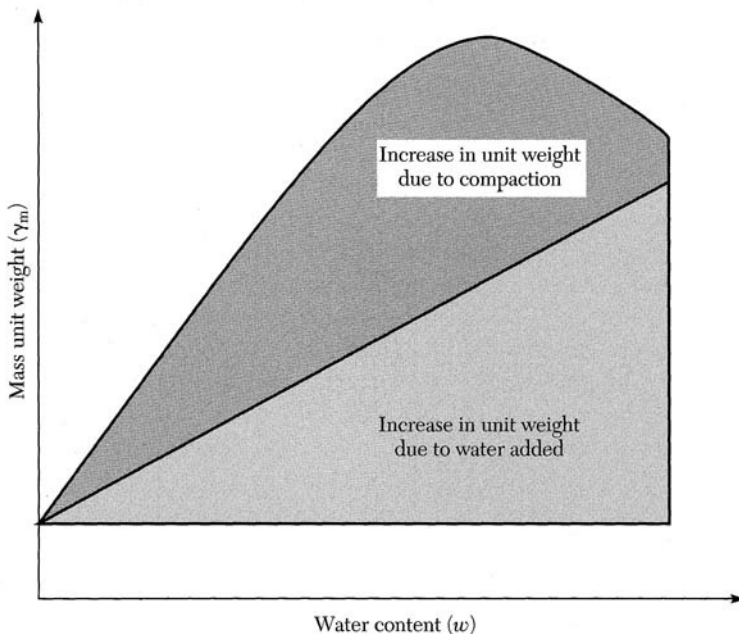


FIGURE 4.1 Graphical illustration of the wet unit weight versus the water content of compacted soil sample.

CE is then calculated as

$$CE = \frac{W_h H_d N_L N_d}{V} \quad (4.1)$$

where W_h is the weight of hammer, H_d is the height of hammer fall, N_L is the number of soil layers, N_d is the number of hammer drops per layer, and V is the volume of the mold.

The process used in compacting cohesive soils can be best illustrated by considering a typical laboratory test. The soil sample is compacted using a standard testing procedure at different water contents. The purpose of adding water is to permit the soil particles to slip relative to one another. Hence, water acts as a lubricant. The wet unit weight of the soil is then measured along with the water content.

$$\gamma_m = \frac{Mg}{V} \quad (4.2)$$

where γ_m is the bulk density, M is the total wet soil mass, V is the total soil volume, and g is the gravitational acceleration. The relationship between wet density and water content can be plotted as shown in Figure 4.1. It is evident from the figure that the wet unit weight is not a proper measure of the compactive effort applied in that it also reflects the weight of the water added. For this reason, the dry unit weight corresponding to given water content is used to assess the degree of compaction attained for a given soil. The dry unit weight can be calculated using phase relationships as follows:

$$\gamma_d = \frac{\gamma_m}{1 + w} \quad (4.3)$$

where w is the water content, and γ_d is the corresponding dry unit weight.

The test results may then be plotted as the dry unit weight versus water content with each test representing a single point on the graph. It is customary to run three to five tests (three to five points). It is recommended that at least four data points be used. The data points are then connected with a smooth curve. For a given compaction procedure, this curve is unique for a given soil type and compactive effort. The peak of the curve corresponds to the optimum dry unit weight and the optimum water content for the compactive effort used in the test. Typically, the optimum water content is a few percent less than the soil's plastic limit. In fact, the optimum water content corresponds to approximately 80% saturation. Hence, it would seem appropriate to plot the dry unit weight versus water content for a given specific gravity of solids G_s and degree of saturation S_r , using the following equation.

$$\gamma_d = \frac{\gamma_w G_s}{1 + w G_s / S_r} \quad (4.4)$$

Note that Eq. (4.4) can be used to plot the curve corresponding to 100% saturation by simply setting $S_r = 1$. This is called the **zero air voids curve** and can be thought of as an envelope for all compaction curves regardless of the compactive

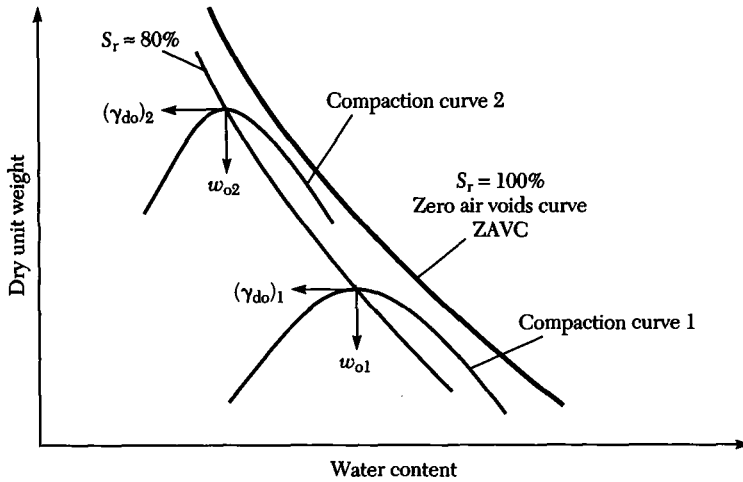


FIGURE 4.2 Schematic representation of compaction and the corresponding zero air voids curves for a typical soil.

effort, soil type, and water content. For a given specific gravity, it represents the absolute maximum dry unit weight that can be achieved for a given water content. These concepts can be best illustrated by considering Figure 4.2. In this case two compactive efforts were used to compact a soil sample at different water contents. The compactive effort for compaction curve 2 is higher than that of curve 1. Note that as the compactive effort increases, the corresponding optimum dry unit weight γ_{do} will increase and the optimum water content w_o will decrease. The implication is that less water is needed to achieve a denser soil.

Although the compaction curve corresponding to the standard test method contains a single peak, some soils may have more complicated curves. Research by Lee and Suedkomp (1972) has shown that four types of compaction curves are possible: (a) one with a single peak, (b) one with an irregular peak, (c) one with a double peak, and (d) one that is almost a straight line with no distinct optimum dry unit weight. These types of compaction curves are illustrated in Figure 4.3. The research program involved a total of 700 tests on 35 different types of natural soils exhibiting different engineering properties. The results indicate that a single peak (Type A) is likely when the liquid limit of the soil being tested is between 30 and 70. Irregularly shaped curves are likely when the liquid limit is less than 30 or more than 70. These curves are to be expected whenever montmorillonite is present. It should be noted that sandy soils and slag will also result in irregularly shaped curves because their liquid limits are less than 30.

4.2 PROPERTIES OF COMPACTED SOILS

The combined effects of compactive effort, type of compaction, and moisture content on a given soil is of utmost importance in controlling soil behavior. For a

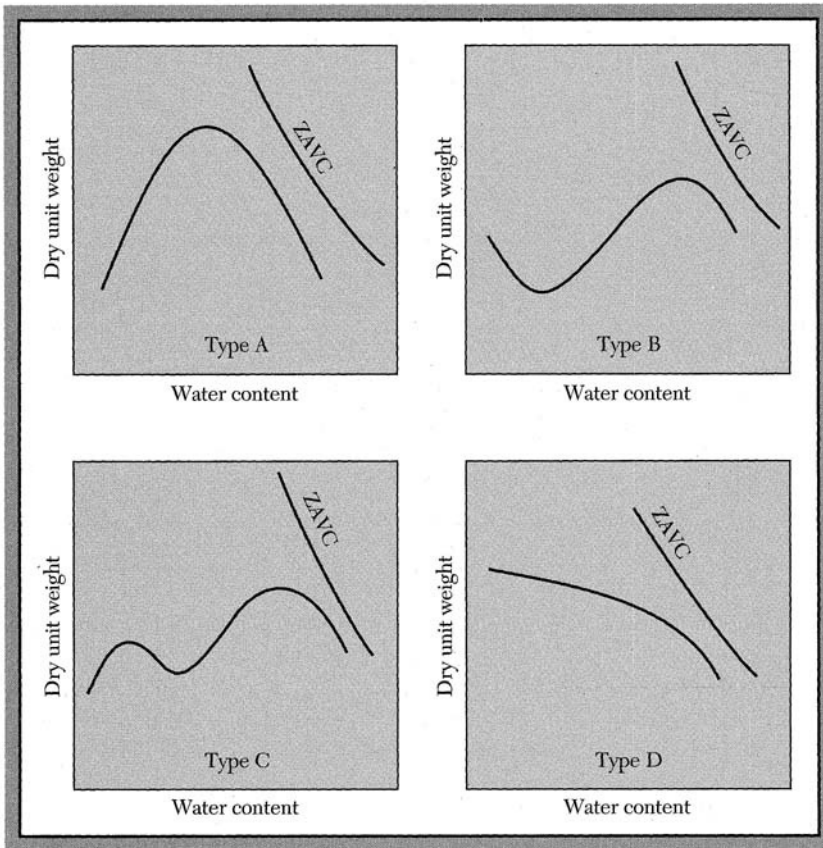


FIGURE 4.3 Schematic representation of four possible types of compaction curves. (After Lee and Suedkamp, 1972.)

given compaction method, the water content may be used to indicate whether the soil is *dry of optimum*, *at optimum*, or *wet of optimum*. Laboratory and field investigations of different soils have shown that soil properties and therefore performance are dependent on the water content at compaction. While the properties of soils dry of optimum are essentially unaffected by the compaction method, those soils wet of optimum are dependent on the method of compaction used. Compaction methods include kneading, vibratory, or static. Studies by Seed and Chan (1959) have shown that soil properties are adversely affected when compacted wet of optimum. It is for this reason that field compaction is normally accomplished for soils when they are dry of optimum. The assessment of compaction and its effects on the engineering properties of soils is very complex and is beyond the scope of this textbook. However, a generalized overview of compaction as it relates to some of the more important soil characteristics is included.

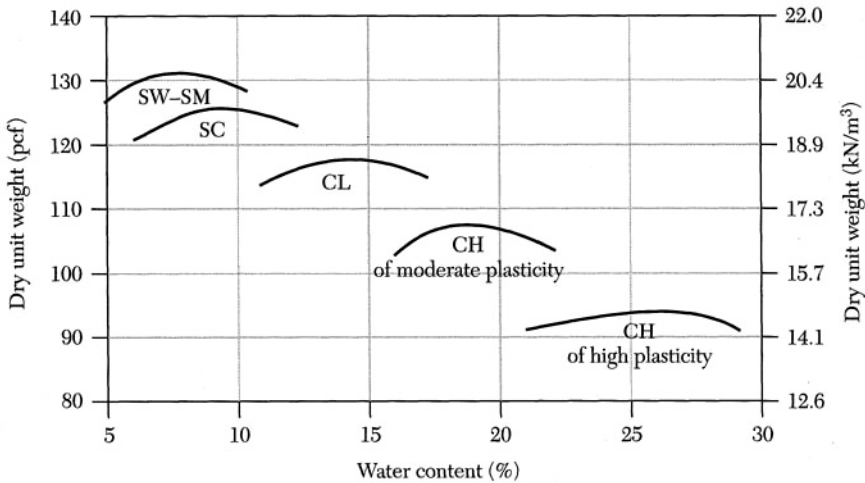


FIGURE 4.4 Proctor compaction curves for typical soils. (United States Department of the Interior, Bureau of Reclamation: *A Water Resources Technical Publication, Report No. 17.*)

The **unit weight** of soil (weight per unit volume) is an important property used as an index to denote soil adequacy in earthwork construction. Using the standard proctor test, the optimum dry unit weights versus water content for several soils are shown along with their soil classifications in Figure 4.4. Clearly, this figure should only serve as a guide; individual soils must be tested to determine their optimum unit weights and corresponding optimum water contents. This is true for all of the engineering properties discussed in this section.

For a given compactive effort, soil permeability (Chapter 5) decreases with increasing water content until the water content approaches full saturation. This occurs when the water content is slightly higher than optimum, after which it remains constant. Recall that the optimum water content for most soils corresponds to about 80% saturation. The coefficient of permeability will also decrease as the compactive effort is increased. This is because smaller voids will result. The coefficient of permeability versus water content for a sandy clay soil is shown in Figure 4.5.

The volume change resulting from adding water to soil during compaction may in some cases be significant. Additionally, remolding sensitive clays may cause substantial loss of strength, as is shown in Figure 4.6. Shrinkage and swelling could lead to disasters. This situation may arise when wetting and drying soil deposits of high plasticity such as montmorillonite clay. The heaving and subsequent cracking of canal linings caused by the saturation of expansive soil is a real problem when dealing with water reservoirs. Figure 4.7 shows the failure of a canal bank in California. It is evident that soil compaction is by no means adequate to assure the proper behavior of soil in a given site. The engineer must not only be certain of the compaction characteristics of the soil but also of its type.

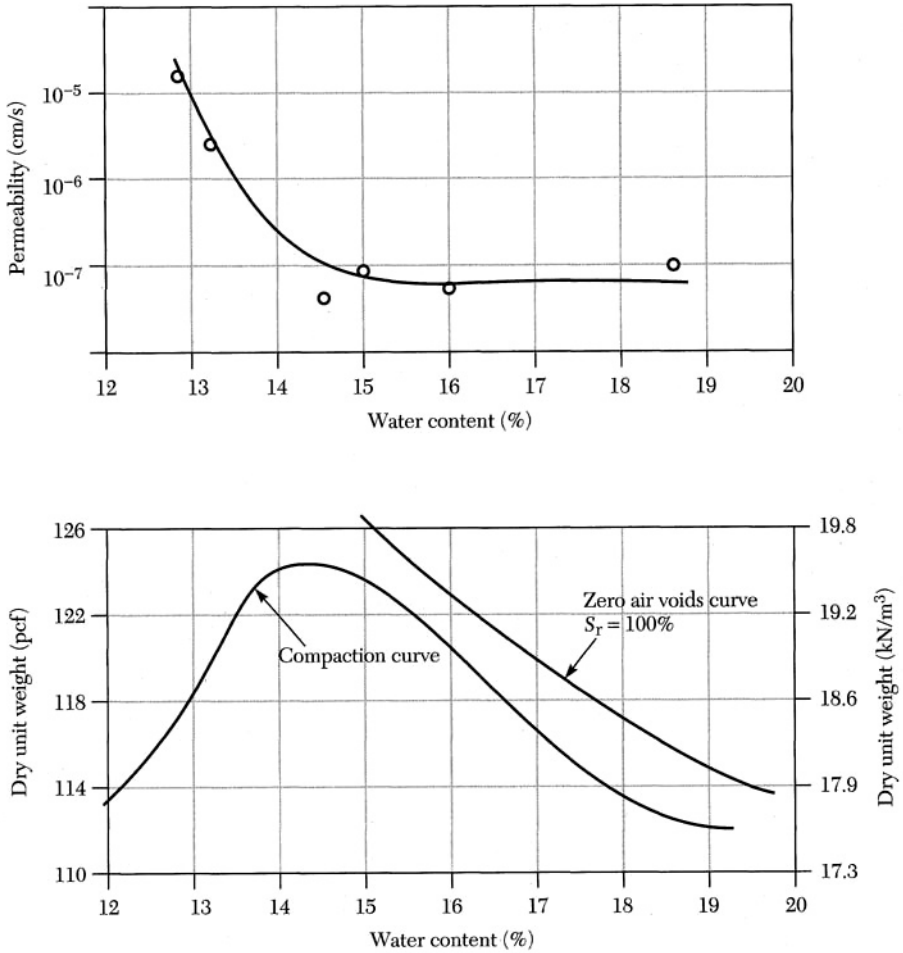


FIGURE 4.5 Effect of water content and compaction on the coefficient of permeability. (Redrawn after Lambe, 1958.)

4.3 FIELD COMPACTION AND GROUND MODIFICATION

4.3.1 General

The primary objective of field compaction is to improve the engineering behavior of soils. Construction on poor soils can be expensive, and it is advantageous to improve its behavior rather than remove it from a given construction site. This includes soils to be used in compacted fills and natural soil deposits. Soil used as fill is generally cohesionless and is excavated from a borrow pit using power shovels and then brought to the site. Cohesive soils are more difficult to compact in the field than are cohesionless soils. Furthermore, their compression characteristics are time-dependent owing to their low permeability. It is often difficult to deter-

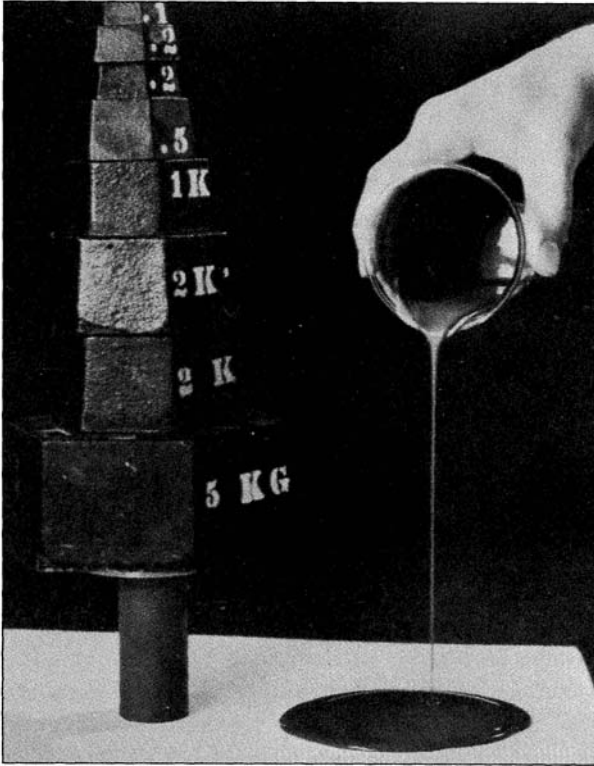


FIGURE 4.6 Illustration showing the strength of undisturbed extrasensitive Canadian clay (left) and extreme strength loss upon disturbance by remolding (right). (Photo courtesy National Research Council of Canada.)

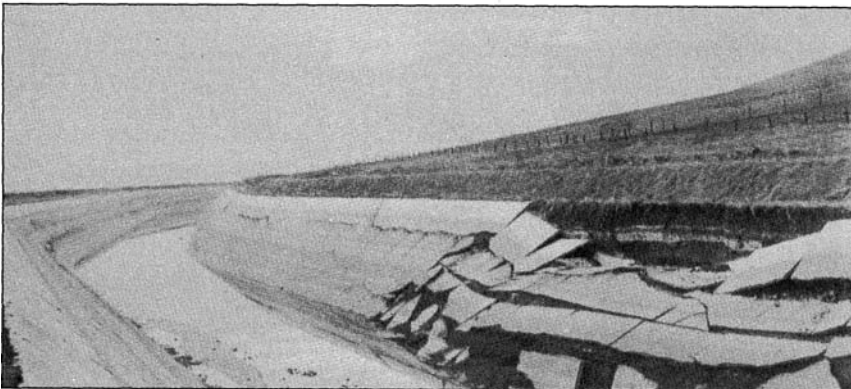


FIGURE 4.7 Failure of a canal bank liner caused by wetting and drying of underlying expansive soils in California. (Courtesy of the U.S. Department of the Interior.)

mine based on behavior whether a given soil is cohesionless or cohesive, because natural soils contain varying amounts of each type. In relative terms, cohesionless soils are more suitable for use as fill materials.

Properties of borrow materials are altered and their densities may be reduced as they are removed from their natural state. In some cases, the natural borrow soil is loose to begin with. The fill material must be placed such that soil densities are properly controlled to assure quality. This is achieved by compacting the fill material to certain unit weights or densities. If the natural soil is not within the desired water content, the soil may have to be dried, wetted, and/or reworked. Field compaction and ground improvement may involve vibrofloatation, chemical stabilization, grouting, ground freezing, biological transformation (root reinforcement), and/or dynamic compaction. Compaction involves several details pertaining to

1. Area, depth, and volume of soil involved
2. Labor versus materials cost
3. Properties and types of soils and intended use
4. Equipment availability
5. Type of existing structure
6. Quality-assurance potential
7. Engineering and construction confidence level

In the United States, there is a natural reluctance to try new and unproven techniques because of potential liability should something go wrong. This tendency has hampered development of new and innovative techniques. Consequently, the majority of ground modification methods were developed outside the United States, with a normal 5- to 10-year time lag before acceptance in the United States. Construction considerations for ground modification projects involve several factors as outlined in Table 4.1.

Field compaction at relatively shallow depths is achieved by first spreading the material using bulldozers, front end loaders, and/or blades. The fill is placed in layers varying in thickness from 6 to 18 inches depending on the type of compaction equipment available. The compaction equipment used varies in size and type. The type used depends on the nature of the project and the soil to be compacted. Smooth-wheel and drum rollers provide 100% coverage under the wheel and a pressure of up to 380 kpa (55 psi). These are generally used for compacting asphalt pavements and subgrades. The pneumatic or rubber-tire roller provides approximately 80% coverage and contact pressures of up to 700 kpa (100 psi). These are suitable for highway fills, embankments, and earth dams. The sheepsfoot roller provides coverage of 8% to 12% and contact pressures of up to 7000 kpa (1000 psi). Sheepsfoot rollers are suitable for compacting cohesive soils. In some cases trucks loaded with fill are routed so that they pass over fill areas to achieve compaction. In addition to the rollers described thus far, hand-operated tampers are also available for compacting fills around foundations and in areas where larger rollers cannot operate. Several examples of equipment used in compacting fill are shown in Figure 4.8.

TABLE 4.1 Assessment of Ground Modification in the United States

| Basic Method | Good Modification Techniques | Construction Assessment | Introduced in the U.S. |
|----------------------------------|------------------------------|-------------------------|------------------------|
| Adhesion | Chemical grouting | E | 1926 |
| | Slurry grouting | E | 1895 |
| | Freezing | D | 1888 |
| Densification | Dynamic deep compaction | E | 1975 |
| | Vibrocompaction | E | 1940 |
| | Compaction grouting | E | 1955 |
| | Compaction by explosives | C | 1960 |
| | Surcharging | E | 1977 |
| Reinforcement | Ground anchors | E | 1961 |
| | Stone columns | E | 1972 |
| | Compaction piles | C | 1960 |
| | Pin piles | C | 1960 |
| | Slurry walls | E | 1962 |
| | Soil nailing | C | 1980 |
| | Geotextiles | C | 1962 |
| Excavation replacement | Slurry excavation | D | 1962 |
| | Jet grouting | C | 1980 |
| | Stone columns | E | 1972 |
| Physical or chemical alterations | Electro-osmosis | A | A |
| | Lime columns | A | A |
| | Lime injection | C | 1960 |
| | Ionic injection | B | 1970 |
| | Ceramic piles | A | A |
| | Microwave piles | A | A |

A = Never utilized on more than five projects.

B = Still in basic research development.

C = Emerging technology.

D = Used when cost and time weigh heavily in its favor.

E = Used with high degree of confidence.

(Adapted from J. P. Welsh, Procs. Intl. Conf. on Deep Foundations, Beijing, China, 1986.)

In areas covered by deep fills and soft or loose soils, compaction is achieved using vibrocompaction, vibroreplacement, or dynamic compaction. These methods generally improve the soil engineering properties, thus allowing buildings to be constructed on relatively inexpensive shallow footings, instead of bypassing the sites with weak soil layers. Dynamic deep compaction can effectively and economically densify and improve unstable soils to permit development.

4.3.2 Dynamic Deep Compaction

This ground modification technique was resurrected by Menard (1970). The dynamic deep compaction technique consists of repeatedly impacting the soil by a heavy weight dropped from heights of up to 120 ft (36.5 m) in a grid pattern. The degree of improvement in density is related to the weight of the object to be

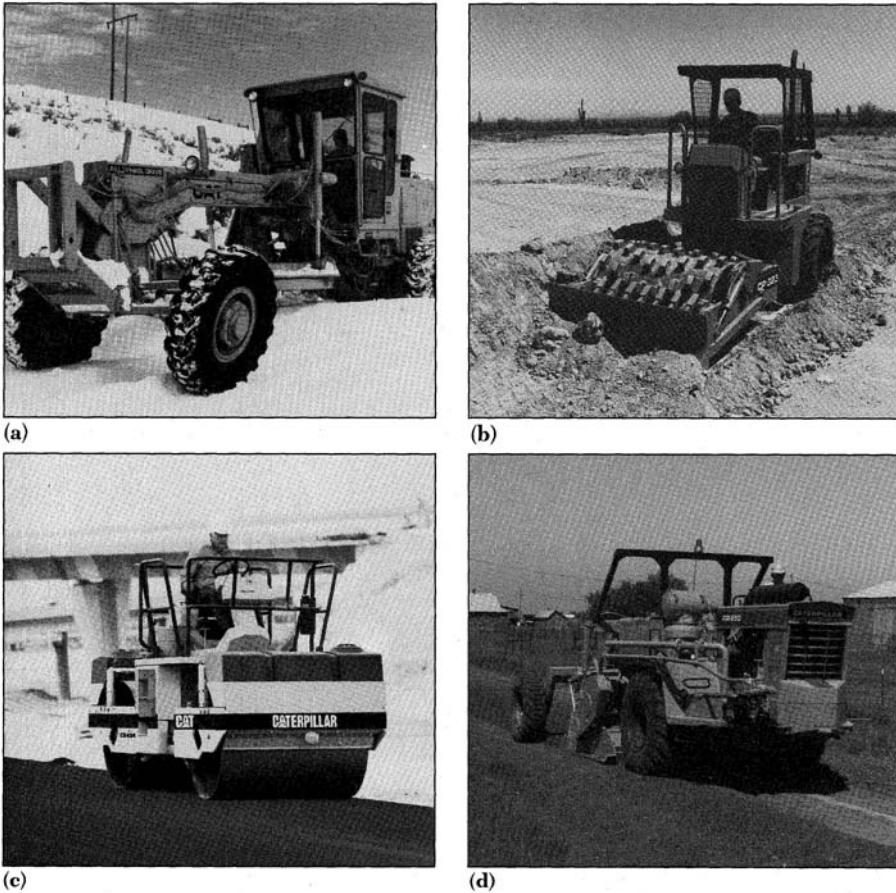


FIGURE 4.8 Examples of equipment used for hauling and compacting fill materials: (a) motor grader spreading and preparing fill subgrade; (b) tamping foot roller and compactor; (c) drum on smooth-wheel roller; and (d) self-propelled rubber-tired roller. (Courtesy of Caterpillar Inc., Peoria, IL.)

dropped, the height of the drop, and soil type. This technique has been successfully used in compacting loose sands, mining spoils, sanitary landfills, collapsible soils, and sinkhole-weakened soils. The energy applied by the impacting weight causes collapse of voids within the cohesionless soil deposit. In cohesive soils, wick drains are used to accelerate dissipation of the pore water pressures developed as a result of impact.

Current practice in the United States involves the use of weights of 10 to 22 tons (9 to 20 tonnes) dropped from heights of up to 110 ft (33.5 m) from specially fitted cranes. The effective of influence due to dynamic compaction can be approximated using the expression (Leonards et al., 1980)

$$D = C \sqrt{wh}$$

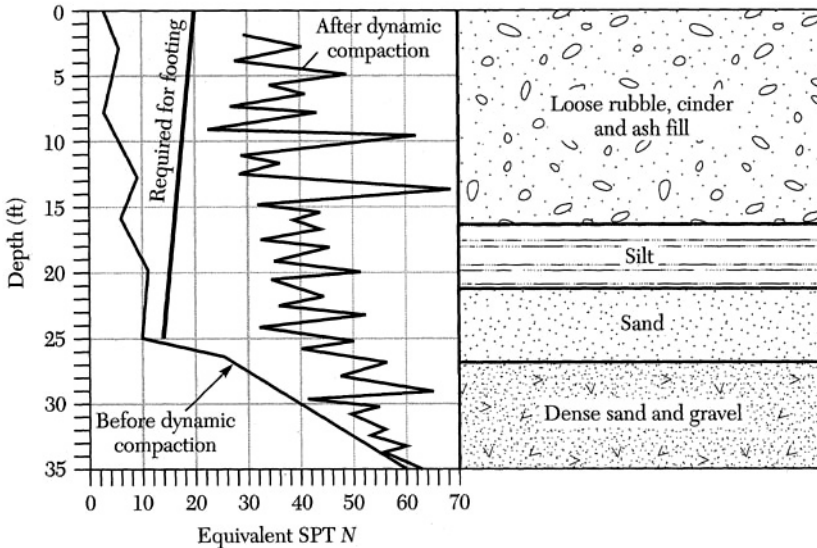


FIGURE 4.9 Site conditions along with required SPT values to support a structure.

where w is the weight to be dropped in metric tons (1 ton = 1000 kg), h is the height of the drop in meters, and D is the depth of influence in meters. Values of C vary from 0.3 to 0.7 depending on soil type. Experience over the past ten years has shown that in landfills, a factor of $C = 0.3$ may be used. For a typical site, the effectiveness of this technique versus depth is normally measured by the penetration resistance, as shown in Figure 4.9.

Economics determines the suitability of this technique for a given site. The types of ground modification problems for which the dynamic modification technique is applicable include

1. Loose, natural granular deposits including collapsible soils
2. Cohesionless and cohesive fills, including building debris
3. Mine spoils
4. Sanitary landfills
5. Soil deposits loosened from underlying limestone formations

When sanitary landfills are used, the site is normally covered initially with 3 to 5 ft (1 to 1.5 m) of granular fill to provide stability to the crane traversing the site. This seemingly simple technique could result in significant increases in strength and appreciable volume reduction of the soil deposit. However, the reader should recognize that each project has its own unique characteristics and must be carefully designed and monitored.

4.3.3 Compaction by Explosive

In the mid 1960s, several projects in the United States were treated utilizing explosives for ground modifications. A case history is rarely seen in the technical lit-

erature despite the fact that the technique is very useful from an economic standpoint. Because of liability and other practical problems, its use is limited to remote areas. From a geotechnical standpoint this technique is limited to sands with less than 15% fines. The technique involves the use of small explosive charges placed on a grid pattern to approximately two thirds of the depth of the zone to be densified. The shock of the explosive can produce relative densities of up to 75%. In the past, the standard penetration test (SPT) was the main testing method available to verify success. Now the SPT method is being replaced by the cone penetration test, which can more accurately and economically verify before and after relative densities and settlements.

A depth limitation has not been established for this technique. Further studies are needed to determine the extent of damage caused to existing structures by vibration. Also, nuisance claims and other legal matters need to be investigated.

4.3.4 Vibrocompaction and Vibroreplacement

This method was developed in Germany over 55 years ago. It was introduced into the United States in the early 1940s, making it the forerunner for ground modification. The use of vibrations to densify clean granular soils is achieved through various methods and equipment. The soil deposit should contain no more than 15% fines. Vibratory surface rollers are normally limited to densifying 3 to 7 ft (1 to 2 m) of soil. Consequently, the effectiveness of densification is limited by energy losses and the vertical nature of the vibrations. The vibrocompaction techniques use depth vibrators, which generate energy within the soil at the required depth. These vibrators contain an electrically driven eccentric weight that produces centrifugal forces in the horizontal plane at frequencies of 1200 to 3000 rpm. The vibrator is normally suspended from a mobile or crawler crane and is lowered into the ground on a predetermined pattern (Figure 4.10). The vibrator is lowered to the desired depth of treatment, then raised in increments of about 1 to 2 ft (0.3 to 0.6 m) per minute. Typically, the basic vibrator length is between 10 and 15 ft (3 to 4.5 m) and weighs approximately 2 tons. Extension tubes are added to permit penetration to the required depth. The diameter of influence of the vibrator is approximately 14 ft.

The action of the vibrator, usually accompanied by water jetting, reduces intergranular forces, causing localized liquefaction. This permits the soil particles to rearrange themselves in more compact configurations. This causes the density to increase, which serves to prevent liquefaction during earthquakes. This technique is well suited for producing earthquake-resistant foundations. The range of spacing for which vibrocompaction is used to achieve a specific level of densification is illustrated graphically in Figure 4.11.

Vibroreplacement usually involves placing stone columns in cohesive soils deposits or when the cohesionless deposits contain more than 20% fines. This technique utilizes the same vibrator, but rather than sand, stones are added and vibrated into the soil. The most recent improvement in this technique is the use of the bottom-feed method, in which stone backfill is fed through a tube to the bottom of the vibrator. The suitability of vibrocompaction and vibroreplacement for

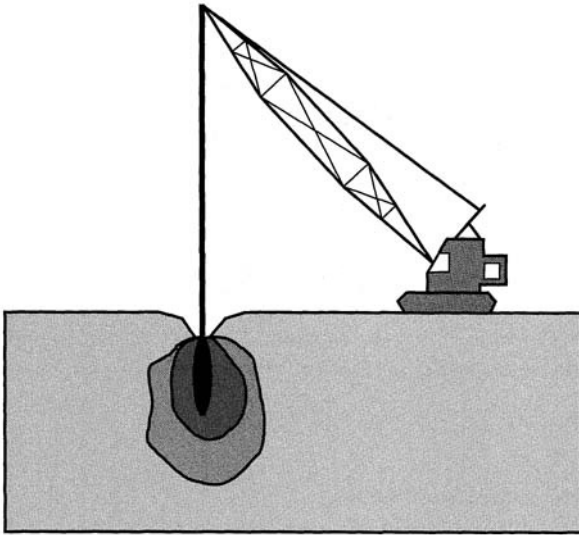


FIGURE 4.10 Typical deep vibrocompaction setup.

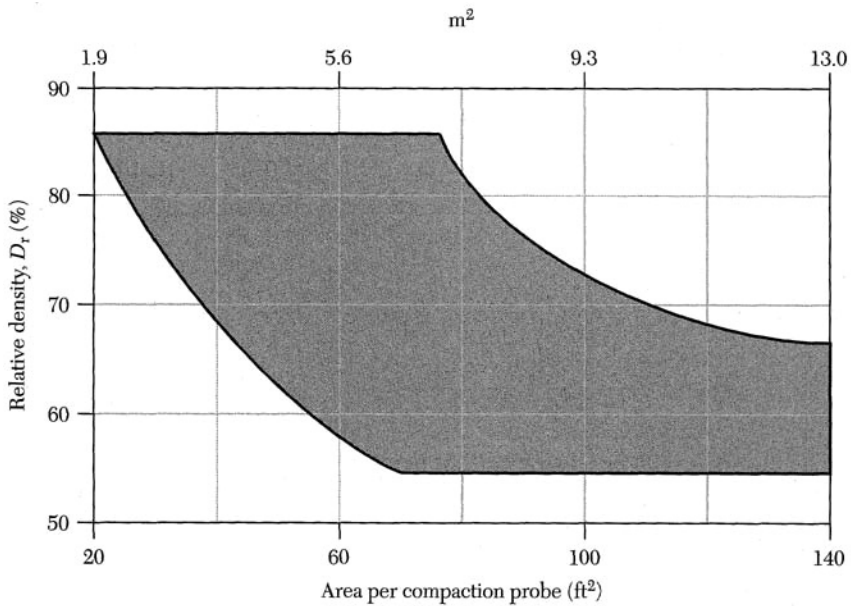


FIGURE 4.11 Envelope for spacing of vibrocenters in clean granular soil deposits.

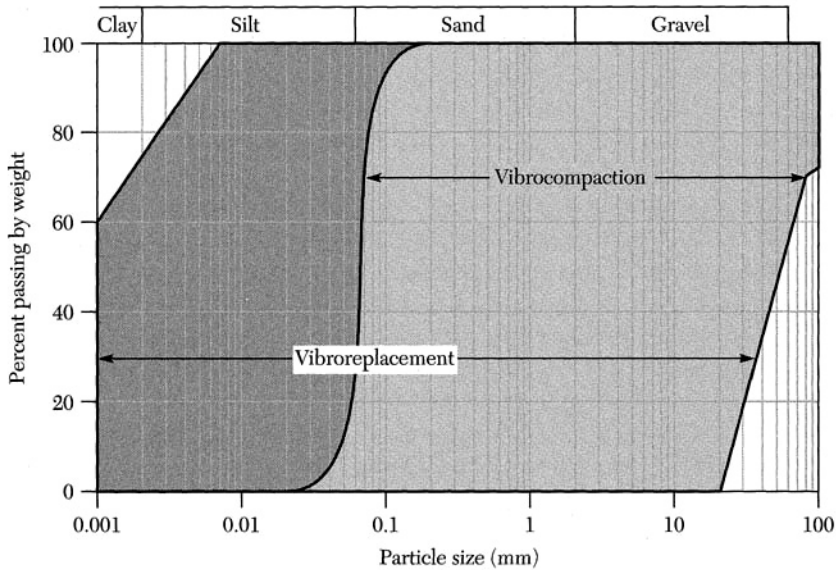


FIGURE 4.12 Grain size distribution curves for soils and suggested technique to be used.

varieties of soil grain sizes is shown in Figure 4.12. These techniques can produce dense soils suitable for the support of spread footings with allowable bearing pressures of 3 to 5 tsf. Relative densities in excess of 85% are achievable to depths of approximately 115 ft.

4.3.5 Grouting

Grouting can generally be described as the injection of pumpable materials into a soil deposit or rock formation to change the physical characteristics of the deposits. As is shown in Figure 4.13, four types of grouting methods are used in ground improvement: compaction grout, chemical grout, slurry grout, and jet grout. All grouting projects involve two basic factors: placing the grout pipes and injecting the grout. These factors are extremely important in ensuring the success of the grouting operation.

Compaction grouting was developed in the United States 35 years ago. This technique is generally used to limit ongoing foundation settlement and settlement resulting from tunneling. More recently, it has been successfully used to improve soil deposits before construction. As with all grouting operations, the proper mix design is essential for compaction grouting. Extensive amounts of water and the grout will behave similarly to a slurry grout. This may result in losing the slurry through fracturing in a given formation.

Chemical grouting involves the injection of properly formulated chemicals into sand deposits containing less than 20% fines. It is used to cement the sand particles, which produce a sandstonelike formation having unconfined compres-

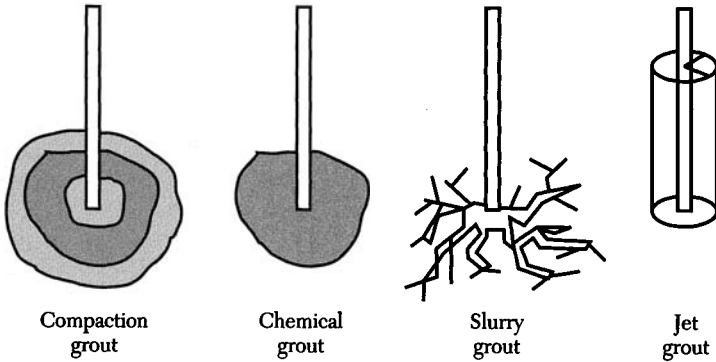


FIGURE 4.13 Types of grouting techniques.

sive strengths in excess of 85,000 psf (4070 kN/m²). Chemical grouting is well suited for structural purposes. Although some additives are toxic, there are non-toxic chemicals that can be used in areas where the water table may be affected.

Slurry grouting is one of the most widely used grouting techniques in the United States. Its use is generally limited to reducing the permeability of rock beneath new dams. The development of ultra-fine grain cements has made possible the use of slurry grouting in granular soils. Expansive soils are often treated using lime slurry grout to fill fissures and to limit potential swelling to less than 1%.

Jet grouting was introduced in Japan in the late 1970s. The basic technique consists of installing a multipassage grout pipe to the desired depth. As the grout pipe is extracted, it is rotated at a controlled rate. Horizontal air/water under high pressure is jetted out to excavate a cavity. This cavity is then filled with appropriate grout through the bottom of the grouting pipe. Jet grouting is applicable to all soils.

4.4 IN-PLACE DETERMINATION OF SOIL DENSITY

Normally, a soil is tested in the laboratory to determine the optimum dry unit weight and the corresponding water content using the standard or modified Proctor compaction or the relative density tests. If more than one type of fill material is to be used, then separate tests must be performed for each. Once the optimum dry unit weight and the corresponding optimum water content are determined, the field dry unit weight is specified. The specified dry unit weight is normally taken as 95% to 98% of the optimum value determined in the laboratory. The reason 100% of optimum is not specified is due in part to the variability of the water content in the field. For convenience, the **percent compaction** is defined as the ratio of the field unit weight γ_{df} to the optimum unit weight γ_{do} as follows.

$$\% \text{ compaction} = \frac{\gamma_{df}}{\gamma_{do}} \times 100 \quad (4.5)$$

The selected percent compaction value is normally related to the type of application at hand. Therefore, fill to be used under or around foundations is normally

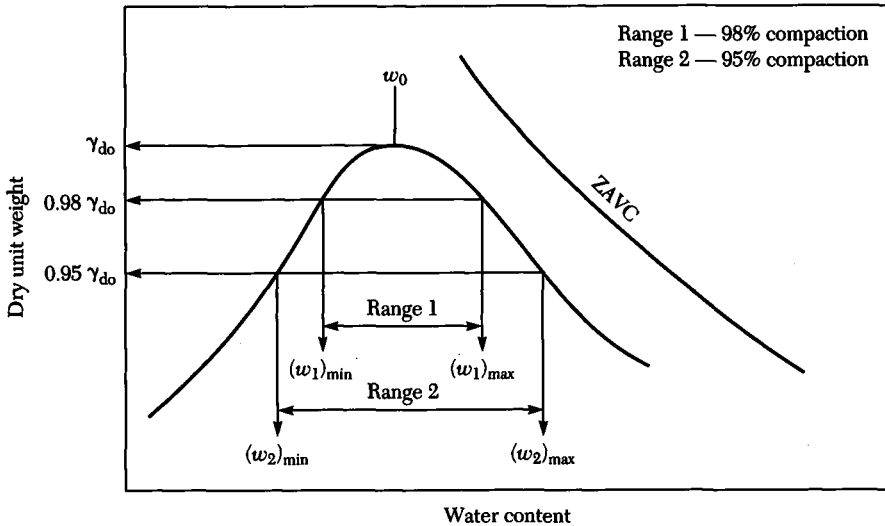


FIGURE 4.14 Schematic diagram showing different water content ranges for different specified field dry unit weights.

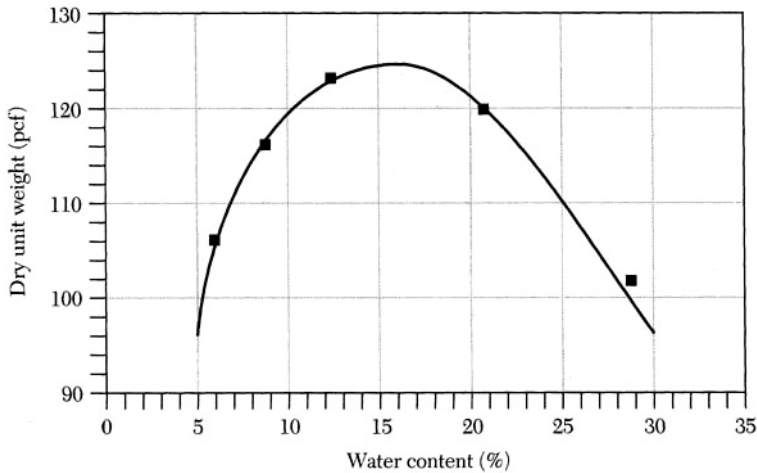
placed at 98% of its optimum unit weight. Note that once a field unit weight is specified, a range of water contents can be used to attain it. This concept is shown in Figure 4.14. It is evident from the figure that the range of water contents corresponding to a high percent compaction is narrower than that for a lower percent compaction. This is precisely what the field technician is provided — a range of water contents rather than a specific optimum value in addition to the optimum dry density and the desired percent compaction.

Field compaction may in some cases exceed the specified percent compaction. In fact in some cases over 100% compaction, as defined by Eq. (4.5), is possible. This is because a higher compactive effort was applied to the soil in the field than was applied in the laboratory. The field technician or engineer must be certain, however, that the soil is compacted to certain unit weights throughout. Therefore, lift thickness and the number of roller passes must be controlled at limiting values. This is done so that the depth of influence of compaction is suitable to assure a minimum unit weight in a given lift. The dry unit weight for a given lift after compaction is determined in the field using a number of standard tests as described in Experiments 18, 19, and 20.

PROBLEMS

- 4.1** The water content of a borrow material is known to be 11.2%. Assuming that 10 lb (4.5 kg) of wet soil is used for a laboratory compaction test, compute how much water must be added to the test sample to bring its water content up to 18%.

- 4.2 A given soil has an optimum water content of 17.3% and an optimum dry density of 112.7 pcf. A sand cone field density test revealed that the in-place unit weight is 111.2 pcf and the soil's water content is 13.4%. Determine whether the field unit weight meets specification if the desired percent compaction is 98%.
- 4.3 Consider the following moisture density curve, then estimate the optimum dry unit weight and the corresponding optimum water content. What is the range of water contents if the degree of compaction specified is 95%?



- 4.4 A standard compaction test was performed on a soil sample having a specific gravity of 2.63 using a $\frac{1}{30}$ ft³ mold. Test results are summarized below.

| Test Number | Water Content of Soil in Mold (%) | Weight of Soil in Mold (lb) |
|-------------|-----------------------------------|-----------------------------|
| 1 | 12.1 | 4.03 |
| 2 | 16.7 | 4.42 |
| 3 | 19.8 | 4.45 |
| 4 | 22.3 | 4.37 |

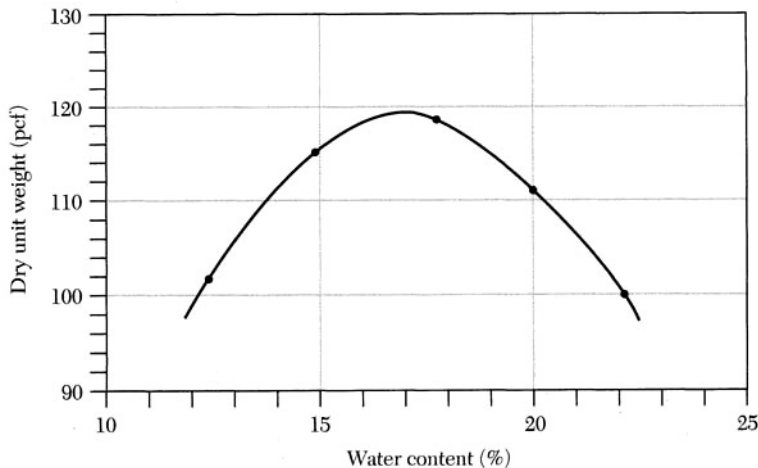
- Establish the wet and dry unit weight and corresponding water contents.
 - Plot the dry unit weight versus the water contents.
 - Determine the optimum dry unit weight and corresponding water content for 95% compaction.
 - Plot the wet unit weight versus the water contents, then determine the optimum wet unit weight and explain why it is higher than the optimum dry unit weight.
 - Plot the 100% and the 80% saturation curves.
- 4.5 Calculate the compactive effort for the standard and modified compaction tests using (a) SI units and (b) British Engineering units.
- 4.6 A proposed earth embankment requires 2,000,000 cubic yards of soil. The soil will be compacted to a bulk unit weight of 125 pcf and a water content of

15.8% when it is placed in the embankment. There are three available borrow pits, designated A, B, and C. The bulk unit weight and corresponding water content of the soil in each pit and transportation cost per cubic yard for the three different soils are as follows.

| Borrow Pit Designation | Bulk Unit Weight (pcf) | Water Content (%) | Cost/yd ³ (\$) |
|------------------------|------------------------|-------------------|---------------------------|
| A | 110.5 | 12.2 | 6.2 |
| B | 107.4 | 15.0 | 5.0 |
| C | 90.0 | 27.4 | 3.5 |

Select the pit from which material should be bought so that the cost is minimized. Ignore compaction costs in making your selection.

- 4.7 Describe briefly the errors associated with the balloon test and the sand cone test for field density determinations.
- 4.8 Determine the depth of influence in meters for a weight of 10 tons when it is dropped a distance of 25 feet.
- 4.9 When vibrocompaction is used, it is necessary to estimate the spacing of vibrocenters in clean granular soil deposits. Estimate the minimum and the maximum spacing if the desired relative density is 65%.
- 4.10 Describe briefly the four different types of grouting methods and their uses.
- 4.11 Suppose you are asked to check earthwork for a construction control job. The laboratory compaction curve for the soil is shown below. Specifications call for compacted unit weight to be at least 98% of the optimum laboratory value and within $\pm 3\%$ of the optimum water content. In the field, you used a balloon test, the volume of the soil excavated was 1162 cm³, and its weight 2253 g wet and 1910 g dry.



- (a) What is the unit weight of the soil in the field?
- (b) What is the field water content?
- (c) What is the percent compaction?

5

Water Flow through Soils

5.0 INTRODUCTION

Water flow through soils is important in a variety of geotechnical engineering problems. Leakage through an earth dam involves the rate of water flow, soil compression and foundation settlement involves drainage of pore water, and the flow pattern of pore water pressures with their influence on shear strength can be responsible for the development of critical stability conditions. Flow can be steady or unsteady. Water flow underneath a large concrete dam or through an earth dam will be unsteady at first, but will stabilize with time to steady flow. Flow will occur in both saturated and unsaturated soils. In this chapter, emphasis will be given to steady-flow conditions in saturated soils.

In general, all voids in soils are connected to neighboring voids. In coarse soils — gravels, sands, and silts — the pores are continuous, with an individual water particle following a path that can deviate erratically but only slightly from smooth curves known as **flow lines**. In clays, a small percentage of the voids may appear to be isolated, although in electron photomicrographs all of the voids are interconnected. The course of water movement involves both gravitational forces on an element of water and the force due to differences of hydrostatic pressure at different points in the soil. Resistance to flow is determined by the soil pore space and properties of the fluid. These topics are introduced in this chapter.

5.1 DARCY'S LAW

The flow of fluids through soils can be illustrated by experimental techniques similar to those used by Darcy (1856). A constant water pressure difference is created between the two ends of a soil sample (Figure 5.1), and the quantity of water flowing through the sample during a certain period of time is measured. The results show that the flow volume Q through the soil in time t is proportional to the soil cross-sectional area A and to the difference in piezometric levels h , and inversely proportional to the length L ; thus,

$$\frac{Q}{t} = q \quad \text{and} \quad q \propto \frac{Ah}{L}$$

or

$$q = \text{constant} \cdot \frac{Ah}{L} \quad (5.1)$$

Rearranging Eq. (5.1) gives

$$\frac{q}{A} = v \quad \text{and} \quad v \propto \frac{h}{L}$$

$$v = (\text{constant}) \frac{h}{L} = ki \quad (5.2)$$

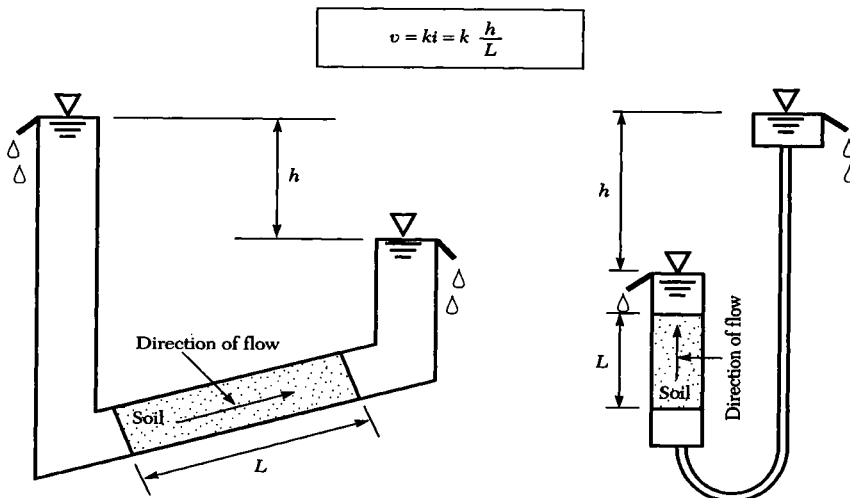


FIGURE 5.1 Flow of water through soils under the effect of gravity.

where v is the discharge velocity, i is the total head lost per unit length of flow path (hydraulic gradient), and k is the Darcy coefficient of permeability. Equation (5.2) is known as *Darcy's law*. The **coefficient of permeability**, or more simply **permeability**, is a soil property that describes how water flows through soils. Note that permeability has units of velocity (m/s) because the hydraulic gradient is dimensionless.

The discharge velocity v is defined as the volume of water that percolates in a unit time across a unit area of a section oriented at right angles to the flow path. This v is a superficial velocity that is convenient for engineering use. The actual **seepage velocity** (also known as the *effective velocity*) v_e of water through the soil pores is greater. For a constant flow rate, write

$$q = vA = v_e A_v = v_e nA \tag{5.3}$$

where A_v is the voids area over the cross-sectional area A in a statistically isotropic porous material and the soil porosity n of a plane section is equal to the volume porosity. The relationship between the soil cross-sectional area, void area, and solids area is illustrated in Figure 5.2. Note that $v = nv_e$.

As used in Darcy's law [Eq. (5.2)], the coefficient of permeability includes the viscosity and unit weight γ_w of the pore fluid; thus,

$$k = \frac{\gamma_w}{\eta} K \tag{5.4}$$

where k is in units of velocity (m/s), and the specific or absolute permeability K is in units of area (m²). For laboratory use it is convenient to take the ratio of k at 20°C to k at some temperature T and rewrite Eq. (5.4) as

$$k_{20} = \frac{\eta_T}{\eta_{20}} \left(\frac{\gamma_{20}}{\gamma_T} \right) k_T \tag{5.5a}$$

For most tests, the ratio of the unit weight at temperature 20°C (γ_{20}) to that at another temperature T (γ_T) is close to unity. This is because the unit weight is not

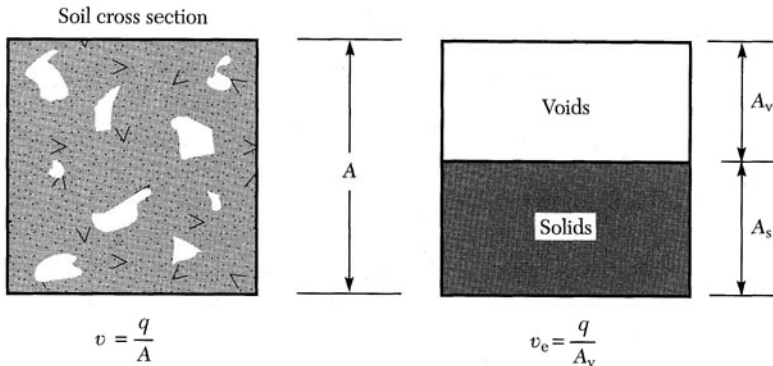


FIGURE 5.2 Discharge and seepage velocities in soils.

significantly affected by temperature changes. Therefore, Eq. (5.5a) is generally expressed as

$$k_{20} = \frac{\eta_T}{\eta_{20}} k_T \quad (5.5b)$$

where the absolute permeability is a constant for a given soil and cancels out. The permeability K characterizes the porous medium in terms of the shape and mean hydraulic radius of its pores and its porosity. To estimate k at other void ratios, Taylor (1948) offers the relationship

$$k_1 : k_2 = \frac{C_1 e_1^3}{1 + e_1} : \frac{C_2 e_2^3}{1 + e_2} \quad (5.6)$$

where the void ratios e_1 and e_2 correspond to k_1 and k_2 , respectively, and the coefficients C_1 and C_2 depend on soil structure and must be determined experimentally. For sands the constants C_1 and C_2 are approximately equal. For silts and clays Eq. (5.6) has a very limited application.

Since Darcy's law was originally developed for clean filter sands, the question arises as to how valid this law is for other soils. Careful experiments have shown that Eq. (5.3) is valid for a wide range of soil types at engineering gradients. In open-graded rock materials and very clean gravels flow may become turbulent and Darcy's law becomes invalid. Taylor (1948) presented information indicating that semiturbulent flow may begin when the effective particle diameter exceeds about 0.5 mm. For fine-grained soils and very small hydraulic gradients, careful investigations (Hansbo, 1960) have shown a nonlinear relationship between v and i (Figure 5.3). Field measurements (Holtz and Broms, 1972) indicated a value of about 1.5 for the exponent n with Swedish clays. If a threshold gradient i_0 exists as shown on Figure 5.3, soil drainage (consolidation) would cease when excess

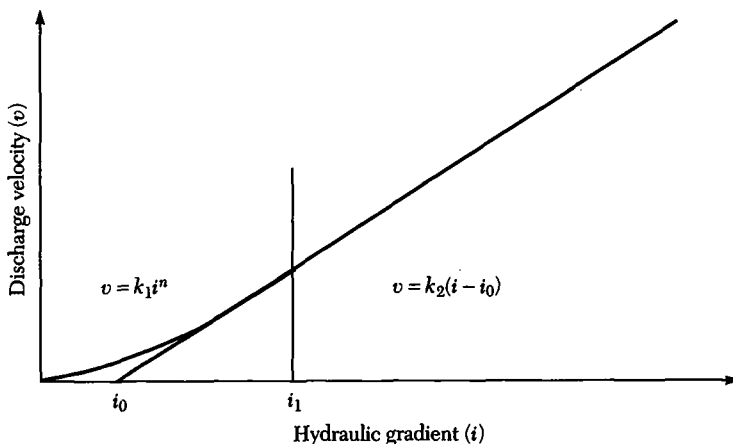


FIGURE 5.3 Discharge velocity versus hydraulic gradient relationship observed in Swedish clays. (After Hansbo, 1960.)

pore pressures in a clay layer have decreased so as to give the threshold gradient throughout the consolidating layer.

5.2 PERMEABILITY MEASUREMENT — LABORATORY

The coefficient of permeability of soil can be determined by any test in which the cross-sectional area, the hydraulic gradient, and the quantity of flow can be measured or can be approximated. Two apparatus types used for determining k of soil samples are illustrated in Figure 5.4. For very permeable soils (clean gravels and sands) the constant-head permeameter is most suitable. For less permeable soils (silts and clays) the falling-head permeameter gives more reliable data. In both types of apparatus (Figure 5.4) gravity forces are responsible for the hydraulic gradient within the sample that causes water to flow through the soil. Several problems associated with the reliability of laboratory tests need to be considered. The permeability of a soil mass is dependent on both its microstructure (i.e., particle size, shape, arrangement, and so on) and its macrostructure (i.e., whether or not stratified, presence of fissures, lenses, etc.). For practical reasons the size of samples taken for laboratory tests is quite small and may not be fully representative. This limitation is overcome by obtaining carefully selected groups of samples. A

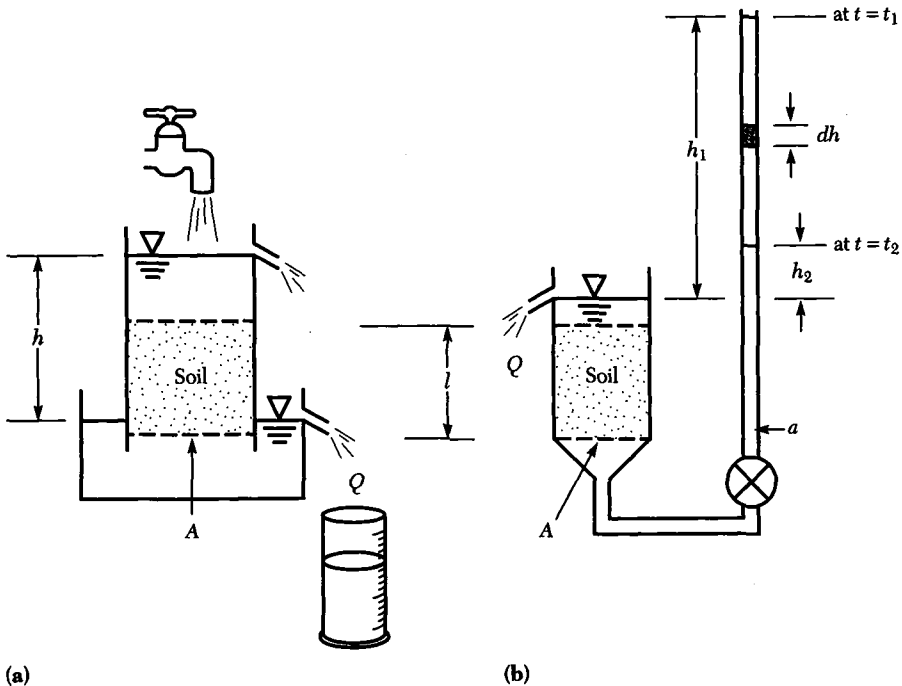


FIGURE 5.4 Measurement of the coefficient of permeability: (a) constant-head test; (b) falling-head test.

second problem involves duplicating field conditions where possible. Changes in temperature and/or pressure may cause air to come out of solution, forming bubbles that block the pores. A backpressure (see Chapter 6) may be applied to force the bubbles back into the solution. The permeant (water) should be similar to the pore water in the field. If the pore fluid contains salts, performing the tests with distilled water can lead to erroneous results.

The constant-head test is used to determine the coefficients of permeability of coarse-grained soils such as clean gravels and sands having k values greater than 10^{-3} cm/s (as shown in Table 5.1). The apparatus used is illustrated in Figure 5.4a with the soil sample contained in a cylindrical mold having a porous stone above and below. Water is allowed to flow through the sample with an overflow arrangement used to maintain a constant head. The water that passes through the sample in time t flows into a container where it is collected and the flow rate q is calculated. The cross-sectional area is the area of the cylinder A , and the hydraulic gradient i is the head h divided by the length of the sample. To obtain a value of k , Eq. (5.2) is rewritten in the form

$$k = \frac{QL}{hAt} = \frac{q}{iA} \quad (5.7)$$

where Q is the quantity of water (cm^3) collected in time t (sec), A is the cross-sectional area of the sample (cm^2), h is the difference in water levels (cm), and L is the flow distance through the sample (cm). If the permeability is very low, time becomes excessive and evaporation during the test can introduce errors in the results.

The falling-head test is used to determine the coefficient of permeability of fine-grained soils having k values too small to enable accurate measurements using the constant-head permeameter. The apparatus used is illustrated in Figure 5.4b with an undisturbed soil sample or with a sample prepared by compaction in a standard mold. Details on equipment and sample preparation are given as part of Experiment 22. The test is conducted by filling the standpipe with de-aired water and allowing seepage to take place through the sample. The height of water in the standpipe is recorded at several time intervals during the test, and the test may be repeated using standpipes of different diameter. If the water level in the standpipe falls an amount dh in time dt , then

$$q = -a \frac{dh}{dt} = kA \frac{h}{L} \quad (5.8)$$

where the hydraulic gradient $i = h/L$, a , and A are the standpipe and sample cross-sectional areas, respectively. Rearranging terms and integrating

$$-\int_{h_1}^{h_2} \frac{dh}{h} = \frac{kA}{aL} \int_{t_1}^{t_2} dt$$

gives

$$-\ln \frac{h_2}{h_1} = \frac{kA}{aL} (t_2 - t_1)$$

Coefficient of permeability k in centimeters per second (log scale)

| | 10^2 | 10 | 1 | 10^{-1} | 10^{-2} | 10^{-3} | 10^{-4} | 10^{-5} | 10^{-6} | 10^{-7} | 10^{-8} | 10^{-9} |
|-------------------------------|---|----|--|-----------|---|---|-----------|-----------|--|--|-----------|---|
| Drainage | Good | | | | | | Poor | | | Practically Impervious | | |
| Soil types | Clean gravel | | Clean sands, clean sand and gravel mixtures | | | Very fine sands, organic and inorganic silts, mixtures of sands, silt and clay, glacial till, stratified clay deposits, and so on | | | | "Impervious" soils, e.g., homogeneous clays below zone of weathering | | |
| | | | | | "Impervious" soils modified by effects of vegetation and weathering | | | | | | | |
| Direct determination of k | Direct testing of soil in its original position — pumping tests; reliable if properly conducted; considerable experience required | | | | | | | | | | | |
| | Constant-head permeameter; little experience required | | | | | | | | | | | |
| Indirect determination of k | | | Falling-head permeameter; reliable; little experience required | | | Falling-head permeameter; unreliable; much experience required | | | Falling-head permeameter; reliable; considerable experience required | | | |
| | Computation from grain size distribution; applicable only to clean cohesionless sands and gravels | | | | | | | | | | | Computation based on results of consolidation tests; reliable; considerable experience required |
| | 10^2 | 10 | 1 | 10^{-1} | 10^{-2} | 10^{-3} | 10^{-4} | 10^{-5} | 10^{-6} | 10^{-7} | 10^{-8} | 10^{-9} |

TABLE 5.1 Permeability and Drainage Characteristics of Soils and Their Methods of Measurement [After A. Casagrande and R. E. Fadum (1940).]

Solve for

$$k = \frac{aL}{A(t_2 - t_1)} \ln \frac{h_1}{h_2} \quad (5.9a)$$

or

$$k = \frac{2.3 aL}{A(t_2 - t_1)} \log \frac{h_1}{h_2} \quad (5.9b)$$

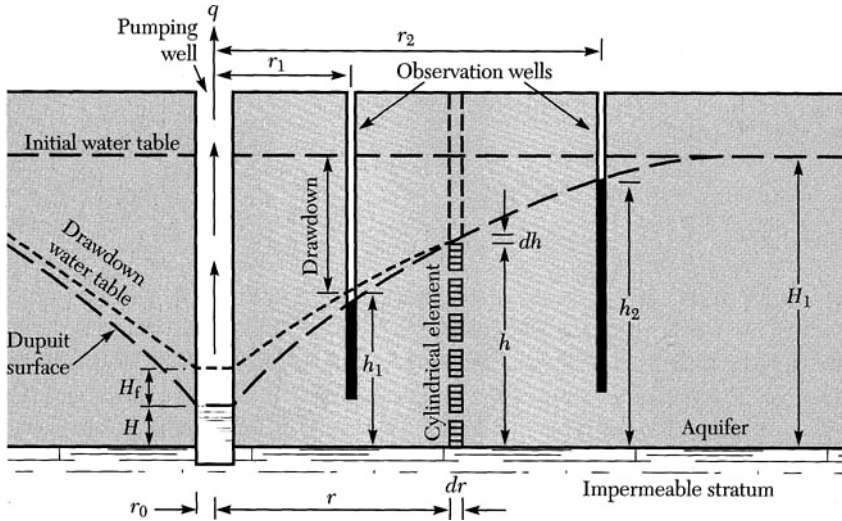
Falling-head tests can be made with flow either upward or downward through the soil sample. The water pressure from downward flow holds the soil in place; however, it may cause migration of fines, leading to clogging. Care must be taken to prevent segregation during sample placement and to prevent the formation of a thin layer of fines at the top or bottom of the specimen. If the measured permeability appears to become smaller during the test, air coming out of solution may be forming bubbles that are partially blocking the pore voids. Use of de-aired water will normally eliminate this problem.

5.3 PERMEABILITY MEASUREMENT—FIELD

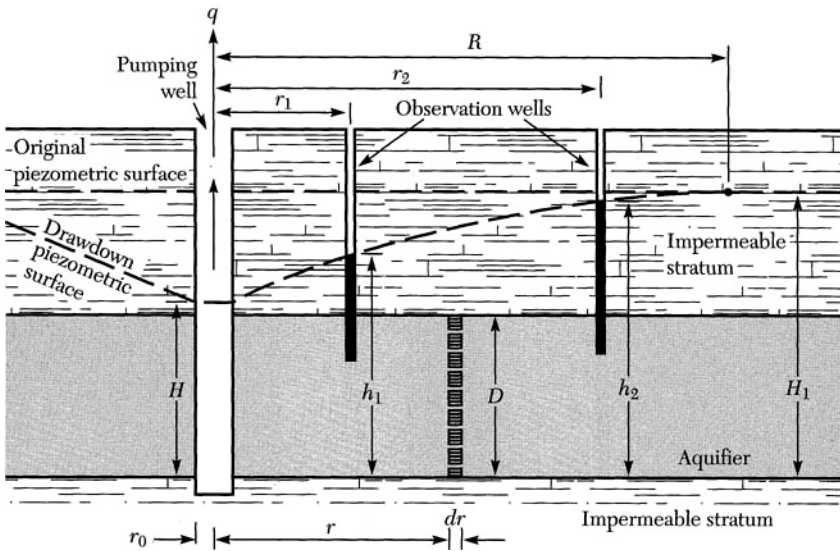
Permeability values from laboratory tests on small samples taken at individual points within large masses may not fully represent field conditions. They do provide a general knowledge of the permeability and when used with consideration of field conditions can be of considerable value. Three general methods are used in determination of the field coefficient of permeability: (1) pumping tests, in which water is pumped from a well at a constant rate and drawdown of the water table is observed in wells placed on radial lines at various distances from the pumped well; (2) tests conducted by observation of the velocity of flow as measured by the rate of travel of a dye or electrolyte from the point of injection to an observation well; and (3) open-end tests, in which water is placed into a drill hole and the rate of seepage is observed under a given load. The pumping tests are relatively high in cost and the results can be difficult to interpret. The rate of seepage between boreholes is limited to more permeable soils. The open-end field permeability tests are more economical, but the results can be considered only as approximations. They do provide the advantage that the permeability of various layers can be tested, rather than only the overall permeability.

5.3.1 Pumping Tests

The unconfined flow pumping test, illustrated in Figure 5.5a, involves pumping from the main well at a constant rate until water levels in the observation wells are observed to be constant, indicating that steady-state conditions have been reached. This may take several days and in some cases longer. The levels in the observation wells and the flow quantity are then noted. It is assumed that the soil is homogeneous and that at zero flow the piezometric surface is horizontal. For ra-



(a)



(b)

FIGURE 5.5 Pumping tests for determination of permeability: (a) unconfined flow; (b) confined aquifer.

dial flow toward wells that fully penetrate the water-bearing strata, Darcy's law and the Dupuit assumption provide the basis for deriving the simple well formula. Dupuit assumed that the hydraulic gradient at any radius is a constant from top to bottom of the water-bearing layer and is equal to the slope of the drawdown water table. This assumption introduces large errors near the well (Figure 5.5a) but is

reasonably accurate at distances from the well greater than 1.0 to 1.5 H_1 . The simple well formula is derived on the basis that the quantity of water flowing toward a well per unit time is $q = kiA$. At a radius r from the well the area through which the water is flowing is $2\pi rh$. Using Dupuit's assumption that $i = dh/dr$, write

$$q = kiA = k \frac{dh}{dr} (2\pi rh) \quad (5.10)$$

Rearranging terms and setting limits gives

$$q \int_{r_1}^{r_2} \frac{dr}{r} = 2\pi k \int_{h_1}^{h_2} h \, dh \quad (5.11)$$

Integrate and solve for k .

$$k = \frac{q}{\pi(h_2^2 - h_1^2)} \ln \frac{r_2}{r_1} \quad (5.12a)$$

$$k = \frac{2.3q}{\pi(h_2^2 - h_1^2)} \log \frac{r_2}{r_1} \quad (5.12b)$$

The reliability of Eq. (5.12) depends on how accurately the assumptions are fulfilled. For slightly sloping water tables, the lower boundary of the water-bearing layer can be drawn parallel to the initial water table with the computation the same as for a level water table.

When an aquifer is confined above and below by impermeable strata (Figure 5.5b) and the piezometric surface is at all radii above the upper surface of the aquifer, a confined flow condition occurs. For steady-state conditions, flow is considered through a cylinder of soil having a radius r , thickness dr , and height h . By pumping at a constant rate q from the well until a steady state of flow is achieved, the height of water in the observation wells at a distance r will be lowered from H_1 to h . Assuming that water flows toward the well in horizontal radial directions, the flow q across the boundary of any cylindrical section of radius r is

$$q = kiA = k \frac{dh}{dr} (2\pi rh) \quad (5.13)$$

Rearranging terms, setting limits as before, and integrating gives

$$k = \frac{q}{2\pi D} \frac{\ln(r_2/r_1)}{(h_2^2 - h_1^2)} = \frac{2.3q}{2\pi D} \frac{\log(r_2/r_1)}{(h_2^2 - h_1^2)} \quad (5.14)$$

Measuring h_1 and h_2 at their corresponding radii, r_1 and r_2 , will give the more accurate values for k . Using the conditions that $h_1 = H$ at $r_1 = r_0$ and that at a large value of $r_2 = R$, h_2 approximates H_1 permits calculation of an approximate value of k without the assistance of observation values. The dimension R , the radius of the well influence, represents the distance beyond which the water table remains close to horizontal. Cedargren (1967) recommended a number of conditions to be followed in order to improve the accuracy of the pumping test. Permeability com-

putations are made using observation wells in various combinations and then taking the average as the best estimate for the large volumes of earth. The well should be pumped to equilibrium under at least two rates of flow so as to provide checks on the accuracy of the permeability determinations. The well pump should have sufficient capacity to lower the water level in the nearest observation well by at least 150 mm.

5.3.2 Field Method Based on Seepage Velocity

An approximate permeability of a coarse-grained soil may be obtained by measurement of the average seepage velocity between two observation wells, as is illustrated in Figure 5.6. Several methods are available for determining the flow velocity. An electrolyte can be placed in the upstream well and galvanometers can be used to detect the time required to pass a known distance through the soil. Radioactivated charges and geiger counters can be used to detect the time required for the charge to travel the distance between the wells. A third method involves placing a dye, such as fluorescein, into the upstream borehole and observing the time taken for it to emerge in a nearby test pit or on banks from which seepage is visible. The average seepage velocity v_e is given by dividing the length L between observation points by the time t required for travel between the two boreholes in Figure 5.6. The soil porosity n is determined for in-place soil conditions and the coefficient of permeability k is calculated:

$$k = v_e n / i \quad (5.15)$$

where $i = h/L$ is the hydraulic gradient. The low rate of groundwater movement should be considered before using this method for determination of the coeffi-

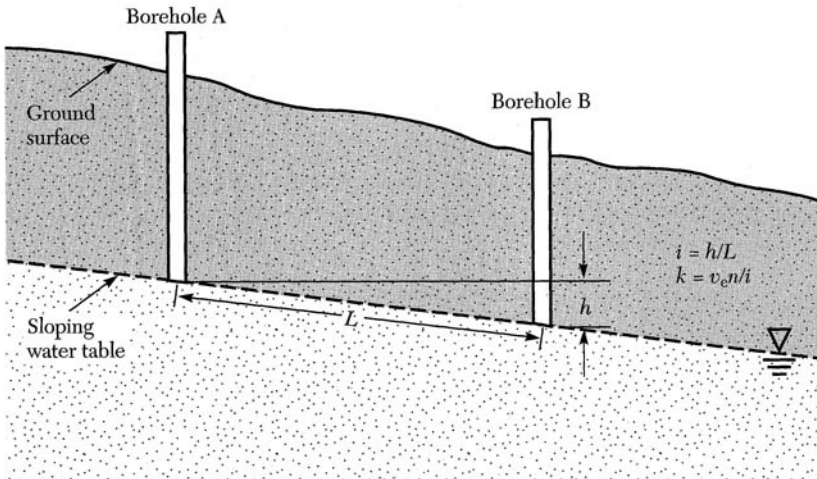


FIGURE 5.6 Permeability measurement based on seepage velocity between boreholes.

cient of permeability. The relationship between permeability, hydraulic gradient, and the rate of water movement through soil having a porosity of 25% is given in Table 5.2. Note that if water is flowing under a hydraulic gradient of 0.05 in a clean sand with a permeability of 10 m/day and a porosity of 25%, the seepage velocity is 2 m/day and the travel time for dye or other tracers is 12 h/m. These travel times place limitations on this field method for measurement of the coefficient of permeability.

5.3.3 Open-End Test for Field Permeability

Open-end tests are based on measuring the amount of water accepted by the ground through the bottom of a pipe or through an uncased section of the borehole. These tests require that clear water be used so that clogging of the soil pores by sediment does not occur. To prevent air from coming out of solution and forming bubbles in the soil pores, the temperature of the water should be higher than the groundwater temperature. The arrangements for testing through the open end of a borehole casing that has been placed to the desired depth and carefully cleaned out to the bottom of the casing are shown in Figure 5.7. The test is conducted by adding water through a measuring device while maintaining a constant head. For locations above the water table, it may be difficult to maintain a constant water level, and surging of a few tenths of a foot at a steady rate of flow for about 5 min is considered to represent an acceptable test by the Bureau of Reclamation. For soils with smaller permeabilities, an additional pressure may be added to the gravity head, as is illustrated in Figure 5.7c and d.

Required data include the flow rate q into the hole, the differential head h , and the internal radius r of the casing. Based on electric-analogy experiments, the

TABLE 5.2 Relationship between Rate of Groundwater Movement and the Coefficient of Permeability (soil porosity $n = 25\%$)

| Coefficient of Permeability, k | | Hydraulic Gradient, i | Seepage Velocity, v_e | Time to Move One Meter | |
|----------------------------------|--------|-------------------------|-------------------------|------------------------|------|
| m/day | cm/s | | | (m/day) | Days |
| 100 | 0.12 | 0.01 | 4 | | 6 |
| | | 0.02 | 8 | | 3 |
| | | 0.05 | 20 | | 1.2 |
| | | 0.10 | 40 | | 0.6 |
| 10 | 0.012 | 0.01 | 0.4 | 2.5 | 60 |
| | | 0.02 | 0.8 | 1.25 | 30 |
| | | 0.05 | 2.0 | 0.50 | 12 |
| | | 0.10 | 4.0 | 0.17 | 4 |
| 1 | 0.0012 | 0.01 | 0.04 | 25 | 600 |
| | | 0.02 | 0.08 | 12.5 | 300 |
| | | 0.05 | 0.20 | 5.0 | 120 |
| | | 0.10 | 0.40 | 2.5 | 60 |

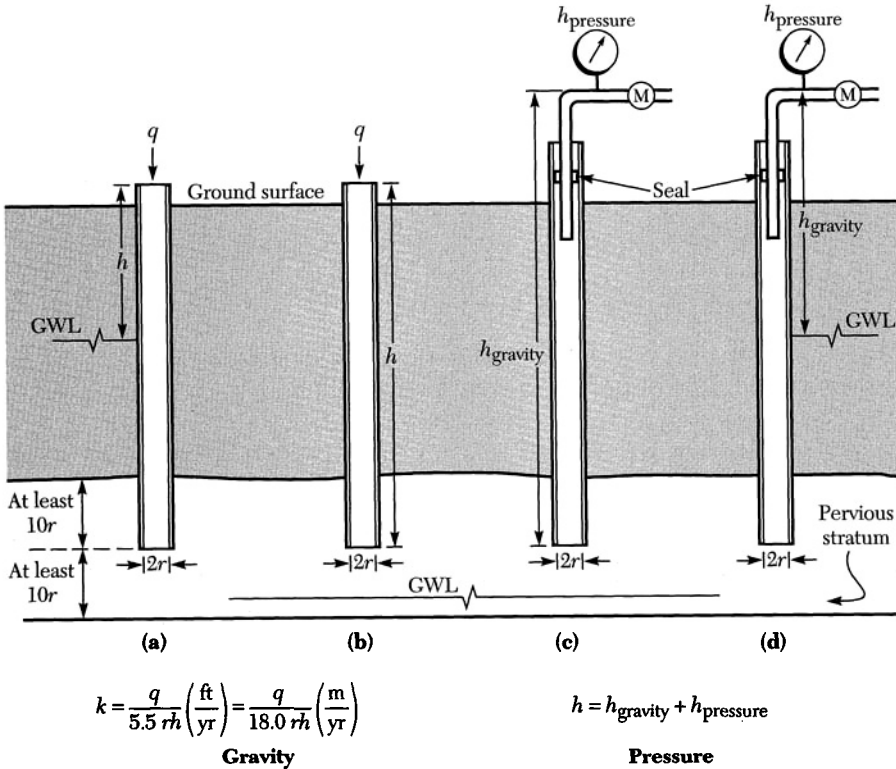


FIGURE 5.7 Open-end field permeability test. (After U.S. Bureau of Reclamation, 1965.)

permeability is computed as

$$k = \frac{q}{5.5 rh} (\text{ft/yr}) = \frac{q}{18 rh} (\text{m/yr}) \tag{5.16}$$

For convenience, the Bureau of Reclamation writes Eq. (5.16) as:

$$k (\text{ft/yr}) = \frac{C_1 q (\text{gal/min})}{h (\text{ft})} \tag{5.17}$$

where values for C_1 vary with casing size and are given in Table 5.3. For gravity tests made below the water table (Figure 5.7) the value for h is the difference in elevation between the water level in the casing and the groundwater level. Above the water table, h is the depth of water in the borehole. For the pressure tests illustrated in Figure 5.7 the applied pressure (1 psi = 2.3 ft or 1 kPa = 0.10 m) is added to the gravity head. Care must be used in all borehole tests so that excessive heads do not split the soil strata and cause high flow rates, giving erroneous permeabilities. A modification of the open-end test involves using packers in boreholes that will remain open. Packers are normally used when isolating a section of a hole when testing bedrock. Details are given in *Design of Small Dams* (U.S. Bureau of Reclamation, 1965).

TABLE 5.3 Values for C_1 in Eq. (5.17)

| Casing Size | C_1 |
|-------------|---------|
| EX | 204,000 |
| AX | 160,000 |
| BX | 129,000 |
| NX | 102,000 |

From Design of Small Dams. U.S. Bureau of Reclamation, 1965, p. 145.

5.4 HYDRAULIC HEADS IN SOIL

When dealing with fluid flow problems in soil, it is practical to express energy, both potential and kinetic, in terms of **head**, which is energy per unit of mass. The following three heads must be considered: *pressure head* (the pressure divided by the unit weight of fluid), *elevation head*, and *velocity head*. The evaluation of forces that govern water movement through soil requires knowledge of the energy changes associated with such movement. Under hydrodynamic conditions, water flows through the soil pores in velocities proportional to the hydraulic gradient. This is described earlier in this chapter as Darcy's law. The most common causes of water flow are water addition due to rainfall, snow melt, or inflow, or water losses resulting from evaporation and outflow. In general, fluid flows are called *turbulent* or *laminar*. **Turbulent flow** results when fluid particles follow highly irregular paths and is accompanied by energy losses proportional to the square of flow velocity. **Laminar flow** results when fluid particles move in smooth, orderly streams accompanied by energy losses proportional to the flow velocity. Turbulent flow rarely occurs in soils (except in rock and coarse gravel deposits). In this section we shall limit our discussion to laminar flow of water through soil masses.

For steady-state fluid flow, Bernoulli gave the total head h as the sum of the pressure head h_p , elevation head h_e , and velocity head h_v . The head at a given point within a saturated soil medium refers to the energy associated with the water particle at that location. The head has dimensions of energy per unit weight of fluid, foot-pounds per pound, or as used in civil engineering, simply feet. Thus, at a given point, we have

$$h = h_p + h_e + h_v = \frac{u}{\gamma_w} + Z + \frac{v^2}{2g} = \text{constant} \quad (5.18)$$

The velocity head in Eq. (5.18) is often ignored when dealing with flow problems through soil. The justification can be made by recognizing that the velocity equals the product of the hydraulic gradient and the coefficient of permeability. Assuming the largest possible value for the coefficient of permeability of soil (3.0 ft/s) and for the hydraulic gradient expected in laminar flow (1.0), gives

$$h_v = \frac{v^2}{2g} = \frac{(ki)^2}{2g} = \frac{(3 \text{ ft/s} \times 1.0)^2}{2(32.2 \text{ ft/s}^2)} = 0.14 \text{ ft}$$

For most soils encountered in practice, the velocity head is significantly smaller than 0.1 ft. This head is far less than the accuracy with which engineers can measure pressure head or elevation head. Engineers dealing with pipe and channel flow define total head as velocity head + pressure head + elevation head; and they define piezometric head as pressure head + elevation head. For flow through soil with its negligible velocity head, the total head and piezometric head are equal. Clearly, the velocity head is extremely small when compared with expected elevation and pressure heads in the field. Hence, it can be ignored. Equation (5.18) is simplified when dealing with fluid flow through soil as follows:

$$h = h_p + h_e = \frac{u}{\gamma_w} + Z \quad (5.19)$$

Equation (5.19) is not valid for problems involving fluid flow through open channels. The meaning of this equation can be best described by considering the soil profile in Figure 5.8. In this case, the total heads at points A and B are determined by establishing an arbitrary datum and measuring the elevations of the two points in question. The pressure heads are illustrated graphically as the water height in the two standpipes above points A and B. Flow between any two points depends only on the difference in total head. Any elevation can be selected as a base of elevation heads. That is, the absolute magnitude of elevation head has little meaning, because it is the difference in elevation head and not the actual elevation head that is of interest, and the difference of elevation head between any two points is the same regardless of where the datum is taken.

In general, it is more appropriate to first determine the elevation and total heads and then compute the desired pressure head by subtracting the elevation head from the total head. The elevation head is the elevation of the water at any point under consideration measured from the datum. At the water surface, the to-

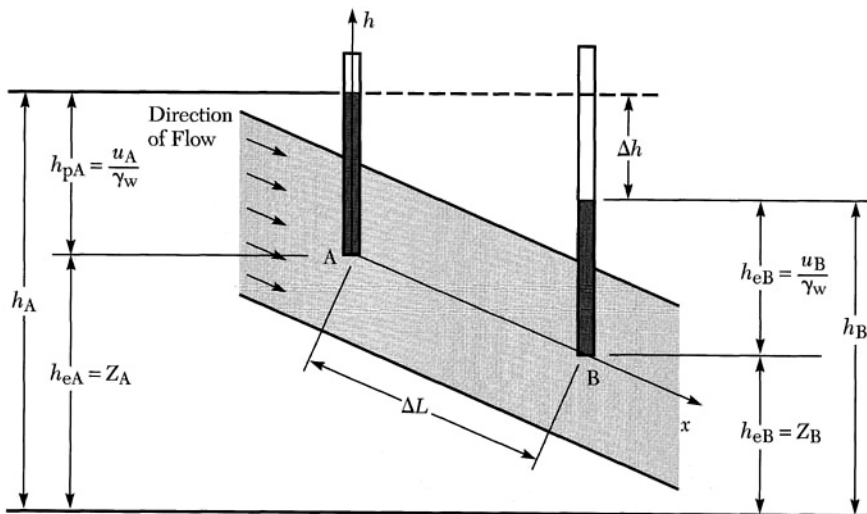


FIGURE 5.8 Graphical illustration of the total head concept.

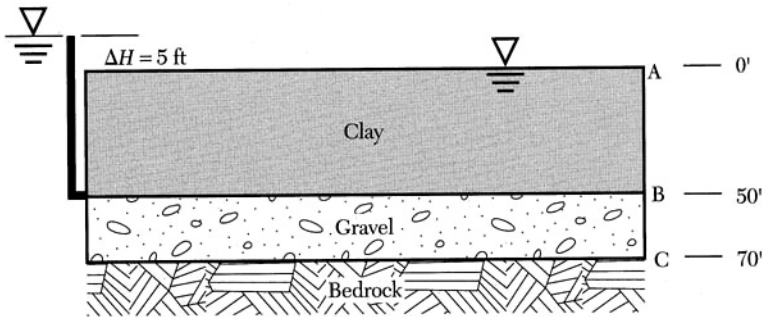


FIGURE 5.9 A soil profile involving a confined aquifer.

tal head is the elevation head, because the pressure head is zero. This concept can be demonstrated graphically for homogeneous and isotropic soils as shown in Figure 5.9.

To draw the elevation head, total head, and pressure head lines for the soil profile, let us assume datum at bedrock. The elevation heads at points A, B, and C are 0 ft, 20 ft, and 70 ft respectively. The total heads at points A, B, and C are $h_A = 70$ ft, $h_B = 70 + 5 = 75$ ft, $h_C = 70 + 5 = 75$ ft. There is a net difference of 5 ft between points A and B, which causes water to flow from point B to A. This is because point B has a higher potential than point A. This difference in head, $\Delta H = 5$, is lost totally in the clay layer. Otherwise the water level at point A would be higher than is shown in Figure 5.9. Note that because points B and C have the same total head, there is no water flow between them. The heads at each point are summarized in Table 5.4. These values are consistent with the information provided and can be illustrated graphically for the entire soil profile as shown in Figure 5.10. The hydraulic gradient within the clay layer is computed as $i = \Delta H/L = 5/50 = 0.10$. This example of flow through porous media illustrates that the *direction of flow is determined by total head difference*. In summary, there are three heads of interest to the geotechnical engineer:

1. *Elevation head*: Its absolute magnitude depends on the location of the datum.
2. *Pressure head*: The pressure head magnitude is of considerable importance, because it indicates the actual pressure in the water. The pressure head is the height to which the water rises in the piezometer above the point under consideration.

TABLE 5.4 Heads for the Aquifer Shown in Figure 5.9

| Point | Elevation Head (ft) | Total Head (ft) | Pressure Head (ft) |
|-------|---------------------|---------------------|-------------------------|
| A | $h_{eA} = 70$ | $h_A = 70$ | $h_{pA} = 70 - 70 = 0$ |
| B | $h_{eB} = 20$ | $h_B = 70 + 5 = 75$ | $h_{pB} = 75 - 20 = 55$ |
| C | $h_{eC} = 0$ | $h_C = 70 + 5 = 75$ | $h_{pC} = 75 - 0 = 75$ |

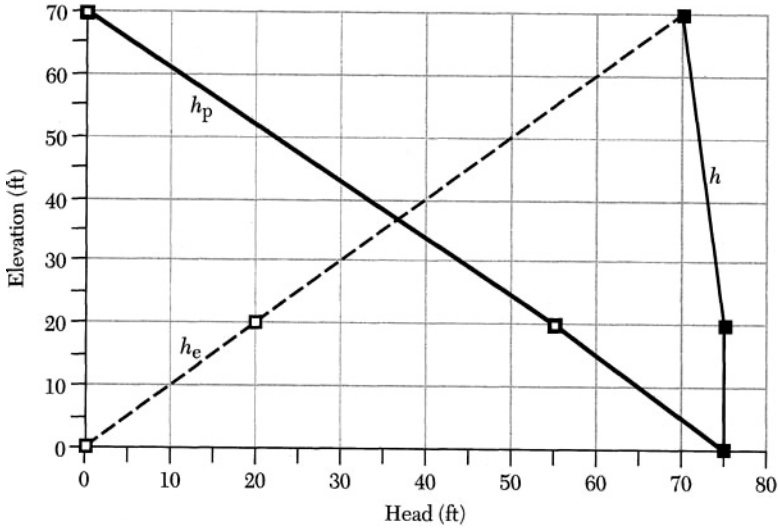


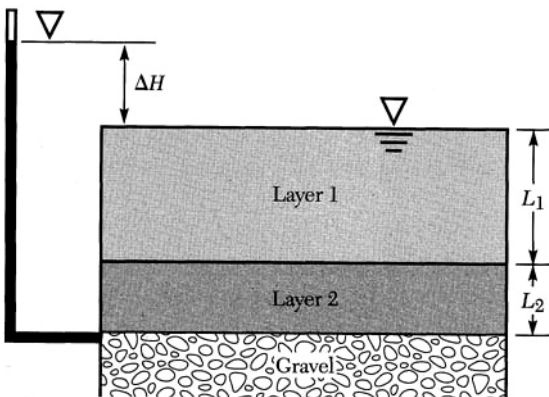
FIGURE 5.10 Graphical representation of the heads for the soil described in Figure 5.9.

3. **Total head:** The total head is the sum of the elevation and pressure heads and is the only head that determines flow and its direction. The total head is used in Darcy's law to compute gradient.

It is the total head difference between two points that determines the gradient to be used in Darcy's law. This concept is valid for one-dimensional as well as two-dimensional flow problems.

EXAMPLE 5.1

Determine the total head loss in each of the soil layers shown in the following figure. Assume that the coefficients of permeability are given as k_1 and k_2 for layers 1 and 2 respectively.



Solution

Denote the total head loss through layer 1 as Δh_1 and that through layer 2 as Δh_2 . The total head loss is then given as the sum of the head losses in each of the two layers. That is

$$\Delta H = \Delta h_1 + \Delta h_2 \quad (\text{a})$$

Because the rate of seepage is the same for layers 1 and 2, then

$$q_1 = q_2$$

or more explicitly,

$$k_1 \frac{\Delta h_1}{L_1} A_1 = k_2 \frac{\Delta h_2}{L_2} A_2 \quad (\text{b})$$

For a unit area, Eq. (b) is simplified to give

$$k_1 \frac{\Delta h_1}{L_1} = k_2 \frac{\Delta h_2}{L_2} \quad (\text{c})$$

Solving Eqs. (a) and (c) for the head loss in each of the two layers gives

$$\Delta h_1 = \frac{\alpha \Delta H}{1 + \alpha} \quad (\text{d})$$

$$\Delta h_2 = \frac{\Delta H}{1 + \alpha} \quad (\text{e})$$

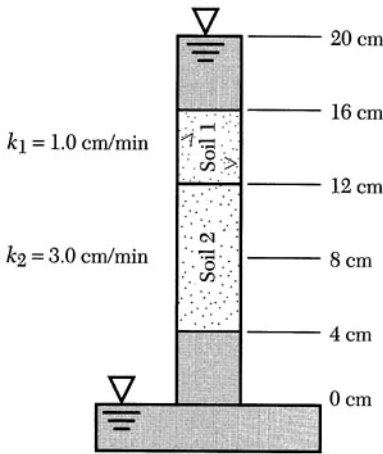
where

$$\alpha = \frac{k_2 L_1}{k_1 L_2} \quad (\text{f})$$

Note that Eqs. (d), (e), and (f) can be derived for problems involving more than two soil layers using the same approach. ■

EXAMPLE 5.2

Consider the following permeameter, then determine the total, elevation, and pressure heads respectively along its elevation. Plot your results.



Solution

Although there is no best way to handle problems of this type, it is always a good idea to follow some specific methodology. In this case, follow the steps outlined below:

Step 1: Establish a datum (reference) at elevation 0 cm, then determine the total head difference. In this case

$$\Delta H = 20 - 0 = 20 \text{ cm}$$

Step 2: Determine the total head loss in layer 1 and layer 2 using results from the preceding example.

$$\alpha = \frac{k_2 L_1}{k_1 L_2} = \frac{3.0 \left(\frac{4}{8} \right)}{1.0} = 1.5$$

$$\Delta h_1 = \frac{\alpha \Delta H}{1 + \alpha} = \frac{1.5(20)}{1 + 1.5} = 12 \text{ cm} \quad \Delta h_2 = \frac{\Delta H}{1 + \alpha} = \frac{(20)}{1 + 1.5} = 8 \text{ cm}$$

Step 3: Determine the elevation head versus height.

Step 4: Determine the total head at elevation 20 cm, 16 cm, 12 cm, 4 cm, and 0 cm. This is because at these elevations the total head is known. Thus

$$h_{20} = h_{e20} + h_{p20} = 20 + 0 = 20 \text{ cm}$$

$$h_{16} = h_{e16} + h_{p16} = 16 + 4 = 20 \text{ cm}$$

$$h_{12} = h_{16} - \Delta h_1 = 20 - 12 = 8 \text{ cm}$$

$$h_4 = h_{12} - \Delta h_2 = 8 - 8 = 0 \text{ cm}$$

$$h_0 = h_{e0} + h_{p0} = 0 + 0 = 0 \text{ cm}$$

Note that head loss occurs only when water flows through soil.

Step 5: Plot the total and elevation heads, then determine the pressure head as

follows:

$$h_{p20} = h_{20} - h_{e20} = 20 - 20 = 0 \text{ cm}$$

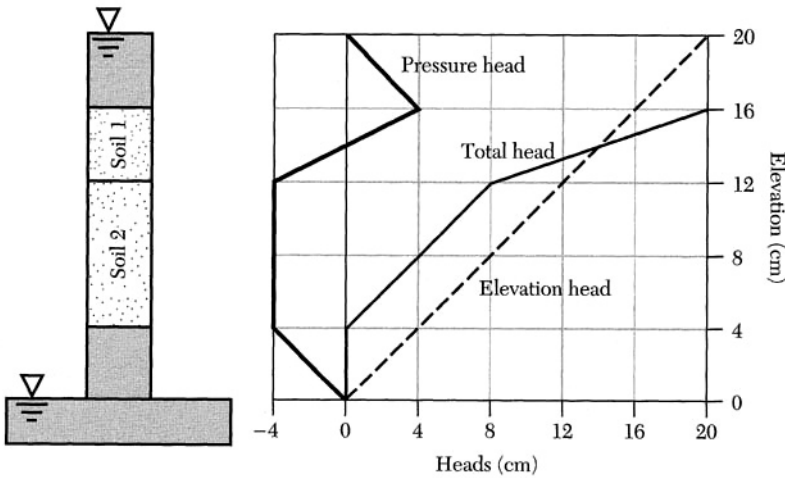
$$h_{p16} = h_{16} - h_{e16} = 20 - 16 = 4 \text{ cm}$$

$$h_{p12} = h_{12} - h_{e12} = 8 - 12 = -4 \text{ cm}$$

$$h_{p4} = h_4 - h_{e4} = 0 - 4 = -4 \text{ cm}$$

$$h_{p0} = h_0 - h_{e0} = 0 - 0 = 0 \text{ cm}$$

The pore water pressure at any elevation can be calculated by multiplying the unit weight of water by the pressure head at that elevation. That is, $u = h_p \gamma_w$. The total head, elevation head, and pressure head versus elevation are shown in the following figure:



Note that the pressure head could be negative. This phenomenon is of theoretical and practical importance. This is especially true when dealing with capillary rise and effective stress. ■

Geotechnical engineers are especially interested in the pressure head because the pore water pressure needed to study soil behavior depends on it. The pressure head at a point can be measured directly or can be computed using principles of fluid mechanics. For most practical problems, the soil in question is non-homogeneous and anisotropic. Consequently, field tests are normally required to determine actual pressure head values. The pressure head or water pressure at a point in the field is determined using a **piezometer**, a word literally meaning “pressure meter.”

5.5 BASIC EQUATION FOR FLUID FLOW IN SOIL

Generally, there are four types of flow problems encountered by geotechnical engineers. These can be explained using the void ratio e and the degree of saturation S_r for a typical soil element. The four flow problems are (1) e and S both constant; (2) e varies and S constant; (3) e constant and S varies; and (4) e and S both vary. Type 1 is *steady flow*, and Types 2, 3, and 4 are *nonsteady flow* situations. Problems of Type 1 involve determination of the amount and rate of fluid flow through semi-infinite saturated soil media under steady-state conditions. The derivation of a mathematical model needed for solving these problems is made possible by **finite element** analysis — considering a soil cube with a volume of $\Delta x \Delta y \Delta z$ as shown in Figure 5.11.

The inflow and the outflow velocities are given for the cube as shown in Figure 5.12. For a saturated incompressible medium and fluid, the quantity of water inflow and outflow per unit time must be equal. That is,

$$Q_{in} = Q_{out}$$

$$v_x \Delta y \Delta z + v_y \Delta x \Delta z + v_z \Delta x \Delta y =$$

$$\left(v_x + \frac{\partial v_x}{\partial x} \Delta x \right) \Delta y \Delta z + \left(v_y + \frac{\partial v_y}{\partial y} \Delta y \right) \Delta x \Delta z + \left(v_z + \frac{\partial v_z}{\partial z} \Delta z \right) \Delta x \Delta y$$

Simplifying and rearranging gives

$$\frac{\partial v_x}{\partial x} + \frac{\partial v_y}{\partial y} + \frac{\partial v_z}{\partial z} = 0 \tag{5.20}$$

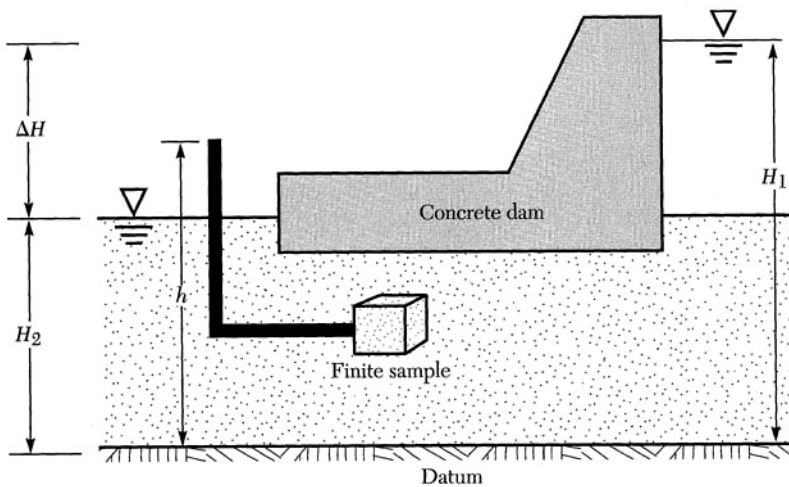


FIGURE 5.11 Cross section of a concrete dam showing a cubic soil element.

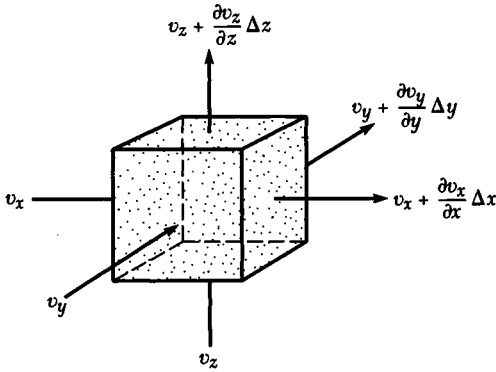


FIGURE 5.12 A saturated cubic soil element showing inflow and outflow velocities. Note that the element dimensions are Δx , Δy , and Δz .

The velocity in a given direction is directly proportional to the hydraulic gradient and the coefficient of permeability in that direction (Darcy's law). That is

$$v_x = k_x \frac{\partial h}{\partial x}$$

$$v_y = k_y \frac{\partial h}{\partial y}$$

$$v_z = k_z \frac{\partial h}{\partial z}$$

Substituting these velocity expressions into Eq. (5.20) gives

$$\frac{\partial}{\partial x} \left(k_x \frac{\partial h}{\partial x} \right) + \frac{\partial}{\partial y} \left(k_y \frac{\partial h}{\partial y} \right) + \frac{\partial}{\partial z} \left(k_z \frac{\partial h}{\partial z} \right) = 0 \quad (5.21)$$

Now, assume that k_x , k_y , and k_z are constant, then Eq. (5.21) can be simplified to give the well-known Laplace's equation for steady-state fluid flow:

$$k_x \frac{\partial^2 h}{\partial x^2} + k_y \frac{\partial^2 h}{\partial y^2} + k_z \frac{\partial^2 h}{\partial z^2} = 0 \quad (5.22)$$

Equation (5.22) can be simplified further by assuming the soil to be isotropic. That is, the coefficient of permeability is the same in all directions. Hence, one can write

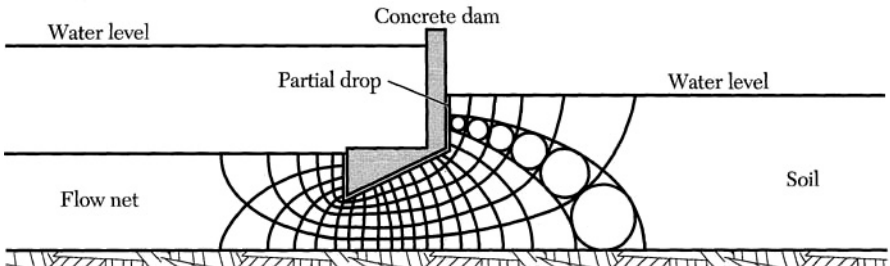
$$\frac{\partial^2 h}{\partial x^2} + \frac{\partial^2 h}{\partial y^2} + \frac{\partial^2 h}{\partial z^2} = 0 \quad (5.23)$$

Most problems involving fluid flow through soil masses are solved using a two-dimensional model rather than the three-dimensional model given by Eq. (5.23).

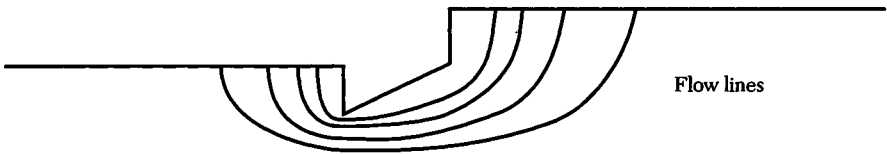
That is,

$$\frac{\partial^2 h}{\partial x^2} + \frac{\partial^2 h}{\partial y^2} = 0 \tag{5.24}$$

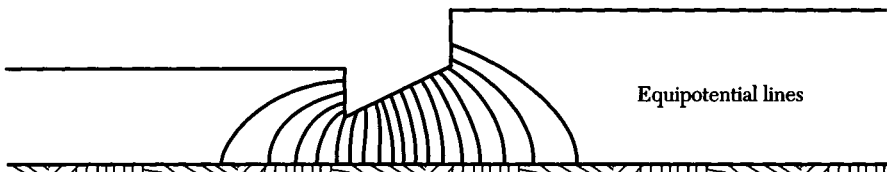
The solution of Laplace’s equation involves two families of curves intersecting at right angles. One family is termed **flow lines**, which represent the paths taken by moving molecules of water. The other family is termed **equipotential lines** or **piezometric lines**, which are lines that indicate points of equal total head. The pattern of flow lines and equipotential lines is called a **flow net**. A typical solution is shown in Figure 5.13. This solution was achieved using a finite element computer program. It shows that the flow net is composed of curvilinear squares in which circles can be drawn to touch each side at one node. That is, the equipotential lines and flow lines are orthogonal. Integration of Eq. (5.24) can be accomplished mathematically for only a few simple cases. Recently, numerical solutions



The flow net and corresponding cross section of a concrete dam with an inclined base.



Flow lines tracing the paths water will follow from one side of the dam to the other.



Lines describing equal total head h under hydrodynamic conditions.

FIGURE 5.13 Typical solution to Laplace’s equation for steady-state fluid flow.

have been used to solve this equation for a variety of practical problems. Generally, flow nets are constructed graphically, by trial and error.

EXAMPLE 5.3

Develop a mathematical expression for the total head for the soil profile shown in Figure 5.8 by directly integrating Laplace's equation for steady-state fluid flow.

Solution

This is a one-dimensional problem. Therefore, Eq. (5.30) is reduced to

$$\frac{\partial^2 h}{\partial x^2} = 0$$

Integrating twice gives

$$h = C_1 x + C_2 \quad (\text{a})$$

where C_1 and C_2 are constants of integration. These constants are determined using the following boundary conditions:

$$\text{at } x = 0 \quad h = h_A$$

$$\text{at } x = \Delta L \quad h = h_B$$

Substituting into Eq. (a) gives

$$h_A = 0 + C_2$$

$$h_B = C_1 \Delta L + C_2$$

Solving for C_1 and C_2

$$C_1 = \frac{h_B - h_A}{\Delta L}$$

$$C_2 = h_A$$

The solution is obtained by substituting C_1 and C_2 into Eq. (a) to give

$$h = \left(\frac{h_B - h_A}{\Delta L} \right) x + h_A$$

This is a simple linear relationship that could have been derived graphically by extending a straight line between the h_A and h_B values in Figure 5.8. ■

5.6 ANALYTICAL METHODS FOR SOLVING FLUID FLOW PROBLEMS

For two- and three-dimensional problems, a theoretical solution is complex, and in some cases is not possible. However, theoretical solutions have been realized for several flow problems. Unfortunately, these are limited in scope and appli-

cation. Complications arise from the presence of nonhomogeneous and/or anisotropic soils. Geometrical problems pertaining to the shapes of dams and impervious boundaries present additional difficulties in the attainment of useful solutions. The best-known theoretical solution is one for flow through an earth dam, which is generally referred to as *unconfined* flow. This solution was made by Kozeny in 1933. A. Casagrande has developed approximations to the Kozeny solution and has also made modifications to the Kozeny equation to account for flow that does not end in a horizontal drain, which is designed to collect seepage downstream.

5.6.1 Fluid Flow Models

Flow problems can be solved by constructing scaled models and analyzing flow patterns. Models are used extensively in engineering practice and serve a rather important purpose in testing the validity of theoretical solutions. The U.S. Waterways Experimental Station in Vicksburg, Mississippi, has some of the largest dam models in the world. Models are also useful to illustrate the fundamentals of fluid flow in a laboratory setting. Students can predict the rate of flow and the pore pressure at various locations in a dam and then compare predicted values with those measured in the model. For example, Figure 5.14 shows flow through a model of an earth dam used at Bradley University. The model consists of sand placed between parallel lucite plates. Steady flow is traced using dye lines. Piezometer tubes are used to determine water pressure and total heads.

Soil models are of limited use in the general solution of flow problems because of the time and effort required to construct them. The geotechnical engineer can sketch many flow nets and investigate the influence of various design features in a shorter period of time than it would take to construct one soil model. Models are also limited in terms of the effects of boundaries on the flow and equipotential lines. This is because the model has impervious boundaries upstream and downstream, whereas in the field such obstacles may not exist.

Laplace's equation for fluid flow also holds for steady-state electrical and heat flow. Although practical difficulties are encountered with heat flow models,

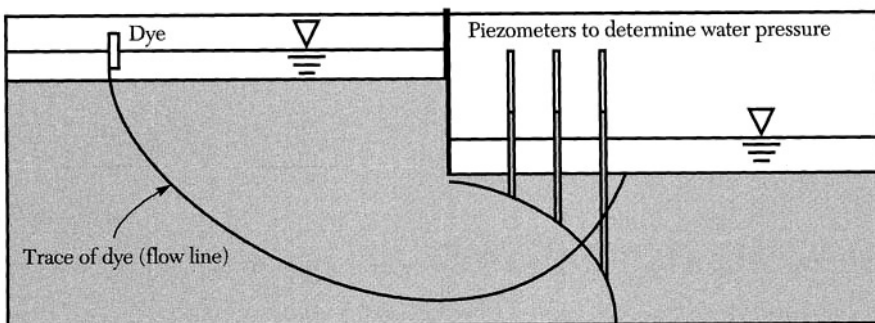


FIGURE 5.14 A typical fluid flow model.

electrical models have been used extensively. In the electrical model voltage corresponds to total head, conductivity to permeability, and current to velocity. Measuring voltage enables one to locate the equipotentials, which can then be used to sketch a flow pattern.

5.6.2 Numerical Methods

The flow net is a valuable tool in that it gives insight into the flow quantity, water pressure, and flow patterns. Laplace's flow equation can be solved numerically using the finite element and finite difference techniques. The advent of high-speed digital computers has greatly increased the use of numerical methods in solving fluid flow problems. Using computers, it is possible to solve and plot the results for many typical flow situations without introducing simplifying assumptions. The engineer can then get an approximate solution to practical problems. Although a complete treatment of this subject is beyond the scope of this textbook, a brief review of the finite difference method is outlined.

Other than the finite element method, the finite difference method is perhaps the main numerical technique employed in geotechnical engineering. This method has been used extensively in the solution of several engineering problems. Use of numerical solutions has been restricted in the past to research projects dealing with variations in soil compression properties (Barden and Berry, 1965), but recently, the numerical solution procedure has found increasing application in practice (Hansen and Nielson, 1965; Desi and Christian, 1977). The basic concept involves discretizing arbitrary continuous functions and replacing them with polynomials whose derivatives are used in approximating mathematical model behavior. The solution of Eq. (5.24) may be viewed as a surface in three-dimensional space. At a given node located at $x = x_j$, $y = y_j$ the surface is defined in terms of the two-dimensional function $h(x_j, y_j)$ as shown in Figure 5.15. Equation (5.24) is replaced with a finite difference formula, which permits direct evaluation of the to-

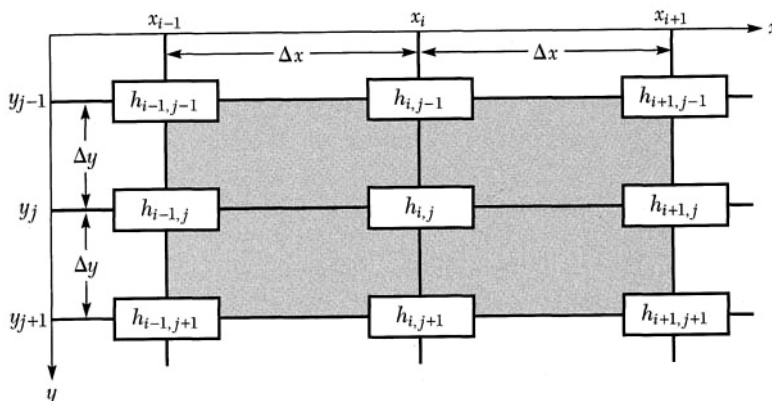


FIGURE 5.15 Schematic representation of the finite difference solution for Laplace's equation.

tal heads. Knowing the boundary head values, it is possible to calculate the heads at all points defined within the soil medium. The second derivative at an arbitrary node (x_i, y_i) can be approximated using a central derivatives approximation as follows (Al-Khafaji and Tooley, 1986):

$$\frac{\partial^2 h}{\partial x^2} \Big|_{x_i, y_j} = \frac{h_{i-1,j} - 2h_{i,j} + h_{i+1,j}}{(\Delta x)^2} \tag{5.25a}$$

$$\frac{\partial^2 h}{\partial y^2} \Big|_{x_i, y_j} = \frac{h_{i,j-1} - 2h_{i,j} + h_{i,j+1}}{(\Delta y)^2} \tag{5.25b}$$

Assuming $\Delta x = \Delta y$, then substituting Eq. (5.25) into (5.24) gives the desired difference formula. Thus

$$\frac{\partial^2 h}{\partial x^2} \Big|_{x_i, y_j} + \frac{\partial^2 h}{\partial y^2} \Big|_{x_i, y_j} = 0 = \frac{h_{i-1,j} - 2h_{i,j} + h_{i+1,j}}{(\Delta x)^2} + \frac{h_{i,j-1} - 2h_{i,j} + h_{i,j+1}}{(\Delta y)^2}$$

$$-4h_{i,j} + h_{i-1,j} + h_{i+1,j} + h_{i,j-1} + h_{i,j+1} = 0 = \begin{matrix} & & \boxed{1} & & \\ & & | & & \\ & & \boxed{-4} & & \\ & & | & & \\ \boxed{1} & & & & \boxed{1} \end{matrix} \tag{5.26}$$

The right-hand side of Eq. (5.26) represents the graphical equivalence of the left-hand side. The reader should be aware that although Δx does not appear in Eq. (5.26), the accuracy of the solution depends on the size of the increment used. The smaller Δx is, the higher the accuracy.

Total heads at various points within the soil medium can be approximated by placing Eq. (5.26) at each node where the total head is not known. This is accomplished by solving a system of linear algebraic equations. Consider Figure 5.16. Steps necessary for analyzing the cross-section shown using the finite difference method are as follows.

Step 1: Divide the cross section into a grid having $\Delta x = \Delta y = 25'$, then number the nodes. Make sure that the profile includes a distance of approximately $3D$ upstream and $3D$ downstream. This will insure that the hydraulic gra-

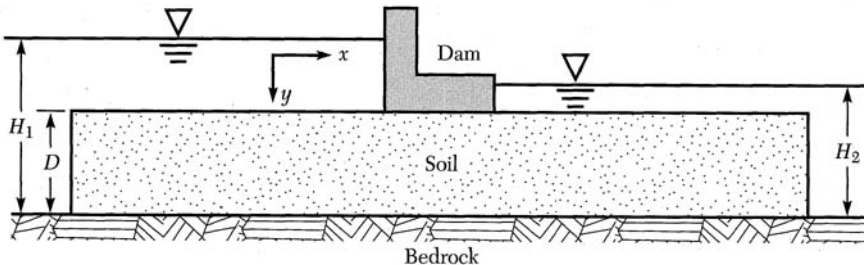
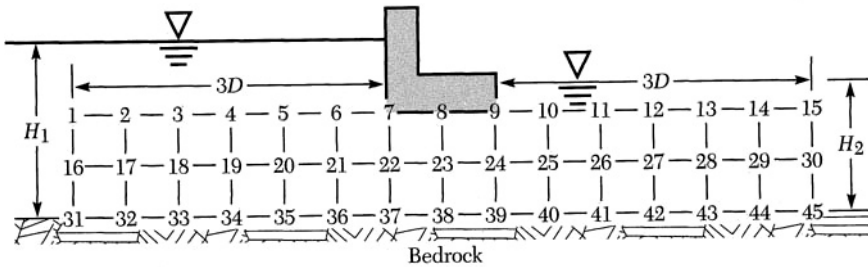


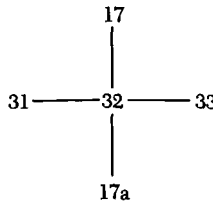
FIGURE 5.16 Typical cross section to be analyzed using the finite difference method.

5.6 ANALYTICAL METHODS FOR SOLVING FLUID FLOW PROBLEMS 159

gradient in the x -direction is zero. This implies that there is no flow. Otherwise, the solution will reflect a situation where there are impermeable boundaries at the left- and right-hand sides. This step is illustrated graphically as follows:



Step 2: Where possible, determine the head at the boundary points. That is, by establishing a datum at bedrock, the total head at nodes 1 through 6 is equal to H_1 . Also, the head at nodes 10 through 15 is equal to H_2 . Consequently, there is no need to place Eq. (5.26) at these nodes. Hence, the system of equations needed for the solution of this problem is reduced to 33 equations with 33 unknown heads. Although Eq. (5.26) can be applied directly at nodes 17 through 29, it must be modified at nodes underneath the dam (7, 8, and 9) and for nodes at bedrock. For example, nodes 32 through 44, Eq. (5.26), are modified as follows:



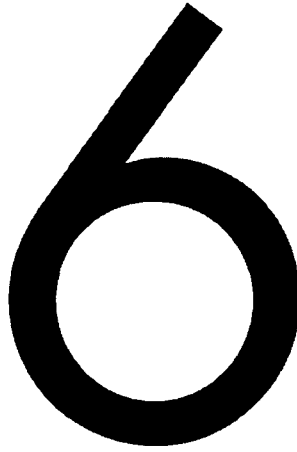
$$h_{31} - 4h_{32} + h_{17} + h_{17a} + h_{33} = 0$$

Note that $h_{17a} = h_{17}$ because the equipotential lines are expected to be perpendicular to bedrock. The equation is rewritten as

$$h_{31} - 4h_{32} + 2h_{17} + h_{33} = 0$$

Similar expressions are developed at nodes located underneath the dam. This is also true at nodes located at the LHS and the RHS of the grid.

- Step 3:** Solve the system of equations for the unknown heads.
- Step 4:** Draw contour lines having equal total heads. These are the equipotential lines.
- Step 5:** Draw the flow lines such that they intersect the equipotential lines at 90° angles. The resulting grid should result in curvilinear squares.



Stresses within a Soil Mass

6.0 INTRODUCTION

Stress imposed on soil due to its own weight or by structural loads is of primary importance to the geotechnical engineer. When a mass of soil is subjected to stresses, it undergoes changes in shape and volume. The changes in effective stresses are significant when dealing with cohesive soils and are less pronounced in cohesionless soils. The effective stress concept, first introduced by Terzaghi in 1920, is the foundation of geotechnical engineering. Terzaghi stated that all measurable effects of compression, distortion, and change in shearing resistance are attributable to changes in the effective stress.

The change in stress within soil masses due to point and line loads and regular and irregular loaded areas acting at the surface of or within soil masses is known as *stress distribution*. Generally, the state of stress within soil masses is of utmost importance in settlement and stability analysis. However, because of the influence of increase in vertical effective stress on consolidation settlement of clay layers, the increase in the vertical stress distribution is of primary importance.

The majority of theories for stress distribution within soil masses assume that the soil is homogeneous (i.e., of the same type), is linearly elastic and obeys Hooke's law, and is isotropic (i.e., properties of the soil are the same in all directions). The first assumption may be correct for soil layers, but not for entire lay-

ered soil profiles. The second assumption is incorrect in that actual soil behavior is nonlinear and inelastic. The third assumption is also incorrect because most soils are anisotropic. Their properties depend on the direction in which they are measured. This is primarily a result of the processes of soil formation and deposition. Fortunately, despite the discrepancies between assumed and actual soil behavior, predicted stress distributions agree reasonably well with observed values. It should be noted that the Principle of Superposition is valid for stress distribution problems. That is, the stress increase caused by any combination of loads can be determined by evaluating the stress increase caused by the individual loads acting separately and then adding them together.

6.1 THE EFFECTIVE STRESS CONCEPT

The reaction of soil masses and rocks to external and/or internal stress is a major factor used in the design of foundations, embankments, slopes, and earth retaining structures. Because soils are a three-phase system involving air, water, and solids, they do not behave in the same fashion as simple one-phase systems such as steel, wood, concrete, and so on. The solids are relatively incompressible and will support static shear stresses. Water is incompressible but offers only time-dependent (viscous) resistance to shear. The gaseous component of soil is compressible and offers no resistance to shear. Failure of a soil mass is governed by the way in which forces are distributed throughout the mass.

6.1.1 Effective Stress Calculation

The agents of force transmission are the soil grains and, in the case of saturated soils, the pore water. Consider a body of material subjected on its surface to a variety of forces, as shown in Figure 6.1. By passing a plane through the body, it is possible to determine the force ΔF acting on a finite area ΔA . The component of force acting in the direction normal to the plane is referred to as ΔF_n , and that in the direction tangent to the plane as ΔF_t . Now define the stress at a point as

$$\text{normal stress} = \sigma = \lim_{\Delta A \rightarrow 0} \frac{\Delta F_n}{\Delta A} \quad (6.1a)$$

$$\text{shear stress} = \tau = \lim_{\Delta A \rightarrow 0} \frac{\Delta F_t}{\Delta A} \quad (6.1b)$$

The implication of Eqs. (6.1) is that the area on which a force acts is reduced to zero. The concept of stress at a point is reduced to accepting the assumption that the smaller the area the smaller the force acting on it will be, and so the ratio of force to area will reach a limiting value. This is in fact a basic assumption of continuum mechanics. Although this concept may present no difficulty when dealing with single-phase materials such as steel, it does present a problem when dealing with soils. Consider Figure 6.2.

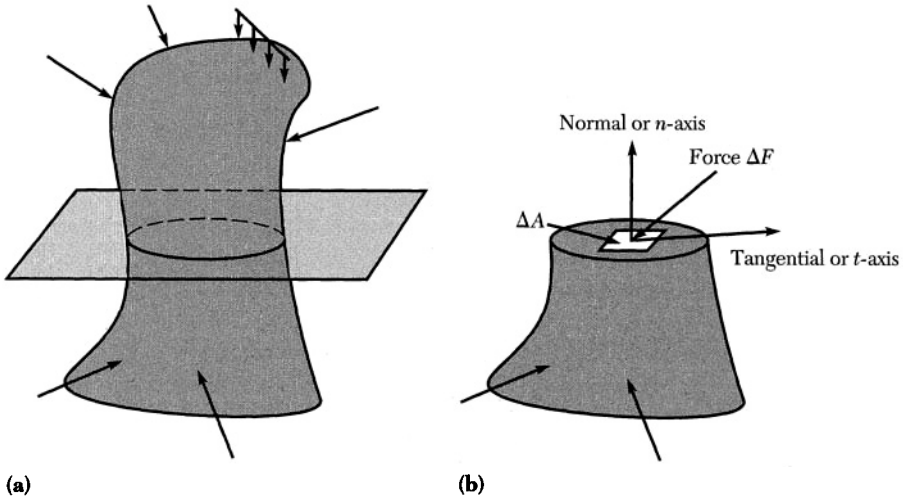


FIGURE 6.1 (a) Solid body subjected to external forces; (b) stress acting on a plane.

An apparently continuous area ΔA in Figure 6.2a is enlarged in Figure 6.2b to illustrate the concept of average stress. Here, it is not meaningless to suggest that stress at a point can actually be defined, the reason being that the force is applied to different grain sizes and voids. Figure 6.2c shows that the stress at a finite area ΔA is in fact an average value of the stress between grains and voids. Stress in a void is zero unless the void is filled with water. In soils that are multiphase systems, this effect is more pronounced than in some other engineering materials. Note that despite this difficulty, the definition of stress at a point within a soil mass is extremely useful. Just remember that it does not exist and that it is defined as an average value.

The presence or absence of water in soil voids is extremely important in the calculation of average normal stress at a point. Water can carry part of the load imposed on a soil before it is squeezed out of the pores. Consider a saturated soil sample subjected to external forces. If no flow is permitted into or out of the sample, then the water must carry part of the force applied in order for the soil volume to remain constant. This is true because soil solids and water are incompressible. Water cannot sustain shear forces but does carry normally applied

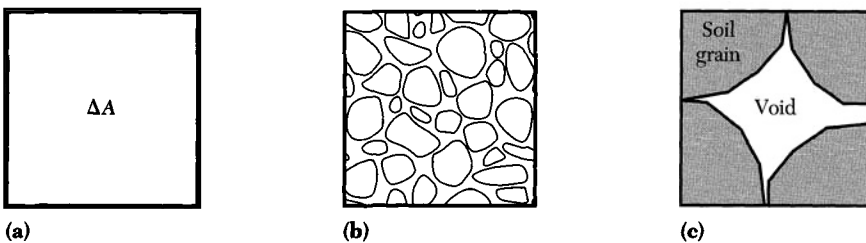


FIGURE 6.2 Stress at a point for soil.

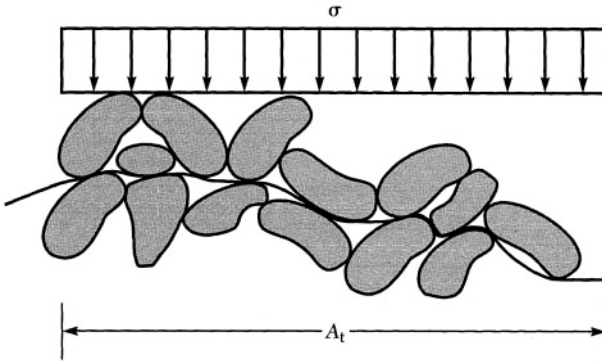


FIGURE 6.3 Side view of a saturated soil mass subjected to an average normal stress.

forces. If water carries some of the normal forces, then the soil skeleton carries less of the normal forces. This concept can be quantified by considering Figure 6.3.



Assume that the solid line shown in Figure 6.3 is a side view of a plane that passes between the soil solid particles rather than through them. Also, suppose that the plane is approximately horizontal, but is wavy, so that it will pass through areas of solid-to-solid contact and through void spaces filled with water. This is a good assumption in that soil particles are generally small when compared with a given soil deposit thickness. A top view of the plane is shown in Figure 6.4.

Now define the following plane related parameters.

A_t = the total horizontal projection of plane.

A_c = the horizontal projection of the contact area between soil solids lying in the plane.

A_w = the horizontal projection of portion of the plane that passes through water.

-  Horizontal projection of the portion of the plane that passes through water
-  Horizontal projection of the contact area between soil solids lying in the plane

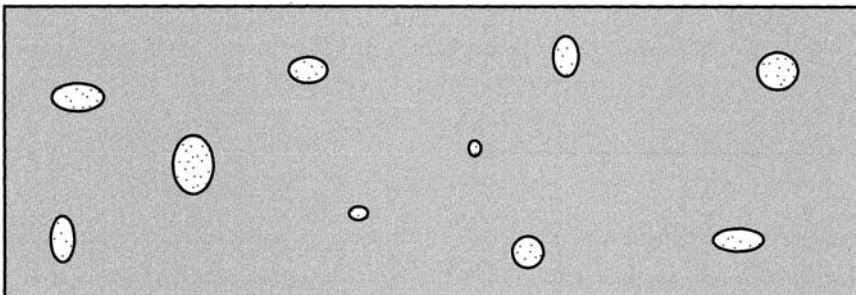


FIGURE 6.4 Top view of plane passing between soil solids within a saturated soil mass.

Using the basic principle of static equilibrium in the vertical direction (the sum of forces in the vertical direction is equal to zero), one can write

$$\Sigma F_n = 0 = \alpha A_t - \sigma^\circ A_c - uA_w \quad (6.2)$$

Where σ° is the average intergranular stress at points of contact and u is the pressure in the water. Because water occupies the pore spaces between the soil solids, this pressure is commonly referred to as the **pore pressure** or **pore water pressure**. Rearranging Eq. (6.2) and dividing by the total area A_t gives

$$\sigma = \sigma^\circ \frac{A_c}{A_t} + u \frac{A_w}{A_t} \quad (6.3)$$

Note that $A_t = A_c + A_w$; then substituting $A_w = A_t - A_c$ into Eq. (6.3) gives

$$\sigma = \sigma^\circ \frac{A_c}{A_t} + u \frac{A_t - A_c}{A_t} \quad (6.4)$$

Although A_c has been measured for a number of soils, its value is extremely small when compared with the total area. It can be assumed to be negligible. The implication is extremely significant in that the intergranular stress must be very large. The quantity $(\sigma^\circ A_c/A_t)$ is defined in terms of the total stress σ and the pore water pressure u . This is indeed what is referred to as **effective stress** $\bar{\sigma}$. Substituting $A_c = 0$ and $\bar{\sigma} = \sigma^\circ A_c/A_t$ into Eq. (6.4) gives the following important relationship.

$$\sigma = \bar{\sigma} + u \quad (6.5)$$

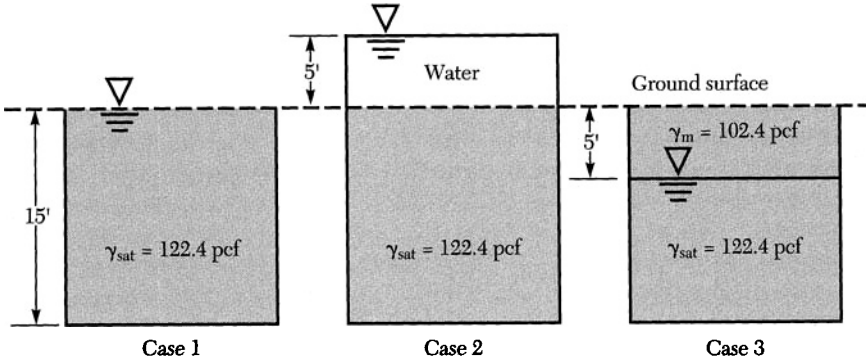
Equation (6.5) defines the *principle of effective stress* and was first developed by Terzaghi. Note that although the average effective normal stress is a fictitious quantity, it is extremely useful in settlement and stability analysis of structures and earth masses. Determination of effective stress for a given soil profile is made indirectly by first calculating the total stress σ , then subtracting the pore water pressure from it. The total stress at a given depth within a soil mass is calculated as the product of the total unit weight and depth. In the case of saturated soils the saturated unit weight is used, and in the case of dry soils the dry unit weight is used. Under hydrostatic conditions, the pore water pressure is calculated as the product of the unit weight of water and depth. The pore water pressure may exist at a higher or lower level than the hydrostatic value. This situation arises when there is flow and the water is said to be under *hydrodynamic conditions*. The principle of effective stress holds under both hydrostatic and hydrodynamic conditions. The pore water pressure is often expressed in a more general form as

$$u = u_{\text{hydrostatic}} + u_{\text{hydrodynamic}} = u_h + u_e \quad (6.6)$$

where u_h is the hydrostatic pore water pressure and u_e is the excess pore water pressure due to hydrodynamic conditions resulting from water flow. Equation (6.6) is important in solving seepage- and settlement-related problems.

EXAMPLE 6.1

Determine the average normal effective stress at the bottom of soil layers shown in the following three cases. Assume that the water table is under a hydrostatic condition (no flow). The unit weight of soil and the corresponding thickness are shown in the following figure.

**Solution****CASE 1**

Assuming that the unit weight of water is 62.4 pcf gives

$$\sigma = \gamma_{\text{sat}}Z = 122.4(15) = 1836 \text{ psf}$$

$$u = \gamma_w Z = 62.4(15) = 936 \text{ psf}$$

$$\bar{\sigma} = \sigma - u = 1836 - 936 = 900 \text{ psf}$$

CASE 2

$$\sigma = 5\gamma_w + 15\gamma_{\text{sat}} = 5(62.4) + 122.4(15) = 2148 \text{ psf}$$

$$u = 20\gamma_w = 20(62.4) = 1248 \text{ psf}$$

$$\bar{\sigma} = \sigma - u = 2148 - 1248 = 900 \text{ psf}$$

Note that although the total normal stress and pore water pressure changed due to rise of the water level above ground surface, the effective stress was unchanged from that of case 1.

CASE 3

$$\sigma = 5\gamma_d + 10\gamma_{\text{sat}} = 5(102.4) + 10(122.4) = 1736 \text{ psf}$$

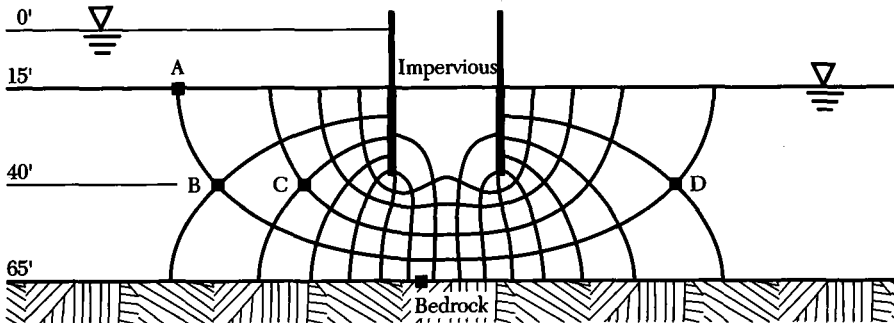
$$u = 10\gamma_w = 10(62.4) = 624 \text{ psf}$$

$$\bar{\sigma} = \sigma - u = 1736 - 624 = 1112 \text{ psf}$$

Note that the effective stress has increased 23.5% while both the total stress and the pore water pressure have decreased. This observation is important in that soil masses may settle or even fail due to lowering the water table. ■

EXAMPLE 6.2

Determine the effective overburden stress at points A, B, C, and D as shown in the following figure. Assume that the water is under a steady-state seepage condition (hydrodynamic). The saturated unit weight of the soil is 122.4 pcf and the elevations of each point are shown on the figure. Ignore the effects of sheet pile weight and assume datum at bedrock.

**Solution**

Consideration of the flow net reveals that there are 15 equipotential drops and the total head drop is 15 feet. The average drop in total head per equipotential drop $\Delta h = 15/15 = 1.0$ ft/drop. That is, in going from point A to point B the total head will drop by 1.0 ft. The total head and elevation head at each point can be used to calculate the pressure head, which permits determination of the effective stress as follows.

POINT A

$$\begin{aligned}
 h_A &= h_{eA} + h_{pA} \\
 h_{eA} &= 50 \text{ ft} \\
 h_{pA} &= \frac{u}{\gamma_w} = \frac{15(\gamma_w)}{\gamma_w} = 15 \text{ ft} \\
 h_A &= 50 + 15 = 65 \text{ ft} \\
 \sigma_A &= 62.4(15) = 936 \text{ psf} \\
 u_A &= 62.4(15) = 936 \text{ psf} \\
 \bar{\sigma}_A &= 936 - 936 = 0 \text{ psf}
 \end{aligned}$$

POINT B

Note that in this case the total head at point B is related to the total head at point A in that the total head at point B is 1.0 ft less than that at A. Now determine the total head at B using the elevation head and pressure head as was the case for point A.

$$\begin{aligned}
 h_B &= h_A - 1.0 = 65 - 1.0 = 64 \text{ ft} \\
 h_{eB} &= 25 \text{ ft} \\
 h_{pB} &= 64 - 25 = 39 \text{ ft} \\
 \sigma_B &= 62.4(15) + 122.4(25) = 3996 \text{ psf} \\
 u_B &= 62.4(39) = 2433.6 \text{ psf} \\
 \bar{\sigma}_B &= 3996 - 2433.6 = 1562.4 \text{ psf}
 \end{aligned}$$

POINT C

Although the elevation is the same at points B, C, and D, their corresponding total head is different. The total head at point C is 2.0 ft less than that at point A (why?).

$$\begin{aligned}
 h_C &= h_A - 2(1.0) = 65 - 2.0 = 63 \text{ ft} \\
 h_{eC} &= 25 \text{ ft} \\
 h_{pC} &= 63 - 25 = 38 \text{ ft} \\
 \sigma_C &= 3996 \text{ psf} \\
 u_C &= 62.4(38) = 2371.2 \text{ psf} \\
 \bar{\sigma}_C &= 3996 - 2371.2 = 1624.8 \text{ psf}
 \end{aligned}$$

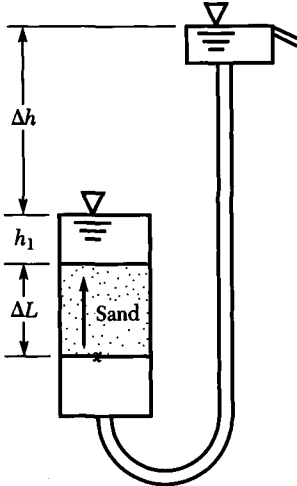
POINT D

$$\begin{aligned}
 h_D &= h_A - 14(1.0) = 65 - 14.0 = 51 \text{ ft} \\
 h_{eD} &= 25 \text{ ft} \\
 h_{pD} &= 51 - 25 = 26 \text{ ft} \\
 \sigma_D &= 25(122.4) = 3060 \text{ psf} \\
 u_D &= 62.4(26) = 1622.4 \text{ psf} \\
 \bar{\sigma}_D &= 3060 - 1622.4 = 1437.6 \text{ psf}
 \end{aligned}$$

Now assume that the water levels on both sides of the sheet piles (no flow) are equal and compute the effective stress at points B, C, and D as $25(60) = 1500$ psf. With flow, the effective overburden pressure is higher at points B and C but is lower at point D. ■

EXAMPLE 6.3

When dealing with flow through soils, engineers are required to assess the equilibrium of soil structures. In practice, a condition could develop whereby the effective overburden is reduced to zero. For a cohesionless soil subjected to a water condition that results into zero effective stress, the strength of the soil becomes zero. This causes what is called a *quick condition* to develop. Determine the height of water Δh necessary to cause a sand boil at point x.

Solution

For a quick condition to occur at point x , the effective stress must be reduced to zero. Applying the basic definition of stress at point x gives

$$\bar{\sigma}_x = \sigma_x - u_x = 0$$

where

$$\begin{aligned}\sigma_x &= \gamma_{\text{sat}} \Delta L + \gamma_w h_1 \\ u_x &= \gamma_w (\Delta h + h_1 + \Delta L)\end{aligned}$$

Substituting, then solving for Δh , gives

$$\Delta h = \frac{\gamma_{\text{sat}} - \gamma_w}{\gamma_w} \Delta L$$

Note that one can determine the **hydraulic gradient** as

$$i = \frac{\Delta h}{\Delta L} = \frac{\gamma_{\text{sat}} - \gamma_w}{\gamma_w}$$

Because a quick condition (sand boil) occurs when the effective stress is reduced to zero, this hydraulic gradient is called the **critical gradient**. That is

$$i_c = \frac{\gamma_{\text{sat}} - \gamma_w}{\gamma_w} = \frac{G_s - 1}{1 + e} \quad (6.7)$$

Careful examination of Eqs. (5.54) and (6.7) reveals that the critical gradient for soil is approximately equal to 1.0. This is because the saturated soil unit weight is approximately twice the unit weight of water. Safe design requires that the hydraulic gradient be kept below i_c . Note that the flow must be vertical and opposite in action to the soil unit weight. In any soil where strength is proportional to effective stress, an upward gradient of γ_b/γ_w will cause zero strength and a quick condition. ■

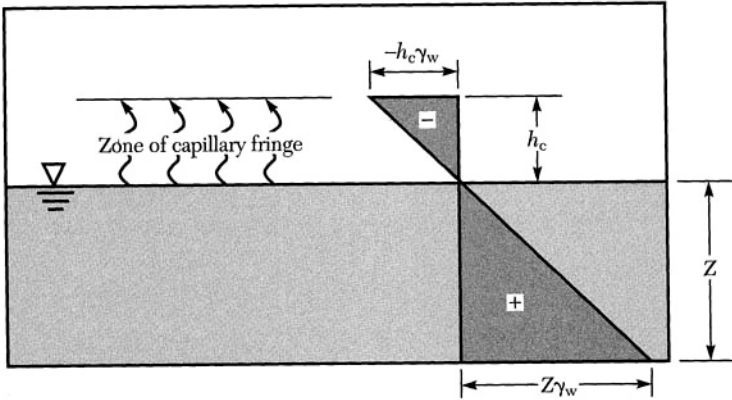


FIGURE 6.5 Capillary rise and corresponding pore water pressure.

6.1.2 Effective Stress Due to Capillary Rise

There is much documentation that a liquid surface resists tensile forces because of the attraction between adjacent molecules in the liquid surface. This attraction, or *surface tension*, is a constant property of any pure liquid at a given temperature. An example of this is shown by water which will rise and remain above the line of atmospheric pressure in a very fine bore or capillary tube (see Chapter 3). This concept is shown graphically in Figure 6.5.

Capillarity enables a dry soil to draw water to elevations above the free water line. The height of water a soil can support is called **capillary head** and is inversely proportional to the 10% finer. Capillary heads for several soils are shown in Table 6.1.

The height to which water rises due to capillarity defines a zone of saturation in which negative pore water pressure will develop. Once the h_c value has been estimated, the maximum pressure is readily estimated as

$$u = -h_c \gamma_w$$

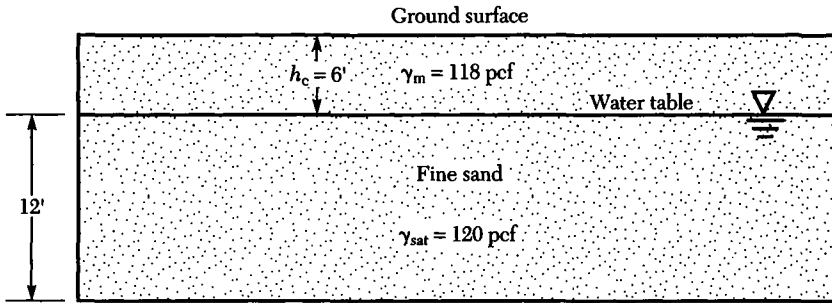
TABLE 6.1 Capillary Heads for Cohesionless Soils

| Soil | Particle Size D_{10} (mm) | Void Ratio | Capillary Head (cm) |
|---------------|--------------------------------|------------|------------------------|
| Coarse gravel | 0.82 | 0.27 | 6.0 |
| Sandy gravel | 0.20 | 0.45 | 28.0 |
| Fine gravel | 0.30 | 0.29 | 20.0 |
| Coarse sand | 0.11 | 0.27 | 60.0 |
| Medium sand | 0.02 | 0.57 | 120.0 |
| Fine sand | 0.03 | 0.36 | 112.0 |
| Silt | 0.006 | 0.94 | 180.0 |

where u is the pore water pressure in the zone of partial saturation and γ_w is the unit weight of water. Within the capillary zone, the effective stress will be greater than the total stress! This conclusion is consistent with Eq. (6.5). This pressure is responsible for preventing shallow vertical cuts in partially saturated fine sand deposits from collapsing. This pore water pressure is normally ignored when dealing with soils, because it is dependent on environmental factors that may change, such as rainfall or evaporation.

EXAMPLE 6.4

Determine the pore water pressure, the total stress, and the effective stress for the following fine sand soil deposit. Note that due to capillarity, water was first encountered at the ground surface (6 ft above the ground water table).



Solution

At depth = 0 ft

$$\sigma = 0$$

$$u = -h_c \gamma_w = -6(62.4) = -374.4 \text{ psf}$$

$$\bar{\sigma} = 0 - (-374.4) = 374.4 \text{ psf}$$

At depth = 6 ft

$$\sigma = 6(118) = 708 \text{ psf}$$

$$u = 0$$

$$\bar{\sigma} = 708 - 0 = 708 \text{ psf}$$

At depth = 18 ft

$$\sigma = 6(118) + 12(120) = 2148 \text{ psf}$$

$$u = 12(62.4) = 748.8 \text{ psf}$$

$$\bar{\sigma} = 2148 - 748.8 = 1399.2 \text{ psf}$$

Generally, fine sand and silt found above the ground water table owe their unconfined strength to capillary tension. Because of this strength, shallow excavations can often be made in such soils with relatively steep side slopes. ■

6.2 MOHR CIRCLE OF STRESS

The state of stress at a point within a solid medium is one of the fundamental concepts covered in courses dealing with mechanics of materials. In this section, these basic concepts are reviewed. Discussion is limited to the two-dimensional state of stress. The basic problem is to formulate relationships between the applied normal and shear stresses acting on a soil element and the resulting normal and shear stresses acting on an arbitrary plane passing through the soil element. Consider Figure 6.6b, which is a two-dimensional representation of a "small" element within a soil medium (Figure 6.6a). Stresses on two mutually perpendicular planes are shown. Assume that the element is sufficiently small so that the stresses can be considered uniform on each of the faces. To determine the stresses on a plane inclined at some angle θ to one face of the element, as shown in Figure 6.6b, static equilibrium requires that the sum of the forces (not stresses) in any direction must be equal to zero. Assuming an element with unit thickness, multiply each stress by the area over which it acts. This requirement can be satisfied in directions normal and parallel to the θ plane.

In most geotechnical engineering applications, the normal stresses are compressive. **Compressive stress** (stress that causes a body to compress in the direction in which the stress acts) is taken as positive and tensile stress as negative. Choose positive shear stress as that stress which creates a clockwise moment about a point just outside the element at the plane considered. Summing forces in the direction normal to the plane defined by θ gives

$$\sigma_{\theta} \left(\frac{\Delta x}{\cos \theta} \right) - \sigma_x (\Delta x \tan \theta) \sin \theta + \tau_{xy} (\Delta x \tan \theta) \cos \theta - \sigma_y (\Delta x) \cos \theta + \tau_{xy} (\Delta x) \sin \theta = 0$$

Solving for σ_{θ} gives

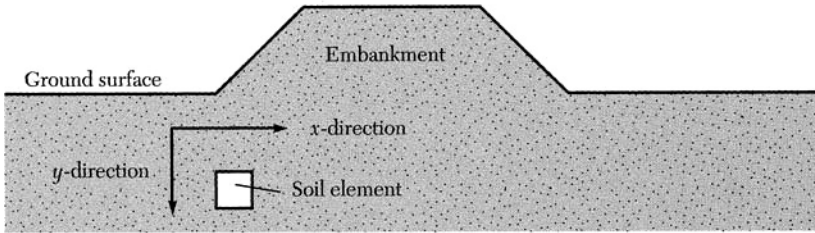
$$\sigma_{\theta} = \left(\frac{\sigma_y + \sigma_x}{2} \right) + \left(\frac{\sigma_y - \sigma_x}{2} \right) \cos 2\theta - \tau_{xy} \sin 2\theta \quad (6.8)$$

Summing forces in the direction of the plane defined by θ gives

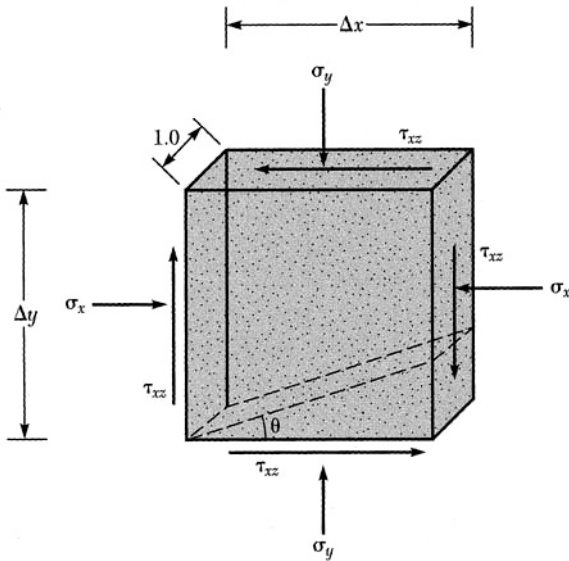
$$\tau_{\theta} \left(\frac{\Delta x}{\cos \theta} \right) + \sigma_x (\Delta x \tan \theta) \cos \theta + \tau_{xy} (\Delta x \tan \theta) \sin \theta - \sigma_y (\Delta x) \sin \theta - \tau_{xy} (\Delta x) \cos \theta = 0$$

Solving for τ_{θ} gives

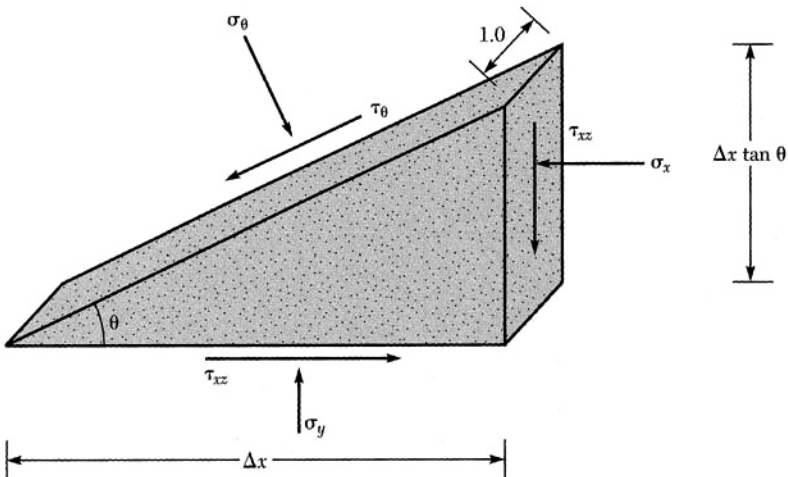
$$\tau_{\theta} = \left(\frac{\sigma_y - \sigma_x}{2} \right) \sin 2\theta + \tau_{xy} \cos 2\theta \quad (6.9)$$



(a) Soil profile



(b) Soil element



(c) Stress on inclined surface

FIGURE 6.6 Stress at a point within a soil mass.

Eqs. (6.8) and (6.9) can be combined by squaring and adding the following terms

$$\left[\sigma_\theta - \left(\frac{\sigma_y + \sigma_x}{2} \right) \right]^2 + \tau_\theta^2 = \left(\frac{\sigma_y - \sigma_x}{2} \right)^2 + \tau_{xy}^2 \quad (6.10)$$

This is the equation of a circle and is referred to as the **Mohr circle**. Eq. (6.10) has the following characteristics.

The circle center is located at

$$\sigma = \frac{(\sigma_y + \sigma_x)}{2} \quad \text{with} \quad \tau = 0$$

and the circle radius is

$$r = \sqrt{\left(\frac{\sigma_y - \sigma_x}{2} \right)^2 + \tau_{xy}^2}$$

Assuming $\sigma_y > \sigma_x$ permits Eq. (6.10) to be shown graphically as in Figure 6.7. The angle 2θ is the counterclockwise angle between the radius vector to point (σ_y, τ_{xy}) and the radius vector to point $(\sigma_\theta, \tau_\theta)$. Note that there are always two planes where no shear stress exists. These directions are referred to as the **principal planes** and the normal stresses acting on them as **principal stresses**. The major principal stress is defined by σ_1 and the minor principal stress by σ_3 . Consideration of Figure 6.7 reveals that the magnitudes of the major and minor principal stresses

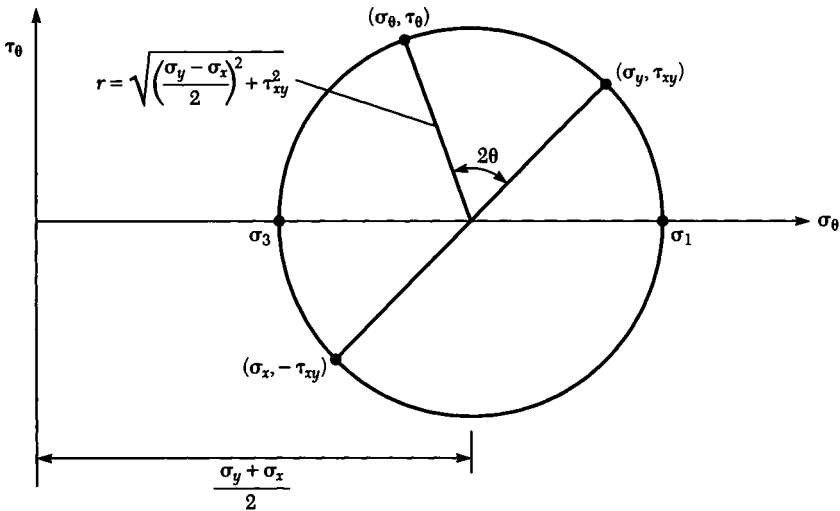


FIGURE 6.7 Mohr circle showing the state of stress on a soil element.

can be determined analytically as

$$\sigma_1 = \left(\frac{\sigma_y + \sigma_x}{2} \right) + \sqrt{\left(\frac{\sigma_y - \sigma_x}{2} \right)^2 + \tau_{xy}^2} \quad (6.11a)$$

$$\sigma_3 = \left(\frac{\sigma_y + \sigma_x}{2} \right) - \sqrt{\left(\frac{\sigma_y - \sigma_x}{2} \right)^2 + \tau_{xy}^2} \quad (6.11b)$$

The principal plane can be determined by sustaining $\tau_\theta = 0$ into Eq. (6.9), then solving for the angle θ . This gives

$$\theta = \frac{1}{2} \tan^{-1} \left(\frac{2\tau_{xy}}{\sigma_y - \sigma_x} \right) \quad (6.12)$$

For the special case where the x - and y -directions are themselves principal directions (only normal stresses exist with zero shear stress), the normal and shear stresses acting on a plane defined by θ are given as

$$\sigma_\theta = \left(\frac{\sigma_1 + \sigma_3}{2} \right) + \left(\frac{\sigma_1 - \sigma_3}{2} \right) \cos 2\theta \quad (6.13a)$$

$$\tau_\theta = \left(\frac{\sigma_1 - \sigma_3}{2} \right) \sin 2\theta \quad (6.13b)$$

where the angle 2θ is measured counterclockwise from the direction of the major principal stress ($\sigma_1, 0$) to the radius vector at $(\sigma_\theta, \tau_\theta)$. Note that the maximum shear stress will always be equal to the radius of the Mohr circle. That is, $\tau_{\max} = (\sigma_1 - \sigma_3)/2$. Knowing the state of stress on any two planes and their orientation permits construction of the Mohr circle shown in Figure 6.7. This circle makes it possible to graphically determine the stresses on planes passing through the same point with any other orientation.

6.3 THE POLE METHOD OF STRESS COMPUTATION

An especially useful point on the Mohr circle is called the *pole* or *origin of planes*. This point, normally designated by the symbol p , is rather unique in that any line drawn through it will intersect the circle at a point representing the state of stress on a plane inclined at the same angle as that of the line. The pole can be found if the major and minor principal stresses and their directions are known. Alternatively, it can be found if the stresses on any two planes and their orientations are known. The validity of the pole can be demonstrated graphically by considering Figure 6.8. In this figure, the stresses acting on two arbitrary planes inclined at α and β through a soil element are known. The corresponding Mohr circle is shown in Figure 6.9. In this case the state of stress acting on the plane inclined at an an-

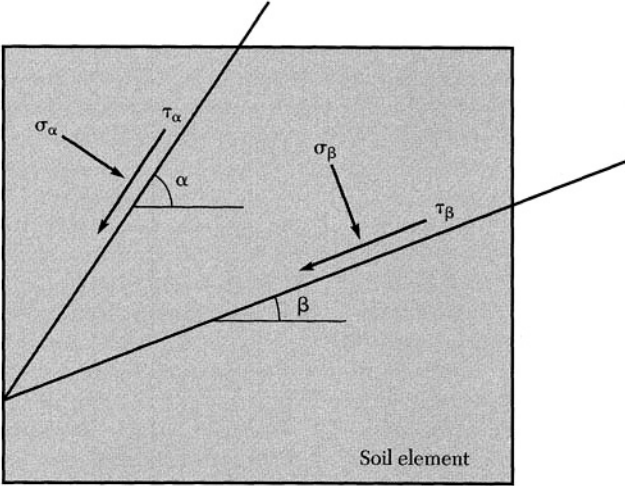


FIGURE 6.8 Stresses acting on two planes within a soil element.

ngle α is given by point 1 and the stress acting on the plane inclined at an angle β is given by point 2. Accordingly, the pole is defined by point p . Recall that the angle 2θ is twice the space angle between the two planes, which are inclined by α and β respectively. That is

$$\theta = \alpha - \beta$$

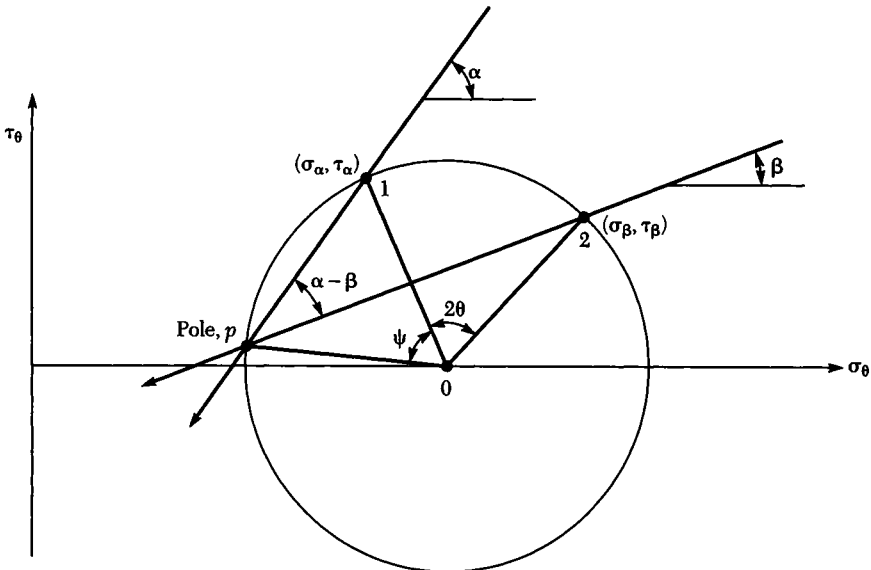


FIGURE 6.9 Mohr circle showing the pole.

If it can be shown that the angle $\angle 1p2$ is equal to θ , then the pole method is validated. From Figure 6.9 note that

$$\begin{aligned}\angle 1p2 &= \angle 1p0 - \angle 2p0 \\ &= \frac{(\pi - \psi)}{2} - \frac{[\pi - (2\theta + \psi)]}{2} \\ &= \theta\end{aligned}$$

The Mohr circle and the pole method of stress computation are important concepts in geotechnical engineering and should be carefully studied. Although all problems dealing with the Mohr circle can be solved analytically, the pole method provides significant insight into applied and resulting stresses on planes of any orientation.

EXAMPLE 6.5

A soil sample is subjected to a horizontal pressure of 50 kN/m^2 and a vertical pressure of 20 kN/m^2 . Determine the normal stress and the shear stress acting on a plane inclined 45° from the horizontal.

Solution

Since there are no shear stresses applied, the applied stresses are principal stresses. The angle $\theta = 135^\circ$ because it is measured from the major principal stress to the normal stress acting on the plane, which is inclined by 45° from the horizontal. Using Eq. (6.6), the normal and shear stresses are computed as

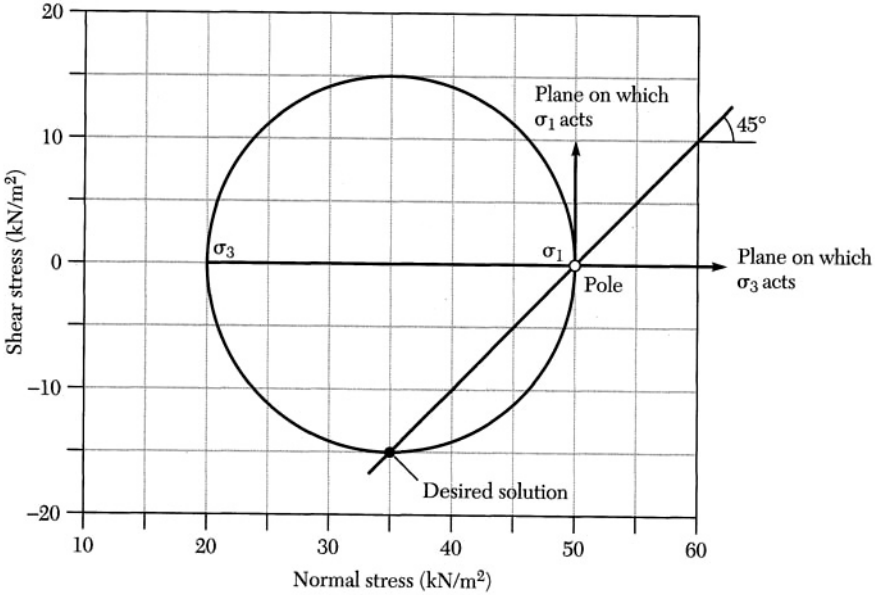
$$\begin{aligned}\sigma_\theta &= \left(\frac{\sigma_1 + \sigma_3}{2} \right) + \left(\frac{\sigma_1 - \sigma_3}{2} \right) \cos 2\theta \\ &= \left(\frac{50 + 20}{2} \right) + \left(\frac{50 - 20}{2} \right) \cos 2(135^\circ) = 35 \text{ kN/m}^2 \\ \tau_\theta &= \left(\frac{\sigma_1 - \sigma_3}{2} \right) \sin 2\theta \\ &= \left(\frac{50 - 20}{2} \right) \sin 2(135^\circ) = -15 \text{ kN/m}^2\end{aligned}$$

EXAMPLE 6.6

Rework Example 6.5 using the pole method.

Solution

Establish the Mohr circle by noting that its center is at $(35, 0)$ and its radius is 15. The pole is found as the point of intersection of the planes upon which σ_1 and σ_3 act. This is shown as follows.



The desired solution is obtained by extending a line through the pole with a slope of 45°. The intersection of this line with the Mohr circle gives the state of stress on the plane that is inclined at 45° from the horizontal. That is, $\sigma_\theta = 35$ and $\tau_\theta = -15$. These values are exactly equal to ones obtained analytically. ■

6.4 STRESS DUE TO A POINT LOAD

Several methods exist for solving the stress distribution problem due to a vertical point load. One of the most important solutions was proposed by Boussinesq in

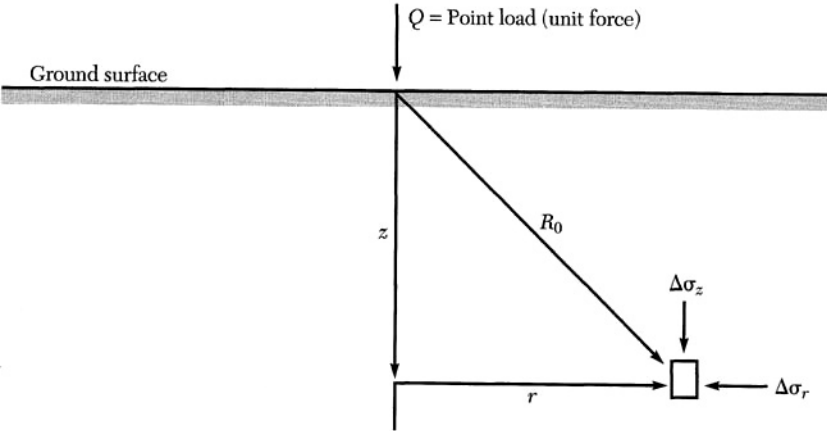


FIGURE 6.10 Typical cross section for a point load applied on an elastic half space.

1883. He assumed that the medium on which the load acts is linearly elastic, homogeneous, and an isotropic half space. For a given soil element within a soil mass, the vertical stress is called the *effective overburden pressure*. When a point load is applied at the ground surface, the increase in normal stress caused by the point load is referred to as the *stress increment*. The vertical and radial stress increments at a given depth z and at a lateral distance r along with the applied point load Q are shown in Figure 6.10. The vertical stress increment $\Delta\sigma_z$ and the radial stress increment $\Delta\sigma_r$, are given by Eqs. (6.14) and (6.15)

$$\Delta\sigma_z = \frac{3Qz^3}{2\pi R_0^5} = \frac{3Qz^3}{2\pi(r^2 + z^2)^{5/2}} \tag{6.14}$$

$$\Delta\sigma_r = \frac{Q}{2\pi R_0^2} \left[\frac{3r^2z}{R_0^3} - (1 - 2\mu) \left(\frac{R_0}{R_0 + z} \right) \right] \tag{6.15}$$

where $R_0 = (r^2 + z^2)^{1/2}$ and μ is Poisson’s ratio. Theoretically, the stress increment at zero depth and zero lateral distance is infinite. Poisson’s ratio ranges from 0 to 0.5 and is only needed for determining the radial stress increments.

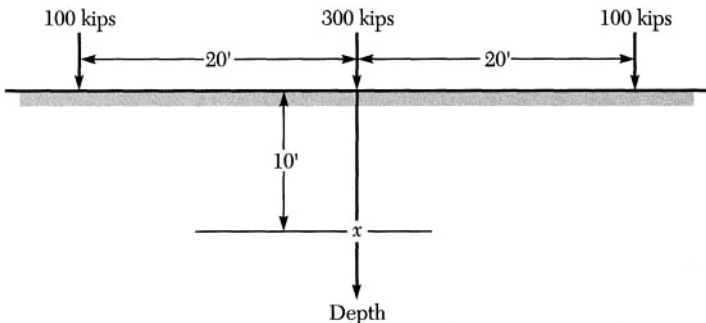
It is customary to express the vertical stress increment in terms of a dimensionless influence factor I_{pz} as given by Eq. (6.16).

$$\Delta\sigma_z = \frac{3z^3Q}{2\pi(r^2 + z^2)^{5/2}} = \frac{3Q}{2\pi z^2 \left[\left(\frac{r}{z} \right)^2 + 1 \right]^{5/2}} = I_{pz} \frac{Q}{z^2} \tag{6.16}$$

The influence factor I_{pz} versus the (r/z) value is shown graphically in Figure 6.11.

EXAMPLE 6.7

Calculate the vertical stress at point x in the following figure due to three point loads acting on the ground surface. Use the Boussinesq procedure.



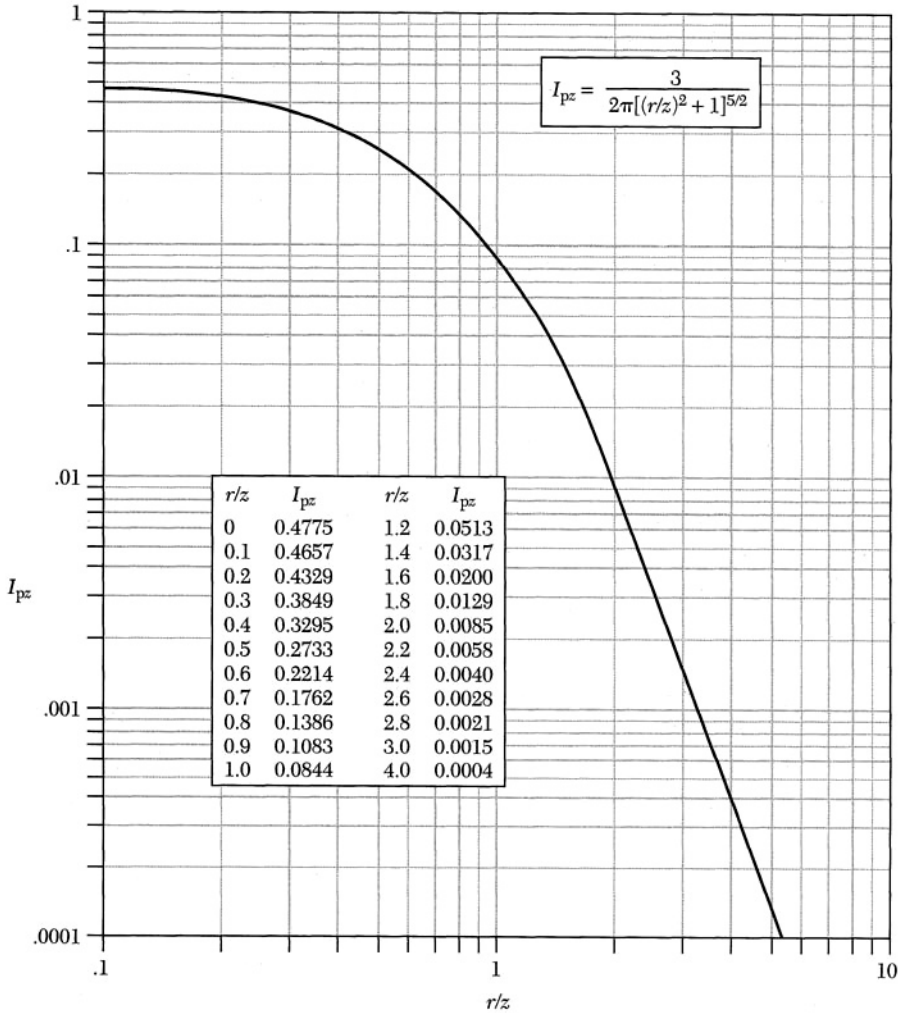


FIGURE 6.11 Influence diagram for vertical stress due to point load acting normal to surface of an elastic half space.

Solution

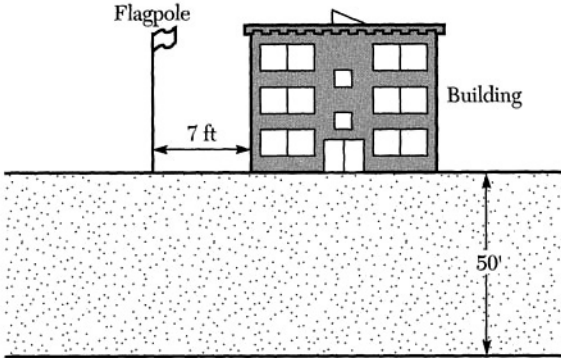
For the 300 kips, $r/z = 0$ and $I_{pz} = 0.4775$. For the 100 kips load, $r/z = 20/10 = 2$, $I_{pz} = 0.0085$. Thus, the vertical stress at point x is given as

$$\Delta\sigma_z = \frac{300(0.4775)}{10^2} + \frac{2(100)(0.0085)}{10^2} = 1.45 \text{ ksf}$$

Generally, the stress increment is required throughout the soil profile and not just at one depth. ■

EXAMPLE 6.8

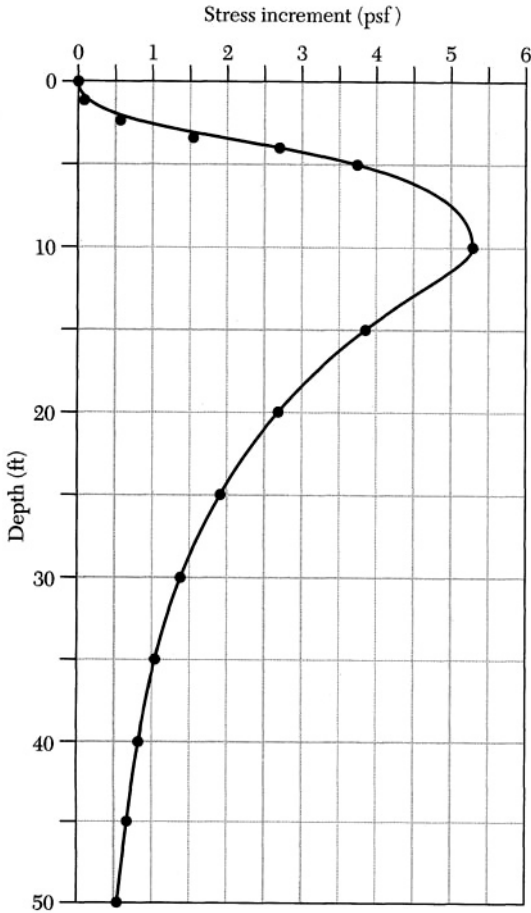
Calculate the maximum vertical stress increment under the edge of the building versus depth due to the flagpole shown in the figure below. Assume the flagpole weighs 3000 lb and use a depth increment of 1 ft to a depth of 10 ft, then use 5 ft.

**Solution**

Note that $r/z = 7/z$ permits the following table to be prepared.

| z ft | r/z | I_{ps} | $\Delta\sigma_z$ (psf) |
|--------|----------|----------|------------------------|
| 0 | ∞ | 0 | 0 |
| 1 | 7 | 3E-05 | 0.081 |
| 2 | 3.5 | 0.0007 | 0.5604 |
| 3 | 2.3333 | 0.0045 | 1.5096 |
| 4 | 1.75 | 0.0144 | 2.6913 |
| 5 | 1.4 | 0.0317 | 3.801 |
| 10 | 0.7 | 0.1762 | 5.2856 |
| 15 | 0.4667 | 0.2918 | 3.8901 |
| 20 | 0.35 | 0.3577 | 2.6825 |
| 25 | 0.28 | 0.3954 | 1.8977 |
| 30 | 0.2333 | 0.4182 | 1.394 |
| 35 | 0.2 | 0.4329 | 1.0601 |
| 40 | 0.175 | 0.4428 | 0.8302 |
| 45 | 0.1556 | 0.4498 | 0.6663 |
| 50 | 0.14 | 0.4548 | 0.5458 |

The resulting vertical stress increment versus depth is shown graphically as follows.



The maximum stress increment is extremely small and will have negligible influence on the existing structure. ■

6.5 STRESS DUE TO AN INFINITE LINE LOAD

The solution for a flexible (not rigid) vertical line load acting on a linearly elastic, homogeneous, isotropic half space was obtained by integrating the Boussinesq equations developed for a vertical point load. This problem is depicted graphically in Figure 6.12. The vertical stress increment $\Delta\sigma_z$ and horizontal stress increments $\Delta\sigma_x$ are given by Eqs. (6.17) and (6.18).

$$\Delta\sigma_z = \frac{2Pz^3}{\pi(z^2 + x^2)^2} \tag{6.17}$$

$$\Delta\sigma_x = \frac{2Px^2z}{\pi(z^2 + x^2)^2} \tag{6.18}$$

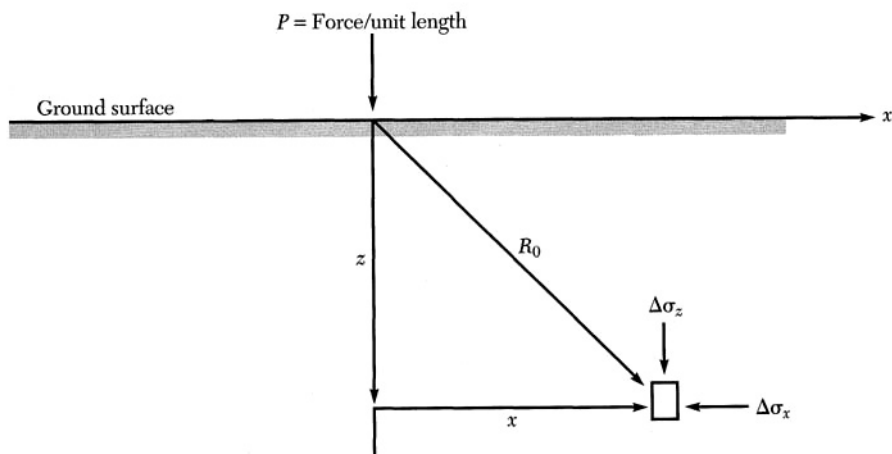


FIGURE 6.12 Line load acting on an elastic half space.

where P is the line load expressed as a unit force per unit length, z is the depth, and x is the lateral distance (measured from the line load) of the point at which the stress increments are required. The stress increments can be expressed in terms of dimensional influence factors by rewriting Eqs. (6.19) and (6.20), respectively.

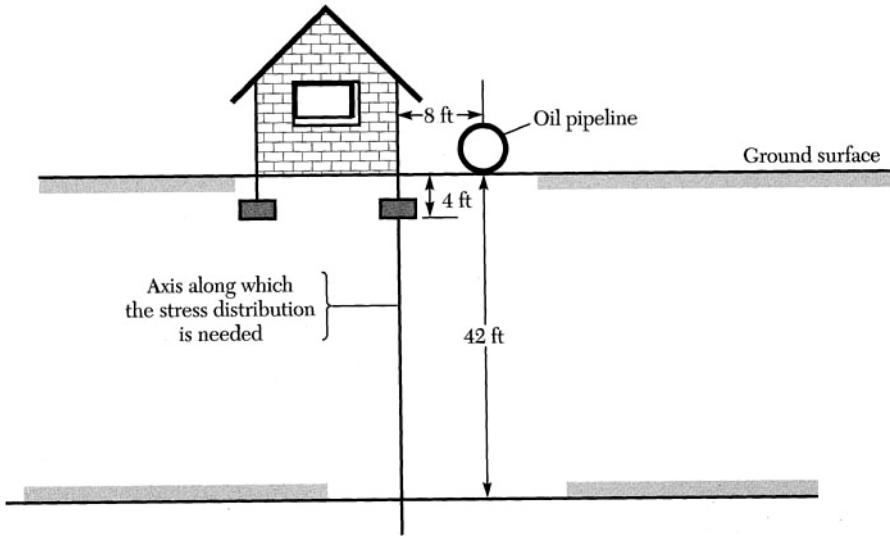
$$\Delta\sigma_z = \frac{2P}{z\pi \left[\left(\frac{x}{z} \right)^2 + 1 \right]^2} = I_{Lz} \frac{P}{z} \quad (6.19)$$

$$\Delta\sigma_x = \frac{2P \left(\frac{x}{z} \right)^2}{z\pi \left[\left(\frac{x}{z} \right)^2 + 1 \right]^2} = I_{Lx} \frac{P}{z} \quad (6.20)$$

where I_{Lz} and I_{Lx} are the influence factors corresponding to the vertical and the horizontal stress increments respectively. The influence factors given by Eqs. (6.19) and (6.20) are shown graphically in Figure 6.13.

EXAMPLE 6.9

An oil pipeline weighing 1500 lb per ft is placed on the ground surface parallel to an existing house. Determine the vertical and horizontal stress distribution versus depth below the house wall footing which is 8 ft from the pipe and 4 ft deep. Assume a depth increment of 2.0 ft and a stratum thickness of 42 ft. The given information is illustrated graphically as follows.



Solution

Note that $P = 1500 \text{ lb/ft}$, $x = 4 \text{ ft}$, $x/z = 4/z$, $\sigma_z = 1500 I_{L1}/z$, and $\sigma_x = 1500 I_{L2}/z$. The solution is obtained using the influence factors given by Eqs. (6.19) and (6.20).

| z | x/z | I_{L1} | I_{L2} | $\Delta\sigma_z$ | $\Delta\sigma_x$ |
|-----|--------|----------|----------|------------------|------------------|
| 4 | 1.0000 | 0.1591 | 0.1591 | 59.66 | 59.66 |
| 6 | 0.6666 | 0.3051 | 0.2033 | 76.28 | 50.83 |
| 8 | 0.5000 | 0.4074 | 0.2037 | 76.39 | 38.19 |
| 10 | 0.4000 | 0.4731 | 0.1892 | 70.97 | 28.38 |
| 12 | 0.3333 | 0.5156 | 0.1718 | 64.45 | 21.48 |
| 14 | 0.2857 | 0.5441 | 0.1554 | 58.30 | 16.65 |
| 16 | 0.2500 | 0.5639 | 0.1409 | 52.87 | 13.21 |
| 18 | 0.2222 | 0.5781 | 0.1284 | 48.18 | 10.70 |
| 20 | 0.2000 | 0.5885 | 0.1177 | 44.14 | 8.83 |
| 22 | 0.1818 | 0.5965 | 0.1084 | 40.67 | 7.39 |
| 24 | 0.1666 | 0.6026 | 0.1003 | 37.66 | 6.27 |
| 26 | 0.1538 | 0.6075 | 0.0934 | 35.05 | 5.39 |
| 28 | 0.1428 | 0.6114 | 0.0873 | 32.75 | 4.68 |
| 30 | 0.1333 | 0.6145 | 0.0819 | 30.73 | 4.10 |
| 32 | 0.1250 | 0.6171 | 0.0771 | 28.93 | 3.61 |
| 34 | 0.1176 | 0.6193 | 0.0728 | 27.32 | 3.21 |
| 36 | 0.1111 | 0.6211 | 0.0690 | 25.88 | 2.88 |
| 38 | 0.1052 | 0.6227 | 0.0655 | 24.58 | 2.59 |
| 40 | 0.1000 | 0.6240 | 0.0624 | 23.40 | 2.34 |
| 42 | 0.0952 | 0.6252 | 0.0595 | 22.33 | 2.13 |

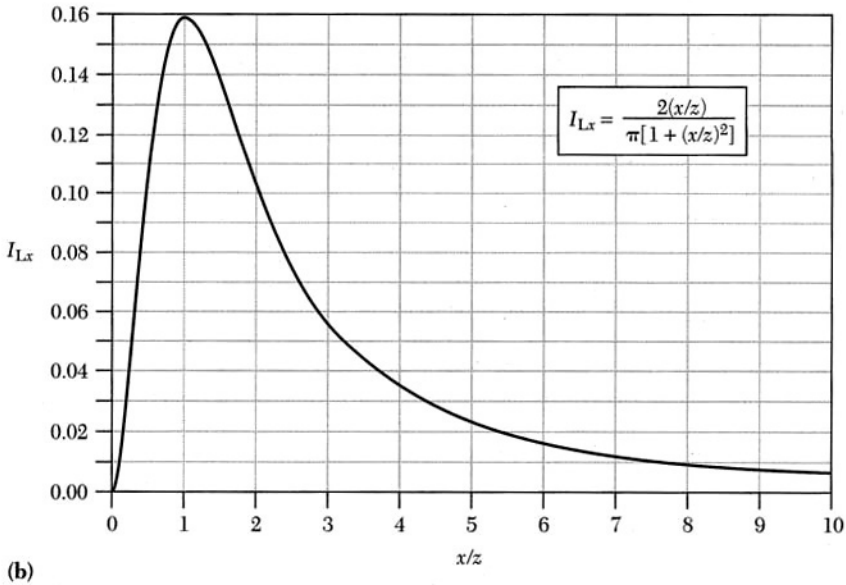
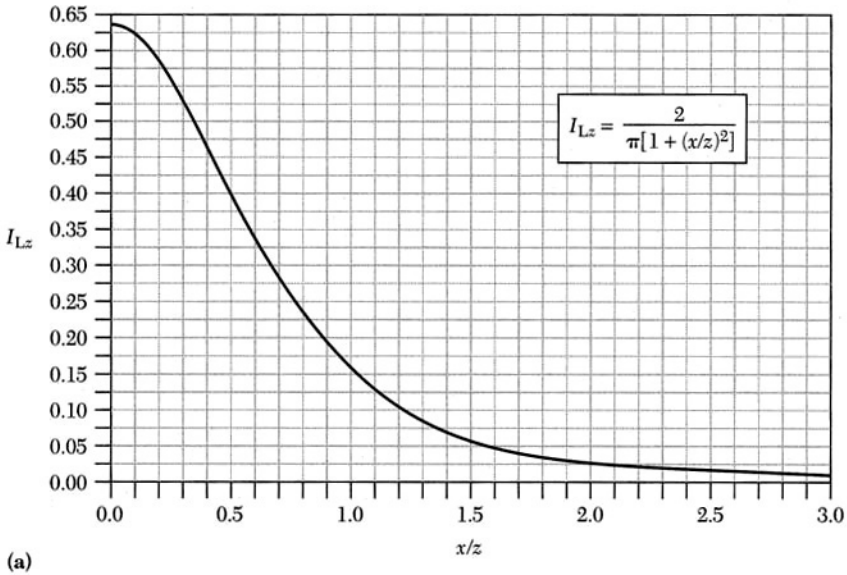
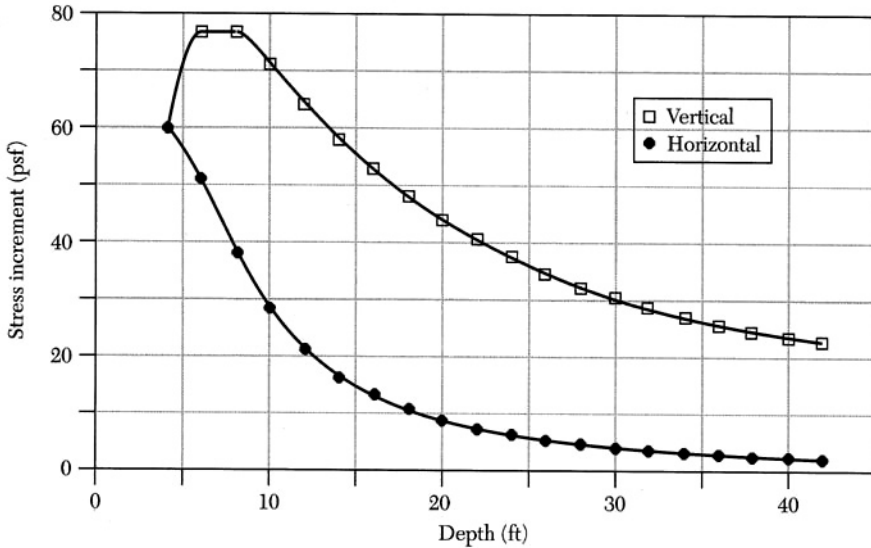


FIGURE 6.13 Influence diagrams due to a line load acting normal to the surface of an elastic half space: (a) vertical stress; (b) horizontal stress.

The horizontal and vertical stress distributions are shown graphically as follows.



6.6 STRESS DUE TO AN INFINITE STRIP LOAD

The solution for a flexible infinite strip load acting vertically on the surface of a linearly elastic, homogeneous, isotropic half space was obtained by integrating the Boussinesq equations developed for a vertical point load. Expressions needed for solving the infinite strip loading problem can be developed by considering Figure 6.14. A solution for the vertical $\Delta\sigma_z$ and horizontal $\Delta\sigma_x$ stress increments can be found in most texts dealing with linear elasticity and are given by Eqs. (6.21) and (6.22) respectively.

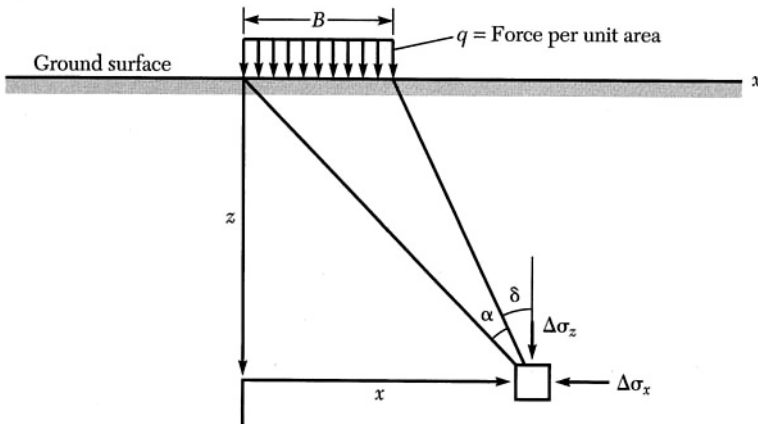


FIGURE 6.14 Infinite strip loading on an elastic half space.

$$\Delta\sigma_z = \frac{q}{\pi} [\alpha + \sin \alpha \cos(\alpha + 2\delta)] \quad (6.21)$$

$$\Delta\sigma_x = \frac{q}{\pi} [\alpha - \sin \alpha \cos(\alpha + 2\delta)] \quad (6.22)$$

where α and δ are angles measured in radians. These angles define the location of the point at which stress increments are desired. The expressions given by Eqs. (6.21) and (6.22) are cumbersome to use, because they require stress at a position identified by angles rather than distances. These angles can be conveniently determined using the following expressions.

$$\alpha = \tan^{-1}\left(\frac{x}{z}\right) - \tan^{-1}\left(\frac{x-B}{z}\right) \quad (6.23)$$

$$\delta = \tan^{-1}\left(\frac{x-B}{z}\right) \quad (6.24)$$

Equations (6.23) and (6.24) make it possible to write a simple computer program for evaluating the stress increments $\Delta\sigma_z$ and $\Delta\sigma_x$ by specifying the coordinates x and z at a point for which the stresses are needed. The stress increment in the y -direction is given by Eq. (6.25):

$$\Delta\sigma_y = 2\mu\alpha \frac{q}{\pi} \quad (6.25)$$

Note that μ is Poisson's ratio and y refers to the direction perpendicular to the cross section shown in Figure. 6.14.

6.7 STRESS DUE TO A LINEARLY INCREASING INFINITE STRIP LOAD

The solution for an infinite vertical load increasing linearly and acting on the surface of a linearly elastic, homogeneous, isotropic half space was obtained by integrating the Boussinesq equations developed for a vertical point load. Needed variables for stress increment computations are illustrated in Figure 6.15. The vertical $\Delta\sigma_z$ and horizontal $\Delta\sigma_x$ stress increments are calculated using Eqs. (6.26) and (6.27).

$$\Delta\sigma_z = \frac{q}{2\pi} \left[\frac{2x\alpha}{B} - \sin 2\delta \right] \quad (6.26)$$

$$\Delta\sigma_x = \frac{q}{2\pi} \left[\frac{2x\alpha}{B} + \sin 2\delta - 2z \ln \left(\frac{R_0^2}{R_1^2} \right) \right] \quad (6.27)$$

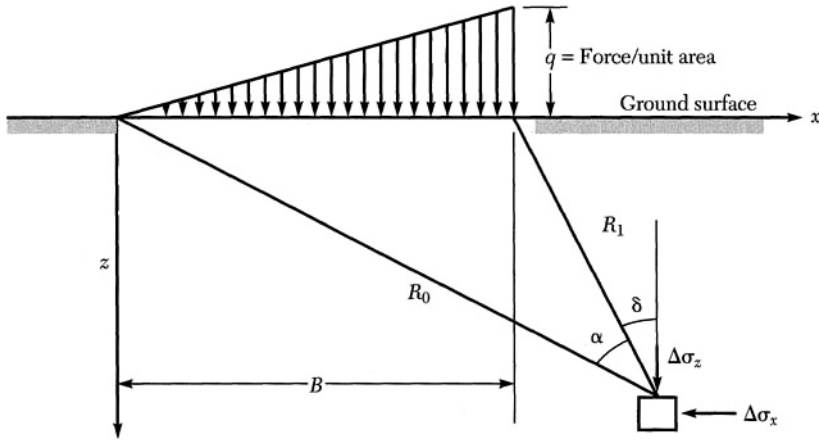


FIGURE 6.15 Linearly increasing strip loading.

Equations (6.26) and (6.27) are cumbersome and not ideal for computer or hand calculations. To simplify their evaluation and programmability, the following expressions are provided.

$$\begin{aligned}
 \alpha &= \tan^{-1}\left(\frac{x}{z}\right) - \tan^{-1}\left(\frac{x-B}{z}\right) \\
 \delta &= \tan^{-1}\left(\frac{x-B}{z}\right) \\
 R_0 &= \sqrt{x^2 + z^2} \\
 R_1 &= \sqrt{(x-B)^2 + z^2}
 \end{aligned}
 \tag{6.28}$$

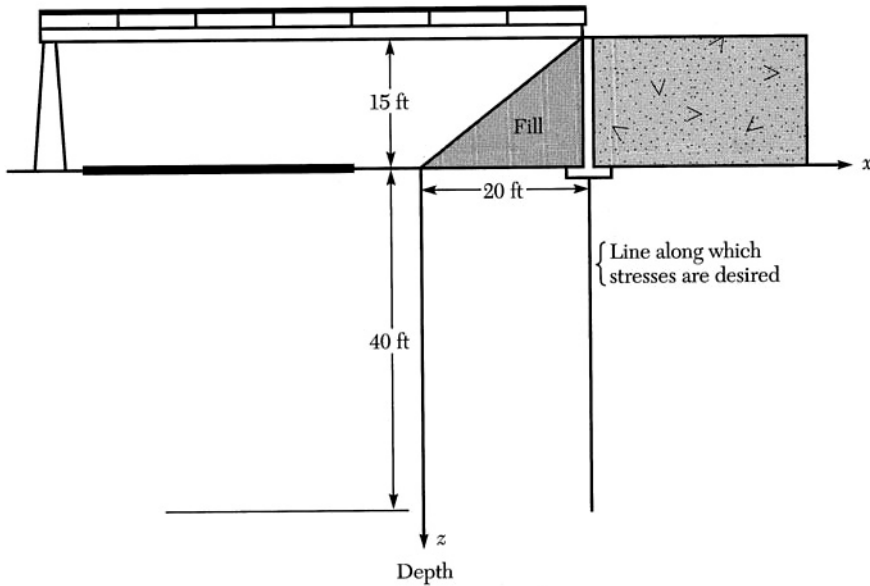
Equation (6.28) permits computation of both vertical and horizontal stresses using coordinates x and z , rather than α and δ .

EXAMPLE 6.10

Calculate the vertical stress increments along a vertical line between the fill and the bridge pier for the highway overpass shown in the following figure. Assume that the fill has a unit weight of 100 pcf. Use a starting depth of 5 ft, final depth of

6.7 STRESS DUE TO A LINEARLY INCREASING INFINITE STRIP LOAD 215

40 ft, and a depth increment of 5 ft. Assume that the fill dimension into the page is sufficiently long to depict an infinite length.

**Solution**

The solution is obtained by first noting that $x = B = 20$ ft and then by performing the following calculations.

$$q = 15(100) = 1500 \text{ psf}$$

$$\alpha = \tan^{-1}(20/z)$$

$$\delta = 0$$

$$\Delta\sigma_z = \left[\frac{2(20)\tan^{-1}(20/z)}{20} - \sin 0 \right] \frac{1500}{2\pi} = \frac{1500}{\pi} \tan^{-1}(20/z)$$

| z | 5 | 10 | 15 | 20 | 25 | 30 | 35 | 40 |
|------------------|--------|--------|--------|--------|--------|--------|--------|--------|
| $\Delta\sigma_z$ | 633.03 | 528.62 | 442.75 | 375.00 | 322.17 | 280.75 | 247.87 | 221.38 |

The stress distribution is shown in the following figure.

7

Volume Change in Soils

7.0 INTRODUCTION

A soil may be considered to be a skeleton of solid particles enclosing **voids** (spaces not occupied by solid mineral matter) that are filled with gas, liquid, or some combination of gas and liquid. Placement of a load on this soil will result in a decrease in volume due to three possible factors: (1) compression of the solid matter, (2) compression of water and air within the voids, and (3) drainage of water and air from the voids. For loads normally encountered in soil masses, the solid matter and pore water, being relatively incompressible, will undergo little volume change. For this reason, the decrease in volume of a saturated soil mass is due almost entirely to drainage of water from the voids. For soils with a low permeability, considerable time may be required for water to drain. This is especially true for deep clay deposits. The gradual adjustment of pore water pressures coupled with escape of water and a slow compression is called **consolidation**. One-dimensional compression occurs in thin clay layers located directly beneath building footings. Engineers are interested in predicting this soil compression and the resulting footing settlement. The measurement of soil properties required for predicting soil volume change and their use in settlement analysis is the subject of this chapter.

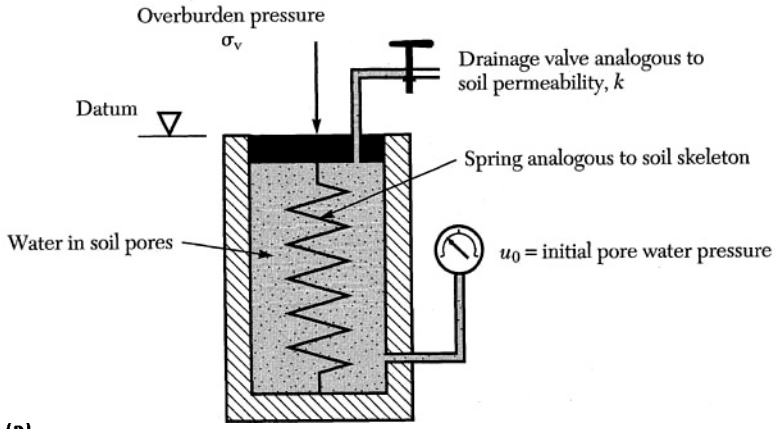
7.1 SOIL COMPRESSIBILITY

Consider an earth fill placed over a soft deposit of clay. The surface will settle uniformly as the clay soil is compressed due to (1) deformation of soil grains, (2) compression of air and water in the voids, and (3) squeezing out water and air from the voids. Compression of the soil particles and water is small at typical engineering loads and can usually be neglected. Below the water table the soil can be considered fully saturated, thus compression of air is neglected. The last item contributes the major portion to volume change of loaded soil deposits. The soil grains rearrange themselves into a more stable and denser configuration as pore water is squeezed out of the soil. The rate of water drainage depends on the soil permeability and the hydraulic gradient. This process, consolidation, is a stress-strain-time phenomenon. Deformation may continue for months, years, or even decades. The amount of particle rearrangement and compression depends on the rigidity of the soil skeleton or soil structure.

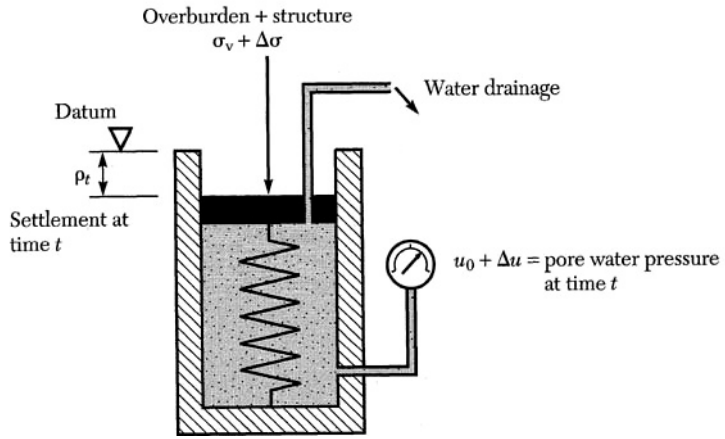
Clay consolidation is readily explained by the spring analogy shown in Figure 7.1. The spring, analogous to the soil skeleton, supports a piston that is loaded vertically by the existing overburden pressure. Water in the cylinder represents water in the soil voids under an initial hydrostatic pore pressure u_0 as shown by the pressure gauge. The drainage valve at the top of the piston is analogous to the soil permeability. At equilibrium, with the valve open, there is no water flow. This situation (Figure 7.1a) is analogous to one where a soil layer is at equilibrium with the weight of all soil layers (overburden pressure) above it. Now the soil layer is loaded by an additional load increment $\Delta\sigma$ giving a total pressure $(\sigma_v + \Delta\sigma)$. Upon application of the load, the additional pressure is immediately transferred to water inside of the cylinder. Because water is relatively incompressible, with the valve at the top of the cylinder closed there will be no drainage and no settlement of the piston. The pressure gauge will read $(u_0 + \Delta u)$ where $\Delta u = \Delta\sigma$. The pore water pressure Δu represents an excess pressure.

If the valve is now partially opened, water drainage under the excess pressure Δu will simulate a fine-grained soil with its low permeability. With time and drainage the water pressure decreases and the load $\Delta\sigma$ will be transferred to the spring. The spring will compress under the additional load, giving a settlement ρ_t to the upper piston (ground surface) at time t . Compression of the spring corresponds to densification of the soil particles. This process will continue until drainage stops, when Δu goes to zero and the total pore water pressure is again hydrostatic. The spring will be at a new equilibrium position under the pressure $(\sigma_v + \Delta\sigma)$ and the piston will display its ultimate settlement ρ_{ult} . At this point the soil skeleton will have reached a new equilibrium void ratio corresponding to the pressure $(\sigma_v + \Delta\sigma)$ — representing the soil overburden pressure and new surface loads.

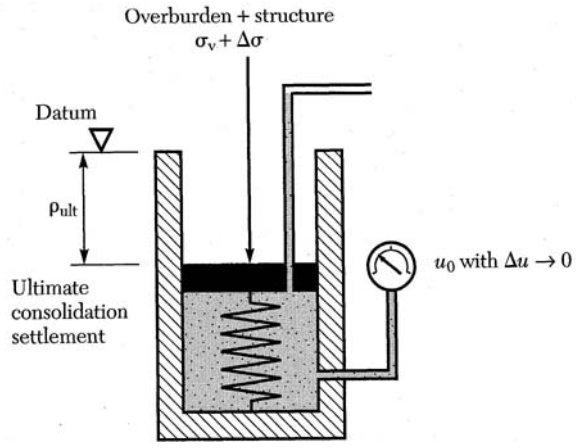
If the surface load were now removed, some expansion would take place but the volume rebound for soils will not be as great as for the preceding compression. A portion of the compression, due to change in relative positions of soil particles, is to a large degree nonelastic. The compression due to deformation of individual particles is predominantly elastic, and these particles are capable of re-



(a)



(b)



(c)

FIGURE 7.1 Spring analogy as applied to soil consolidation: (a) at equilibrium under an overburden pressure σ_v ; (b) consolidation under a pressure $(\sigma_v + \Delta\sigma)$; (c) at equilibrium under a pressure $(\sigma_v + \Delta\sigma)$ representing an overburden plus surface load.

gaining their original shape, which is responsible for some volume rebound. Another type of strain rebound, which occurs in fine-grained soils, involves small amounts of water held by particle surface forces. When pressure is increased some of this water is squeezed out. When the pressure is decreased these forces cause water to be drawn in. This time-dependent phenomenon, known as *swelling*, can be of practical importance for certain soil deposits.

7.2 CONSOLIDATION AND OEDOMETER TEST

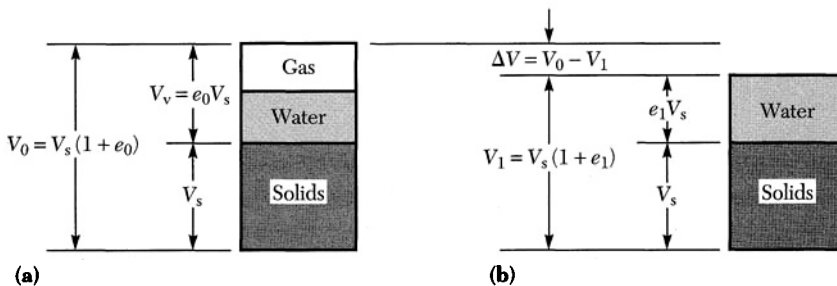
7.2.1 One-Dimensional Compression

A soil sample has been obtained from the soft clay deposit referred to in the previous section. Initial soil conditions can be described by its volume V_0 and void ratio e_0 as illustrated in Figure 7.2. Placement of an earth fill increases the vertical stresses and causes drainage of water from the soil pores until a new equilibrium void ratio e_1 is attained. With a uniform surface load (fill) the soil compression will be one-dimensional and only surface settlement results from the decrease in volume. The volumetric strain $\Delta V/V_0$ can be represented by $\Delta e/(1 + e_0)$ as shown in Figure 7.2. For a uniform clay deposit, one-dimensional compression, and a unit area A , the volumetric strain will equal the ratio of settlement ΔH to the initial clay layer thickness H_0 , thus

$$\frac{\Delta V}{V_0} = \frac{\Delta HA}{H_0 A} = \frac{\Delta e}{1 + e_0} \quad (7.1)$$

The question now arises as to how to relate change in void ratio Δe to the increase in effective vertical stress $\Delta \bar{\sigma}_v$, due to the fill. A laboratory oedometer test on a sample obtained from the clay deposit is the answer.

The soil specimen is placed in either a fixed-ring or floating-ring consolidometer (Figure 7.3). All specimen movement relative to the ring container is downward in the fixed-ring container. In the floating-ring container, compression



$$\frac{\Delta V}{V_0} = \frac{V_0 - V_1}{V_0} = \frac{V_s(1 + e_0) - V_s(1 + e_1)}{V_s(1 + e_0)} = \frac{e_0 - e_1}{1 + e_0} = \frac{\Delta e}{1 + e_0}$$

FIGURE 7.2 One-dimensional compression: (a) initial conditions; (b) compressed conditions.

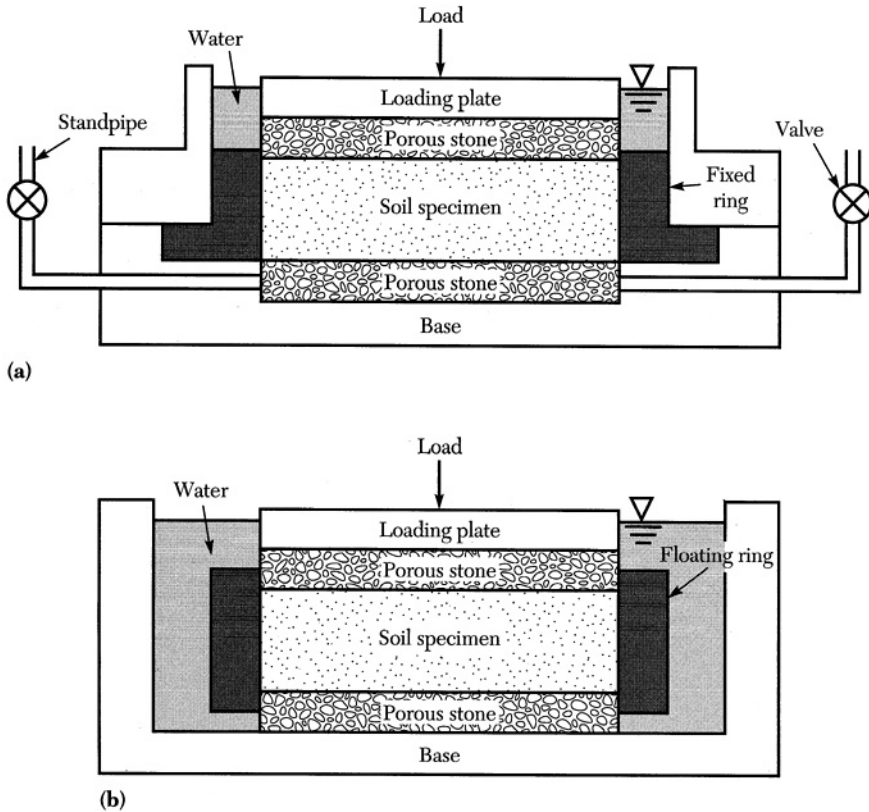


FIGURE 7.3 Consolidometers: (a) fixed-ring; (b) floating-ring.

is toward the middle from both top and bottom. This gives a smaller value for friction between the soil specimen and container wall. Use of a specimen diameter-to-height ratio of 2.75 or greater helps minimize the effect of ring friction. The fixed-ring container is more easily adapted for permeability tests, hence the selection of a soil container type and loading unit is based on laboratory needs and personal preference. The load is often applied in increments so that each increment equals the previous consolidation pressure (load-increment ratio of $(P_2 - P_1)/P_1 = 1$). For each load increment a curve of compression versus time is obtained. The duration of each increment is usually 24 hours in the conventional oedometer test. At the end of each load increment the void ratio of the soil sample is determined. Data from a series of load and unload increments, presented as a plot of void ratio versus pressure, are illustrated by the curve in Figure 7.4. An alternate form for data presentation replaces void ratio with vertical strain ϵ_v , equal to $\Delta e/(1 + e_0)$. The choice is based on convenience and later use of the data.

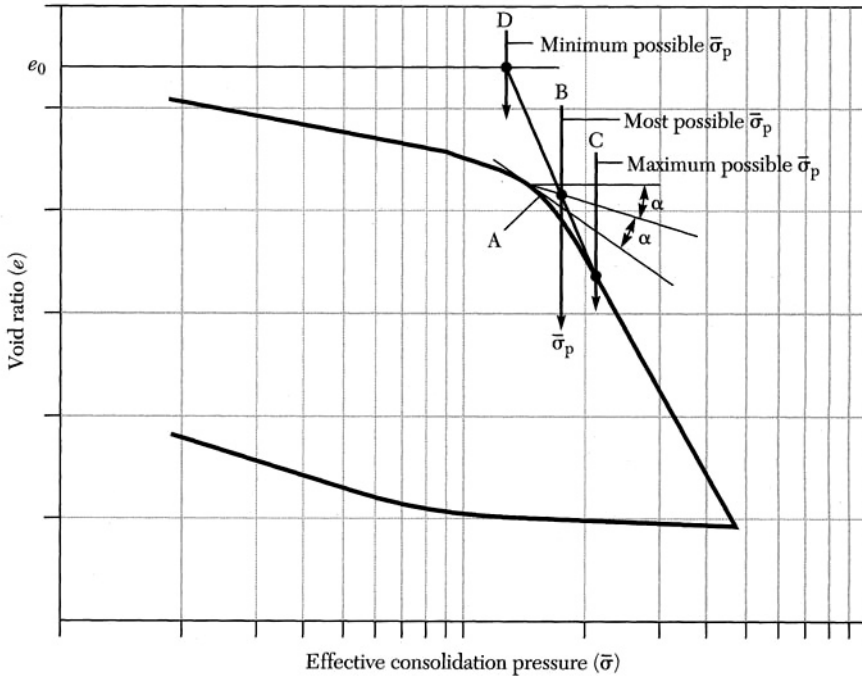


FIGURE 7.4 Laboratory compressibility curve showing the Casagrande (1936) method for determining the most probable preconsolidation pressure.

7.2.2 Consolidation Theory

The soft clay deposit with an earth fill described in Section 7.1 may be illustrated as shown in Figure 7.5a. Prior to placement of the earth fill, all pore pressures were hydrostatic relative to the groundwater table. Placement of the earthfill increases the stresses in the clay by $\Delta\sigma$. If no drainage occurs during soil placement, the increase in load will be carried initially by the pore water as illustrated by the rectangular pressure diagram (curve t_0) in Figure 7.5c. Total pore pressure u in the clay will include both hydrostatic (u_h) and excess (u_e) pressures, thus

$$u = u_h + u_e \tag{7.2}$$

After placement of the earth fill, drainage from the clay commences immediately with the rate dependent on soil permeability and the hydraulic gradient. The upper one half of the clay layer drains upward and the lower one half drains downward until all excess pore pressures have dissipated (curve t_∞ in Figure 7.5c). With drainage of pore water, one-dimensional volume change (surface settlement) would be observed.

Consider a vertical section through a thin horizontal slice of the consolidating clay (Figure 7.5d). Water flows upward through the layer at a rate v . With the unbalanced hydrostatic pressure equal to $(\partial u / \partial z) dz$, Darcy's law (Section 5.1) re-

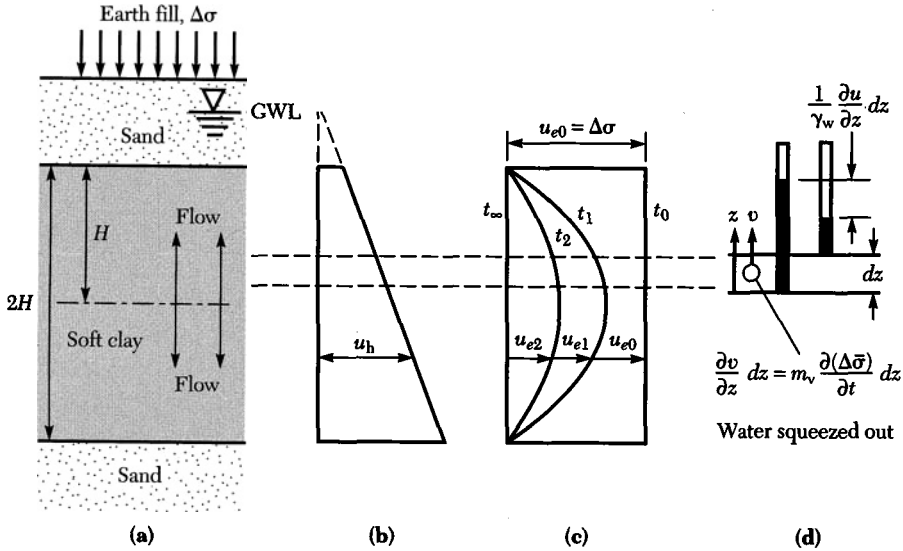


FIGURE 7.5 Soil consolidation: (a) soil profile; (b) hydrostatic pore pressure; (c) excess pore pressure; (d) horizontal slice through consolidating layer.

quires that

$$v = -ki = -k \frac{\partial u}{\partial z} = -k \frac{1}{\gamma_w} \frac{\partial u}{\partial z} \tag{7.3}$$

For the range in stress from σ_1 to $(\sigma_1 + \Delta\sigma)$, the change in void ratio may be written as

$$e_1 - e = \Delta e = a_v \Delta\sigma \tag{7.4}$$

where a_v represents the **coefficient of compressibility** (Figure 7.6). Substitution into Eq. (7.1) gives

$$\frac{\Delta e}{1 + e_1} = \frac{a_v}{1 + e_1} \Delta\sigma = m_v \Delta\sigma \tag{7.5}$$

where m_v is the **coefficient of volume compressibility**. It represents the compression of clay, per unit of original thickness, due to a unit increase in pressure. In a consolidating compressible layer with thickness equal to unity, the quantity of water that leaves the layer per unit of time exceeds that which enters it by an amount equal to the corresponding volume decrease of the layer. By use of Eq. (7.5), write

$$\frac{\partial v}{\partial z} = m_v \frac{\partial(\Delta\bar{\sigma})}{\partial t} \tag{7.6}$$

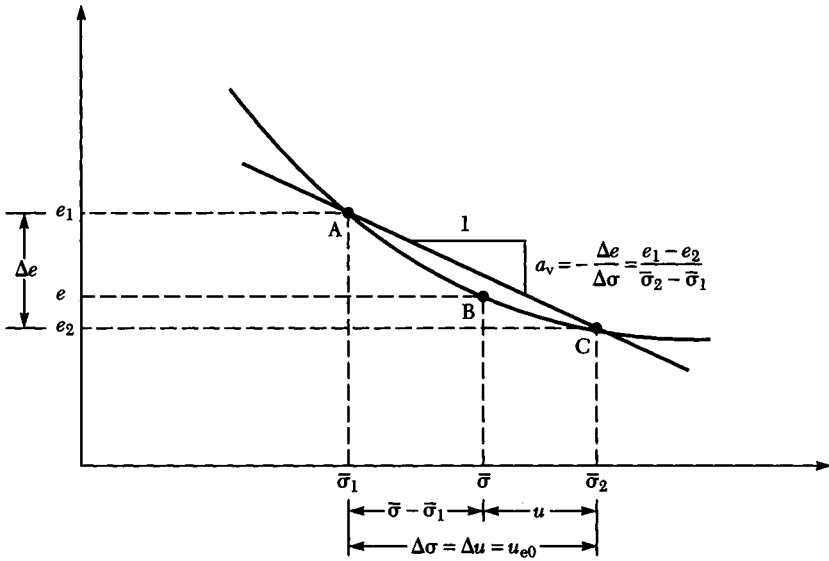


FIGURE 7.6 Laboratory compression curve.

Since $\Delta\sigma$ is constant and equals $(\Delta\bar{\sigma} + u_e)$, write

$$\frac{\partial \Delta\bar{\sigma}}{\partial t} = -\frac{\partial u}{\partial t}$$

whence

$$\frac{\partial v}{\partial z} = -m_v \frac{\partial u}{\partial t}$$

Combining this equation with Eq. (7.3) gives

$$\frac{\partial v}{\partial z} = -m_v \frac{\partial u}{\partial t} = -\frac{k}{\gamma_w} \frac{\partial^2 u}{\partial z^2}$$

or

$$\frac{\partial u}{\partial t} = \frac{k}{\gamma_w m_v} \frac{\partial^2 u}{\partial z^2} = c_v \frac{\partial^2 u}{\partial z^2} \tag{7.7}$$

where $k(\text{cm}/\text{sec})/\gamma_w (\text{g}/\text{cm}^3) \cdot m_v(\text{cm}^2/\text{g}) = c_v (\text{cm}^2/\text{s})$ is the **coefficient of consolidation**. Equation (7.7) is Terzaghi's one-dimensional consolidation equation. This equation must satisfy the hydraulic boundary conditions. These conditions include: (1) at $t = 0$ and at any distance z from the impervious clay surface the excess pore pressure is equal to $\Delta\sigma$; (2) for $t > 0$ at the upper and lower drainage surfaces the excess pore pressure is zero; (3) for any time t at the center of the clay

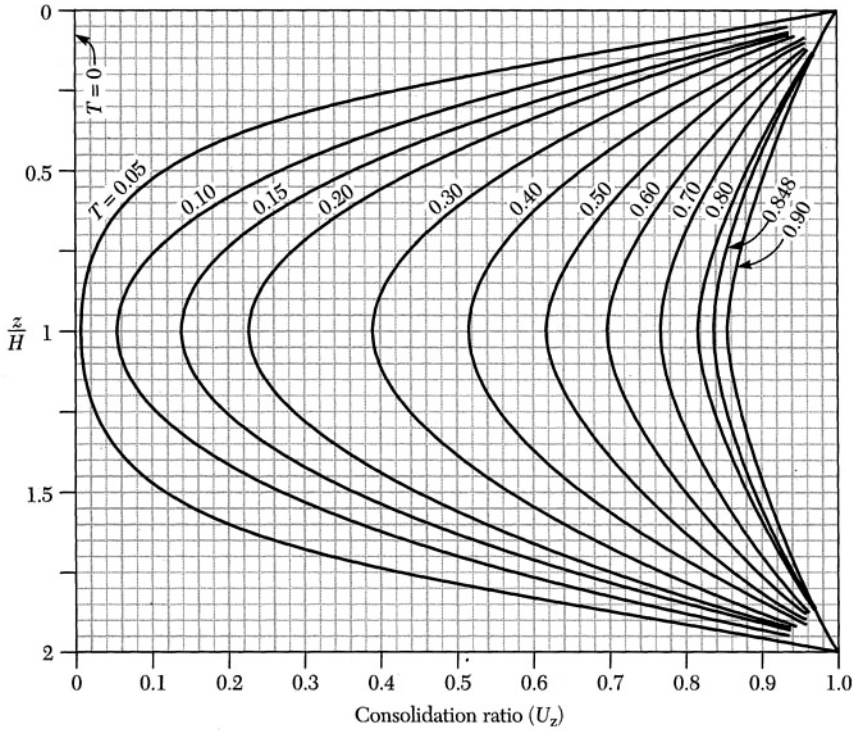


FIGURE 7.7 Consolidation as a function of depth and time factor. (After Taylor, 1948.)

layer the hydraulic gradient is zero (that is $\partial u / \partial z = 0$); and (4) after a very great time ($t = \infty$), at any value z , the excess pore pressure is zero.

Using the preceding boundary conditions Taylor (1948) provided a mathematically rigorous solution to Eq. (7.7), which is represented in Figure 7.7. For convenience, the solution is presented in terms of a dimensionless depth ratio z/H and a consolidation ratio U_z expressed as

$$U_z = \frac{e_1 - e}{e_1 - e_2} \tag{7.8}$$

where e is some intermediate void ratio as shown in Figure 7.6. In terms of stresses and pore pressures Eq. (7.8) can be rewritten as

$$U_z = \frac{\bar{\sigma} - \bar{\sigma}_1}{\bar{\sigma}_2 - \bar{\sigma}_1} = \frac{\bar{\sigma} - \bar{\sigma}_1}{\Delta\sigma} = \frac{u_i - u}{u_i} = 1 - \frac{u}{u_i} \tag{7.9}$$

where $\bar{\sigma}$ and u are intermediate values corresponding to e and u_i is the initial excess pore pressure due to the applied stress $\Delta\sigma$. Examination of Eq. (7.9) shows that U_z is zero at the start of loading and gradually increases to 1 (or 100 %) as the void ratio decreases from e_1 to e_2 . At the same time, for a constant total stress, the

effective stress increases from $\bar{\sigma}_1$ to $\bar{\sigma}_2$ with dissipation of excess pore pressures from u_i to zero.

The consolidation ratio U_z represents the degree or percentage of consolidation at a point in the consolidating clay layer. For any real time after start of loading and at any point in the consolidating layer Figure 7.7 permits calculation of U_z (and therefore u and $\bar{\sigma}$). The time factor $T_v = c_v(t/H^2)$, where t is time and H equals the length of the longest drainage path. Information needed includes c_v from the oedometer test, total thickness of the layer, and the boundary drainage conditions. Settlement calculations require the use of an average degree of consolidation

$$U = \frac{1}{\Sigma H} \int_0^{\Sigma H} U_z dz \tag{7.10}$$

where ΣH represents thickness of the entire consolidating layer. This average value of U corresponds to the ratio of the area outside the T curve in Figure 7.7 to the total area. The integration has been done mathematically with the results summarized in Figure 7.8. Settlement at time t for the clay layer illustrated in Figure

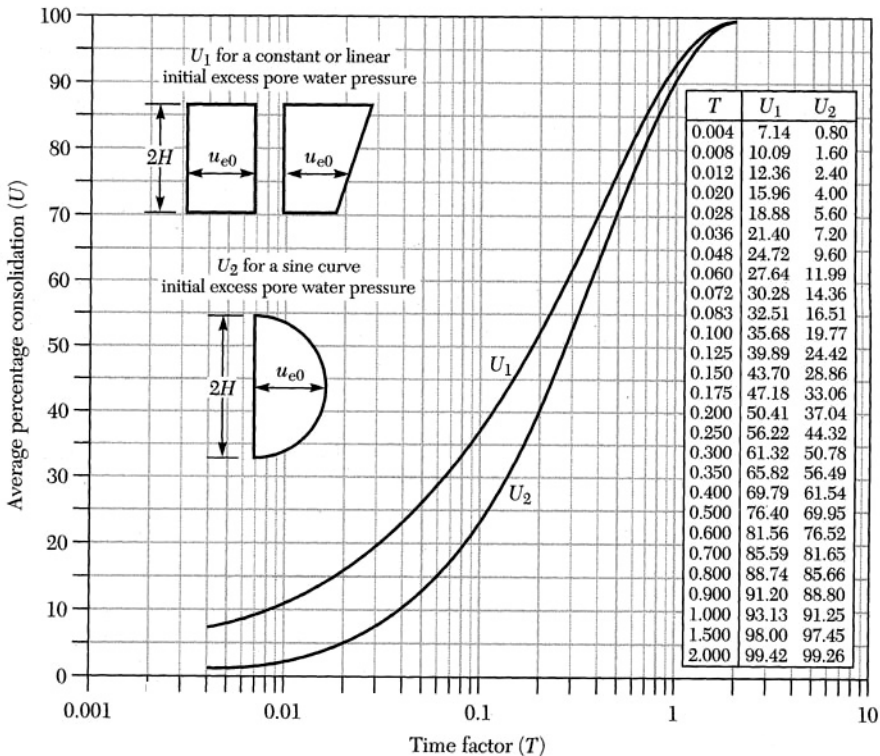


FIGURE 7.8 Relationship between average degree of consolidation U and time factor T for a uniform load applied to a doubly drained soil.

7.5 will be

$$\rho_t = U\rho_{ult} \quad (7.11)$$

where ρ_{ult} is the ultimate consolidation settlement under the uniform surface load.

7.2.3 Maximum Past Vertical Pressure

The initial portion of the curve in Figure 7.4 has a relatively flat slope and represents a reloading (reconsolidation) of the soil sample. At a pressure close to the maximum past consolidation pressure, $\bar{\sigma}_p$, the curve exhibits a much steeper slope and continues at close to a straight line. Depending on soil type and its geologic history, the change in slope can be quite large. An increase in vertical stress to a level greater than what the soil has experienced in the past causes the soil structure to seek a new equilibrium void ratio. The soil is considered to be normally consolidated when the **preconsolidation pressure** $\bar{\sigma}_p$ (the greatest effective stress to which the soil has been subjected) just equals the existing effective vertical overburden pressure $\bar{\sigma}_0$. Settlement prediction requires that the preconsolidation pressure be determined. Several procedures have been proposed with the Casagrande (1936) method illustrated in Figure 7.4. The point of maximum curvature (minimum radius) on the consolidation curve is selected by eye (point A in Figure 7.4). A horizontal line and a line tangent to the curve are drawn through point A. The angle between these lines is bisected with a third line. The intersection of this bisector with an upward extension of the straight line portion of the curve gives location B, the most probable value for the preconsolidation pressure $\bar{\sigma}_p$. The minimum possible value for $\bar{\sigma}_p$ is given by location D, the intersection of a horizontal line through the initial void ratio e_0 and the upward extension of the straight line portion of the consolidation curve. The maximum possible $\bar{\sigma}_p$ corresponds to location C, where the straight line leaves the curve. Casagrande's (1936) method for determination of $\bar{\sigma}_p$ requires that the compression curve show a fairly well-defined minimum radius of curvature. In some cases the load increment ratio for the oedometer test may have to be reduced in the vicinity of $\bar{\sigma}_p$ in order to better define the break in the curve. Poor samples, which have been partially remolded during sampling, require other procedures.

The effects of sample disturbance on laboratory compression curves are illustrated in Figure 7.9 by data representing a good and a poor sample. Sample disturbance decreases the void ratio (or increases the strain) at a given consolidation stress and makes it difficult to define the point of minimum radius. This decreases the estimated value of $\bar{\sigma}_p$ based on the Casagrande method. Experience indicates that thin-wall samplers give field samples with a minimum of disturbance. Most disturbance probably occurs before the tube is opened and the sample extruded. Block samples have repeatedly been shown to be superior to better quality tube samples. To allow for some sample disturbance, Schmertmann (1955) developed the method for reconstructing the in situ compression curve illustrated in Figure 7.9. The procedure requires an oedometer test with an unload-reload cycle after reaching the virgin compression curve. The unload-reload cycle should encompass the current overburden pressure $\bar{\sigma}_0$ and the maximum past overburden pres-

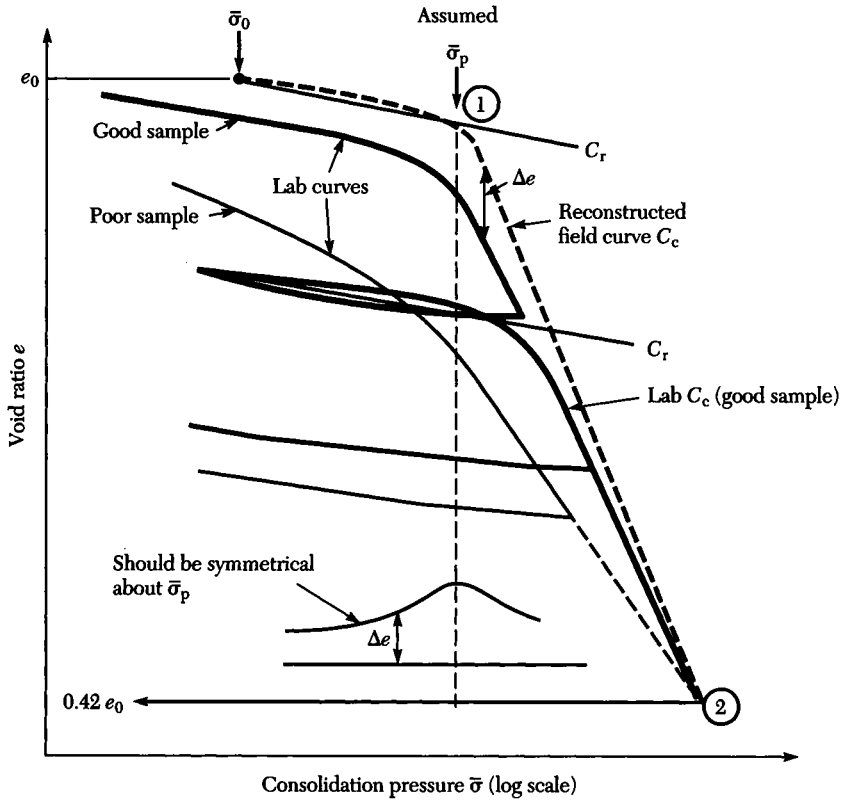


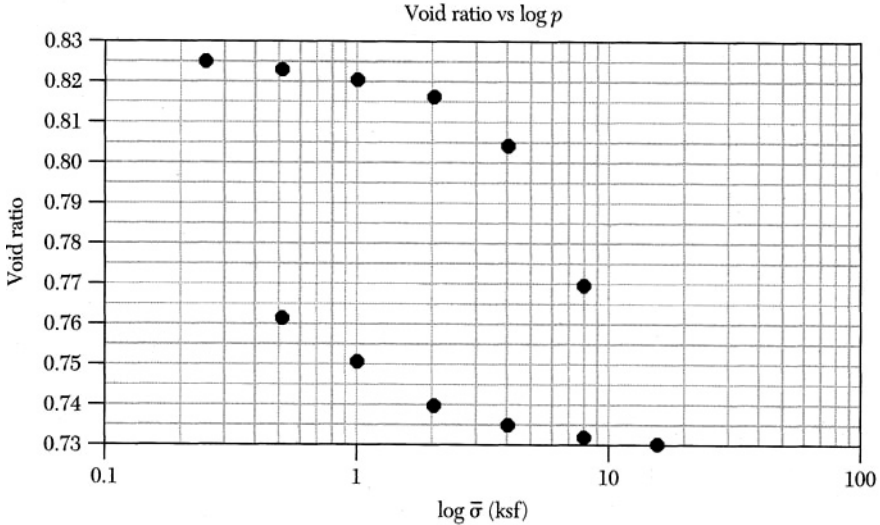
FIGURE 7.9 Reconstruction of in situ compression curve using Schmertmann's (1955) method.

sure $\bar{\sigma}_p$. Draw in the recompression line representing the recompression index C_r , and draw a parallel line through the in situ condition $(e_0, \bar{\sigma}_p)$. Assume a trial $\bar{\sigma}_p$ based on the Casagrande method and locate point 1 as shown in Figure 7.9. Next draw a line through point 1 and the intersection of the laboratory curve with $0.42 e_0$. The value, $0.42 e_0$, is based on experimental evidence showing that laboratory curves with varying degrees of disturbance will approximately intersect the field curve at 42% of e_0 . Now sketch in the trial compression curve and plot values of Δe (difference between the trial and laboratory curves) versus $\log \sigma$ as shown at the bottom of Figure 7.9. The correct value of $\bar{\sigma}_p$ corresponds to the trial compression curve giving the most symmetrical curve of Δe versus $\log \sigma$. The assumed value of $\bar{\sigma}_p$ in Figure 7.9 should be increased slightly to make the curve representing Δe more symmetrical.

EXAMPLE 7.1

A consolidation test was performed on a soil sample that was retrieved from 30 ft deep in a clay layer. The saturated clay layer extends from ground surface to 100 ft

deep. The void ratio versus consolidation pressure is shown below. If the consolidation sample has an initial void ratio of 0.83 and a specific gravity of 2.65, then determine its stress history.



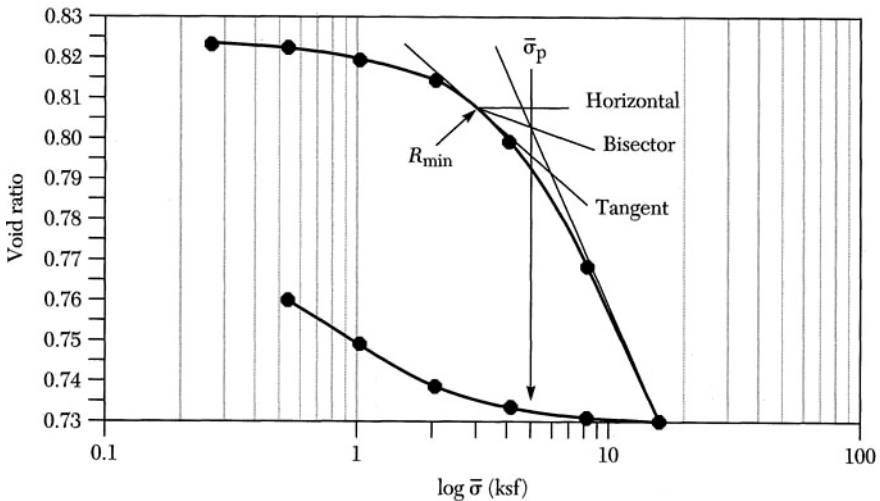
Solution

Calculate the effective overburden pressure at the depth where the sample was retrieved as

$$\gamma_{\text{sat}} = \frac{(e + G_s)}{(1 + e)} \gamma_w = \frac{(0.83 + 2.65)}{1 + 0.87} (62.4) = 118.7 \text{ pcf}$$

$$\bar{\sigma}_{30} = 30(118.7 - 62.4) = 1689 \text{ psf}$$

Determine the maximum past pressure using the procedure described in Figure 7.4. This is done on the following figure.



The maximum past pressure is approximately 5000 psf. This is substantially larger than the effective overburden of 1689 psf. Hence, the soil is overconsolidated. ■

7.2.4 Curve-Fitting Methods

The one-dimensional consolidation behavior observed in the oedometer test on an undisturbed soil sample is described by Terzaghi's consolidation equation

$$\frac{\partial u}{\partial t} = \frac{k(1+e)}{a_v \gamma_w} \frac{\partial^2 u}{\partial z^2} \quad (7.12)$$

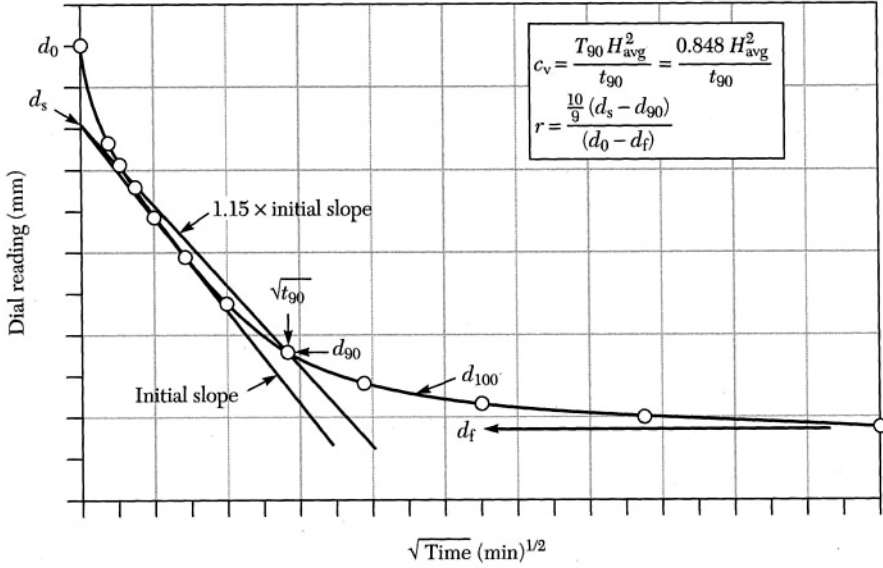
where $k(1+e)/a_v \gamma_w = k/m_v \gamma_w = c_v$ is the coefficient of consolidation, k is the coefficient of permeability, $a_v = -\Delta e/\Delta \bar{\sigma}$ is the coefficient of compressibility, e is the void ratio, and γ_w is the unit weight of water. With a decreasing void ratio both k and a_v decrease rapidly, however, the ratio k/a_v and c_v remain fairly constant over a considerable range of pressures. The Terzaghi (1943) theory does include the following simplifying assumptions: (1) the soil is saturated and homogeneous, (2) the pore water and soil particles are incompressible relative to the soil skeleton, (3) water drainage and compression are one-dimensional, (4) vertical strains are small in comparison with thickness of the sample, and (5) the time lag of compression is caused entirely by the low soil permeability. This permits secondary compression to be handled separately (Section 7.2.5). These assumptions are reasonable for most soils in the oedometer test.

A typical set of dial readings (Figure 7.10), shows change in sample thickness with time during one load increment. Two curve-fitting methods are included for determination of the coefficient of consolidation. The square root of time method (Figure 7.10a) requires that a tangent to the straight line portion of the curve be extended back to intersect zero time, giving the corrected zero point d_s . Through d_s draw a straight line having a slope 1.15 times the initial slope. Theoretically, this straight line will intersect the observed compression-time curve at 90% of total compression for that load increment. According to the Terzaghi theory the coefficient of consolidation is computed from

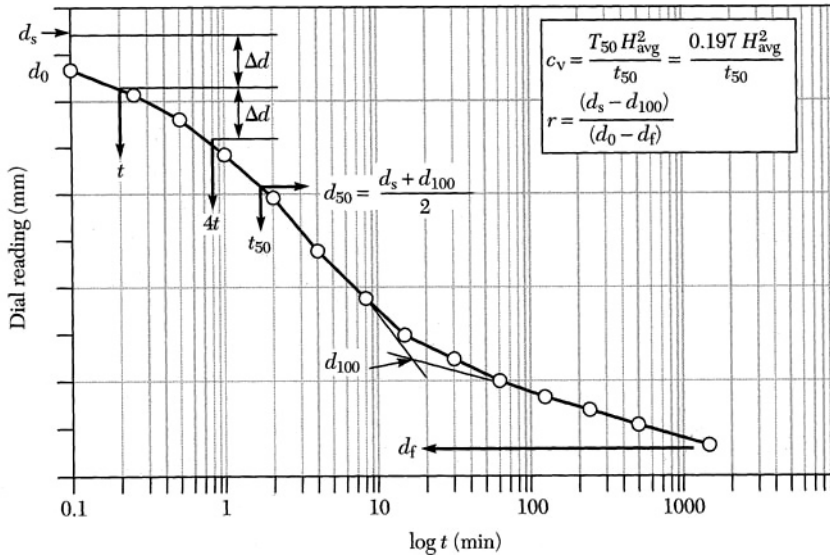
$$c_v = \frac{T_v H^2}{t} \quad (7.13)$$

where T_v is the time factor and equals 0.848 for 90% consolidation, t is the time corresponding to d_{90} , and H equals one half the average sample thickness for the load increment.

The log of time method (Figure 7.10b) requires that tangents be drawn to the two straight line portions of the observed curve. The intersection of these two tangents defines the d_{100} point. The corrected zero point d_s is located by selecting two points on the initial part of the curve indicated by t and $4t$ (Figure 7.10b) and locating point d_s on the horizontal line above point t at a distance equal to the vertical distance between points t and $4t$. This relationship recognizes that the early portion of the curve approximates a parabola. The 50% compression point is



(a)



(b)

FIGURE 7.10 Determination of the coefficient of consolidation and primary compression ratio: (a) square root of time method; (b) log of time method.

halfway between d_s and d_{100} . Using Eq. (7.13) with $T = 0.197$ for 50% compression, t corresponding to d_{50} , and H equal to one half the average sample thickness for the load increment gives the coefficient of consolidation c_v .

These curve-fitting methods contain steps that appear to partially compensate for differences between actual and theoretical soil behavior. The square root method places emphasis on the early stages of consolidation and may give larger c_v values compared to the log time method, which emphasizes the latter stages of consolidation. A correction for the initial point is often required because of equipment limitations or the presence of a small amount of air in the specimen. Continued secondary compression after dissipation of excess pore pressures may require an arbitrary determination of d_{90} or d_{100} . If the soil exactly followed the Terzaghi theory, c_v from the two curve-fitting methods would be identical and the primary compression ratio

$$r = \frac{d_s - d_{100}}{d_0 - d_f} = \frac{\text{primary compression}}{\text{total compression for the load increment}} \quad (7.14)$$

would equal unity. Because of secondary compression and any immediate deformation due to gas compression, the primary compression ratio is always less than unity ($r = 0.7 \pm 0.2$ for typical normally consolidated clays).

7.2.5 Secondary Compression

Soil compression that continues after excess pore water pressures have dissipated (Figure 7.11) is called *secondary compression*. It takes place at a constant effective

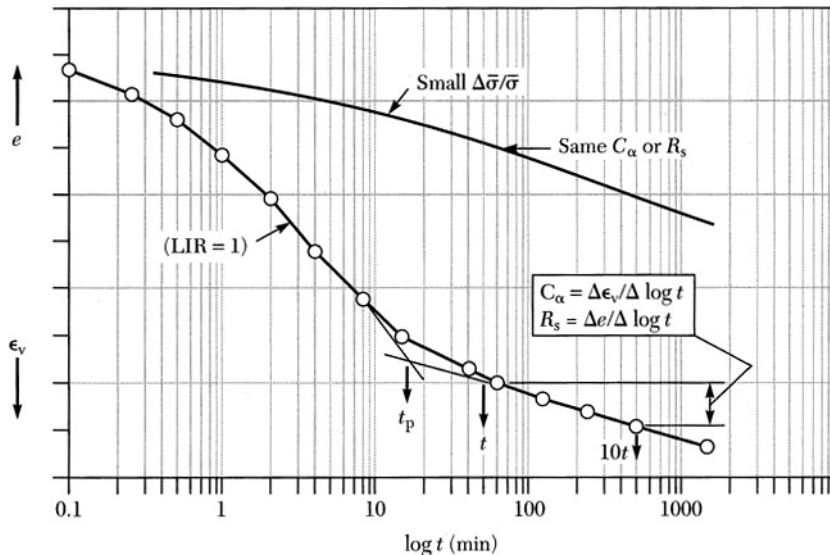


FIGURE 7.11 Soil compression for a small load increment ratio (LIR = 0.25, upper curve) and a large load increment ratio (LIR = 1, lower curve).

tive stress. A small excess pore pressure associated with the very small drainage during compression is difficult to measure. The usual assumption is that secondary compression does not start until after primary compression has been completed. This arbitrary division is convenient for field settlement computations. It is also assumed that a straight line represents the relationship between compression and log time (Figure 7.10b), at least over one or two time cycles for most clays. The rate of secondary compression (secondary compression index C_{α}) can be defined as the change in void ratio, Δe , per log cycle of time

$$C_{\alpha} = \frac{\Delta e}{\Delta \log t} \quad (7.15)$$

or by the change in vertical strain, $\Delta \epsilon_v$, per log cycle of time (modified secondary compression index, $C_{\alpha\epsilon}$)

$$C_{\alpha\epsilon} = \frac{\Delta \epsilon_v}{\Delta \log t} \quad (7.16)$$

Because strain is based on the initial sample thickness and $\Delta \epsilon_v = \Delta e / (1 + e_0)$, note that $C_{\alpha\epsilon} = C_{\alpha} / (1 + e_0)$. The two curves in Figure 7.11 represent both a small (LIR = 0.25) and a large load increment ratio (LIR = 1). Soil compression for the large load increment ratio follows the Terzaghi (1943) theory reasonably well during primary compression. The typical S-shaped compression curve does not develop for the small load increment ratio, whereas the rate of secondary compression (C_{α} or $C_{\alpha\epsilon}$) appears to remain the same for both large or small load increment ratios. Several assumptions commonly made in estimating secondary field settlements include the following: (1) C_{α} is independent of time (during the normal service life), (2) C_{α} is independent of soil layer thickness, (3) C_{α} is independent of the load increment ratio, and (4) the ratio C_{α}/C_c is approximately constant over the usual range of engineering pressures for many normally consolidated clays. The range of C_{α}/C_c values reported by Mesri and Godlewski (1977) for inorganic soils was 0.025 to 0.06. Limited experimental data suggest that C_{α} will increase with increasing temperature and therefore temperature can be a factor in laboratory testing.

The two curves shown in Figure 7.12a for a normally consolidated clay illustrate the influence that secondary compression has on the void ratio–logarithm of pressure curves. The lower dashed curve represents compression data obtained for a load increment duration of 24 h. The corresponding dial reading–logarithm of time curves for two load increments are shown in Figure 7.12b. The straight line portion of the curves following d_{100} represent secondary compression occurring during the 24-h period. The upper curve in Figure 7.12a would be obtained if the load increment were increased at the end of primary consolidation. The assumed loading path (Figure 7.12a) appears to represent soil compression behavior for the 24-h duration load increments. It is normally recommended that the compression curve corresponding to the end of primary consolidation be used to determine the maximum past pressure. This can be accomplished by applying incremental loads at the end of primary consolidation or by correction of the standard 24-h incremental test data as illustrated in Figure 7.12a.

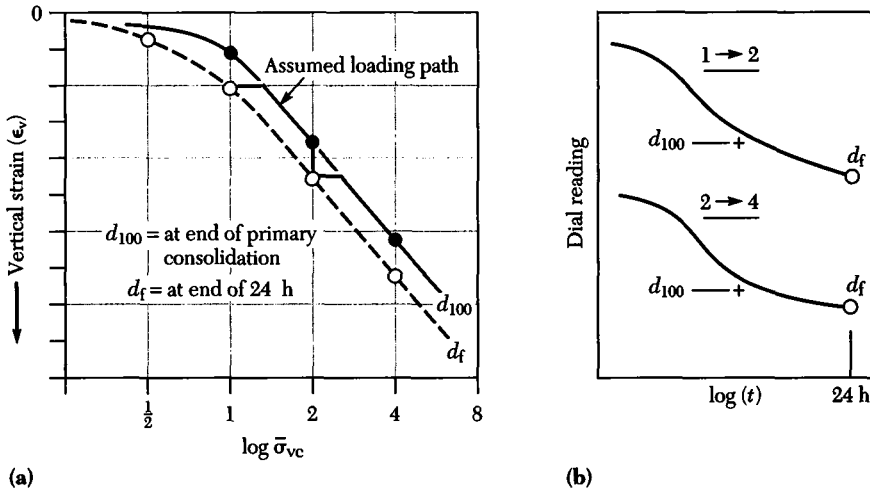


FIGURE 7.12 Correction of oedometer test data to obtain end of primary consolidation compression curve: (a) compression curve; (b) dial reading versus $\log t$.

Secondary field compression over a period of many years will permit the development of a maximum past pressure as illustrated in Figure 7.12a. The older the soil deposit, the greater will be the stress increment required to bring the clay to the compression curve corresponding to the end of primary compression. Measurement of this quasi-preconsolidation pressure requires very-high-quality soil samples and a well-defined compression curve. Laboratory results should be combined with knowledge of the past geologic soil history in determination of the maximum past pressure.

7.3 CONSTANT-RATE-OF-STRAIN CONSOLIDATION

The constant-rate-of-strain (CRS) oedometer test was initially developed as a rapid means of determining the preconsolidation pressure. With introduction of the basic theory (Wissa et al., 1971) the technique was extended to measurement of the coefficient of consolidation c_v , the coefficient of permeability k , and the coefficient of volume compressibility m_v . Sample boundary conditions are similar to those in the conventional oedometer test except for one-way drainage of pore water to the top (Figure 7.13a). The soil specimen, with porous stones at the top and bottom, is confined laterally by a similar type of ring (Figure 7.14). In place of incremental loading, the specimen is loaded at a constant rate of strain chosen so that excess pore pressures u_b at the undrained base of the specimen (Figure 7.13a) do not exceed 5% to 10% of the total vertical stress, σ_a (Sandbaekken et al., 1985). The ASTM standard (designation: D 4186-82) recommends a pore pressure ratio $u_b/\bar{\sigma}_a$ of between 3% and 20%. Prior to start of continuous loading, a vertical stress close to $\bar{P}_0/4$ is applied to the specimen in one increment. Thereafter the vertical stress will increase dependent on the rate of strain. Sandbaekken et al. (1985) re-

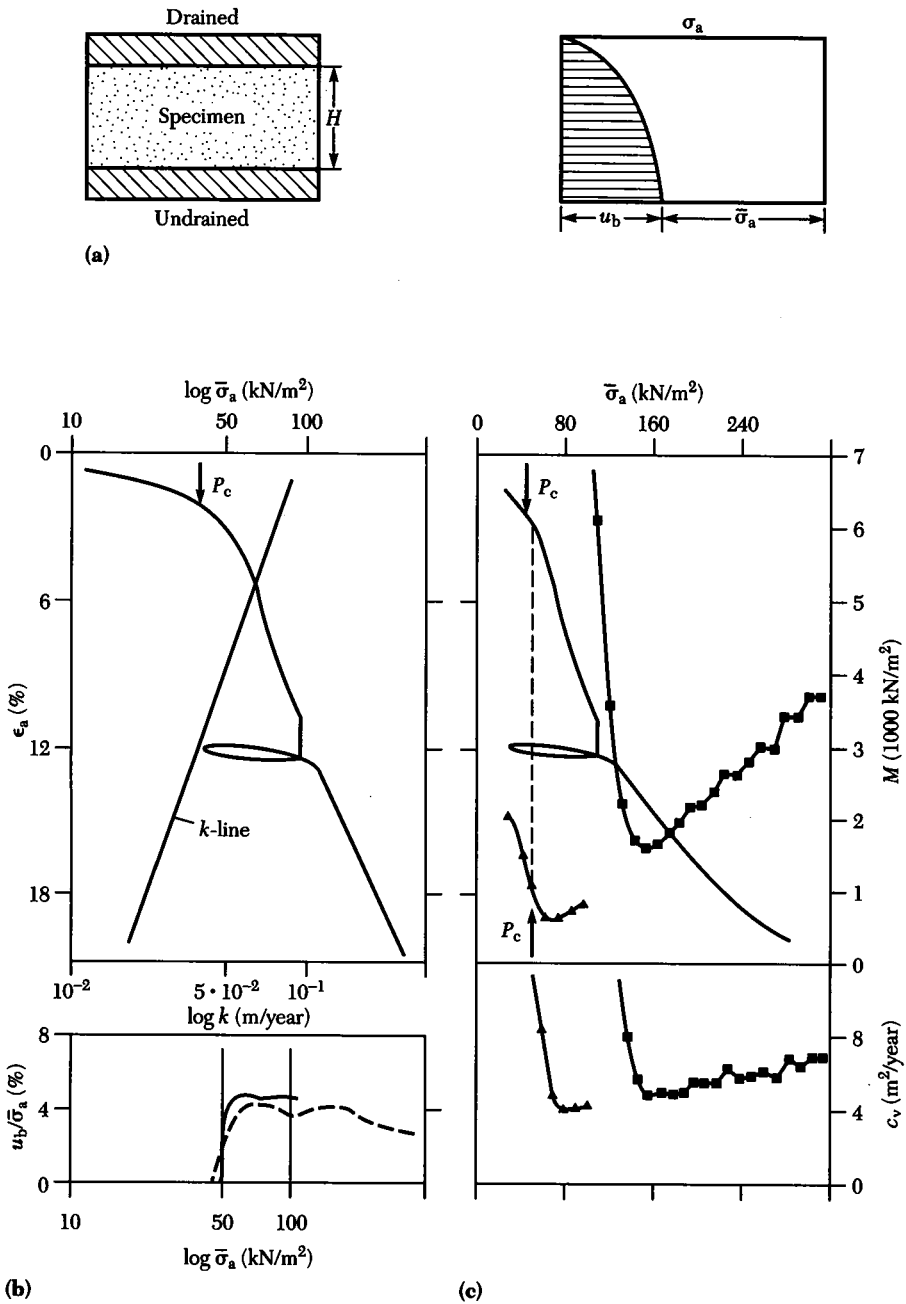
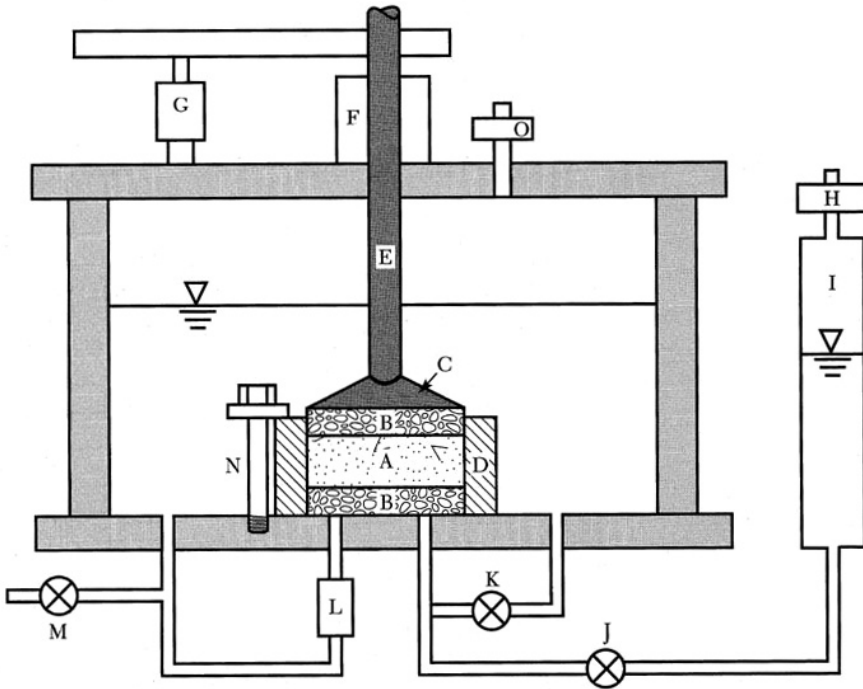


FIGURE 7.13 Constant-rate-of-strain (CRS) oedometer test on a soft plastic clay: (a) stress distribution in a CRS oedometer specimen; (b) stress-strain curve, k -line, and excess pore pressure (semilog plot); (c) stress-strain curve, constrained modulus, and coefficient of consolidation (linear scale). (After Sandbaekken *et al.*, 1985.)

7.3 CONSTANT-RATE-OF-STRAIN CONSOLIDATION 263



- | | |
|-------------------------------------|---|
| (A) Soil specimen | (I) Burette |
| (B) Porous stones | (J) Valve for permeability test |
| (C) Loading platen | (K) Back pressure valve |
| (D) Consolidation ring | (L) Differential pressure transducer |
| (E) Loading piston | (M) Valve to water reservoir |
| (F) Low friction seal | (N) Fastening post for consolidation ring |
| (G) Displacement transducer | (O) Cell pressure regulator |
| (H) Regulator for permeability test | |

FIGURE 7.14 Schematic diagram for the constant-rate-of-strain consolidation test equipment. (After Armour and Dmievich, 1985.)

ported that for many clays a rate of axial strain of 0.5%/h to 1%/h maintains the ratio of pore pressure to total axial stress between 2% and 7% throughout the test. Readings of time, total axial load, axial displacement, and excess pore pressure, taken every 5 to 10 min, provide the data needed for the test results illustrated in Figure 7.13.

Data interpretation for the CRS oedometer test involves several assumptions. First, the pore pressure distribution in the specimen (Figure 7.13a) is assumed to be parabolic. This permits calculation of the average effective stress $\bar{\sigma}_a$ in the sample as

$$\bar{\sigma}_a = \sigma_a - \frac{2}{3} u_b \quad (7.17)$$

8

Shear Strength of Soils

8.0 INTRODUCTION

The application of load or stress on soil below a foundation, or in a slope, until deformations become unacceptably large is described as **failure**. For this reason, the limiting value of shear stress is often based on a maximum allowable strain or deformation. Shear strength may be defined as the ability of soil to sustain load without undue distortion or failure in the soil mass. The allowable deformation will often control the design of structures, because the usual factors of safety result in shear stresses much less than those that would cause collapse or failure.

A number of stress-strain tests are available for measuring the shear strength of soils. Laboratory tests are designed to permit application of stress to a soil sample with measurement of the resulting deformation and pore water pressures. The more common methods include direct shear, unconfined compression, and triaxial tests. In certain field situations the water content of clays and some silts does not change for an appreciable time after application of stress. This undrained condition permits use of the vane shear test and penetrometers for evaluation of shear strength. This chapter describes the main features of the more common methods used to evaluate the shear strength of soils.

8.1 SOIL DEFORMATION BEHAVIOR AND STRENGTH

Soil materials deform when subjected to a change in stress. Consider a saturated soil element initially under the stresses σ_1 , σ_2 , and σ_3 as shown in Figure 8.1a. When stresses are increased by $\Delta\sigma_1$, $\Delta\sigma_2$, and $\Delta\sigma_3$, a simultaneous rise in pore water pressure Δu occurs. For an all-around increase in stress, $\Delta\sigma_1 = \Delta\sigma_2 = \Delta\sigma_3 = \Delta\sigma$, the ratio

$$B = \frac{\Delta u}{\Delta\sigma} \tag{8.1}$$

defines the pore pressure coefficient B . For a soil that is fully saturated before application of $\Delta\sigma$, B equals 1.0 (Figure 8.1b), for a dry soil B equals zero, and for a partially saturated soil the value of B falls between zero and unity. These changes in stress and pore water pressures cause the material to undergo certain deformations. If drainage is permitted, excess pore pressures dissipate and a decrease in volume occurs (Figure 8.1c). These stress-strain relationships for soil materials are complex. Certain limiting stress and/or strain levels are related to soil strength. Excessive deformations in soil masses result largely from slippage between soil particles. Localized shear deformations along some surfaces are associated with soil shear strength. Soil deformation behavior, shear strength, and measurement of these properties are described in the following sections.

8.1.1 Stress-Strain Relationships

The stress-strain behavior of soils depends greatly on whether the water content can adjust itself to the state of stress. Two limiting conditions are recognized: (1) drained, under which slowly applied stresses permit drainage such that no excess pore pressures develop, and (2) undrained, under which no dissipation of excess pore pressure can occur during the application of stresses. These limiting conditions may not be fully realized in the field, but they do provide a guide to the behavior of soil masses for changing stresses. Consider first the drained condition with an all-around stress σ_3 acting on the soil sample, as is illustrated in Fig-

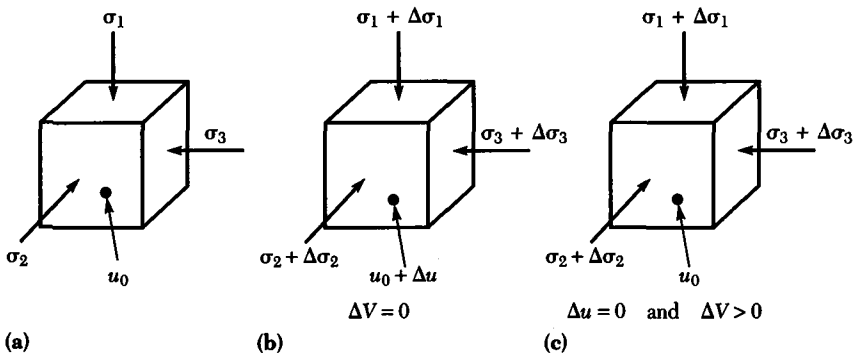


FIGURE 8.1 A soil element under a change in stress.

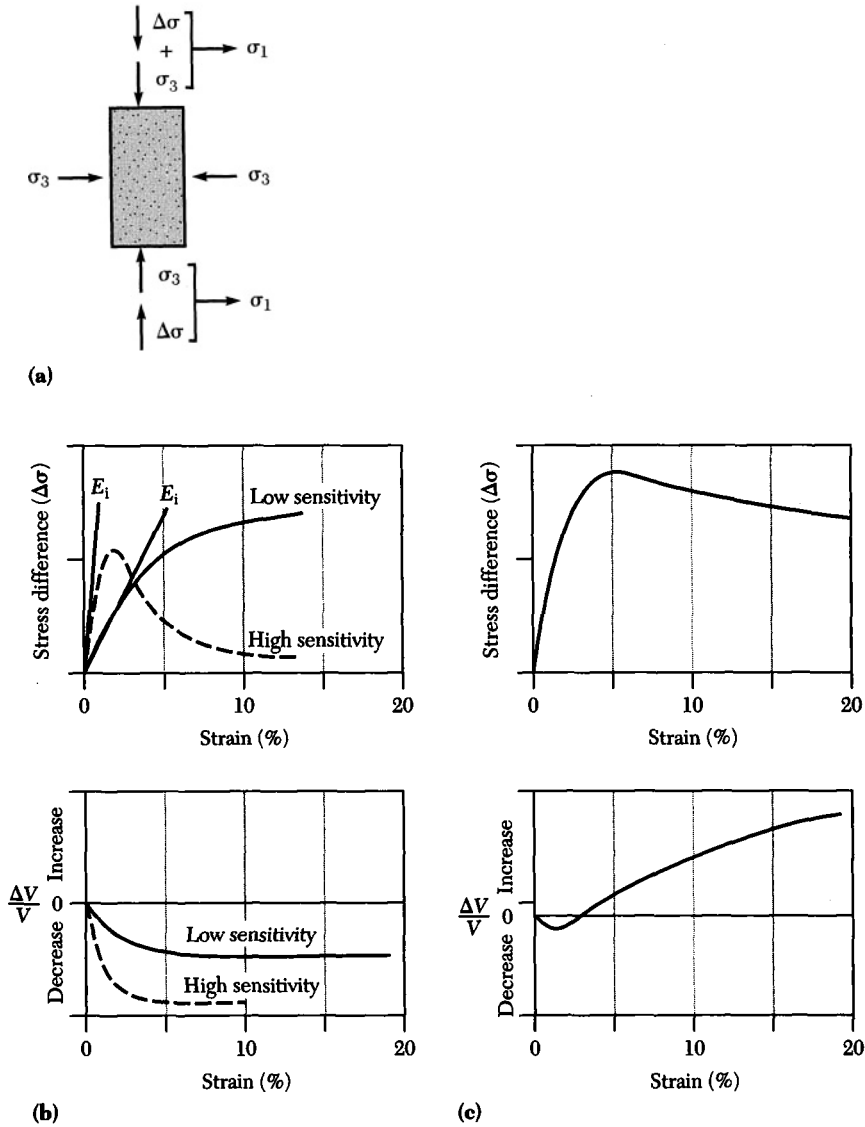


FIGURE 8.2 Saturated soil behavior with an increase stress difference $\Delta\sigma$ for drained conditions: (a) principal stresses acting on sample; (b) loose sand or normally consolidated clay; (c) dense sand or highly overconsolidated clay.

ure 8.2a. The soil will consolidate or swell until the stress is carried entirely by an effective stress σ'_3 within the sample. For an isotropic soil the strains will be equal in all directions. This volume change is not shown in Figure 8.2.

With the soil at equilibrium under an all-around stress σ_3 , the axial stress is slowly increased such that no appreciable pore pressures are permitted to develop. The soil will begin to deform with additional drainage from the soil. The

behavior of loose sands and normally consolidated low-sensitivity clays are represented by the solid curves in Figure 8.2b. A highly sensitive clay is represented by the dashed curves. Note that the stress difference increases to a peak value and then drops along with a larger decrease in volume for the sensitive soil. The initial slopes of both curves are defined as the initial tangent modulus E_t . For small strains, these stress-strain relations approximate those for an elastic material. For dense sand and highly overconsolidated clay, loaded in a like manner, the soil behavior will change as shown in Figure 8.2c. For dense soils, axial deformation initially causes a small decrease in volume followed by a volume increase associated with rearrangement of particles. This tendency for dense soils to increase in volume with increasing deformation is known as **dilatancy**.

The undrained condition occurs when no dissipation of excess pore pressure is permitted during load application. Let the soil mass shown in Figure 8.3a consolidate under an all-around pressure σ_3 until the confining pressure is carried entirely by an effective stress σ'_3 within the sample. The volume change associated with this consolidation is not shown in Figure 8.3. Now, with the sample undrained, let the stress difference increase. For a loose sand or soft normally consolidated clay the deformation behavior is represented by the solid curves in Figure 8.3b. The dashed curves refer to a highly sensitive clay. The pore water pressure will increase with an increase in stress difference. The ratio $\Delta u/\Delta\sigma$ for pore pressure increase Δu due to stress difference $\Delta\sigma$ defines the pore-pressure coefficient A . The experimental relation between A and strain is given by the lower curves in Figure 8.3b. For the loose sands and insensitive normally loaded clays, note that A increases with strain and approaches unity. For very loose sand and sensitive clay, the soil structure may collapse with strain, giving A values greater than unity, as shown by the dashed curve in Figure 8.3b.

For dense sand or highly overconsolidated clay, loaded in a similar manner, the soil behavior will change as shown in Figure 8.3c. A larger stress difference is required to deform the soil. The pore pressure will increase at small strains and then decrease to negative values relative to atmospheric pressure. This decrease in pore pressure develops when soil dilatancy and a volume increase cannot take place because sample drainage is prevented. The pore-pressure coefficient A will be positive at low strains, then decrease to negative values at larger strains. At a critical void ratio, intermediate to the densities illustrated in Figure 8.3, the undrained soil will develop very small or negligible changes in pore pressure. The initial slopes of the stress-strain curves in Figure 8.3 represent the initial tangent modulus E_{iu} for the soil in a consolidated-undrained state. The stress-strain relations illustrated in Figures 8.2 and 8.3 will vary depending on the initial degree of saturation and the method of compaction for compacted soils.

8.1.2 Mohr-Coulomb Failure Criterion

Stress-strain behavior for typical soils, illustrated in Figures 8.2 and 8.3, shows that failure is not always clearly defined. The peak stress difference is normally taken as failure. With plastic soils the stress difference may continue to increase for strains exceeding 20%. In this case it is convenient to define failure at some ar-

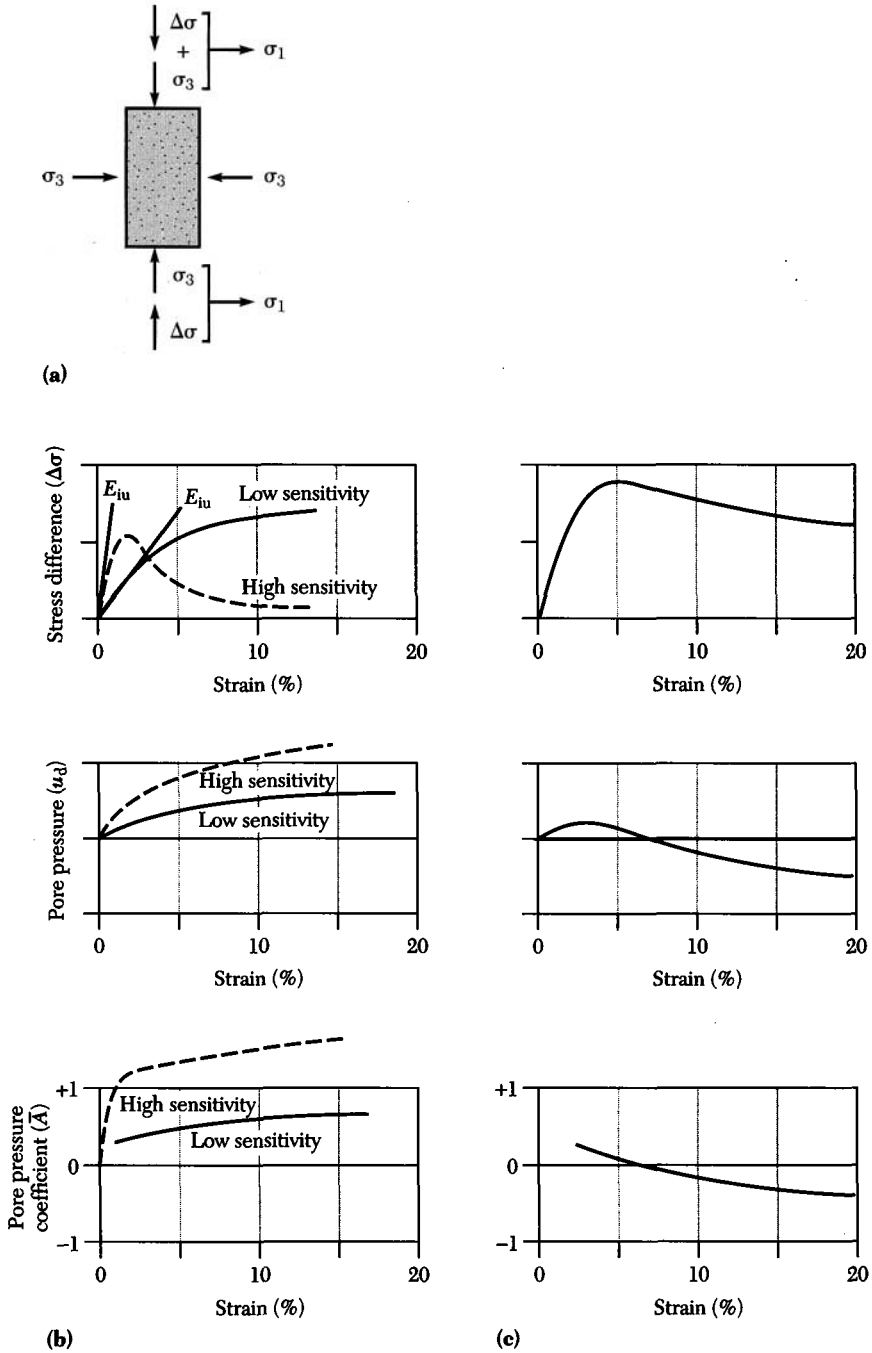


FIGURE 8.3 Saturated soil behavior with an increase stress difference $\Delta\sigma$ for undrained conditions: (a) principal stresses acting on sample; (b) loose sand or normally consolidated clay; (c) dense sand or highly overconsolidated clay.

bitrary strain, 15% or 20%, or at a strain at which the function of the structure may be impaired. Soil strength is now taken as the maximum or yield stress or the stress at some strain acceptable to the engineer. For design applications it is common to use these measured strengths to determine soil strength parameters common to the Mohr-Coulomb failure criterion.

The stresses acting on the soil sample at failure are used to construct Mohr stress circles with normal stress on the horizontal axis and shear stress on the vertical axis. Total (T) or effective (E) stresses may be used depending on the basis on which the strength parameters are to be defined. It is convenient to work with only the top half of the Mohr stress circles. For loose sand (Figure 8.4a) with positive pore pressures, note that the effective stress circle is displaced to the left. The drained condition, with no pore pressures, gives a larger stress circle at failure. Two or more stress circles, based on effective stress, define a limiting or **Mohr failure envelope** with a slope defined by the angle of internal friction $\bar{\phi}$ (Figure 8.4a). For cohesionless soils this envelope passes through the origin. For dense sand (undrained condition) with dilatancy and negative pore pressures, note that the effective stress circle is displaced to the right (Figure 8.4b). For the drained condition the smaller circle represents both total and effective stresses. Again a Mohr failure envelope is defined, with the slope determined by the angle of internal friction $\bar{\phi}$. The dependence of $\bar{\phi}$ on the initial sand density or void ratio will be discussed in Section 8.3.1.

Mohr failure envelopes for cohesive soils are dependent on whether the soil is normally consolidated or overconsolidated. Again, stresses acting on the soil sample at failure (Figures 8.2 and 8.3) are used to construct Mohr stress circles. Total (T) or effective (E) stresses are used depending on which basis the strength parameters are to be defined (Figure 8.5). For normally consolidated cohesive soils the envelopes pass through the origin and are similar to those for cohesionless materials. Within the overconsolidated stress range larger Mohr circles raise the envelope, giving a vertical axis intercept or cohesion. The relationships between total and effective Mohr stress circles and the failure envelopes are illustrated in Figure 8.5. The break in the total stress envelope (point z) occurs to the right of the break for the effective stress envelope. In practice, Mohr failure envelopes are determined by tests on several samples consolidated over the working range of the field problem.

8.2 MEASUREMENT OF SOIL STRESS-STRAIN PROPERTIES

Several different tests have come into common use for measurement of soil stress-strain properties, each designed to observe a particular type of deformation or loading condition. Confined soil compression behavior is measured with the oedometer test (Section 7.2). Triaxial soil compression permits measurement of both distortion and volumetric deformation. Direct shear involves primarily soil distortion with some volumetric deformation. Special laboratory tests may use hollow soil cylinders, a vane shear apparatus, cone penetration devices, and/or

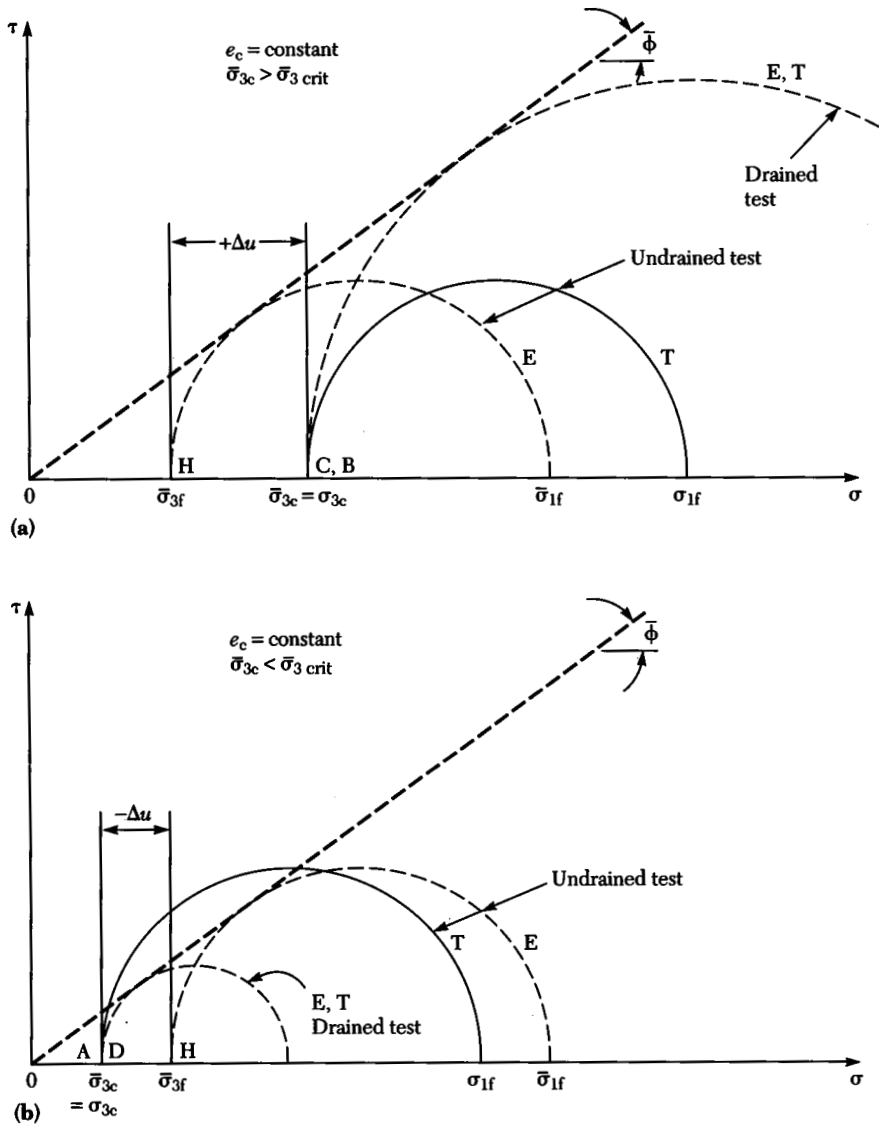


FIGURE 8.4 Mohr failure envelopes for drained and undrained cohesionless soils in triaxial compression: (a) loose sand; (b) dense sand.

cyclic stress applications. The more common test methods are described in the following sections.

8.2.1 Direct Shear

The direct shear test may involve shearing of rectangular, hollow, or solid cylindrical soil samples. Using the apparatus illustrated in Figure 8.6a, a normal load is

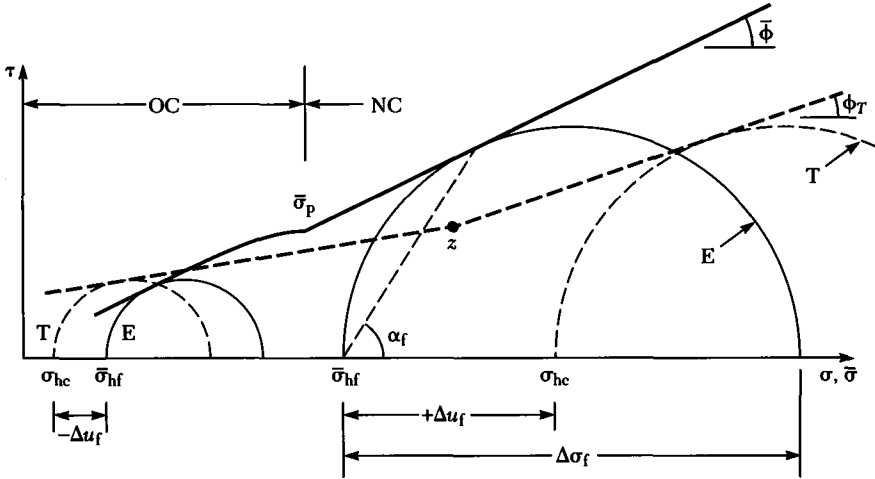


FIGURE 8.5 Mohr failure envelopes for cohesive soils including stresses over both normal and overconsolidated conditions.

applied to the soil sample in the shear box through a rigid loading cap. In cohesive soils drainage may or may not be permitted under the applied normal stress. Next a shear load is applied while the horizontal displacement of the upper soil container and the vertical movement of the loading cap are measured. The rate of shear displacement is about one percent per minute except for drained tests on cohesive soils, which require much slower rates. Shear resistance develops along the predetermined surface through the mechanism of internal friction within the soil. Dividing the shear force and the normal force by the nominal area of the sample gives the shear stress and normal stress on the failure plane. A series of these tests are required, each with the same initial void ratio or soil structure. Typical results (Figure 8.6b) show a shear stress versus displacement curve for each test with $\sigma_{v1} < \sigma_{v2} < \sigma_{v3}$. Vertical movement of the loading cap (Figure 8.6b) shows that sand dilatancy is suppressed with an increase in normal stress. Plotting the peak point from each stress-displacement curve against the normal stress gives the Mohr failure envelope and angle of internal friction shown in Figure 8.6c.

The observed shearing stresses may be corrected for work done by displacement against the applied normal stress. Consider Figure 8.7, which shows both shear strength and increase in sample thickness versus shear displacement. For an increment of displacement $\delta\Delta$ the work done against the normal stress σ_v equals $\sigma_v \delta V = \tau_d \delta\Delta$. Rearrangement gives $\tau_d/\sigma_v = \delta V/\delta\Delta$. Now consider the ratio

$$\frac{\text{frictional strength}}{\text{normal stress}} = \frac{(\tau - \tau_d)}{\sigma_v} = \left(\frac{\tau}{\sigma_v} - \frac{\delta V}{\delta\Delta} \right)_{\text{max}} = \tan \phi_f \quad (8.2)$$

The maximum value of this ratio equals the tangent of the “angle of internal friction.” Experimental results (Bishop, 1950) on a dense sand showed that the increase in shear strength (as measured by ϕ) with density was due primarily to

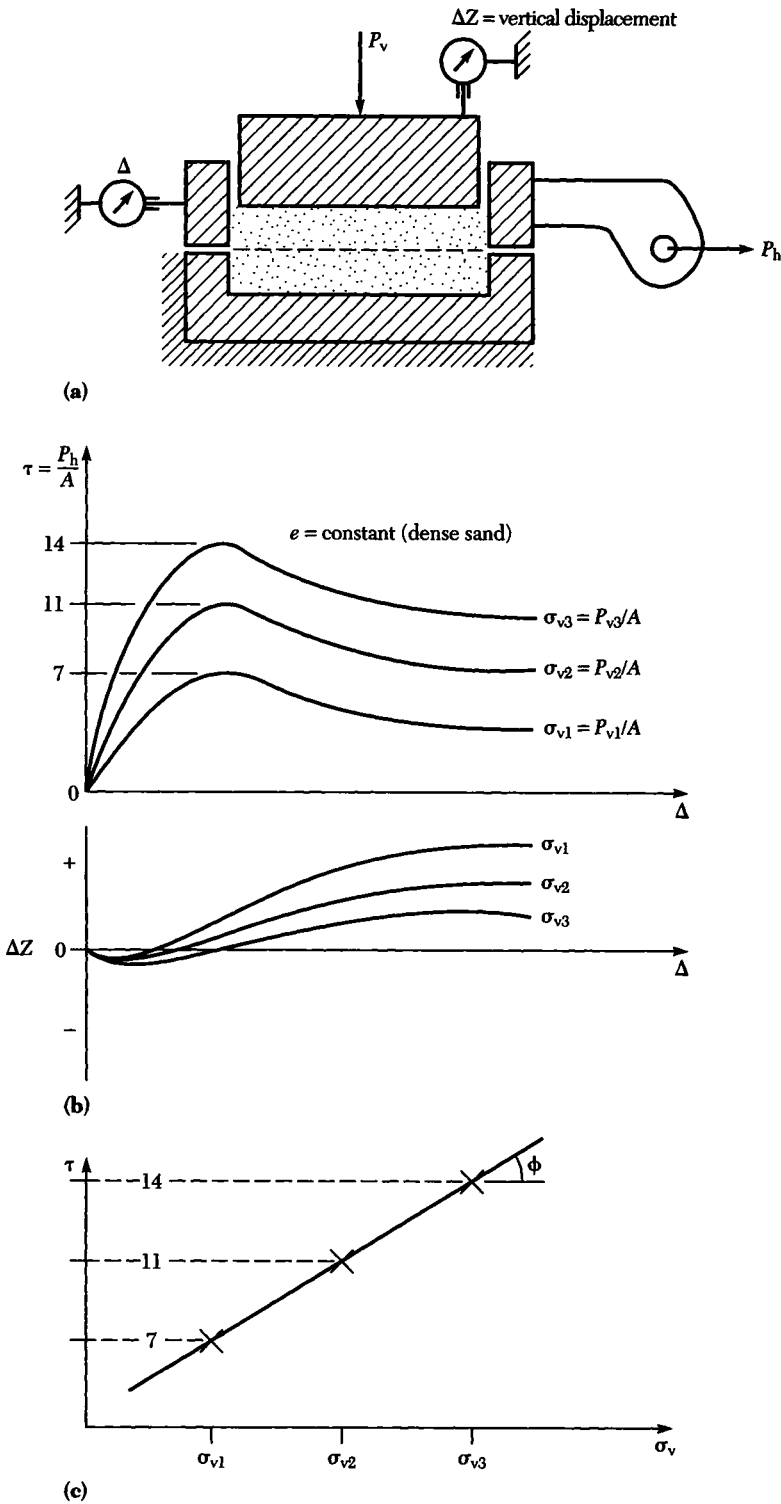
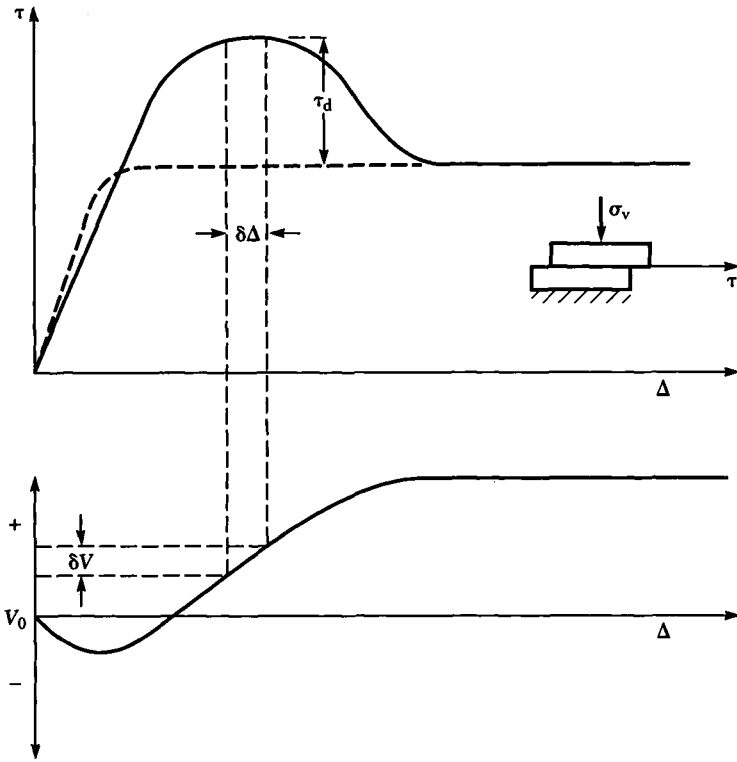


FIGURE 8.6 Direct shear test and typical results: (a) cross-sectional diagram of test apparatus; (b) experimental results; (c) Mohr failure envelope for sand specimen at the same initial density.



σ_v denotes normal stress
 τ denotes shear strength
 τ_d denotes shear stress necessary to cause sample to dilate against the normal stress
 For displacement $\delta\Delta$, work done against normal stress is

$$\sigma_v \cdot \delta V = \tau_d \cdot \delta\Delta$$

Hence $\frac{\tau_d}{\sigma_v} = \frac{\delta V}{\delta\Delta}$

$$\frac{\text{Frictional strength}}{\text{Normal stress}} = \frac{\tau - \tau_d}{\sigma_v}$$

$$= \frac{\tau}{\sigma_v} - \frac{\delta V}{\delta\Delta} = \tan \phi_f$$

FIGURE 8.7 Derivation of an expression for separation of the frictional dilatancy components of shear strength for samples tested in a shear box under drained conditions. (After Bishop, 1950.)

sample dilation and the work done in overcoming frictional forces (measured by ϕ_f) was almost unchanged.

The direct shear test has several advantages and disadvantages. First, the test is inexpensive, fast, and simple for granular soils. The failure plane is predetermined, based on sample orientation in the test apparatus, and stresses on the failure plane are measured directly. This means that the angle of rotation for principal stresses can only be determined after the Mohr-Coulomb failure envelope is known. The problem of controlling drainage limits the test to drained conditions

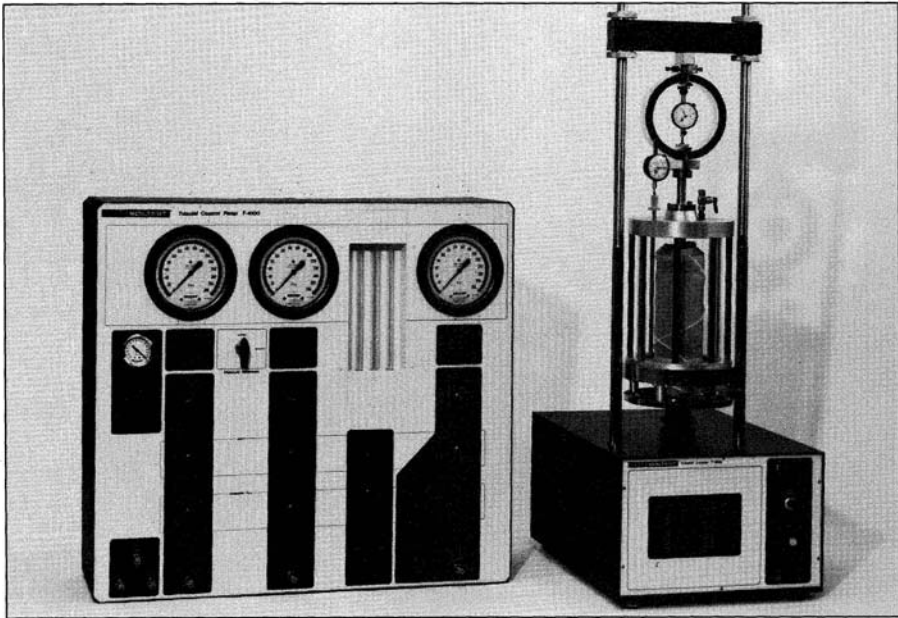


FIGURE 8.8 Triaxial apparatus. (Courtesy of Soiltest, Inc.)

for fine-grained soils. For highly plastic clays the undrained condition may be approximated with a relatively rapid loading rate. Another test limitation involves stress concentrations at sample boundaries. This leads to highly nonuniform stresses within the test specimen. The combination of principal stress rotation and stress concentrations at sample boundaries makes it difficult to simulate in situ loading conditions. For this and other reasons the triaxial test has been developed.

8.2.2 Triaxial Tests

The triaxial test should, theoretically, permit independent control of the three principal stresses (Figure 8.1), so that soil behavior could be observed for generalized states of stress. Mechanical problems related to high compressibility of the soil skeleton and the magnitude of shear strains required to cause failure make independent control too complicated except for special research tests. In practice, cylindrical soil samples are examined in an axially symmetric ($\sigma_1 \geq \sigma_2 = \sigma_3$) stressed state. The cylindrical soil sample, with a loading cap on the top (Figure 8.8), is surrounded by a watertight rubber membrane and enclosed in a cell where a hydrostatic stress state (isotropic case) is created by liquid pressure. A nonhydrostatic state (anisotropic case) can be created by application of an additional axial load. For the second part of the test the sample is axially loaded, by the ram acting on the top cap, until failure takes place in the $\sigma_1 > \sigma_2 = \sigma_3$ stress state. The axial stress is the major principal stress (σ_1), with the intermediate and minor principal stresses (σ_2 and σ_3 , respectively) both being equal to the fluid pressure in the cell. Connections to the sample end caps and porous disk (Figure 8.8) permit ei-

TABLE 8.1 Loading and Drainage Conditions for Triaxial Tests

| | Unconsolidated-Undrained Test | Consolidation Tests | | |
|------------|-------------------------------------|----------------------------------|--|--|
| | | Consolidation Phase | CU | CD |
| σ_3 | Held constant | Held constant | Held constant | Held constant |
| σ_1 | Gradually increased from σ_3 | Equal to σ_3 [*] | Gradually increased from σ_3 | Very gradually increased from σ_3 |
| u | Drainage lines closed | Drainage lines open† | No water permitted to escape. Pore pressure measured for effective stress tests. | Drainage lines open |

*Unless anisotropic consolidation is to be effected.

†In back-pressured tests, pressure is supplied to pore lines, but drainage is permitted.

(After U.S. Navy, 1982)

ther drainage of water and air from the soil voids or, alternatively, the measurement of soil pore water pressures under conditions of no drainage. Test classification is defined by the drainage conditions permitted during each stage of the triaxial test. **Unconsolidated-undrained (UU)** tests involve no sample drainage during application of the all-around stress or during application of the deviator stress. **Consolidated-undrained (CU)** tests permit full drainage and consolidation under application of the all-around stress with no drainage allowed during application of the deviator stress. **Consolidated-drained (CD)** tests permit drainage throughout the test so that full consolidation occurs under the all-around stress and no excess pore pressures develop during application of the deviator stress. These loading and drainage conditions for triaxial tests are summarized in Table 8.1.

Triaxial Apparatus

The triaxial apparatus most frequently used consists of the cell (Figure 8.8) and its accessories. A general layout for a triaxial test unit (Figure 8.9) includes the triaxial cell, which can be loaded by the motor-driven loading press, by deadweights suspended on the hangar, or by the air-operated double-acting piston on the top of the loading frame. Axial loads on the sample are measured by the load ring or force transducer and axial sample strain is measured with the dial gauge and/or displacement transducer. Pore water pressures in the sample are measured using the null-indicator and manometer and/or the pressure transducer shown below the cell. Two valve selector blocks provide connections for the cell pressure and pore pressure, respectively. Each block has outlets to a pressure (screw) control, Bourdon gauge, constant pressure (cell) source, water supply, and air pressure. A mercury pressure manometer, between the two valve blocks, can accurately mea-

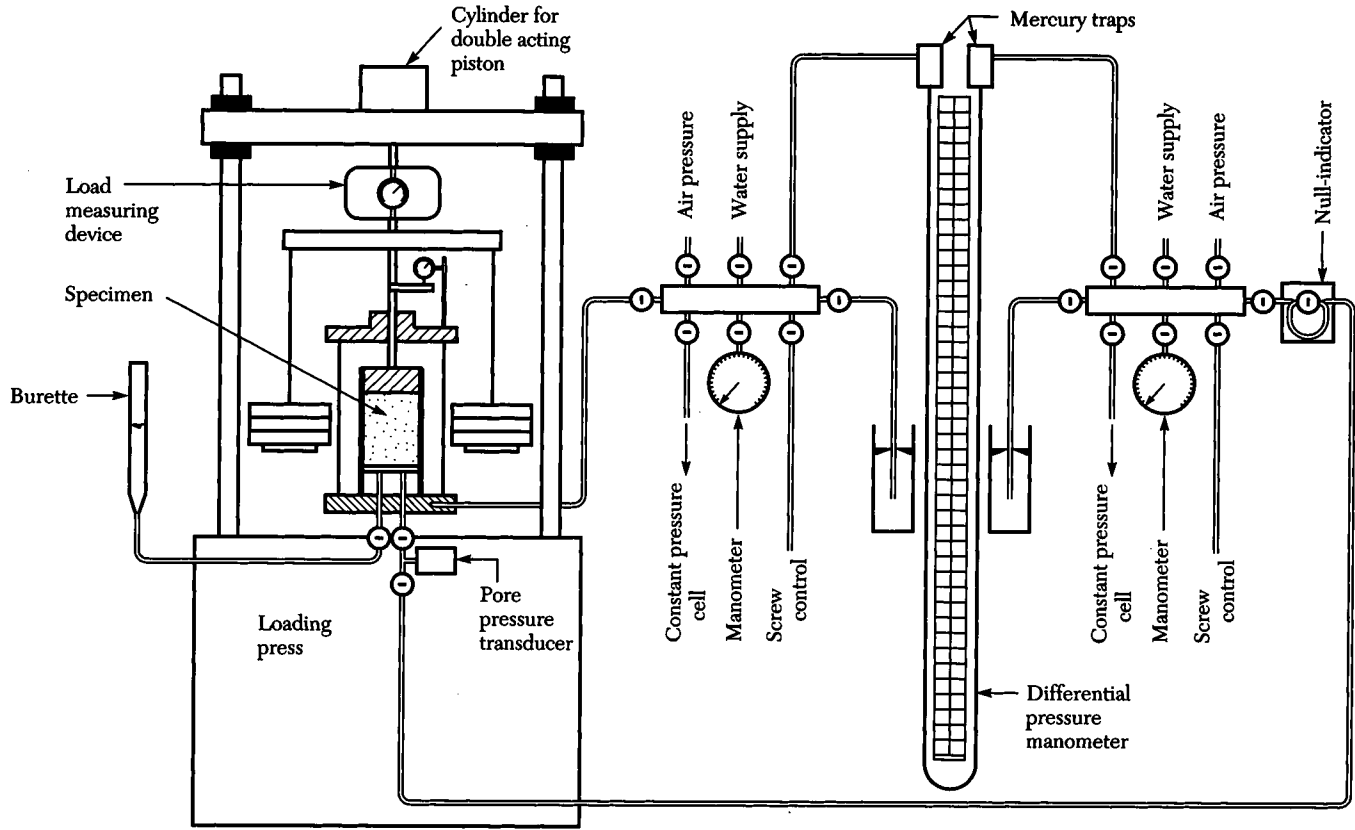


FIGURE 8.9 General layout of a typical triaxial test unit. (After Berre, 1981.)

sure the difference between the cell and pore pressures independently of any back pressure. Two traps prevent mercury from escaping into the valve blocks. In addition to the usual measuring devices, the triaxial unit can also be equipped with electronic transducers for automatic data logging.

Stress Paths

Field deformation and strength behavior of a soil element are dependent on how stresses change during construction and the service life of an embankment, foundation, or retaining wall. Loadings imposed on a laboratory sample will attempt to duplicate stresses anticipated for a similar soil element in the field. To do so, consider first the definitions

$$p = (\sigma_1 + \sigma_3)/2 \text{ or } \bar{p} = \bar{\sigma}_1 + \bar{\sigma}_3/2$$

and

$$q = (\sigma_1 - \sigma_3)/2 = \bar{q}$$

describing the stress point illustrated in Figure 8.10a. A change in stress can be shown by a series of stress circles, or more conveniently by a series of stress points defining a stress path. This stress path can represent effective stresses (ESP) or total stresses (TSP). The case illustrated in Figure 8.10b represents a constant minor principal stress σ_3 with an increasing major principal stress σ_1 on a total stress basis. Both total and effective stress paths are shown in Figure 8.10c summarizing the results of an undrained axial compression (CU) test on a normally consolidated Weald clay. Mohr stress circles are not shown for convenience. The soil sample was initially consolidated under an all-around pressure σ_3 equal to 206.8 kPa and then brought to failure by increasing the axial load. Note that σ_3 remained constant, $\bar{\sigma}_3$ decreased with an increase in pore pressure, and both σ_1 and $\bar{\sigma}_1$ increased with an increase in the compression load, their difference being equal to the pore pressure. The q_f versus p_f points represent soil failure or the K_f line. The slope of the K_f line

$$\bar{\alpha} = \tan^{-1} \frac{q_f}{\bar{p}_f}$$

can be converted to an angle of internal friction using the geometrical relationship

$$\bar{\phi} = \sin^{-1} (\tan \bar{\alpha})$$

For the Weald clay represented in Figure 8.10c the slope $\bar{\alpha} = 20.5$ degrees. The intercept or cohesion \bar{c} equals zero for a normally consolidated clay.

Various stress systems encountered in the field may include axial compression under a footing or an embankment, axial extension (decrease in axial pressure) below an excavation, or lateral extension (decrease in lateral pressure) for the active case behind a retaining wall. The first case, illustrated for a circular footing in Figure 8.10d, shows the vertical stresses increasing more than the horizontal stresses. The principal stress directions remain unchanged on the center

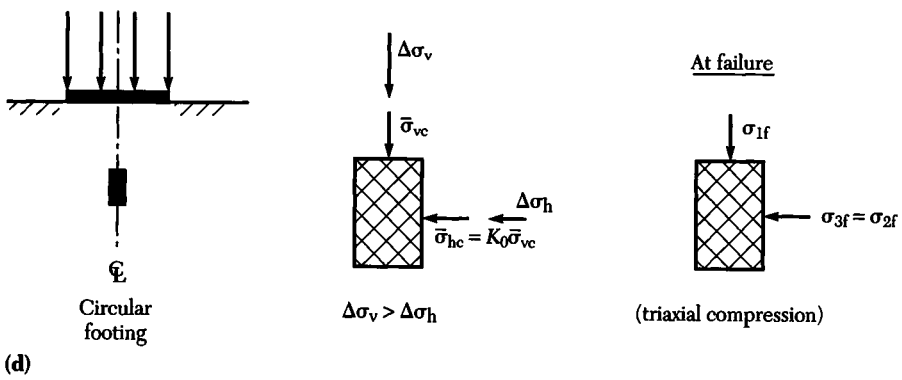
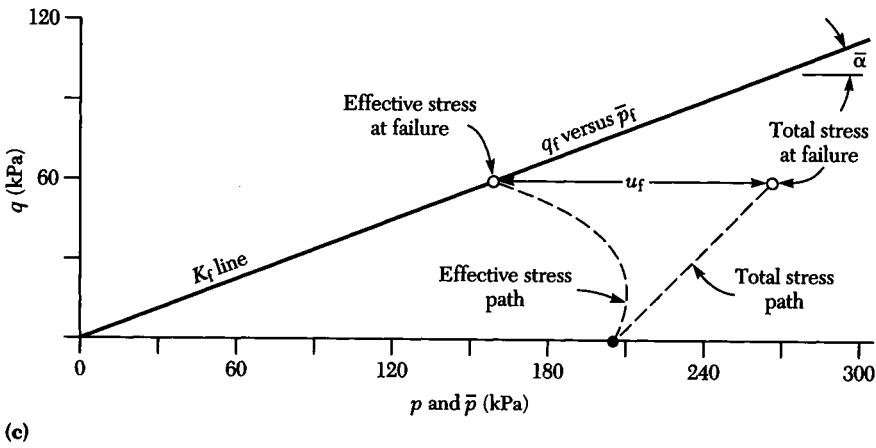
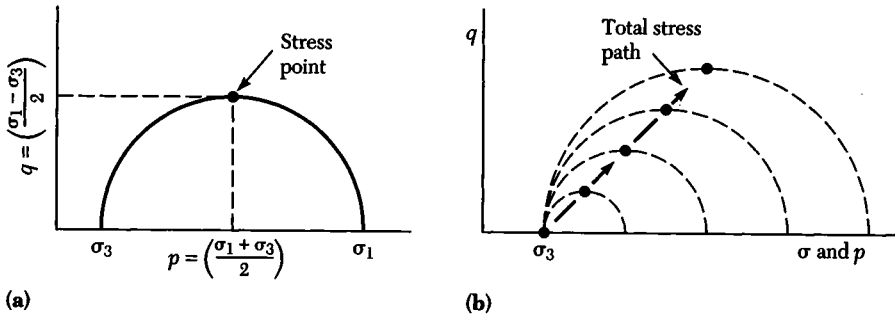


FIGURE 8.10 Stress paths: (a) definitions of p and q ; (b) constant σ_3 with an increasing σ_1 ; (c) undrained axial compression loading of a normally consolidated clay; (d) field problem along with its laboratory model.

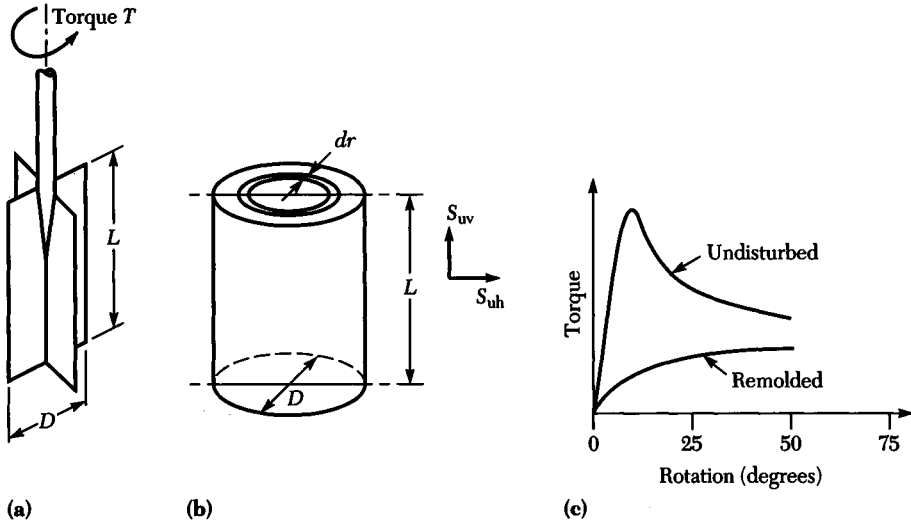


FIGURE 8.11 The vane shear test: (a) four-bladed vane; (b) right cylindrical shear surface; (c) torque curves for a typical soft sensitive clay.

line with the applied stress system modeled by triaxial compression ($\sigma_2 = \sigma_3$). Note that hydrostatic (isotropic) consolidation was illustrated in Figure 8.10c. The field stress conditions would be more closely modeled using nonhydrostatic (anisotropic) consolidation; that is, the axial stress would be different from the cell pressure ($K_0 \neq 1$). This condition can be duplicated in the triaxial cell using the hangar system with deadweights (Figure 8.9) to create the anisotropic stress state.

8.2.3 Vane Shear Strength

In soils with low permeabilities (most clays and some silts) there are many problems in which the water content of the soil does not change for an appreciable time after application of a stress. That is, undrained conditions prevail and the $\phi = 0$ concept assumes practical importance. This condition permits other types of tests to be used advantageously for evaluating the cohesion c . Among the several types the **vane shear test** is the most versatile and widely used, both in the laboratory on very weak or remolded clays and in the field on soft deposits of clay or silt. An added advantage is that the vane (Figure 8.11a) can be attached to the bottom of a vertical rod, placed into the boring, and pushed into a soft soil deposit without appreciable disturbance. The assembly is then rotated, and the relation between torque and angular rotation is determined (Figure 8.11c).

The vane shears a right cylindrical surface with closed ends as shown in Figure 8.11b. If the vertical undrained shear strength is S_{uv} and the horizontal undrained shear strength is S_{uh} , then the torque T required to shear the soil is

$$T = \underbrace{\pi D \frac{D}{2} L S_{uv}}_{\text{sides}} + \underbrace{4\pi S_{uh} \int_0^{D/2} r^2 dr}_{\text{ends}} \quad (8.3)$$

where D and L are the cylinder diameter and length, respectively, and r is the radius as shown in Figure 8.11b. Rearrangement of terms gives

$$T = \pi \frac{D^2}{2} \left(LS_{uv} + \frac{D}{3} S_{uh} \right) = \pi \frac{D^2}{2} S_{uv} \left(\frac{L}{D} + \frac{S_{uh}}{3S_{uv}} \right) \quad (8.4)$$

This equation in two unknowns, S_{uv} and S_{uh} , can be solved if the torque is found for two vanes with different length to diameter ratios. It is often incorrectly assumed for field deposits that $S_{uv} = S_{uh} = S_u$ and

$$T = \pi \frac{D^2}{2} S_u \left(L + \frac{D}{3} \right) \quad (8.5)$$

Clay particles tend to become oriented perpendicular to the direction of the major principal stress during deposition and subsequent consolidation, resulting in horizontal layering or bedding. Parallel orientation of particles alters the undrained strength, with greater difficulty in reorientation of particles and higher strengths being observed when the shear surface is normal to the plane of particles. This directional variation of the undrained shear strength is illustrated in Figure 8.12a in terms of stress-strain curves for an overconsolidated clay. The variation in strength due to orientation of the failure plane for a near-parallel particle configuration is illustrated in Figure 8.12b. This directional variation of the undrained strength was represented in terms of the horizontal (S_{uh}) and vertical (S_{uv}) undrained shear strengths and inclination angle θ by Casagrande and Carrillo (1944), thus

$$S_{u0} = S_{uh} + (S_{uv} - S_{uh}) \sin^2 \theta \quad (8.6)$$

Bjerrum (1972) has reported that the undrained shear strength measured by field vane tests should be corrected before use in stability problems. The correction factor is given as a function of the soil plasticity index in Figure 8.13 with $S_{u,field} = \mu S_{u,vane}$.

8.2.4 Other Methods for Shear Strength Measurement

The preceding sections and experiments have been limited to the more conventional methods of shear strength measurement. Several additional laboratory and field tests are briefly described in this section.

Laboratory Tests

Direct Simple Shear Simple shear tests are used to determine directly the shear modulus and, for cyclic loading, can be used in evaluating the liquefaction potential of a sand. The cylindrical soil sample, about 75 mm in diameter by 10 mm high, is confined by a flexible wire-reinforced rubber membrane. This permits application of a fairly homogeneous state of shear stress, thus stress concentrations associated with the direct shear apparatus (Section 8.2.1) are avoided.

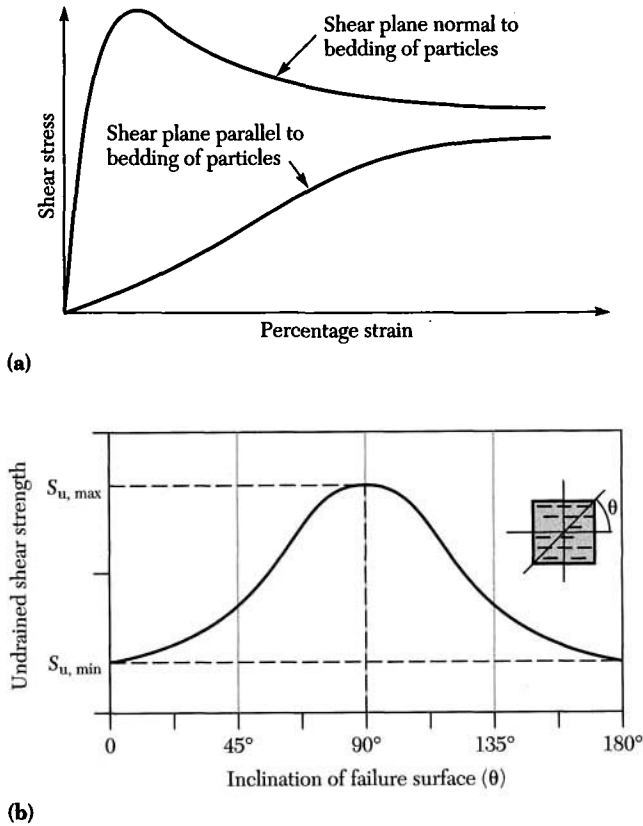


FIGURE 8.12 Undrained shear strength of anisotropic soils: (a) particle orientation effect on stress-strain curves for an overconsolidated clay; (b) directional shear strength relationship for a well-oriented clay fabric.

Initial stress conditions, shown in Figure 8.14a, for direct simple shear (DSS) are the same as for the direct shear test (Experiment 25). With application of the shear stress (τ_{hv}) the soil sample sides are forced to rotate through an angle γ (Figure 8.14b). Complementary stresses are necessary for equilibrium. The Mohr stress circle (Figure 8.14c) enlarges with application of the shear stress until it becomes tangent to the Mohr failure envelope, circle *f*.

For the stresses shown in Figure 8.14b, the pole *P* is found by extending a line from $(\sigma_1, -\tau_{hv})$ horizontally to where it intersects the Mohr failure circle. Lines drawn from the pole represent the orientation of different stress states within the soil sample. The failure plane is represented by line *PF*. The orientation of σ_1 planes, when τ_{hv} is negative, is represented by the line *P* σ_{1f} . For a cyclic simple shear test, the pole is located at *P'* when the shear stress becomes positive. The line *P'* σ_1 gives the new orientation of the principal plane with a negative θ , the angle of principal stress rotation.

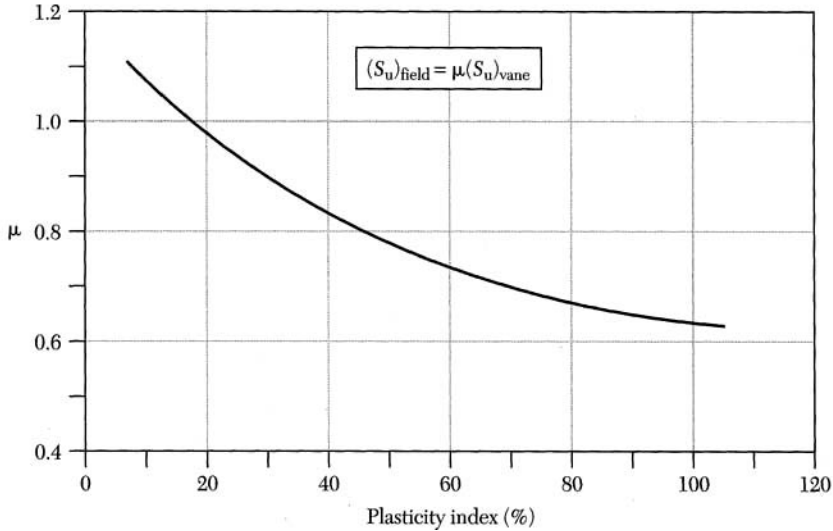


FIGURE 8.13 Vane strength correction factor for soft clays. (After Bjerrum, 1972.)

Hollow Cylinder and Plane Strain Tests The state of stress encountered in many geotechnical problems (long retaining walls, strip footings, etc.) involves an intermediate principal stress σ_2 that falls between the major (σ_1) and minor (σ_3) principal stresses. In the triaxial test σ_2 can only be equal to σ_1 or σ_3 . These special tests, the hollow cylinder and plane strain test, provide a great deal more flexibility in that various combinations of σ_1 , σ_2 , and σ_3 can be applied to the soil sample. The schematic diagram (Figure 8.15a) shows how these stresses are applied to the hollow soil sample in terms of σ_a , σ_b , and σ_z . For the plane strain test (Figure 8.15b) σ_1 and σ_3 can be increased while the ends are fixed during measurement of σ_2 . Details on the hollow cylinder test procedures have been presented by Kirkpatrick (1957) and Wu et al. (1963). The plane strain apparatus along with the test procedures are described by Cornforth (1964). These tests have been used primarily for research rather than practical engineering applications.

Field Methods

Problems associated with soil sampling and laboratory testing have been responsible for the development and use of a number of field methods. The more common methods include the vane shear (Section 8.2.4), the standard penetration test (SPT), the Dutch cone penetrometer (CPT), and the pressure meter test (PMT). Brief descriptions of the last three field methods are given in this section.

Standard Penetration Test (SPT) In the United States the standard penetration test, conducted with an ordinary split sampling spoon (Figure 8.16a), is the most widely used of the field methods. The test is usually performed every 1 m of depth starting at about 1 m below the ground surface. After the spoon reaches the bottom of the drill hole, the sampler is driven 150 mm (6 in.) into undisturbed soil by

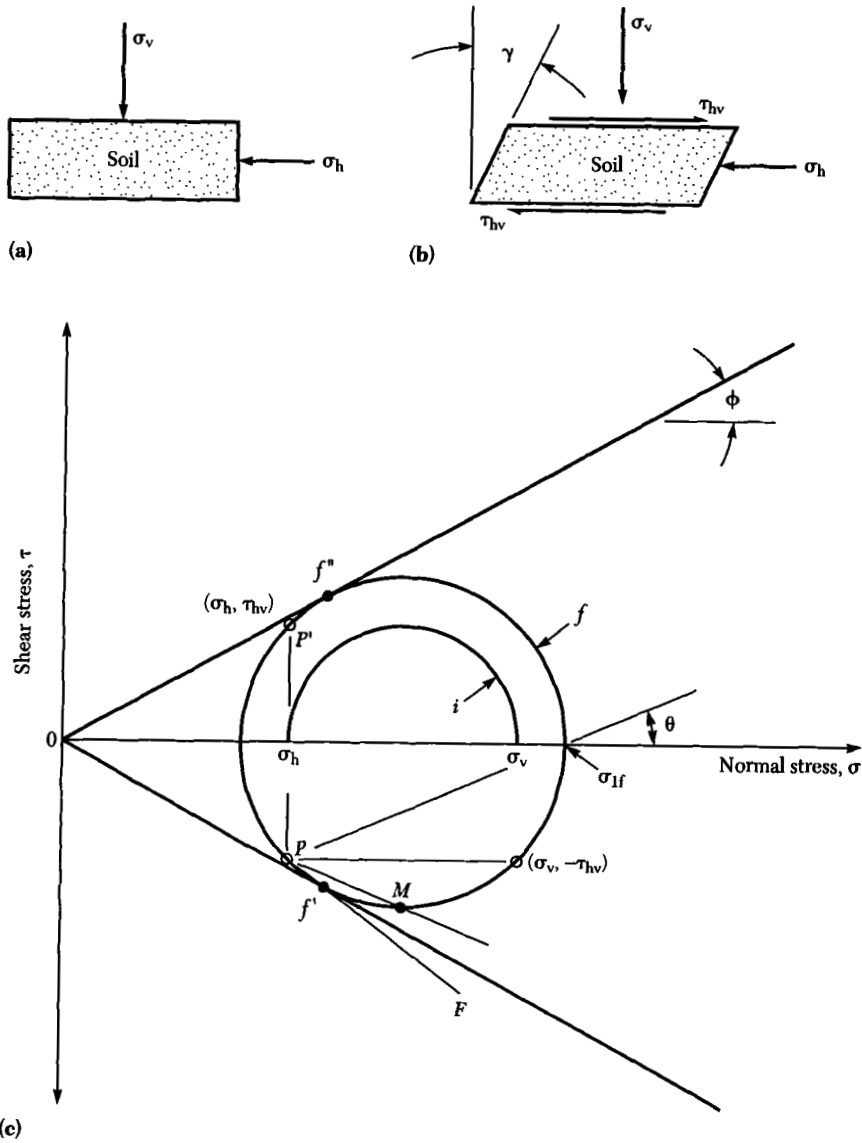


FIGURE 8.14 Simple shear on a cylindrical specimen with a wire-reinforced rubber membrane: (a) initial conditions; (b) sample after placement of shear stresses on top and bottom; (c) Mohr stress circles and failure envelopes.

dropping a 63.5-kg (140-lb) mass from a height of 760 mm (30 in.), and the blow count is recorded. The **blow count** for the next two 150-mm increments is reported as the **penetration resistance** (or *penetration count*) N unless the last increment cannot be completed (blow count >100 or rock is encountered). In this case the blow count for the last 305 mm is used for N . The boring log shows “re-

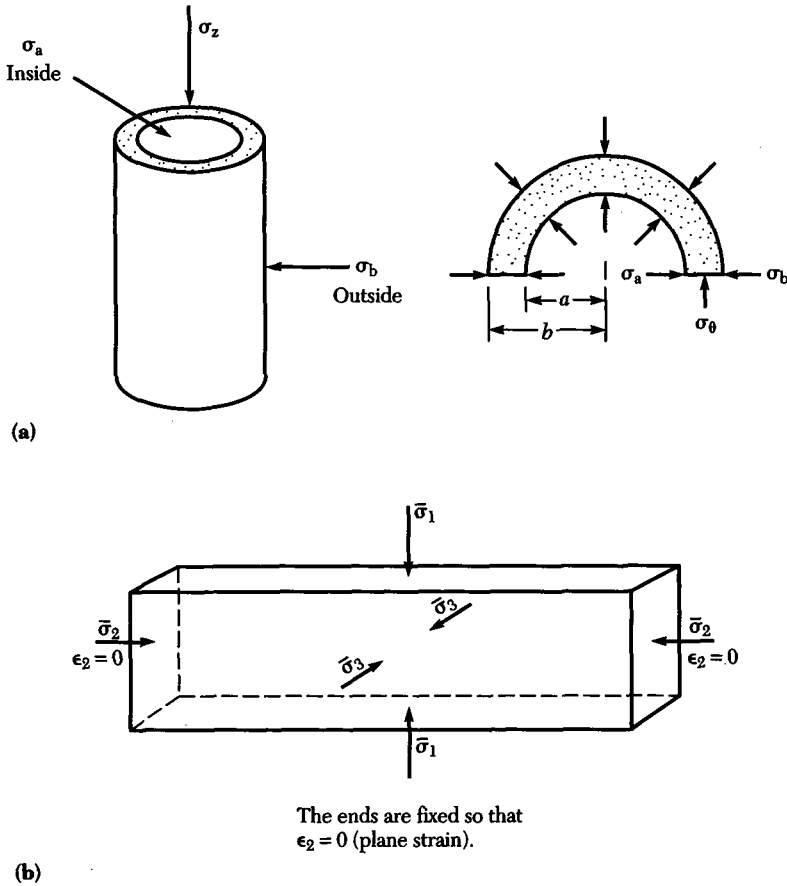
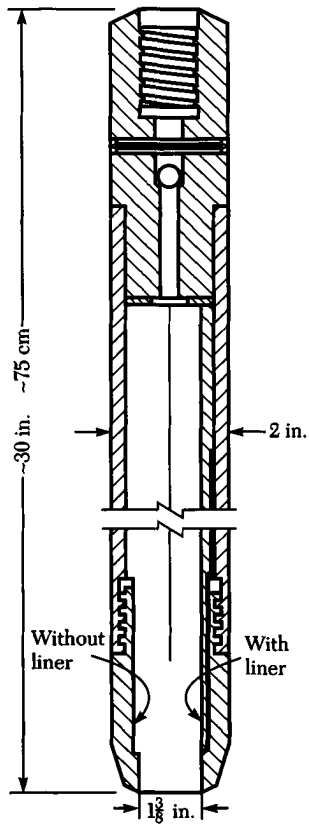


FIGURE 8.15 Special laboratory tests: (a) hollow cylinder test; (b) plane strain compression test.

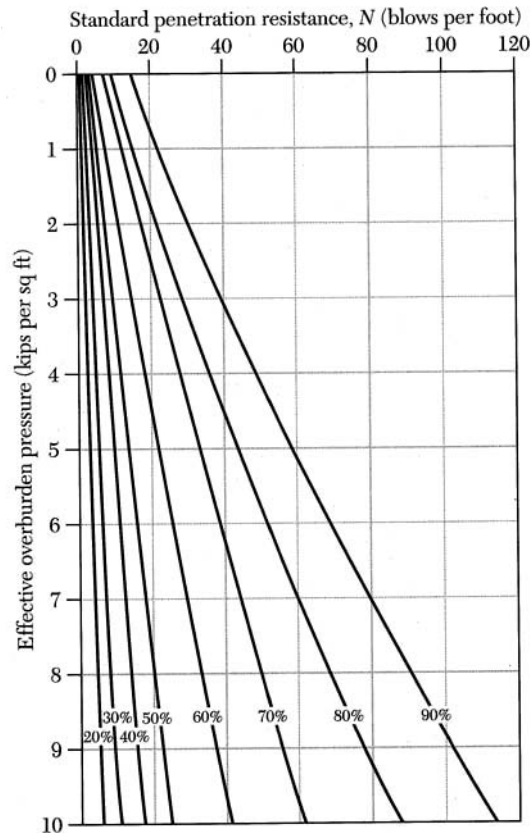
fusal” if the blow count exceeds 100. A correlation of standard penetration resistance with relative density for sand and with the unconfined compressive strength for clay is given in Table 8.2. Determination of the clay shear strength on the basis of penetration resistance can be very unreliable. The N values do give useful preliminary indications of consistency for clay, and the information is in some cases sufficient for final design.

In granular (fine-grained) deposits the standard penetration resistance at the level where N is measured is influenced by the effective vertical stress, density of

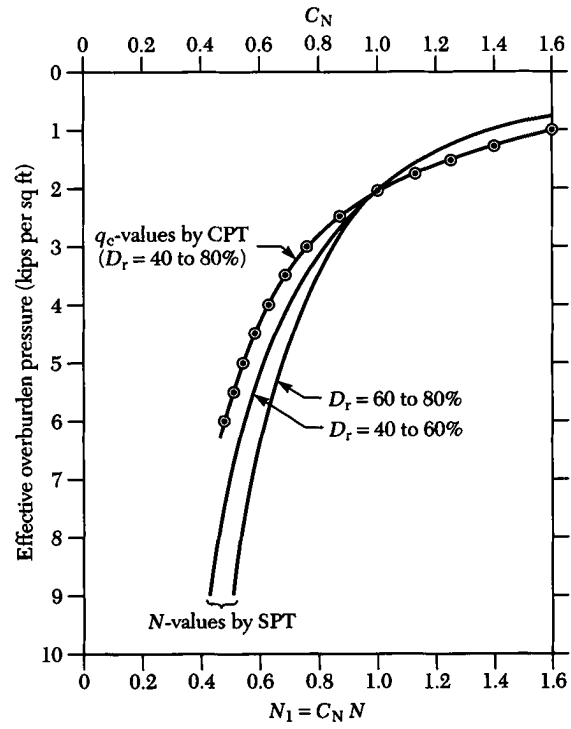
FIGURE 8.16 Standard penetration test (SPT): (a) split-spoon sampler; (b) relationship between standard penetration resistance, relative density, and effective overburden pressure (after Gibbs and Holtz, 1957); (c) curves for determination of C_N (after Seed et al., 1983).



(a)



(b)



(c)

TABLE 8.2 Standard Penetration Test*

| Relative Density of Sand | | Strength of Clay | | |
|---|------------------|---------------------------------------|--|-------------|
| Penetration Resistance N (blows/305 mm) | Relative Density | Penetration Resistance (blows/305 mm) | Unconfined Compressive Strength (kN/m ²) | Consistency |
| 0–4 | Very loose | <2 | <24 | Very soft |
| 4–10 | Loose | 2–4 | 24–48 | Soft |
| 10–30 | Medium | 4–8 | 48–96 | Medium |
| 30–50 | Dense | 15–30 | 96–192 | Stiff |
| >50 | Very dense | >30 | >388 | Hard |

*From Terzaghi and Peck, 1948.

the soil, stress history, gradation, and other factors. Gibbs and Holtz (1957) recognized the effect of effective overburden pressure in their correlation between N and relative density (Figure 8.16b). Their work showed that stiffness and weight of the drill rods connecting the sampler to the ground surface, where driving takes place, did not affect the blow count. A normalized penetration resistance N_1 was used by Seed et al. (1983) in the evaluation of liquefaction potential of sand deposits. The measured penetration resistance is corrected to an effective overburden pressure of 95.76 kPa (1 ton/sq ft) by the relationship

$$N_1 = C_N N$$

where C_N is a function of the effective overburden pressure at the depth where the penetration test was conducted. Values of C_N may be read from the chart shown in Figure 8.16c.

Dutch Cone Penetrometer Test (CPT) The CPT test involves pushing a standard cone at a rate of 1 to 2 m/min into the soil stratum of interest (Figure 8.17a), followed by advancing the cone and friction sleeve together for readings of point resistance q_c and friction on the sleeve jacket f_c . Forces on the penetrometer are measured either mechanically or electrically using transducers. The 60-degree cone has a diameter of 35.7 mm with a projected area of 10 sq cm. The friction sleeve includes an area of 150 sq cm. The equipment for a CPT test can be truck-mounted with an opening in the truck floor for pushing the cone and drill rods via use of a hydraulic ram system. Reactions generally do not exceed 100 kN.

The data are usually presented as point resistance q_c and friction ratio F_r (Figure 8.17b) where

$$F_r = \frac{\text{friction resistance}}{\text{point resistance}} = \frac{q_t - q_c}{q_c} = \frac{q_f}{q_c} \quad (8.7)$$

The ratio between frictional and point resistance is one aid in differentiating between various soil types. Clean sands generally exhibit very low ratios (low friction component in comparison to point resistance), and an increase in the clay content will result in a higher ratio (Figure 8.17b). The cone resistance is related to the undrained shear strength for cohesive soils because undrained conditions develop

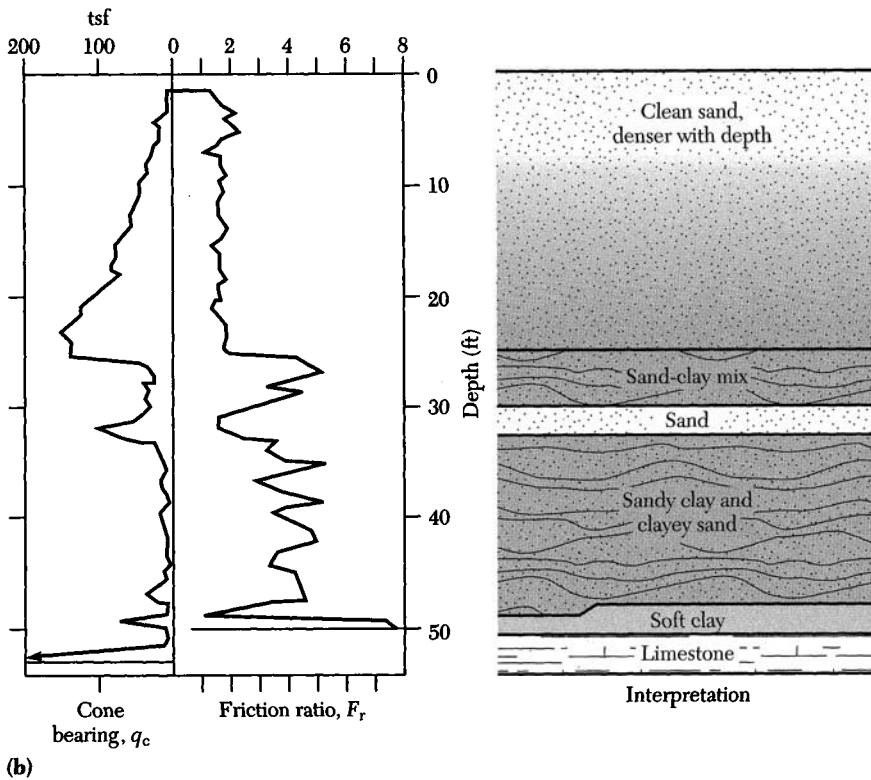
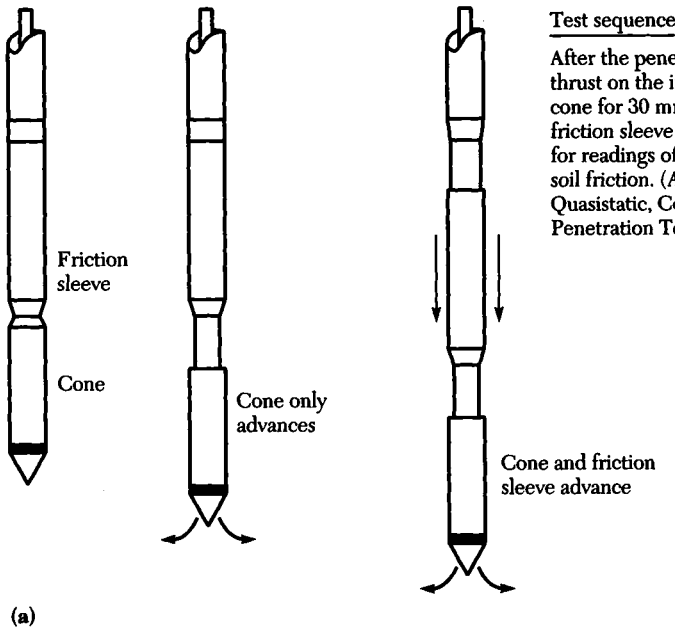


FIGURE 8.17 Dutch cone penetrometer test (NAVFAC DM-7.1, 1982): (a) mechanical cone with friction sleeve; (b) cone penetration test results.

TABLE 8.3 Correlation Between the SPT and CPT Tests

| Soil Type | q_c/N^* |
|--|-----------|
| Silts, sandy silts, slightly cohesive silt-sand mixtures | 2 |
| Clean, fine to medium sands and slightly silty sand | 3.5 |
| Coarse sands and sands with little gravel | 5 |
| Sandy gravel and gravel | 6 |

*Units of q_c are kg/cm^2 or tons/ft^2 ; units of N are blows/ft.
(From Schmertmann, 1970.)

for the steady loading conditions. Correlations have been developed for the CPT test with bearing capacity, relative density of sands, strength and sensitivity of clays, and overconsolidation. Schmertmann (1970) has presented a correlation between the cone point resistance and the SPT N values as summarized in Table 8.3.

Pressure Meter Test (PMT) The Menard pressure meter (Figure 8.18) is a special borehole dilatometer that is used for in situ measurements of stress-strain and strength properties of soils adjacent to the borehole. The test may be repeated for each meter of depth, hence information can be obtained for the various soil strata. The pressure meter consists of an inflatable probe, composed of two coaxial cells, and a pressure-volume control device that allows a given pressure to be applied to the wall of the borehole while observations are made on the resulting borehole expansion. The results depend greatly on the quality and accuracy of the drilled borehole in which the probe is placed.

For the standard test, the pressure in the probe is increased up to the limiting pressure in about 10 to 20 increments, the pressure at each stage being kept constant for no longer than 2 minutes. At each stage, volume readings are taken at 30 s, 1 min, and 2 min after the pressure was increased. Pressure meter test results (Ladanyi, 1973) on a frozen (temperature $\approx -0.2^\circ\text{C}$) varved clay of low to medium plasticity, composed of clay layers 12 to 25 mm thick and silt layers 25 to 75 mm thick, are illustrated in Figure 8.19. The volume of fluid V_m injected into the measuring cell from the start of pressure application is plotted in Figure 8.19a. The applied pressure p_c has been corrected for the piezometric head and the extension resistance of the unloaded probe.

Data interpretation is based on the true pressure meter curve, such as would be obtained in the ideal test starting from the original ground pressure p_0 . The true pressure meter curve represents a relationship of the form

$$\Delta V = f(p_c - p_0) \quad (8.8)$$

where p_0 is the original total lateral ground pressure at the level of the test, and

$$\Delta V = V_m - V_{m0} \quad (8.9)$$

where V_{m0} is the volume of liquid forced into the probe up to $p_c = p_0$. The true pressure meter curve is obtained by adjusting the origin from O to O' as shown in Figure 8.19a. The pressure meter modulus E_p may be calculated from the initial

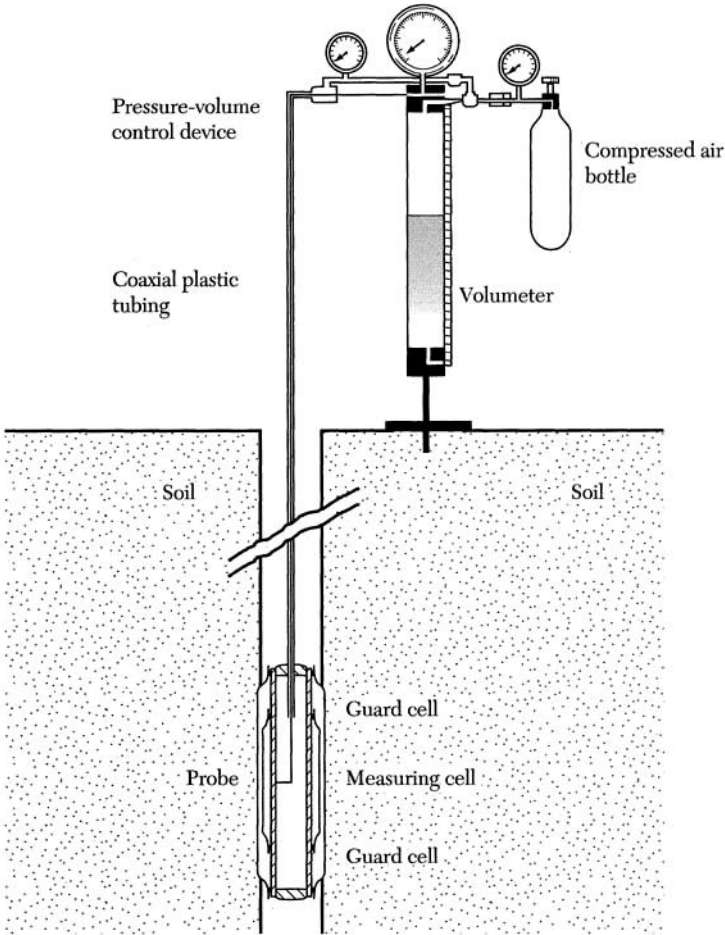


FIGURE 8.18 Menzies pressure meter type G and the test setup.

straight line portions of the pressure meter curve using the relation

$$E_p = \frac{3\Delta p}{\Delta(\Delta V/V)} \tag{8.10}$$

The stress-strain curve (Figure 8.19b) is obtained following the method outlined by Ladanyi (1973). From any two points ($i, i + 1$) of the true pressure meter curve, the corresponding mobilized strength $q_{i,i+1}$ is defined as the principal stress difference, thus

$$q_{i,i+1} = (\sigma_1 - \sigma_3)_{i,i+1} \tag{8.11}$$

and the corresponding average shear strain, defined as the *principal normal strain difference*, is

$$\gamma_{i,i+1} = (\epsilon_1 - \epsilon_3)_{i,i+1} \tag{8.12}$$

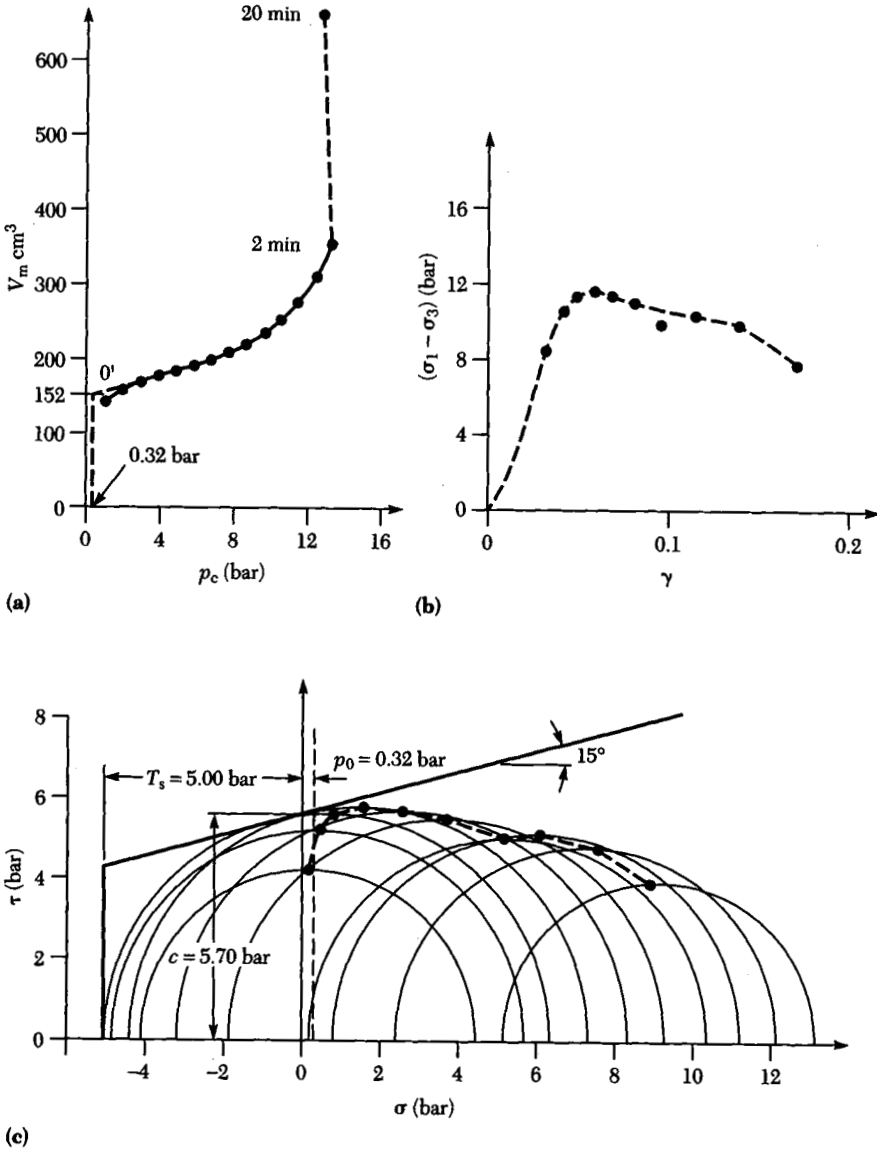


FIGURE 8.19 Pressure meter test results: (a) the pressure meter curve; (b) stress-strain curve; (c) vector curve. (From Ladanyi, 1973.)

The principal stress difference is given by

$$(\sigma_1 - \sigma_3)_{i,i+1} = \frac{(P_i - P_{i+1})}{[\ln(\Delta V/V)_i - \ln(\Delta V/V)_{i+1}] / 2} \quad (8.13)$$

and the principal normal strain difference by

$$(\epsilon_1 - \epsilon_3)_{i,i+1} = [(\Delta V/V)_i + (\Delta V/V)_{i+1}] / 2 \quad (8.14)$$

where p and ΔV denote the coordinates of the true pressure meter curve at points i and $i + 1$ and the current volume V of the borehole is defined by

$$V = V_0 + \Delta V \quad (8.15)$$

in which

$$V_0 = V_{\text{empty}} + V_{m0} \quad (8.16)$$

is the volume of the measuring section of the probe at the moment when the pressure in the probe has attained the original ground pressure p_0 . Ladanyi (1973) recommends that p_0 should be determined independent of the test. The stress-strain curve obtained by this procedure is shown in Figure 8.19b.

Mohr stress circles and vector curves (Figure 8.19c) are prepared based on the known major principal stress σ_1 (equal to the applied radial stress) and the principal stress difference $(\sigma_1 - \sigma_3)$. For any interval $i, i + 1$ of the pressure meter curve

$$\sigma_1 = (P_{c,i} + P_{c,i+1})/2 \quad (8.17)$$

and

$$\sigma_3 = \sigma_1 - q_{i,i+1} \quad (8.18)$$

where p_c is the applied radial stress and $(\sigma_1 - \sigma_3)_{i, i+1}$ is the stress difference defined by Eq. (8.13). The sequence of stress circles in Figure 8.19c shows the variation of $(\sigma_1 - \sigma_3)/2$ with $(\sigma_1 + \sigma_3)/2$. The first two or three circles, which increase in diameter but remain concentric, show a pseudoelastic behavior. The next two or three circles correspond to the peak strength of the soil. The remaining circles show increasing plastic deformation. In Figure 8.19c, the Mohr circle plots have been used only for estimating the lower limits of the frozen soil tensile strength T_s and the cohesion c . To estimate the two parameters, the Mohr circles were enclosed by the Coulomb envelope and a vertical tension cutoff. The friction angle of 15 degrees was assumed for the silty soil based on other information.

8.3 SHEAR STRENGTH OF SOIL MATERIALS

8.3.1 Cohesionless Soils

Cohesionless soil is a frictional material in which a number of soil properties may increase the frictional resistance. These same properties also lead to an increase in the measured angle of internal friction $\bar{\phi}$. A list of these properties is given in Table 8.4 along with their effect on $\bar{\phi}$. Void ratio or soil density has the major effect, with the lower void ratio (higher density) giving the higher shear strength. This effect is illustrated in Figure 8.20 for several soil types. Note that as the void ratio decreases (density increases), the angle of internal friction $\bar{\phi}$ increases for each soil type. If two sands have the same relative density, the soil that has a well-graded particle size distribution (for example, an SW soil compared to an SP soil) has the larger $\bar{\phi}$. Sands containing particles with a greater surface roughness generally will have the greater $\bar{\phi}$. Wet sands will often show a $\bar{\phi}$ 1 to 2 degrees lower

TABLE 8.4 Soil Properties Affecting the Angle of Internal Friction $\bar{\phi}$

| Property | Effect on $\bar{\phi}$ |
|---------------------------------|---|
| Void ratio, e | $e \downarrow$ $\bar{\phi} \uparrow$ |
| Grain size distribution | $C_u \uparrow$ $\bar{\phi} \uparrow$ |
| Particle angularity, A | $A \uparrow$ $\bar{\phi} \uparrow$ |
| Particle surface roughness, R | $R \uparrow$ $\bar{\phi} \uparrow$ |
| Water content, w | $w \uparrow$ $\bar{\phi} \downarrow$ |
| Maximum particle size | No effect for constant e Slight |
| Intermediate principal stress | No effect for constant e $\bar{\phi}_{ps} \geq \bar{\phi}_{\tau\epsilon}$ |

than dry sand. The influence of the intermediate principal stress on $\bar{\phi}$ is shown by special tests such as the plane strain or hollow cylinder test. Ladd et al. (1977) summarized research showing that $\bar{\phi}$ in plane strain is larger than $\bar{\phi}$ in triaxial shear by 2 to 4 degrees in loose sands and by 4 to 9 degrees in dense sands. Increased shear resistance for the plane-strain condition may come about because the soil particles have less freedom for movement around adjacent particles, so there is greater interlocking.

The volume change (dilatancy) accompanying shear deformation in sand involves a shear stress required to provide energy for the expansion as shown in Fig-

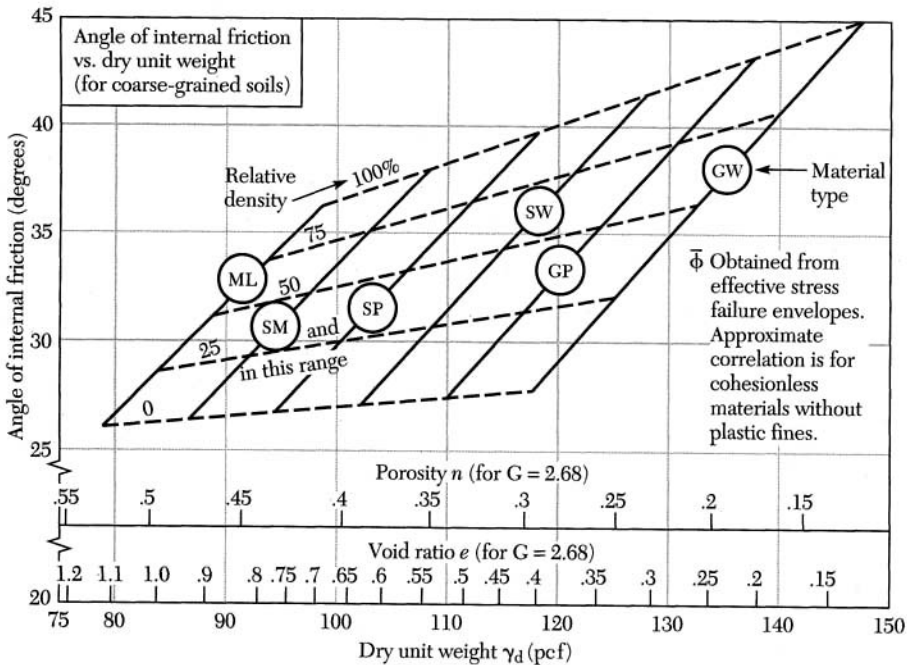


FIGURE 8.20 Correlations between the angle of internal friction and the dry density, void ratio, porosity, and soil classification. (After U.S. Navy, 1982.)

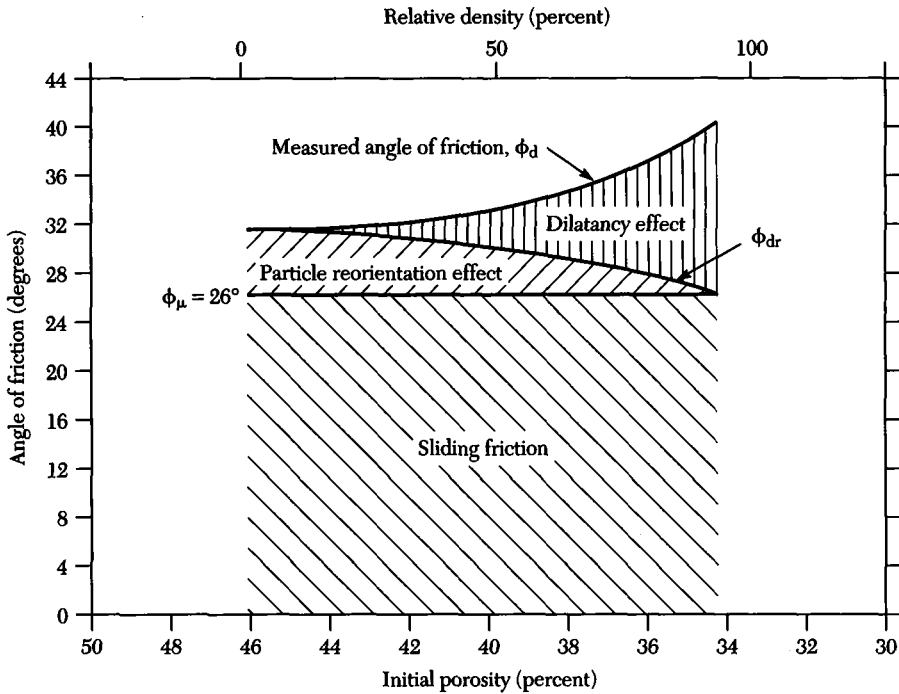


FIGURE 8.21 Particle reorientation and dilatancy effects on the measured angle of friction ϕ_d for a sand. (After Lee and Seed, 1967.)

ure 8.7. Application of Eq. (8.2) for direct shear tests or for triaxial tests, the relation (Lee and Seed, 1967)

$$\tan^2(45 + \phi_{dr}/2) = \left(\frac{\sigma_1}{\sigma_3} - \frac{dV}{V\dot{\epsilon}_1} \right)_f \tag{8.19}$$

provides the angle of friction ϕ_{dr} computed after the dilatancy component has been deducted. In Eq. (8.19) σ_3 is the confining pressure, dV is the incremental increase in volume, V is the sample volume, and $\dot{\epsilon}_1$ is the incremental increase in axial strain. Application of Eq. (8.19) to a series of strength tests conducted at different void ratios permitted Lee and Seed (1967) to obtain the relative values of ϕ_d , ϕ_{dr} , and ϕ_μ shown in Figure 8.21. When dilatancy effects were accounted for in dense sand, the observed friction angle was reduced to a value equal to that for sliding of the mineral grains, ϕ_μ . For larger void ratios, the angle of friction, after reduction for soil dilatancy, exceeded that of the mineral grains. As indicated on Figure 8.21, for most of the void ratio range, the three components of shear strength are (1) strength mobilized by frictional resistance, (2) strength developed by energy required to rearrange and reorient soil particles, and (3) strength developed from energy required to cause expansion or dilation of the sand.

The concepts represented in Figure 8.21 correspond to relatively low pressures. As confining pressures were increased (up to 6.9 MPa), data from drained

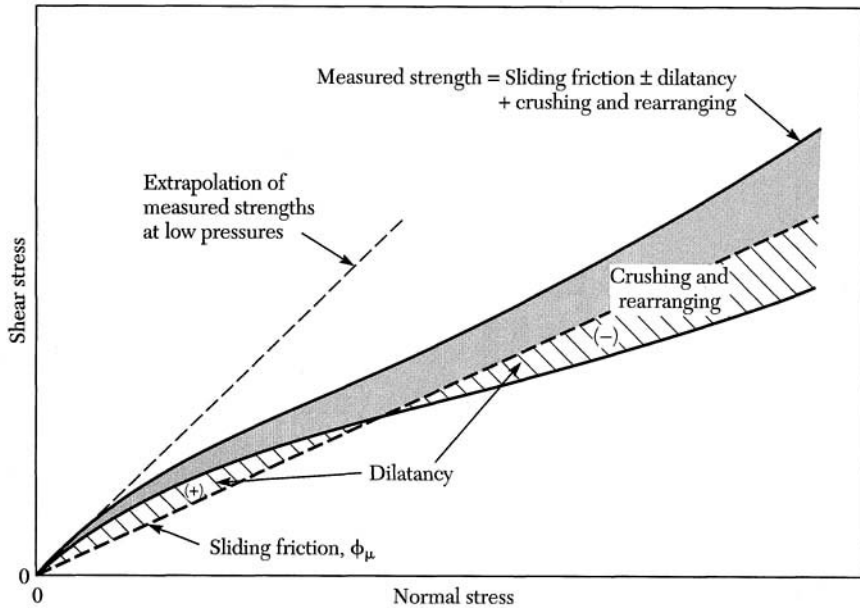


FIGURE 8.22 A schematic of drained test results on sand showing the contribution of sliding friction, dilatancy, and particle crushing to the observed Mohr failure envelope. (After Lee and Seed, 1967.)

tests showed a significant curvature and a progressive flattening of the failure envelope. Examination of particles after testing showed that additional volume decrease and densification was due to crushing of particles at the high pressures. This additional factor, particle crushing at high pressures, is similar to that of remolding or rearranging of particles in loose sands. In tests at high confining pressures, energy will be absorbed during crushing of sand particles, causing the observed friction angle, corrected for dilatancy effects, to be greater than ϕ_μ , the angle of sliding friction. The Mohr failure envelope, shown in Figure 8.22, illustrates these concepts, thus

$$\begin{aligned} \text{measured shear strength} &= \text{strength due to sliding friction} \\ &+ \text{dilatancy effects} \\ &+ \text{crushing and rearranging effects} \end{aligned}$$

As illustrated in Figure 8.22, the dilatancy effect can be positive or negative depending on whether the sample volume increases or decreases during shear. The effect of particle crushing and rearranging shown at low normal stresses will be small for dense sands.

Experimental data on sands (Lee and Seed, 1967) and on concrete and rock (Skempton, 1961) show that the failure envelope becomes progressively flatter with increasing pressure. At higher pressures, this failure envelope approaches the intrinsic line of the solid substance comprising the particles of the porous material. At a pressure sufficiently high to cause complete yielding of the particles

the envelope becomes coincidental with the intrinsic failure line. Voids in the porous material are eliminated at this point. The shape of the failure envelope (Figure 8.23b and c) is controlled by changes in the contact area ratio, $a = A_s/A$, between particles under pressure. When the soil porosity is comparatively high, a given pressure increment $\Delta\sigma$ will cause a comparatively high increase in contact area Δa . As the porosity is progressively reduced the ratio $\Delta a/\Delta\sigma$ becomes smaller. At a pressure σ^* , corresponding to zero porosity and $a = 1$, the ratio $\Delta a/\Delta\sigma$ becomes zero and the slope of the failure envelope falls to the value ψ . This behavior is illustrated in Figure 8.23, where τ_1 corresponds to the intrinsic line and τ_d represents the failure envelope from drained tests on the porous material.

When the ratio σ/σ^* is small, Coulomb's equation is applicable, thus

$$\tau_d = \bar{c} + \bar{\sigma} \tan \bar{\phi} \quad (8.20)$$

where \bar{c} is the cohesion and $\bar{\phi}$ is the angle of internal friction. With higher pressures τ_1 is given by

$$\tau_d = ak + \bar{\sigma} \tan \psi \quad (8.21)$$

where a is the contact area ratio, k is the intrinsic cohesion, and ψ is the angle of intrinsic friction of the solid. For all positive values of $\bar{\sigma}$,

$$\tau_1 = k + \bar{\sigma} \tan \psi \quad (8.22)$$

as shown in Figure 8.23. Typical values for k and ψ are listed in Table 8.5.

TABLE 8.5 Intrinsic Shear Strength Parameters

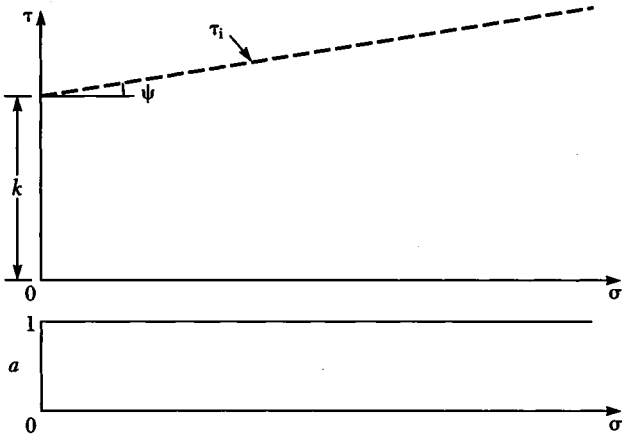
| Solid | k | | ψ |
|-----------|---------------------|-------------------|---------|
| | kgf/cm ² | MN/m ² | Degrees |
| Rock salt | 450 | 44.1 | 3.5 |
| Calcite | 1900 | 186.3 | 8 |
| Quartz | 9500 | 931.7 | 13.25 |

(After Skempton, 1961.)

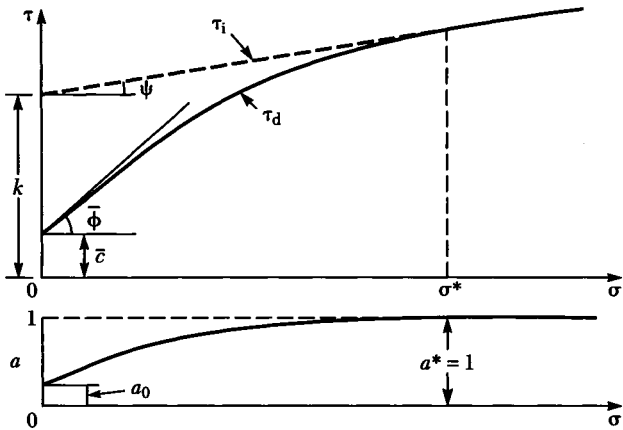
8.3.2 Cohesive Soils

Components of Shear Resistance

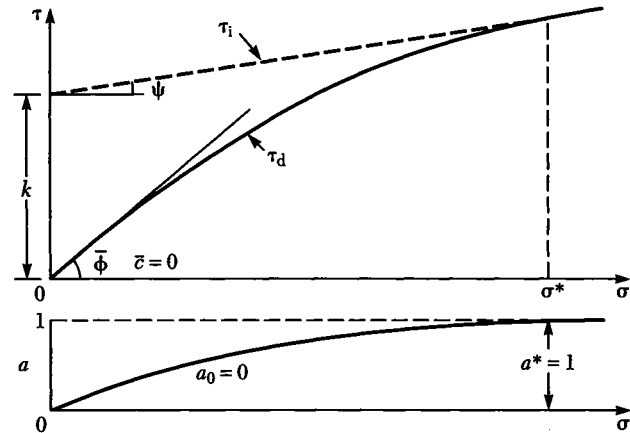
Sliding between particles is the primary mechanism of deformation within a soil mass. A soil's resistance to deformation is dependent on the attractive forces that act among the surface atoms of particles and the interlocking of particles, which is largely a function of packing density. The attractive forces lead to chemical bond formation at points of contact of the surfaces. The strength and number of bonds that form at the interface between two particles are influenced very much by the physical and chemical nature of the surfaces of the particles. The total shear resistance will be proportional to the normal force that is pushing the two particles to-



(a) Solids



(b) Cohesive porous materials



(c) Cohesionless porous materials

FIGURE 8.23 Intrinsic shear strength at high pressure. (After Skempton, 1961.)

gether. If the normal force decreases, the strength or the number of bonds or both decrease and the total shear resistance decreases. The several components involved in shear resistance may be labeled as *cohesion*, *dilatancy*, and *friction*. While these terms are widely used in soil mechanics, they may mean different things to different people.

Cohesion describes the shear resistance that can be mobilized between two adjacent particles that stick or cohere to each other without the need for normal forces pushing the particles together. If the normal force were decreased to zero, there would still be a measurable shear resistance. In this case, we say that there is *true cohesion* between the soil particles. Various types of cohesion are illustrated in Figure 8.24. Flocculation cohesion is shown in Figures 8.24a and b. Clay particles approach each other and stick by van der Waals forces when enough electrolyte is added to a soil-water suspension. Marine clays and some lake clays are linked by this type of electrical force. Edge-to-face linkage occurs in clay-water systems when the positively charged edge of one clay particle is attracted to the negatively charged face of another particle. Cohesion from flocculation is probably weak and sensitive to changes in the environment.

Individual clay crystals can become more or less permanently linked together as illustrated in Figures 8.24c and d. Drying can bring adjacent clay sheets close enough together for the exchangeable potassium ions to fit tightly into holes and

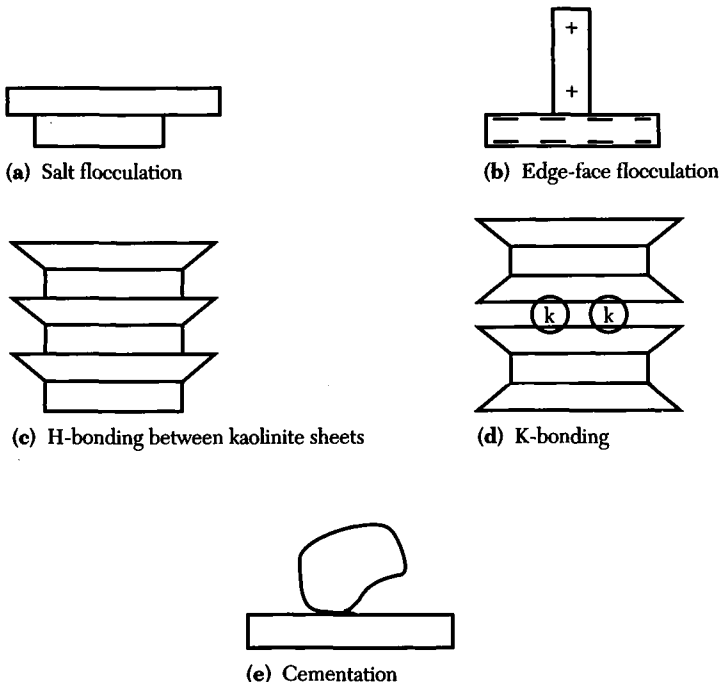


FIGURE 8.24 Several cohesion types that may occur in a soil mass.

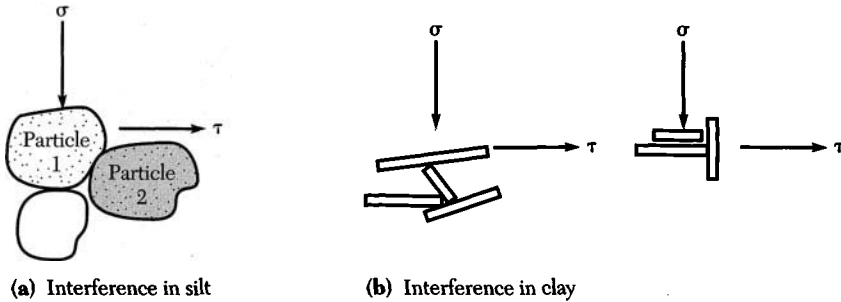


FIGURE 8.25 Soil dilatancy.

thus become nonexchangeable and serve as a permanent linkage between the clay crystals. Adjacent soil particles can become cemented together as illustrated in Figure 8.24e. On drying, naturally occurring materials in the pore water—carbonates, iron oxides, silicates, aluminates, and certain organic matter—tend to precipitate soluble cementing materials at particle contact points. Many soil stabilization materials function, at least in part, by this process. In general, cohesion, unlike the other two components of shear resistance, will be mobilized at very low strains and can be destroyed before the other components of strength become active.

During shear displacements the moving particles tend to interfere with each other both electrically and physically. If the interference results in a tendency toward a volume increase, a higher shear resistance will be mobilized. Consider the three particles in Figure 8.25a. If the three particles lie along a horizontal shear surface, particle 1 must move vertically in order to move horizontally relative to particle 2. This requires a larger applied horizontal stress than if particle 1 moved only along a smooth horizontal surface. Thus the soil in Figure 8.25a has a higher shear resistance because of a physical or geometric interference. The added shear resistance from dilatancy can be computed as illustrated in Figure 8.7 for a sample tested in a shear box under drained conditions.

Frictional resistance is commonly expressed in terms of the coefficient of friction f . If N is the normal force across a surface, the maximum shear force on this surface is $T_{\max} = Nf$. An alternate way to express frictional resistance involves use of a friction angle ϕ_{μ} defined such that $\tan \phi_{\mu} = f$. The geometric interpretation of ϕ_{μ} is shown in Figure 8.26a. This figure involves two basic laws of frictional behavior. First, the shear resistance between two masses is proportional to the normal force between the masses. Second, the shear resistance between two masses is independent of the dimensions of the two masses. The second law can be demonstrated by pulling a brick over a flat surface. The force T_{\max} (Figure 8.26a) will be the same whether the brick rests on a face or on an edge.

Most particle surfaces, on a submicroscopic scale, show some roughness such that two solids will be in contact only where high points (asperities) touch one another. The actual contact area is a very small fraction of the apparent contact area (Figure 8.26b). The normal stresses across these contacts will be extremely high

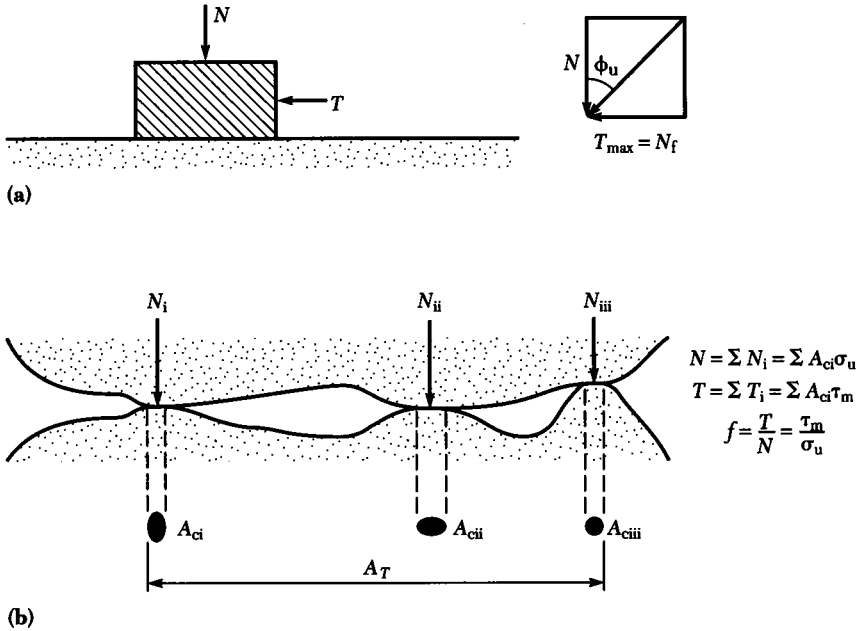


FIGURE 8.26 Soil friction: (a) friction angle; (b) frictional resistance on a microscopic scale.

and under a small load may reach the yield strength σ_u of the material at these sites. The actual contact area A_c will be

$$A_c = \frac{N}{\sigma_u} \tag{8.23}$$

where N is the normal force and σ_u is the normal stress required to cause yielding (i.e., plastic flow). With σ_u a fixed quantity, an increase in total normal force between the particles means a proportional increase in contact area. The high contact stress causes the two surfaces to adhere at the contact points (chemical bonds). The adhesive strength of these points provides the shear resistance. The maximum possible shear force T_{max} is

$$T_{max} = sA_c \tag{8.24}$$

where s is the shear strength of the contact surface and A_c is the actual area.

These concepts lead to the relation

$$T_{max} = N \frac{s}{\sigma_u} \tag{8.25}$$

Note that s and σ_u are material properties and T_{max} is proportional to N . The ratio s/σ_u should equal the friction factor f . The surfaces of soil particles are contaminated with water molecules, various ions, and other materials. At the particle contact points these contaminants are largely squeezed out. For smooth quartz

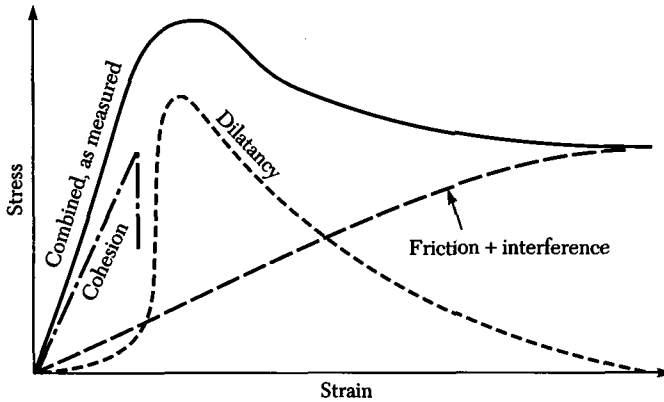


FIGURE 8.27 Combination of cohesion, dilatancy, and friction + interference.

the friction varies from about $f = 0.2$ to $f = 1.0$, depending on surface cleanliness (Bromwell, 1966; Dickey, 1966). As the surface becomes rougher the value of f becomes independent of surface cleanliness. Most quartz particles in natural soils have rough surfaces and a value of $f = 0.5$ ($\phi_\mu = 26$ degrees).

The components of shear resistance have been described individually. The measured shear resistance will be some combination of the components similar to the stress-strain curve illustrated in Figure 8.27. The cohesion is mobilized at small strains and with continued strain is quickly destroyed. Particle interference causes a tendency for volume increase and additional shear resistance. After some strain there is no further tendency for volume increase and the dilatancy component disappears. Only particle interference remains when the stress-strain curve becomes horizontal. Skempton (1964) labels this value as the residual soil strength. As shear occurs clay particles tend to align themselves with their long axes parallel to the direction of shear. Lambe (1960) describes how cohesion can exist at larger strains and manifest itself as increased friction and dilatancy.

Drained Shear Strength Behavior

To evaluate the shear resistance available at a particular point within a soil mass, information is needed on (1) the existing effective stresses at that point and how these effective stresses may change in the future, and (2) a relationship between effective stress and shear resistance. The second step introduces certain limitations in that (1) there is no unique relationship between effective stress and shear resistance, and (2) in many problems, it is difficult to predict with any high degree of certainty the changes in effective stress that may occur in the future. A useful and simple formulation for the shear resistance involving effective stress is

$$\tau_{ff} = f(\bar{\sigma}_{ff}) \quad (8.26)$$

The form of this relation is illustrated in Figure 8.28. The curve representing Eq. (8.26) may have a slight curvature. For engineering purposes it is approxi-

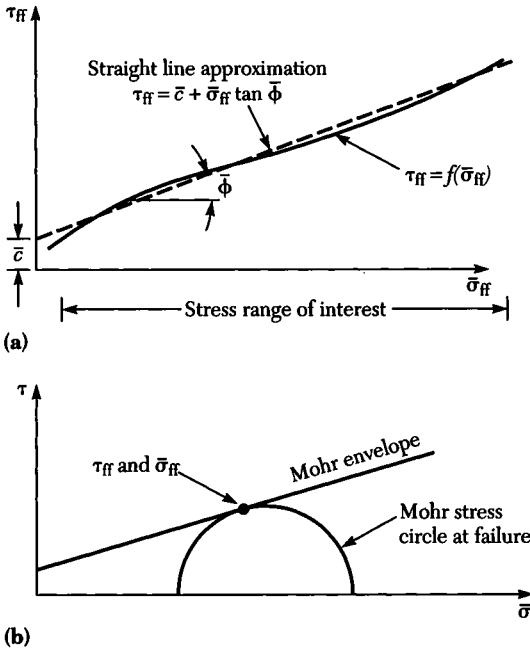


FIGURE 8.28 Shear strength: (a) relation between τ_{ff} and $\bar{\sigma}_{ff}$; (b) Mohr stress circle at failure.

mated by a straight line over the range of $\bar{\sigma}_{ff}$ values of interest (Figure 8.28a), thus

$$\tau_{ff} = \bar{c} + \bar{\sigma}_{ff} \tan \bar{\phi} \tag{8.27}$$

The values of \bar{c} and $\bar{\phi}$ used to describe this curve (Mohr envelope) will depend upon the range of $\bar{\sigma}_{ff}$ values selected, the soil composition, and the type and proportion of colloidal and granular particles. The double subscript notation defines both the stress direction (on the plane of tangency of the Mohr envelope) and the time of failure. The quantity $\bar{\sigma}_{ff}$ is defined in terms of σ_{ff} , the total normal stress on the plane of tangency of the Mohr envelope at the time of failure, and u_f , the pore pressure at the time of failure; thus

$$\bar{\sigma}_{ff} = \sigma_{ff} - u_f \tag{8.28}$$

The shear stress at failure defined by Eq. (8.27) describes one of several possible relations between shear strength and effective stress. This problem is illustrated in Figure 8.29. Assume that the circle gives the state of stress in a triaxial sample at the time of failure. Four possible shear failure stresses are illustrated in the figure. The shear stress τ_{ff} is defined by Eq. (8.27). The shear stress τ_{ff} on the failure plane at failure is determined on the basis of the slope of the plane of maximum distortion. The shear stress τ_{bf} on the plane of maximum obliquity (maximum $\tau/\bar{\sigma}$) corresponds to the point of tangency for a straight line through the origin. The maximum shear stress at failure τ_{mf} corresponds to $(\bar{\sigma}_1 - \bar{\sigma}_3)/2$. The

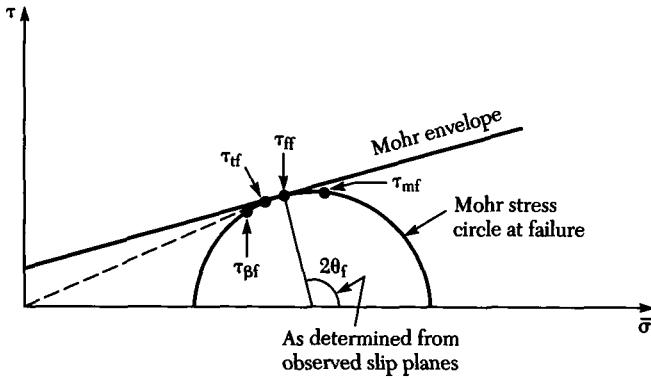


FIGURE 8.29 Definition of failure.

differences between τ_{if} , τ_{ff} , and τ_{mf} are seldom great, and usually all points would fall within the range of experimental error. Gibson (1953) has shown that it is possible to distinguish between τ_{if} and τ_{ff} . If the failure plane could be identified, then τ_{ff} and not τ_{if} should be used as the shear strength. In research work the choice is a matter of which theory is believed to be more correct. When shear strength data is to be used with conventional methods of stability analysis, the definition of strength used must be suited to the problem. When dealing with shear strength in terms of effective stresses, τ_{if} (i.e., the Mohr envelope) should be used; when dealing with undrained strength, τ_{mf} should be used.

Thus far, the peak shear resistance has been defined as the shear strength of the clay without further qualification. At this stage a shear test is normally stopped. For natural soils, and particularly for overconsolidated clays, the stress-strain curve will drop off somewhat following the peak, showing what may be called a *residual strength* that the clay maintains for large displacements. Field evidence (Skempton, 1964) indicates that this residual strength remains constant over shear displacements (landslide) of many feet. A direct shear test conducted on a normally and overconsolidated clay will give results illustrated in Figure 8.30. The strength envelopes are assumed to be of the form represented by Eq. (8.27)

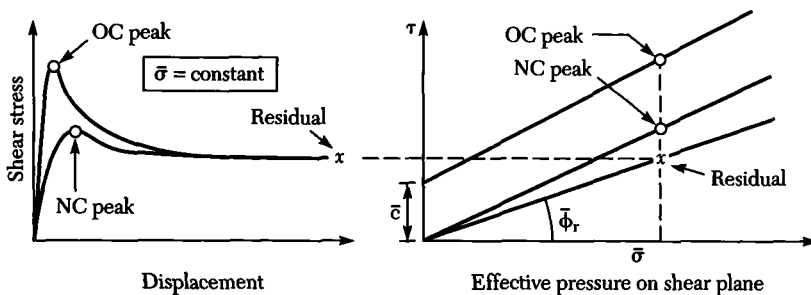


FIGURE 8.30 Simplified shear behavior of normally (NC) and an overconsolidated (OC) clay.

with parameters \bar{c} and $\bar{\phi}$ being dependent on whether peak or ultimate failure stresses are of interest. Test results (Skempton, 1964) show that the residual cohesion \bar{c}_r is very small and probably not significantly different from zero. The angle of shear resistance $\bar{\phi}$ also decreases, in some clays by as much as 10 degrees.

During the shear process, overconsolidated clays tend to expand after passing the peak strength. The increase in water content along the shear surface corresponds to the drop in strength from the peak value. Skempton (1964) describes the formation of thin bands or domains in which flaky clay particles become oriented in the direction of shear displacement along the failure surface. Particles lying parallel to each other will develop a lower shear strength compared to particles with a random orientation. Available data (Skempton, 1964) suggest that the residual strength of a clay, under a given effective stress, will be the same whether the clay has been normally or overconsolidated as indicated in Figure 8.30. This behavior would suggest that the angle $\bar{\phi}_r$ should be constant for a given clay regardless of the clay's consolidation history.

Support for this view is provided in Figure 8.31, where the ultimate (residual) angles of shearing resistance for a number of normally and overconsolidated clays are plotted against the clay fraction (percentage of particles, by weight, finer than 2 mm). No differences between the two conditions are observed. For clay contents approaching 100%, the ultimate friction angles are the same as $\bar{\phi}_\mu$ for the clay minerals. When the soil consists of a mixture of clay and silt (or sand) parti-

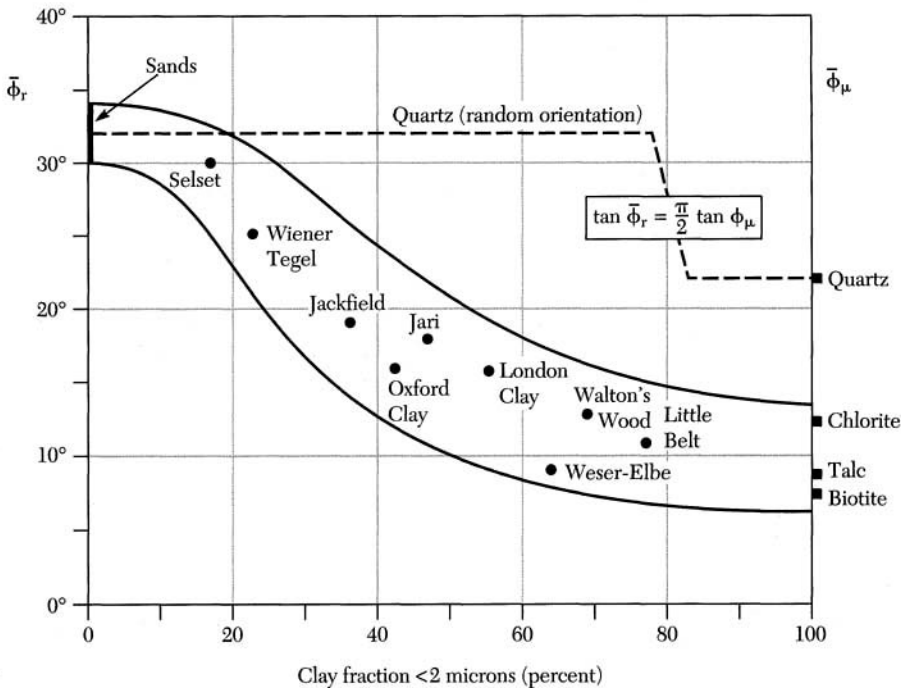


FIGURE 8.31 Relation between $\bar{\phi}_r$ and $\bar{\phi}_\mu$ clay content. (From Skempton, 1964.)

TABLE 8.6 Clay Consistency

| Consistency | Unconfined Compressive Strength, q_u | |
|-------------|--|-------------------|
| | kg/cm ² | kN/m ² |
| Very soft | <0.25 | <25 |
| Soft | 0.25–0.5 | 25–50 |
| Medium | 0.5–1.0 | 50–100 |
| Stiff | 1.0–2.0 | 100–200 |
| Very stiff | 2.0–4.0 | 200–400 |
| Hard | >4.0 | >400 |

cles, the value of $\bar{\phi}_r$ will be raised above the value of $\bar{\phi}_\mu$ for the clay particles, indicating that the more spherical silt (or sand) particles contribute some measure of their higher angle of shear resistance and interfere with full orientation of the clay particles.

Undrained Shear Strength Behavior

The undrained shear strength of clay is determined by tests in which no overall water content change is permitted to occur during application of the stresses. Soil consistency is conveniently described by the load per unit area at which unconfined cylindrical samples fail in undrained compression. Fine-grained soils, in the natural state, show a different consistency depending on how the deposit was formed and conditions that may have existed during the geologic history of the deposit. Desiccation or **weathering** cause stiff surface layers to form over a uniform soft soil deposit. An entire soil stratum may be overconsolidated as a result of pressures exerted by previous loads—for example, thick deposits of soil that were later removed by erosion. The consistency of these soils is conveniently described in terms of the unconfined compressive strength, q_u , as in Table 8.6. Stress-strain curves for these soils may exhibit variations ranging from brittle to plastic behavior. Most normally and slightly overconsolidated clays show a considerable loss in strength when remolded. A high degree of sensitivity is commonly associated with a saturated soil having a well-developed skeleton structure or leaching of soft marine clays (glacial clays deposited in salt water that have been subsequently uplifted). Soil sensitivity (S_t) is defined as the ratio of undisturbed to remolded undrained strength at the same water content, thus

$$S_t = \frac{S_u (\text{undisturbed})}{S_u (\text{remolded})} \quad (8.29)$$

The vane test (Section 8.2.4) may be used to evaluate sensitivity of those soils in which the remolded unconfined specimen cannot stand without excessive deformation. A classification of clays based on sensitivity is given in Table 8.7.

In comparatively uniform normally consolidated clays, the undrained shearing resistance will increase approximately linearly with depth. For this condition,

TABLE 8.7 Clay Sensitivity

| Condition | Clay |
|--------------------|------|
| Insensitive | <2 |
| Low sensitivity | 2-4 |
| Medium sensitivity | 4-8 |
| High sensitivity | 8-16 |
| Quick | >16 |

the ratio of undrained strength c_u to the effective overburden pressure p_0 is reasonably constant. The ratio c_u/p_0 appears to be correlated with the plasticity index PI as shown in Figure 8.32. Bishop and Henkel (1962) suggest that any test results not conforming with Figure 8.32 should be reexamined relative to both laboratory test and sampling techniques. If a clay deposit is known to be normally consolidated, values for c_u for the various depths can be estimated on the basis of the plasticity index and the overburden pressure. On the other hand, if values of c_u and PI have been determined, the relationship can be used to estimate the degree of overconsolidation.

The effect of strain rate on the undrained behavior of clays is summarized in Figure 8.33. Increasing the rate at which a soil is sheared increases the undrained strength, with the effect being larger in soils compacted dry of optimum water content or in stiff saturated soils. There is general agreement that undrained strength is less in tests of long duration (several months) as compared to tests of conventional duration (several minutes). In cases where pore pressures have been measured during undrained tests at various loading rates (Richardson and Whitman, 1964), the results indicate that changes in undrained strength are due to differences in induced pore pressures. Smaller induced pore pressures were ob-

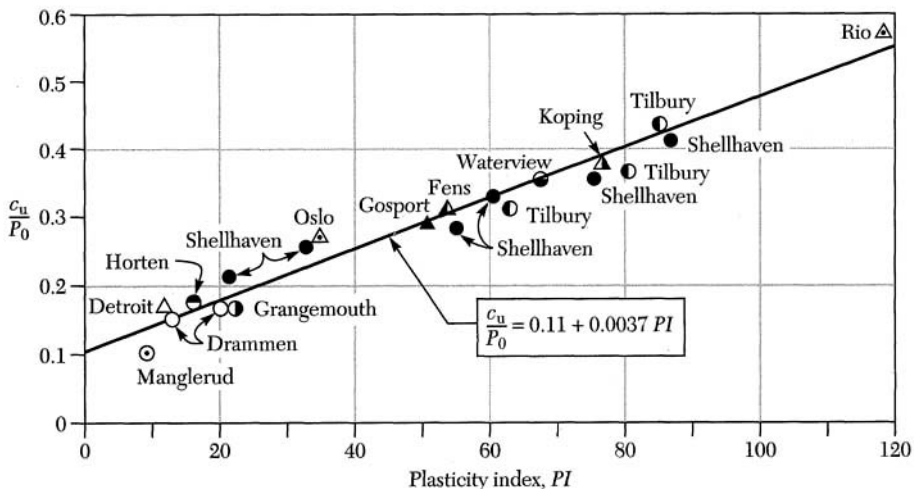


FIGURE 8.32 Relationship between c_u/P_0 and PI for normally consolidated clays. (After Skempton, 1957.)

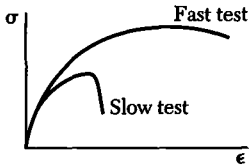
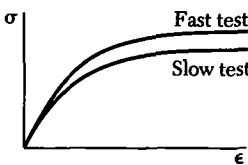

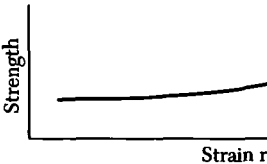
| Brittle Failure | Plastic Failure |
|--|--|
| Failure by splitting or pronounced failure planes | Failure by bulging |
| <p>Occurs where there are large negative pore pressures in unconfined compression tests.</p> <ol style="list-style-type: none"> 1. Soils compacted dry of optimum water content. 2. Stiff saturated soils. | <p>Occurs in triaxial tests with large chamber pressures, or where there are small negative pore pressures in unconfined compression tests.</p> <ol style="list-style-type: none"> 1. Soils compacted wet of optimum water content. 2. Soft saturated soils. |
| <p>Strain-at-failure affected by strain-rate</p>  | <p>Strain-at-failure independent of strain-rate</p>  |
| <p>Large strain-rate effect</p>  | <p>Moderate strain-rate effect</p>  |

FIGURE 8.33 Undrained soil behavior for different loading rates. (From Whitman, 1960.)

served for increasing rates of strain. Where the pore pressures that existed at failure were positive or slightly negative, a plastic type of behavior was usually encountered (Whitman, 1960). In contrast, where large negative pore pressures existed at failure, the brittle type of failure was observed. When confining pressures were applied to ensure positive pore pressures at failure, the plastic type of behavior was observed. The exact cause of the viscous-type behavior during plastic failures appears to be associated with the structural viscosity of an assemblage of mineral particles. More research is needed in this area.

PROBLEMS

8.1 A direct shear test is conducted on a dense sample of sand. The initial void ratio was 0.75. The shear box was 75 mm square, and initially the specimen height was 10 mm. The following data were collected during shear. Com-

pute the data needed and plot curves similar to those shown in Figure 8.6.

| Time Elapsed (min) | Vertical Load (kN) | Horizontal Displacement (mm) | Thickness Change (mm) | Horizontal Load (N) |
|--------------------|--------------------|------------------------------|-----------------------|---------------------|
| 0 | 2.25 | 8.89 | 3.56 | 0 |
| 0.5 | 2.25 | 8.82 | 3.54 | 356 |
| 1 | 2.25 | 8.63 | 3.52 | 721 |
| 2 | 2.25 | 8.44 | 3.51 | 1014 |
| 3 | 2.25 | 7.92 | 3.53 | 1428 |
| 4 | 2.25 | 7.18 | 3.59 | 1655 |
| 5 | 2.25 | 6.38 | 3.63 | 1770 |
| 6 | 2.25 | 5.49 | 3.65 | 1744 |

(After Taylor, 1948.)

- 8.2 A drained triaxial compression test is conducted on a sample of dense sand. The initial area of the test specimen was 10 cm² and its initial height was 71 mm. The initial void ratio was 0.60. The following data were observed during shear. First, calculate the average area of the specimen, assuming it is a right circular cylinder at all times during the test. Then make the calculations needed to plot the axial stress versus axial strain curves for this test. Assuming $\bar{c} = 0$, what is $\bar{\phi}$?

| Time Elapsed (min) | Chamber Pressure (kPa) | Strain Dial Giving ΔH (mm) | Buret Giving ΔV (cc) | Axial Load (N) |
|--------------------|------------------------|------------------------------------|------------------------------|----------------|
| 0 | 205 | 5.08 | 2.00 | 0 |
| | 205 | 5.21 | 1.91 | 182 |
| | 205 | 5.33 | 1.86 | 374 |
| 45 | 205 | 5.69 | 1.92 | 641 |
| | 205 | 6.10 | 2.13 | 787 |
| 90 | 205 | 7.06 | 2.80 | 921 |
| | 205 | 8.10 | 3.66 | 970 |
| | 205 | 9.12 | 4.56 | 983 |
| 240 | 205 | 10.21 | 5.40 | 970 |
| | 205 | 12.90 | 7.30 | 898 |
| 460 | 205 | 15.3 | 8.09 | 814 |

(After Taylor, 1948.)

- 8.3 Two sandy soils are compacted to the same relative density. Sand A is well graded with angular particles. Sand B has a uniform gradation and has rounded particles.
- Which sand will have the larger void ratio?
 - Which sand will have the larger friction angle?

- 8.4 The stresses acting on the plane of maximum shearing stress through a given point in a sand stratum are as follows: total normal stress = 264.8 kN/m^2 ; pore water pressure = 93.8 kPa ; and shear stress = 90.3 kN/m^2 . Failure is occurring in the region surrounding the point. Determine the normal effective stress and the shearing stress on the failure plane, the friction angle of the sand, and the major and minor principal effective stresses.
- 8.5 A saturated sand, at a given density, is tested in a triaxial CU test. The sand at this density has $\bar{\phi} = 30$ degrees, and the effective critical confining pressure equals 490.3 kN/m^2 . At the end of consolidation, the effective minor principal stress equals 147.1 kN/m^2 and the chamber pressure equals 735.5 kN/m^2 . Evaluate the initial and failure conditions by drawing total and effective stress circles, labeling all parts and values.
- 8.6 An undrained triaxial test on a compacted soil sample, with a cell pressure of 250 kPa , gave the following results. The pore pressure within the sample was zero before application of the cell pressure.

| Strain (%) | σ_1 (kN/m^2) | u (kN/m^2) |
|------------|--------------------------------|-------------------------|
| 0.0 | 250 | 100 |
| 2.5 | 417 | 125 |
| 5.0 | 600 | 125 |
| 7.5 | 767 | 100 |
| 10.0 | 875 | 67 |
| 15.0 | 1000 | 8 |
| 20.0 | 1042 | -50 |

- (a) Determine the pore pressure coefficient B and state whether or not the soil was saturated.
- (b) Plot the variation of deviator stress with strain.
- (c) Plot the variation of the pore pressure coefficient A with strain.
- 8.7 Explain why permeability of a cohesive soil sample and the rate at which it is sheared have an important effect on shear strength.
- 8.8 An unconfined compression test on a saturated clay specimen gave a compressive strength of 146 kN/m^2 . The value of A at failure was -0.2 and the effective stress shear strength parameters were $\bar{c} = 7.0 \text{ kN/m}^2$ and $\bar{\phi} = 24$ degrees. What was the initial value of the pore pressure u_0 in the unconfined soil specimen before testing? What is the undrained shear strength?
- 8.9 An undisturbed soil sample 50 mm in diameter and 100 mm in height was tested in a triaxial cell. The sample sheared under an additional axial load of 725 N with a vertical deformation of 18 mm . The failure plane was inclined at 51 degrees to the horizontal and the cell pressure was 300 kPa . Determine Coulomb's equation for the soil shear strength in terms of total stress.
- 8.10 Another undisturbed soil sample was tested in a shear box under the same drainage conditions as those in Problem 8.9. If the box area was 4500 mm^2 and the normal load was 625 N , what would you predict for the failure shear stress?

- 8.11 Why does the pore pressure coefficient A at failure differ for overconsolidated, normally consolidated, and sensitive clays?
- 8.12 A normally consolidated clay with effective shear strength parameters $\bar{c} = 0$ and $\bar{\phi} = 24$ degrees was tested in the conventional undrained, consolidated-undrained, and drained triaxial tests. In each test, the cell pressure was held constant at 200 kN/m^2 .
- (a) What was the compression strength $(\sigma_1 - \sigma_3)$ of the specimen in the undrained test when the pore pressure at failure was 135 kN/m^2 ?
 - (b) What was the pore pressure at failure in the consolidated-undrained test for a compressive strength of 175 kN/m^2 ?
 - (c) What was the compressive strength in the drained test if the back pressure was maintained at 50 kPa ?
- 8.13 A saturated, normally consolidated clay sample, obtained from a block sample, is trimmed to form a triaxial test specimen. This specimen is placed in a triaxial cell. The measured suction (u_0) equals 39 kPa . The cell is filled with water and a cell pressure of 75 kPa applied. An undrained triaxial test with pore pressure measurements gave the following data:

$$\bar{c} = 0 \quad \bar{\phi} = 26 \text{ degrees} \quad A_r = -0.2$$

Compute the undrained shear strength of the clay sample.

- 8.14 In a slow triaxial test on an overconsolidated clay, the engineer accidentally closed a valve, thus preventing sample drainage after completing part of the test. The error was discovered after plotting the data. What difference, if any, does this make relative to the results? List any assumptions made in solving the problem.
- 8.15 Two vanes, A and B, are used to measure the undrained shear strength at the same depth in a clay layer. Vane dimensions and maximum recorded torques are

| Vane | Length (mm) | Diameter (mm) | Maximum Torque (Nm) |
|------|-------------|---------------|---------------------|
| A | 150 | 50 | 52.4 |
| B | 50 | 50 | 26.15 |

Find the values of the undrained shear strength on horizontal and vertical planes at this depth.

- 8.16 After all-around consolidation with a cell pressure of 200 kPa , the initial degree of saturation for a clay triaxial sample was observed to be close to 97 percent. Estimate the back pressure needed to increase the degree of saturation to 100 percent (assume Henry's coefficient of solubility equals 0.02 and atmospheric pressure is equal to 100 kPa).
- 8.17 In the consolidated-undrained triaxial test, two soil specimens were loaded to failure after consolidation under all-around pressures of 196.1 and 392.3 kN/m^2 . The results are

| Sample | σ_3 (kN/m ²) | σ_1 at Failure (kN/m ²) | u_0 at Failure (kN/m ²) |
|--------|------------------------------------|---|--|
| 1 | 196.1 | 343.2 | 137.3 |
| 2 | 392.3 | 686.5 | 275.6 |

Calculate

- (a) the values c and ϕ for total stresses,
 - (b) the values \bar{c} and $\bar{\phi}$ for effective stresses,
 - (c) the shear and normal stress on the failure plane in sample 2.
- 8.18** Strength tests conducted on samples of a stiff overconsolidated clay gave lower strengths for CD tests than for CU tests. Explain this behavior.
- 8.19** A clay soil sample was obtained from a depth of 10 m. Soil physical properties include $LL = 65$, $PL = 30$, and $\gamma_{\text{sat}} = 17.8 \text{ kN/m}^3$. The groundwater level coincides with the ground surface. Estimate the undrained shear strength S_u of this normally consolidated clay.
- 8.20** For structures placed on clays of low, medium, and high sensitivity, would you use the same factor of safety? Will the temporary or permanent nature of these structures affect your decision? Explain.
- 8.21** Why might the angle of the failure plane observed in a triaxial test on a remodeled soil sample differ from that predicted from a Mohr diagram at failure? Assume that all data derived from the test are correct.

9

Lateral Earth Pressure

9.0 INTRODUCTION

Earth pressure is the force per unit area exerted by the soil on a structure. Its magnitude depends on the physical properties of the soil, the nature of the soil–structure interface, and possible modes of deformation of the structural system. In the case of cohesive soils, the earth pressure is influenced by the time-dependent nature of soil properties.

Generally, an element of soil in the ground is acted on by three principal stresses. However, in most earth pressure problems, plain strain is assumed and only the major and minor principal stresses are required: (1) a vertical principal stress and (2) a horizontal principal stress. The horizontal stress is linearly related to the vertical stress by a proportionality constant called the **coefficient of earth pressure**. However, the resulting pressure is dependent on the theories used and the assumptions made relative to the nature of the structure, the soil, and the soil–structure interface. This chapter is devoted to the study of several earth pressure theories.

9.1 EARTH PRESSURE AT REST

Consider the soil element within the large soil mass depicted in Figure 9.1. Assuming that the soil mass is completely dry, then at depth z the soil element is

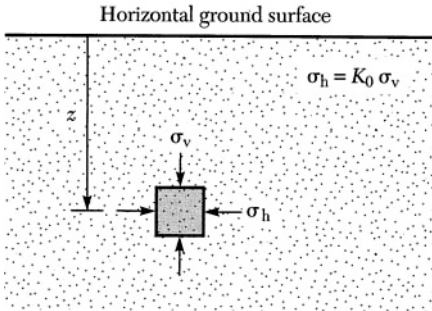


FIGURE 9.1 Interpretation of the coefficient of earth pressure at rest for dry soil.

subjected to a vertical effective stress $\bar{\sigma}_v$ and a horizontal stress of $\bar{\sigma}_h$. Note that for this special case, there are no shear stresses acting on the horizontal and the vertical planes. Because there is no water present within the soil profile, the total vertical stress is equal to the effective stress. This implies that the total horizontal stress is equal to the effective horizontal stress. This is because the horizontal effective stress in a given soil mass is related linearly to the vertical effective stress. The ratio of the effective horizontal stress $\bar{\sigma}_h$ to the vertical stress $\bar{\sigma}_v$, is called the **coefficient of earth pressure at rest**, K_0 . That is

$$K_0 = \frac{\bar{\sigma}_h}{\bar{\sigma}_v} \quad (9.1)$$

Generally, the value of K_0 is less than 1.0. Several researchers have studied this important coefficient and have concluded that for most soils K_0 is between 0.4 to 0.6. For granular soil, the coefficient of earth pressure at rest was found to be a function of the effective angle of internal friction $\bar{\phi}$ as given by Eq. (9.2).

$$K_0 = 1 - \sin \bar{\phi} \quad (9.2)$$

For cohesive soils, the coefficient of earth pressure at rest can be approximated in terms of the angle of internal friction $\bar{\phi}$ and the overconsolidation ratio, OCR, as given by Eq. (9.3).

$$K_0 = (0.95 - \sin \bar{\phi}) \sqrt{\text{OCR}} \quad (9.3)$$

Note that the OCR is the ratio of the maximum past pressure to the effective overburden pressure. For normally consolidated soils, the OCR value is 1.0.

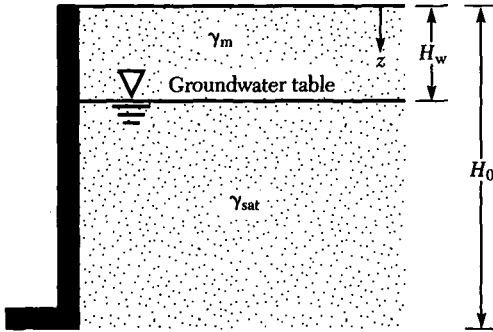
Estimation of the coefficient of earth pressure at rest is by no means an exact science. In fact, when dealing with compacted soils, estimates of K_0 based on Eqs. (9.1) and (9.2) might be appreciably lower than the actual field values.

For the purpose of earth pressure calculations, it is often necessary to deal with soil profiles that include a water table behind a retaining structure. In such cases, the effective vertical stress is computed, then used in computing the effective horizontal stress. At a given depth, the total horizontal stress is computed as the sum of the horizontal effective stress and the pore water pressure. The total

horizontal stress distribution can then be used to compute the total horizontal force acting on the earth-retaining structure in question.

EXAMPLE 9.1

For the earth retaining wall shown below, compute the total horizontal earth pressure. The wall is completely rigid and frictionless.



Solution

Because the wall is rigid, this implies the soil backfill is in a state of elastic equilibrium. The soil is at rest. Also, because the wall is frictionless, there are no shear stresses between the wall and the soil backfill. Therefore, the effective vertical and horizontal stresses at any depth z are principal stresses and are given as follows.

For $0 \leq z \leq H_w$

$$\begin{aligned}\bar{\sigma}_v &= \gamma_m z = \sigma_v \\ \bar{\sigma}_h &= K_0 \bar{\sigma}_v = K_0 \gamma_m z\end{aligned}$$

For $H_w \leq z \leq H_0$

$$\begin{aligned}\bar{\sigma}_v &= \gamma_m H_w + (z - H_w)(\gamma_{\text{sat}} - \gamma_w) \\ \bar{\sigma}_h &= K_0 \bar{\sigma}_v = K_0 \gamma_m H_w + K_0 (z - H_w)(\gamma_{\text{sat}} - \gamma_w)\end{aligned}$$

Therefore, the total horizontal stress (lateral earth pressure) at any depth is computed by including the corresponding pore water pressure. Thus,

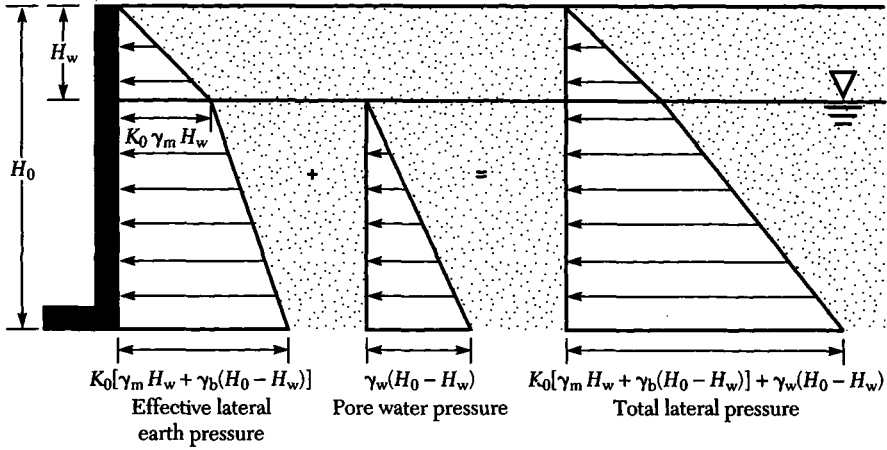
For $0 \leq z \leq H_w$

$$\sigma_h = \bar{\sigma}_h = K_0 \gamma_m z$$

For $H_w \leq z \leq H_0$

$$\sigma_h = \bar{\sigma}_h + u = K_0 \gamma_m H_w + K_0 (z - H_w)(\gamma_{\text{sat}} - \gamma_w) + \gamma_w (z - H_w)$$

Note that the pore water pressure is not multiplied by the coefficient of earth pressure at rest. These pressures are shown graphically as follows.



Note that the total force per unit width acting on the wall is equal to the area under the total earth pressure diagram. ■

9.2 RANKINE'S EARTH PRESSURE THEORY

9.2.1 Introduction

The analysis and design of retaining structures such as walls, cofferdams, basement walls, and bulkheads require a thorough knowledge of the lateral forces acting between the structure and the soil mass they help support. Earth pressure theories involve three possible states of stress, namely *at rest*, *active*, and *passive*. These states of stress can be examined using Figure 9.2. If the wall does not move away from or toward the soil element shown in Figure 9.2, then the state of stress corresponds to the *at rest condition* discussed in the preceding section. If the wall

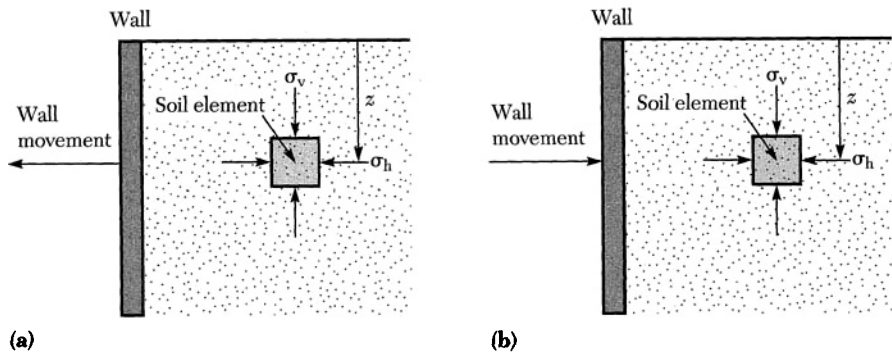


FIGURE 9.2 Illustration of the earth pressure states of stress: (a) active state; (b) passive state.

moves away from the element, the horizontal stress will decrease to some limiting value when the soil mass fails. This is depicted in Figure 9.2a and is referred to as the *active state of stress*. However, if the wall moves toward the soil element, then the horizontal stress will increase to some limiting value when the soil mass fails, and the state of stress is termed the *passive state of stress*. Note that in all three cases, the vertical stress remains constant because the weight of material remains constant. Hence, the effective horizontal stress may be expressed in terms of the effective vertical stress and three distinct earth pressure coefficients. That is,

$$\bar{\sigma}_{h0} = K_0 \bar{\sigma}_v \quad (9.4a)$$

$$\bar{\sigma}_{ha} = K_a \bar{\sigma}_v \quad (9.4b)$$

$$\bar{\sigma}_{hp} = K_p \bar{\sigma}_v \quad (9.4c)$$

where K_0 is the coefficient of earth pressure at rest, K_a is the coefficient of active earth pressure, and K_p is the coefficient of passive earth pressure. The earth pressure coefficients represent limiting values of stress, which are dependent on wall movement. The total horizontal stresses corresponding to the three states of stress described by Eq. (9.4) can be expressed in terms of the pore water pressure u as given by Eq. (9.5).

$$\sigma_{h0} = \bar{\sigma}_{h0} + u = K_0 \bar{\sigma}_v + u \quad (9.5a)$$

$$\sigma_{ha} = \bar{\sigma}_{ha} + u = K_a \bar{\sigma}_v + u \quad (9.5b)$$

$$\sigma_{hp} = \bar{\sigma}_{hp} + u = K_p \bar{\sigma}_v + u \quad (9.5c)$$

For a wall height H , active earth pressures are associated with wall movements of about $H/500$. Passive earth pressures are associated with wall movements of approximately $H/100$ (H = height of wall). Note that it is not necessary for the whole wall to move in order to achieve these states of stress; it is only necessary for the wall to tilt, as will be discussed later. Determination of the earth pressure on a wall can be calculated from the triangular earth pressure distribution described in Example 9.1. The main difference is how to evaluate K_a and K_p .

The simplest theory proposed for earth pressure calculations is Rankine's. It assumes a smooth vertical wall and plane failure surfaces. The smooth wall implies that there are no shear stresses acting on horizontal and vertical planes. Therefore, the horizontal and vertical stresses are principal stresses. Because a limiting state of stress is being considered, Rankine's theory is easily visualized in terms of Mohr's diagram and a failure envelope as shown in Figure 9.3. Note that the failure envelope is defined in terms of the effective strength parameters, namely the cohesion \bar{c} and the angle of internal friction $\bar{\phi}$. For the active state and the passive state, the soil starts from the at rest condition. As the wall moves away from the mass (active case), the horizontal stress will decrease until the soil mass behind the wall fails (i.e., the Mohr stress circle becomes tangent to the failure envelope). However, as the wall moves toward the soil mass (passive case), the horizontal stress increases. It exceeds the vertical stress and continues to increase until failure again occurs in the soil mass. Again the Mohr stress circle is tangent to the strength (failure) envelope.

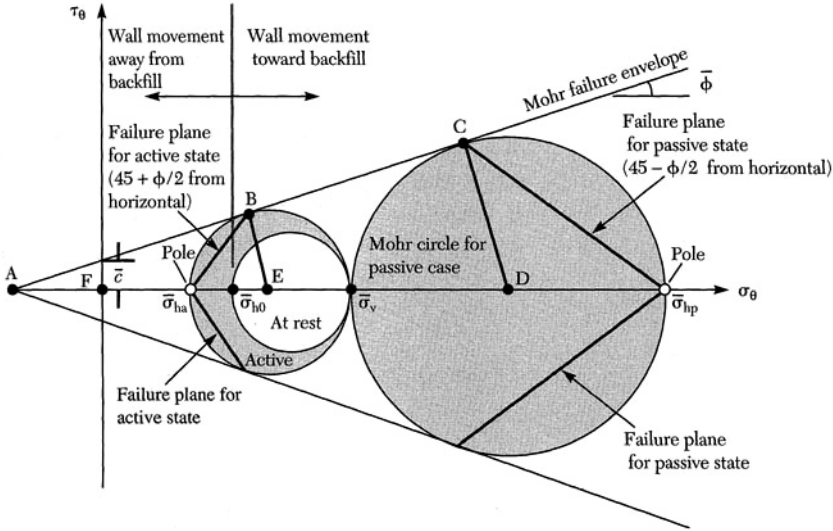


FIGURE 9.3 Mohr circles for Rankine's state of earth pressure within any soil mass.

9.2.2 Rankine's Active State of Stress

In the active case, $\bar{\sigma}_{ha}$ is the minor principal stress and $\bar{\sigma}_v$ is the major principal stress. In the passive case, $\bar{\sigma}_{hp}$ is the major principal stress and $\bar{\sigma}_v$ is the minor principal stress. Note that $\bar{\sigma}_{ha}$ can be determined graphically from Figure 9.3. Alternatively, it can be determined using relationships between the major and minor principal stresses. For the active case, the relationship between $\bar{\sigma}_v$ and $\bar{\sigma}_{ha}$ can be determined using Figure 9.3 as follows.

$$\sin \bar{\phi} = \frac{\overline{BE}}{\overline{AE}} = \frac{\overline{BE}}{\overline{AF} + \overline{FE}} = \frac{\frac{(\bar{\sigma}_v - \bar{\sigma}_{ha})}{2}}{\frac{(\bar{\sigma}_v + \bar{\sigma}_{ha})}{2} + \frac{\bar{c}}{\tan \bar{\phi}}}$$

or more simply

$$\bar{\sigma}_v \sin \bar{\phi} - \bar{\sigma}_{ha} \sin \bar{\phi} + 2\bar{c} \cos \bar{\phi} = \bar{\sigma}_v - \bar{\sigma}_{ha}$$

Collecting terms, then solving for $\bar{\sigma}_{ha}$ gives

$$\bar{\sigma}_{ha} = \frac{1 - \sin \bar{\phi}}{1 + \sin \bar{\phi}} \bar{\sigma}_v - \frac{2\bar{c} \cos \bar{\phi}}{1 + \sin \bar{\phi}}$$

Using trigonometric identities, write

$$\tan^2(45 - \bar{\phi}/2) = \frac{1 - \sin \bar{\phi}}{1 + \sin \bar{\phi}} \quad \text{and} \quad \tan(45 - \bar{\phi}/2) = \frac{\cos \bar{\phi}}{1 + \sin \bar{\phi}}$$

Substitution gives the desired relationship between the minor and major principal stresses for the active state of stress as

$$\bar{\sigma}_{ha} = \tan^2(45 - \bar{\phi}/2) \bar{\sigma}_v - 2\bar{c} \tan(45 - \bar{\phi}/2) \tag{9.6}$$

The Rankine coefficient of active earth pressure is defined as

$$K_a = \tan^2(45 - \bar{\phi}/2) \tag{9.7}$$

Substituting Eq. (9.7) into (9.6) gives

$$\bar{\sigma}_{ha} = \bar{\sigma}_v K_a - 2\bar{c} \sqrt{K_a} \tag{9.8}$$

Note that for cohesionless soils Eq. (9.8) can be modified by substituting $\bar{c} = 0$, which gives

$$\bar{\sigma}_{ha} = \bar{\sigma}_v K_a \tag{9.9}$$

The vertical effective overburden pressure can be computed in terms of the effective unit weight of the soil and depth. Therefore, the active earth pressure acting on a frictionless wall of height H_0 can be determined for cohesive and cohesionless soils as shown in Figure 9.4. Examination of this figure reveals that for cohesive soils, the active earth pressure is negative to a depth z_0 . At this depth the horizontal pressure is zero. Hence, for a cohesive soil with an effective unit weight of γ' , substitute $\bar{\sigma}_{ha} = 0$ and $\bar{\sigma}_v = \gamma'z_0$ into Eq. (9.8), then solve for z_0 , which yields

$$z_0 = \frac{2\bar{c}}{\gamma'} \sqrt{K_a} = \frac{2\bar{c}}{\gamma'} \tan(45 - \bar{\phi}/2)$$

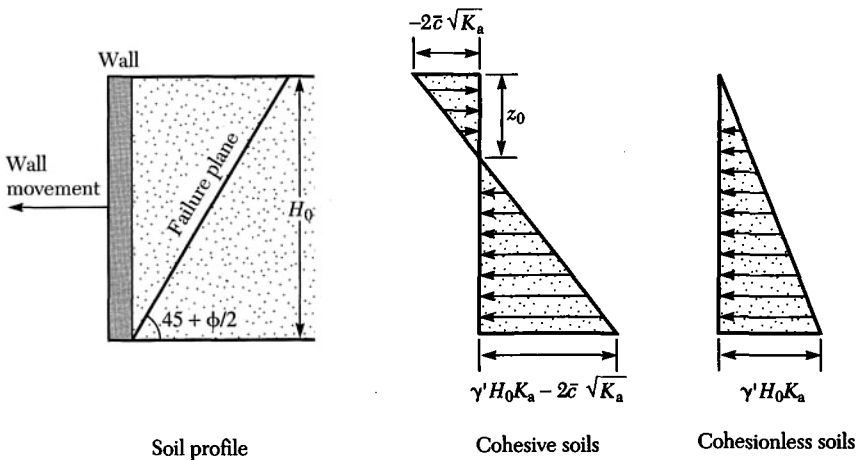


FIGURE 9.4 Graphical illustration of the Rankine active earth pressure acting on a frictionless wall.

Note that the earth pressure in cohesive soil is generally calculated using the positive component of the active earth pressure. That is, the earth pressure above z_0 is ignored because tension cracks will form between the soil and wall.

9.2.3 Rankine's Passive State of Stress

In the passive case, $\bar{\sigma}_{hp}$ is the major principal stress and $\bar{\sigma}_v$ is the minor principal stress. Note that $\bar{\sigma}_{hp}$ can be determined graphically using Figure 9.3. Alternatively, the relationship between $\bar{\sigma}_v$ and $\bar{\sigma}_{hp}$ can be determined using Figure 9.3 as follows.

$$\sin \bar{\phi} = \frac{\overline{CD}}{\overline{AD}} = \frac{\overline{CD}}{\overline{AF} + \overline{FD}} = \frac{\frac{(\bar{\sigma}_{hp} - \bar{\sigma}_v)}{2}}{\frac{(\bar{\sigma}_{hp} + \bar{\sigma}_v)}{2} + \frac{\bar{c}}{\tan \bar{\phi}}} \quad (9.10)$$

Solving Eq. (9.10) for the passive earth pressure gives

$$\bar{\sigma}_{hp} = \frac{1 + \sin \bar{\phi}}{1 - \sin \bar{\phi}} \bar{\sigma}_v + \frac{2 \bar{c} \cos \bar{\phi}}{1 - \sin \bar{\phi}}$$

Using trigonometric identities, write

$$\tan^2(45 + \bar{\phi}/2) = \frac{1 + \sin \bar{\phi}}{1 - \sin \bar{\phi}} \quad \text{and} \quad \tan(45 + \bar{\phi}/2) = \frac{\cos \bar{\phi}}{1 - \sin \bar{\phi}}$$

Substitution gives the desired relationship between the minor and major principal stresses for the active state of stress as

$$\bar{\sigma}_{hp} = \tan^2(45 + \bar{\phi}/2) \bar{\sigma}_v + 2 \bar{c} \tan(45 + \bar{\phi}/2) \quad (9.11)$$

The Rankine coefficient of passive earth pressure is defined as

$$K_p = \tan^2(45 + \bar{\phi}/2) \quad (9.12)$$

Substituting Eq. (9.12) into (9.11) gives

$$\bar{\sigma}_{hp} = \bar{\sigma}_v K_p + 2 \bar{c} \sqrt{K_p} \quad (9.13)$$

Note that for cohesionless soils Eq. (9.13) can be modified by substituting $\bar{c} = 0$, which gives

$$\bar{\sigma}_{hp} = \bar{\sigma}_v K_p \quad (9.14)$$

Note that the vertical effective overburden pressure is computed in terms of the effective unit weight of the soil and depth. Therefore, the passive earth pressure acting on a frictionless wall of height H_0 can be determined for cohesive and cohesionless soils as shown in Figure 9.5. Examination of Figure 9.5 reveals that for both cohesive and cohesionless soils, the active earth pressure is positive along the wall.

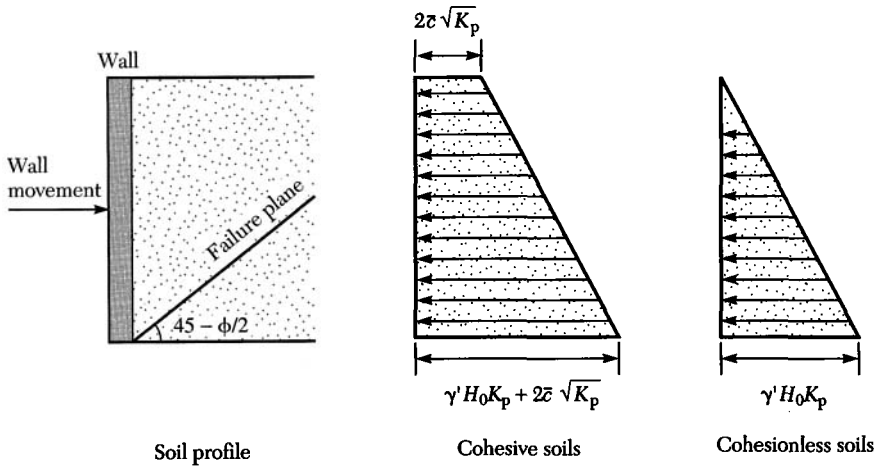


FIGURE 9.5 Graphical illustration of the Rankine passive earth pressure acting on a frictionless wall.

9.2.4 General Comments on Rankine's Earth Pressure Theory

Consideration of Eqs. (9.7) and (9.12) reveals that the Rankine coefficient of active earth pressure is related to the passive coefficient as

$$K_a = \frac{1}{K_p} \tag{9.15}$$

Equation (9.15) is significant in that according to Figure 9.3, the coefficient of *active* earth pressure is smaller than the *at rest* coefficient, which is generally between 0.4 and 0.6. The implication is that the passive coefficient of earth pressure will always be greater than 1.0 irrespective of the soil mass being considered. If one assumes an average of 0.5 for the coefficient of active earth pressure, then the passive value is 2.0.

If a large uniform surcharge q is placed on a backfill, it will increase the vertical stress at every point by q . In such cases, the increase in horizontal pressure due to the surcharge is computed by an amount of $K_a q$ or $K_p q$ depending on the state of stress being considered. If water is present behind the wall, then the pore water pressure is added to the active or passive earth pressures. That is, the earth pressure coefficient for water is unity. This is why it is necessary to provide proper drainage for retaining walls.

The Rankine coefficients for active and passive earth pressure can be considered as limiting values of an otherwise continuous function. In fact, the at rest coefficients correspond to intermediate states of stress that can be changed to either the active or the passive state by simply moving a wall away from or toward the backfill. This concept is shown graphically in Figure 9.6.

Note that it is not necessary for the whole wall to move for the states described in Figure 9.6 to develop. Instead, if the wall tilts, then it is possible to

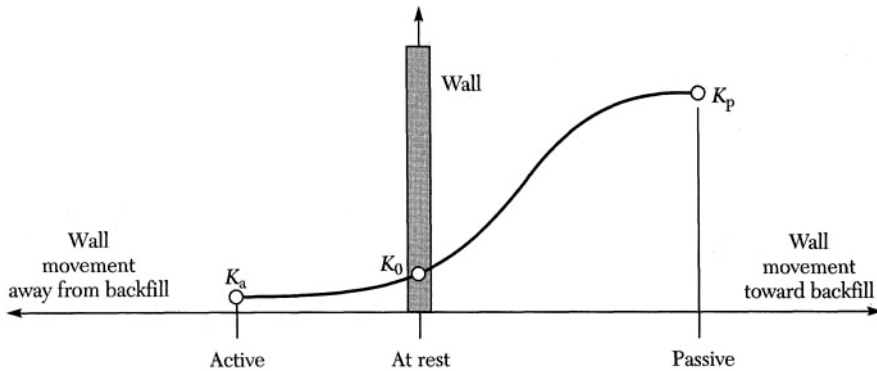
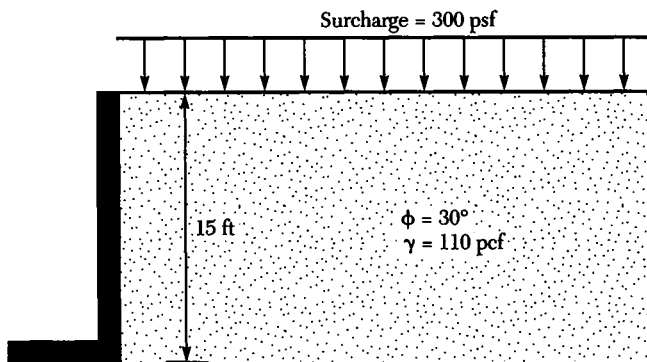


FIGURE 9.6 Possible states of earth pressure within a soil mass.

achieve an active or a passive state of stress depending on the direction of tilt (that is, away from or toward the backfill).

EXAMPLE 9.2

Calculate the total force acting on the wall shown below assuming (a) an active state and (b) a passive state of stress. The soil is relatively dry with a mass unit weight of 110 pcf.



Solution

Because the soil is sand, the coefficients of active and passive earth pressures are computed using Eqs. (9.7) and (9.12) as follows.

$$K_a = \tan^2(45 - 30/2) = 1/3$$

$$K_p = \tan^2(45 + 30/2) = 3.00$$

For this profile, the effective stresses are equal to the total stresses. Hence, the active and the passive horizontal earth pressures at the base of the wall are com-

puted as

$$\sigma_{ha} = 15(110)(1/3) + 350(1/3) = 666.67 \text{ psf}$$


$$\sigma_{hp} = 15(110)(3) + 350(3) = 6000 \text{ psf}$$

Note that at the top of the wall, the horizontal earth pressure is equal to the product of the surcharge and the corresponding coefficients of earth pressure. That is

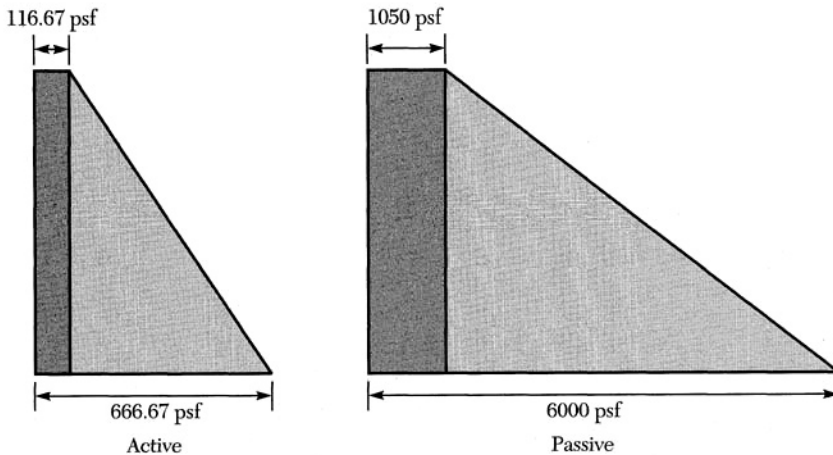
$$\sigma_{ha} = 350(1/3) = 116.67 \text{ psf}$$

$$\sigma_{hp} = 350(3) = 1050 \text{ psf}$$

These pressures are shown as follows.

 Surcharge

 Overburden



The resultant earth forces acting on the wall, in the event that an active or a passive state of stress exists, are computed as the areas enclosed by the diagrams just shown. Thus

$$E_a = 15 \left(\frac{116.67 + 666.67}{2} \right) = 5875 \text{ lb}$$

$$E_p = 15 \left(\frac{1050 + 6000}{2} \right) = 52,875 \text{ lb}$$

where E_a and E_p are the active and passive forces respectively. ■

EXAMPLE 9.3

Rework the problem described in Example 9.2 assuming that the soil is totally saturated, with a saturated unit weight of 122.4 pcf.

Solution

Because the soil is sand, the coefficient of active and passive earth pressures are computed using Eqs. (9.7) and (9.12) as follows.

$$K_a = \tan^2(45 - 30/2) = 1/3$$

$$K_p = \tan^2(45 + 30/2) = 3.00$$

For this profile, the effective stresses are not equal to the total stresses. Hence, the effective active and passive horizontal earth pressures at the base of the wall are computed as

$$\bar{\sigma}_{ha} = 15(122.4 - 62.4)(1/3) + 350(1/3) = 416.67 \text{ psf}$$

$$\bar{\sigma}_{hp} = 15(122.4 - 62.4)(3) + 350(3) = 1950 \text{ psf}$$

Note that at the top of the wall, the horizontal effective earth pressure is equal to the product of the surcharge and the corresponding coefficients of earth pressure. That is

$$\bar{\sigma}_{ha} = 350(1/3) = 116.67 \text{ psf}$$

$$\bar{\sigma}_{hp} = 350(3) = 1050 \text{ psf}$$

Also note that at the top the effective and total stresses are equal because the pore water pressure is zero at ground surface. The total horizontal stresses at the bottom are computed by first calculating the pore water pressure, then using Eqs. (9.5b) and (9.5c), which gives

$$\sigma_{ha} = \bar{\sigma}_{ha} + u = 416.67 + 15(62.4) = 1352.67 \text{ psf}$$

$$\sigma_{hp} = \bar{\sigma}_{hp} + u = 1950 + 936 = 2886 \text{ psf}$$

The resultant earth forces acting on the wall in the event that an active or a passive state of stress exists are computed as the areas enclosed by the pressure distributions. Thus

$$E_a = 15 \left(\frac{116.67 + 1352.67}{2} \right) = 11,020 \text{ lb}$$

$$E_p = 15 \left(\frac{1050 + 2886}{2} \right) = 29,520 \text{ lb}$$

where E_a and E_p are the active and passive forces, respectively. Note that the active force almost doubled and the passive force was reduced by almost one half. ■

9.3 COULOMB'S EARTH PRESSURE THEORY**9.3.1 Introduction**

Unlike Rankine's theory, Coulomb's theory assumes a rough wall. As in the case of Rankine's theory, a plane failure surface was assumed. The effect of wall rough-

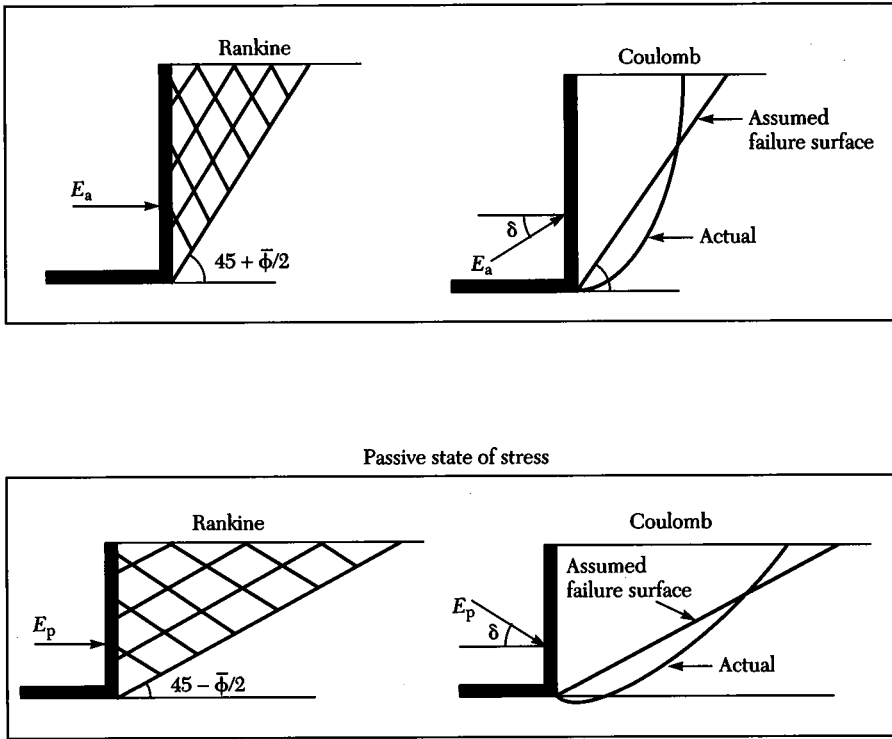


FIGURE 9.7 Comparison of failure surface and earth pressures using Rankine's and Coulomb's theories.

ness is to introduce shear stresses between the back of the wall and the soil that change the direction of the principal planes. This changes both the appearance of the failure surface from that assumed by Rankine and the inclination of the resultant earth pressure force as shown in Figure 9.7. The figure reveals that, rather than describing the state of stress at every point of the backfill, Coulomb assumed that failure will occur along a single surface. Therefore, the minimum (active) force and the maximum (passive) force between the wall and a soil wedge can be determined without considering stresses within the wedge.

In the active case the soil mass moves down relative to the wall. The shear stresses therefore act down on the wall and the resultant force E_a on the wall is inclined at an angle δ below the horizontal. For the passive case the soil mass moves up relative to the wall. The shear stresses therefore act upward on the wall, and the resultant force E_p on the wall is inclined at δ above the horizontal, where δ is the angle of friction between the soil and the wall. This is related to the effective

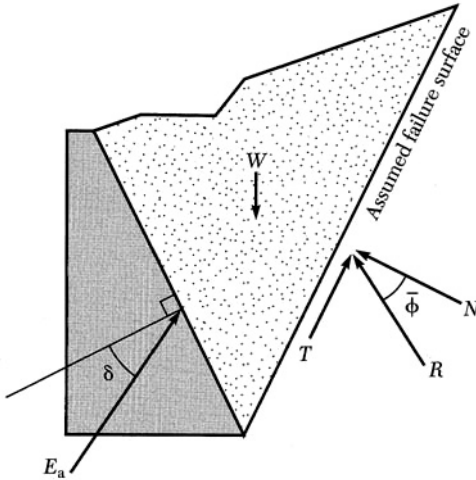


FIGURE 9.8 Determination of the active force for cohesionless soils.

angle of internal friction of the soil mass. Values of $\delta/\bar{\phi}$ range from 0.30 to 1.0 depending on the nature of the wall material and the backfill.

9.3.2 Coulomb's Active Earth Pressure

Because Coulomb approximated the actual curved failure surface by a straight line, the resultant force can be determined from a consideration of the free body diagram. That is, using the concepts of static equilibrium and the force polygon associated with a trial failure mass, it is possible to evaluate the earth pressure. Consider the free body diagram of an assumed failure mass in a cohesionless backfill as shown in Figure 9.8.

The direction and magnitude of W is known. It is the weight of the failure mass acting downward. The direction of R is known but not its magnitude. The resultant of the shear force T and normal force N acting on the assumed failure sur-

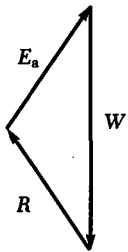


FIGURE 9.9 Force polygon for the active case of cohesionless dry soils.

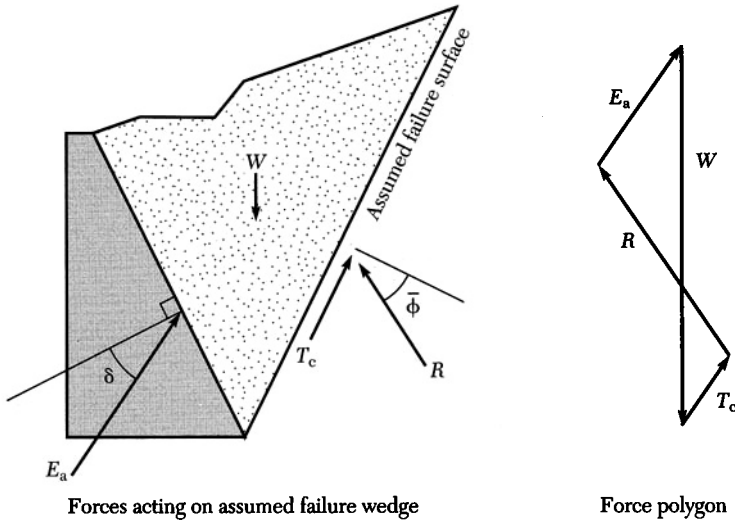


FIGURE 9.10 Determination of the active resultant force for cohesive soils.

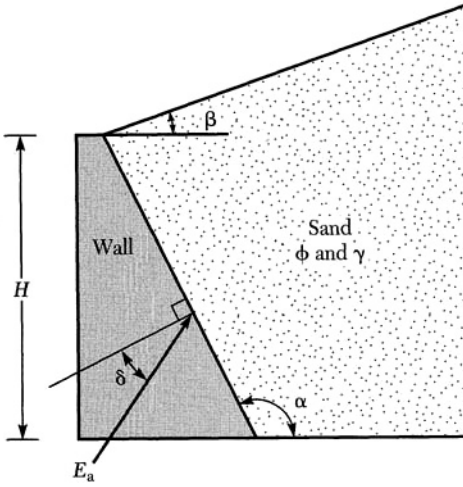
face is inclined at an angle $(90^\circ - \bar{\phi})$ to the failure surface. Finally, the direction of E_a , the active earth pressure force, is known. It is inclined downward from a line normal to the wall at an angle δ , the angle of wall friction. With this information a force polygon was constructed as shown in Figure 9.9. It is now possible to scale off the value of E_a . Different failure surfaces must be assumed until the maximum value of E_a is found. Note that the inclination of the failure surface is no longer at $(45^\circ + \bar{\phi}/2)$.

Similarly, the active resultant force in a cohesive backfill can be determined from a consideration of the free body diagram of a trial failure mass and a force polygon. Cohesion introduces another force, whose magnitude and direction is known, along the assumed failure surface as shown in Figure 9.10. Note that the adhesion force on the back of the wall was ignored.

Note that T_c is the force acting on the assumed failure surface due to the soil's cohesion. Its magnitude is equal to the cohesion multiplied by the length of the assumed failure surface. The directions of R , E_a , W , and T_c are known. Also, the magnitudes of T_c and W are known. For a given assumed failure surface, the magnitude of the active force per unit width is easily determined.

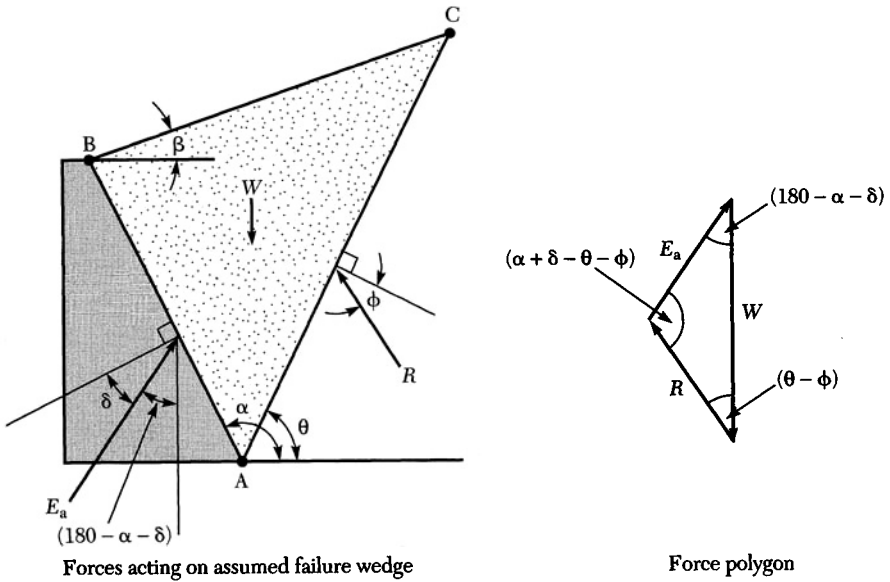
EXAMPLE 9.4

Develop an expression for the coefficient of active earth pressure using the Coulomb method of force polygons for the following profile. Assume that the soil is dry and cohesionless.



Solution

First assume a failure surface and the associated free body diagram. This is shown along with the force polygon as follows.



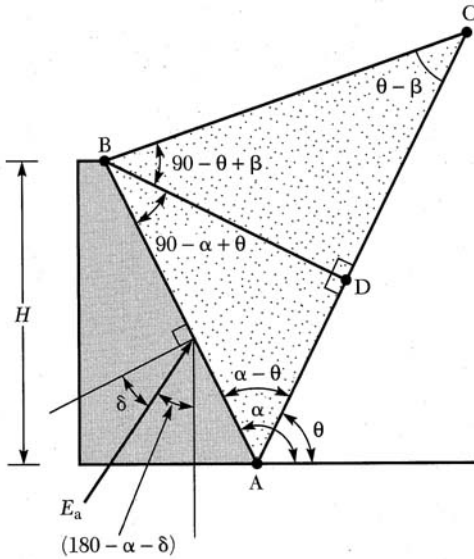
Using the law of sines, write

$$\frac{E_a}{\sin(\theta - \phi)} = \frac{W}{\sin(\alpha + \delta - \theta - \phi)}$$

Solving for E_a gives

$$E_a = \frac{W \sin(\theta - \phi)}{\sin(\alpha + \delta - \theta - \phi)}$$

Note that for a given problem, the angles ϕ , α , and δ are known. Hence, the relationship between the resultant force corresponding to the active earth pressure and the failure angle θ is known. However, the weight W is clearly a function of θ . The value of W is determined by considering the following figure.



The weight can be expressed as the area of the wedge ABC multiplied by the unit weight of soil. That is,

$$W = \frac{(\overline{AD} + \overline{CD}) \overline{BD}}{2} \gamma$$

However,

$$\begin{aligned} \frac{\overline{AB}}{\overline{CD}} &= \frac{H}{\cos(\alpha - 90)} = \frac{\overline{BD}}{\sin(\alpha - \theta)} \Rightarrow \overline{BD} = \frac{\sin(\alpha - \theta)}{\cos(\alpha - 90)} H \\ \frac{\sin(90 - \theta + \beta)}{\overline{AD}} &= \frac{\sin(\theta - \beta)}{\overline{BD}} \Rightarrow \overline{CD} = \frac{\sin(90 - \theta + \beta)}{\sin(\theta - \beta)} \frac{\sin(\alpha - \theta)}{\cos(\alpha - 90)} H \\ \frac{\overline{AD}}{\sin(\alpha - 90)} &= \frac{\overline{BD}}{\sin(\alpha - \theta)} \Rightarrow \overline{AD} = \frac{\sin(\alpha - 90)}{\sin(\alpha - \theta)} \frac{\sin(\alpha - \theta)}{\cos(\alpha - 90)} H \end{aligned}$$

Therefore,

$$W = \frac{H^2}{2} \gamma \left(\frac{\sin(\alpha - 90)}{\sin(\alpha - \theta)} + \frac{\sin(90 - \theta + \beta)}{\sin(\theta - \beta)} \right) \left(\frac{\sin(\alpha - \theta)}{\cos(\alpha - 90)} \right)^2$$

Consequently, the resultant force corresponding to the active earth pressure for any failure plane with a slope of θ from the horizontal is given by

$$E_a = \frac{\gamma H^2}{2} \left[\left(\frac{\sin(\theta - \phi)}{\sin(\alpha + \delta - \theta - \phi)} \right) \left(\frac{\sin(\alpha - 90)}{\sin(\alpha - \theta)} + \frac{\sin(90 - \theta + \beta)}{\sin(\theta - \beta)} \right) \left(\frac{\sin(\alpha - \theta)}{\cos(\alpha - 90)} \right)^2 \right]$$

The orientation of the failure plane that corresponds to the active case is determined by satisfying the following condition.

$$\frac{\partial E_a}{\partial \theta} = 0$$

The maximum E_a value is determined by substituting the angle that satisfies the above condition, which gives

$$E_a = \frac{\gamma H^2}{2} \left[\frac{\cos^2(90 + \phi - \alpha)}{\cos^2(\alpha - 90) \cos(\alpha - 90 + \delta) \left(1 + \sqrt{\frac{\sin(\delta + \phi) \sin(\phi - \beta)}{\cos(\alpha - 90 + \delta) \cos(\alpha - 90 - \beta)}} \right)^2} \right]$$

or more simply

$$E_a = \frac{\gamma H^2}{2} K_a$$

where

$$K_a = \left[\frac{\cos^2(90 + \phi - \alpha)}{\cos^2(\alpha - 90) \cos(\alpha - 90 + \delta) \left(1 + \sqrt{\frac{\sin(\delta + \phi) \sin(\phi - \beta)}{\cos(\alpha - 90 + \delta) \cos(\alpha - 90 - \beta)}} \right)^2} \right]$$

Note that for $\alpha = 90^\circ$, $\delta = 0$, and $\beta = 0$, the preceding expression reduces to the expression derived for the Rankine value given by Eq. (9.7). ■

9.3.3 Coulomb's Passive Earth Pressure

The resultant passive force can once again be determined from a consideration of the free body diagram. Consider the free body diagram for an assumed failure mass in a cohesionless backfill as shown in Figure 9.11. The passive earth pressure force can be determined using force polygons similar to the one shown in the figure. This is accomplished by trying different failure surfaces until the minimum value of E_p is found. Note that the inclination of the failure surface is no longer at $(45^\circ - \phi/2)$. Similarly, the passive resultant force in a cohesive backfill can be ap-

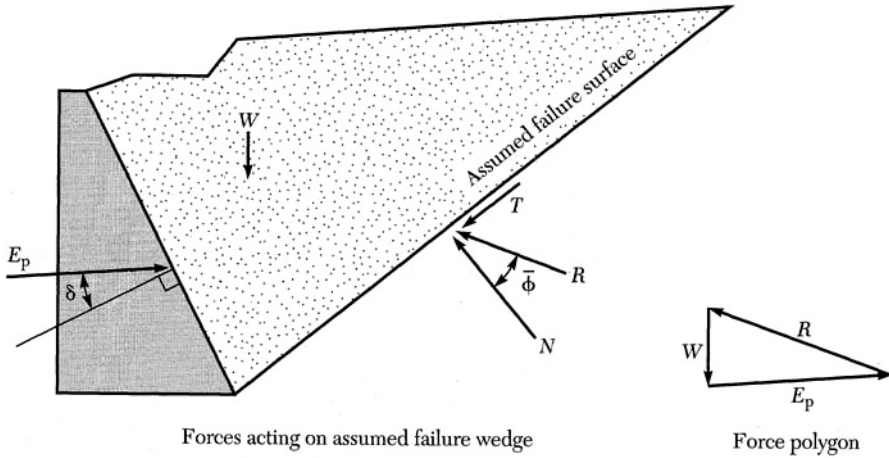


FIGURE 9.11 Determination of the passive resultant force for cohesionless soils.

proximated from a consideration of the free body diagram of a trial failure mass and a force polygon that includes the cohesion force T_c as shown in Figure 9.12.

Note that T_c is the force acting on the assumed failure surface due to the soil's cohesion. Its magnitude is equal to the cohesion multiplied by the length of the assumed failure surface. The directions of R , E_a , W , and T_c are known. Furthermore, the magnitudes of T_c and W are known. For an assumed failure surface, the magnitude of the active force per unit width is determined. Again, several force polygons must be constructed to arrive at the actual E_p . For this case, the critical failure plane is associated with the minimum value of E_p .

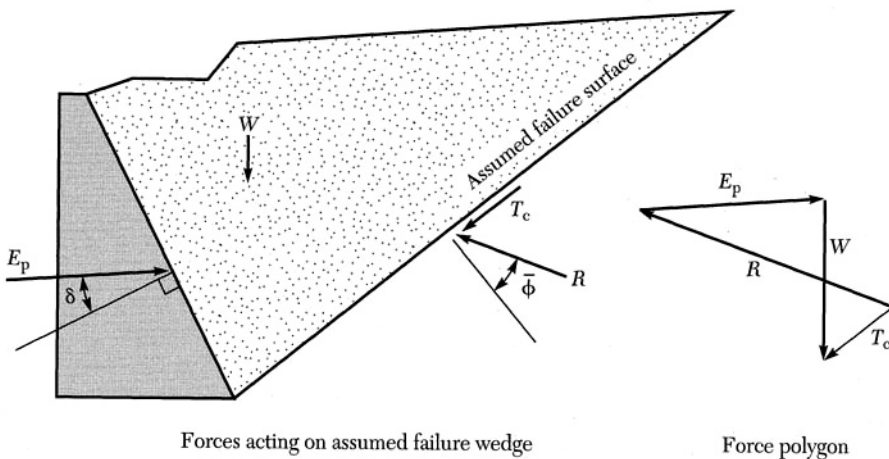


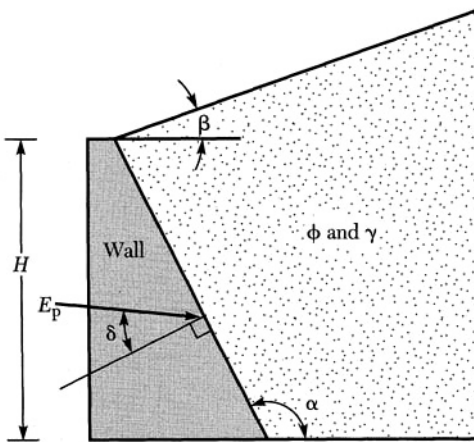
FIGURE 9.12 Determination of the passive resultant force for cohesive soils.

372 CHAPTER 9 LATERAL EARTH PRESSURE

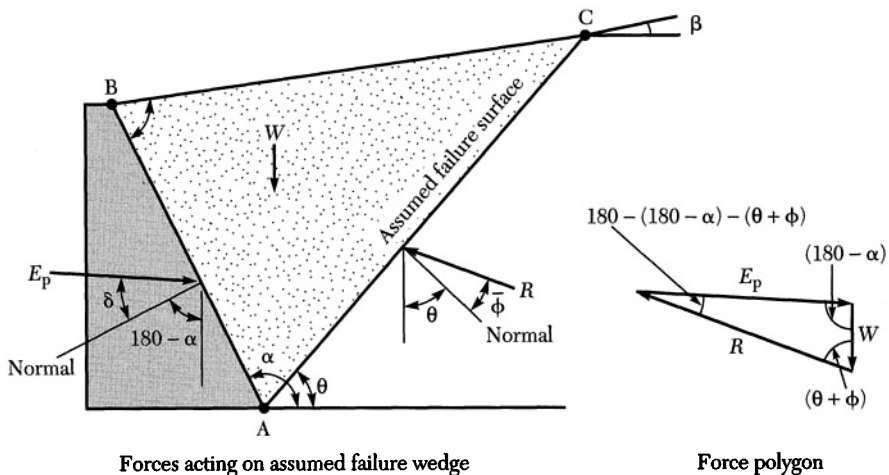
Considering Figures (9.9) through (9.12) clearly shows that Coulomb's method is not limited to horizontal soil backfills or vertical walls. In fact, it is also possible to include point, line, and strip loads in the analysis.

EXAMPLE 9.5

Develop an expression for the coefficient of active earth pressure using the Coulomb method of force polygons for the following soil profile. Assume the soil is dry and cohesionless.

**Solution**

First, assume a failure surface that defines the associated free body diagram. This is shown along with the force polygon as follows.



10

Bearing Capacity

10.0 INTRODUCTION

Bearing capacity may be defined as the ability of the soil to carry a load without failure within the soil mass. Failure in geotechnical engineering is a relative term in that it is not as well defined as is the case in structural engineering. Bearing capacity failure relates to the concept of excessive settlement without any increase in applied pressure. This chapter is a brief introduction into the bearing capacity of shallow and deep foundations.

Shallow foundations are defined as any footing that has a width equal to or greater than the depth at which it is buried (Figure 10.1a). *Deep foundations* are defined as any footing that has a width that is smaller than the depth to which it extends (Figure 10.1b). These two definitions are significant in that the theories pertaining to each are different. Generally, a shallow footing has a relatively large load-bearing area, which makes it possible to transfer the load from a column or a wall to the underlying soil mass. That is, the stress at the footing-soil interface is controlled by how large the area is. In deep foundations, such as piles, the load from the structure is transferred to the underlying soil either by the friction at the pile surface to the surrounding soil and/or through the tip of the pile to a hard stratum in which it is embedded. Both shallow and deep foundation systems must satisfy the following three basic requirements.

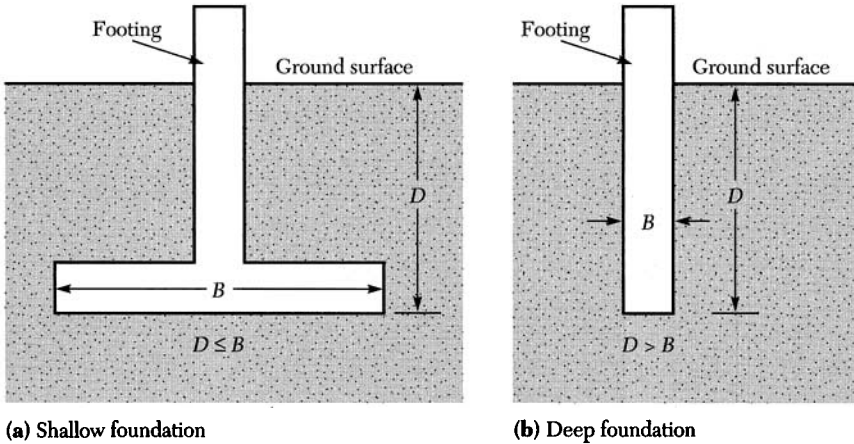


FIGURE 10.1 Types of foundation systems.

1. The total and differential settlements must be sufficiently small to ensure that the structure will not be damaged by foundation movements.
2. The applied pressure must be sufficiently less than the bearing capacity to assure foundation safety.
3. The foundation must be constructed so that adjacent structures are not damaged during construction.

Unfortunately, available mathematical analyses have limitations and do not fully predict soil behavior. This is why, in the design of foundations, a large factor of safety must be used relative to bearing capacity failure. There are approximate theories suitable for computation of the bearing capacity for a foundation.

10.1 FACTOR OF SAFETY

The factor of safety (FS) is of central importance in conventional design of foundation systems. It is also the focus of much criticism. There are several definitions for the factor of safety depending on the type of problem being analyzed.

1. Ratio of ultimate strength in a component to the actual stress.
2. Ratio of maximum safe load to normal service load.
3. Ratio of driving moment to resisting moment when dealing with instability analysis.
4. Ratio of mean strength to mean load.
5. Ratio of computed strength to the corresponding computed load.

When dealing with bearing capacity, the factor of safety is defined as the ratio of the calculated bearing pressure to the applied bearing pressure. The computed value is referred to as the ultimate bearing capacity q_{ult} . This is related to the angle of internal friction and cohesion of a given soil. The inherent variability

in soil properties accounts for variation of strength, which causes variations in q_{ult} (of, say, Δq_{ult}) and in the applied stress q_a (of, say, Δq_a) from computed values. The lowest probable ultimate bearing capacity ($q_{ult} - \Delta q_{ult}$) and the largest probable bearing pressure ($q_a + \Delta q_a$) must satisfy the inequality $q_{ult} - q_a > 0$ to avoid failure. Thus,

$$q_{ult} - \Delta q_{ult} \geq q_a + \Delta q_a$$

or

$$q_{ult} \left(1 - \frac{\Delta q_{ult}}{q_{ult}} \right) \geq q_a \left(1 + \frac{\Delta q_a}{q_a} \right)$$

The minimum factor of safety is then given by Eq. (10.1).

$$FS = \frac{q_{ult}}{q_a} = \frac{\left(1 + \frac{\Delta q_a}{q_a} \right)}{\left(1 - \frac{\Delta q_{ult}}{q_{ult}} \right)} \quad (10.1)$$

One must have some idea of the variations in soil properties as well as variations in loading. For example, assuming a variation of 25% in the computed q_{ult} and q_a gives a factor of safety of

$$FS = \frac{q_{ult}}{q_a} = \frac{\left(1 + \frac{\Delta q_a}{q_a} \right)}{\left(1 - \frac{\Delta q_{ult}}{q_{ult}} \right)} = \frac{1 + 0.25}{1 - 0.25} = 1.67$$

This value corresponds to the factor of safety used in the design of steel structures. With soils, the properties are not that well known, so a larger factor of safety is normally used. Structural loads are known well enough for design purposes so that a 25% variation in the expected bearing pressure is suitable. However, the calculated ultimate bearing pressure is dependent on soil properties, footing type, the theory being used, and, in some cases, good judgment. Therefore, if one is to assume a 50% variation in the calculated q_{ult} value and a 25% variation in the applied pressure, the corresponding factor of safety is given as

$$FS = \frac{q_{ult}}{q_a} = \frac{\left(1 + \frac{\Delta q_a}{q_a} \right)}{\left(1 - \frac{\Delta q_{ult}}{q_{ult}} \right)} = \frac{1 + 0.25}{1 - 0.5} = 2.5$$

Normally, the factor of safety used in determining the allowable bearing pressure is taken to be 3.0. This is equivalent to a variation of 58.3% in q_{ult} and a variation of 25% in q_a . Furthermore, the bearing pressure used in design is called the allow-

able bearing pressure q_{all} (or simply q_a). In bearing capacity problems, the allowable bearing capacity (also called *allowable bearing pressure*) is given by

$$q_a = \frac{q_{\text{ult}}}{\text{FS}}$$

In slope stability problems, a factor of safety of 1.3 to 1.5 is generally used because the loading and soil properties are controlled.

The proper design of foundations requires that both settlement and strength factors be considered. The fallacy that only bearing capacity be considered could be dangerous. The implication is that once an allowable bearing pressure is determined, the corresponding settlement can be calculated. The allowable settlement value should be checked. In some cases, the allowable bearing pressure, based on bearing capacity, must be reduced so that the settlement is not excessive.

10.2 TERZAGHI'S BEARING CAPACITY THEORY FOR SHALLOW FOUNDATIONS

The failure mechanism of a foundation when the bearing capacity of the soil is exceeded usually takes place in four stages. The first stage involves a downward movement of soil beneath the foundation. The second stage is described by a localized cracking of the soil around the perimeter of the foundation. Stage three involves formation of a cone-shaped wedge of soil beneath the footing that forces the soil downward and outward. Finally, a continuous surface of shear may develop.

In 1943, Terzaghi proposed a theory for the bearing capacity of shallow foundations based on a model developed by Prandtl (1921). His solution involved several assumptions: uniform soil, $D_f \leq B$, water level below zone II (Figure 10.2), vertical concentric load, and negligible vertical friction and cohesion forces along the sides of the footing. This theory is based on the supposition that a footing penetrating a soil mass will generally result in the development of three distinct zones. These zones of plastic equilibrium after failure of the soil beneath a continuous footing are shown in Figure 10.2. Zone I is in a state of elastic equilibrium with a boundary assumed at ϕ to the horizontal, zone II represents a zone of radial shear, and zone III represents a passive Rankine zone.

To evaluate Q_{ult} , the ultimate capacity of the footing, consider the forces acting on the wedge ABC as shown in Figure 10.3. The value of the passive earth pressure resultant is E_p shown in Figure 10.3 the resultant of shear stresses associated with ϕ and the normal stresses along AB and AC. Note that the resultant is at ϕ to the normal and AC is at ϕ to the horizontal, and E_p acts in the vertical direction. Summing forces in the vertical direction gives

$$\Sigma F_x = 0 = Q_{\text{ult}} + \frac{B^2}{4}\gamma - 2E_p - cB \tan \phi$$

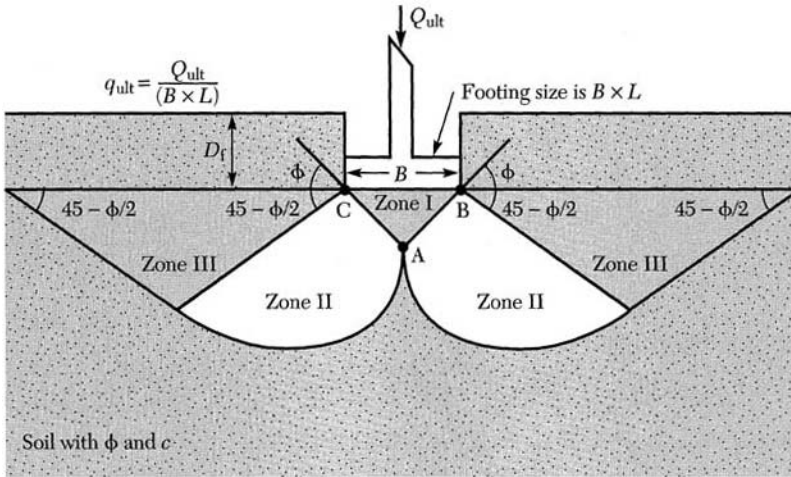


FIGURE 10.2 Bearing capacity failure zones.

where γ is the unit weight of the soil. Therefore, solving for Q_{ult} gives

$$Q_{ult} = -\frac{B^2}{4}\gamma + 2E_p + cB \tan \phi \tag{10.2}$$

Hence, the ultimate bearing capacity is given by

$$q_{ult} = \frac{Q_{ult}}{B \times L} = -\frac{B}{4L}\gamma + \frac{2}{L}E_p + \frac{c}{L} \tan \phi \tag{10.3}$$

All terms are known in Eq. (10.3) except E_p . Terzaghi solved for E_p by assuming the curved surface of sliding in zone II consists of a logarithmic spiral with the equation $r = r_0 e^{\theta \tan \phi}$. For a given soil with an angle of internal friction ϕ , the value of r is the radius of the spiral for a given angle θ . The solution for E_p can be found in most textbooks on foundation engineering and is omitted for lack of space.

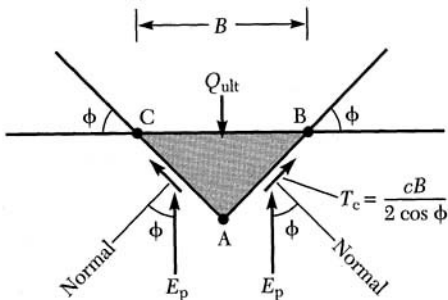


FIGURE 10.3 Terzaghi's bearing capacity analysis of zone I.

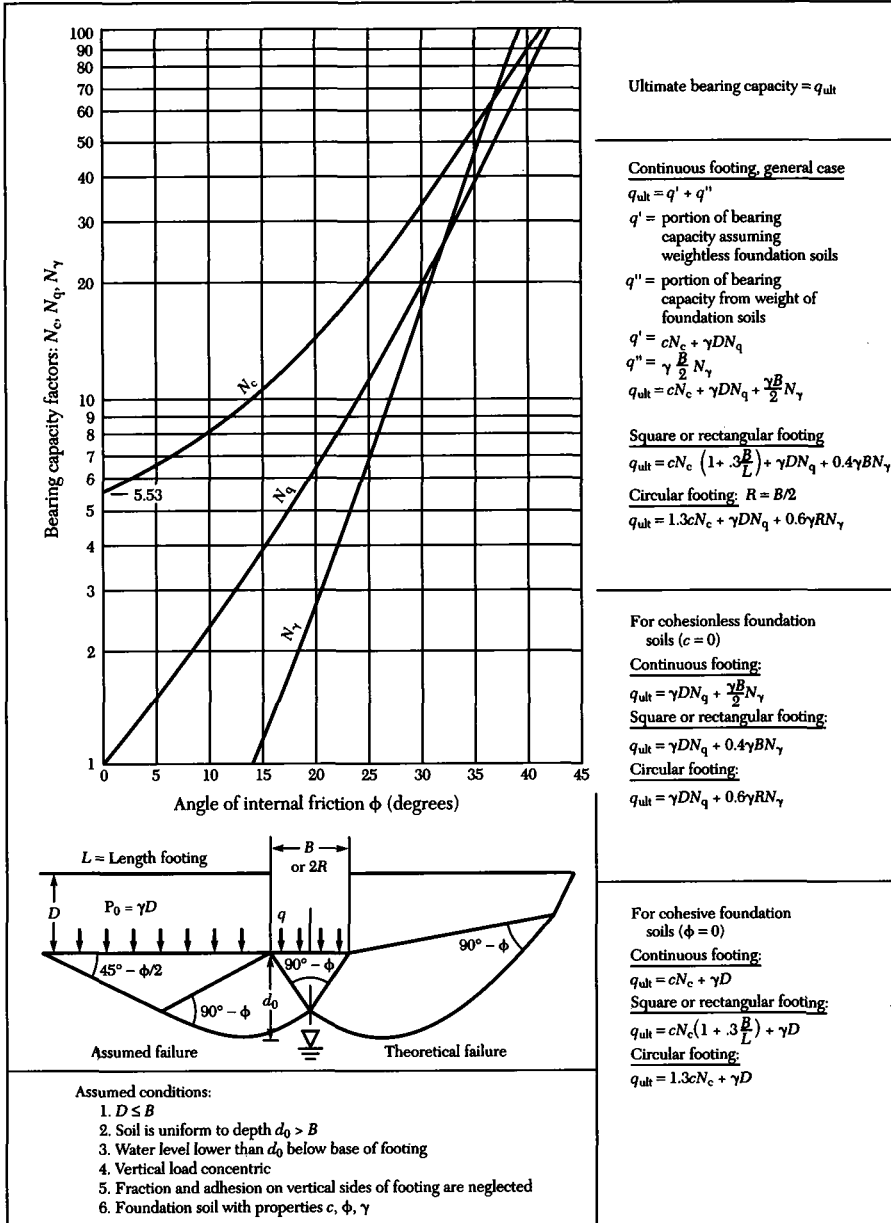


FIGURE 10.4 Terzaghi's ultimate bearing capacity factors of shallow footing assuming general shear failure. (After U.S. Navy NAVFAC DM-7.1, 1982.)

Terzaghi developed expressions for E_p and rewrote Eq. (10.3) in terms of bearing capacity factors for the general shear failure condition. His solution is

$$q_{ult} = cN_c + qN_q + \frac{1}{2}\gamma BN_\gamma \tag{10.4}$$

where N_c , N_q , and N_γ are the bearing capacity factors, c is soil cohesion, B is footing width, γ is soil unit weight, and q is the overburden pressure at the footing base ($q = D_f\gamma$). Equation (10.4) is Terzaghi's ultimate bearing capacity equation for general shear failure. Terzaghi provided a chart showing the bearing capacity factors as functions of the angle of internal friction for the soil as shown in Figure 10.4.

As in the case for retaining walls, the magnitude of strains preceding failure in a soil mass are assumed to be very small (i.e., the soil behaves "plastically"). This may be approximately correct for dense sand or stiff clay but not for loose sand or soft clay. The stress-strain and load settlement behavior for different soil types found in the field is shown in Figure 10.5.

For loose sand and soft clay, the footing sinks into the ground before the state of plastic equilibrium is reached along the entire failure surface. Bearing capacity failures of the first type are called *general shear* failures, because the shear strength of the soil is mobilized along the entire failure surface. *Local shear* failure occurs when the shear strength is only mobilized along a limited (local) portion of the failure surface at any time. Currently, there are no bearing capacity theories for local shear failures, because there are no limiting zones of failure that can be clearly defined. An approximate value may be obtained by assuming the cohesion and friction are equal to two thirds of their actual values, and then solving for bearing capacity factors N'_c , N'_q , and N'_γ , as shown in Figure 10.6.

The Terzaghi equation for ultimate bearing capacity is modified for the local shear failure condition as given by Eq. (10.5).

$$q_{ult} = \frac{2}{3}cN'_c + qN'_q + \frac{1}{2}\gamma BN'_\gamma \tag{10.5}$$

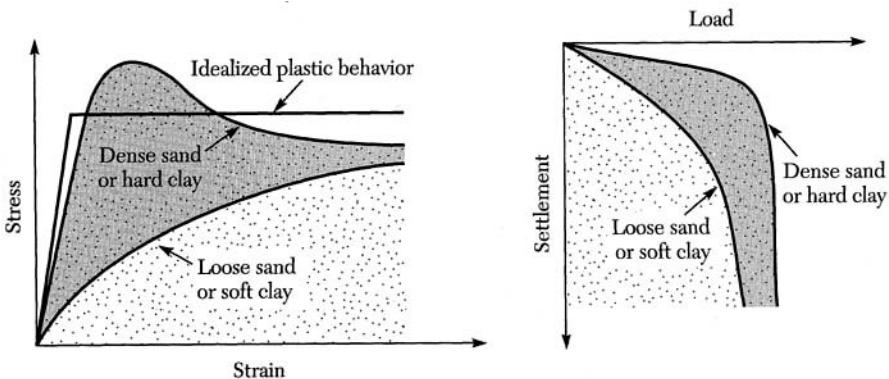


FIGURE 10.5 Stress-strain and load deformation behavior of different soils.

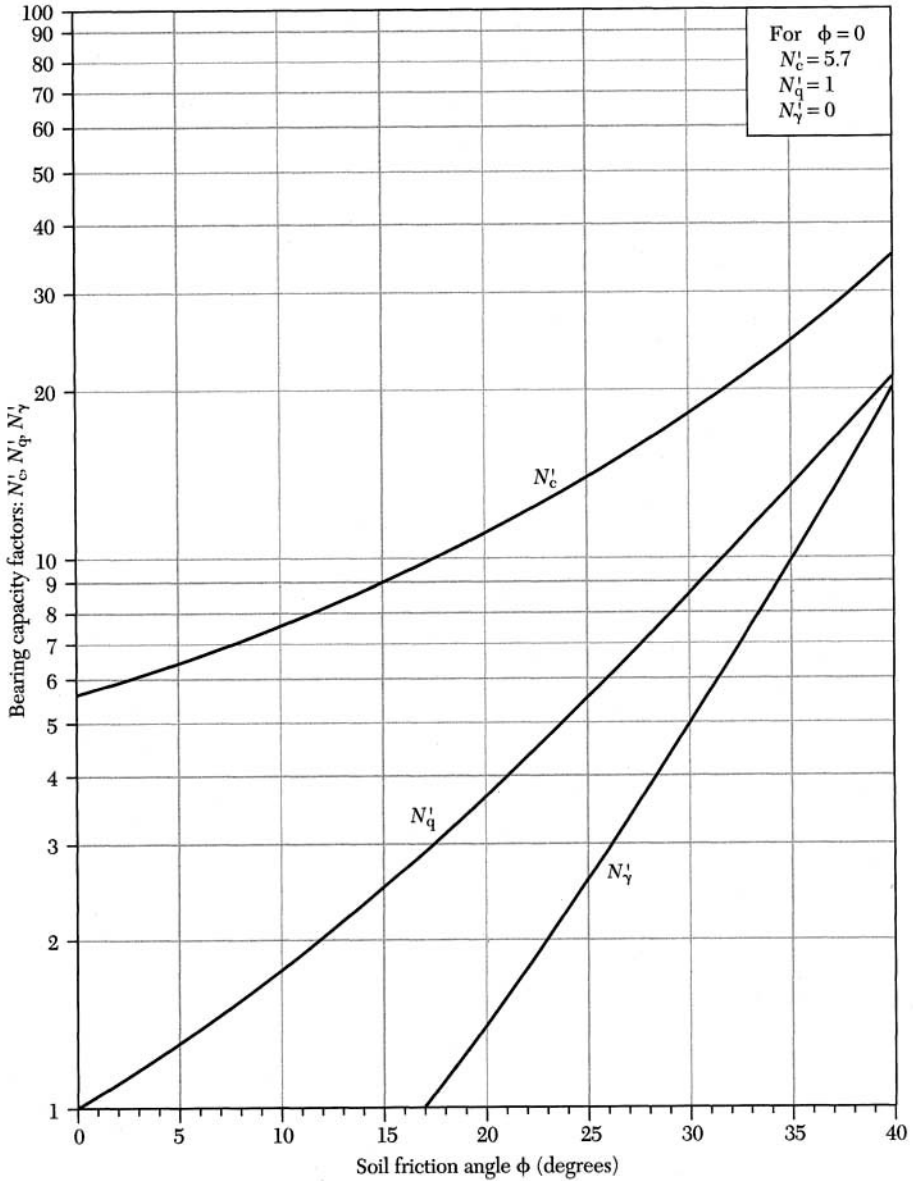


FIGURE 10.6 Terzaghi's ultimate bearing capacity factors of shallow footings assuming local shear failure. (Adapted from Terzaghi, 1943.)

Table 10.1 Terzaghi's Ultimate Bearing Capacity Equations

| Type of Shallow Footing | General Shear Failure | Local Shear Failure |
|-----------------------------|--|---|
| Long $B \times \infty$ | $q_{ult} = cN_c + qN_q + \frac{1}{2} \gamma B N_\gamma$ | $q_{ult} = \frac{2}{3} cN'_c + qN'_q + \frac{1}{2} \gamma B N'_\gamma$ |
| Rectangular $B \times L$ | $q_{ult} = \left(1 + 0.3 \frac{B}{L}\right) cN_c + qN_q + 0.4 \gamma B N_\gamma$ | $q_{ult} = \left(1 + 0.3 \frac{B}{L}\right) cN'_c + qN'_q + 0.4 \gamma B N'_\gamma$ |
| Square $B \times B$ | $q_{ult} = 1.3 cN_c + qN_q + 0.4 \gamma B N_\gamma$ | $q_{ult} = 1.3 cN'_c + qN'_q + 0.4 \gamma B N'_\gamma$ |
| Circular Diam. $= D$ | $q_{ult} = 1.3 cN_c + qN_q + 0.3 \gamma B N_\gamma$ | $q_{ult} = 1.3 cN'_c + qN'_q + 0.3 \gamma B N'_\gamma$ |
| | Find N_c , N_q , and N_γ using Figure 10.4 with ϕ . | Find N'_c , N'_q , and N'_γ using Figure 10.6 with $\phi = \tan^{-1} \left(\frac{2}{3} \tan \phi \right)$. |

Note that the reduced angle of internal friction to be used with Figure 10.6 must be computed using the angle of internal friction ϕ for the soil as follows.

$$(\phi)_{\text{for local shear}} = \tan^{-1} \left(\frac{2}{3} \tan \phi \right)$$

Because the general bearing capacity equation [Eq. (10.4)] was developed for a long shallow footing, it is necessary to modify it when dealing with footings of finite length and width. Terzaghi modified the general ultimate bearing capacity equations for square and circular footings and introduced several correction factors. A summary of all of Terzaghi's equations is shown in Table 10.1. Terzaghi's ultimate bearing capacity equations have been refined through the effort of several investigators. Most notable among them are Meyerhof, Vesic, and Hanson.

EXAMPLE 10.1

A strip footing 6 ft wide is to be placed at a depth of 4 ft in a moist soil that has the following characteristics: $\gamma_m = 100$ pcf, $c = 750$ psf, $\phi = 25^\circ$. Determine the allowable bearing capacity of the foundation assuming a factor of safety of 3.0 and a general shear failure.

Solution

Using Figure 10.4, with $\phi = 25$, read $N_c = 21.5$, $N_q = 12$, and $N_\gamma = 7$. Substituting into Eq. 10.4 gives

$$q_{ult} = 750(20.5) + 100(4)(12) + \frac{1}{2}(100)(7) = 20,525 \text{ psf}$$

The allowable bearing pressure is given as

$$q_a = \frac{20,525}{3.0} = 6842 \text{ psf}$$

Note that this value is relatively high if settlement of the footing is to be limited to a reasonable value. ■

EXAMPLE 10.2

Design a square footing to carry a column load of 250 kips with a factor of safety of 2.5. The footing is to be placed 3.5 ft below ground surface. The clay soil beneath the footing is homogeneous with an unconfined compressive strength of q_u of 2.2 ksf and a unit weight of 105 pcf. The soil is assumed to have $\phi = 0$ and general shear failure is expected.

Solution

Using Figure 10.4 with $\phi = 0$ and $c_u = q_u/2 = 1.10$ ksf gives $N_c = 5.53$, $N_q = 1.0$, and $N_\gamma = 0$. Using Table 10.1, select the equation for a square footing.

$$q_{ult} = 1.3(1.10)(5.53) + \frac{105}{1000}(3.5) + 0 = 8.275 \text{ ksf}$$

$$q_a = \frac{8.275 \text{ ksf}}{2.5} = 3.31 \text{ ksf}$$

Consequently,

$$q_a = 3.31 \text{ ksf} = \frac{Q_a}{A} = \frac{250}{A} \Rightarrow A = 75.5 \text{ ft}^2$$

The footing size $B = \sqrt{A} = 8.7$ ft square or $8\frac{3}{4}$ ft \times $8\frac{3}{4}$ ft. ■

10.3 EFFECT OF GROUNDWATER TABLE AND ECCENTRICITY

Terzaghi's ultimate bearing capacity equation was based on several simplifying assumptions. For the special case, where the groundwater table is either above the footing or falls within the failure zone II of the footing, Terzaghi's equation must be corrected. Figure 10.7 provides modified ultimate bearing capacity equations with appropriate correction factors for water table location within a given soil profile.

In some cases, either a footing or the force it transmits is inclined by an angle α from the horizontal. There are other practical problems where the applied force acting on a horizontal footing is eccentric. In all such cases, Figure 10.8 can be used to adjust the bearing capacity equation developed by Terzaghi. Note that the modified ultimate bearing capacity equations are given in Figure 10.8. These equations are suitable for only continuous footings.

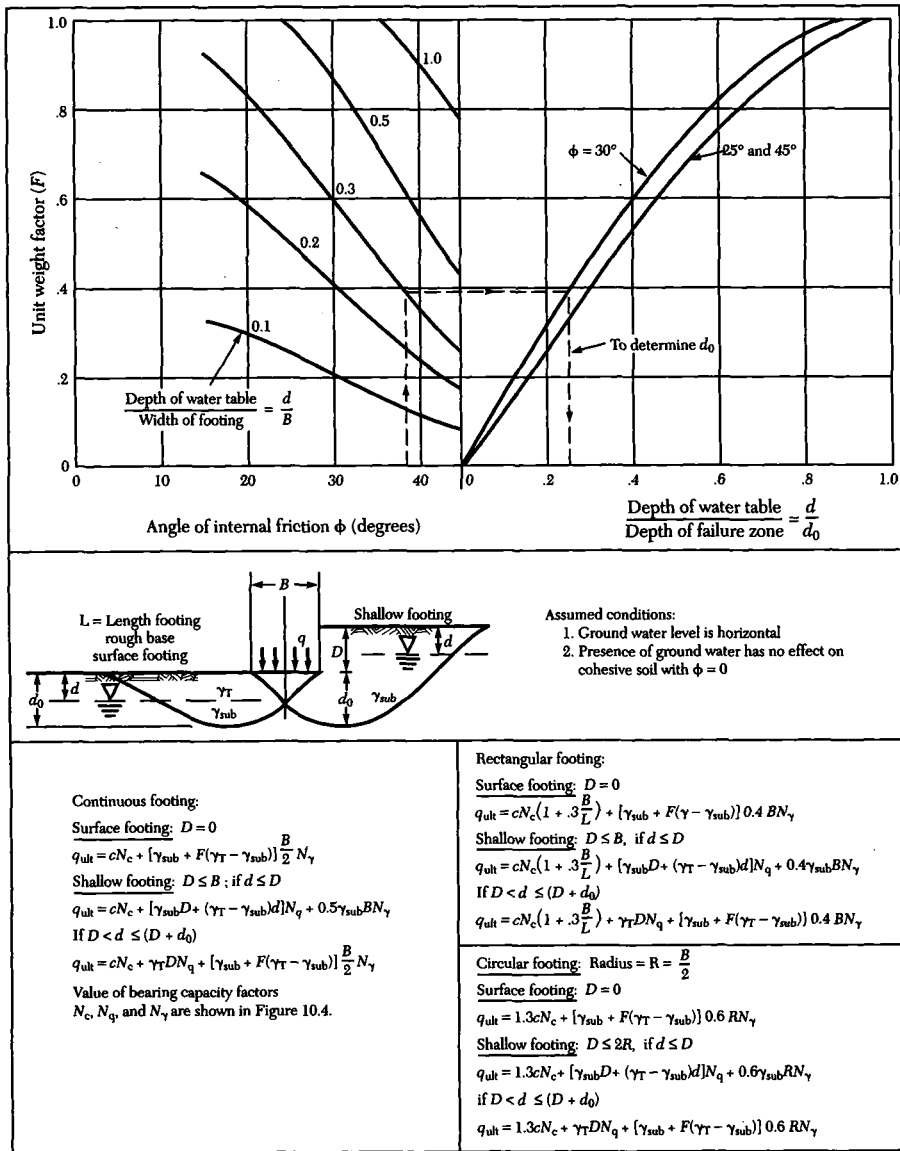


FIGURE 10.7 Ultimate bearing capacity with groundwater effect. (After U.S. Navy, NAVFAC DM-7.)

10.4 ULTIMATE BEARING CAPACITY ON TWO-LAYER COHESIVE SOIL

There are several practical problems where a proposed shallow footing is placed within a soft clay layer below which exists a harder clay layer. In some cases, the opposite may be true. In both of these cases, it is assumed that the clay layers are

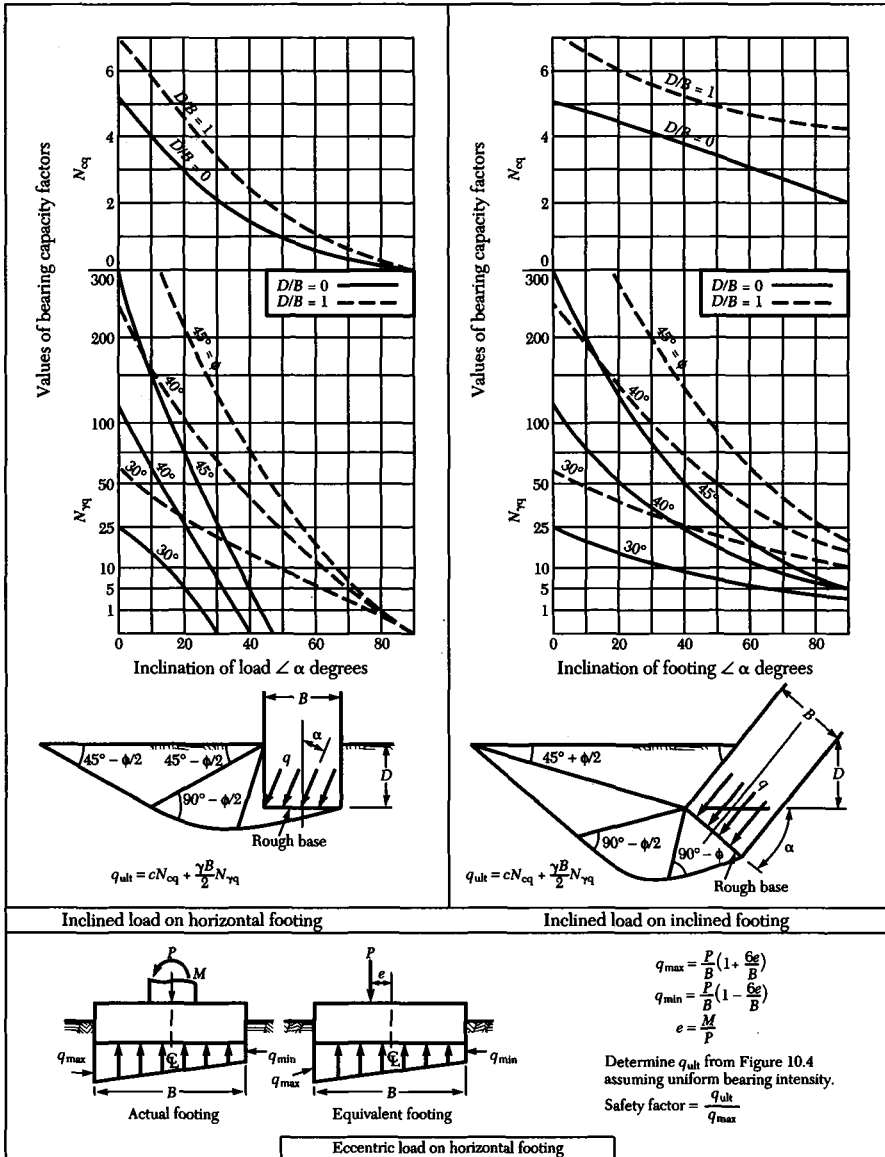


FIGURE 10.8 Ultimate bearing capacity with eccentric or inclined loads. (After U.S. Navy, NAVFAC DM-7.)

unconsolidated and undrained ($\phi = 0$). Furthermore, the cohesion of the two clay layers may be constants with depth or may vary within each layer. All of these cases are described fully in Figure 10.9. (Note that the modified ultimate bearing capacity equations are included in Figure 10.9 for continuous and a rectangular footings.)

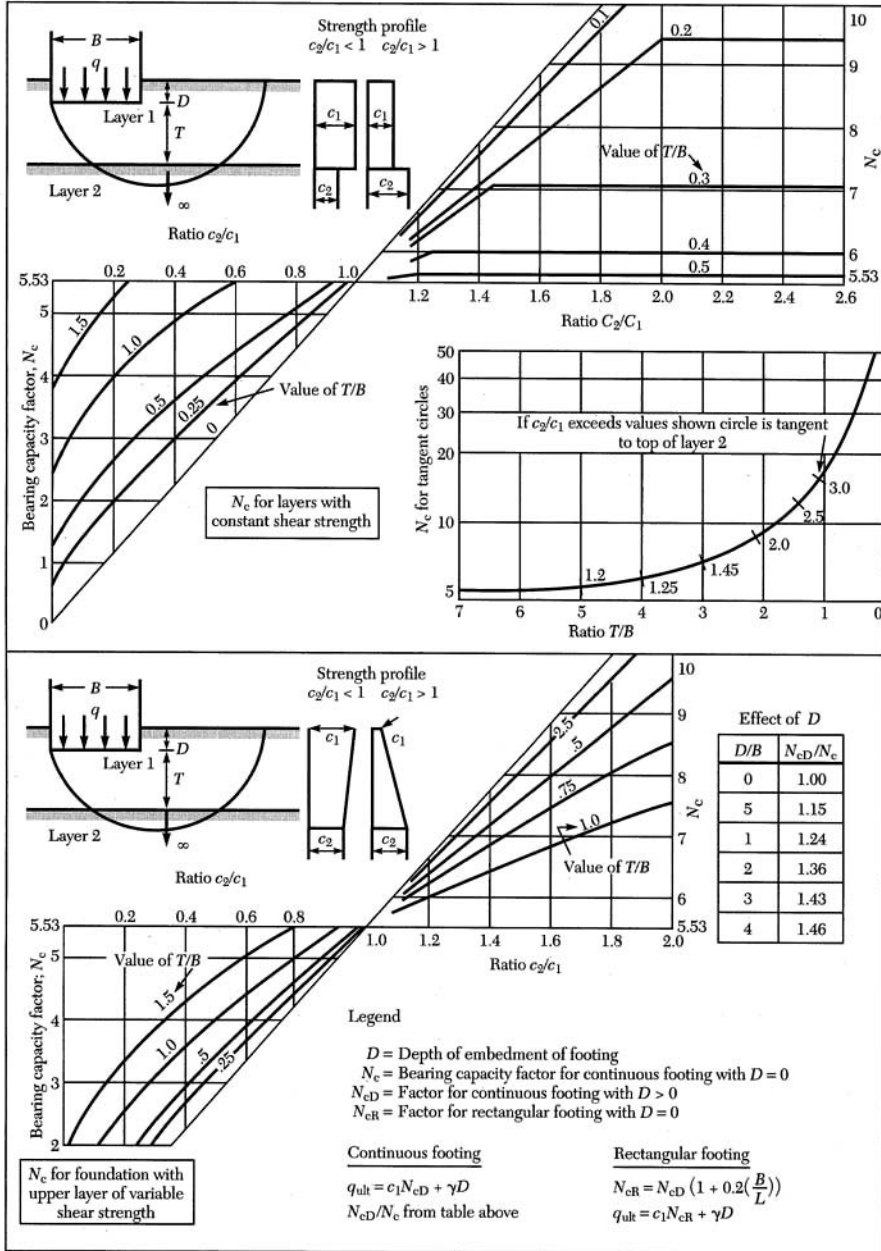


FIGURE 10.9 Ultimate bearing capacity on two cohesive soils ($\phi = 0$). (After U.S. Navy, NAVFAC DM-7.)

10.5 NOMINAL BEARING PRESSURE

Nominal bearing pressures are allowable bearing pressures that are based primarily on good judgment and experience. Nominal bearing pressures are often used for preliminary design estimates. They may also be used when an elaborate soils investigation is not justified. These bearing pressures provide a suitable “check” on allowable bearing pressures calculated from bearing capacity factors and the corresponding factors of safety. Nominal bearing pressures for several types of bearing material are given in Table 10.2. These values are intended to provide a reasonable safety factor against ultimate failure and to avoid detrimental settlement of individual footings. Note that the nominal guide for selection of allowable bearing pressures based on the values given in Table 10.2 is computed as follows.

$$q_a = \frac{Q}{(B + 1.16 H)(L + 1.16 H)} \leq \text{nominal value} \quad (10.6)$$

where L is the length of the footing, Q is the applied load, and H is the depth from the footing base to a weaker soil stratum as shown in Figure 10.10. (*Note:* Nominal bearing pressures must always be used with extreme caution.)

10.6 ALLOWABLE SETTLEMENT VERSUS ALLOWABLE BEARING PRESSURE

Once the ultimate bearing capacity of a footing is determined, it is customary to design for an allowable bearing pressure of approximately 33% of the ultimate. The settlement is generally limited to prescribed values pertaining to the nature of a structure and its intended function. For example, the allowable differential settlement for a radar station may be less than 0.1 in. and the settlement for an oil tank may be 4 in. Typically, for concentric footings

$$q_{\text{allowable}} = \frac{q_{\text{ultimate}}}{\text{FS}}$$

and for eccentric footings

$$q_{\text{maximum}} = \frac{q_{\text{ultimate}}}{\text{FS}}$$

These definitions of the factor of safety ignore allowable settlement and its corresponding allowable pressure. Although conventional wisdom suggests that the ultimate bearing capacity is independent of footing size for clay, practical requirements for limiting settlement tend to suggest that the allowable pressure is a function of footing width. The allowable loading intensity versus footing size for a footing within a clay layer is illustrated graphically in Figure 10.11. Using settlement as the criterion for controlling bearing pressure, then a small footing size would require a greater pressure intensity to produce a given settlement value. This intensity is significantly reduced as the footing size is increased. This is because the pressure caused by the footing extends to a much greater depth. For co-

TABLE 10.2 Nominal Bearing Capacity Pressures for Spread Foundations*

| Type of Bearing Material | Consistency in Place | Allowable Bearing Pressure (tons per sq ft) | |
|--|-------------------------|---|---------------------------|
| | | Ordinary Range | Recommended Value for Use |
| Massive crystalline igneous and metamorphic rock: granite, diorite, basalt, gneiss, thoroughly cemented conglomerate (sound condition allows minor cracks) | Hard, sound rock | 60 to 100 | 80 |
| Foliated metamorphic rock: slate, schist (sound condition allows minor cracks) | Medium hard, sound rock | 30 to 40 | 35 |
| Sedimentary rock: hard cemented shales, siltstone, sandstone, limestone without cavities | Medium hard, sound rock | 15 to 25 | 20 |
| Weathered or broken bedrock of any kind except highly argillaceous rock (shale) | Soft rock | 8 to 12 | 10 |
| Compaction shale or other highly argillaceous rock in sound condition | Soft rock | 8 to 12 | 10 |
| Well-graded mixture of fine- and coarse-grained soil: glacial till, hardpan, boulder clay (GW-GC, GC, SC) | Very compact | 8 to 12 | 10 |
| Gravel, gravel-sand mixtures, boulder-gravel mixtures (GW, GP, SW, SP) | Very compact | 7 to 10 | 8 |
| | Medium to compact | 5 to 7 | 6 |
| | Loose | 3 to 6 | 4 |
| Coarse to medium sand, sand with little gravel (SW, SP) | Very compact | 4 to 6 | 4 |
| | Medium to compact | 3 to 4 | 3 |
| | Loose | 2 to 3 | 2 |
| Fine to medium sand, silty, or clayey medium to coarse sand (SW, SM, SC) | Very compact | 3 to 5 | 3 |
| | Medium to compact | 2 to 4 | 2.5 |
| | Loose | 1 to 2 | 1.5 |
| Fine sand, silty, or clayey medium to fine sand (SP, SM, SC) | Very compact | 3 to 4 | 3 |
| | Medium to compact | 2 to 3 | 2 |
| | Loose | 1 to 2 | 1.5 |
| Homogeneous inorganic clay, sandy or silty clay (CL, CH) | Very stiff to hard | 3 to 6 | 4 |
| | Medium to stiff | 1 to 3 | 2 |
| | Soft | .5 to 1 | .5 |
| Inorganic silt, sandy or clayey silt, varved silt-clay-fine sand (ML, MH) | Very stiff to hard | 2 to 4 | 3 |
| | Medium to stiff | 1 to 3 | 1.5 |
| | Soft | .5 to 1 | .5 |

*After U.S. Navy, NAVFAC DM-7.

hesionless soils, the corresponding load intensity versus footing width is shown in Figure 10.12. For a cohesionless soil deposit and for a very small footing size, the allowable intensity is zero. Also, its bearing capacity is dependent on footing size.

Once the relationships between load intensity and footing size are established as shown in Figures 10.11 and 10.12, the settlement versus footing size for

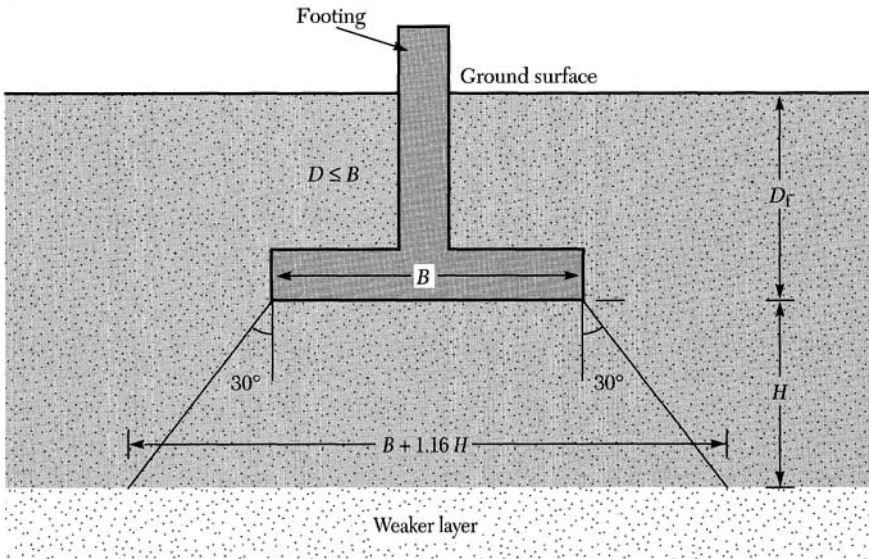


FIGURE 10.10 Definition of terms used in nominal bearing capacity.

several assumed intensity values can be plotted. These values must be less than the allowable bearing pressure as shown in Figure 10.13. The implication of Figure 10.13 is that for a given allowable settlement value, it is possible to determine the appropriate footing size with an intensity equal to or less than the allowable bearing pressure.

EXAMPLE 10.3

Establish a curve relating the allowable bearing pressure based on settlement and the allowable bearing capacity of a shallow footing ranging in size from (0.5 ft ×

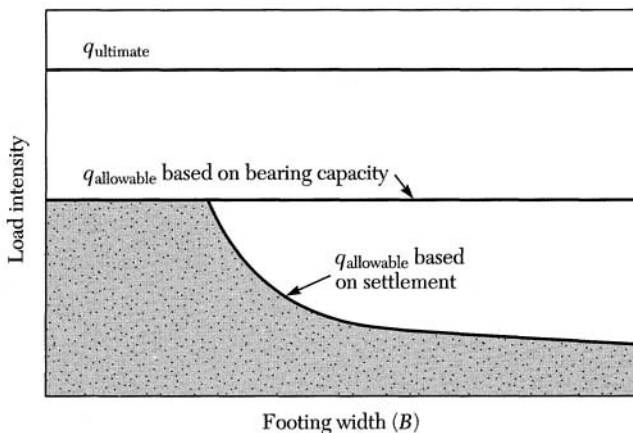


FIGURE 10.11 Allowable bearing pressure for cohesive soils.

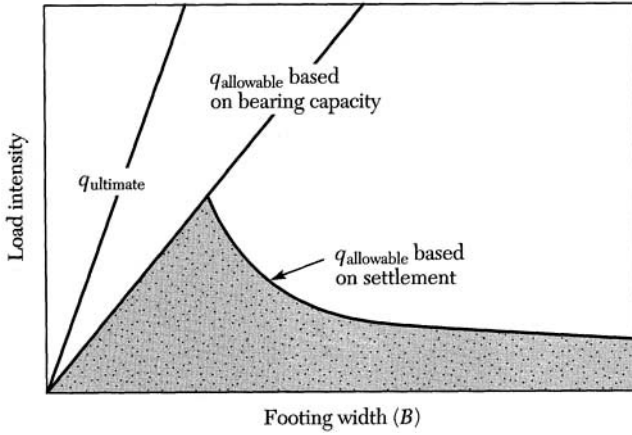


FIGURE 10.12 Allowable bearing pressure for cohesionless soils.

0.5 ft) to (20 ft \times 20 ft). Assume an allowable bearing pressure of one-third the ultimate bearing capacity and a maximum allowable settlement of 3 in. (note that this value is excessive but was selected to show how critical settlement is). The footing is to be placed at a depth of 4 ft below the ground surface. Assume deep bedrock as compared with footing width. The soil was found to have $\gamma_{sat} = 122.4$, $c_c = 0.3$, $e_0 = 0.8$, $c_u = 800$ psf, and an allowable bearing capacity of 2000 psf.

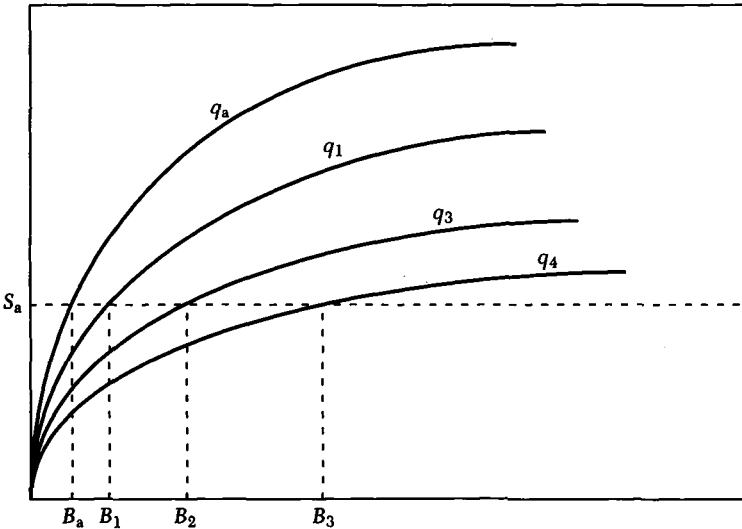
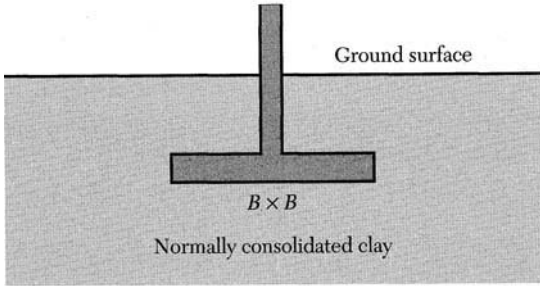


FIGURE 10.13 Allowable bearing pressure based on settlement and allowable bearing capacity.



Solution

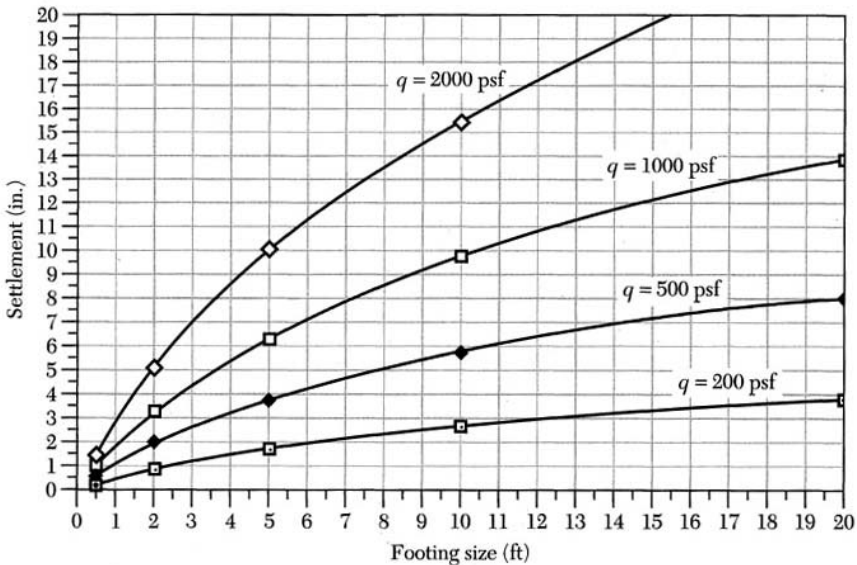
The settlement for each footing size is computed using stresses based on the Boussinesq equation. Compute the stress increments to a depth of $4B$, then subdivide the clay layer as shown below.

contact pressure (psf) = 200
 footing width (ft) = 0.5

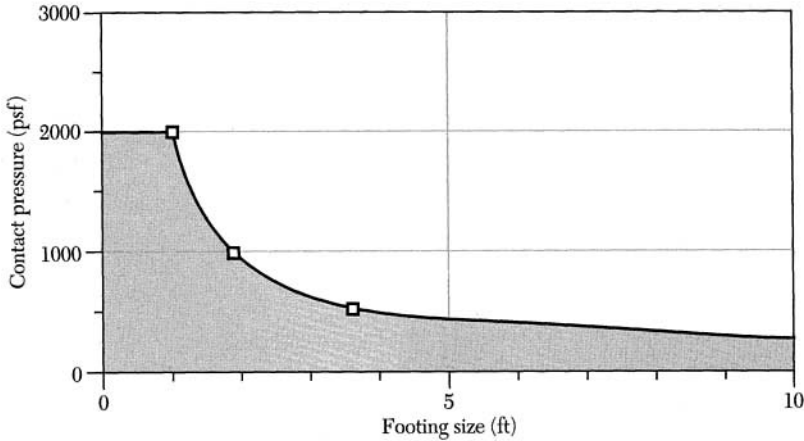
| Layer | H_{0i} | $\Delta\sigma_z$ | $\bar{\sigma}_0$ | $m = C_c H_0 / (1 + e_0)$ | $m \log(1 + \Delta\sigma_z / \bar{\sigma}_0)$ |
|-------|----------|------------------|------------------|---------------------------|---|
| 1 | 0.25 | 170 | 247.5 | 0.0416 | 0.00944658 |
| 2 | 0.25 | 104 | 262.5 | 0.0416 | 0.0060297 |
| 3 | 0.25 | 52 | 277.5 | 0.0416 | 0.00310305 |
| 4 | 0.25 | 30 | 292.5 | 0.0416 | 0.001764 |
| 5 | 1 | 17 | 330 | 0.1666 | 0.00363447 |

$\Delta H = 0.02397779$ ft

This procedure is repeated and the results are summarized in the following figure.



If the settlement is to be limited to 3.0 in., draw a horizontal line through 3.0 inches and read the corresponding footing sizes and contact pressures. These values can be plotted as shown below.



Examination of this figure reveals that although the allowable bearing capacity is 2000 psf this value is permissible only if the footing size is approximately 1.5 ft \times 1.5 ft! Larger footing sizes dictate that the allowable bearing pressure be reduced to approximately 500 psf, if settlement is to be limited to less than 3.0 in. ■

10.7 BEARING CAPACITY OF DEEP FOUNDATIONS

10.7.1 Uses of Deep Foundations

Deep foundations are generally slender structural members used to transfer loads to suitable soil strata. They are used when shallow footings are not feasible because of weak soil layers at shallow depths or because of the large magnitude of the expected load to be transferred. **Piles** are perhaps the oldest form of recognizable foundations. Inhabitants of Switzerland 12,000 years ago drove wooden piles into the soft bottoms of shallow lakes and erected their houses on them. Piles today are used for several purposes as shown in Figure 10.14.

When a pile is loaded, the load Q is carried partly by skin friction Q_f , and partly by point bearing Q_p . When most of the load carried by a pile is transmitted to its lower end or point, then it is termed a *point-bearing* or *end-bearing* pile. If most of the load is transferred through the pile shaft to the soil, then the piles are termed *friction* piles. These are described in Figure 10.15. Again, it should be emphasized that all piles derive their support from both skin friction and point bearing, but the division into *end bearing* or *friction* has become convenient terminology.

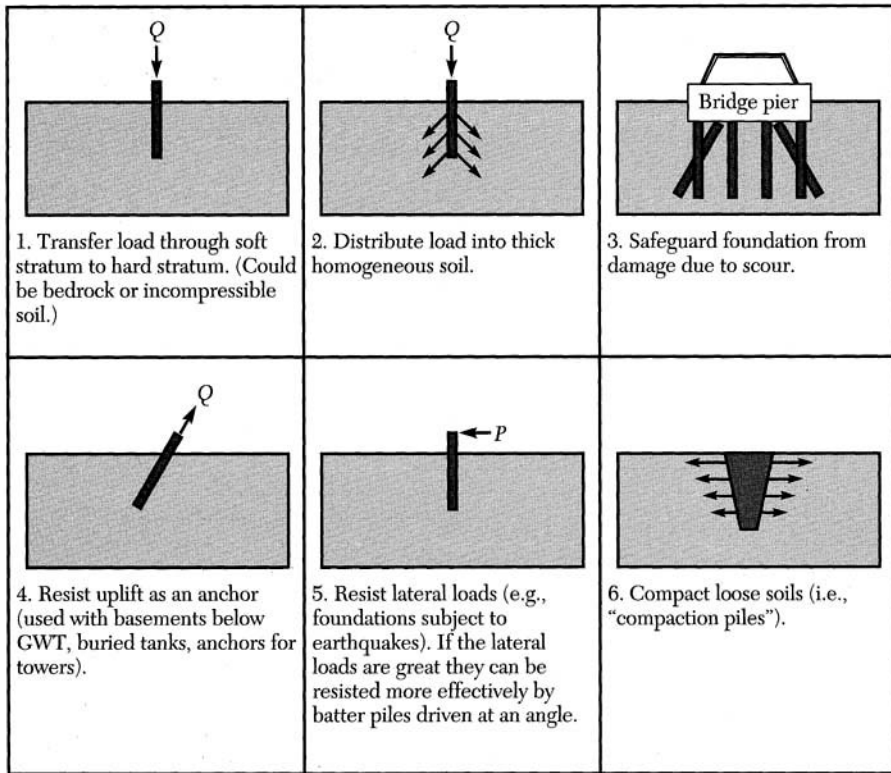


FIGURE 10.14 Types and uses of piles.

When piles are installed, either they displace the soil to accommodate the volume of the pile or the soil is removed and the void formed is occupied by the pile. That is, the pile either *displaces* or *replaces* the soil. Piles installed in the former method are termed *displacement* piles while those installed by the latter method are termed *nondisplacement* piles. This may be viewed as another criterion for classifying deep foundation systems. Pile foundations must satisfy five requirements.

1. The pile (foundation) must possess sufficient structural strength to carry the applied loads.
2. It must be possible to install the piles without damage to them.
3. The soil must be able to develop the required resistance to transfer the load.
4. The total and differential settlements of the foundation must be less than the permissible settlement of the structure the foundation is supporting.
5. It must be possible to install the foundation without damage to adjacent structures.

To design pile foundations that satisfy these requirements, one must know the following.

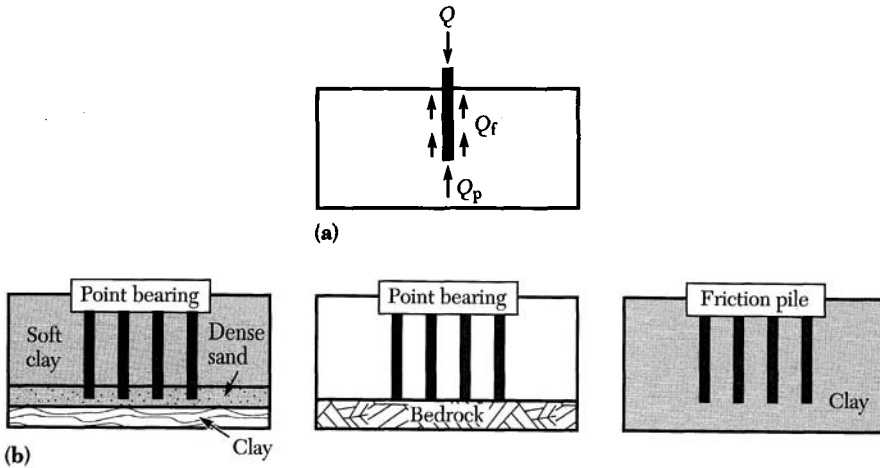


FIGURE 10.15 Types of piles: (a) a typical pile; (b) friction and point-bearing piles.

1. The magnitude and direction of loads on the pile.
2. The soil characteristics, including depth to the GWT and depth to the bearing strata, if applicable.
3. The cost of materials and installation.
4. The types of piles and driving equipment available.
5. The locations and characteristics of adjacent structures.
6. The building code requirements.

To satisfy requirements (1) and (2), the allowable stresses for the various types of piles available must be known. Several materials have been used as piles. These include timber piles, precast concrete (including prestressed concrete), structural steel piles, pipe piles, plain concrete, and composite piles.

10.7.2 Prediction of Bearing Capacity of a Single Pile in Clay

There are two main design considerations: (1) the ultimate load the pile (or pile group) can carry or its bearing capacity (Q_{ult}) and (2) how much settlement will occur under the working loads. Design variables under the engineer's control are the number and length of piles.

One of the most basic methods for determining pile-bearing capacity is based on the assumption of vertical equilibrium of static forces. That is,

$$Q_{ult} = Q_f + Q_p - W \quad (10.7)$$

where

Q_{ult} = ultimate load on pile

Q_f = skin friction along the pile shaft

Q_p = point resistance

W = weight of pile or weight above the volume of soil where the pile is now situated (usually negligible compared to the pile load)

Therefore,

$$Q_{ult} = Q_f + Q_{pt} = qA_p + fA_s \quad (10.8a)$$

$$Q_{ult} = qA_p + \sum fA_s \quad (10.8b)$$

where

q = unit tip resistance

A_p = area of point

f = unit shaft resistance (friction or adhesion)

A_s = area of the shaft

Now, q is merely the bearing capacity of a deep foundation, and therefore it is a simple matter of obtaining the appropriate bearing capacity factors to use in the following formula.

$$q = cN_c + 0.5B\gamma N_\gamma + D\gamma N_{qp}$$

where N_c , N_γ , and N_{qp} are bearing capacity factors for deep circular or square foundations, D is pile depth of embedment, and B is pile diameter. However, values of N_{qp} seem to be the cause of most divergence between available theories. For clay with $\phi = 0$,

$$N_\gamma = 0 \quad \text{and} \quad N_{qp} = 1 \Rightarrow q = cN_c + \gamma D$$

The term γD is small and can be neglected, so

$$q = cN_c$$

For deep foundations, the *generally accepted* value of N_c is 9. Therefore, the unit tip resistance is given by

$$q = 9c_u \quad (10.9)$$

The unit skin friction for clay and sand may be computed in terms of c and an adhesion factor α as follows.

$$f = \alpha c_u \quad (10.10)$$

McClelland (1974) provided a relationship for the adhesion factor in terms of the undrained cohesion of a given soil as shown in Figure 10.16. Generally, the adhesion factor ranges from 0.25 to 1.25 depending on the type of soil. Consequently, the ultimate capacity of a given pile is given by substituting Eqs. (10.9) and (10.10) into (10.8). This yields

$$Q_{ult} = 9c_u A_p + \sum \alpha c_u A_s \quad (10.11)$$

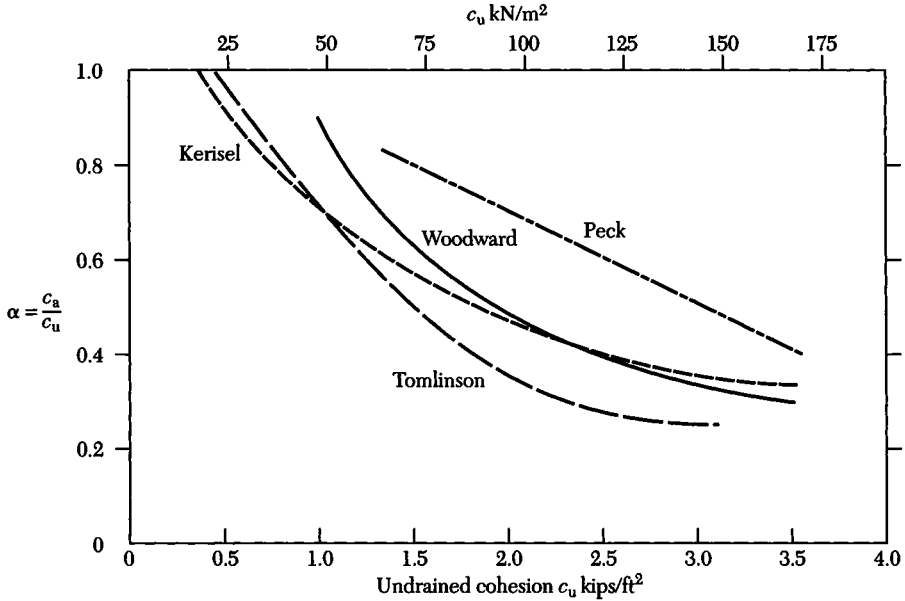
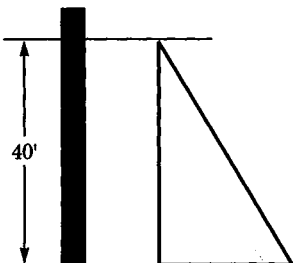


FIGURE 10.16 Values for the adhesion factor α . (McClelland, 1974.)

Note that if the pile is driven into a soil with a variable undrained shear strength, then Eq. (10.11) can still be used by applying different α -values to the different surface areas of the pile. The reader should be aware that computations for the ultimate capacity of piles can be a very tedious and a complex problem. Generally, pile load tests are performed in the field in order to assess the actual capacity of a given pile. This is true when several piles are required for important projects. The procedure just described is meant to introduce the reader to the concept of determining pile capacity.

EXAMPLE 10.4

Consider the following concrete-filled steel pipe pile with a diameter of 1.0 ft and $\gamma_{sat} = 120$ pcf was driven into clay with $c = 1.5$ ksf and $\phi = 0$. Estimate the ultimate capacity.



Solution

Given $c_u = 1.5$ ksf implies that $\alpha = 0.50$.

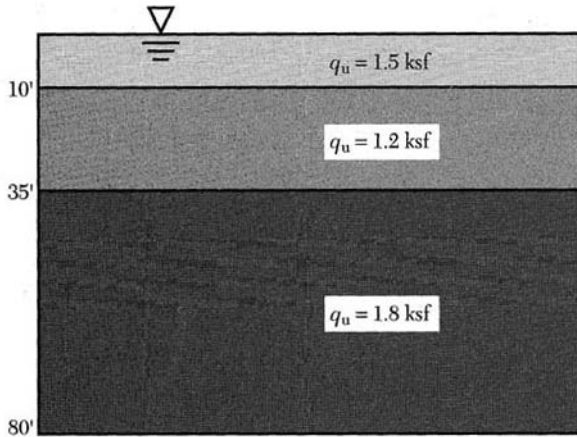
$$Q_{ult} = A_p(9c_u) + A_s\alpha c_u$$

$$Q_{ult} = \frac{\pi}{4}(1)(9)(1.5) + \pi(1)(40)(0.5)(1.5)$$

$$Q_{ult} = 11 + 94 = 105 \text{ kips} \quad \blacksquare$$

EXAMPLE 10.5

A friction pipe pile 50 ft long is to be driven into the soil profile shown. Estimate its ultimate load capacity if the average unit weight for all of the clay layers is 129.4 pcf. Assume a pile diameter of 1.5 ft.

**Solution**

For a friction pile ignore the end bearing. For the three different soil layers and Figure 10.16 read

$$\alpha_1 = 0.83 \quad \alpha_2 = 0.90 \quad \alpha_3 = 0.75$$

Now compute

$$Q_{ult} = \sum_{i=1}^3 \bar{\alpha}_i c_{ui} = 0.83(0.75)[1.5\pi(10)] + 0.9(0.6)[1.5\pi(25)] + 0.75(0.9)[1.5\pi(15)]$$

$$Q_{ult} = 140.7 \text{ kips} \quad \blacksquare$$

10.7.3 Prediction of Bearing Capacity of a Single Pile in Sand

For sands, it is virtually impossible to take an “undisturbed” sample. The value of ϕ is assessed in the lab by densifying the samples to in situ densities, then using

the results as in situ values. In so doing, the effects of natural cementation and fabric are not accounted for. Penetration tests have been developed to overcome these shortcomings as well as provide immediate and frequent values of in situ properties.

Meyerhoff (1956) relates results of the standard penetration test to the pile tip unit resistance and skin resistance. He concluded that

$$q = 4N \text{ (tsf)}$$

Vesic (1970) found that the following relationship is very good for large depths and slightly conservative for shallow depths:

$$f_{\text{avg over } D} = N_{\text{avg}} D / 1000 \text{ (tsf)}$$

where N_{avg} is the average value of N over depth D , and so

$$Q_{\text{ult}} = (4N)A_p + N_{\text{avg}} DA_s / 1000 \quad (10.12)$$

where the areas are in ft^2 and Q_{ult} in tons. However, Meyerhoff suggested that for normal displacement piles

$$f_{\text{avg}} = N_{\text{avg}} / 50 < 1 \text{ tsf}$$

and for nondisplacement piles

$$f_{\text{avg}} = N_{\text{avg}} / 100 < \frac{1}{2} \text{ tsf}$$

Therefore Eq. (10.12) is modified to give

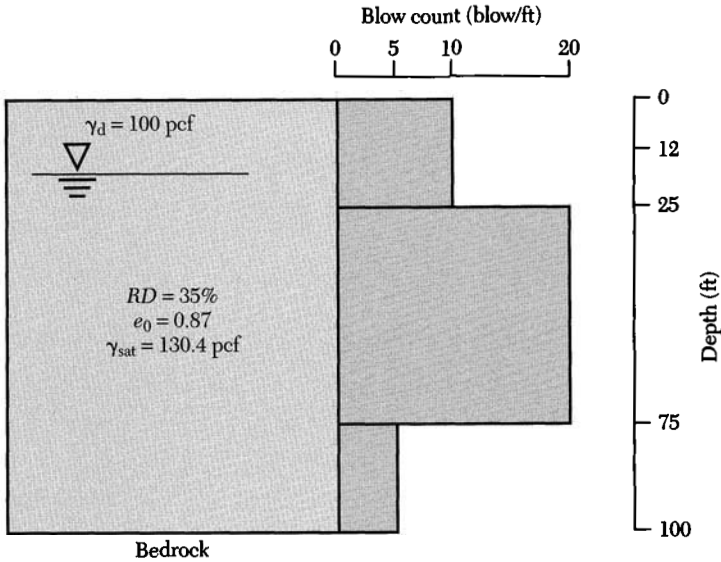
$$Q_{\text{ult}} = (4N)A_p + N_{\text{avg}} A_s / (50 \text{ or } 100) \quad (10.13)$$

Vesic examined Meyerhoff's method [Eq. (10.13)] and concluded that it was good for $D = 30$ to 50 ft and conservative for depths of less than 30 ft.

The reader should be aware that the ultimate capacity of piles driven into sand is affected by several factors that are not included in Eq. (10.12). The procedure just described is meant to introduce the reader to the concept of estimating pile capacity.

EXAMPLE 10.6

A round displacement pile is to be driven into the soil profile shown. Determine the length of pile required that will have an ultimate load capacity of 450 kips. Assume the pile has a cross-sectional area of $\pi \text{ ft}^2$.



Solution

Assume that D is the depth of pile penetration. Then

$$Q_{\text{ult}} = 4NA_p + \frac{N_{\text{avg}}A_s}{50}$$

$$A_p = \frac{\pi d^2}{4} \Rightarrow d = \sqrt{\frac{4A}{\pi}} = 2 \text{ ft}$$

$$A_s = 2\pi D$$

Take $D = 24 \text{ ft}$

$$Q_{\text{ult}} = 4(10)(\pi) + \frac{10(2\pi(24))}{50} = 155.8 \text{ tons} = 311.6 \text{ kips} < 450 \text{ kips}$$

Take $D = 25 \text{ ft}$

$$Q_{\text{ult}} = 4(20)(\pi) + \frac{10(2\pi(25))}{50} = 282.7 \text{ tons} = 565.5 \text{ kips} > 450 \text{ kips}$$

Select a pile depth of 25 feet. ■

10.7.4 Prediction of Bearing Capacity for a Drilled Caisson in Clay

Analysis of drilled caissons in cohesive soils is similar to that of piles. However, there is a significant difference between the two when estimating the bearing capacity factor N_c and the unit skin friction f . Generally, the bearing capacity in clay is given as

$$Q_{\text{ult}} = 9\omega c_u A_b + \alpha c_u A_s$$

where c_u is the cohesion, A_b is the area of the base, A_s is the area of the shaft surface, and ω and α are determined from field tests. Generally, $\omega = 0.75$ for fissured clay and $\alpha = 0.4$ to 0.6 . These values are influenced by the following factors.

1. Method of pier construction
2. Soil disturbance
3. Reliability of laboratory tests

The skin friction component of the ultimate bearing capacity of drilled caissons in clay is ignored as being very small, because a drilled caisson does not compact the surrounding soil. Skempton (1951) gives the ultimate bearing capacity as

$$q_{\text{ult}} = \frac{Q_{\text{ult}}}{A_p} = c_u N_c \quad (10.14)$$

where $N_c = 7.7$ for $D/d_b = 1$ and $N_c = 9$ for $D/d_b > 4$, for an average of 8.4 (where D is the depth of the caisson and d_b is the diameter of its base). Thus, assuming a factor of safety of 3.0 , the allowable capacity is given by

$$\frac{Q_{\text{all}}}{A_p} = \frac{8.4}{3} c_u = \frac{8.4}{3} \frac{q_u}{2} = 1.4 q_u \quad (10.15)$$

where q_u is the unconfined compressive strength of the clay at the bottom of caisson. Equation (10.15) implies that the allowable bearing pressure at the tip of the caisson should be 1.4 times the unconfined compressive strength.

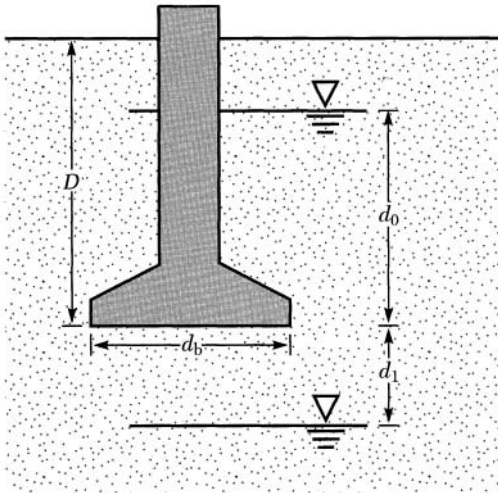
10.7.5 Prediction of Bearing Capacity for a Drilled Caisson in Sand

The ultimate bearing capacity (psf) is given directly in terms of the standard penetration test index N as follows.

$$\frac{Q_{\text{ult}}}{A_p} = 2N^2 d_b R_w + 6(100 + N^2) DR'_w \quad (10.16)$$

Note that if D is greater than d_b then use $D = d_b$, where d_b is the diameter of the caisson's bell and Q_{ult} is in pounds. The values of the correction factors R_w for the water table are given as follows.

$$R_w = 1 - 0.5 \frac{d_0}{D} \quad R'_w = 0.5 + 0.5 \frac{d_1}{D} \quad (10.17)$$



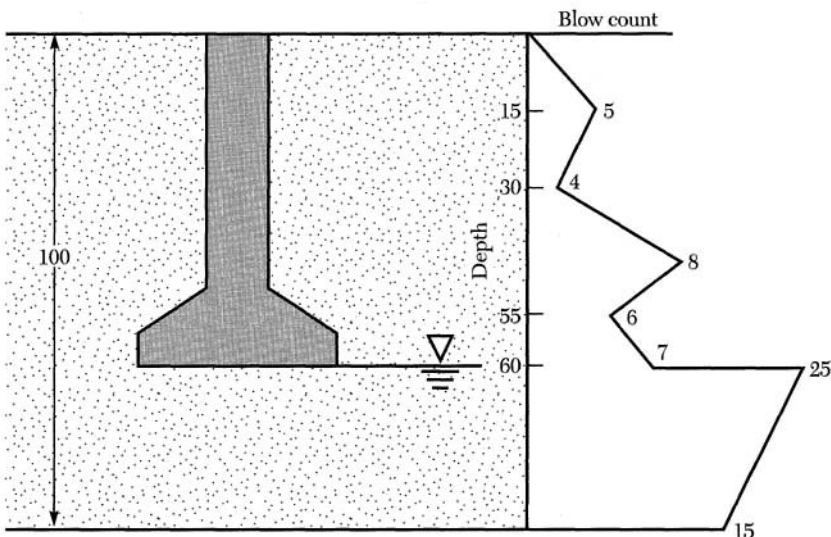
A second expression for the allowable bearing capacity for a settlement of one inch is given as

$$\frac{Q_{all}}{A_p} = 1440(N - 3) \left(\frac{d_b + 1}{2d_b} \right)^2 R'_w \quad (10.18)$$

where Q_{all} is given in pounds and d_1 is less than or equal to d_b .

EXAMPLE 10.7

A round drilled caisson with a bell 9 ft in diameter is to be placed 60 ft below ground surface as shown in the profile. Determine the ultimate load capacity. Also determine the ultimate load capacity if the settlement is to be limited to 1.0 in.



Solution

The ultimate capacity of a caisson is generally determined by ignoring the skin friction component of the capacity. Therefore,

$$\frac{Q_{\text{all}}}{A_p} = 1440(N - 3) \left(\frac{d_b + 1}{2d_b} \right)^2 R'_w$$

where

$$R_w = 1 - 0.5 \frac{d_0}{D} = 1.0 \quad R'_w = 0.5 + 0.5 \frac{d_1}{D} = 0.5$$

$$N = \frac{25 + 15}{2} = 20$$

$$d_b = 9 \text{ ft}$$

$$D = 60 \text{ ft} \quad (\text{since } D > B, \text{ then use } D = B = 9 \text{ ft})$$

$$\frac{Q_{\text{ult}}}{A_p} = 2(20)^2(9)(1.0) + 6[100 + (20)^2](9)(0.5) = 20,700 \text{ pounds}$$

$$Q_{\text{ult}} = 20.7(4.5^2\pi) = 1317 \text{ kips}$$

Assuming a factor of safety of 3.0, then

$$Q_{\text{all}} = \frac{1317}{3} = 439 \text{ kips}$$

For settlement of 1.0 in., the allowable capacity is given by

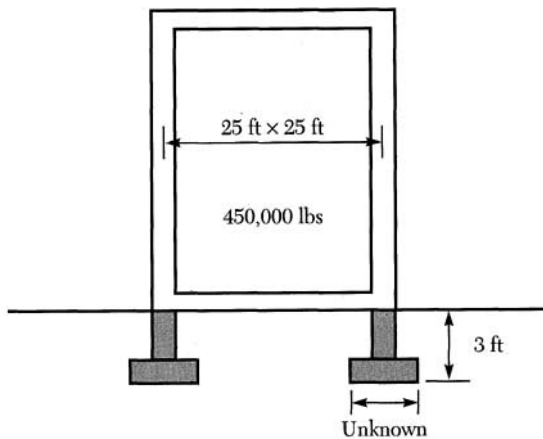
$$\frac{Q_{\text{all}}}{A_p} = 1440(20 - 3) \left(\frac{9 + 1}{2(9)} \right)^2 (0.5) = 3778 \text{ pounds}$$

$$Q_{\text{all}} = 3.778(4.5^2\pi) = 240 \text{ kips} \quad \blacksquare$$

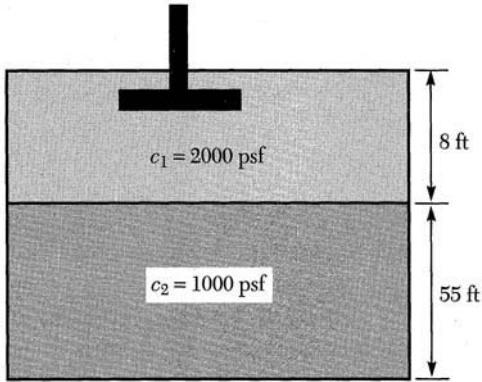
PROBLEMS

- 10.1** A strip footing 5 ft wide is to be placed at a depth of 4 ft in a moist soil that has the following characteristics: $\gamma_m = 112$ pcf, $c = 750$ psf, $\phi = 32^\circ$. Determine the allowable bearing capacity of the foundation assuming a factor of safety of 3.0 and a general shear failure.
- 10.2** A square footing 1.5 m wide is to be placed at a depth of 1.2 m in a moist soil that has the following characteristics: $\gamma_m = 17.6$ kN/m³, $c = 50$ kN/m² psf, $\phi = 30^\circ$. Determine the allowable bearing capacity of the foundation assuming a factor of safety of 3.0 and a general shear failure.
- 10.3** A circular footing 5 ft wide is to be placed at a depth of 4 ft in a moist soil that has the following characteristics: $\gamma_m = 17.9$ kN/m³, $c = 73$ kN/m², $\phi = 27^\circ$. Determine the allowable bearing capacity of the foundation assuming a factor of safety of 2.5 and a general shear failure.

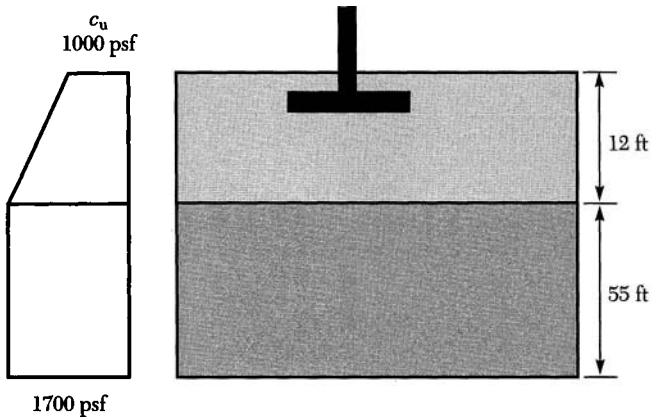
- 10.4** A strip footing 5 ft wide is to be placed at a depth of 4 ft in a moist soil that has the following characteristics: $\gamma_m = 100$ pcf, $c = 750$ psf, $\phi = 25^\circ$. Determine the allowable bearing capacity of the foundation assuming a factor of safety of 3.0 and a local shear failure.
- 10.5** A square footing 1.5 m wide is to be placed at a depth of 1.2 m in a moist soil that has the following characteristics: $\gamma_m = 17.6$ kN/m³, $c = 50$ kN/m², $\phi = 30^\circ$. Determine the allowable bearing capacity of the foundation assuming a factor of safety of 3.0 and a local shear failure. The water table is at the footing base.
- 10.6** A square footing 5 ft wide is to be placed at a depth of 4 ft in a moist soil that has the following characteristics: $\gamma_m = 107$ pcf, $c = 500$ psf, $\phi = 30^\circ$. Determine the allowable bearing capacity of the foundation assuming a factor of safety of 3.0 and a local shear failure. The water table is at footing base and the load is inclined at 10° from the vertical.
- 10.7** A footing-reinforced concrete silo is shown below. The structure will be placed on the perimeter of a round footing, the bottom of which will be 3 ft beneath the surface of the poorly compacted fill. What footing width would you recommend for this structure? What is the safe bearing capacity at this width? State the assumptions you make and use a factor of safety of 2.5. Assume $\gamma_m = 107$ pcf, $c = 500$ psf, $\phi = 20^\circ$.



- 10.8** Design a square footing to carry a column load of 1200 MN with a factor of safety of 2.5. The footing is to be placed at 1.5 m below ground surface. The clay soil beneath the footing is homogeneous, with an unconfined compressive strength q_u of 120 kN/m² and a unit weight of 18.0 kN/m³. The soil is assumed to have $\phi = 0$ and general shear failure is expected.
- 10.9** A square footing 5 ft wide is to be placed at a depth of 4 ft in the soil shown. Assuming that $\gamma_m = 107$ pcf, determine the allowable bearing capacity of the foundation assuming a factor of safety of 3.0.



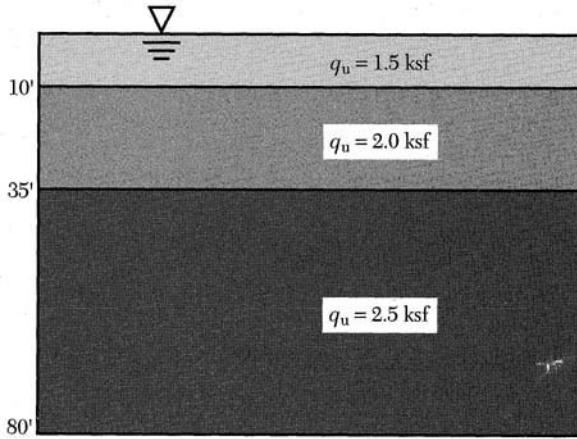
- 10.10** A square footing 5 ft wide is to be placed at a depth of 4 ft in the soil shown below. Assuming that $\gamma_m = 107$ pcf for both layers, determine the allowable bearing capacity of the foundation assuming a factor of safety of 3.0.



- 10.11** Establish a curve for the allowable bearing capacity of shallow square footings ranging in size from 5 ft \times 5 ft to 15 ft \times 15 ft. Assume an allowable bearing pressure of one-third the ultimate bearing capacity and a maximum allowable settlement of 1.0 in. The footing is to be placed at a depth of 4 ft from ground surface. Assume a deep bedrock as compared with footing width. The soil was found to have $\gamma_{sat} = 122.4$, $c_c = 0.12$, $e_0 = 0.85$, $c_u = 1450$ psf, and $\phi = 0$.
- 10.12** Establish a curve relating the allowable bearing pressure based on settlement and the allowable bearing capacity of a shallow footing ranging in size from 5 ft \times 5 ft to 15 ft \times 15 ft. Assume an allowable bearing pressure of one-third the ultimate bearing capacity and a maximum allowable settlement of 1.0 in. The footing is to be placed at a depth of 4 ft below the ground surface. Assume deep bedrock as compared with the footing width.

The soil has $\gamma_{\text{sat}} = 122.4$, $\phi = 30$, an average $N = 20$ blows/ft, and it is mostly coarse sand.

- 10.13 A concrete-filled steel pipe pile with a diameter of 1.0 ft and $\gamma_{\text{sat}} = 120$ pcf was driven into a clay layer with $c_u = 1.5$ ksf and $\phi = 0$. Estimate the pile's ultimate capacity.
- 10.14 A concrete-filled steel pipe pile with a diameter of 0.3 mm and $\gamma_{\text{sat}} = 18.5$ kN/m³ pcf was driven into a clay layer with $c_u = 72$ kN/m² and $\phi = 0$. Estimate the pile's ultimate capacity.
- 10.15 A friction pipe pile 50 ft long is to be driven into the soil profile shown. Estimate its ultimate load capacity if the average saturated unit weight for the three clay layers is 124.4 pcf. Assume a pile outer diameter of 1.5 ft.





Slope Stability

11.0 INTRODUCTION

Slope failures are similar to bearing capacity and lateral earth pressure failures in that they involve movement along a surface within the soil mass. Generally, failure occurs due to natural or man-made causes. Natural failures primarily occur because of stresses imposed by weight of the soil mass itself and by changing soil properties. Man-made failures occur when the slope is physically altered. Irrespective of the mechanism causing failure, a slope fails when the imposed stresses exceed the shear strength of the soil along the failure surface. This is depicted in Figure 11.1.

The purpose of stability analysis is to determine the factor of safety corresponding to a potential failure surface. The shape of the failure surface may be quite irregular, depending on the homogeneity of the material involved within the failed region. This is particularly true in natural slopes, where weaker materials dictate the location of failure surfaces. In the case of a homogeneous material, the most critical failure surface will be cylindrical, because a circle gives the least area along the failure surface. This surface offers the least resistance to the driving force. If a large circle cannot be developed, such as when a slope has a depth much smaller than its length, the most critical failure surface will be a plane parallel to the slope. If weak soil layers exist, the most critical failure surface may consist of a series of planes passing through the weak strata. A combination of plane, cylindrical, and other irregular failure surfaces may also be possible.

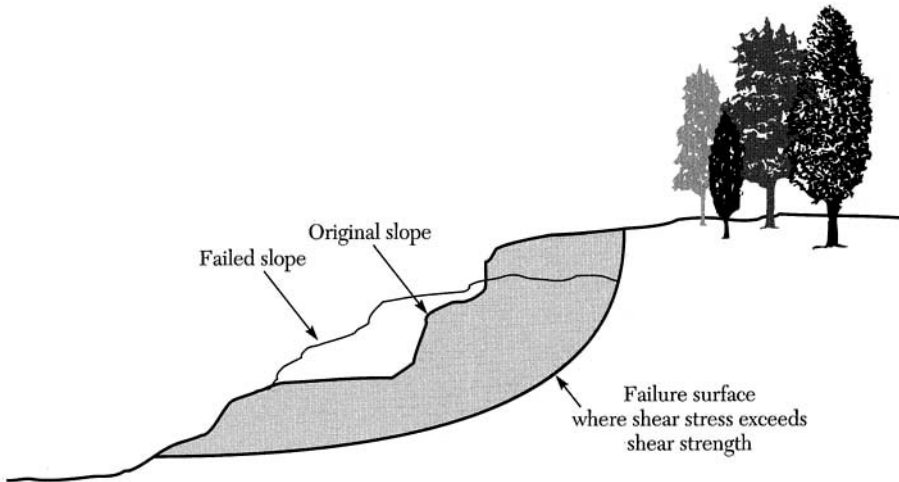


FIGURE 11.1 Typical slope failure.

11.1 SLOPE TYPES AND FAILURE THEORIES

Natural and man-made slopes are generally classified as either finite or infinite. All other classifications can be viewed as variations of these two basic slope types. A finite slope is one with a “top” and a “toe”; that is, there is a “break” in the slope. The stability of a finite slope can be analyzed by considering the equilibrium of forces acting on a potential failure surface. The degree of complexity of the stability analysis of a finite slope depends on the nature of the materials comprising the slope and the loading conditions associated with a potential failure surface. An infinite slope is one with a constant slope of determinate extent and with a relatively shallow depth. In most cases the soil is assumed to be homogeneous, but, an infinite slope may also consist of nonhomogeneous materials. Typical finite and infinite slopes are shown in Figure 11.2. (Note that although there is no such thing as an infinite slope, the analysis pertaining to such slopes assumes that the slope is infinite in extent.)

There are several theories used to determine the stability of a slope, all of which assume that the soil mass is in a state of plastic equilibrium at failure. That is, once failure has occurred along a surface in the slope, the shear and normal stresses on this surface will not increase or decrease. Of course, real soil behavior differs from this ideal material behavior, as was illustrated earlier in Figure 10.5. Another assumption common to the majority of slope stability analyses is that the “end effects” of the slope can be ignored. This assumption allows the slope to be analyzed in two dimensions. Three-dimensional slope stability analysis techniques are available but are rarely used, because the two-dimensional analysis techniques are adequate for solving most practical problems.

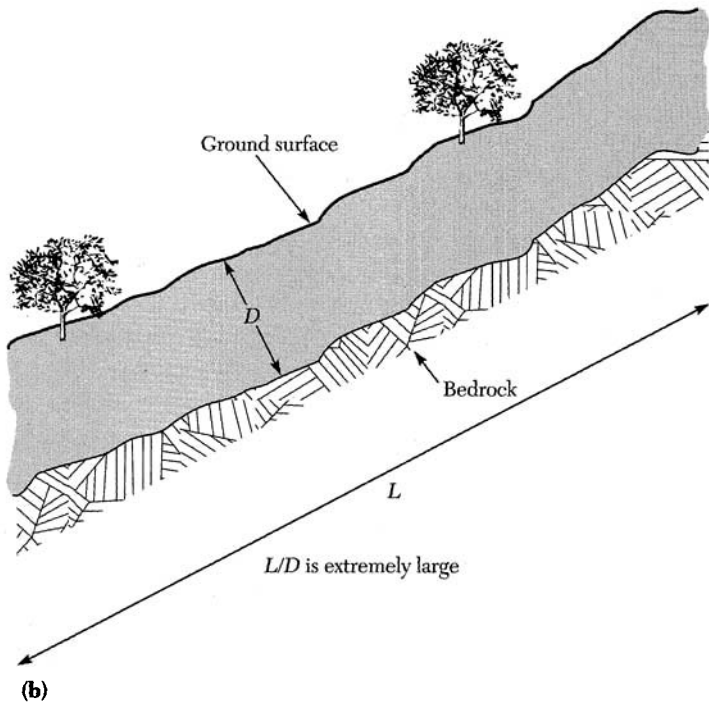
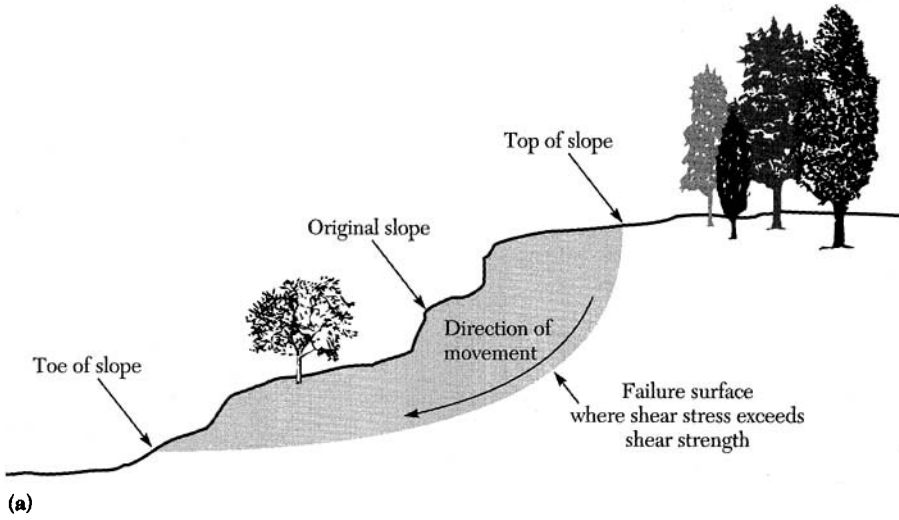


FIGURE 11.2 Types of slopes: (a) finite slope; (b) infinite slope.

11.2 CAUSES OF INSTABILITY

Failures of natural and man-made slopes are generally attributable to any activity that results in either an increase in soil stress or a decrease in soil strength. The specific causes of slope instability are varied and depend on the nature of the soil, pore water pressure, climate, and stress within the soil mass (static and dynamic). Specific examples that cause a net increase in stresses include an increase in the unit weight of the soil through rainfall, loads imposed by fills or structures at the top of a slope or excavation at the toe of a slope, movement of water levels (such as rapid drawdown in a reservoir), earthquakes, and water pressure in cracks within the slope. These are shown in Figure 11.3.

Furthermore, activities that contribute to a net increase in stress along a potential failure surface include excavation at the toe of the slope, thawing of frozen soil, vibration of saturated loose fine-grained soils, and changes in soil properties

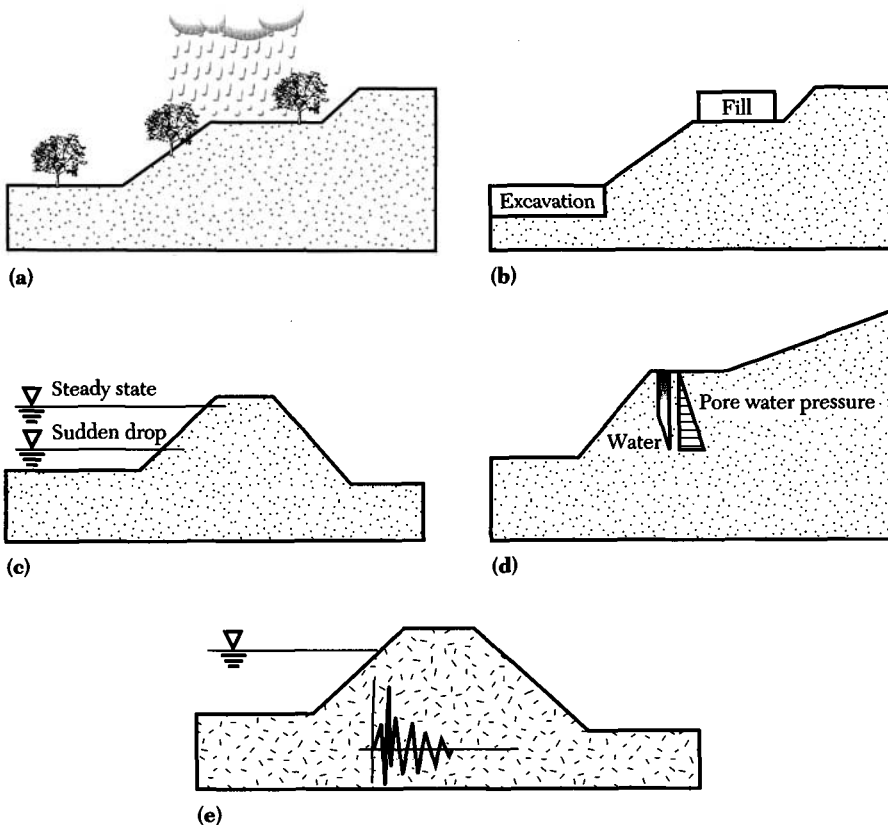


FIGURE 11.3 Examples of activities that cause a net increase in stresses: (a) rain storm; (b) fill/excavation; (c) seepage/rapid drawdown; (d) water in cracks; (e) earthquakes.

due to consolidation. Note that it is extremely critical that different drainage conditions be analyzed when man-made slopes are constructed.

The necessary requirements for stability analyses include knowledge of several factors. These include the slope geometry and underlying soil, the soil properties (c , ϕ , γ), water pressure, the magnitude and location of external loads, and the earthquake potential at the given site. The possible modes of failure of earth dams during earthquakes include loss of freeboard, piping through cracks induced by ground motion, and overtopping of the dam. Design considerations due to potential seismic activity are not always possible because of present lack of knowledge relative to their occurrence and expected magnitude. Therefore defensive design measures such as an increased factor of safety and an assumed earthquake magnitude are often used when dealing with slopes in seismic areas.

11.3 STABILITY OF INFINITE SLOPES IN COHESIONLESS SOILS

When dealing with cohesionless soil deposits, the cohesion is zero and soil shear strength is derived from normal stresses and the angle of internal friction. This is also true when a total or effective stress analysis is used. An infinite slope is assumed to fail along a plane that is parallel to the inclination of the slope. Failure is caused by the weight component acting parallel to the slope. The stability of an infinite slope may be analyzed by considering the forces acting on a typical vertical slice of unit width in the slope. Consider the partially submerged slice shown in Figure 11.4. The slice base has an area equal to unity and is acted upon by a side force H , slice weight W , force T tangential to the base, effective normal force \bar{N} , and pore water force U . No vertical forces along the sides of the prism are shown, because the depth of the failure surface D is assumed to be a constant. The pressure head is designated by h_p . The factor of safety against sliding can be defined as the ratio of the resisting force F_R to the driving force F_D (causing failure). That is

$$FS = \frac{F_R}{F_D} \quad (11.1)$$

The force causing failure is the component of weight parallel to the slope. Hence

$$F_D = W \sin \beta = \gamma D \cos \beta \sin \beta \quad (11.2)$$

Note that the weight of the slice is equal to the product of the unit weight of the soil γ and the slice volume ($1 \times D \times \cos \beta$). The force resisting failure is associated with the strength of the soil along the base of the slice. Recall that the shear strength of cohesionless soil is related to the angle of internal friction ϕ and the effective normal stress by

$$\tau = \bar{\sigma} \tan \bar{\phi} = (\sigma - u) \tan \bar{\phi} \quad (11.3)$$

Recall that the slice area A is unity. This implies that $T = \tau$, $N = \bar{\sigma}$, and $U = u$. Therefore, substituting these values into Eq. (11.3) and noting that the resisting force is equal to T gives

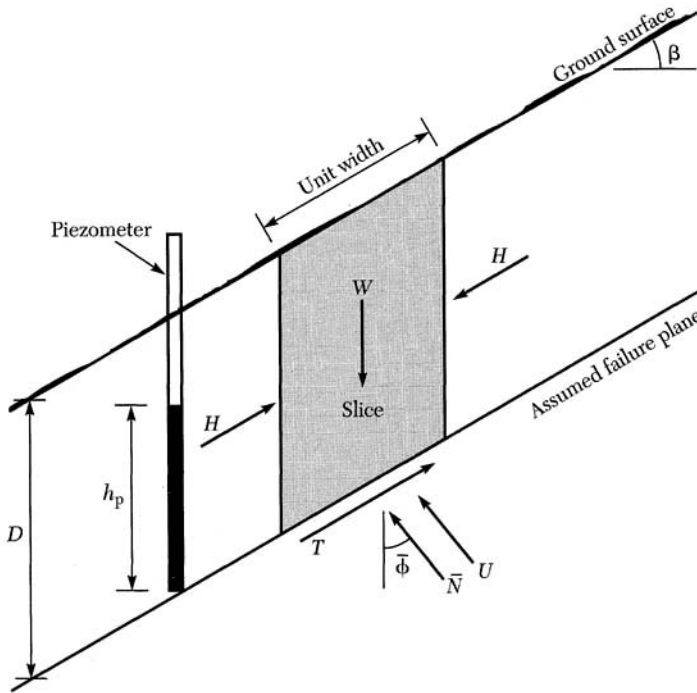


FIGURE 11.4 Free body diagram showing forces acting on a typical soil slice within an infinite slope.

$$F_R = (W \cos \beta - \gamma_w h_p) \tan \bar{\phi}$$

or more simply

$$F_R = (\gamma D \cos^2 \beta - \gamma_w h_p) \tan \bar{\phi} \quad (11.4)$$

Substituting Eqs. (11.4) and (11.2) into Eq. (11.1) yields the desired expression for the factor of safety.

$$FS = \frac{(\gamma D \cos^2 \beta - \gamma_w h_p) \tan \bar{\phi}}{\gamma D \cos \beta \sin \beta} = \frac{\tan \bar{\phi}}{\tan \beta} \left(1 - \frac{h_p \gamma_w}{D \gamma \cos^2 \beta} \right) \quad (11.5)$$

Equation (11.5) provides a general expression for determining the safety of an infinite slope irrespective of the drainage conditions. However, one must substitute the proper expression for the pressure head, which is a function of the direction of flow.

It is now possible to examine several potential problems that might be encountered in a field situation. These include slopes with or without seepage. Consider the following examples.

EXAMPLE 11.1

Derive a general expression for the factor of safety of an infinite slope assuming the soil is dry cohesionless material.

Solution

For a dry soil the pressure head is equal to zero. Therefore, substituting $h_p = 0$ into Eq. (11.5) gives:

$$FS = \frac{\tan \bar{\phi}}{\tan \beta} \left(1 - \frac{0}{D\gamma \cos^2 \beta} \right) = \frac{\tan \bar{\phi}}{\tan \beta} \quad (11.6)$$

This equation implies that failure will occur when the slope angle is equal to the angle of internal friction of the soil. ■

EXAMPLE 11.2

Derive a general expression for the factor of safety of an infinite slope assuming a saturated cohesionless soil with a drainage blanket at its base.

Solution

This situation may arise due to rainfall if the soil is drained at its base, then water will flow vertically but with a pore water pressure of zero. The pressure head is again equal to zero. Therefore, substituting $h_p = 0$ into Eq. (11.5) yields the same expression given for the dry soil. This situation is depicted in Figure 11.5. Note that the horizontal lines are equipotential lines. On any such line, the total head is the same. However, since the pore water pressure is zero, then the total head is equal to the elevation head. ■

EXAMPLE 11.3

Derive a general expression for the factor of safety of an infinite slope assuming the soil is a saturated cohesionless soil with a drainage blanket at its top.

Solution

This situation is depicted in Figure 11.6. The head is determined as $h_p = D - D_w$ where D_w is the thickness of the drainage blanket. Note that $\gamma = \gamma_{\text{sat}}$, and substituting into Eq. (11.5) yields the factor of safety given by Eq. (11.7).

$$FS = \frac{\tan \bar{\phi}}{\tan \beta} \left(1 - \frac{(D - D_w)\gamma_w}{D\gamma_{\text{sat}} \cos^2 \beta} \right) \quad (11.7)$$

Other flow directions can be assumed, including flow parallel to the slope and flow where the water level is depressed below the ground surface. In all cases, Eq. (11.5) can be modified by substituting the appropriate pressure head value. ■

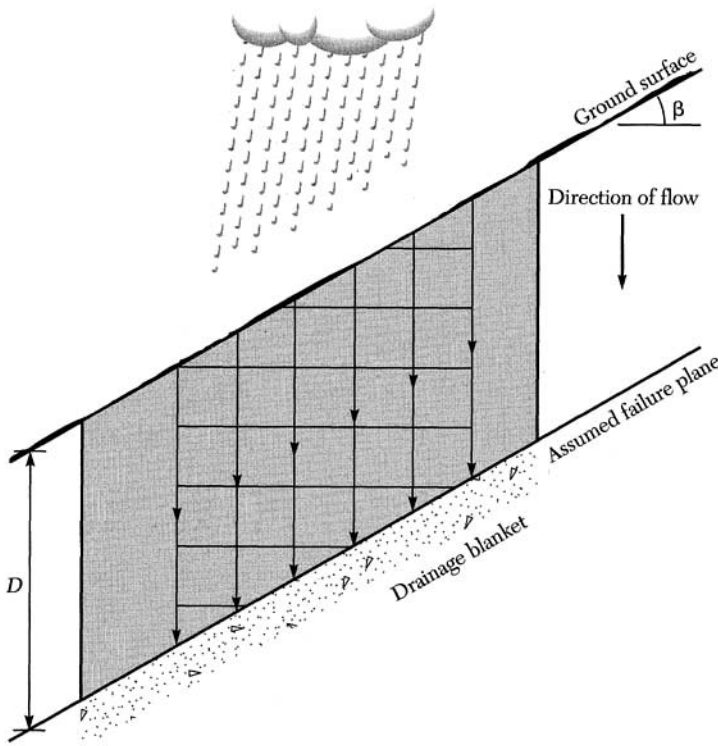


FIGURE 11.5 Analysis of an infinite slope with a drainage blanket at its base.

11.4 STABILITY OF INFINITE SLOPES IN COHESIVE SOILS

The stability of an infinite slope in cohesive soil can be assessed by including the cohesion in the analysis. The effect of seepage on the stability of an infinite slope is assessed by considering a vertical slice of unit base area with a constant head at a given depth, as was done in Section 11.3. Note that Figure 11.4 can be used if one assumes that the shear force has both a frictional and a cohesive component.

Consideration of Figure 11.4 reveals that the slice has an area equal to unity at its base and is acted upon by a horizontal force H , a slice weight W , a tangential force T , an effective normal force \bar{N} , and a pore water force U . The pressure head is designated by h_p and the factor of safety is defined by Eq. (11.1). The force causing failure is the weight component parallel to the slope. Hence

$$F_D = W \sin \beta = \gamma D \cos \beta \sin \beta \tag{11.8}$$

Note that the slice weight equals the product of the unit weight of the soil γ and the volume of the slice ($1 \times D \times \cos \beta$). The force resisting failure is associated with the effective shear strength of the soil along the base of the slice. Recall that

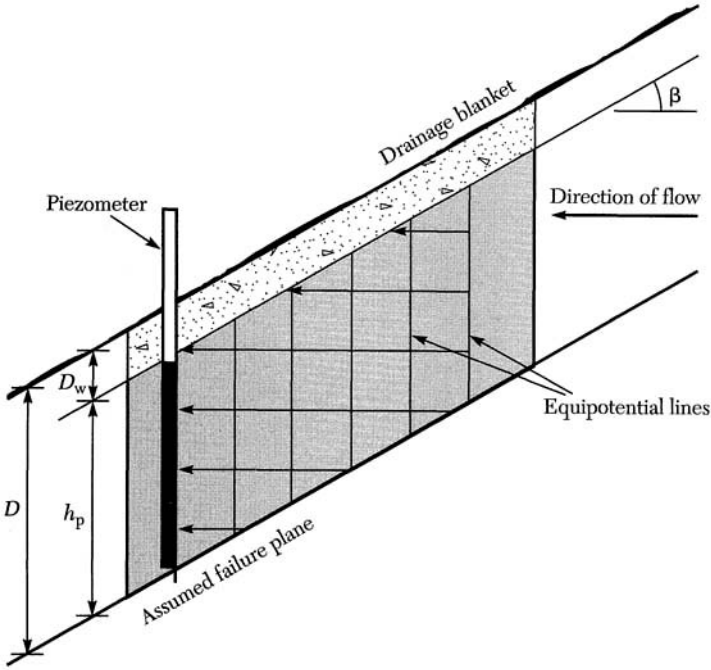


FIGURE 11.6 Analysis of an infinite slope with a drainage blanket at its top.

the shear strength of cohesive soil is dependent on the effective angle of internal friction $\bar{\phi}$, the effective cohesion, and the effective normal stress as follows.

$$\tau = \bar{c} + \bar{\sigma} \tan \bar{\phi} = \bar{c} + (\sigma - u) \tan \bar{\phi} \quad (11.9)$$

Recall that the slice area A is unity. This implies that $T = \tau$, $\bar{N} = \bar{\sigma}$, and $U = u$. Substituting these values into Eq. (11.9) and noting that the resisting force is equal to T gives

$$T = F_R = \bar{c} + (W \cos \beta - \gamma_w h_p) \tan \bar{\phi}$$

or more simply

$$F_R = \bar{c} + (\gamma D \cos^2 \beta - \gamma_w h_p) \tan \bar{\phi} \quad (11.10)$$

Substituting Eqs. (11.8) and (11.10) into Eq. (11.1) yields the desired expression for the factor safety for slopes in cohesive soils.

$$FS = \frac{\bar{c} + (\gamma D \cos^2 \beta - \gamma_w h_p) \tan \bar{\phi}}{\gamma D \cos \beta \sin \beta}$$

or

$$FS = \frac{\bar{c}}{\gamma D \cos \beta \sin \beta} + \frac{\tan \bar{\phi}}{\tan \beta} \left(1 - \frac{h_p \gamma_w}{D \gamma \cos^2 \beta} \right) \quad (11.11)$$

Equation (11.11) provides a general expression for determining the safety of an infinite slope in cohesive soils irrespective of the drainage conditions. Note that for a cohesionless soil the cohesion is zero and Eq. (11.11) reduces to Eq. (11.5). Also, for a slope in cohesive soil and undrained conditions, the friction angle will be close to zero. In that case the factor of safety is given as

$$FS = \frac{\bar{c}}{\gamma D \cos \beta \sin \beta} = \frac{c}{\gamma_{\text{sat}} D \cos \beta \sin \beta} \quad (11.12)$$

Note that in this case, the critical depth where the failure surface is located can be determined by substituting $FS = 1$ into Eq. (11.12). Furthermore, different seepage conditions can be analyzed using the procedure described earlier for cohesionless soils.

EXAMPLE 11.4

For an infinite slope at an angle of 30° from the horizontal, determine the factor of safety against failure if $\phi = 32^\circ$, $c = 22 \text{ kN/m}^2$, and $\gamma_m = 18.4 \text{ kN/m}^3$. The soil extends to a depth of 7 m and is partially saturated.

Solution

Since the soil is partially saturated, the pressure head is zero. Therefore substituting into Eq. (11.11) gives

$$FS = \frac{22}{18.4(7) \cos 30^\circ \sin 30^\circ} + \frac{\tan 32^\circ}{\tan 30^\circ} \left(1 - \frac{0}{18.4(7) \cos^2 30^\circ} \right) = 1.48 \quad \blacksquare$$

11.5 STABILITY OF HOMOGENEOUS SLOPES

When dealing with slopes in homogeneous soil deposits, it is possible to derive a general expression similar to those developed for infinite slopes. All other cases require use of approximate numerical or graphical techniques. The factor of safety in all approximate methods of analysis for finite slopes is defined in terms of moments about the center of an assumed circular failure arc. This concept is illustrated graphically in Figure 11.7. The analysis of a finite slope in any soil can be made by first assuming a failure surface defined by a circle with a radius R . The weight of the failure mass W is determined along with its center of gravity. The radius and the angle θ defining the failure arc are used to compute the arc length L as

$$L = \frac{\theta}{360} (2\pi R) \quad (11.13)$$

The overturning moment OM and the resisting moment RM are then computed.

$$OM = WX$$

$$RM = RTL$$

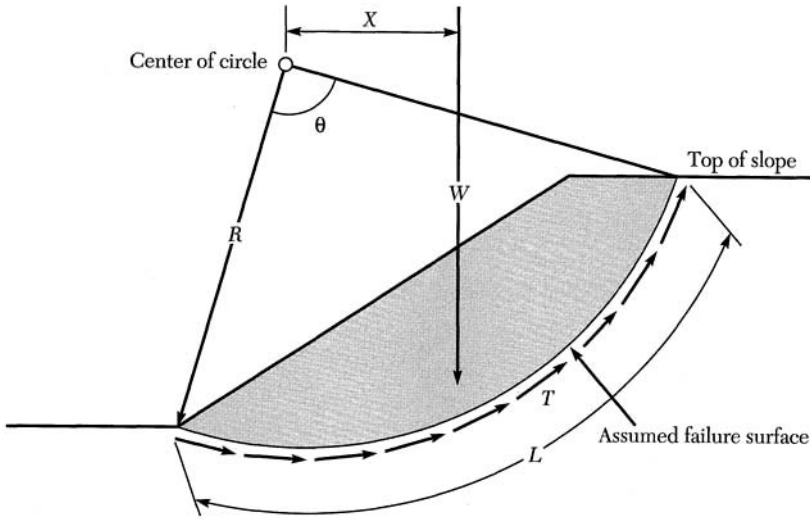


FIGURE 11.7 Typical cross section of a finite homogeneous slope.

The factor of safety is then defined as the ratio of RM to OM.

$$FS = \frac{RM}{OM} = \frac{RTL}{WX} \quad (11.14)$$

Thus far, the factor of safety has been calculated for only one failure surface. To determine the minimum factor of safety we must calculate the FS for many trial failure surfaces by assuming other radii and centers. The proper factor of safety corresponds to the lowest value computed for all of the assumed failure surfaces. This concept is depicted in Figure 11.8. Here, a grid representing the centers of all circles to be investigated is first specified. The radius at each of the nodes is varied so that the lowest factor of safety for circles with radii ranging from bedrock to the top of the slope is normally investigated. The lowest value is then placed at the node j ($j = 1, 2, \dots, m$), where m is the number of nodes in the grid. This procedure is repeated for each node, after which contours of equal factors of safety are drawn and the lowest factor of safety is determined. For the case shown in Figure 11.8, the soil cross section involves stratified soil layers. The individual soil layer i is homogeneous within its thickness L_i . The implication is that the weight of each stratum within the assumed failure surface must be determined separately. The factor of safety for a given center j is then given by

$$(FS)_j = \frac{RM}{OM} = R_j \frac{\sum_{i=1}^n T_i L_i}{\sum_{i=1}^n W_i X_i} \quad j = 1, \dots, m \quad (11.15)$$

Equation (11.15) involves a significant number of computations. Hence, this procedure is better suited for computer applications.

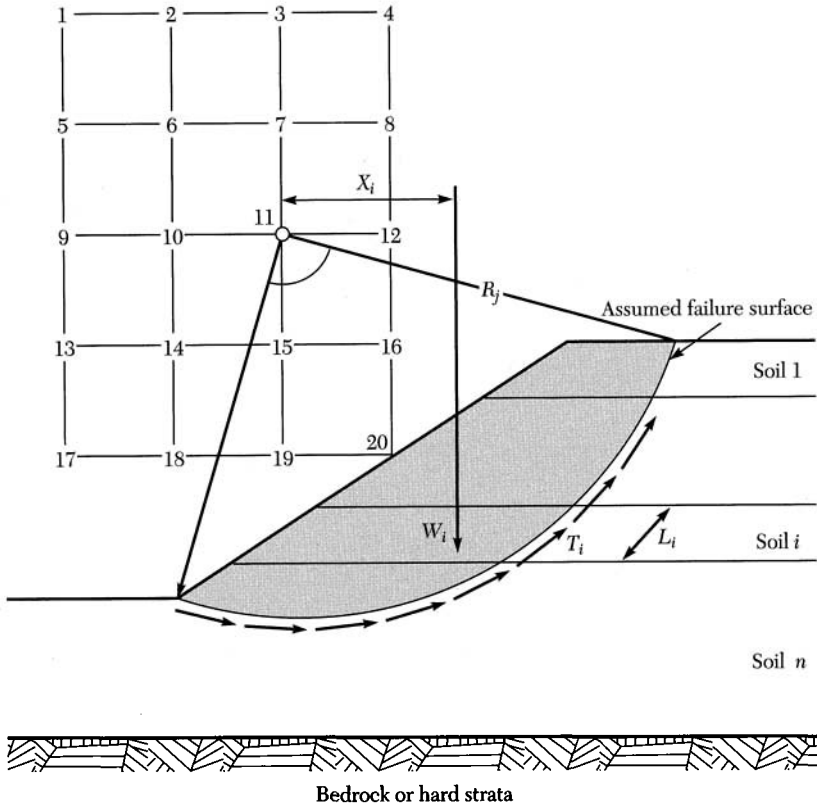


FIGURE 11.8 General method of analysis of finite slopes.

The stability of homogeneous finite slopes can be determined using stability charts. Typical stability charts for homogeneous clay slopes developed by D. W. Taylor (1948) are shown in Figures 11.9 and 11.10. These charts have been extended to include the influence of surcharge loadings, submergence, and tension cracks as shown in Figure 11.11. These charts have one thing in common, they apply to finite slopes in homogeneous soils. Nonhomogeneous soils require a more elaborate analysis.

11.6 METHOD OF SLICES FOR NONHOMOGENEOUS SLOPES

11.6.1 Total Stress Analysis

Not all materials are going to be a clay with $T = c = \text{constant}$ along the failure surface. Therefore, we must look at materials with $s = c + \sigma \tan \phi$. Note that it is also possible to use effective stress strength parameters. Stability chart solutions are available for soils with these strength characteristics as shown in Figure 11.12. This chart is extended to include the influence of surcharge loadings, submer-

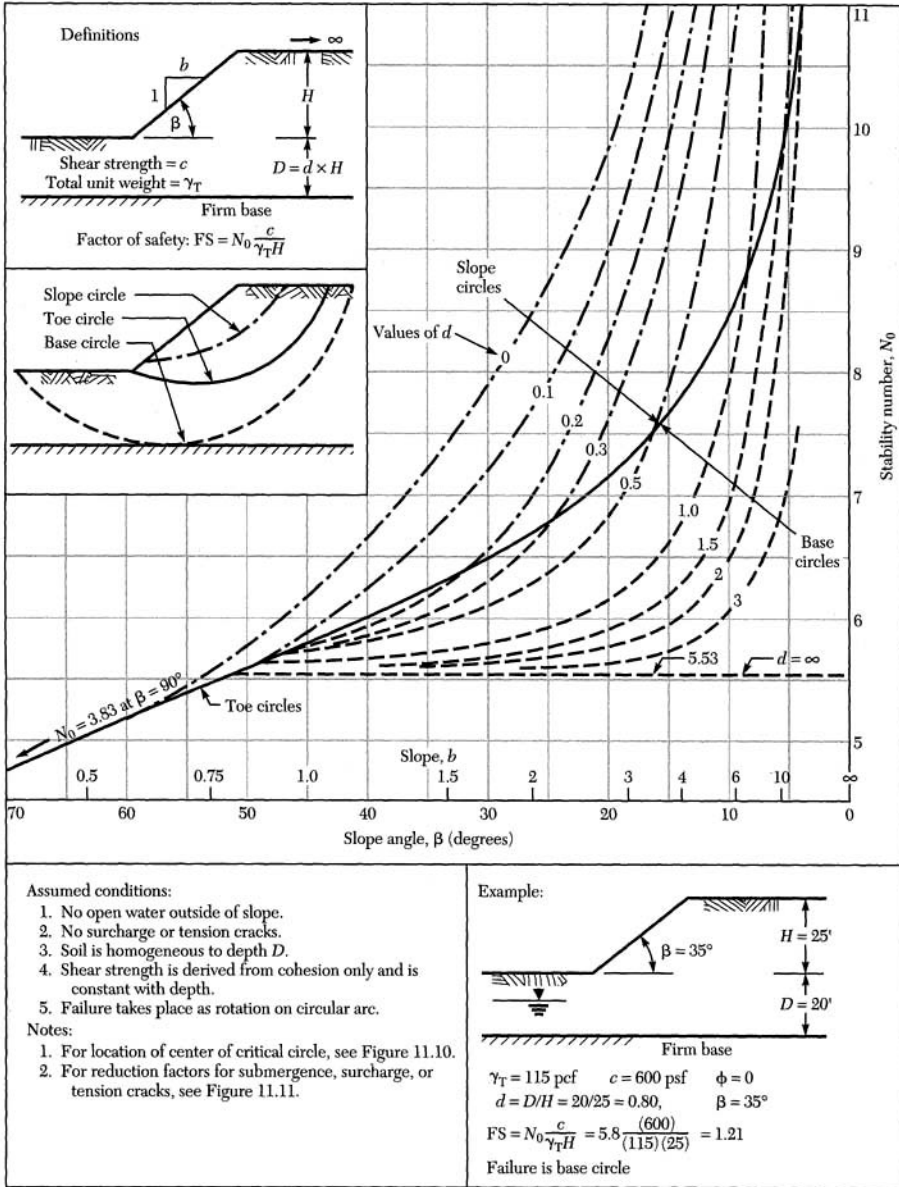


FIGURE 11.9 Stability analysis for slopes in cohesive soils ($\phi = 0$). (After NAVFAC DM-7, "Design Manual—Soil Mechanics, Foundations, and Earth Structures," Dept. of the Navy, March 1971.)

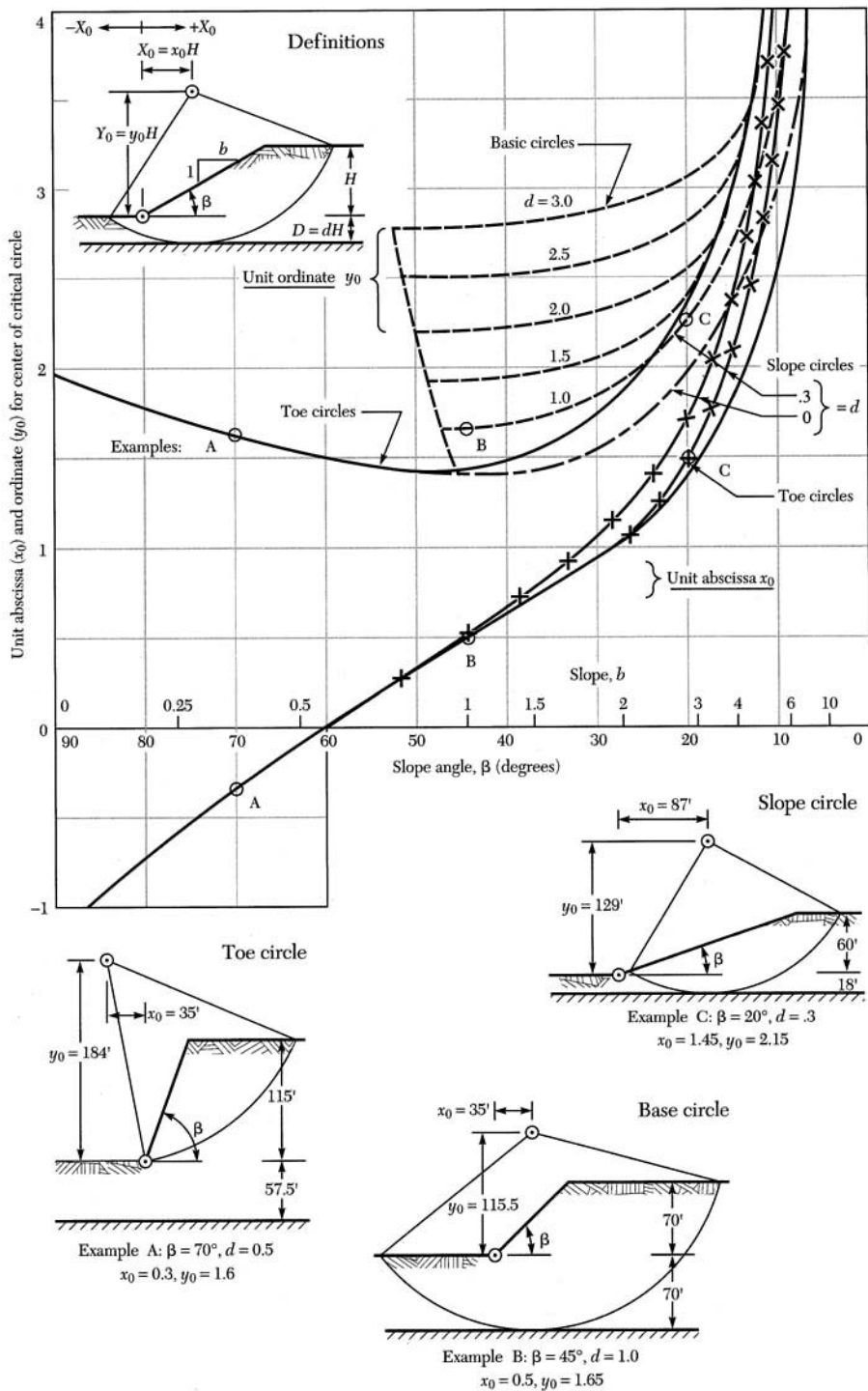


FIGURE 11.10 Center of critical circle, slope in cohesive soil. (After NAVFAC DM-7, "Design Manual—Soil Mechanics, Foundations, and Earth Structures," Dept. of the Navy, March 1971.)

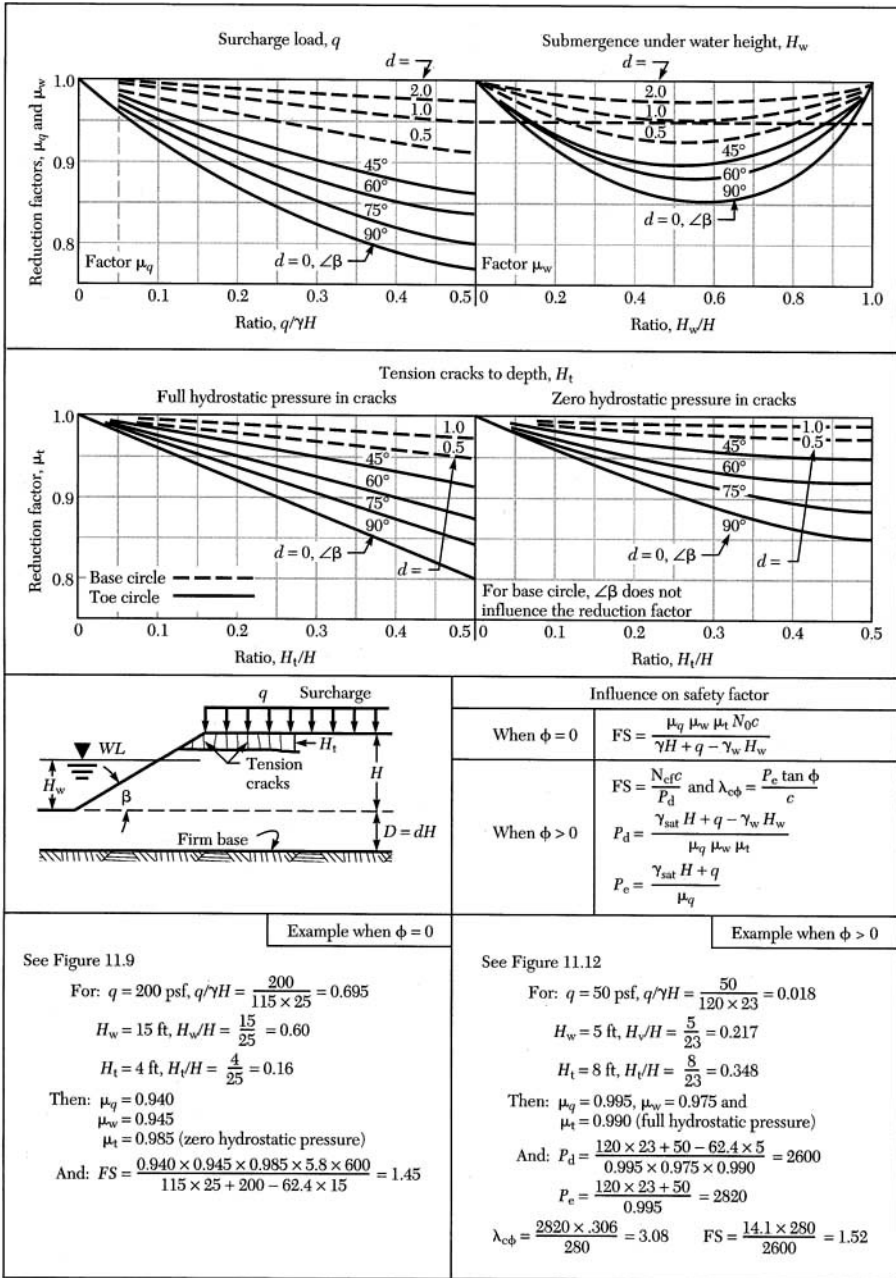


FIGURE 11.11 Influence of surcharge, submergence, and tension cracks of stability. (After NAVFAC DM-7, "Design Manual—Soil Mechanics, Foundations, and Earth Structures," Dept. of the Navy, March 1971.)

gence, and tension cracks in Figure 11.11. The method of slices deals with slopes in soils with variable shear strength along the failure surface.

The method is extremely versatile and is based on dividing a failure mass into several vertical slices. Consider the problem using total stress strength parameters (strength = $\tau = c + \sigma \tan \phi$). This assumption generally implies that the pore water pressure is not known. Consider the finite slope shown in Figure 11.13. The factor of safety against stability failure is defined as before using Eq. (11.14). Assuming the failure mass consists of vertical slices only, the free body diagram for the i th slice can be determined as shown in Figure 11.14.

Since the slice is statically indeterminate, assume that the resultant of E_L and S_L is equal to the resultant of E_R and S_R and that their lines of action coincide. This assumption is not a bad one, especially if the failure mass is subdivided into several slices. Consequently, the overturning moment is determined as follows.

$$OM = \sum_{i=1}^n W_i X_i = R \sum_{i=1}^n W_i \sin \alpha_i \quad (11.16)$$

The corresponding resisting moment RM is given by

$$RM = R \sum_{i=1}^n L_i T_i = R \sum_{i=1}^n L_i (c_i + \sigma_i \tan \phi_i) \quad (11.17)$$

For a unit slice thickness, the normal stress σ_i is related to the component of the weight in the direction normal to the base of the slice W_{ni} . That is, $\sigma_i = W_{ni} \sin \alpha_i$. Therefore, substituting into Eq. (11.17) and simplifying gives

$$RM = R \sum_{i=1}^n L_i c_i + L_i W_i \cos \alpha_i \tan \phi_i \quad (11.18)$$

The factor of safety is now determined as

$$FS = \frac{RM}{OM} = \frac{\sum_{i=1}^n L_i c_i + L_i W_i \cos \alpha_i \tan \phi_i}{\sum_{i=1}^n W_i \sin \alpha_i} \quad (11.19)$$

Equation (11.19) is applicable when using total strength parameters. Several computer programs utilizing this technique are available. Hand calculations are cumbersome and inefficient when more than a few circles are examined.

11.6.2 Effective Stress Analysis

Consider the situation in which the soil is either totally or partially submerged and there is steady-state seepage. The strength of the soil along the failure surface is now given by the effective shear strength parameters \bar{c} and $\bar{\phi}$ as $\tau = \bar{c} + \bar{\sigma} \tan \bar{\phi}$. This implies that the pore water pressure is known or can be predicted. This is

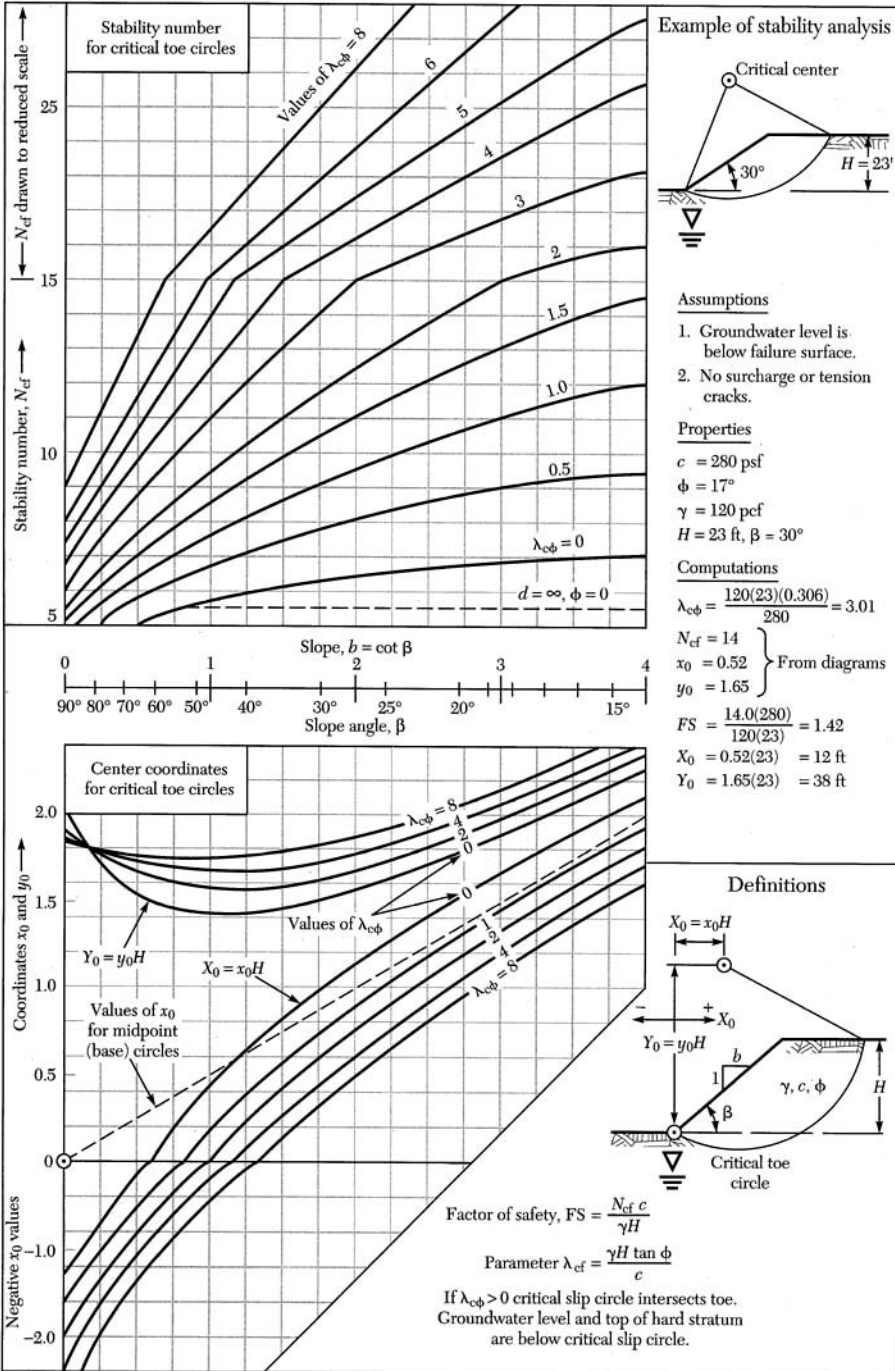


FIGURE 11.12 Stability analysis for slopes with ϕ and c . (After NAVFAC DM-7, "Design Manual—Soil Mechanics, Foundations, and Earth Structures," Dept. of the Navy, March 1971.)

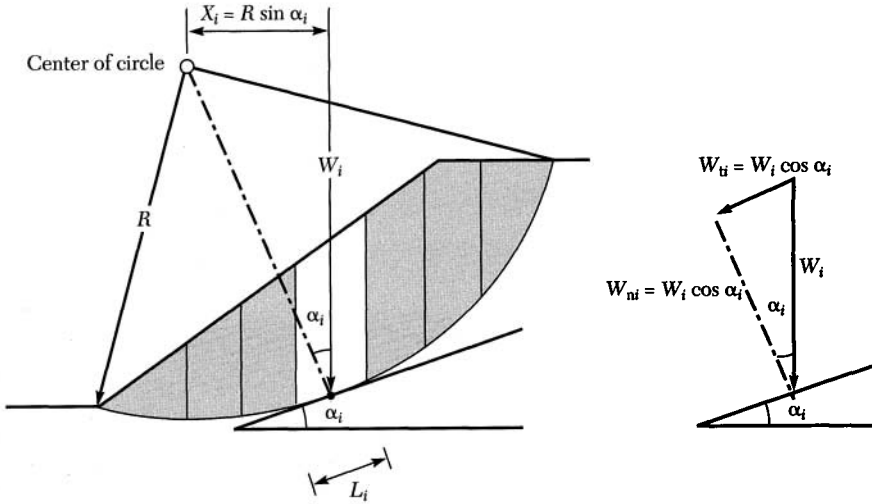


FIGURE 11.13 Finite slope stability analysis using total stress.

generally the case in that the pore water pressure can be approximated using a piezometer or a flow net. An expression for the factor of safety can be derived using Figure 11.15. The factor of safety is once again given by Eq. (11.14). Therefore, the resisting moment is determined by examining a typical free body diagram for a slice as shown in Figure 11.16.

Note that Figure 11.16 represents a slice with a unit thickness. Therefore, the pore water pressure $u_i = U_i/L_i$, and the normal effective stress acting on the slice base is given by

$$\bar{\sigma}_i = \frac{\bar{N}_i}{L_i} = \frac{N_i - U_i}{L_i} = \frac{W_i \cos \alpha_i}{L_i} - u_i \tag{11.20}$$

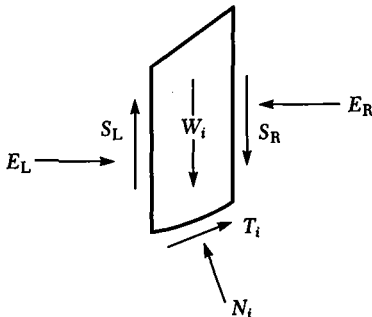


FIGURE 11.14 Free body diagram for a typical slice.

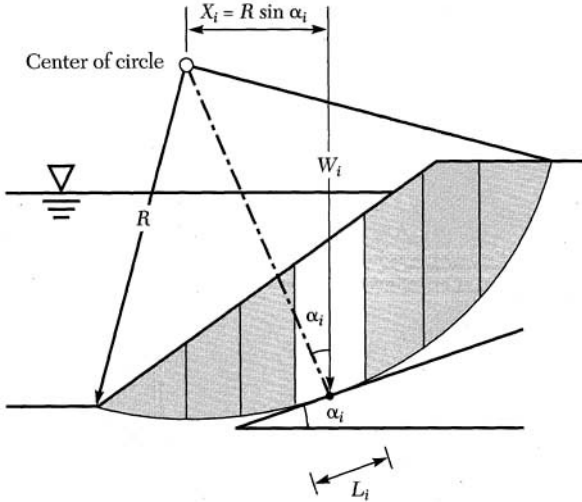


FIGURE 11.15 Finite slope stability analysis using effective stress.

The resisting moment is then given by

$$RM = R \sum_{i=1}^n L_i T_i = R \sum_{i=1}^n L_i (\bar{c}_i + \bar{\sigma}_i \tan \bar{\phi}_i) \quad (11.21)$$

Substituting Eq. (11.20) into (11.21) gives

$$RM = R \sum_{i=1}^n L_i \left(\bar{c}_i + \left(\frac{W_i \cos \alpha_i}{L_i} - u_i \right) \tan \bar{\phi}_i \right)$$

which simplifies to

$$RM = R \sum_{i=1}^n L_i \bar{c}_i + (W_i \cos \alpha_i - u_i L_i) \tan \bar{\phi}_i \quad (11.22)$$

The overturning moment can be evaluated by considering the total unit weights and boundary water pressures. For the cross section under consideration, the total unit weights and boundary water pressures are evaluated by considering the free body of the entire failure mass shown in Figure 11.17. The resultant U_3 of the boundary water pressure distribution along the circular failure surface is normal to the failure surface and, therefore, passes through the center of the trial failure circle. Consequently, it does not have any influence on the OM. Thus, the OM is given as

$$OM = -U_1 X_1 - U_2 X_2 + R \sum_{i=1}^n W_{si} \sin \alpha_i \quad (11.23)$$

Substituting Eqs. (11.22) and (11.23) into (11.14) yields the desired factor of safety

U_i = pore water pressure force
 W_{wi} = weight of water
 W_{si} = weight of soil

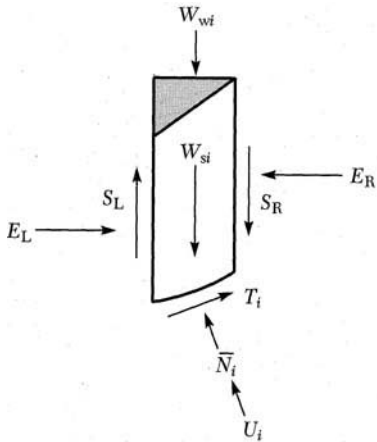


FIGURE 11.16 Free body diagram for a typical slice using effective stress.

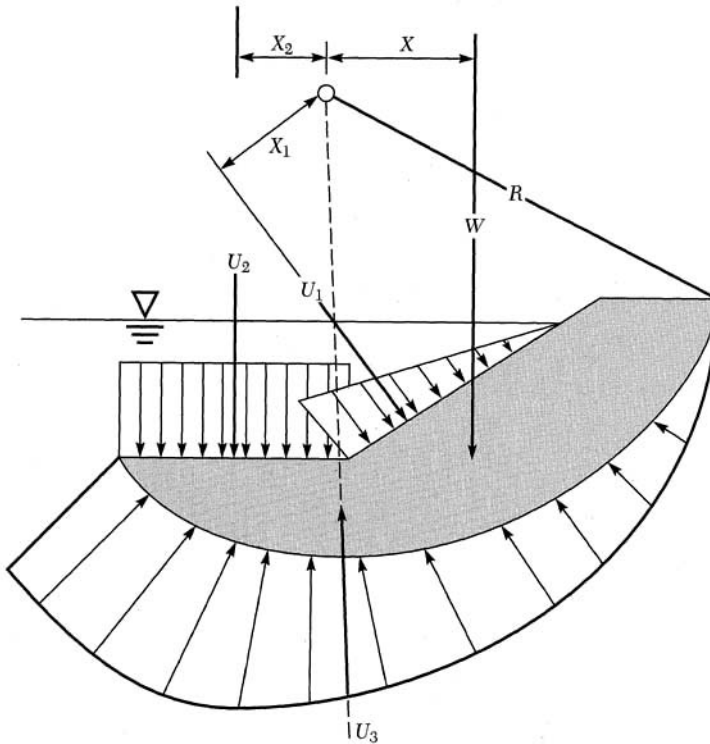


FIGURE 11.17 Boundary water pressure resultant.

$$FS = \frac{RM}{OM} = \frac{R \sum_{i=1}^n L_i \bar{c}_i + (W_i \cos \alpha_i - u_i L_i) \tan \bar{\phi}_i}{-U_1 X_1 - U_2 X_2 + R \sum_{i=1}^n W_{si} \sin \alpha_i} \quad (11.24)$$

When hand calculations are used, tabular summary sheets are generally used. Otherwise, computer programs are used for analyzing the majority of practical problems. One such computer program is called GARDS.

GARDS was developed as a user-friendly, interactive computer program to guide a permit reviewer through the customary steps of evaluating the stability of earth dike systems used in the land disposal of hazardous wastes. Section 264.221(d) of 40 CFR, Part 264, Land Disposal Regulations published in the *Federal Register* states: "A surface impoundment must have dikes that are designed, constructed, and maintained with sufficient structural integrity to prevent massive failure of the dikes." The program contains several subroutines (subprograms). These include REAME (Rotational Equilibrium Analysis of Multilayered Embankments: Y. H. Huang, University of Kentucky), SEEP (Hydraulics Analysis: K. S. Wong and J. M. Duncan, Virginia Polytechnic Institute), "Settlement," and "Liquefaction."

The GARDS software package consists of several distinct blocks. Each block is a program in itself and is called by the user through the use of menu displays. The main command structure of the GARDS program is as follows.

1. Control Block
2. Input Block
3. Input Data Check and Edit Block
4. Hydraulics Analysis Block
5. Slope Stability Analysis Block
6. Settlement Analysis Block
7. Liquefaction Analysis Block
8. Summary Output Block

The automatic search routine for this analysis is based upon selection of a trial central block defined by the user. Stability analyses may be performed using any of the six hydraulic boundary conditions described earlier and may employ unconsolidated-undrained (UU), consolidated-undrained (CU), or consolidated-drained (CD) soil strength parameters.

The results of a rotational analysis are presented as a tabulation of all factors of safety less than 2.5, along with the corresponding coordinates of the various failure arc centers, radii, and associated hydraulic boundary conditions. A graphics subroutine plots the dike section, the most critical circle passing through it, the factor of safety, and other pertinent project information.

11.7 WEDGE METHOD OF ANALYSIS

In some soil deposits, existing weak planes will force failure of a slope to occur along a planar failure surface that is not parallel to the slope or through a noncir-

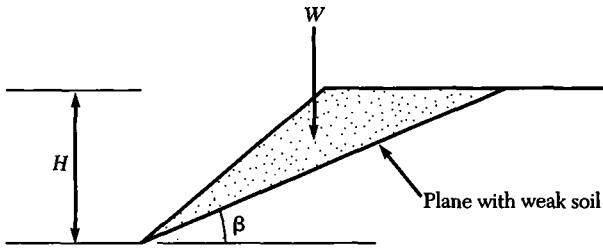


FIGURE 11.18 Typical cross section for a finite dam with a weak layer.

cular failure surface consisting of more than one planar failure surface. In the first case the factor of safety may be determined by considering the weight component along the failure surface and the shear resistance along the failure plane. Consider the slope shown in Figure 11.18. The factor of safety for the wedge shown in the figure is given by Eq. (11.1) in terms of the driving and resisting forces: Using total strength parameters, write

$$F_D = W \sin \beta$$

$$F_R = T(\text{area}) = (\text{area})(c + \sigma \tan \phi)$$

$$F_R = \frac{cH}{\sin \beta} + W \cos \beta \tan \phi$$

Substituting the expressions for F_D and F_R into Eq. (11.1) gives the appropriate factor of safety.

$$FS = \frac{F_R}{F_D} = \frac{\frac{cH}{\sin \beta} + W \cos \beta \tan \phi}{W \sin \beta} \quad (11.25)$$

Equation (11.25) is a simple expression that can be used when one weak layer is present. For the more general case, the analysis is more complex.

11.8 RECOMMENDED FACTORS OF SAFETY

Table 11.1 gives factors of safety suggested by various sources for mining operations (D'Appolonia Consulting Engineers, 1975; *Federal Register*, 1977; Mine Branch, Canada, 1972; National Coal Board, 1970). All of these factors are based on the assumptions that the most critical failure surface is used in the analysis, that strength parameters are reasonably representative of the actual case, and that sufficient construction control is ensured. There is no substitute for a sound subsurface investigation and for a credible laboratory program for soil property determination. The lower the uncertainty, the lower the factor of safety required to ensure safety.

TABLE 11.1 Factors of Safety Suggested for Mining Operations

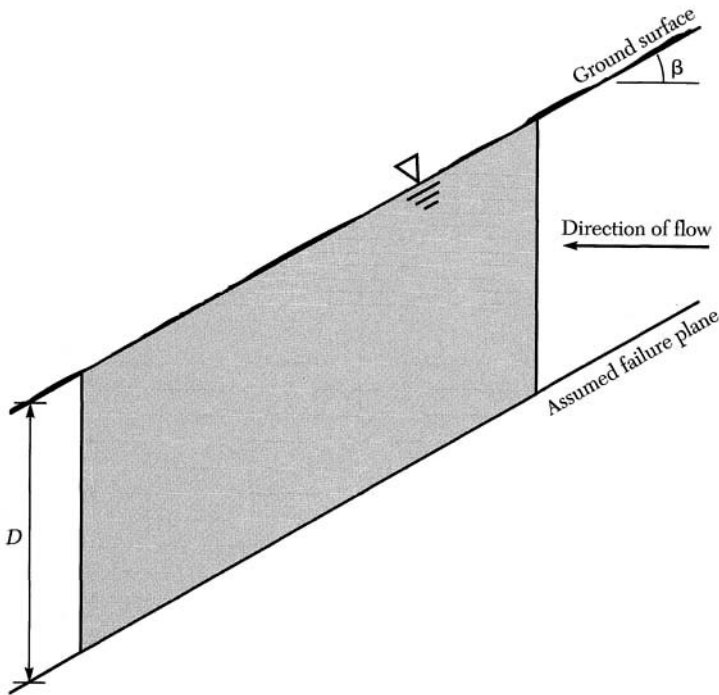
| United States (<i>Federal Register</i> , 1977) | | Minimum Safety Factor |
|---|---|-----------------------|
| I | End of construction | 1.3 |
| II | Partial pool with steady seepage saturation | 1.5 |
| III | Steady seepage from spillway or decant crest | 1.5 |
| IV | Earthquake (cases II and III with seismic loading) | 1.0 |
| | Design is based on peak shear strength parameters | 1.5° 1.3† |
| | Design is based on residual shear strength parameters | 1.3° 1.2† |
| | Analyses that include the predicted 100-year return period accelerations applied to the potential failure mass | 1.2° 1.1† |
| | For horizontal sliding on base of dike in seismic areas assuming shear strength of fine refuse in impoundment reduced to zero | 1.3° 1.3† |

*Where there is a risk of danger to persons or property.

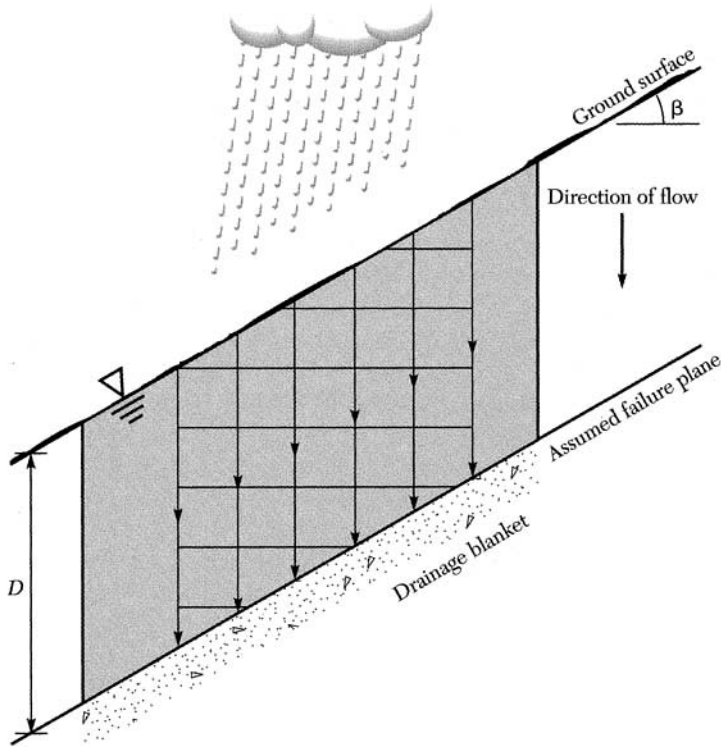
†Where no risk of danger to persons or property is anticipated.

PROBLEMS

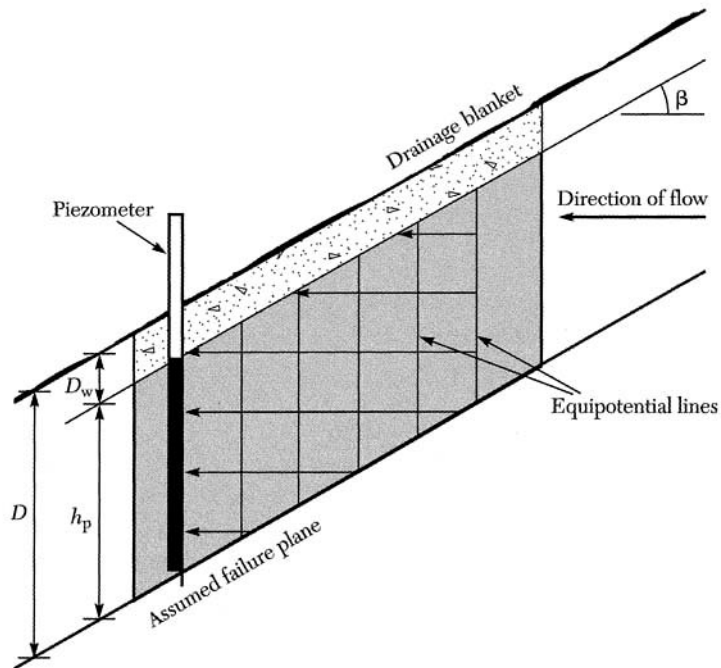
11.1 Derive a general expression for the factor of safety of an infinite slope assuming that the soil is a homogeneous saturated sand. The direction of flow was found to be as shown in the following figure.



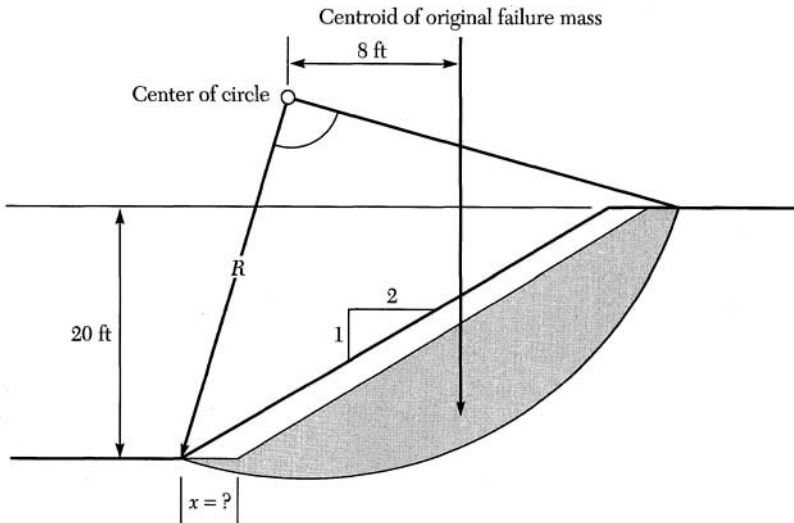
11.2 Derive a general expression for the factor of safety of an infinite slope assuming that the soil is a homogeneous saturated clay. The direction of flow was found to be as shown in the following figure.



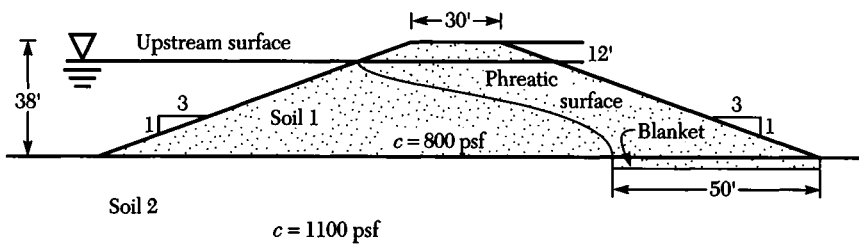
11.3 Derive a general expression for the factor of safety of an infinite slope assuming that the soil is a saturated cohesive soil with a drainage blanket at its top.



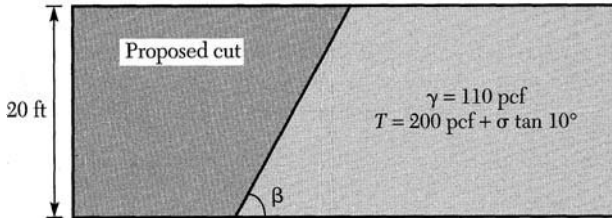
- 11.4 Derive a general expression for the factor of safety of the infinite slope shown in Problem 11.1 assuming the soil is a homogeneous saturated clay.
- 11.5 Derive a general expression for the factor of safety of an infinite slope assuming a cohesionless soil and flow at angle α from the horizontal.
- 11.6 The shear strength in unconfined compression c_u required to achieve a factor of safety of 1.1 along the circular failure surface for the slope shown is 600 psf. The area of the failure mass is 1700 sq ft and its centroid is at a horizontal distance of 8 ft from the center of the failure surface. What is the minimum distance X that the slope can be cut back parallel to itself if the new factor of safety is to be 1.0? (Assume the failure surface is the same before and after excavation.)



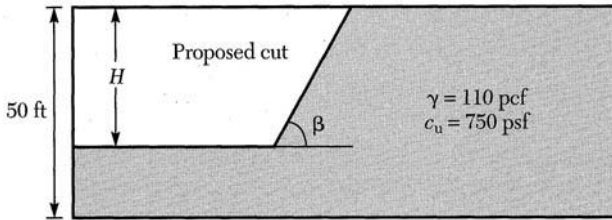
- 11.7 Use the method of slices to determine the factor of safety against failure for the trial circle and embankment shown. The failure mass should be divided into 10 slices with a circle having a radius of 125 ft located immediately above the toe on the upstream side of the embankment. Interpolate equipotential lines along the trial failure surface as required. Determine the pressure heads h_p from a knowledge of the intersection of an equipotential line with the line of seepage.



- 11.8 Repeat Problem 11.7 assuming the circle is located immediately above the toe downstream.
- 11.9 A cut is to be made in the cohesive soil at the site shown. If the design factor of safety is 1.5 with respect to the height of the slope, what is the maximum slope angle β to which the slope can be cut?



- 11.10 A cut is to be made in the cohesive soil at the site shown. What is the maximum depth of cut H that can be made if the slope angle β is equal to 35° ?



EXPERIMENT 1

Refraction Survey

Purpose

The refraction survey provides wave propagation velocities and soil profile information for in situ soil materials below the uppermost earth layers. Depths to different soil strata and rock can be determined on the basis of differences in compression wave velocities.

Equipment

Refraction seismograph
Geophone with connecting cable and accessories
Tamper (hammer) and switch with 60 m of cable
Measuring tape

Field Procedure

Select the "course" over which each test is to be conducted. This would be from where the geophone is pushed firmly into contact with the earth and the last tamping (or hammering) point. Since the calculation methods presented here apply only to horizontally layered soil and rock strata, avoid areas that include inclined strata. Disturbed earth locations should be avoided for a course location, as they will give erratic results. Hard surfaces such as concrete, blacktop, and dense gravel roads should also be avoided for the same reason. A course should have a constant earth grade between its ends. More advanced work (Richart et al., 1970;

Dobrin, 1976; U. S. Dept. of the Army, 1979) includes two field layouts for inclined subsurface layers.

The tamping (or hammering) point spacing will vary with the accuracy required and the site geologic conditions. For normal soil conditions, 1.5-m intervals from 1.5 m to 15 m and 3-m intervals thereafter are typical. Course length is determined by the depth required. The usual length is about four times the depth tested. After the course is completed in one direction, the geophone is moved to the last hammering point and a reversed course is run back toward the point where the first course geophone was placed.

Tamping (or hammering) technique involving solid, equal blows gives sharp, well-shaped waves, which are easily timed. Glancing, weak blows should be avoided. If the ground is soft it may be necessary to hammer on some solid object such as a metal plate or block of wood. Two- to three-second spacing between blows gives the seismograph operator sufficient time to check each wave. With inexperienced operators, approximately three to eight hammer blows may be needed for each reading.

Seismograph adjustments (gain) may be required at each new distance from the geophone to show the wave on the screen. The first wave to reach the geophone is used for timing purposes. Near the critical distance a change in the wave shape and a decrease in the wave amplitude is often observed. The gain must be increased enough to recognize the smaller wave, which is used for timing. A check against missing the smaller wave is to look back over the sweep when needed.

A vertical mark on the sweep is used as a reference in determining the delay time between the hammer blow and wave arrival at the geophone. Instructions for reading available equipment should be checked with the course instructor before taking field data. Delay time and hammer point distance should be recorded as illustrated in Figure E1.1.

Numerical Example

Field time and distance data obtained at the site are tabulated on the data and calculation sheet (Figure E1.1). These data are plotted with delay time on the vertical axis and hammer point distance on the horizontal axis (Figure E1.2). Next, straight velocity lines are drawn through an average of the points. Distance data for the reversed course are plotted from right to left, giving the second set of velocity lines in Figure E1.2. Material variations and changes in the subsurface or surface profiles may cause the points to vary from a straight line. Each straight line indicates a layer of the same material.

For the reversed course, velocity lines should close; that is, when lines for the same layer are extended forward they will cross the opposite time axis at the same time as the first course. This is shown by the third layer lines in Figure E1.2. This rule holds only when the material in each layer through which the wave passes remains uniform. Data points that do not lie on the straight velocity lines are usually the result of variations in the material or depth of the material through which the wave passes.

452 EXPERIMENT 1 REFRACTION SURVEY

| | |
|--------------------------|----------------------|
| Site location _____ | |
| Weather conditions _____ | |
| Project no. _____ | Date _____ |
| Seismic survey by _____ | Instrument no. _____ |

Data

| Distance (m) | Time (ms) | Distance (m) | Time (ms) | Distance (m) | Time (ms) |
|--------------|-----------|--------------|-----------|--------------|-----------|
| 0 | 0 | 90 | 55.4 | | |
| 6 | 7.6 | 84 | 54.3 | | |
| 12 | 15.2 | 78 | 53.2 | | |
| 18 | 22.8 | 72 | 52.1 | | |
| 24 | 30.2 | 66 | 51.0 | | |
| 30 | 33.4 | 60 | 50.0 | | |
| 36 | 36.7 | 54 | 46.6 | | |
| 42 | 40.0 | 48 | 43.3 | | |
| 48 | 43.3 | 42 | 40.0 | | |
| 54 | 46.6 | 36 | 36.7 | | |
| 60 | 50.0 | 30 | 33.4 | | |
| 66 | 51.0 | 24 | 30.2 | | |
| 72 | 52.1 | 18 | 22.8 | | |
| 78 | 53.2 | 12 | 15.2 | | |
| 84 | 54.3 | 6 | 7.6 | | |
| 90 | 55.4 | 0 | 0 | | |

Results

| V_1 | V_2 | V_3 | X_{c1} | X_{c2} | D_1 | D_2 |
|---------|----------|----------|----------|----------|-------|--------|
| 790 m/s | 1830 m/s | 5490 m/s | 23.7 m | 60.3 m | 7.5 m | 19.7 m |

Remarks

| |
|-----------------------------------|
| <i>Depth bedrock about 27.2 m</i> |
| |
| |

$$D_1 = 0.5 X_{c1} [(V_2 - V_1)/(V_2 + V_1)]^{1/2}$$

$$D_2 = 0.5 X_{c2} [(V_3 - V_2)/(V_3 + V_2)]^{1/2} + (D_1/V_1) \{ [V_3(V_2^2 - V_1^2)]^{1/2} - V_2(V_3^2 - V_1^2)^{1/2} \} / (V_3^2 - V_2^2)^{1/2}$$

FIGURE E1.1 Data and calculation sheet (horizontal layers).

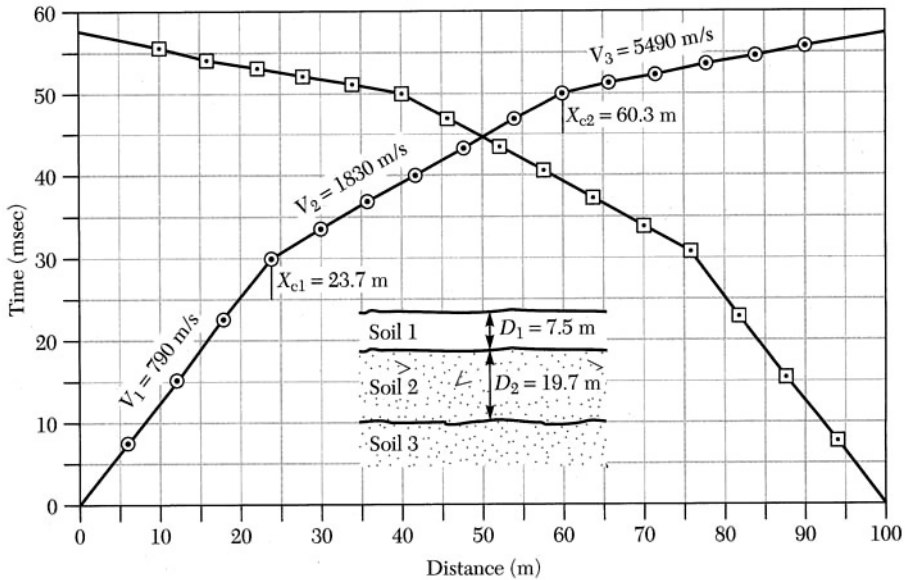


FIGURE E1.2 Travel-time plot for direct and head waves.

Depths are computed from the time-distance graph using velocities of the materials and the points at which the velocity lines change slope (crossover distance). The graph will show a velocity line for each soil strata. Equations for calculation of depths D_1 and D_2 are given on the data and calculation sheet (Figure E1.1) in terms of the crossover distances (X_{c1} and X_{c2}) and velocities (V_1 , V_2 , and V_3). Depths determined from the first course will agree with the reversed course only if the layers are parallel to the ground surface.

Interpretation of the velocities provided by the time-distance graph requires some knowledge of the area tested. Other sources of information include borings, soil profiles, road cuts, construction excavations, and well logs. Use of the seismic method with these other sources provides an economical method for extending information over a larger area. Velocities for the different soil strata are indicative of how compact or cemented the material is and what kind of material is present. More dense or compact materials are indicated by higher velocities, as is shown in Table 1.2. More advanced techniques can provide information on inclined strata and both Young's and the shear moduli for subsurface materials.

DISCUSSION QUESTIONS

Some questions are not covered in the text and may require outside reading.

1. The compression wave velocity of fresh water is given as 1480 m/s in Table 1.2. Will compression wave velocities less than 1480 m/s be observed below the groundwater table? Explain.

2. Compression wave velocities observed for soil and rock strata are related to their density, Young's modulus, and Poisson's ratio. What additional information would be needed to evaluate E and G for the soils at your test site? Explain.
3. For inclined soil and rock strata, measured velocities V_2 and V_3 , and so on, are called *apparent velocities*. They are true or actual velocities only when the strata are of uniform thickness. Describe how the true velocity for layer 2 and the true dip angle might be determined for the inclined strata shown Figure E1.3.

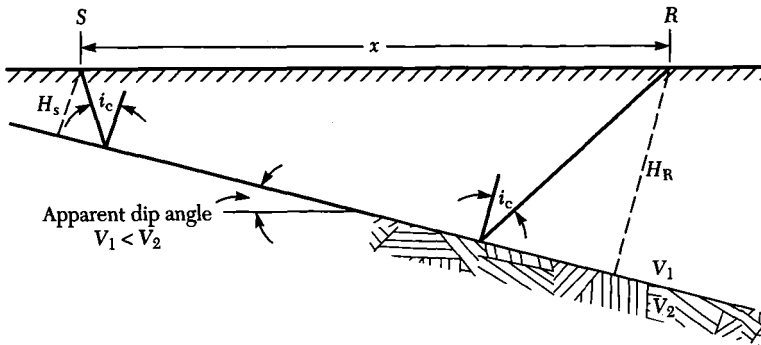


FIGURE E1.3 Sketch of an inclined soil strata.

Glossary

Absorbed water Water held mechanically in a soil mass and having physical properties not much different from ordinary free water at the same temperature and pressure.

Adhesion Shearing resistance between soil and another material such as steel, concrete, etc., under zero externally applied pressure.

Adsorbed water Water in a soil held by physiochemical forces. Its physical properties are substantially different from absorbed water at the same temperature and pressure.

Aeolian deposits Wind-deposited material such as dune sands and loess soil deposits.

Alluvium soil Soil that has been transported in suspension by flowing water and subsequently deposited by sedimentation.

Angle of friction Angle whose tangent is the ratio of the maximum shear stress that resists slippage between two solid bodies at rest and the normal stress across the contact surfaces.

Angle of internal friction Angle between the axis of normal stress and the tangent to the Mohr envelope at a point corresponding to a given failure-stress in soil.

Angle of obliquity Angle between the direction of the resultant stress acting on a given plane and the normal stress to that plane.

Angle of repose Angle between the horizontal and the maximum slope that soil assumes through natural processes. It generally applies to dry granular soils.

Anisotropic soils Soils having different properties in different directions.

Aquifer Groundwater reservoir found in a water-bearing geologic formation.

Area ratio of a sampling spoon A measure of the volume of soil displaced by a sampling spoon, sampler, or sampling tube.

Bedrock The continuous body of rock of relatively great thickness that underlies the overburden soils.

Bentonitic clay Soil with a high content of montmorillonite clay that is characterized by high swelling potential.

Berm A break in the continuity of a given soil slope.

Biaxial compression Compression caused by application of normal stresses in two perpendicular directions.

Biaxial state of stress State of stress resulting when one of the three principal stresses is zero.

Blow count *See Penetration resistance.*

Body force Force such as that of gravity whose effect is distributed throughout a body.

Boulders Usually rounded shapes with an average dimension of 12 in. (305 mm) or more that result when rocks are fragmented by weathering or abrasion.

California bearing ratio The ratio of force per unit area required to penetrate a soil mass with a 3-in.² (19-cm²) circular piston approximately 2 in. (51mm) in diameter at the rate of 0.05 in. (1.3 mm)/min, to that required for corresponding penetration of a standard material. The ratio is usually determined at 0.1-in. (2.5-mm) penetration, although other penetrations are sometimes used.

Capillarity The rise of water in the interstices of soil or rock voids due to capillary forces.

Capillary fringe zone The zone above free water elevation where water is held by capillary action.

Capillary head The potential, expressed in head of water, that causes water to flow by capillary action.

Capillary rise The height above a free water elevation to which water will rise due to capillary action.

Clay soil Fine-grained soil finer than 0.002 mm (0.005 mm in some cases) that exhibits plasticity within a range of water contents. It usually exhibits considerable strength depending on the presence of other soil materials when air-dried.

Cobble A rock fragment, usually rounded, with an average diameter of 3 to 12 in. (75 to 305 mm).

Coefficient of compressibility The rate of change of void ratio relative to applied pressure. It applies to cohesive soils.

Coefficient of consolidation A soil parameter utilized in the theory of consolidation that contains physical constants of a soil affecting its rate of volume change.

Coefficient of earth pressure The ratio of principal stresses at a given point in a soil mass.

(active) The minimum ratio of minor principal stress to major principal stress. This is applicable where soil mass has yielded sufficiently to develop a lower limiting value of minor principal stress.

(at rest) The ratio of minor principal stress to major principal stress. This is applicable where soil mass is in its natural state without having been permitted to yield or compress.

(passive) The maximum ratio of major principal stress to minor principal stress. This is applicable where soil mass has been compressed sufficiently to develop an upper limiting value of major principal stress.

Coefficient of permeability The rate of discharge of water under laminar flow conditions through a unit cross-sectional area of a porous medium such as soil under a unit hydraulic gradient and standard temperature and pressure conditions.

Coefficient of uniformity The ratio D_{60}/D_{10} , where D_{60} is soil particle diameter corresponding to 60% finer and D_{10} is particle diameter corresponding to 10% finer on the grain-size curve.

Coefficient of viscosity The shearing force per unit area required to maintain a unit difference in velocity between two parallel layers of a fluid situated a unit distance apart.

Coefficient of volume compressibility The compression of a solid layer per unit of original thickness due to a given unit increase in pressure. It is numerically equal to the coefficient of compressibility a_v divided by one plus the void ratio e .

Cohesion Normally applies to cohesive soils and is defined as shear resistance at zero normal stress.

(apparent) Cohesion in fine granular soils caused by capillary forces.

Cohesionless soil Any air-dried soil that exhibits little or no strength when unconfined and has significant cohesion when submerged.

Cohesive soil Any air-dried soil that exhibits considerable strength when unconfined and has little or no cohesion when submerged.

Colloidal particles Small soil particles whose surface activity has an appreciable influence on their properties.

Compaction The densification of a soil through mechanical means.

Compaction curve The curve showing the relationship between dry unit weight and water content of a soil for a given compactive effort.

Compaction test Laboratory compacting procedure in which a soil mass at a known water content is placed in a specified manner into a mold of standard dimensions, subjected to a standard compactive effort, and the resulting dry unit weight is determined.

Compressibility Property of soil and rock pertaining to their susceptibility to decrease in volume when subjected to external load.

Compression curve See **Pressure-void-ratio curve**.

Compression index The slope of the linear portion of the void-ratio-pressure curve on a semilog plot. It applies to cohesive soils.

Compressive strength The load per unit area at which an unconfined cylindrical soil specimen will fail in a simple compression test.

Compressive stress Normal stress that causes a body to compress in the direction in which the stress acts.

Consistency The relative ease with which a soil mass can be deformed.

Consolidated-drained test A test in which soil is completely consolidated under confining pressure; additional axial stress is then applied in such a manner that even a fully saturated soil of low permeability can adapt itself completely to the changes in stress due to the additional stress.

Consolidated-undrained test, consolidated quick test A test in which essentially complete consolidation under vertical stress or under the confining pressure is followed by a shear at constant water content.

Consolidation The process of gradual reduction in volume of a soil mass resulting from an increase in compressive stress.

(**initial**) A sudden reduction in volume of a soil mass under applied loads due principally to expulsion and compression of gas in the soil voids preceding primary consolidation.

(**primary**) The reduction in volume of a soil mass caused by the application of a sustained load. It is caused principally by squeezing out water from void spaces present in a soil mass and accompanied by a transfer of the load from water to soil solids.

(**secondary**) The reduction in volume of a soil mass caused by application of a sustained load and due principally to the adjustment of the internal structure of the soil mass after most of the load has been transferred from pore water to soil solids.

Consolidation test A test in which the soil specimen is laterally confined in a ring and is compressed vertically between porous stones.

Core drilling A rotary drilling technique that cuts out cylindrical rock samples.

Critical gradient *See Hydraulic gradient.*

Deformation A change in the shape or size of a solid body due to external factors.

Degree of consolidation The ratio, expressed as a percentage, of the amount of consolidation at a given time within a soil mass to the total amount of consolidation expected under a given stress condition.

Degrees of freedom The minimum number of independent coordinates required in a mechanical system to define completely the positions of all parts of a system at any instant of time.

Degree of saturation The degree to which the voids in a soil mass contain fluid (water, gas, or oil). Usually expressed as the ratio of water volume to total void volume.

Deviator stress The difference between the major and minor principal stresses applied in a triaxial test.

Dewatering The removal of pore water and/or pore pressures as a technique for soil improvement.

Diamond drilling *See Core drilling.*

Dilatancy The phenomenon of expansion of cohesionless soils when subjected to shearing deformation.

Direct shear test Shear test in which soil or rock under an applied normal load is stressed to failure by moving one section of a soil sample relative to the other section.

- Discharge velocity** Rate of discharge of liquid through a porous medium per unit of total area perpendicular to direction of flow.
- Drawdown** The vertical distance corresponding to free water elevation fall due to removal of free water.
- Ductility** Condition in which material can sustain permanent deformation without losing its ability to resist applied external load.
- Effective diameter** Soil particle diameter corresponding to 10% finer on the grain-size curve.
- Effective force** The force transmitted through a soil mass by intergranular pressures.
- Effective pressure, effective stress** The average normal force per unit area transmitted from grain to grain of a soil mass.
- Effective size** *See* **Effective diameter**.
- Eigenvalues** Values that force the determinant of a square matrix to equal zero.
- Eigenvectors** Solutions to a system of dependent linear algebraic equations.
- Elasticity** Property of material that returns to its original form after applied force is removed.
- Elastic limit** Point on a stress-strain curve separating elastic from inelastic behavior.
- Elastic state of equilibrium** State of stress within a soil mass where internal resistance of mass is not fully mobilized.
- Equipotential line** *See* **Piezometric line**.
- External force** A force that acts across an external surface of soil elements.
- Failure** Exceeding the maximum strength of material.
- Failure criterion** Mechanical condition under which solid materials fail by fracturing or by deforming beyond some specified limit. Specification may be expressed in terms of stresses, strains, rate of change of stresses, rate of change of strains, or some combination of these parameters.
- Fatigue** Decrease of material strength by repetitive loading.
- Fill** Man-made deposits of natural soils or rock products and waste materials.
- Filter** A layer or combination of layers of pervious materials used to provide drainage yet prevent the movement of soil particles due to flowing water.
- Fines** Portion of a soil finer than a No. 200 U.S. standard sieve (0.075 mm).
- Finite element** One of the regular geometric shapes into which a body is subdivided for the purpose of numerical analysis.
- Flow channel** That part of a flow net bounded by two adjacent flow lines.
- Flow curve** The locus of points obtained from a standard liquid limit test and plotted on a semilog graph representing water content as ordinate on an arithmetic scale and the number of blows as abscissa on a logarithmic scale.
- Flow index** The slope of the flow curve obtained from a liquid limit test, expressed as the difference in water contents at 10 blows and at 100 blows.

Flow line The path a particle of water follows in its course of seepage through soil under laminar flow conditions.

Flow net A graphical representation of flow lines and equipotential (piezometric) lines used in solution of seepage related problems.

Footing Portion of a structure that transmits loads directly to the soil.

Foundation Part of a structure that transmits load to soil or rock.

Free water Water that is free to move through a soil mass under the influence of gravity.

Freezing index The number of degree-days between the highest and lowest points on the cumulative degree-days-time curve for one freezing season.

Frost action Freezing and thawing of moisture in soil masses and the resultant effects on these masses and on structures with which they are in contact.

Frost heave The raising of a surface due to the freezing of water and subsequent formation of ice in the underlying soil or rock.

Glacial till Material deposited by glaciers, usually composed of a wide range of particle sizes.

Gradation Graph showing the proportions by mass of a soil or fragmented rock distributed in specified particle-size ranges.

Grain-size analysis Soil test used in determining grain-size distribution.

Grain-size distribution *See Gradation.*

Gravel Rounded or semirounded particles of rock that pass a 3-in. (76.2-mm) sieve and are retained on a No. 4 U.S. standard sieve (4.75 mm).

Gravitational water, groundwater *See Free water.*

Ground water level The level below which the rock and subsoil, to unknown depths, are saturated.

Hardness Resistance of a given material to indentation or scratching.

Hardpan A hard impervious soil layer which does not become plastic when mixed with water and limits the downward movement of water and roots.

Head Pressure at a point in a liquid, expressed in terms of vertical distance of a point below the surface of liquid.

Heave Movement of soil caused by expansion or displacement resulting from phenomena such as moisture absorption, removal of pressure, driving of piles, frost action, and/or loading of an adjacent area.

Heterogeneous soil mass A soil mass having different properties at different points.

Homogeneous soil mass A soil mass having the same properties at different points.

Horizon One of the layers of a soil profile, distinguished principally by its texture, color, structure, and chemical content. These include the "A" horizon, the uppermost layer of a soil profile from which inorganic colloids and other soluble materials have been leached; the "B" horizon, the layer of a soil profile in which material leached from the overlying "A" horizon is accumulated; and the "C" horizon, which is an undisturbed parent material from which the overlying soil profile has been developed.

Humus A brown or black material formed by the partial decomposition of vegetables, animal remains, and organic fraction of soil.

Hydraulic gradient The loss of hydraulic head per unit distance of flow.

(critical) Hydraulic gradient at which the intergranular pressure in a soil mass is reduced to zero by the upward flow of water.

Hydrostatic pressure A state of stress in which all the principal stresses are equal and there is no shear stress. It is determined as the product of unit weight of liquid and difference in elevation between a given point and free water elevation.

Influence value Portion of a mathematical expression that contains combinations of independent variables arranged in dimensionless form.

Intergranular pressure *See Stress.*

Isochrome A curve showing distribution of excess pore water pressure at a given time during the consolidation process.

Isotropic soil mass A soil mass having the same properties in all directions.

Kaolin A clay containing a high percentage of kaolinite.

Laminar flow Liquid flow in which head loss is proportional to the first power of the velocity.

Landslide The downward and outward sliding or movement of a soil mass of earth or rock, or a mixture of both.

Leaching The removal in solution of soluble materials by percolating or moving water.

Line of seepage The upper free water surface of the zone of seepage.

Linear expansion The increase in one dimension of a soil mass, expressed as a percentage of that dimension at the shrinkage limit, when the water content is increased from the shrinkage limit to any given value.

Linear shrinkage Decrease in one dimension of a soil mass, expressed as a percentage of the original dimension, when the water content is reduced from a given value to the shrinkage limit.

Liquefaction The sudden large decrease in shearing resistance of a cohesionless soil. It is caused by a collapse of structure by shock or other type of strain and is associated with a sudden but temporary increase in fluid pressure.

Liquid limit The water content at which a pat of soil, cut by a groove of standard dimensions, will flow together for a distance of 1/2 in. (12.7 mm) under the impact of 25 blows in a standard liquid limit apparatus.

Liquidity index The ratio, expressed as a percentage, of the natural water content of a given soil sample minus its plastic limit to its plasticity index.

Loam A mixture of sand, silt, or clay, or a combination of any of these, with organic matter.

Loess A uniform aeolian deposit of silty material having an open structure and relatively high cohesion due to cementation of grains. A characteristic of loess deposits is that they can stand with nearly vertical slopes.

Mechanical analysis *See Grain-size analysis.*

Modulus of elasticity The ratio of stress to strain for a material under given loading conditions. It is equal to the slope of the tangent or the secant of a stress–strain curve.

Modulus of volume change *See Coefficient of volume compressibility.*

Mohr circle A graphical representation of the stresses acting on various planes at a given point in a solid body.

Mohr failure envelope The envelope of a sequence of Mohr circles representing different stress conditions at failure for a given material.

Moisture content The ratio, expressed as a percentage, of the weight of water in a given soil mass to the weight of solid particles.

Moisture-density curve *See Compaction curve.*

Moisture-density test *See Compaction test.*

Muck Stone, dirt, debris, or an organic soil of low consistency.

Mud A mixture of soil and water in a fluid state.

Normal force A force directed normal to a surface element upon which it acts.

Normally consolidated soil Soil that has never been subjected to an effective pressure greater than the existing effective overburden pressure.

Open cut An excavation through rock or soil made through a hill or other topographic feature to facilitate the passage of a highway, railroad, or waterway along an alignment that varies in topography. It can be comprised of single slopes or multiple slopes.

Optimum moisture content, optimum water content Water content at which a soil can be compacted to a maximum dry unit weight using a specific compactive effort.

Organic soil Soil with a high organic content, normally greater than 25% by weight. In general, organic soils are highly compressible and have poor load-sustaining properties.

Outcrop Exposed portions of bedrock at ground surface.

Overburden Loose soil that overlies bedrock; also refers to all material overlying point of interest in a given soil deposit.

Overconsolidated soil Soil that has been subjected to an effective pressure greater than the existing effective overburden pressure.

Parent rock Rock from which a soil has been derived.

Peat Fibrous organic matter in various stages of decomposition, generally dark brown to black in color and of spongy consistency.

Penetration resistance Number of blows required to drive a standard sampler a distance of 1.0 ft into soil using a hammer weighing 140 lb falling a 30-in. distance.

Percent compaction The ratio, expressed as a percentage, of dry unit weight of a soil to maximum dry unit weight obtained in a laboratory compaction test.

Percent consolidation *See Degree of consolidation.*

Percent saturation *See Degree of saturation.*

Perched water table Groundwater separated from an underlying body of groundwater by a concave and relatively impervious soil or rock layer. It is located at a higher elevation than the groundwater table.

Percolation Movement, under hydrostatic pressure, of water through soil or rock, excluding movement through large openings such as caves and solution channels.

Permafrost Perennially frozen soil found at varying depths.

Permanent strain The strain remaining in a solid relative to its initial condition after application and removal of stress greater than its yield stress.

Permeability The capacity of soil and rock to conduct liquid or gas.

pH An index of the acidity or alkalinity of a solution expressed in terms of the logarithm of the reciprocal of the hydrogen ion concentration.

Phreatic line *See* **Line of seepage**.

Phreatic water *See* **Free water**.

Piezometer An instrument for measuring pressure head in soil deposits.

Piezometric line Line along which water will rise to the same elevation in a standpipe.

Pile Relatively slender structural element that is driven or otherwise introduced into soil for the purpose of providing vertical or lateral support for a structure.

Piping The progressive removal of soil particles from a deposit by percolating water, leading to the development of channels and ultimately failure.

Pit An excavation in the surface of the earth from which ore is obtained as in large open-pit mining or as an excavation made for test purposes.

Plane stress A state of stress in a solid body in which all stress components normal to a certain plane are equal to zero.

Plasticity The property of a soil that allows it to be deformed beyond the point of recovery without cracking or appreciable volume change.

Plasticity index Numerical difference between the liquid limit and the plastic limit.

Plastic limit The water content corresponding to an arbitrary limit between the plastic and the semisolid states of consistency of a soil. It is equivalent to the water content, expressed in percentage, at which a soil will begin to crumble when rolled into a thread 1/8 in. (3.2 mm) in diameter.

Pore pressure, pore water pressure Pressure transmitted through pore water in saturated soil deposits.

Porosity The ratio of volume of voids in a rock or soil to its total volume.

Potential drop The difference in total head between two equipotential lines.

Preconsolidation pressure The greatest effective stress to which a soil has been subjected.

Preloading The densification of a soil by placement of a temporary surface load.

Pressure-void-ratio curve A curve representing the relationship between effective stress and void-ratio of a soil as obtained from a consolidation test. The curve has a characteristic shape when plotted on semilog paper with pressure on the log scale.

Principal plane Each of three mutually perpendicular planes through a point in a soil mass on which shearing stress is zero.

Principal stress The stress normal to one of three mutually perpendicular planes on which shear stresses at a point in a body are zero.

Proctor curve *See* **Compaction curve.**

Progressive failure Formation and development of localized fractures that, after additional stress increase, eventually form a continuous rupture surface and thus lead to failure after steady deterioration of a soil deposit or rock.

Protective filter *See* **Filter.**

Quick condition Condition in which water is flowing upward with sufficient velocity to significantly reduce the bearing capacity of a localized area within a given soil deposit through a decrease in intergranular pressure.

Quick test *See* **Unconsolidated-undrained test.**

Quicksand *See* **Quick condition.**

Radius of influence of a well Distance from the center of a well to the closest point at which the piezometric level is not lowered when pumping has produced the maximum steady rate of flow.

Relative density The ratio of the difference between the void-ratio of a cohesionless soil in the loosest state and any given void-ratio to the difference between void-ratios in the loosest and in the densest states.

Remolded soil Soil that has had its natural structure modified by mechanical manipulation.

Remolding sensitivity The ratio of the unconfined compressive strength of an undisturbed specimen of soil to the unconfined compressive strength of a specimen of the same soil after remolding at unaltered water content.

Residual soil Soil derived in place by weathering of the underlying material.

Residual strain *See* **Permanent strain.**

Rock Any naturally formed and cemented aggregate of mineral matter occurring in large masses or fragments.

Sand Soil particles that will pass the No. 4 (4.75-mm) sieve and be retained on the No. 200 U.S. standard sieve.

Sand boil The ejection of sand and water resulting from piping.

Saturation curve *See* **Zero air voids curve.**

Seepage The infiltration or percolation of water through rock or soil. The term seepage is usually restricted to the very slow (laminar flow) movement of groundwater.

Seepage force The frictional drag of water flowing through voids or interstices in soil, causing an increase in the intergranular pressure.

Seepage line *See* **Line of seepage.**

Seepage velocity The rate of water seepage through a porous medium, such as soil, per unit area of void space perpendicular to the direction of flow.

Sensitivity ratio *See* **Remolding sensitivity.**

Shear failure Failure in which movement caused by shearing stress in a soil or rock mass is of sufficient magnitude to seriously endanger the safety of a structure.

Shear stress, shearing stress *See* **Stress.**

Shrinkage index The numerical difference between the plastic and shrinkage limits.

Shrinkage limit The maximum water content at which a reduction in water content will not cause a decrease in volume of a soil mass.

Shrinkage ratio The ratio of a given volume change, expressed as a percentage of the dry volume, to the corresponding change in water content above the shrinkage limit, expressed as a percentage of the weight of an oven-dried soil sample.

Silt Material passing the No. 200 U.S. standard sieve that is nonplastic or very slightly plastic and exhibits little or no strength when air-dried.

Slow test *See Consolidated-drained test.*

Soil Sediments or other unconsolidated accumulations of solid particles produced by the physical and chemical disintegration of rocks, and which may contain organic matter.

Soil horizon *See Horizon.*

Soil mechanics The application of the laws and principles of mechanics and hydraulics to engineering problems dealing with soil as an engineering material.

Soil profile Vertical section of soil, showing the nature and sequence of various layers, as developed by deposition or weathering, or both.

Soil stabilization Chemical or mechanical treatment designed to improve stability of a soil mass or to otherwise enhance its engineering properties.

Specific gravity of solids Ratio of the weight in air of a given volume of solids at a stated temperature to the weight in air of an equal volume of distilled water at a given temperature.

(**apparent**) Ratio of the weight in air of a given volume of solid matter including its impermeable pores or voids at a given temperature to the weight in air of an equal volume of distilled water at the same temperature.

(**bulk**) Ratio of the weight in air of a given volume of a material including both permeable and impermeable voids at a given temperature to the weight in air of an equal volume of distilled water at the same temperature.

Specific surface The surface area per unit of volume of soil particles.

Stability The condition of a structure or a mass of material when it is able to support applied loads for a long time without suffering any significant deformation or movement.

Standard penetration resistance *See Penetration resistance.*

Stiffness The ratio of change of force to the corresponding change in translation deflection of an elastic element.

Stone Crushed or naturally angular particle of rock that will pass a 3-in. (75-mm) sieve and be retained on a No. 4 (4.75-mm) U.S. standard sieve.

Strain The change in length per unit of length in a given direction.

Streamline flow *See Laminar flow.*

Strength Maximum stress that a material can withstand without failing for any given type of loading.

Stress The ratio of force to area upon which it acts.

Subsidence Sinking of a part of the earth's crust and downward displacement of the overburden (rock, soil, or both) lying above an underground excavation.

Tangible stress *See Stress.*

Test pit *See Pit.*

Texture The arrangement in space of soil particles and of the boundaries between these particles within a soil mass.

Thixotropy The property of a material that enables it to stiffen in a relatively short time, but upon agitation or manipulation to change to a very soft consistency or to a fluid of high viscosity. The process is completely reversible.

Time factor Dimensionless factor, utilized in the theory of consolidation, containing physical constants of a soil stratum influencing its rate of consolidation.

Till Unstratified glacial drift of clay, sand, gravel, and boulders.

Topsoil Dark surface soil, usually containing organic matter.

Toughness index The ratio of the plasticity index to the flow index.

Transported soil Soil transported from the place of its origin by wind, water, or ice.

Triaxial compression Compression caused by the application of normal stresses in three perpendicular directions to a soil specimen.

Tunnel A man-made underground passage constructed without removing the overlying rock or soil.

Turbulent flow Flow in which a water particle may move in any direction with respect to any other particle, and in which the head loss is approximately proportional to the second power of the velocity.

Unconfined or uniaxial compressive strength *See Compressive strength.*

Unconsolidated-undrained test A soil test in which the water content of the test specimen remains practically unchanged during the application of the confining pressure and the additional axial force.

Underconsolidated soil deposit A deposit that is not fully consolidated under the existing effective pressure.

Undisturbed sample A soil sample that has been obtained by methods in which precaution has been taken to minimize disturbance.

Uniaxial compressive strength *See Compressive strength.*

Unit weight Weight per unit volume.

Vane shear test A shear test in which a rod with thin radial vanes at the end is forced into the soil and the resistance to rotation of the rod is determined.

Varved clay Alternating thin layers of silt or fine sand and clay formed by variations in sedimentation during the various stages of deposition and formation, often exhibiting contrasting colors when partially dried.

Viscous flow *See Laminar flow.*

Void Space in a soil or rock mass not occupied by solid mineral matter. This space may be occupied by air, water, or other gaseous or liquid material.

Volumetric shrinkage The decrease in volume, expressed as a percentage of the soil mass when dried, of a soil mass when water content is reduced from a given percentage to its shrinkage limit.

Water content *See* **Moisture content.**

Weathering The process of disintegration and decomposition of rock as a consequence of exposure to the atmosphere, to chemical action, and/or to the action of frost, water, and heat.

Zero air voids curve The curve showing the zero air voids dry unit weight as a function of water content.

References

Acker III, W. L. 1974. *Basic Procedures for Soil Sampling and Core Drilling*. Acker Drill Co., Inc., Scranton, PA.

Al-Khafaji, A. W. N. 1979. "Decomposition effects on engineering properties of fibrous organic soils." Ph.D. Dissertation, Michigan State University, East Lansing, MI.

Al-Khafaji, A. W. N. 1991. *Geotek-Pro 2.0: Geotechnical Software for MS-DOS Personal Computers*. National Laboratories, Inc., Evansville, IN.

Al-Khafaji, A. W. N. and Andersland, O. B. 1981. "Ignition test for soil organic content measurement." *Journ. of the Geotechnical Engr. Div. ASCE*, Vol. 107, No. GT4, pp. 465–479.

Al-Khafaji, A. W. N. and Tooley, J. R. 1986. *Numerical Methods in Engineering Practice*. Holt, Rinehart and Winston, New York.

American Association for State Highway and Transportation Officials. 1986 *Standard Specifications for Transportation Materials and Methods of Sampling and Testing*, 14th ed. Washington, D. C., Specifications: T 87; T 88; T 89; T 90; T 92; T 99; T 180; T 191; T 205; T 208; T 215; T 216; T 217; T 232; T 233; T 238; T 265; T 854.

Armour, D. W. and Drnevich, V. P. 1985. "Improved techniques for the constant-rate-of-strain consolidation test." ASTM Symposium on Consolidation of Soils, Laboratory Testing.

ASTM Standards. 1990. Sec. 4, Vol. 04.08, *Soil and Rock; Dimension Stone; Geosynthetics*. American Society for Testing and Materials, Designation: C 127; D 70; D 421; D 422; D 427; D 698; D 854; D 1556; D 1557; D 1586; D 1587; D 2166; D 2167; D 2216; D 2434; D 2435; D 2573; D 2922; D 2937; D 3080; D 3441; D 4180; D 4186; D 4253; D 4254; D 4318;

- Barden, L. and Berry, P. L. 1965. "Consolidation of normally consolidated clay." *Jour. of the Soil Mech. and Found. Div., ASCE*, Vol. 91, No. SM5.
- Barnes, H. E. 1952. "Soil investigation employing a new method of layer-value determination for earth-resistivity interpretation." *Highway Research Board Bull.* 65, pp. 26–36.
- Bazaraa, A. R. 1967. "Use of the standard penetration test for estimating settlement of shallow foundation on sand," Ph.D. Thesis, University of Illinois, Urbana.
- Berre, Toralv. 1981. "Triaxial testing at the Norwegian Geotechnical Institute." Norwegian Geotechnical Institute Publ. No. 134, Oslo, Norway.
- Bishop, A. W. 1950. "Discussion on measurement of shear strength of soils." *Geotechnique* Vol. 2, pp. 113–116.
- Bishop, A. W. and Eldin, A. K. G. 1950. "Undrained triaxial tests on saturated sands and their significance in the general theory of shear strength." *Geotechnique*, Vol. 2, pp. 13–32.
- Bishop, A. W. and Henkel, D. J. 1962. *The Measurement of Soil Properties in the Triaxial Test*. Edward Arnold Ltd., London.
- Bjerrum, Laurits. 1972. "Embankments on soft ground." Proc. ASCE Specialty Conf. on Performance of Earth and Earth-Supported Structures American Society of Civil Engineers, New York, Vol. II, pp. 1–54.
- Boussinesq, J. 1885. *Application des Potentiels a l'Etude de l'Equilibre et due Mouvement des Solides Elastiques*. Gauthier-Villars, Paris.
- Bromwell, L. G. 1966. "The friction of quartz in high vacuum." Sc.D. Thesis, M.I.T., Cambridge, MA.
- Casagrande, A. 1948. "Classification and identification of soils." *Trans. ASCE*, Vol. 113, pp. 901–930.
- Casagrande, A. and Carrillo, N. 1944. "Shear failure of anisotropic materials." *Contributions to Soil Mechanics, 1941–1953*. Boston Society of Civil Engineers, Boston.
- Casagrande, A. and Fadum, R. E. 1940. "Notes on soil testing for engineering purposes." Harvard Univ. Grad. School of Engineering Publ. 268, Cambridge, MA.
- Cedargren, H. R. 1967. *Seepage, Drainage, and Flow Nets*. Wiley, New York.
- Chamberlain, E. J. 1981. "Frost susceptibility of soil, review of index tests." U. S. Army Corps of Engineers, Cold Regions Research and Engineering Laboratory, Hanover, NH, CRREL Monograph 81-2.
- Cornforth, D. H. 1964. "Some experiments on the influence of strain conditions on the strength of sand." *Geotechnique*, Vol. 14, pp. 143–167.
- D'Appolonia Consulting Engineers, Inc. 1975. "Engineering and design manual—coal refuse disposal facilities." Mining Enforcement and Safety Administration, U. S. Dept. of the Interior.
- Darcy, H. 1856. *Les Fontaines Publiques de la Ville de Dijon* (The public water supply of the city of Dijon). Dalmont, Paris.
- Davis, E. H. and Poulos, H. G. 1968. "The use of elastic theory for settlement prediction under three-dimensional conditions." *Geotechnique*, Vol. 18, pp. 67–91.
- Desai, S. D. and Christian, J. T. 1977. *Numerical Methods in Geotechnical Engineering*. McGraw-Hill, New York.

- Dickey, J. W. 1966. "Frictional characteristics of quartz." S. B. Thesis, M. I. T., Cambridge, MA.
- Dobrin, M. 1976. *Introduction to Geophysical Prospecting*, 3rd ed. McGraw-Hill, New York.
- Federal Register. 1977. "Part II, tile 30—mineral resources." Office of Surface Mining Reclamation and Enforcement, U. S. Dept. of the Interior, Ch. VII, Part 715.
- Fisk, H. N. 1947. "Fine-grained alluvial deposits and their effects on Mississippi River activity." 2, Waterways Exp. Sta., Vicksburg, Mississippi.
- Gibbs, H. J. and Holtz, W. G. 1957. "Research on determining the density of sand by spoon penetration test." Proc. 4th ICSMFE, Vol. I, pp. 35–39.
- Gibson, R. E. 1953. "Experimental determination of the true cohesion and angle of internal friction in clays." Proc. 3rd Int. Conf. Soil Mechanics, Vol. 1, pp. 126–130.
- Gibson, R. E. and Henkel, D. J. 1954. "Influence of duration of test at constant rate of strain on measured 'drained strength.'" *Geotechnique*, Vol. IV, pp. 6–15.
- Grim, R. E. 1953. *Clay Mineralogy*. McGraw-Hill, New York.
- Hansbo, S. 1960. "Consolidation of clay with special reference to the influence of vertical sand drains." Proc. 18, Swedish Geotechnical Inst., Stockholm.
- Hansen, J. B. 1970. "A revised and extended formula for bearing capacity." Danish Geotechnical Institute, Bulletin 28, Copenhagen.
- Hansen, B. and Nielson, H. K. 1965. "Settlement calculations for a tunnel construction in Gothenburg clay." Proc. 6th ICSMFE, Vol. 2, pp. 77–85.
- Harr, M. E. 1966. *Foundations of Theoretical Soil Mechanics*. McGraw-Hill, New York.
- Holtz, R. D. and Broms, B. B. 1972. "Long-term loading tests at Ska-Edeby, Sweden." Proc. ASCE Specialty Conf. on Performance of Earth and Earth-Supported Structures. Purdue University, Vol. 1, Part I, pp. 435–464.
- Huang, Y. H. 1983. *Stability Analysis of Earth Slopes*. Van Nostrand Reinhold Company, Inc., New York.
- Hvorslev, M. J. 1949. *Subsurface Exploration and Sampling of Soils for Civil Engineering Purposes*. Waterway Experimental Station, Vicksburg, Mississippi.
- Janbu, N. Bjerrum, L., and Kjaernsli, B. 1956. *Veiledning ved l sning av fundamenteringsopp-gaver*. Norges Geotekniske Institute Publikasjon Nr. 16, Oslo.
- Kelly, W. P., Jenny, H., and Brown, S. M. 1936. "Hydration of minerals and soil colloids in relation to crystal structure." *Soil Science*, Vol. 41, p. 259.
- Kirkpatrick, W. M. 1957. "The condition of failure for sands." Proc. 4th ICSMFE, London, Vol. 1, pp. 172–178.
- Ladanyi, B. 1973. "Evaluation of in situ creep properties of frozen soils with the pressuremeter." *Permafrost*. North American Contribution to the 2nd Int. Conf., National Academy of Sciences, Washington, DC, pp. 310–318.
- Ladd, C. C., Foote, R., Ishihara, K., Schlosser, F., and Poulos, H. G. 1977. "Stress-deformations and strength characteristics." State-of-the-Art Report, Proc. 9th ICSMFE, Tokyo, Vol. 2, pp. 421–494.
- Lambe, T. W. 1951. *Soil Testing for Engineers*. John Wiley & Sons, Inc., New York.

- Lambe, T. W. 1958. "The engineering behavior of compacted clay." *Journ. of the Soil Mech. and Found. Div.*, ASCE, Vol 84, No SM2, pp 1655-1 to 1655-35.
- Lambe, T. W. 1960. "A mechanistic picture of shear strength in clay." Res. Conf. on Shear Strength of Cohesive Soils, ASCE, Boulder, CO, pp. 555-580.
- Lee, K. L. and Seed, H. B. 1967. "Drained strength characteristics of sands." *Journ. of the Soil Mech. and Found. Div.*, ASCE, Vol. 93, No. SM6, pp. 117-141.
- Lee, P. Y. and Suedkamp, R. J. 1972. "Characteristics of irregularly shaped compaction curves of soils." *Highway Research Record No. 381*, Washington, DC.
- Leonards, G. A., Cutter, W. A., and Holtz, R. D. 1980. "Dynamic compaction of granular soils." *Journ. of the Geotechnical Engr. Div.*, ASCE, Vol. 106, No. 1, pp. 35-44.
- McClelland, B. 1972. "Design of deep penetration piles for ocean structures." *International Geotechnical Engineering Division*, ASCE, Vol 100, No. GT7, pp. 705-747.
- Mclean, F. G. et al. 1975. "Influence of mechanical variables on the SPT," 6th PSC, ASCE, Vol. 1, New York.
- Menard, L. and Broise, Y. 1975. "Theoretical and practical aspects of dynamic consolidation." *Geotechnique*, Vol. 15, No. 1, pp. 3-18.
- Mesri, G. and Godlewski, P. M. 1977. "Time- and stress-compressibility interrelationship." *Journ. of the Geotechnical Engr. Div.*, ASCE, Vol. 103, No. GT5, pp. 417-430.
- Metson, A. J. 1956. "Methods of chemical analysis for soil survey samples." Bull. 12, Soil Bureau, New Zealand Dept. of Scientific and Industrial Research, p. 145.
- Meyerhof, G. G. 1956. "Penetration tests and bearing capacity of cohesionless soils." *Journ. of the Soil Mech. and Found. Div.*, ASCE, Vol 82, SM1, pp. 1-19.
- Meyerhof, G. G. 1974. "Ultimate bearing capacity of footings on sand layer overlaying clay." *Canadian Geotechnical Journ.*, Vol. 11, No. 2, pp. 224-229.
- Mines Branch. 1972. "Tentative design guide for mine waste embankments in Canada." Department of Energy, Mines, and Resources, Canada.
- Mitchell, J. K. 1976. *Fundamentals of Soil Behavior*. John Wiley & Sons, Inc., New York.
- Moore, R. W. 1961. "Geophysics efficient in exploring the subsurface." *Journ. of the Soil Mech. and Found. Div.*, ASCE, Vol. 87, No. SM3: Pt. 1, pp. 69-100.
- National Coal Board. 1970. "Soil heaps and lagoons." Technical Handbook, London.
- Newmark, N. M. 1942. "Influence charts for computation of stresses in elastic foundations." University of Illinois Engineering Experiment Station Bulletin, Series No. 338, Vol. 61, No. 92, Urbana, IL, reprinted 1964.
- Osterberg, J. O. 1957. "Influence values for vertical stresses in a semi-infinite mass due to an embankment loading." Proceedings of the Fourth International Conference on Soil Mechanics and Foundation Engineering, London, Vol. I, pp. 393-394.
- Perloff, W. H. and Baron, W. 1975. *Soil Mechanics*. Ronald Press, New York.
- Pitts, J. 1984. *A Manual of Geology for Civil Engineers*. Wiley, New York.
- Prandtl, L. 1921. "Über die eindringungsfestigkeit (Harte) plastischer baustoffe und die festigkeit von schneiden." *Zeitschrift für Angewandte Mathematik und Mechanik*, Vol. 1, No. 1, pp. 15-20.

- Richardson, A. M., Jr. and Whitman, R. V. 1964. "Effect of strain-rate upon undrained shear resistance of saturated remolded fat clay." *Geotechnique*, Vol. 13, No. 4, pp. 310–346.
- Richart, F. E., Jr., Hall, J. R., Jr., and Woods, R. D. 1970. *Vibrations of Soils and Foundations*. Prentice-Hall, Englewood Cliffs, NJ.
- Sandbaekken, G., Berre, T., and Lacasse, S. 1985. "Oedometer testing at the Norwegian Geotechnical Institute." ASTM Symposium on Consolidation of Soils, Laboratory Testing.
- Schmertmann, J. H. 1955. "The undisturbed consolidation of clay." *Trans. ASCE*, Vol. 20, p. 201.
- Schmertmann, J. H. 1970. "Static cone to compute static settlement over sand." *Journ. of the Soil Mech. and Found. Div.*, ASCE, Vol. 96, No. SM3, pp. 1011–1043.
- Schmertmann, J. H., Hartman, J. P., and Brown, P. R. 1978. "Improved strain influence factor diagram." *Journ. of the Geotechnical Engr. Div.*, ASCE, Vol. 104, No. GT8, pp. 1131–1135.
- Scott, R. F. 1963. *Principles of Soil mechanics*. Addison Wesley, Reading, MA.
- Seed, H. B. and Chan, C. K. 1959. "Structure and strength characteristics of compacted clays." *Journ. of the Soil Mech. and Found. Div.* ASCE, Vol. 85, No. SM5, pp. 87–128.
- Seed, B. H., Idriss, I. M., and Arango, I. 1983. "Evaluation of liquefaction potential using field performance data." *Journ. of the Geotechnical Engr. Div.*, ASCE, Vol. 109, No. 3, pp. 458–482.
- Skempton, A. W. 1953. "The colloidal activity of clays" Proceedings of the Third International Conference on Soil Mechanics and Foundation Engineering, Vol. I, pp. 57–61.
- Skempton, A. W. 1957. "Discussion: The planning and design of the new Hong Kong Airport." *Proc. Inst. Civ. Engrs.*, London, 7, pp. 305–307.
- Skempton, A. W. 1961. "Effective stress in soils, concrete and rocks." *Pore Pressure and Suction in Soils*. Butterworths, London, pp. 4–16.
- Skempton, A. W. 1964. "Long-term stability of clay slopes." Fourth Rankine Lecture. *Geotechnique*, Vol. XIV, pp. 77–101.
- Skempton, A. W. and Henkel, D. J. 1953. "The post-glacial clays of the Thames Estuary at Tilbury and Shellhaven." *Proc. 3rd ICSMFE*, Switzerland, Vol. I, p. 302.
- Taylor, D. W. 1948. *Fundamentals of Soil Mechanics*. Wiley, New York.
- Technical Procedures Committee of ASCE. 1962. *Subsurface Investigation for Design and Construction of Foundation of Buildings*. New York.
- Terzaghi, K. 1943. *Theoretical Soil Mechanics*. Wiley, New York.
- Terzaghi, K. 1952. "Permafrost." *Journ. of the Boston Society of Civil Engineers*, Vol. XXXIX, No. 1, pp. 1–50.
- Terzaghi, K. and Frolich, O. K. 1936. *Theorie der setzung von tonschichten: eine einfuehrung in die analytische tonmechanik*. Deuticke, Leipzig.
- Terzaghi, K. and Peck, R. 1948. *Soil Mechanics in Engineering Practice*. John Wiley and Sons, Inc., New York.
- U. S. Bureau of Reclamation. 1965. *Design of Small Dams*. U. S. Government Printing Office, Washington, D. C.

- U.S. Dept. of Commerce. 1960. *The Identification of Rock Types*. U.S. Government Printing Office, Washington, DC.
- U.S. Dept. of the Interior. 1974. *Earth Manual*. U.S. Government Printing Office, Washington, DC (reprinted 1980).
- U.S. Dept. of the Army. 1979. *Geophysical Exploration*. Engineering Manual, EM 1110-1-1802, Washington, DC.
- U.S. Dept. of the Navy. 1982. *Soil Mechanics*. NAVFAC Design Manual DM-7.1, Alexandria, VA.
- Vesic, A. S. 1963. "Bearing capacity of deep foundations in sand." Highway Research Record No. 39, National Academy of Sciences, pp. 112–153.
- Welsh, J. 1986. "In situ testing for ground modification techniques." *Use of In situ Tests in Geotechnical Engineering*. ASCE Geotechnical Special Publication No. 6, New York, pp. 322–335.
- Welsh, J. 1986. "Construction consideration for ground modification projects," Proc., Intl. Conf. on Deep Foundation, Beijing, China.
- Whitman, Robert V. 1960. "Some considerations and data regarding the shear strength of clays." Research Conf. on Shear Strength of Cohesive Soils, ASCE, Boulder, CO, pp. 581–614.
- Wilson, S. D. and Mikkelsen, P. E. 1978. "Field instrumentation." Ch. 5 in *Landslides, Analysis and Control*, ed. by R. L. Schuster and R. J. Krizek, National Academy of Sciences, Washington, D. C., Special Report 176.
- Wissa, A. E. Z., Christian, J. T., Davis, E. H., and Heiberg, S. 1971. "Consolidation at constant rate of strain." *Journ. of the Soil Mech. and Found. Div.*, ASCE, Vol. 97, No. SM10, pp. 1393–1413.
- Wu, T. H., Loh, A. K., and Malvern, L. E. 1963. "Study of failure envelope of soils." *Journ. of the Soil Mech. and Found. Div.*, ASCE, Vol. 89, No. SM1, pp. 145–181.

Appendix A

SI Units and Conversion Factors

SI Units

SI Base Units

| Base Unit | Name | Symbol |
|-----------|----------|--------|
| Length | meter | m |
| Mass | kilogram | kg |
| Time | second | s |

SI Prefixes

| Multiplication Factor | Prefix | SI Symbol |
|-----------------------|--------|-----------|
| 1,000,000,000 | giga | G |
| 1,000,000 | mega | M |
| 1,000 | kilo | k |
| 0.001 | milli | m |
| 0.000 001 | micro | μ |
| 0.000 000 001 | nano | n |

SI Derived Units

| Quantity | Derived SI Unit | Name | Symbol |
|-----------------|-----------------------------------|--------|------------------------|
| Area | square meter | — | m ² |
| Volume | cubic meter | — | m ³ |
| Density | kilogram per cubic meter | — | kg/m ³ |
| Force | kilogram-meter per second squared | newton | N |
| Pressure | newton per meter squared | Pascal | Pa or N/m ² |
| Work and energy | newton-meter | joule | J |
| Power | joule per second | watt | W |

Conversion Factors**Length**

| This Quantity | Multiplied by This Quantity | Gives This Quantity |
|------------------|-----------------------------|---------------------|
| centimeters (cm) | 3.937×10^{-1} | inches |
| centimeters (cm) | 3.281×10^{-2} | feet |
| centimeters (cm) | 6.214×10^{-6} | miles |
| meters (m) | 3.937×10^1 | inches |
| meters (m) | 3.281 | feet |
| meters (m) | 1.094 | yards |
| meters (m) | 6.214×10^{-4} | miles |
| inches (in.) | 2.540 | centimeters |
| inches (in.) | 2.540×10^{-2} | meters |
| feet (ft) | 3.048×10^{-1} | meters |
| feet (ft) | 3.048×10^{-4} | kilometers |
| feet (ft) | 1.894×10^{-4} | miles |
| feet of water | 6.243×10^1 | pounds/sq ft |
| feet of water | 4.335×10^{-1} | pounds/sq in. |
| yards | 9.144×10^{-1} | meters |

Area

| This Quantity | Multiplied by This Quantity | Gives This Quantity |
|--------------------|-----------------------------|---------------------|
| square centimeters | 1.550×10^{-1} | square inches |
| square centimeters | 1.076×10^{-3} | square feet |
| square meters | 1.550×10^3 | square inches |
| square meters | 1.076×10^1 | square feet |
| square meters | 2.471×10^{-4} | acres |
| square meters | 3.861×10^{-7} | square miles |
| square feet | 9.290×10^{-2} | square miles |
| square feet | 3.587×10^{-8} | square miles |

Volume

| This Quantity | Multiplied by This Quantity | Gives This Quantity |
|----------------------|------------------------------------|----------------------------|
| cubic centimeters | 6.102×10^{-2} | cubic inches |
| cubic centimeters | 3.531×10^{-5} | cubic feet |
| cubic centimeters | 1.308×10^{-6} | cubic yards |
| cubic centimeters | 2.642×10^{-4} | gallons |
| cubic centimeters | 1.000×10^{-3} | liters |
| cubic centimeters | 1.057×10^{-3} | quarts |
| cubic meters | 6.102×10^4 | cubic inches |
| cubic meters | 1.000×10^3 | liters |
| cubic meters | 2.642×10^2 | gallons |
| cubic meters | 3.531×10^1 | cubic feet |
| cubic inches | 1.639×10^{-2} | liters |
| cubic inches | 4.329×10^{-3} | gallons |
| cubic inches | 1.639×10^{-5} | cubic meters |
| cubic feet | 2.832×10^{-2} | cubic meters |
| cubic feet | 7.48052 | gallons |
| cubic feet | 2.832×10^1 | liters |

Force

| This Quantity | Multiplied by This Quantity | Gives This Quantity |
|----------------------|------------------------------------|----------------------------|
| dynes | 2.248×10^{-6} | pounds-force |
| dynes | 2.248×10^{-9} | kip |
| dynes | 1.124×10^{-9} | short tons |
| newtons | 1.000×10^5 | dynes |
| newtons | 2.248×10^{-1} | pounds-force |
| newtons | 2.248×10^{-4} | kip |
| newtons | 1.000×10^{-3} | kilonewtons |
| long tons (metric) | 2.240×10^3 | pounds-force |
| pounds | 4.448×10^5 | dynes |
| pounds | 4.448 | newtons |
| pounds | 1.600×10^1 | ounces |
| short tons | 2.000×10^3 | pounds-force |

Mass

| This Quantity | Multiplied by This Quantity | Gives This Quantity |
|----------------------|------------------------------------|----------------------------|
| grams | 2.205×10^{-3} | pounds-mass |
| kilograms | 2.2046 | pounds-mass |
| kilograms | 6.852×10^{-2} | slugs |
| pounds-mass | 4.5359×10^2 | grams |
| pounds-mass | 4.5359×10^{-1} | kilograms |
| pounds-mass | 3.1081×10^{-2} | slugs |

Velocity

| This Quantity | Multiplied by This Quantity | Gives This Quantity |
|----------------------|------------------------------------|----------------------------|
| cm/s | 1.969 | ft/min |
| cm/s | 3.281×10^{-2} | ft/s |
| cm/s | 3.600×10^{-2} | km/h |
| cm/s | 2.237×10^{-2} | miles/h |
| m/s | 3.281 | ft/s |
| m/s | 3.600 | km/h |
| m/s | 2.237 | miles/h |
| ft/min | 1.829×10^{-2} | km/h |
| ft/min | 3.048×10^{-1} | m/min |
| ft/min | 1.136×10^{-2} | miles/h |
| ft/s | 1.097 | km/h |
| ft/s | 1.829×10^1 | m/min |
| ft/s | 6.818×10^{-1} | miles/h |

Pressure

| This Quantity | Multiplied by This Quantity | Gives This Quantity |
|---|------------------------------------|-----------------------------|
| kilonewtons/m ² (kN/m ²) | 1.450×10^{-1} | lb/in. ² |
| kilonewtons/m ² (kN/m ²) | 2.088×10^1 | lb/ft ² |
| kilonewtons/m ² (kN/m ²) | 2.088×10^{-2} | kip/ft ² |
| kilonewtons/m ² (kN/m ²) | 3.346×10^{-1} | feet of water |
| pounds-force/sq ft | 1.602×10^{-2} | feet of water |
| pounds-force/sq ft | 4.788 | Pascals (N/m ²) |
| pounds-force/sq in. | 2.307 | feet of water |
| pounds-force/sq in. | 6.895×10^3 | Pascals (N/m ²) |

Density

| This Quantity | Multiplied by This Quantity | Gives This Quantity |
|------------------------------|------------------------------------|-----------------------------|
| kg/m ³ | 6.243×10^{-2} | pounds-mass/ft ³ |
| pounds-mass/ft ³ | 1.602×10^1 | kg/m ³ |
| pounds-mass/in. ³ | 2.768×10^4 | kg/m ³ |

Unit Weight

| This Quantity | Multiplied by This Quantity | Gives This Quantity |
|----------------------|------------------------------------|----------------------------|
| kN/m ³ | 3.685×10^{-3} | lb/in. ³ |
| kN/m ³ | 6.368 | lb/ft ³ |
| lb/ft ³ | 1.570×10^{-1} | kN/m ³ |

INDEX

| <u>Index Terms</u> | <u>Links</u> | | |
|--|--------------|---------|-----|
| A | | | |
| A-line | 94 | 523 | |
| AASHTO soil classification system | 102–106 | | |
| activity, A_c | 15 | 89–90 | 108 |
| aggregate, soil | 77 | | |
| alluvium | 17 | | |
| angle of internal friction, ϕ | 311 | 313 | |
| <i>See also</i> shear strength | | | |
| correlation with e | 334 | | |
| for clay minerals | 345 | | |
| with soil classification | 334 | | |
| summary of factors affecting | 334 | | |
| anisotropic soil properties | 168 | 321–323 | |
| area ratio (sampling), AR | 52 | | |
| Atterberg limits. <i>See also</i> liquid limit | | | |
| plastic limit, shrinkage limit | | | |
| flow index | 511 | 513 | |
| liquid limit, LL | 88 | 510 | |
| device | 508–509 | | |
| flow curve | 509–510 | | |
| flow index, I_f | 511 | 513 | |
| multipoint test | 507 | 509–510 | |
| one-point test | 507 | 511 | |
| ratio | 95 | | |
| test description | 507–513 | | |
| liquidity index, LI | 88–89 | | |

Index Terms

Links

Atterberg limits (*Cont.*)

| | | | |
|---------------------------------------|---------|---------|---------|
| plastic limit, <i>PL</i> | 88–89 | 94 | |
| test description | 515–518 | | |
| plasticity chart | 89 | 94 | 518 |
| plasticity index, <i>PI</i> | 15 | 88–89 | 517–518 |
| shrinkage limit, <i>SL</i> | 88 | | |
| test description | 519–525 | | |
| soil classification, use in | 94–95 | 103–106 | |
| toughness index, <i>I_t</i> | 511 | 513 | |
| auger | | | |
| Iwan | 44–45 | | |
| rotary bucket | 47 | | |
| ship | 45–46 | | |
| augite | 6 | | |

B

Bearing capacity

| | | | |
|------------------------|---------|-----|--|
| analysis | 396 | | |
| corrections for | | | |
| eccentricity | 401 | 403 | |
| geometry | 396 | | |
| inclination | 403 | | |
| defined | 392 | | |
| equations | 400 | | |
| factor of safety | 393–395 | | |
| factors | 397–400 | | |
| failure zones | 396 | | |
| groundwater, effect of | 401–402 | | |
| layered soils | 404 | | |
| nominal | 405–407 | | |
| reduced | 74 | | |
| Terzaghi's theory | 395–397 | | |

Index Terms

Links

| | | | |
|--|---------|---------|-----|
| Bernouli's equation | 145 | | |
| bog | 19 | | |
| borderline classification | 94 | | |
| boring | | | |
| auger | 43 | | |
| depth of | 34 | | |
| number of | 35 | | |
| records of | 59–62 | | |
| samplers | | | |
| Denison | 54 | | |
| split-spoon | 48 | | |
| stationary piston | 53 | | |
| tube | 47–48 | | |
| samples | | | |
| intervals | 36 | | |
| type | 36 | | |
| spacing of | 35 | | |
| boulders | 75 | | |
| Bousinesq method. <i>See also</i> stress distribution. | | | |
| influence charts | 206 | 210–211 | 220 |
| | 228 | | |
| integrated over areas | 221–226 | | |
| point load | 204–206 | | |
| C | | | |
| Caissons | 417–419 | | |
| in clay | 417 | | |
| in sand | 418 | | |
| calcite | 6 | 8 | |

Index Terms

Links

| | | | |
|-----------------------------------|---------|---------|-----|
| capillarity | | | |
| capillary pressure | 196 | | |
| capillary rise, h_c | 68–69 | 151 | 196 |
| capillary zone | 196 | | |
| effect of | 196 | | |
| effective stress | 196 | | |
| frost action | 71–72 | | |
| surface tension, T | 67–69 | 196 | |
| capillary rise, h_c | 68–69 | 151 | 196 |
| carbonation | 5 | | |
| Casagrande, | | | |
| determination of preconsolidation | | | |
| pressure | 249 | 254 | |
| liquid limit, test for | 89 | 507–513 | |
| log-time fitting method | 258 | 575 | |
| cations | 12 | | |
| chemical decomposition | 9 | | |
| clay | 76–77 | 93 | 95 |
| consistency | 88 | 95 | 346 |
| index properties | 64 | | |
| permeability, k | 31 | 70 | 119 |
| sensitivity | 118 | 308 | 310 |
| | 346–347 | | |
| structure | 14 | | |
| swelling | 118 | | |
| varved | 19 | 21 | |
| clay minerals | 11 | 345 | 518 |
| activity | 15 | 89–90 | 108 |
| common clay minerals | 11–13 | | |
| crystal structure | | | |
| octahedral | 12 | | |
| tetrahedral | 12 | | |

Index Terms

Links

clay minerals (*Cont.*)

| | | | |
|-------------------------------|---------|---------|---------|
| halloysite | 12–13 | 89 | |
| illite | 11 | 13 | 89 |
| kaolinite | 11 | 13 | 89 |
| montmorillonite | 12–13 | 89 | |
| silica sheet | 11–12 | | |
| soil structure | | | |
| dispersed | 14 | | |
| flocculated | 14 | | |
| cobble | 75 | | |
| coefficient of | | | |
| active earth pressure, K_a | 356–358 | | |
| compressibility, a_v | 250 | 258 | |
| consolidation, c_v | 251 | 257–258 | 264 |
| determination of | 257–258 | 575 | 614 |
| concavity, C_z | 94 | 476 | 478 |
| earth pressure at rest, K_0 | 353–354 | | |
| passive earth pressure, K_p | 360–362 | | |
| permeability, k | 31 | 70 | 118–119 |
| | 133–144 | | |
| consolidation test | 264 | | |
| field measurement | 139–144 | | |
| laboratory tests | 559–567 | | |
| open-end tests | 139 | 143–144 | |
| pumping tests | 139–142 | | |
| solubility, Henry's | 607 | | |
| uniformity, C_u | 94 | 475–476 | 478 |
| volume compressibility, m_v | 250 | 258 | |
| wall friction δ | 374–377 | | |
| cohesion | 14 | 337–340 | 342 |

Index Terms

Links

| | | |
|--|---------|---------|
| cohesionless soils | 333–337 | |
| Coulomb analysis | 364–370 | |
| earth pressure at rest, K_0 | 354 | 359 |
| failure of | 308 | 312 |
| infinite slope stability | 428–429 | |
| wall friction, coefficient of δ | 366 | |
| cohesive soils | 337–348 | |
| active earth pressure | 358–360 | |
| components of shear resistance | 337–342 | |
| compressibility | 250–251 | |
| Coulomb analysis | 367 | |
| drained shear strength behavior | 342–346 | |
| overconsolidation | 249 | 254–255 |
| sample disturbance | 255 | |
| shrinkage | 519–525 | |
| slope stability | | |
| center of critical circle | 437 | |
| curved surface | 436 | |
| infinite slopes | 431–433 | |
| $\phi = \text{zero}$ analysis | 436 | |
| collapsing soils | 21 | 109 |
| compaction | 113 | |
| benefits of | 113 | |
| by explosive | 124–125 | |
| curve | 116 | |
| line of optimums | 116 | |
| optimum dry unit weight | 115–116 | |
| optimum water content | 116 | |
| dynamic | 122 | |
| effort | 114–115 | |
| impact | 114 | |
| kneading | 114 | 117 |

Index Terms

Links

| | | | |
|---|---------|---------|---------|
| compaction (<i>Cont.</i>) | | | |
| lift thickness | 121 | | |
| objectives | 119 | | |
| percent | 128–129 | 547 | 553 |
| | 557 | | |
| relative density | 128 | 540–544 | |
| static | 117 | | |
| theory | 113–116 | | |
| vibratory | 117 | 122 | 125 |
| zero air voids curve | 115–117 | 532–533 | 538 |
| compaction equipment | | | |
| motor grader | 123 | | |
| sheepsfoot rollers | 121 | | |
| smooth wheel roller | 121 | 123 | |
| tamping foot roller | 123 | | |
| rubber tired roller | 121 | 123 | |
| compaction tests | | | |
| curves | 116–118 | | |
| field density | 128–129 | | |
| Proctor test (modified) | 128 | 535–539 | |
| Proctor test (standard) | 118 | 128 | 530–534 |
| compactive effort | 115 | | |
| compressibility | 245 | | |
| coefficient of a_v | 250 | | |
| coefficient of volume m_v | 250 | | |
| compression | | | |
| index, C_c | 255 | 273–274 | |
| primary compression ratio, r | 258–259 | | |
| secondary | 279–280 | | |
| compression indices | | | |
| modified secondary, $C_{\alpha \epsilon}$ | 260 | | |
| recompression, C_r | 255 | 273–274 | |

Index Terms

Links

| | | | |
|--|---------|---------|-----|
| compressibility (<i>Cont.</i>) | | | |
| secondary, C_α | 259–260 | | |
| typical values | 260 | | |
| concavity coefficient of, C_z | 94 | 476 | 478 |
| cone penetration test. <i>See</i> Dutch cone penetration test. | | | |
| confining pressure. <i>See</i> triaxial tests. | | | |
| consistency limits | 88 | | |
| <i>See also</i> Atterberg limits. | | | |
| consolidated-undrained triaxial test. <i>See</i> triaxial tests | | | |
| consolidation | 244 | | |
| average degree of, U | 253 | | |
| boundary conditions | 251–252 | | |
| coefficient of, c_v | 251 | 257–258 | 575 |
| constant-rate-of-strain, CRS | 261–264 | | |
| degree of, U_z | 252–253 | | |
| effect of sample disturbance | 254–255 | | |
| percent | 252 | | |
| primary | 281 | 574 | |
| secondary | 279–280 | | |
| spring analogy | 245–246 | | |
| Terzaghi's 1-D theory | 249–253 | | |
| boundary conditions | 251–252 | | |
| derivation | 249–253 | | |
| solution | 252 | | |
| time factor | 252–253 | 257–259 | |
| test | 247–249 | 568–577 | |
| <i>See also</i> oedometer test. | | | |
| theory | 249–253 | | |

Index Terms

Links

| | | | |
|--|---------|---------|---------|
| consolidation (<i>Cont.</i>) | | | |
| time factor, T_v | 252–253 | | |
| time rate of | 278 | 281 | |
| numerical solution | 281–285 | | |
| consolidation parameters | | | |
| coefficient of | | | |
| compressibility, a_v | 250 | 258 | |
| consolidation, c_v | 251 | 257–258 | 264 |
| | 574–576 | | |
| volume compressibility, mv | 250 | 258 | 264 |
| compression index, C_c | 255 | 273–274 | |
| consolidation ratio, U_z | 252–253 | | |
| modified secondary compression index, $C_{\alpha\epsilon}$ | 260 | | |
| oedometer modulus, M | 264 | | |
| percent of consolidation, U_z | 252 | | |
| recompression index, C_r | 255 | 273–274 | |
| secondary compression index, C_α | 260 | | |
| consolidation settlement | | | |
| calculation of | 273–274 | | |
| multilayered soil | 295–297 | | |
| preconsolidation pressure, $\bar{\sigma}_p$ | 249 | 254–255 | |
| time rate | 281 | | |
| ultimate | 272–274 | | |
| consolidation testing | | | |
| CRS oedometer test | 261–264 | | |
| data presentation | 249 | 255 | 258 |
| | 262 | 571–573 | 575–576 |
| fixed-ring | 248 | 570 | 572 |
| floating-ring | 248 | | |
| test details | 568–577 | | |

Index Terms

Links

| | | | |
|------------------------------------|---------|---------|---------|
| consolidometer (oedometer) | | | |
| fixed-ring | 248 | 570 | 572 |
| floating-ring | 248 | | |
| CU-tests | 317 | | |
| Culmann's method | 376–378 | | |
| curve-fitting methods | 257–259 | | |
| Casagrande's | 258 | 575 | |
| Taylor's | 258 | 575 | |
| D | | | |
| Darcy's law | 31 | 133–134 | 153 |
| | 161–164 | 249 | |
| decomposition, degree of, X_{di} | 91 | | |
| deep foundations | | | |
| caissons | 417–419 | | |
| in clay | 417 | | |
| in sand | 418 | | |
| piles | 410–416 | | |
| friction | 410 | | |
| point-bearing | 410 | 412–413 | 415–416 |
| degree of saturation, S_r | 79 | 87 | |
| delta | 17 | | |
| Denison sampler | 54 | | |
| density | 10 | 79 | 106–107 |
| dry | 541 | 577 | |
| index, I_d | 542–543 | | |
| in-place determination | 128 | 545–558 | |
| maximum | 542–543 | | |
| minimum | 542–543 | | |
| nuclear method | 556–558 | | |
| optimum | 116–118 | 534 | 539 |
| | 546 | | |

Index Terms

Links

| | | |
|---|---------|-------------|
| density (<i>Cont.</i>) | | |
| relative, D_r | 106–107 | 540–544 |
| rubber balloon method | 551–555 | |
| sand cone method | 545–550 | |
| dewatering | 113 | |
| dilatancy. <i>See</i> soil characteristics. | | |
| direct shear test | 312–316 | 585–590 |
| discharge velocity, v | 133–134 | |
| dispersed-type structure | 13–14 | 76 |
| dispersion cups | 483–484 | |
| distortion (immediate) settlement | 265–267 | 269 |
| disturbed sampling | 47 | |
| drainage, blanket | 174–176 | 431–432 |
| dunes | 20 | |
| dupuit assumption | 140 | |
| dutch cone penetration test, CPT | 267–268 | 324 328–330 |
| correlation with SPT test | 330 | |

E

Earth pressure

active

| | | |
|---|---------|-----|
| coefficient of active earth pressure, K_a | 356–358 | 370 |
| cohesive soils | 358–359 | |
| pressure distribution | 375 | |

at-rest

| | | |
|--------------------------------------|---------|--|
| coefficient of earth pressure, K_0 | 353–354 | |
|--------------------------------------|---------|--|

cohesive soils

354

Coulomb theory

| | | |
|--------------------|---------|---------|
| active | 364–367 | |
| cohesionless soils | 365–367 | |
| cohesive soils | 366 | 371 |
| passive | 367 | 370–371 |

Index Terms

Links

Earth pressure (*Cont.*)

| | | | |
|---|---------|---------|-----|
| Culmann construction. <i>See</i> Culmann's method | | | |
| effect of water | 384–385 | | |
| failure surfaces | | | |
| Coulomb | 365–367 | | |
| log spiral method | 374 | | |
| Rankine | 365 | | |
| horizontal pressure | | | |
| distribution of | 359–361 | 384 | |
| effective | 384 | | |
| log spiral method | 374–375 | | |
| passive | 360–362 | 373 | |
| calculation | 360–361 | 363 | 371 |
| coefficient of passive earth pressure K_p | 357 | 360 | 362 |
| | 373 | | |
| cohesive soils | 360 | | |
| pressure distribution | 375 | | |
| retaining walls | 385–386 | | |
| point of application | 382 | | |
| Rankine theory | 358–362 | | |
| assumptions | 357 | 361 | |
| earth pressure coefficients | 361–362 | | |
| wall friction, coefficient of δ | 374–377 | | |
| effective grain size, D_{10} | 69 | 94 | |
| effective stress | 151 | 188 | 191 |
| | 196 | | |
| Eigenproblem method | 285–295 | | |
| epidote | 6 | | |
| equipotential | | | |
| drop | 165 | | |
| line | 154 | 165–166 | |

Index Terms

Links

| | | | |
|---|---------|---------|-----|
| erosion | 9 | | |
| esker | 21 | | |
| excess pore water pressure, u_e | 191 | 249 | |
| exchange capacity | 12–13 | | |
| expansive soils | 21 | 108 | |
| exploration | | | |
| geophysical | 38 | | |
| resistivity | 41 | | |
| seismic | 39 | | |
| soil | 33 | | |
| F | | | |
| factor of safety | | | |
| bearing capacity | 393–395 | | |
| infinite slope stability | 428–429 | 432–433 | |
| method of slices | 439 | 444 | |
| recommended | 445–446 | | |
| sliding | 27 | | |
| trial failure circle | 434 | | |
| failure theory. <i>See</i> Mohr-Coulomb | | | |
| strength | | | |
| feldspars | 5 | 11 | |
| fill | 23 | | |
| fine-grained soil | 22 | | |
| finite difference method | 157–159 | 281–284 | |
| finite element method | 157 | | |
| flocculated-type structure | 13–14 | 76 | |
| floodplain | 17 | | |
| flow index I_f | 511 | 513 | |
| flow line | 31 | 132 | 154 |
| | 165–166 | | |

Index Terms

Links

| | | | |
|--|---------|---------|---------|
| flow nets | 154 | 161–162 | 164–167 |
| and anisotropic permeability | 168–170 | | |
| construction of | 156 | 165–166 | |
| drawing rules | 165–166 | | |
| electric analogy | 156–157 | | |
| equipotential drops | 165 | | |
| equipotential lines | 154 | 165–166 | |
| flow channels | 165 | | |
| flow quantity calculation | 166–167 | | |
| seepage force | 178 | | |
| fluid flow | | | |
| laminar | 145 | | |
| turbulent | 145 | | |
| foundation engineering | 1 | | |
| foundations. <i>See also</i> shallow foundations. | | | |
| caissons | 417–419 | | |
| deep | 392–393 | | |
| piles | 410–416 | | |
| settlement | 398 | 407–408 | |
| shallow | 393–394 | 395 | |
| types | 392 | 411–412 | 417 |
| friction angle. <i>See also</i> shear strength; angle of internal friction | | | |
| measurement, ϕ | | | |
| direct shear test | 314 | 585 | |
| triaxial test | 319 | 598 | 610 |
| mineral-to-mineral, ϕ_{μ} | 340–342 | | |
| peak | 333–337 | 344 | |
| residual, ϕ_r | 342 | 344–345 | |
| Friction ratio, F_r | 328 | | |
| Frictional resistance | 340–342 | | |

Index Terms

Links

Frost

| | |
|-------------------------------|-------|
| action | 70–72 |
| heave | 72 |
| ice layers | 70–71 |
| susceptibility | 72–75 |
| Frozen soils. See also frost. | 2 |

G

| | | | |
|-----------------------------|---------|-----|-----|
| gap- (or skip-) graded soil | 475–476 | | |
| GARDS program | 444 | | |
| geologic cycle | 75 | | |
| geophysical methods | 38 | | |
| geotechnical engineering | 1 | | |
| glacial soils | 15 | 20 | |
| gradation | | | |
| poorly graded | 475–476 | | |
| skip- (or gap-) graded | 475 | | |
| well-graded | 475–476 | | |
| gradient | | | |
| hydraulic, i | 133 | 135 | 137 |
| | 164–165 | | |
| threshold, i_0 | 135 | | |
| grain shape | | | |
| effect on, $\bar{\phi}$ | 334 | | |
| types | | | |
| angular | 76 | | |
| rounded | 76 | | |
| subangular | 76 | | |
| subrounded | 76 | | |
| well rounded | 76 | | |

Index Terms

Links

| | | | |
|--------------------------|---------|---------|-----|
| grain size | 75–76 | | |
| analysis | 472–479 | 482–492 | |
| curve | 491–492 | | |
| distribution | 475–476 | | |
| effect on shear strength | 334 | | |
| effective, D_{10} | 94 | 476 | |
| hydrometer method | 482–492 | | |
| mechanical analysis | 472 | | |
| passing, percent | 475 | 478–479 | |
| poorly graded | 475–476 | | |
| retained, percent | 475 | 478–479 | |
| sieve analysis | 75 | 482 | 485 |
| | 491–492 | 541 | |
| skip- (or gap-) graded | 475–476 | | |
| uniformly graded | 475–476 | | |
| well graded | 475–476 | | |
| granular soil | 23 | 107 | |
| gravel | 22 | 76 | |
| ground modification | 119 | 122 | |
| ground water | | | |
| artesian | 57–58 | | |
| perched | 58 | | |
| table | 59 | | |
| group index, GI | 103 | | |
| grouting | 122 | 127–128 | |
| H | | | |
| halloysite | 12 | 13 | 67 |
| | 89 | | |
| hardness, rocks | 56 | | |

Index Terms

Links

| | | | |
|---|---------|---------|---------|
| head | | | |
| capillary | 196 | | |
| elevation | 145–147 | | |
| pressure | 145–148 | 151 | |
| total | 145–148 | 164–166 | |
| velocity | 145–146 | | |
| height ratio factor | 92 | | |
| hornblende | 6 | | |
| humus | 11 | | |
| hydration | 5 | | |
| hydraulic gradient, i | 133 | 137 | 164–165 |
| hydrometer method | 75 | 482–492 | |
| hydroxyls | 11 | 12 | |
| I | | | |
| ice layers | 70–71 | | |
| igneous | 5 | | |
| ignition test | 90 | 526–529 | |
| illite | 11 | 13 | 89 |
| immediate settlement | 265–270 | | |
| index | | | |
| activity, A_c | 15 | 89 | |
| density, I_d | 592 | | |
| flow, I_f | 511 | 513 | |
| liquidity, LI | 88 | 517–518 | |
| plasticity, PI | 88 | 94 | 517–518 |
| toughness, I_t | 511 | | |
| index properties | 64 | | |
| influence charts. <i>See</i> Stress distribution. | | | |
| circular loaded area | 220 | | |
| line load | 210–211 | | |
| Newmark's | 228 | | |

Index Terms

Links

influence charts (*Cont.*)

| | |
|--------------------------|-------|
| point load | 206 |
| rectangular loaded area | 223 |
| interlayer water | 67 |
| iron ore | 6 |
| isomorphous substitution | 12 |
| isotherm | 70–71 |
| isotropic soil | 308 |

K

| | | | |
|---------------------------------|---------|----|----|
| K_0 | 353 | | |
| clays | 354 | | |
| defined | 354 | | |
| relation to, $\bar{\phi}$ | 354 | | |
| sands | 354 | | |
| kame | 21 | | |
| kaolin | 6 | 11 | |
| kaolinite | 11 | 13 | 89 |
| K_f | 319–320 | | |
| Mohr-Coulomb, relationship with | 319–320 | | |
| parameters | 319 | | |
| Kozeny equation | 156 | | |

L

| | |
|---|---------|
| lacustrine deposits | 17 |
| landform | 1 |
| lateral earth pressure at rest, coefficient | |
| of, K_0 | 354 |
| lattice water | 67 |
| Laplace's equation | 153–154 |
| limestone | 16 |

Index Terms

Links

| | | | |
|--|---------|---------|---------|
| limits, Atterberg | 88 | | |
| liquid, <i>LL</i> | 88–89 | 94 | 507–513 |
| one-point test | 507 | 511 | |
| multipoint test | 507 | 509–510 | |
| plastic, <i>PL</i> | 88–89 | 94 | 515–518 |
| shrinkage, <i>SL</i> | 88 | 519–525 | |
| line of optimums. <i>See</i> compaction curve | | | |
| liquid limit, <i>LL</i> . <i>See</i> Atterberg limits. | | | |
| liquid limit ratio | 95 | | |
| liquidity index | 88 | 517–518 | |
| LIR. <i>See</i> load-increment ratio. | | | |
| <i>LL</i> . <i>See</i> Atterberg limits. | | | |
| load increment ratio, LIR | 248 | 570 | 580 |
| loess | 20 | | |
| M | | | |
| magma | 5 | | |
| marine sediments | 19 | | |
| marsh | 19 | | |
| metamorphic rock | 5 | | |
| mica | 6 | | |
| microcline | 6 | | |
| mineral fraction, X_m | 90 | | |
| modified compression index, secondary, $C_{\alpha c}$ | 260 | | |
| modified Proctor test | 128 | | |
| modulus | | | |
| oedometer, <i>M</i> | 264 | | |
| tangent | 308–310 | | |
| Young's | 56 | 308 | 310 |

Index Terms

Links

| | | | |
|--|---------|-------|-----|
| Mohr circle | | | |
| failure plane | 344 | | |
| pole method | 201–203 | | |
| Mohr circle of stress | 198–201 | 344 | 618 |
| Mohr-Coulomb strength | | | |
| criterion | 309–311 | | |
| parameters | 311–313 | | |
| Mohr failure envelope. <i>See also</i> shear strength. | | | |
| clays | 311 | 313 | 610 |
| effect of overconsolidation pressure | 311 | 313 | |
| K_f line | 319–320 | | |
| sands | 311–312 | 618 | |
| moisture-density test | 530 | 535 | |
| montmorillonite | 11–13 | 15–16 | 67 |
| | 89 | | |
| moraine | 21 | | |
| N | | | |
| NC. <i>See</i> normally consolidated soils. | | | |
| Newmark's chart | 228 | | |
| N-value. <i>See</i> standard penetration test | | | |
| normally consolidated soils, defined | 254 | | |
| Nuclear density meters | 556 | | |
| O | | | |
| octahedral sheet | 12 | | |
| octahedral unit | 11 | | |
| oedometer. <i>See</i> consolidometer. | | | |
| oedometer modulus, M | 264 | | |

Index Terms

Links

| | | | |
|--|---------|---------|-----|
| oedometer test | | | |
| consolidation | 247–249 | 568–577 | |
| constant-rate-of-strain, CRS | 261–264 | | |
| “quick” | 579–584 | | |
| one-dimensional | | | |
| compressibility | 245–247 | | |
| consolidation theory | 249–254 | | |
| optimum water content | 116 | | |
| organic fraction, X_f | 67 | 90 | 527 |
| organic matter | 11 | 90 | |
| organic soil | 4 | 11 | 22 |
| | 66 | 75 | 90 |
| peat | 19 | 75 | 90 |
| | 93 | | |
| orthoclase | 6 | | |
| outwash, glacial | 22 | | |
| overconsolidated soils | | | |
| defined | 254 | | |
| settlement calculations | 273–274 | | |
| overconsolidation ratio, OCR | | | |
| defined | 354 | | |
| effect on K_0 | 354 | | |
| oxidation | 5 | | |
| P | | | |
| particle shape. <i>See also</i> grain shape. | | | |
| effect on shear strength | 334 | | |
| particle surface roughness effect on | | | |
| shear strength | 334 | | |
| peat | 19 | 75 | 90 |
| | 93 | | |

Index Terms

Links

| | | | |
|---|---------|---------|---------|
| penetration test standard, SPT | 49 | 267 | 324 |
| | 327–328 | | |
| permeability | | | |
| absolute (specific), K | 134 | | |
| anisotropic materials | 169–170 | | |
| coefficient of, k | 31 | 70 | 118–119 |
| | 133–135 | 138 | 264 |
| measurement of | 136–137 | 139–144 | 559–567 |
| of stratified soils | 163–164 | | |
| typical values, chart | 138 | | |
| permeameter | | | |
| constant-head | 136–137 | 559–563 | |
| falling-head | 136–137 | 139 | 564–567 |
| permeant | 137 | | |
| phase diagram | 10 | 77–78 | |
| phase relations | 10 | 78–80 | |
| <i>PI</i> See Atterberg limits; plasticity index. | | | |
| piezometer | 59 | 147 | 151 |
| piezometric | | | |
| head | 146 | | |
| level | 37 | 133 | |
| lines | 154 | | |
| surface | 139 | 141 | |
| Piles | | | |
| displacement | 411–412 | | |
| friction | 410 | | |
| in clay | 413–414 | | |
| in sand | 415–416 | | |
| non-displacement | 411–412 | | |
| point-bearing | 410 | 412–413 | 415–416 |
| plastic limit, PL | 88–89 | 94 | 515–518 |

Index Terms

Links

| | | | |
|---|---------|---------|---------|
| plasticity | | | |
| chart | 94 | | |
| A-line | 94 | 523 | |
| U-line | 94 | 523 | |
| index, PI | 15 | 88–89 | 517–518 |
| point resistance, q_c | 328 | | |
| Poisson's ratio | 205 | 213 | |
| pole. <i>See also</i> Mohr's circle. | 201–203 | | |
| poorly-graded soil | 475–476 | | |
| pore pressure parameters | | | |
| A parameter | 606–607 | | |
| \bar{A} parameter | 309–310 | 606–607 | |
| B parameter | 307 | 606 | |
| effect of saturation on B | 307 | 607 | |
| pore water pressure | | | |
| back pressure | 607 | | |
| excess u_e | 191 | 249 | |
| hydrostatic, u_k | 191 | 249 | |
| porosity, n | 10 | 79 | 87 |
| preconsolidation pressure | | | |
| Casagrande construction | 249 | | |
| determination of | 249 | 255 | |
| effect of sample disturbance | 255 | | |
| factors effecting determination of | 254–255 | 584 | |
| methods to evaluate | 249 | 254–255 | |
| quasi-preconsolidation pressure | 261 | | |
| Schmertmann's method | 255 | | |
| pressure meter test, PMT | 324 | 330–333 | |
| primary compression ratio, r | 259 | | |
| primary consolidation. <i>See</i> consolidation | | | |
| principle planes. <i>See</i> stress. | | | |
| proctor test. <i>See</i> compaction tests. | | | |

Index Terms

Links

| | |
|---------------|---------|
| profile, soil | 22–24 |
| pumping tests | 139–141 |
| pycnometer | 493–495 |

Q

| | | |
|-------------|-----|-----|
| quartz | 6 | |
| quick clays | 22 | |
| quicksand | 179 | 195 |

R

Rankine analysis. *See also* earth pressure.

| | | |
|---|---------|---------|
| active state | 358–360 | |
| passive state | 360–361 | |
| recompression index, C_r | 255 | 273–274 |
| refraction survey | 40–41 | 450–454 |
| residual soils | 5 | 15–17 |
| resistivity | | |
| exploration | 41–43 | |
| meter | 43 | |
| retainer | | |
| lad sample | 48 | |
| spring valve | 48 | |
| trap valve | 48 | |
| retaining walls | 385–386 | |
| rock quality designator, RQD | 55 | |
| rocks, mineral composition | 6 | |
| rollers. <i>See</i> compaction equipment. | | |

S

| | |
|----------|----|
| salinity | 67 |
|----------|----|

Index Terms

Links

| | | | |
|-----------------------------|---------|---------|---------|
| sampler | | | |
| Denison | 54–55 | | |
| Shelby tube | 52–53 | | |
| solid tube | 47 | | |
| split spoon | 48 | | |
| stationary piston | 53 | | |
| thin-wall tube | 52 | | |
| sand | 22 | 76 | 93 |
| sand boil | 179 | 195 | |
| sand cone method | 545–550 | | |
| saturation degree of, S_r | 79 | 87 | 577 |
| Schmertmann method | 255 | | |
| secondary compression | 259 | | |
| sedimentary rock | 5–6 | 8 | |
| seepage | | | |
| Bernouli's equation | 145 | | |
| Darcy's law | 31 | 133–134 | 153 |
| | 161–164 | | |
| anisotropic soil | 168–170 | | |
| discharge velocity, v | 134 | | |
| equipotential lines | 154 | 165–166 | |
| flow nets | 154 | 161–162 | 164–167 |
| force | 178–179 | | |
| hydraulic gradient, i | 133 | 137 | 164–165 |
| Laplace's equation | 153–154 | | |
| transformed section | 169 | | |
| velocity, v_s | 134 | 142 | |
| seismic survey | 39–41 | | |
| sensitivity | | | |
| defined | 346 | 592 | |
| example of | 308 | 310 | 596 |
| typical values of | 347 | | |

Index Terms

Links

| | | | |
|---|---------|---------|---------|
| settlement, S | 25 | 92 | |
| calculations | 272–274 | | |
| components of | 265 | | |
| consolidation | 244 | 247–261 | |
| as a function of time | 253–254 | 277–278 | |
| of multiple layers | 295 | | |
| distortion (immediate) | 265 | | |
| immediate | 265–271 | | |
| overconsolidated soils | 249 | 254–255 | 273–274 |
| Schmertmann’s method | 268–271 | | |
| secondary compression | 279 | | |
| shallow foundations. <i>See</i> shallow foundations | | | |
| ultimate | 272–276 | | |
| shallow foundations | | | |
| bearing capacity | 395–400 | | |
| settlement | 398 | | |
| shape factor, N_f/N_c | 167 | | |
| shear strength | | | |
| angle of internal friction, ϕ | 334 | | |
| clays | | | |
| drained strength parameters | 342–343 | 612 | |
| effective stress analysis | 439 | 441–444 | |
| total stress analysis | 435–439 | | |
| unconfined compression | 346 | 596 | |
| vane | 321–322 | 619 | |
| cohesion, c | 337 | 339 | 342 |
| cohesionless soils | 333 | 339 | |
| definition | 306 | | |
| dilatancy | 309 | 315 | 342 |
| drained | 307 | 342 | 618 |
| envelope Mohr failure | 311–313 | 343 | 618 |

Index Terms

Links

| | | | |
|---|---------|---------|---------|
| shear strength (<i>Cont.</i>) | | | |
| factors of safety | 27 | 432–433 | 445–446 |
| failure | 306 | 344 | |
| failure angle, α_f | 313 | | |
| failure criteria | | | |
| compressive strength | 309 | | |
| maximum principle stress difference | 308 | 310 | |
| maximum principle stress ratio | 343–344 | | |
| friction | 340–342 | | |
| intrinsic | 338–339 | | |
| parameters | | | |
| c | 345 | 598 | |
| intrinsic | 337 | 339 | |
| ϕ | 345 | 598 | |
| residual | 344–345 | | |
| undrained | 307 | 344 | 346–348 |
| | 585 | 594 | |
| shear strength tests. <i>See also</i> triaxial tests. | | | |
| direct shear | 312–315 | | |
| direct simple shear | 322–323 | | |
| typical results | 314 | 590 | |
| vane | 321 | 324 | 619–621 |
| sheet structure | 11 | | |
| Shelby tube | 52–53 | | |
| shrinkage | | | |
| limit, <i>SL</i> | 88 | 519–525 | |
| linear, <i>LS</i> | 519 | 523 | |
| ratio, <i>R</i> | 519 | 522–523 | |
| volumetric, <i>VS</i> | 519 | 523 | |
| sieve analysis | 75 | 482 | 485 |
| | 491–492 | 541 | |
| silica sheet | 11–12 | | |

Index Terms

Links

| | | | |
|-----------------------------|---------|---------|----|
| silicate | 11 | | |
| silt | 22 | 76 | 93 |
| sinkhole | 17 | | |
| site | | | |
| conditions | 37 | | |
| geology | 36 | | |
| seismicity | 36 | | |
| slope | | | |
| failure | 425 | | |
| homogeneous | 433–435 | | |
| infinite | 428–433 | | |
| instability, causes of | 427–429 | | |
| types | 425–426 | | |
| slope failure | 425 | | |
| slope stability | 44 | 433 | |
| center of critical circle | 437 | | |
| effective stress | 439 | 442–444 | |
| infinite slope | 428–433 | | |
| influence of | | | |
| submergence | 438 | | |
| surcharge | 438 | | |
| tension cracks | 438 | | |
| method of slices | 435 | 439 | |
| $\phi = \text{zero}$ method | 436 | | |
| pore pressures | 441–443 | | |
| total stress | 441 | | |
| wedge method of analysis | 444–445 | | |
| soil(s) | 1 | 64 | 75 |
| aggregate | 77 | | |
| borings | | | |
| depth | 34–35 | | |

Index Terms

Links

| | | | |
|--------------------------|---------|--------|-----|
| soil(s) (<i>Cont.</i>) | | | |
| number | 35–36 | | |
| spacing | 35–36 | | |
| classification | 90 | 93–106 | |
| coarse-grained | 93 | | |
| cohesive | 65 | | |
| collapsible | 21 | 109 | |
| composition | 5 | | |
| consistency | 64 | 86 | 346 |
| density | 545–550 | | |
| electrical resistivities | 42 | | |
| expansive | 21 | | |
| exploration | 34 | | |
| resistivity exploration | 41–43 | | |
| scope of | 34 | | |
| seismic survey | 39–41 | | |
| field sample collection | 455–456 | | |
| fine-grained | 93 | | |
| glacial origin | 20–21 | | |
| granular | 66 | | |
| identification | 89 | | |
| improvement, types | 113 | | |
| investigation program | 38 | | |
| organic | 11 | 22 | 66 |
| | 75 | 90 | 526 |
| profile | 22–24 | | |
| reconnaissance | 34 | | |
| residual | 9 | 15–17 | |
| samples | | | |
| depth interval | 36 | | |
| disturbed | 36 | 47 | |
| types | 36 | | |

Index Terms

Links

| | | | |
|--------------------------|---------|---------|---------|
| soil(s) (<i>Cont.</i>) | | | |
| undisturbed | 36 | 50 | 591 |
| sensitivity | 64 | 86 | 120 |
| | 308 | 310 | 346–347 |
| | 592 | | |
| transported | 17–20 | | |
| water | 17–19 | | |
| wind | 19–20 | | |
| water | 65 | | |
| absorbed | 66 | | |
| content ω | 65 | 79 | 87 |
| | 458–459 | 462–465 | |
| density | 500 | 504 | |
| free | 65–66 | | |
| interlayer | 67 | | |
| lattice | 67 | | |
| oriented | 66 | | |
| salinity | 466–470 | | |
| unfrozen, ω_u | 66 | | |
| water transported | 17–19 | | |
| wind transported | 19–20 | | |
| soil characteristics | | | |
| compressibility | 245–247 | 250 | |
| dilatancy | 309 | 315 | 335–337 |
| | 340 | 342 | |
| permeability | | | |
| absolute (specific), K | 134 | | |
| anisotropic materials | 169–170 | | |
| coefficient of, k | 31 | 70 | 118–119 |
| | 133–135 | 138 | 264 |
| measurement of | 136–137 | 139–144 | 559–567 |

Index Terms

Links

| | | | |
|---------------------------------------|---------|-----|-----|
| soil characteristics (<i>Cont.</i>) | | | |
| of stratified soils | 163–164 | | |
| typical values, chart | 138 | | |
| soil classification | | | |
| AASHTO system | 102–106 | | |
| Unified system (USCS) | 93–101 | | |
| soil improvement | | | |
| compaction | 113 | | |
| dewatering | 113 | | |
| grouting | 127 | | |
| preloading | 113 | | |
| soil mechanics | 1 | 2 | |
| solids | | | |
| unit weight | 78 | | |
| volume of | 499 | 504 | |
| specific gravity, G_s | 80 | 87 | 92 |
| | 495–496 | 500 | 522 |
| apparent | 493 | 495 | |
| average | 541 | 543 | |
| correction factor, α | 485–486 | | |
| specific surface | 13 | 15 | 86 |
| spread footing | 28 | | |
| stability analysis | | | |
| charts | 436–438 | 440 | |
| effective stress | 439–444 | | |
| infinite slope | 428–433 | | |
| method of slices | 435 | | |
| total stress | 435–439 | | |
| wedge method | 444–445 | | |
| standard penetration test, SPT | 49 | 267 | 324 |
| | 327–328 | | |
| correlation with CPT tests | 330 | | |

Index Terms

Links

| | | | |
|--|---------|---------|-----|
| standard Proctor tests. <i>See</i> compaction tests. | | | |
| strain influence diagram | 271 | | |
| strength parameters | 444 | 598 | 612 |
| | 617 | | |
| stress | | | |
| at a point | 188–189 | 204–206 | |
| due to surface loads | 204–233 | | |
| effective | 188 | 191 | 196 |
| | 610 | | |
| Mohr's circle, derivation | 198–201 | | |
| paths | 319–320 | | |
| plane (two-dimensional) | 198 | | |
| principal planes | 200–201 | | |
| principal stresses | 200 | | |
| intermediate | 324 | | |
| major | 200 | 324 | |
| minor | 200 | 324 | |
| total | 191 | | |
| stress distribution | | | |
| Bousinesq theory | 204–205 | | |
| circular load | 218–220 | | |
| influence charts | | | |
| circular loaded area | 220 | | |
| line load | 210–211 | | |
| Newmark's | 228 | | |
| point load | 206 | | |
| rectangular loaded area | 223 | | |
| line load | 208–211 | | |
| long embankment | 217–218 | | |
| point load | 204–206 | | |

Index Terms

Links

| | | | |
|--------------------------------------|---------|-----|---------|
| stress distribution (<i>Cont.</i>) | | | |
| rectangular load | 221–223 | | |
| strip load | 212–213 | | |
| triangular load | 216–217 | | |
| stress ratio. <i>See</i> , K_f | | | |
| stress-strain behavior | | | |
| confined compression | 307 | 576 | 584 |
| direct shear | 312–316 | 590 | |
| drained | 307–308 | 315 | |
| examples | 308 | 310 | 314–315 |
| | 398 | | |
| triaxial test | 316–321 | | |
| undrained | 307 | 310 | 596 |
| volumetric | 308 | 315 | |
| structure | 13–14 | | |
| dispersed-type | 13 | | |
| flocculated-type | 13 | | |
| macrostructure | 136 | | |
| microstructure | 136 | | |
| surface of sliding, observation of | 27–28 | | |
| surface tension, T | 67–69 | 196 | |
| swelling of soils | 118 | | |

T

| | | | |
|---|-------|--|--|
| tamping foot roller. <i>See</i> compaction equipment | | | |
| tension cracks | | | |
| retaining walls | 360 | | |
| slopes | 438 | | |
| tetrahedral unit | 11–12 | | |
| thaw-weakening | 72 | | |
| threshold gradient, i_0 | 135 | | |

Index Terms

Links

| | | | |
|--|---------|---------|---------|
| till | 20 | | |
| toughness index, I_t | 511 | | |
| triaxial tests | | | |
| apparatus | 317–319 | | |
| consolidated-drained, CD | 317 | 612–618 | |
| consolidated-undrained, CU | 317 | 598–610 | |
| unconsolidated-undrained, UU | 317 | | |
| tube capillary | 69 | | |
| U | | | |
| U-line | 94 | 523 | |
| unconfined compression | | | |
| test | 591–596 | | |
| test machine | 592 | | |
| undisturbed sampling | 47 | 50 | |
| undrained strength | | | |
| from field tests | | | |
| Dutch cone penetration test, CPT | 267–268 | 324 | 328–330 |
| standard penetration test, SPT | 49 | 267 | 324 |
| | 327–328 | | |
| measurement. <i>See also</i> triaxial, tests | | | |
| direct shear test | 312–315 | 585 | |
| unconfined compression test | 591–596 | | |
| vane shear test | 321–322 | 346 | 619–622 |
| strain rate effect | 348 | | |
| Unified Soil Classification System | 5 | 93–101 | |
| uniformity coefficient of, C_u | 94 | 475–476 | 478 |
| unit weight | 78 | 107 | 118 |
| bouyant | 79 | | |
| bulk | 78 | 87 | 108 |
| | 502–504 | 534 | |
| dry | 500 | 502–504 | 534 |

Index Terms

Links

| | | | |
|--|---------|-----|-----|
| unit weight (<i>Cont.</i>) | | | |
| effective | 79 | | |
| of solids | 78 | | |
| optimum | 534 | 539 | 542 |
| | 546 | | |
| saturated | 79 | 87 | 500 |
| | 502–504 | | |
| water | 78 | 80 | 134 |
| USCS. <i>See</i> Unified Soil Classification System. | | | |
| V | | | |
| Van der Waals forces | 13 | | |
| vane shear test | 321 | 324 | |
| Bjerrums correction factor | 322 | 324 | |
| varved clay | 19 | 21 | |
| vermiculite | 13 | | |
| vertical strain | | | |
| area correction | 594 | 609 | 615 |
| use in settlement calculations | 268 | 272 | |
| viscosity, η | 486 | | |
| void ratio, e | 10 | 79 | 87 |
| | 107 | 500 | 504 |
| | 574 | | |
| effect on shear strength | 334 | | |
| maximum | 107 | 542 | |
| minimum | 107 | 541 | |
| voids volume of, V_v | 78 | | |

Index Terms

Links

W

water

| | | |
|-----------|---------|-----|
| absorbed | 66 | |
| density | 500 | 504 |
| salinity | 466–470 | |
| viscosity | 561–562 | |
| volume of | 499 | 504 |

water content

| | | | |
|------------------|---------|---------|-----|
| determination of | 458–459 | 462–465 | |
| optimum | 534 | 539 | 542 |
| pore, w | 65 | 79–80 | |
| unfrozen, w_u | 66 | | |

water pressure. *See* pore water pressure.

| | | | |
|-------------|----|----|-------|
| water table | 24 | 30 | 57–59 |
|-------------|----|----|-------|

| | | | |
|-------------------------|----|----|--|
| water transported soils | 15 | 17 | |
|-------------------------|----|----|--|

waves

| | | | |
|-------------|-------|-----|--|
| compression | 39 | 42 | |
| direct | 39–40 | | |
| head | 40 | 453 | |

| | | | |
|------------|---|---|----|
| weathering | 5 | 9 | 56 |
|------------|---|---|----|

| | | | |
|--|-----|-----|--|
| | 346 | 475 | |
|--|-----|-----|--|

| | | | |
|-------------|----|-----|-----|
| weight unit | 78 | 107 | 115 |
|-------------|----|-----|-----|

well graded. *See* grain size distribution.

| | | | |
|------------------|---------|--|--|
| well graded soil | 475–476 | | |
|------------------|---------|--|--|

| | | | |
|------------------------------|----|--|--|
| Wenner electrode arrangement | 43 | | |
|------------------------------|----|--|--|

| | | | |
|--------------------|-------|--|--|
| wind-laid deposits | 19–20 | | |
|--------------------|-------|--|--|

Y

| | | | |
|----------------------|----|-----|--|
| Young's modulus, E | 56 | 453 | |
|----------------------|----|-----|--|

| | | | |
|------------------------|-----|--|--|
| initial tangent, E_i | 308 | | |
|------------------------|-----|--|--|

| | | | |
|-------------------------------------|-----|--|--|
| initial tangent undrained, E_{iu} | 310 | | |
|-------------------------------------|-----|--|--|

Index Terms

Links

Young's modulus, E (*Cont.*)

shear

453

Z

Zero air voids curve

115–117

532–533

538